DOT/FAA/TC-16/23

Federal Aviation Administration
William J. Hughes Technical Center
Aviation Research Division
Atlantic City International Airport
New Jersey 08405

Mode I (G1c) Fracture Toughness of Composite Sandwich Structures for Use in Damage Tolerance Design and Analysis: Vol. I Static Testing Including Effects of Fluid Ingression

September 2017

Final Report

U.S. Department of Transportation
Federal Aviation Administration

NOTICE

Technical Report Documentation Page

1. Report No.	2. Government Accession No.	3. Recipient's Catalog No.
DOT/FAA/TC-16/23		

4. Title and Subtitle	5. Report Date
MODE I (G1C) FRACTURE TOUGHNESS OF COMPOSITE SANDWICH STRUCTURES FOR USE IN DAMAGE TOLERANCE DESIGN AND ANALYSIS: VOL. I STATIC TESTING INCLUDING EFFECTS OF FLUID INGRESSION	September 2017
	6. Performing Organization Code

7. Author(s)	8. Performing Organization Report No.
John S. Tomblin, Waruna Seneviratne, and Shawn Denning	

9. Performing Organization Name and Address	10. Work Unit No. (TRAIS)
National Institute for Aviation Research Wichita State University Wichita, KS 67260	
	11. Contract or Grant No.

12. Sponsoring Agency Name and Address	13. Type of Report and Period Covered
U.S. Department of Transportation Federal Aviation Administration FAA Northwest Mountain Regional Office 1601 Lind Ave SW Renton, WA 98057 USA	
	14. Sponsoring Agency Code AIR-100

15. Supplementary Notes

The Federal Aviation Administration William J. Hughes Technical Center Aviation Research Division CORs were Lynn Pham and Curtis Davies.

16. Abstract

This report, Volume I, contains results of Mode I static testing of composite sandwich structures. It is the first of a set of three volumes. The second volume contains results of Mode I fatigue testing, and the third volume contains supplemental results of Mode I static testing of sandwich variables not tested in Volume I. In this volume, the influence of sandwich parameters, such as facesheet thickness, core type, cell size, and core density, on the onset of damage growth of sandwich composites was investigated using single-cantilever beam static testing for Mode I fracture toughness of the core-facesheet disbond. To investigate the influence of fluid ingression and entrapped fluids in sandwich structures, test specimens were conditioned in a hydraulic oil (i.e., Skydrol®) and water mixture. The fluid ingression and facesheet thickness of all the studied variables increased fracture toughness significantly. Other variables, such as cell size, core type, and core density, had a minimal effect on fracture toughness. The information gathered through this research will be instrumental in developing analytical methods and validating finite element analysis procedures to further investigate the damage growth mechanics in composite sandwich structures. The data can also be used in the design of sandwich structures constructed of similar materials and geometries tested here.

17. Key Words	18. Distribution Statement
Composite sandwich, Fluid ingression, Mode I testing, Damage tolerance	This document is available to the U.S. public through the National Technical Information Service (NTIS), Springfield, Virginia 22161. This document is also available from the Federal Aviation Administration William J. Hughes Technical Center at actlibrary.tc.faa.gov

19. Security Classif. (of this report)	20. Security Classif. (of this page)	21. No. of Pages	22. Price
Unclassified	Unclassified	445	

ACKNOWLEDGEMENTS

This research program was funded by the FAA William J. Hughes Technical Center in Atlantic City, NJ. The authors would like to thank Curtis Davies of the FAA William J. Hughes Technical Center and Dr. Larry Ilcewicz of the FAA Seattle Aircraft Certification Office for their technical guidance. Also, the support from Cessna Aircraft, Bombardier Aerospace, Hawker Beechcraft, and Spirit AeroSystems is appreciated.

The authors would also like to thank the NIAR Composites and Structures Laboratory staff for their commitment and hard work; namely, Upul Palliyaguru, Janith Senaratne, Tharindu Jayaratne, Chee-Kuen Chan, Jason Koehn, Errick Robles, Jeffery Robles, and Benjamin Coon for their support during fabrication, testing, and data reduction.

TABLE OF CONTENTS

LIST OF FIGURES

LIST OF TABLES

LIST OF ABBREVIATIONS, SYMBOLS, AND ACRONYMS

5%/max	The 5% offset or max load GIC
D5528	ASTM Standard for Mode I Interlaminar Fracture Toughness of Unidirectional Fiber-Reinforced Polymer Matrix Composites
β	Geometric correction parameter
δ	End displacement of cantilever beam
Δa	Additional crack length required to correct for cantilever beam not being perfectly built-in
σ	Stress
ε	Strain
a	Crack length
a_o	Prescribed crack length
b	Specimen width
A	Adhesive interface disbond failure
B	y-intercept
C	Compliance
E	Stiffness
F	Large displacement correction factor
G	Strain energy release rate
Gc	Fracture toughness or critical strain energy release rate
I	Second moment of inertia of cantilever beam
L	Length of specimen
M	Moment applied to cantilever beam
P	Load applied to cantilever beam
S	Interlaminar facesheet delamination failure
t	Distance from bottom surface of cantilever beam to load line in piano hinge
U	Strain energy
V	Volume
x	Axial direction of cantilever beam
y	Normal to axial direction of cantilever beam
ADL	Allowable damage limit
AGATE	Advanced General Aviation Transport Experiments
APO	Adhesive pullout failure
CDT	Critical damage threshold
DCB	Double-cantilever beam
ETD	Elevated-temperature dry
ETW	Elevated-temperature wet
GAG	Ground-air-ground
GIC	Mode I fracture toughness
GIC (NL)	Mode I fracture toughness measured at nonlinear onset of crack growth
GIC (VIS)	Mode I fracture toughness measured at visual onset of crack growth
GIC (5%/max)	Mode I fracture toughness measured at 5% offset or max load
HX	Hexagonal core
NASA	National Aeronautical and Space Administration
NL	Nonlinear onset of crack growth

OX	Over-expanded core
PO	Pullout failure
RTD	Room temperature dry
RTW	Room temperature wet
SCB	Single-cantilever beam
SERR	Strain energy release rate
VIS	Visual onset of crack growth

EXECUTIVE SUMMARY

The influence of sandwich parameters, such as facesheet thickness, core type, cell size, and core density, on the onset and damage growth rate of sandwich composites was investigated using single-cantilever beam static testing for Mode I fracture toughness of the core-facesheet disbond. To investigate the influence of fluid ingression and entrapped fluids in sandwich structures, test specimens were conditioned in a hydraulic oil (Skydrol®) and water mixture.

The fluid-ingression phenomenon in composites is a concern relative to sandwich structures. Inadequate design details or poor material selection can result in microcracks during ground-air-ground (GAG) cycling that consequently coalesce to form transverse matrix cracks, leading to moisture ingression into the subsequent composite and adhesive layers and, finally, into the core. Impact damage on sandwich structures exacerbates the fluid-ingression phenomenon as a result of localized transverse cracks, delaminations, disbonds, and core damages. Thermo-mechanical loads during GAG cycling could cause local buckling on the compression side of sandwich structures, which results in localized Mode I stresses that may result in further delamination/disbond growth, thus creating more passageways for fluid migration. Additionally, trapped water in sandwich cells translates into vapor during high temperatures, thus increasing the internal pressure and causing core disbonds and fractures. In some cases, the damage growth resulting from these two mechanisms is stable and occurs over a period of several flights, but it may not be readily detected on the ground when the thermo-mechanical and internal vapor pressure loads are released. Although the damage size continues to grow in such cases, the structure will continue to carry loads until it reaches a critical damage threshold (CDT), at which point the unstable damage growth triggers catastrophic failure. Unless such damage is detected and repaired prior to reaching the CDT, GAG cycling effects will increase the size of damage and threaten the structural integrity and safety of the aircraft.

For tests performed in this study, the fluid ingression and facesheet thickness increased facture toughness significantly. Other variables, such as cell size, core type and core density, had a minimal effect on fracture toughness. The information gathered through this research will be instrumental in developing analytical methods and validating finite element analysis procedures to further investigate the damage growth mechanics of composite sandwich structures. The data can also be used in the design of sandwich structures constructed with similar materials and the geometries tested here.

1. INTRODUCTION

Over the past 25 years, the use of advanced composite materials in aircraft primary structures has increased significantly. In 1994, with the Advanced General Aviation Transport Experiments (AGATE) program, the National Aeronautics and Space Administration (NASA) and the FAA revitalized the use of composites in both general and commercial aviation. Driven by the demand for fuel-efficient, lightweight, and high-stiffness structures with fatigue durability and corrosion resistance, large modern commercial aircraft are designed with more than 50% composite materials. Because of the key differences between metal and composite damage mechanics and durability concerns, the certification philosophy for composites must meet rigorous structural integrity, safety, and durability requirements. Despite the many advantages of composites, composite structural certification becomes challenging because of a lack of experience with large-scale structures, complex interactive failure mechanisms, sensitivity to temperature and moisture, and scatter in the data, especially fatigue.

The current research effort was designed to investigate the fluid-ingression phenomenon in sandwich structures and the resulting progressive damage growth caused by ground-air-ground (GAG) cycling. Inadequate design details, poor material selection, and operational damages can cause fluid ingression into the core. Impact damage on sandwich structures exacerbates the fluid-ingression phenomenon as a result of localized transverse cracks, delaminations, disbonds, and core damages. Thermo-mechanical loads during GAG cycling could cause local buckling on the compression side of a sandwich structure, resulting in localized Mode I stresses that may result in further delamination/disbond growth, thus creating more passageways for fluid migration. Additionally, trapped water in sandwich cells translates into vapor during high temperatures, thus increasing the internal pressure and causing core disbonds or fractures. In some cases, the damage growth resulting from these two mechanisms is stable and occurs over a period of several flights, but it may not be readily detected on the ground when the thermo-mechanical and internal vapor pressure loads are released. Although the damage size continues to grow in such cases, the structure will continue to carry loads until it reaches a critical damage threshold (CDT), at which point the unstable damage growth triggers catastrophic failure. Unless such damage is detected and repaired prior to reaching the CDT, GAG cycling effects will increase the size of damage and threaten the structural integrity and safety of the aircraft.

This investigation used single-cantilever beam (SCB) static testing for Mode I fracture toughness of core-facesheet construction because the failure modes included core, disbonds, and adhesive. The influence of sandwich parameters, such as facesheet thickness, core size, core density, and cell size, on the onset and the damage growth rate of sandwich composites were investigated. Furthermore, the influence of the fluid-ingression on damage initiation due to entrapped fluids in sandwich structures was investigated. The flow chart (see figure 1) demonstrates how the data generated in this program will result in guidance for durability and damage tolerance of sandwich composite structures.

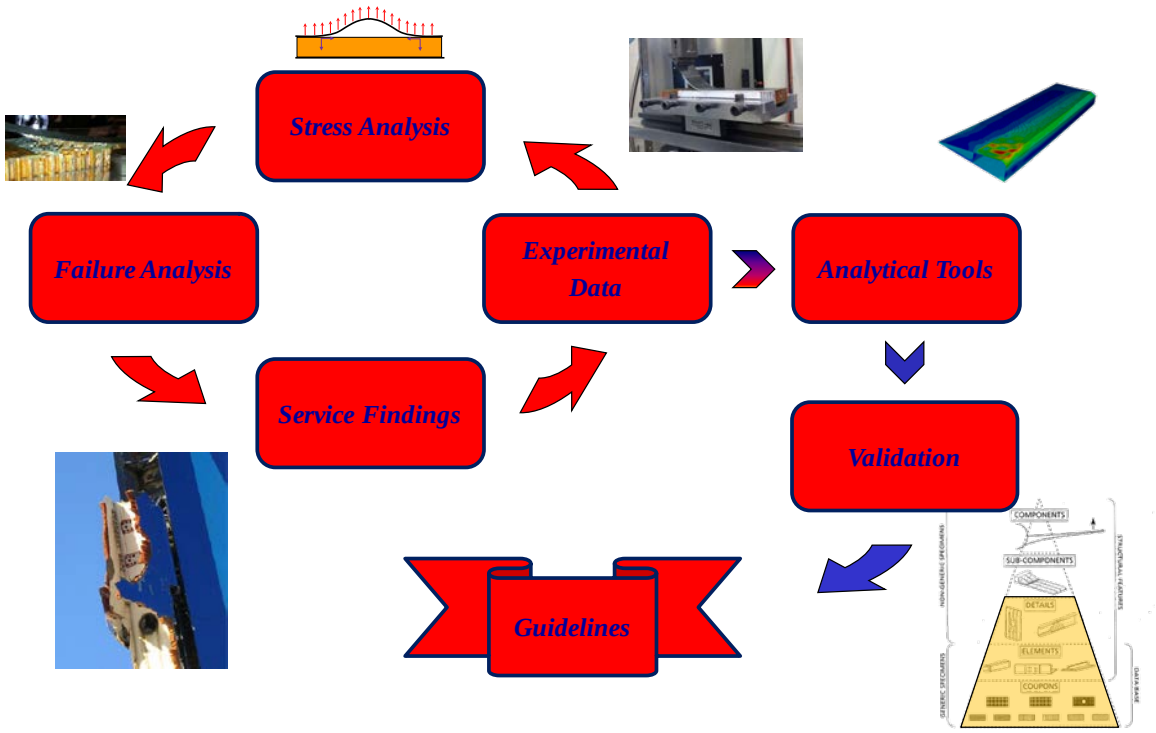

Figure 1. Objective of current research program

The onset of damage propagation and the CDT are functions of the stress level for a particular damage configuration. Typically, certification programs adopt a "no-growth" damage-tolerant design concept, whereby a composite structure is required to demonstrate the ability to contain intrinsic manufacturing defects, and the maximum allowable service damage(s) in adverse operational conditions and throughout the design life of the structure (i.e., the allowable damage limit [ADL] is selected so that the fatigue stress level corresponding to the limit load of the structure will not cause the onset of damage propagation prior to a life corresponding to the design service goal). In contrast, a "stable-growth" damage-tolerant design concept must consider damage growth only if the following apply:

- Damage growth is stable or an arrest mechanism is in place prior to the damage reaching CDT.
- Damage growth can be predicted through analysis and can be verified by testing.
- Two inspection intervals occur prior to the damage reaching the CDT, if applicable.

Because the onset of damage propagation depends on several design parameters, such as load spectrum/severity, damage configuration, damage location with respect to the primary load path, environmental exposure, facesheet thickness, core density or cell size of sandwich construction, and fracture toughness, the application of load-enhancement factors to a structure that exhibits stable damage growth during testing may significantly alter its fatigue life. Damage-tolerance substantiation through a stable-growth approach for a specific structure requires great confidence at the onset (initiation) and during the growth rate (propagation), and knowledge of the factors influencing both initiation and propagation. It was found in the literature that through

experimental validation, the fracture toughness of an adhesive or the core can be used to predict crack initiation [1]. The influence of key parameters—such as initial damage configuration, fracture toughness at different altitudes and environmental conditions, facesheet thickness, core type, cell size, and core density at both initiation and during propagation—must be studied in detail and incorporated into the certification process to mitigate risks associated with a stable-growth approach.

The data contained in this report and the subsequent two volumes encompass the information regarding the fracture toughness of sandwich structures, and the influence of core and facesheet parameters provides an understanding of the sandwich structure design space and the failure mechanism. The data in this report contain the results of Mode I testing under static load for different composite sandwich variables, including fluid ingression. Volume 2 contains data from Mode I testing under fatigue loading for the same sandwich parameters and fluid ingression as in Volume I for static loads. Volume 3 examines additional sandwich parameters under static loads on Mode I fracture toughness.

Crack growth can be characterized by three modes [2, 3]: Mode I (opening mode), Mode II (sliding or in-plane shear mode), and Mode III (tearing or out-of-plane shear mode), as shown in figure 2. It is common that combinations of these three modes are present at a crack tip unless care is taken to isolate them, especially during coupon-level testing. Both volumes of the test report focus on Mode I (opening mode) fracture toughness of sandwich structures. Sandwich structures often fail in a mixture of dominant failure modes (e.g., in the case of debond in core-to-facesheet interface, facesheet tends to buckle outwards because of the pressure differential at cruising altitude and cause mixed-mode [predominantly Modes I and II] stresses at crack tip). To evaluate the structural behavior of sandwich construction, Mode I loading configuration was selected because of its simplicity in comparison with Mode II or mixed-mode test configurations. Mode I (GIC) opening mode is considered a material property. For the tests performed here, GIC has a broader meaning. It should be understood more as a structural property of a given sandwich construction. Different failure modes are encountered and, therefore, a strict definition of a material property does not apply.

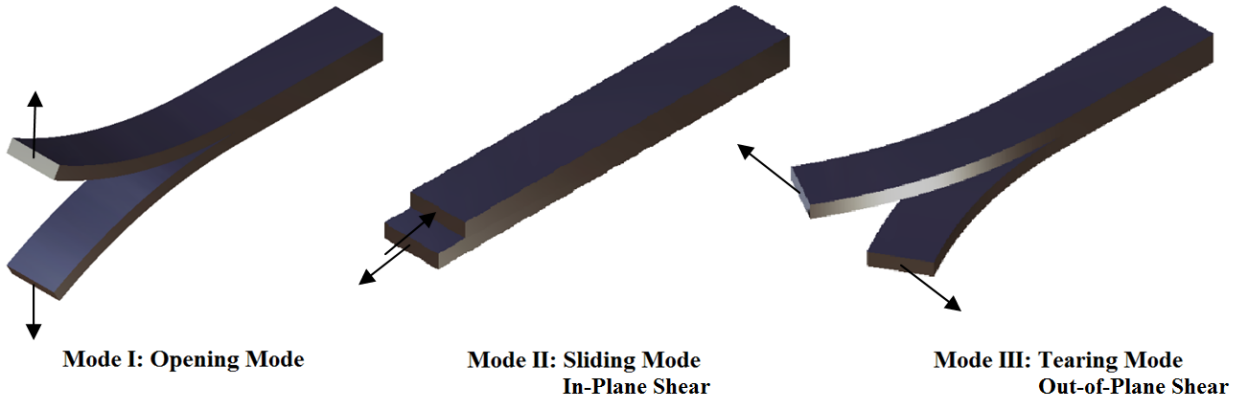

Figure 2. Fracture modes

2. EXPERIMENTAL PROCEDURE

The primary objective of this program was to determine the Mode I fracture toughness of several sandwich composite material systems. Therefore, it was imperative to develop and use a test configuration that isolated Mode I crack propagation and mitigated Mode II-/Mode III-induced crack growth. Because of the lack of standardized test methods and validated data-reduction techniques involving Mode I tests of sandwich structures, a preliminary investigation was conducted to evaluate the feasibility of two test configurations: 1) a double-cantilever beam (DCB) test, and 2) an SCB test. Both of these test configurations are shown in figure 3. The DCB test for a sandwich structure is a modification of the existing ASTM standard D5528, Mode I Interlaminar Fracture Toughness of Unidirectional Fiber-Reinforced Polymer Matrix Composites. Because the D5528 data-reduction technique is not directly applicable to the current sandwich specimen, it required modification to address the current test procedure. Therefore, the existing data-reduction methodologies for similar specimens [4–6] were reviewed and modified to suit the sandwich test configurations.

(a) DCB (b) SCB

Figure 3. Test configurations: (a) DCB and (b) SCB [7]

Preliminary DCB tests indicated large rotation of the free end because of the asymmetric nature of the sandwich specimen configuration (i.e., crack along the facesheet-core interface, as seen in figure 4). This potentially added a significant amount of Mode II stresses resulting in mixed-mode loading at the crack tip. When the free end was stabilized by two rollers to prevent rotation, unsymmetrical bending loads caused core rupture through the thickness and crack propagation along the lower facesheet, a failure known as kinking, which can be seen in figure 5. Both of these DCB test configurations were deemed unacceptable for sandwich specimen testing.

After preliminary DCB trials, SCB tests based on the work of Cantwell and Davies [8, 9] were selected for the remainder of the tests included in the current phase of the research, and the specimen sizing guidelines presented by Ratcliffe [10] were evaluated to determine the valid range of crack lengths for each specimen configuration. The sandwich SCB test configuration used for this research program is discussed next.

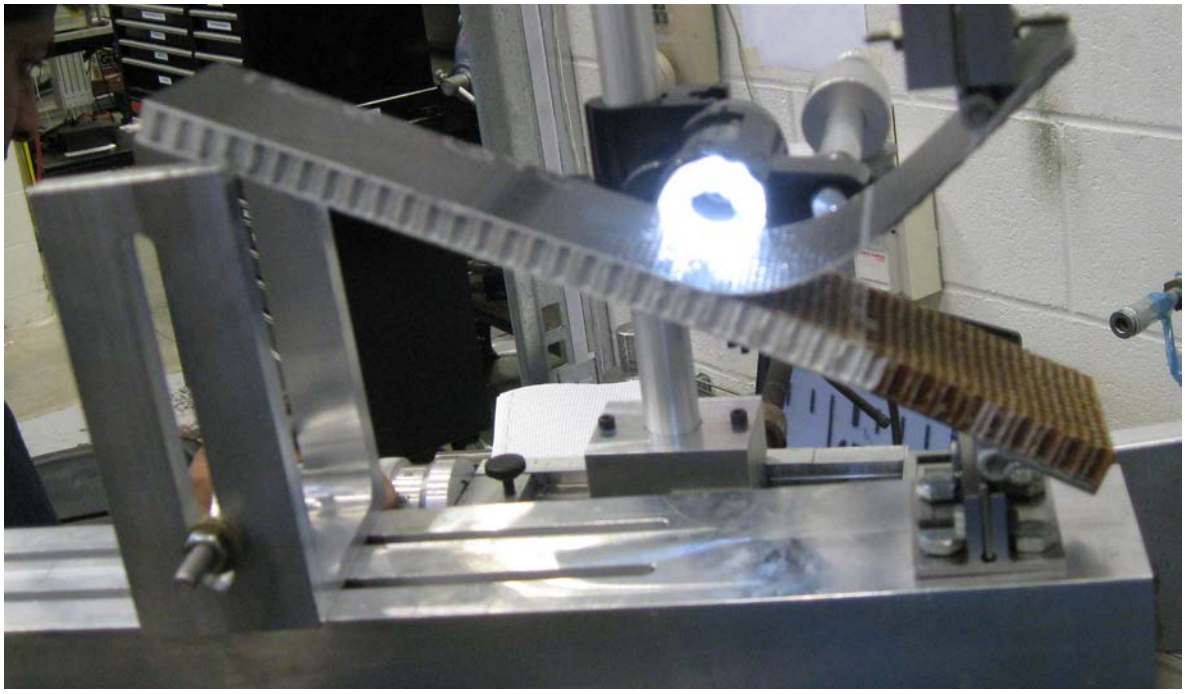

Figure 4. Large rotation of unstabilized DCB test on sandwich structure

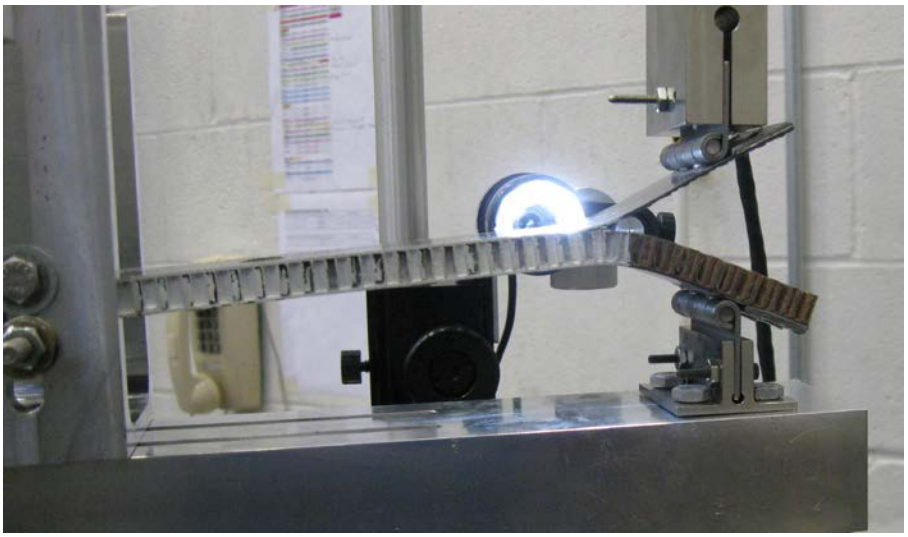

(a) Test setup

(b) Kinking and core rupture

Figure 5. Kinking of stabilized DCB test on sandwich structure: (a) test setup and (b) kinking and core rupture

Because of the complex damage mechanics, a detailed failure analysis was conducted for each test specimen. Preliminary tests conducted on the sandwich specimens indicated that failure initiation can occur either along the bondline or within the core, right below the fillets. Although it was possible that the crack could initiate within the composite facesheet, it was unlikely because the facesheet fracture toughness is significantly higher than that of the core.

Additionally, preliminary tests revealed that two primary progressive fracture paths are possible, as shown in figure 6:

1. Crack propagation along the bondline (core-facesheet interface).
2. Crack propagation along the bondline for a short distance, then migration into the core directly below the fillets.

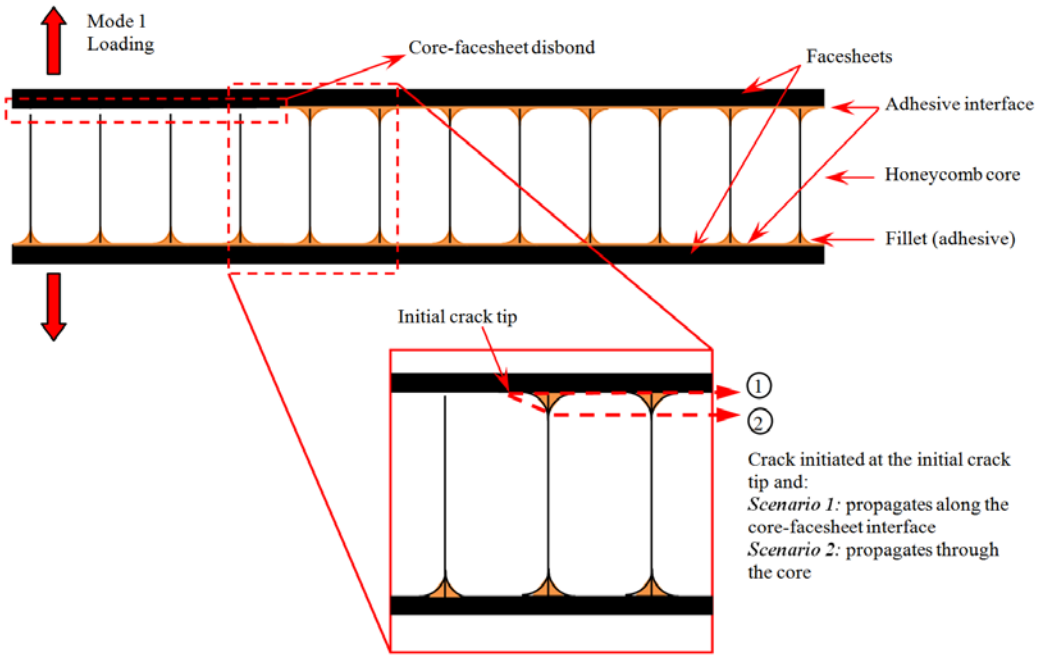

Figure 6. Primary progressive fracture paths for sandwich structures

In addition to these two primary failure modes, the following secondary failure modes were observed:

1. Adhesive pullout: flatwise tensile failure of adhesive underneath the fillet region (very common)
2. Kinking: crack propagation along the bondline for a short distance, core rupture through the thickness, and crack propagation along the opposite bondline (common in DCB, not common in SCB)
3. Core pullout or adhesion failure of the cell wall interface (not common)
4. Delamination of the facesheet (not common)

Because of the complex nature of progressive damage growth, any combination of the previously mentioned primary failure modes is possible. Detailed failure modes for the sandwich specimen configurations studied in this investigation are discussed in the results section of this report.

2.1 SCB TEST ON SANDWICH STRUCTURE

The primary difference between SCB and DCB test configurations on sandwich structures is that the underside of the SCB specimen is secured to a sliding foundation, whereas the top facesheet is loaded out-of-plane (Mode I), as shown in figure 7.

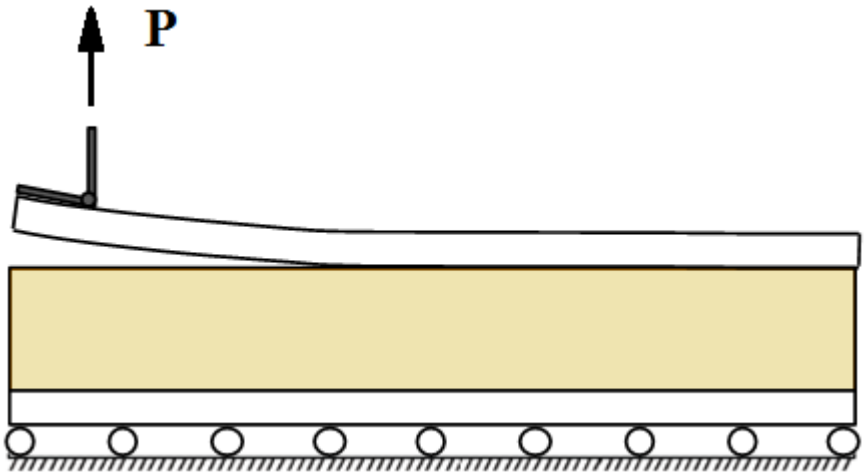

Figure 7. Schematic of SCB test configuration on sandwich structure

2.1.1 Test Fixture

The SCB diminishes the effects of unsymmetric loading of sandwich specimens and the effects of stiffness mismatch. It also reduces the effects of mode mixity, which can be further mitigated by creating a very long loading arm, thus reducing the component of force in the shear direction, or by placing the specimen on a sliding foundation, which releases the force in the shear direction every time it overcomes static friction. The latter was used in the design of this test configuration. The clamping method could be carried out in many ways. For example, each specimen could be perfectly bonded to the sliding foundation; however, this is illogical and time and cost intensive. Instead, an adjustable clamping system was used, as shown in figure 8. The test fixture holds the bottom facesheet while loading the hinge bonded to the top facesheet where the prescribed crack is located, as shown in figure 9.

Figure 8. Sliding SCB test fixture design

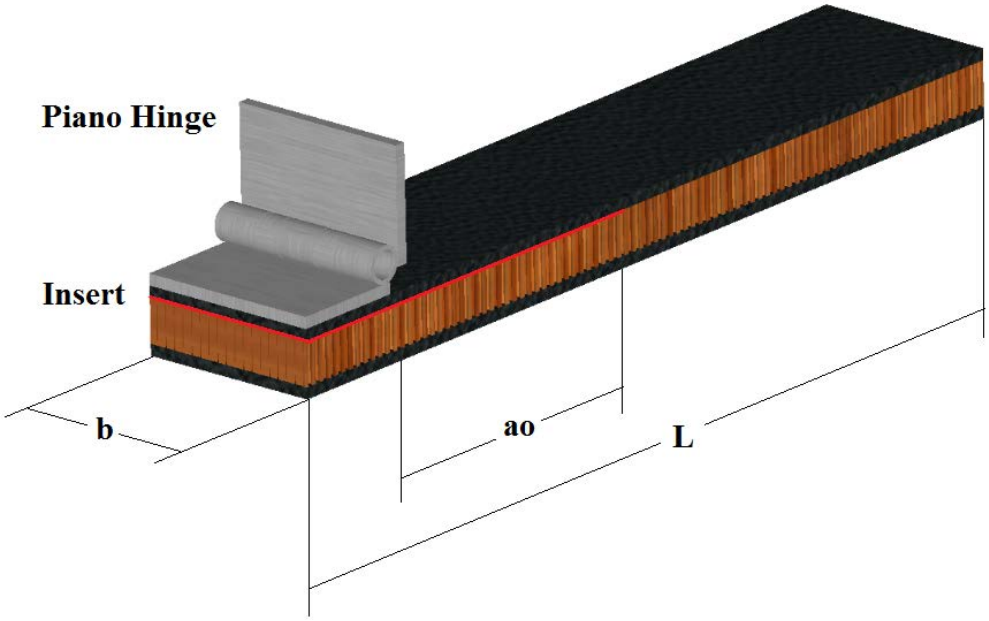

Figure 9. SCB geometry of sandwich specimen

2.1.2 Specimen Sizing

The 4-ply facesheet specimens underwent large displacements during testing. The modified correction factor (F) based on the ASTM D5528 test configuration could properly adjust the Mode I fracture toughness (GIC); however, it does not adjust the corresponding displacements. Because nonlinear displacements are required to properly determine the maximum and minimum displacements for cyclic loading, an additional adjustment was needed.

To reduce the large deflection and attain an accurate nonlinear displacement, coupons were resized to reduce the prescribed crack length, prolonging the onset of large deflection if the prescribed crack length was still long enough to ensure that bending was the primary form of loading. Methods presented by Ratcliffe [10] were used to determine a modified prescribed crack length (a_o) of the shortened specimens. A new prescribed crack length of 1″, referred to as "shortened," was selected. The sizing study shown in figure 10 indicates the length of cracks with the black lines as the initial crack length (a_o), as per Radcliffe [10].

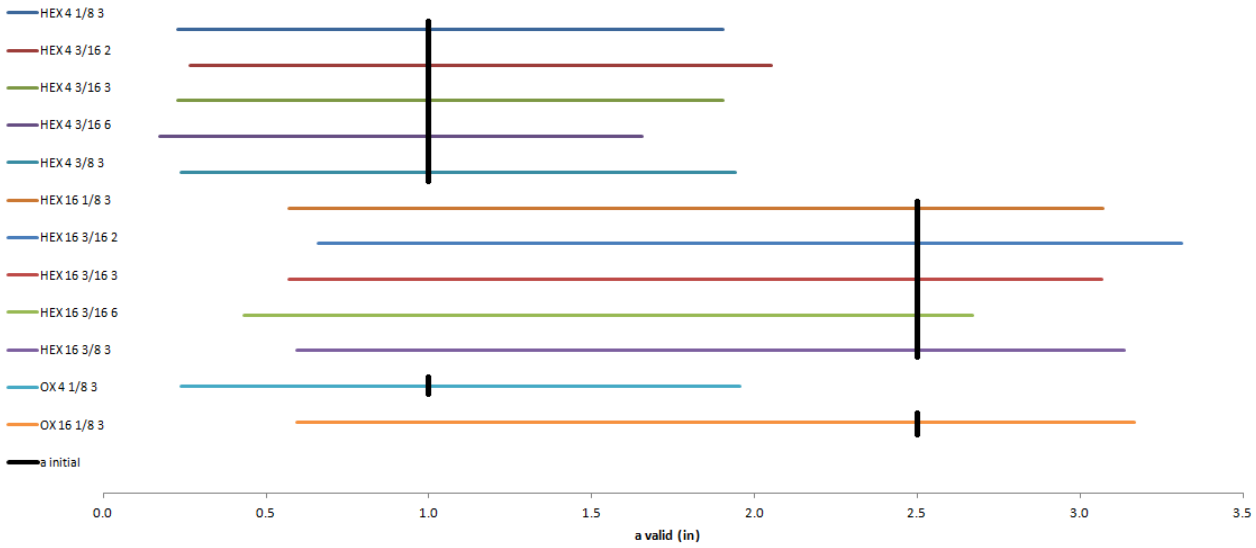

Figure 10. Valid crack growth range for 4-ply sandwich specimens

2.2 TEST MATRIX

Experiments proposed in the current task were carried out using Cytec AS4/E7K8 plain-weave facesheets bonded to Hexcel HexWeb® HRH-10 aramid fiber/phenolic honeycomb, using Cytec FM 300 film adhesive. Table 1 shows the test matrix for determining the Mode I fracture toughness of sandwich specimens using the SCB test configuration.

Table 1. Static test matrix for SCB sandwich specimens

Core Material	Core Type	Core Thickness (in)	Facesheet	Cell Size (in)	Core Density (lb/ft^3)	Number of Static Test Specimens			
						Baseline	Fluid-Ingressed	Extended Fluid-Ingressed	Water-Ingressed
HRH-10	HX	0.5	4-ply $[0/45]_S$	1/8	2.0				
					3.0	6			
					3.0*	3	6	1	
					6.0				
				3/16	2.0	6			
					2.0*	3	6	1	
					3.0	6			
					3.0*	3	6	1	
					6.0	6			
					6.0*	3	6	2	
				3/8	2.0				
					3.0	6			
					3.0*	3	6	2	
					6.0				
			16-ply $[0/45]_{4S}$	1/8	2.0				
					3.0	6	6	2	4
					6.0				
				3/16	2.0	6	6	2	4
					3.0	6	6	2	3
					6.0	6	6	1	4
				3/8	2.0				
					3.0	6	6	2	4
					6.0				
	OX	0.5	4-ply	3/16	2.0				
					3.0	6			
					3.0*	3	6	2	
					6.0				
			16-ply	3/16	2.0				
					3.0	6	6	1	4
					6.0				
Total Specimens						204			

* a_o = 1 inch; OX = over-expanded core ; HX = hexagonal core;

As shown in table 1, two different core types (hexagonal and over-expanded), three different cell sizes (1/8″, 3/16″, and 3/8″), and three different core densities (2, 3, and 6 pcf) were selected with two different facesheet thicknesses (4 and 16 plies). This matrix includes as-fabricated (baseline), fluid-ingressed, and water-ingressed specimens. Fluid-ingressed specimens were conditioned in a mixture of water and Skydrol® LD-4 hydraulic oil, as outlined in the procedure described in appendix A. An additional subtask determined the appropriate conditioning parameters. The test matrix was reduced so that a design of experiments model could be used for evaluating other (untested) combinations within the design space considered in table 1. The nomenclature shown in figure 11 was used to uniquely identify different specimen configurations.

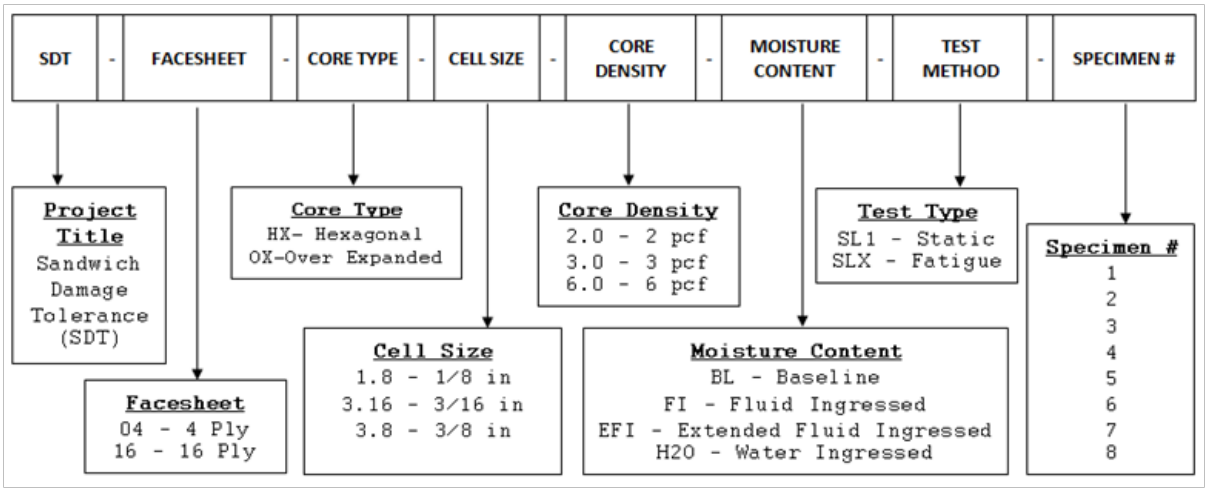

Figure 11. Sandwich specimen nomenclature

SCB sandwich specimens were 2″ x 10″ with a prescribed length (a_o) of 2.5″. For several configurations, specimens with an a_o of 1″ were included after the original prescribed crack length was deemed unacceptable.

Figure 12 shows the basic core geometry for both a hexagonal core (HX) and an over-expanded core (OX). Note that the OX cell size is the normal HX cell size before expansion to a rectangular shape. The typical nomenclature for core designation is material–cell size–density (i.e., HRH-10–1/8–3.0), indicating HRH-10 hexagonal honeycomb material with a 1/8″ cell size and a 3.0 lb/ft^3 (pcf) density. It is important to recognize that the mechanical properties of the sandwich structure are influenced by the ribbon direction in addition to the previously mentioned core parameters.

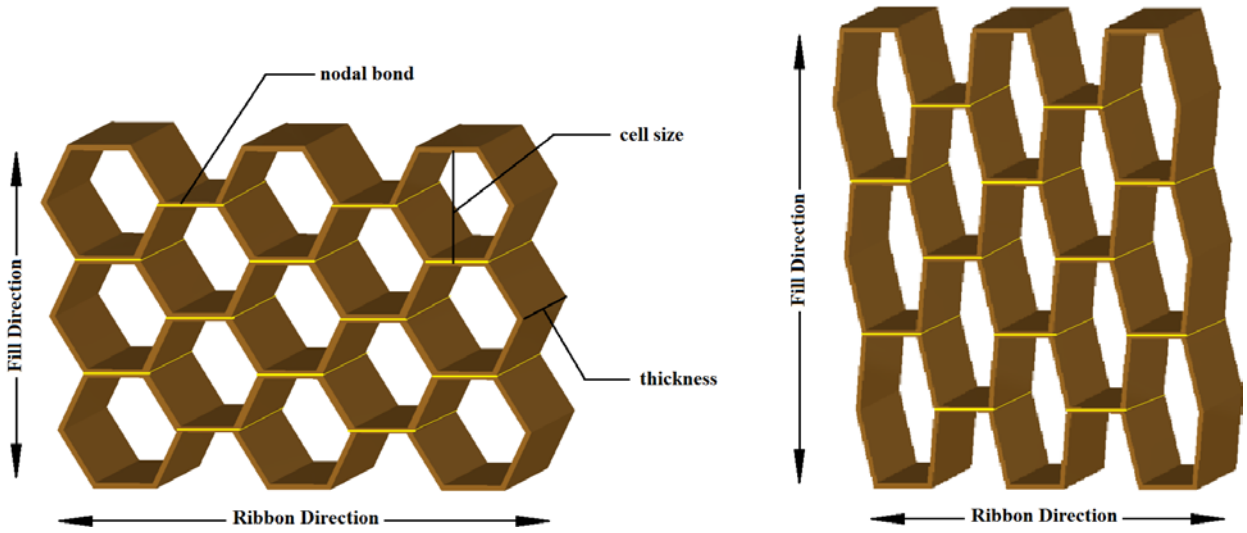

(a) HX (b) OX

Figure 12. Core geometry: (a) HX and (b) OX

2.2.1 Environmental Conditioning

Baseline specimens were tested as fabricated with no drying or additional fluid ingression. Fluid-ingressed specimens were conditioned either in a Skydrol-water solution or in a water bath. Standard Skydrol-water fluid ingression took place for 45 days, and extended fluid ingression took place for 165 days. Water-ingressed specimens were conditioned in a deionized water bath for 45 days.

When hydraulic oil was mixed with water and exposed to elevated temperatures (i.e., more than 120 °F) for an extended period of time, a chemical reaction released phosphoric acid, which deteriorated the adhesive interface in bonded structures. Aircraft control surfaces that extensively use sandwich structures are frequently exposed to hydraulic oil, and the previously mentioned conditions are highly probable. Therefore, it was vital to determine the effect on sandwich structures that are exposed to this volatile mixture.

To produce a viable solution, water and Skydrol were mixed in a 50:50 ratio by volume, placed in an elevated temperature of 160 °F for preconditioning, and agitated for 2 weeks. The mixture was then kept at room temperature, and the acidity level was monitored daily. During preconditioning, the elevated temperature acted as a catalyst and accelerated the chemical reaction that produced phosphoric acid. Following preconditioning, the solution maintained a steady pH level of approximately 3 at room temperature, indicating a stable fluid mixture for conditioning the fluid-ingressed specimens (see figure 13).

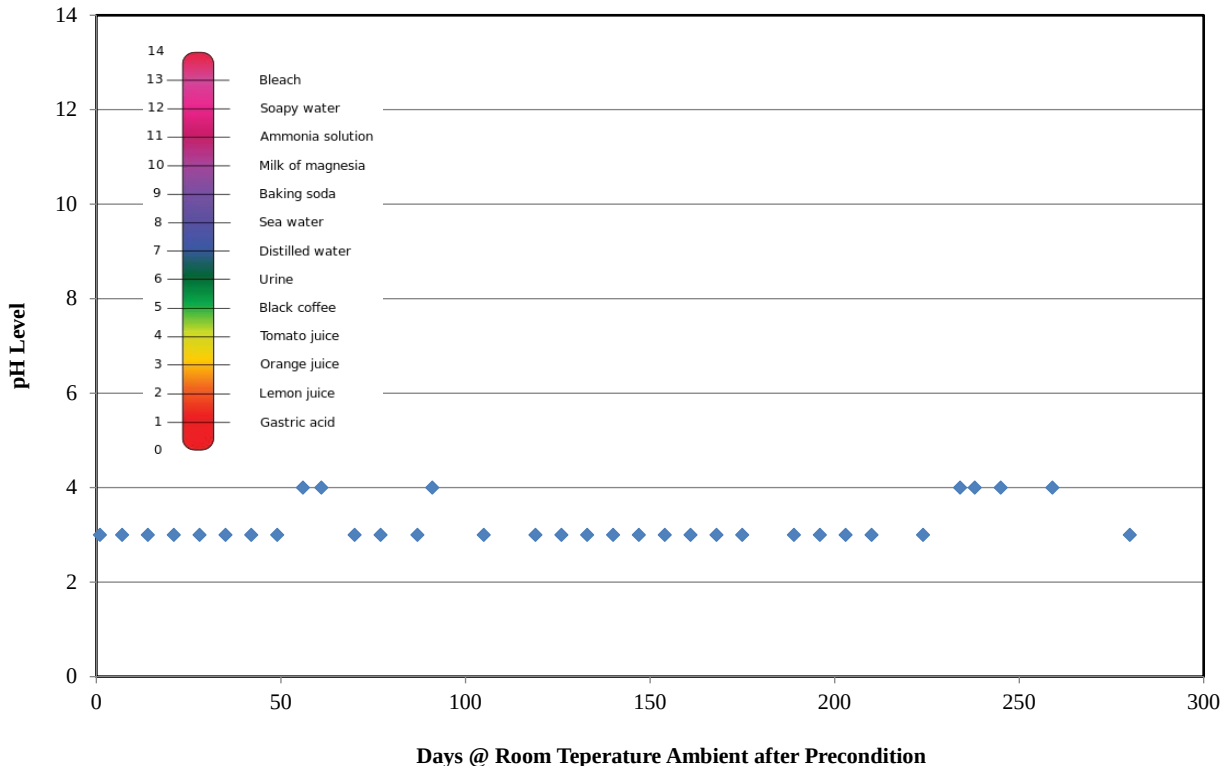

Figure 13. Acidity of Skydrol-water mixture used for environmental conditioning

2.2.2 Supplemental Testing

In addition to the sandwich SCB tests outlined in table 1, DCB test configurations were selected for determining the fracture toughness of the composite material and the adhesive system used for sandwich construction. Table 2 shows the test matrix for evaluating the fracture toughness of the laminate and adhesive using a modified ASTM D5528 test configuration. This includes the baseline specimens tested at room temperature dry (RTD) and 180 °F elevated-temperature dry (ETD), as well as fluid-ingressed specimens tested at room temperature wet (RTW) and elevated-temperature wet (ETW). DCB fatigue tests were carried out using a procedure developed for ASTM round-robin testing conducted at the National Institute for Aviation Research at Wichita State University for determining crack propagation. Table 3 shows the test matrix for evaluating flatwise tension (FWT) strength using the ASTM for Flatwise Tensile Strength of Sandwich Constructions (C297). The results are in appendix F (not used in this report); however, the data will be needed for any future finite element method analyses of sandwich structures.

Table 2. Test matrix for DCB laminate and adhesive fracture toughness

Material	Description	Layup Sequence	Test Condition	Number of Static Test Specimens	
				Baseline	Fluid-Ingressed
AS4/E7K8 PW	Laminate	$[0/45]_{4S}$	RTD	6	
			RTW		6
			ETD	6	
			ETW		6
AS4/E7K8 PW and FM300	Adhesive	$[0/45/0/45/FM300]_S$	RTD	6	
			RTW		6
			ETD	6	
			ETW		6
Total Specimens				48	

Table 3. Test matrix for flatwise tension of sandwich specimens

Material	Core Type	Core Thickness (in)	Facesheet	Cell Size (in)	Core Density (lb/ft^3)	Number of Static Test Specimens	
						Baseline	Fluid-Ingressed
HRH-10	HX	0.5	4-ply $[0/45]_S$	1/8	2.0		
					3.0	6	6
					6.0		
				3/16	2.0	6	6
					3.0	6	6
					6.0	6	6
				3/8	2.0		
					3.0	6	6
					6.0		
	OX			3/16	2.0		
					3.0	6	6
					6.0		
Total Specimens						72	

2.3 TEST PROCEDURE

It is important to note that the procedure involved in testing sandwich composite specimens for strain energy release rate (SERR or G) has no engineering standard dictating proper methodology. Therefore, a new procedure was developed by modifying the existing procedure for testing laminate DCB specimens.

Fracture toughness was measured using the SERR, because it is the most applicable for the specimens' test configuration and geometry. Furthermore, fracture toughness is often represented graphically by a resistance curve, or R curve. The fracture behavior of a material for a given mode is studied by developing a resistance curve that can be used to predict the load required for propagation. This curve is traditionally the SERR plotted against the crack extension for a given material. The R curve provides a basic description of how a fracture behaves in a particular material, because it depicts the energy required for a crack to propagate. Furthermore, an R curve can predict the stable/unstable regions of the propagation by superimposing the driving force against crack length on the R curve, as shown in figure 14 [2].

The R curves for two types of materials are shown here. The first case, as shown in figure 14(a) is a material with a flat R curve, indicating brittle behavior. The crack does not extend for the first stress level and becomes unstable as the driving force increases. The second case, shown in figure 14(b), is a material with a rising R curve, indicating ductile behavior. The crack propagates slowly with increasing stress until it reaches a critical point and then becomes unstable as the rate of change in the driving force exceeds the slope of the R curve.

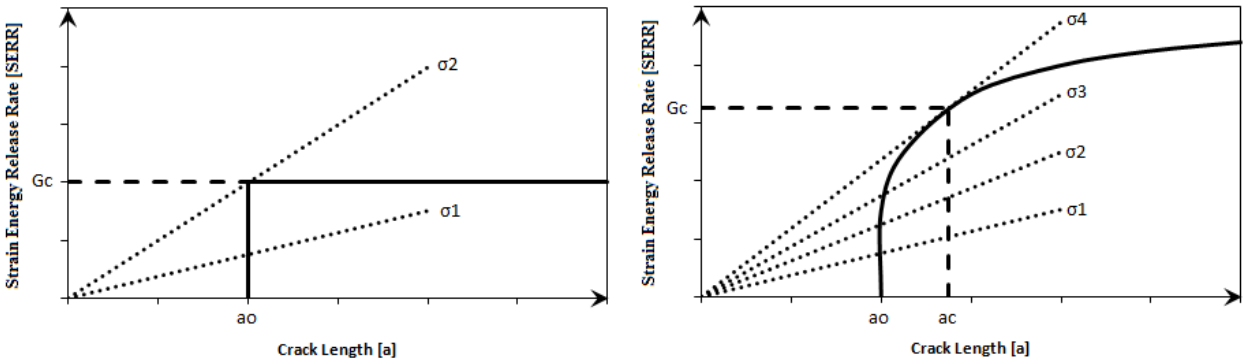

(a) Flat R curve

(b) Rising R curve

Figure 14. Schematic diagrams of driving force/R curve [2]: (a) flat R curve and (b) rising R curve

2.3.1 Static Test Procedure

The static test procedure was based very closely on the ASTM standard for Mode I Interlaminar Fracture Toughness of Unidirectional Fiber-Reinforced Polymer Matrix Composites (D5528). Excluding the test specimen configuration (SCB versus DCB) and data-reduction method, the test procedures are nearly identical.

Similar to the practices prescribed in the D5528 standard, the side of each specimen was painted white so that the crack propagation could be clearly visible. Because the edge was not planar, but rather contoured with the honeycomb core, shadowing and depth played a part in visually determining the crack tip location and crack propagation; therefore, crack length was a subjective measurement. Crack tip was monitored using a traveling digital microscope set at a magnification of 20x, as shown in figure 8.

One key difference in the test setup was the SCB test fixture. The specimens were clamped into the test fixture in the widthwise direction at two different torque values, which were determined after several trials, so that the facesheets would not be damaged. The clamping torque for thick-facesheet specimens was 35 in-lbs and 20–25 in-lbs for the thin-facesheet specimens.

As recommended in the D5528 standard, the specimen was preloaded to produce a natural (sharp) crack tip. The test was conducted under displacement control mode with a crosshead speed of 4 mm/min (except for the shortened specimens, for which the crosshead speed was 2 mm/min) while continuously recording the load and actuator displacement. Actuator displacement was assumed to be equal to the crack-opening displacement (δ). The crack was then propagated for approximately 5 mm, and the data collected during this phase were used for determining the fatigue load (discussed in Volume II of this research). The specimen was then reloaded, and the crack was propagated for approximately 50 mm.

Three distinct values of Mode I fracture toughness, or GIC, were determined from the SCB sandwich test. The first and most conservative was the nonlinear GIC (NL) (Mode I fracture toughness measured at nonlinear onset of crack growth), which was based on the load at onset of nonlinearity in the load-versus-displacement curve. The second and most subjective was the visual GIC (VIS), which corresponds to the load at which the crack initiates (visible crack). Lastly, the 5% offset or max load GIC (5%/max) was determined by plotting the intersection of the load-versus-displacement curve and a 5% radial offset curve or the maximum load, whichever occurred first. These three values and all propagation points were then plotted, producing a resistance curve, as shown in figure 15. The D5528 standard procedure includes details for determining these three GIC values.

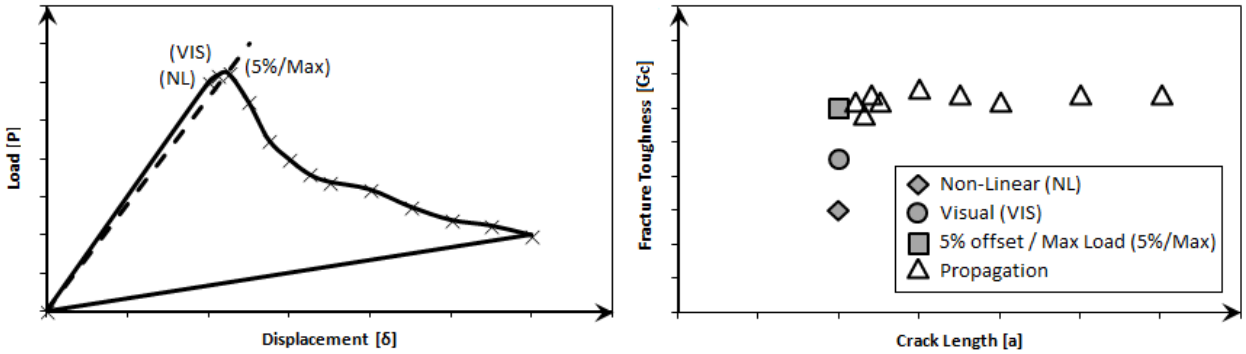

Figure 15. Sample load vs. displacement diagram and resistance curve

2.4 DATA REDUCTION

2.4.1 GIC Derivation

The SERR, or G, is energy dissipated during crack growth normalized by the newly created fracture surface and can be determined using several data-reduction methodologies. The most common data-reduction scheme is derived from the Euler-Bernoulli beam theory [11, 12].

The SERR is a material (and geometric) constant that characterizes the amount of energy required to open the crack. It is best to start the derivation process in its simplest form [2]:

$$G = \beta \frac{\partial U}{\partial a} \tag{1}$$

First, we look at strain energy, which is defined as the volume integral [11, 12]:

$$U = \frac{1}{2} \int_V \sigma \varepsilon \, dV \tag{2}$$

Consider these relationships and assume that stiffness and cross-sectional area remain constant [11, 12]:

$$\varepsilon = \frac{\sigma}{E} \tag{3}$$

Then,

$$U = \frac{1}{2E} \int_V \sigma^2 \, dV \tag{4}$$

$$\sigma = \frac{My}{I} \tag{5}$$

$$U = \frac{1}{2E} \int_V \frac{M^2 y^2}{I^2} \, dV \tag{6}$$

$$I = \int_A y^2 \, dA \tag{7}$$

$$U = \frac{1}{2EI} \int_x M^2 \, dx \tag{8}$$

Consider only the beam from the crack tip to the end load and the following relationship:

$$M = P\,(a - x) \tag{9}$$

$$U = \frac{1}{2EI}\int_0^a [P(a-x)]^2\,dx \tag{10}$$

Solve for strain energy:

$$U = \frac{P^2 a^3}{6EI} \tag{11}$$

Normalize by the crack front width:

$$\beta = \frac{1}{b} \tag{12}$$

Solve for the critical strain energy release rate:

$$GIC = \beta \frac{\partial U}{\partial a} = \frac{P^2 a^2}{2EIb} \tag{13}$$

Consider crack-opening displacement derived from the Euler-Bernoulli beam theory [11, 12]:

$$\delta = \frac{Pa^3}{3EI} \tag{14}$$

Substituting, the critical strain energy release rate's final form is obtained as:

$$GIC = \frac{3P\delta}{2ba} \tag{15}$$

2.4.2 Δ*a* Crack-Tip Rotation Correction

Euler-Bernoulli beam theory has many assumptions; one of them is being perfectly built-in or clamped. This implies that the crack front is perfectly normal to the loading direction and that there is no rotation or displacement. In reality, however, the crack front does rotate and may be displaced vertically. To remedy this issue, the crack is theoretically lengthened by Δa to the point where the crack front would be normal to the loading direction. When this adjustment is applied to beam theory, it is called the modified beam theory.

Start by considering the displacement derived by Euler-Bernoulli beam theory [11, 12]:

$$\delta = \frac{Pa^3}{3EI} \tag{16}$$

Consider compliance:

$$C = \frac{\delta}{P} \tag{17}$$

$$C = \frac{a^3}{3EI} \tag{18}$$

Rewrite:

$$C^{1/3} = \left(\frac{1}{3EI}\right)^{1/3} a + 0 \tag{19}$$

Consider the function of a line:

$$y = mx + B \tag{20}$$

Ideally the *y*-intercept would be zero, and the line would intersect the origin; however, because the beam is not perfectly built-in (displacement and rotation at the crack tip do not equal zero), the curve does not intersect the origin. Therefore, additional terms are added to the equations to shift the experimental data set and force the curve to intercept the origin.

Increase the crack length by Δa:

$$\delta = \frac{P(a + \Delta a)^3}{3EI} \tag{21}$$

Consider compliance and rewrite:

$$C^{1/3} = \left(\frac{1}{3EI}\right)^{1/3} (a + \Delta a) + B \tag{22}$$

Solve for Δa, where B is obtained empirically:

$$(3CEI)^{1/3} - B(3EI)^{1/3} - a = \Delta a \tag{23}$$

Set $C^{1/3}$ and a to zero (forcing the function to pass through the origin):

$$B(3EI)^{1/3} = \Delta a \tag{24}$$

Solve either analytically or graphically using a plot similar to figure 16.

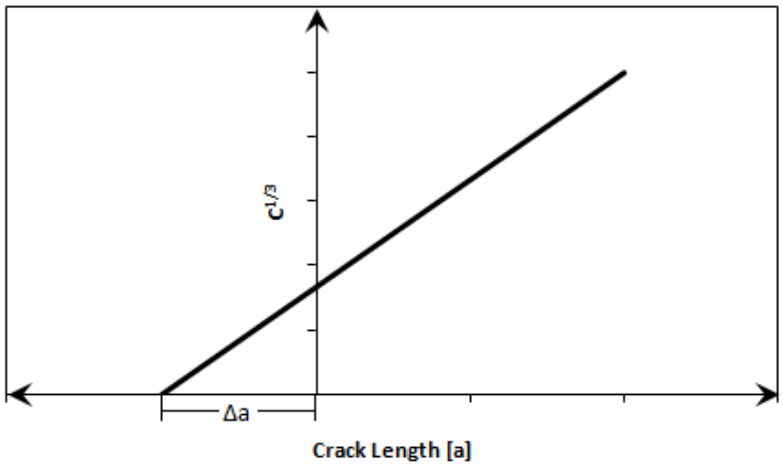

Figure 16. Graphical solution for Δ*a*

2.4.3 *F* Large Deflection Correction

Another assumption associated with beam theory entails small deflections. This implies that the tip deflection cannot be larger than 1/10 of the beam length. Large deflection causes two distinct issues. First is the direction of load application. Because the load is applied through a piano hinge, the loading direction is always perfectly normal to the crack front. The second is an artificial shortening of the moment arm. To remedy this issue, a correction factor *F* is applied to reduce the moment arm or rather the force felt at the crack tip.

Start by considering the correction factor *F* presented by the ASTM standard. The first term refers to shortening because of the beam in large deflection, and the second refers to shortening because of the piano hinge in large deflection:

$$F = 1 - \frac{3}{10}\left(\frac{\delta}{a}\right)^2 - \frac{3}{2}\left(\frac{\delta t}{a^2}\right) \tag{25}$$

Because the ASTM standard refers to DCBs, and because δ refers to the total displacement (which is displacement of both the top and bottom beams), the δ in the previous equation must be replaced with 2δ:

$$F = 1 - \frac{3}{10}\left(\frac{2\delta}{a}\right)^2 - \frac{3}{2}\left(\frac{2\delta t}{a^2}\right) \tag{26}$$

Reducing yields:

$$F = 1 - \frac{6}{5}\left(\frac{\delta}{a}\right)^2 - 3\left(\frac{\delta t}{a^2}\right) \tag{27}$$

To further validate the correction factor, it was compared to an analytical model developed by Williams [13]; the two solutions are shown in figure 17.

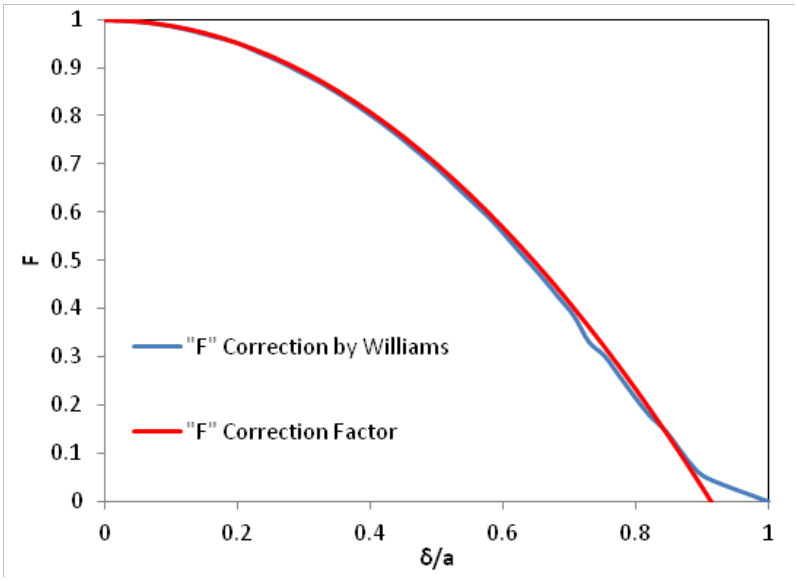

Figure 17. Comparison of correction factor (*F*) and analytical solution

2.5 FAILURE MODES

2.5.1 Adhesive Interface Disbond

An adhesive interface disbond, or adhesion failure, occurs when a crack is formed between the adhesive and the facesheet (see figure 18). This failure mode is typically an indication of poor adhesion of film adhesive to the prepreg material during the co-cure process. In this report, this failure is identified by the letter A.

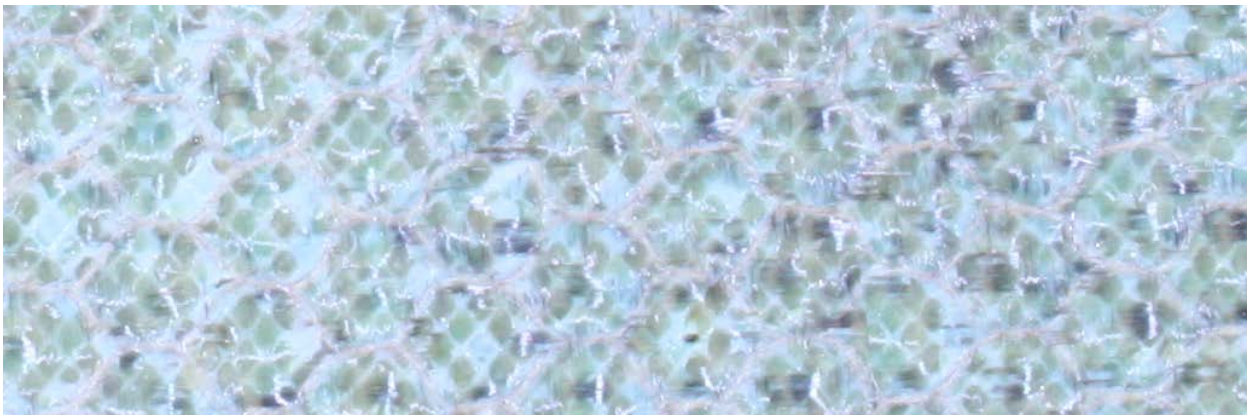

(a) Adhesive interface failure surface

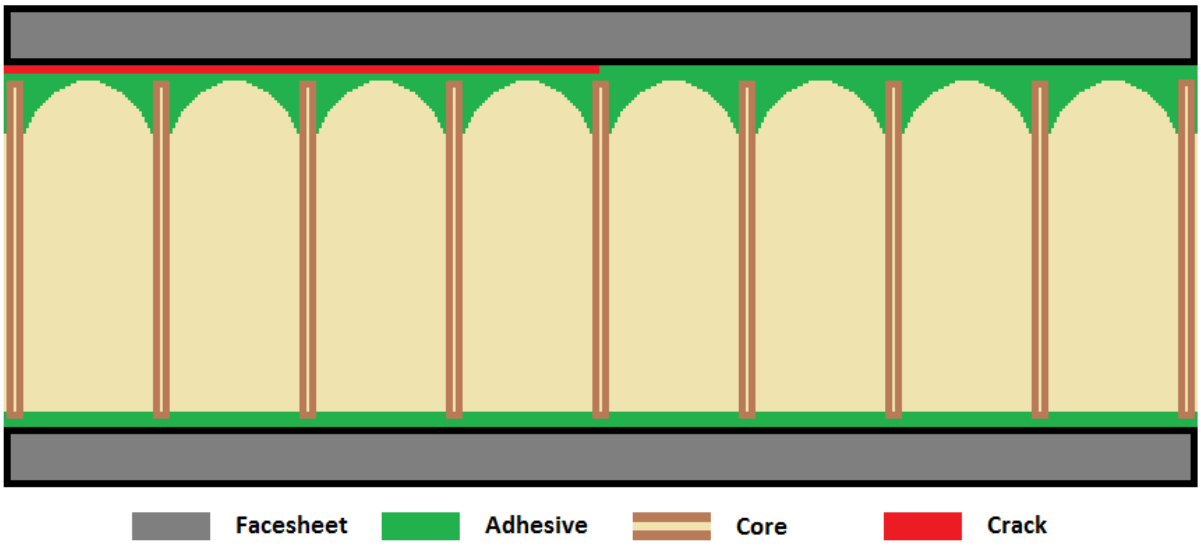

(b) Side view

Figure 18. Image of adhesive interface disbond: (a) adhesive interface failure surface and (b) side view

2.5.2 Adhesive Pullout Failure

Adhesive pullout failure (APO), or simply pullout failure (PO), occurs when a crack is formed within the adhesive (see figure 19). This type of failure rarely takes place on its own and is most often in combination with an adhesive interface disbond.

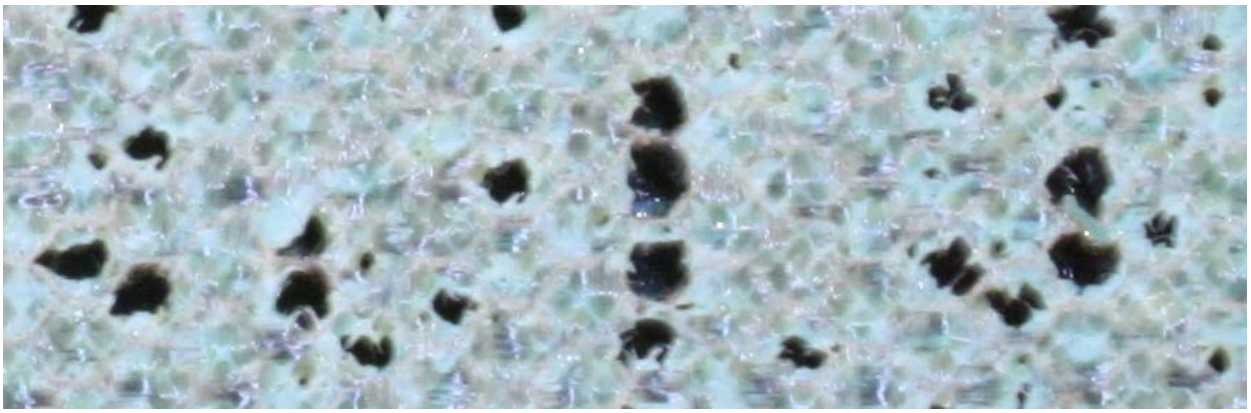

(a) PO surface

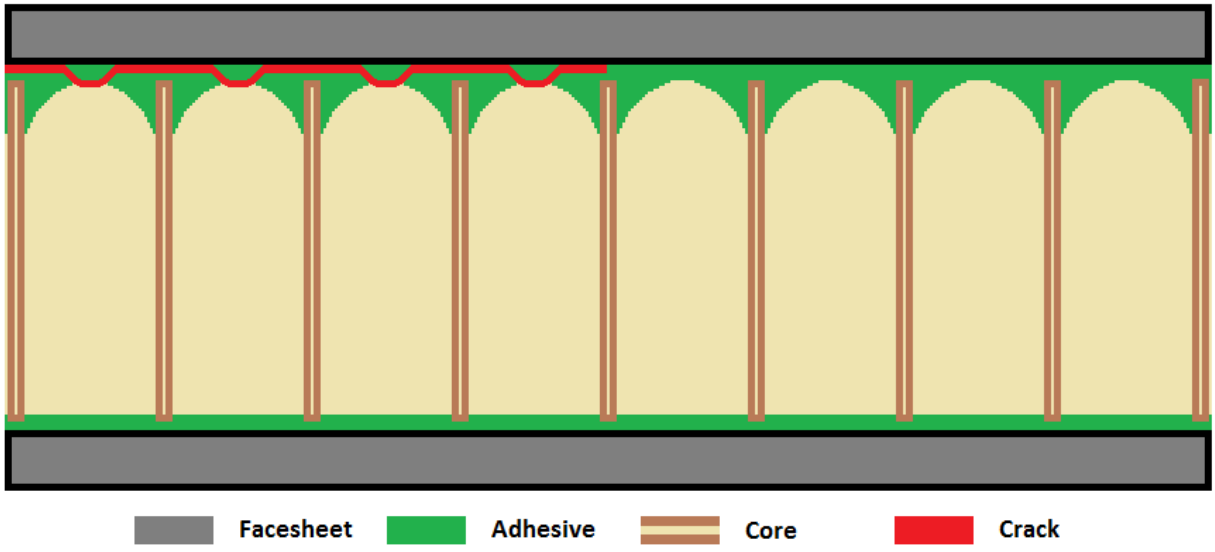

(b) Side view

Figure 19. Adhesive pullout failure: (a) PO surface and (b) side view

2.5.3 Tensile Core Failure

Tensile core failure, or simply core failure, occurs when a crack is formed within the core (see figure 20). Soon after initiation, the crack propagates into the core and often stayes there. In this report, core failure is identified by the letter C.

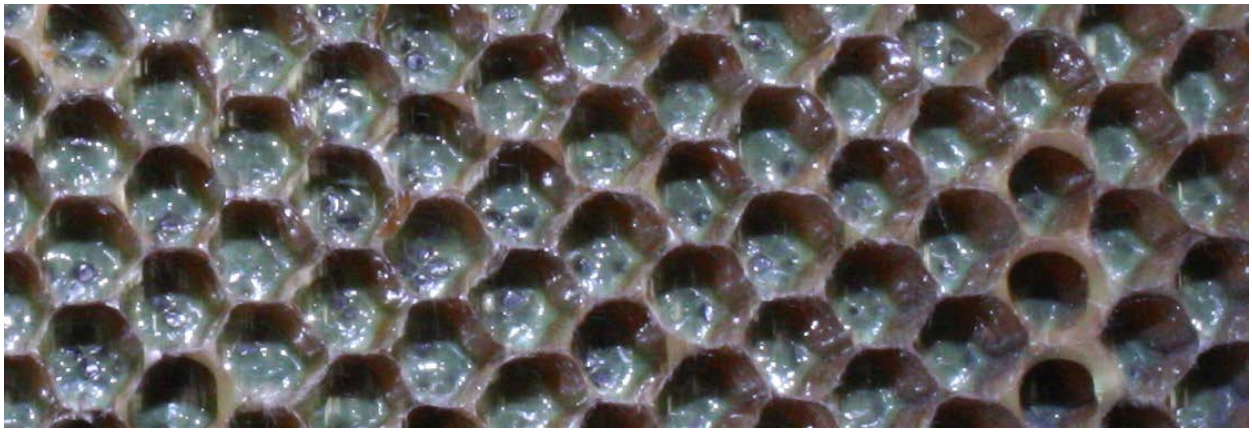

(a) Tensile core failure surface

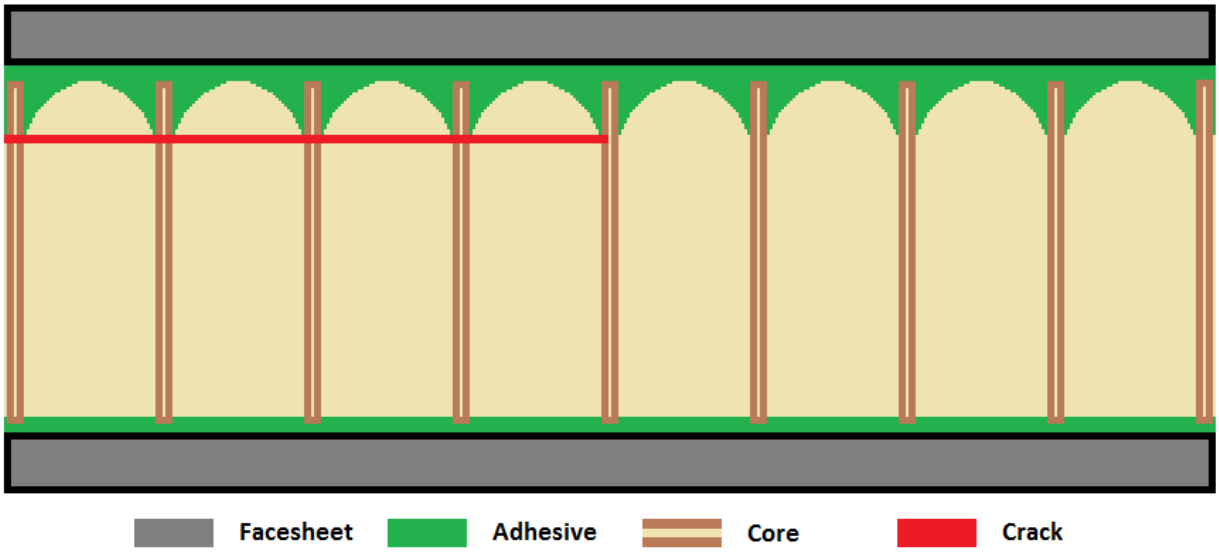

(b) Side view

Figure 20. Tensile core failure (a) surface and (b) side view (core failure)

2.5.4 Tensile Core PO

Tensile core PO occurrs when a crack is formed between the adhesive and the core (see figure 21). This type of failure mode was not seen during this investigation but can occur because of improper core preparation (i.e., rough cut/dry sanded core).

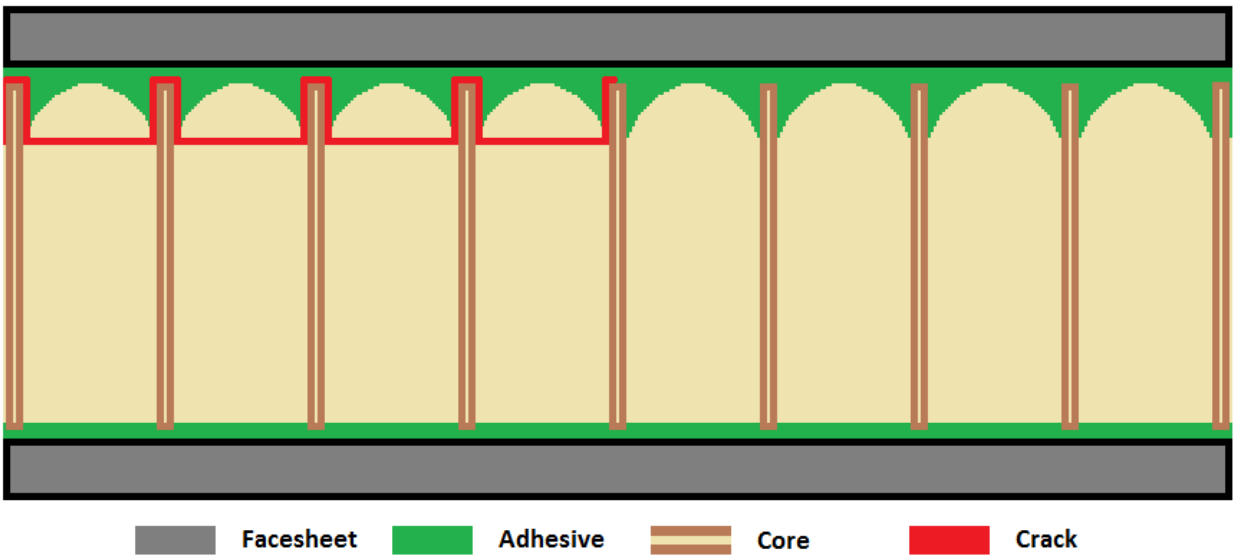

Figure 21. Tensile core PO

2.5.5 Adherend First Ply Facesheet Delamination

An adherend first-ply facesheet delamination, or adherend failure, is very rare and occurs when a crack is formed within the first-ply of the composite facesheet and propagates through the laminate.

2.5.6 Interlaminar Facesheet Delamination

Typically, interlaminar facesheet delamination forms on very thick facesheets (see figure 22) and occurs when a crack is formed within the laminate. This crack is predominantly caused by shear (Mode II) loads during the bending of a facesheet. In this report, interlaminar facesheet delamination is identified by the letter S.

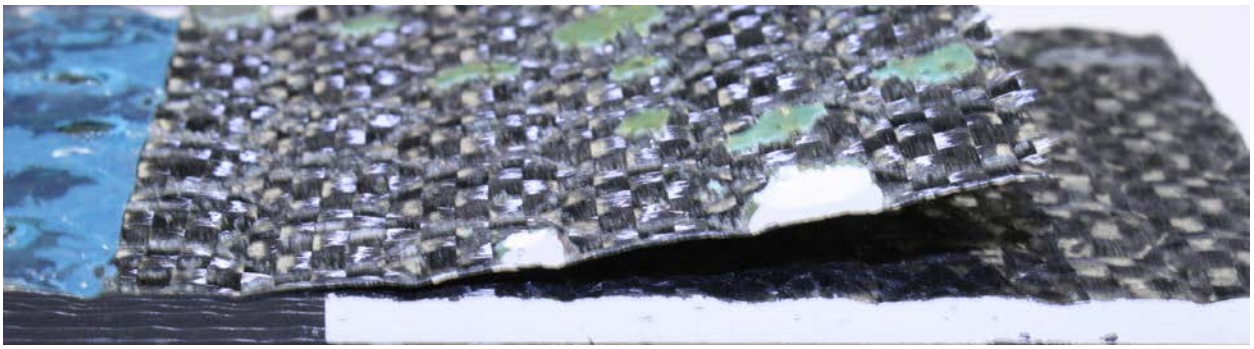

(a) Interlaminar facesheet delamination failure (S) surface

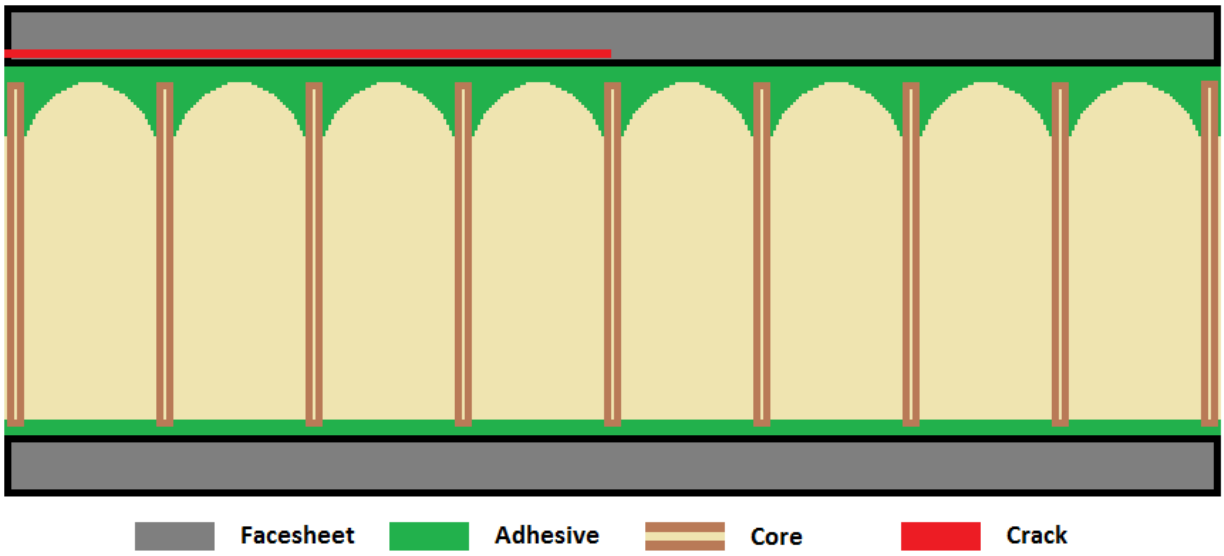

(b) Side view

Figure 22. Interlaminar facesheet delamination: (a) failure (S) surface and (b) side view

3. RESULTS AND DISCUSSION

Tables 4 and 5 show the average Mode I fracture toughness obtained for different sandwich parameters and environmental conditions. Note that the data reported here are for the natural crack tip. Pre-crack (Teflon™ film) data were recorded and reduced, but they were not included in this report. Figures 23–25 show a graphical comparison of the results. Test data include the GIC values for different facesheet thicknesses, core types, cell sizes, core densities, and different environments. It is important to note that several other variables can contribute to GIC, such as ribbon direction, fabrication technique, and prescribed crack location with respect to cell walls. These additional variables are investigated through a supplemental test matrix, and the results are included in volume III of this report series. The discussion and conclusions in this volume are based solely on the results included in this report.

Although the master summary tables and charts show a comparison of GICs, the effects of the aforementioned variables on GIC are coupled across different variables and required detailed

data analysis for determining each variable's impact. This section discusses, in detail, the impact of the following sandwich parameters on GIC:

- Facesheet thickness
- Core type
- Cell size
- Core density
- Environmental conditioning
- Prescribed crack length

Detailed results, including failure modes, are found in appendices B through E for 4-ply HX, 16-ply HX, 4-ply OX, and 16-ply OX, respectively. In these appendices, the progressive failure modes are compared against the SERR as the crack propagates so that the change in SERR can be attributed to the corresponding change in failure mode(s), as shown in figure 26.

Table 4. Master summary (English units)

Core Type	Facesheet	Cell Size (in)	Core Density (lb/ft^3)	GIC ($in\text{-}lb/in^2$)											
				Baseline			Fluid-Ingressed			Extended Fluid-Ingressed			Water-Ingressed		
				NL	VIS	5%/max	NL	VIS	5%/max	NL	VIS	5%/max	NL	VIS	5%/max
HX	4-ply $[0/45]_S$	1/8	2.0												
			3.0	0.622	1.538	2.086	-	-	-	-	-	-	-	-	-
			3.0*	*1.149*	*3.437*	*3.644*	*1.004*	*4.710*	*4.407*	*0.422*	-	*3.725*	-	-	-
			6.0												
		3/16	2.0	0.605	1.945	2.020	-	-	-	-	-	-	-	-	-
			2.0*	*1.067*	-	*3.317*	*0.880*	*2.834*	*2.707*	*1.064*	-	*2.499*	-	-	-
			3.0	0.604	2.153	2.325	-	-	-	-	-	-	-	-	-
			3.0*	*1.362*	*3.058*	*3.740*	*0.979*	*3.590*	*3.491*	*0.994*	-	*4.393*	-	-	-
			6.0	0.596	2.012	2.349	-	-	-	-	-	-	-	-	-
			6.0*	*1.020*	*3.246*	*2.993*	*0.695*	*4.206*	*4.834*	*0.547*	-	*5.379*	-	-	-
		3/8	2.0												
			3.0	0.788	3.149	3.030	-	-	-	-	-	-	-	-	-
			3.0*	*0.868*	*2.028*	*2.533*	*0.552*	*3.685*	*4.022*	*1.044*	-	*4.578*	-	-	-
			6.0												
	16-ply $[0/45]_{4S}$	1/8	2.0												
			3.0	1.912	4.603	5.475	1.201	6.226	6.393	1.950	-	6.809	3.740	-	7.633
			6.0												
		3/16	2.0	2.128	4.437	4.931	1.566	5.142	5.331	2.320	-	4.598	1.537	-	5.398
			3.0	2.305	4.961	4.842	2.501	5.713	6.151	2.475	-	8.602	3.093	-	6.050
			6.0	1.722	5.121	5.645	1.315	6.039	5.983	1.558	-	5.962	1.714	-	9.650
		3/8	2.0												
			3.0	1.567	2.813	2.877	2.052	5.263	6.816	2.298	-	5.906	2.178	-	6.366
			6.0												
OX	4-ply	3/16	2.0												
			3.0	0.583	1.712	2.195	-	-	-	-	-	-	-	-	-
			3.0*	*1.088*	-	*3.131*	*0.850*	*3.262*	*3.211*	*0.797*	-	*3.433*	-	-	-
			6.0												
	16-ply	3/16	2.0												
			3.0	1.541	5.483	6.017	1.206	4.973	5.074	1.149	-	5.022	1.849	-	4.743
			6.0												

* a_o = prescribed crack length of 1″ and is shown in italics; NL = nonlinear onset of crack growth; VIS = visual onset of crack growth

Table 5. Master summary (SI units)

Core Type	Facesheet	Cell Size (mm)	Core Density (kg/m^3)	GIC (KJ/m^2)											
				Baseline			Fluid-Ingressed			Extended Fluid-Ingressed			Water-Ingressed		
				NL	VIS	5%/max	NL	VIS	5%/max	NL	VIS	5%/max	NL	VIS	5%/max
HX	4-ply $[0/45]_S$	3.2	32												
			48	0.109	0.269	0.365	-	-	-	-	-	-	-	-	-
			48*	*0.201*	*0.602*	*0.638*	*0.176*	*0.825*	*0.772*	*0.074*	-	*0.652*	-	-	-
			96								-				
		4.8	32	0.106	0.341	0.354	-	-	-	-	-	-	-	-	-
			32*	*0.187*	-	*0.581*	*0.154*	*0.496*	*0.474*	*0.186*	-	*0.438*	-	-	-
			48	0.106	0.377	0.407	-	-	-	-	-	-	-	-	-
			48*	*0.239*	*0.536*	*0.655*	*0.171*	*0.629*	*0.611*	*0.174*	-	*0.769*	-	-	-
			96	0.104	0.352	0.411	-	-	-	-	-	-	-	-	-
			96*	*0.179*	*0.568*	*0.524*	*0.122*	*0.737*	*0.847*	*0.096*	-	*0.942*	-	-	-
		9.6	32												
			48	0.138	0.551	0.531	-	-	-	-	-	-	-	-	-
			48*	*0.152*	*0.355*	*0.444*	*0.097*	*0.645*	*0.704*	*0.183*	-	*0.802*	-	-	-
			96												
	16-ply $[0/45]_{4S}$	3.2	32												
			48	0.335	0.806	0.959	0.210	1.090	1.120	0.342	-	1.192	0.655	-	1.337
			96												
		4.8	32	0.373	0.777	0.864	0.274	0.900	0.934	0.406	-	0.805	0.269	-	0.945
			48	0.404	0.869	0.848	0.438	1.000	1.077	0.433	-	1.506	0.542	-	1.059
			96	0.302	0.897	0.989	0.230	1.058	1.048	0.273	-	1.044	0.300	-	1.690
		9.6	32												
			48	0.274	0.493	0.504	0.359	0.922	1.194	0.402	-	1.034	0.381	-	1.115
			96												
OX	4-ply	4.8	32												
			48	0.102	0.300	0.384	-	-	-	-	-	-	-	-	-
			48*	*0.191*	-	*0.548*	*0.149*	*0.571*	*0.562*	*0.140*	-	*0.601*	-	-	-
			96											-	
	16-ply	4.8	32												
			48	0.270	0.960	1.054	0.211	0.871	0.889	0.201	-	0.879	0.324	-	0.831
			96												

* a_o = prescribed crack length of 1″and is shown in italics; NL = nonlinear onset of crack growth; VIS = visual onset of crack growth

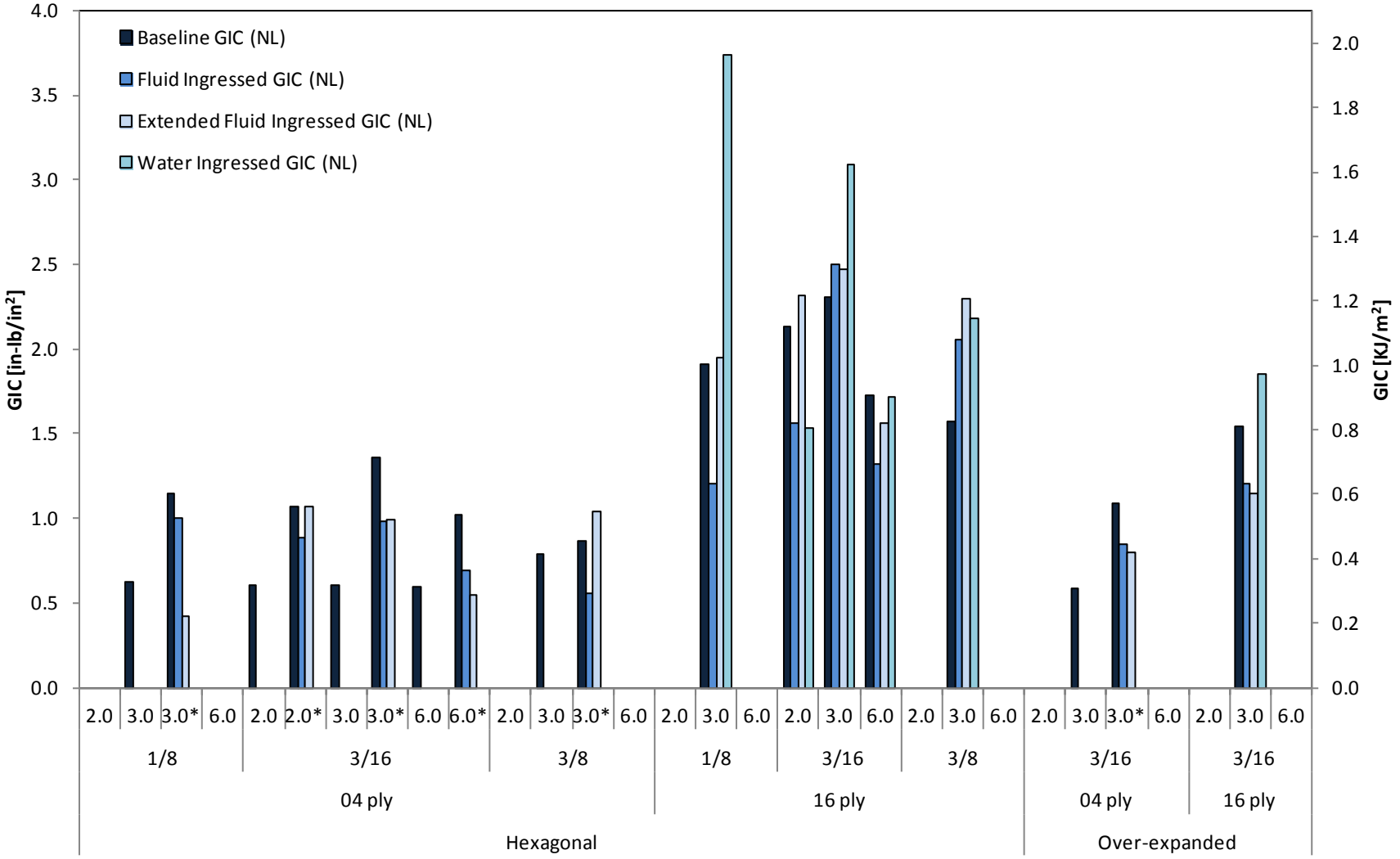

Figure 23. GIC (NL) master summary (* a_o = prescribed crack length of 1″)

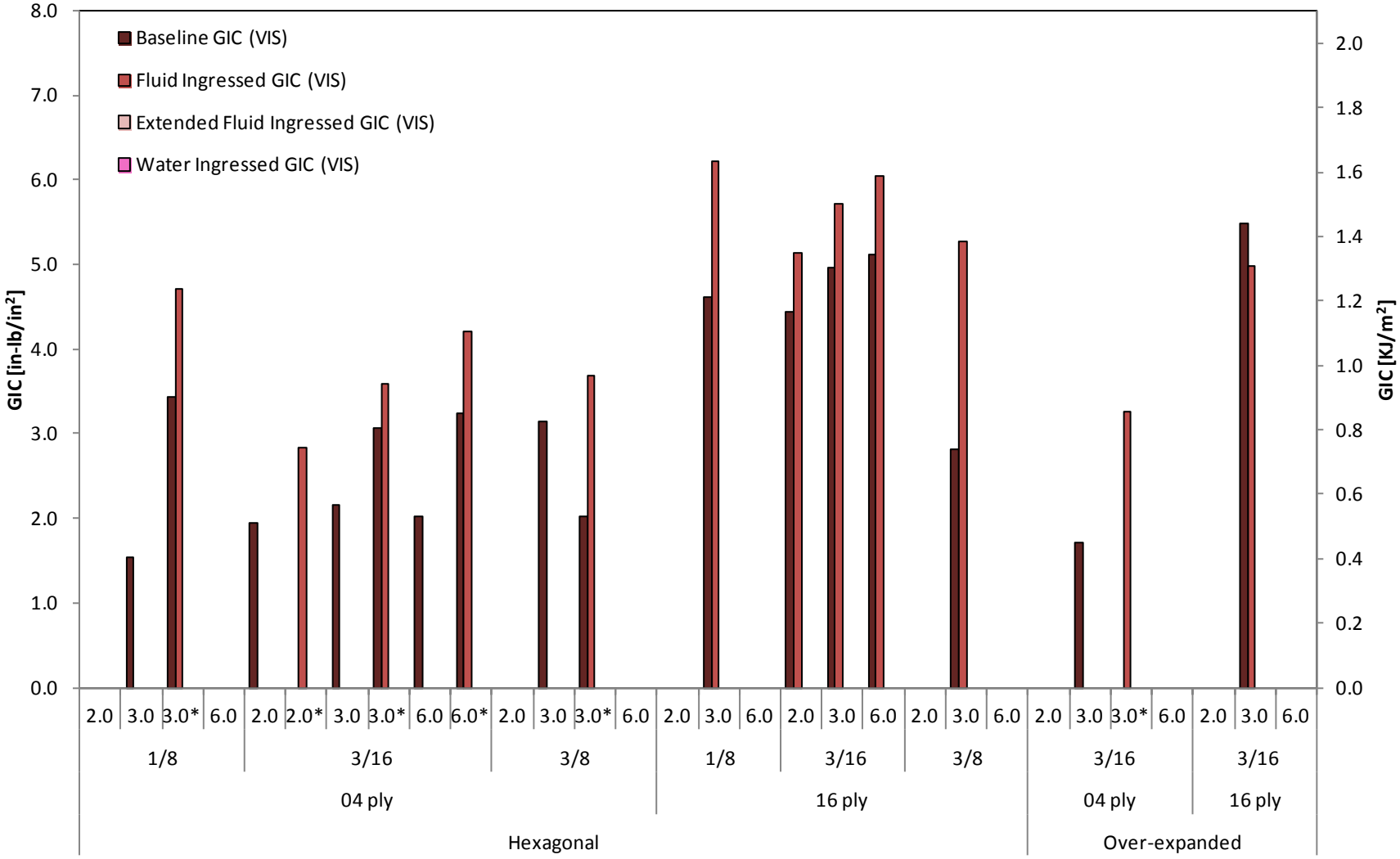

Figure 24. GIC (VIS) master summary (* a_o = prescribed crack length of 1″)

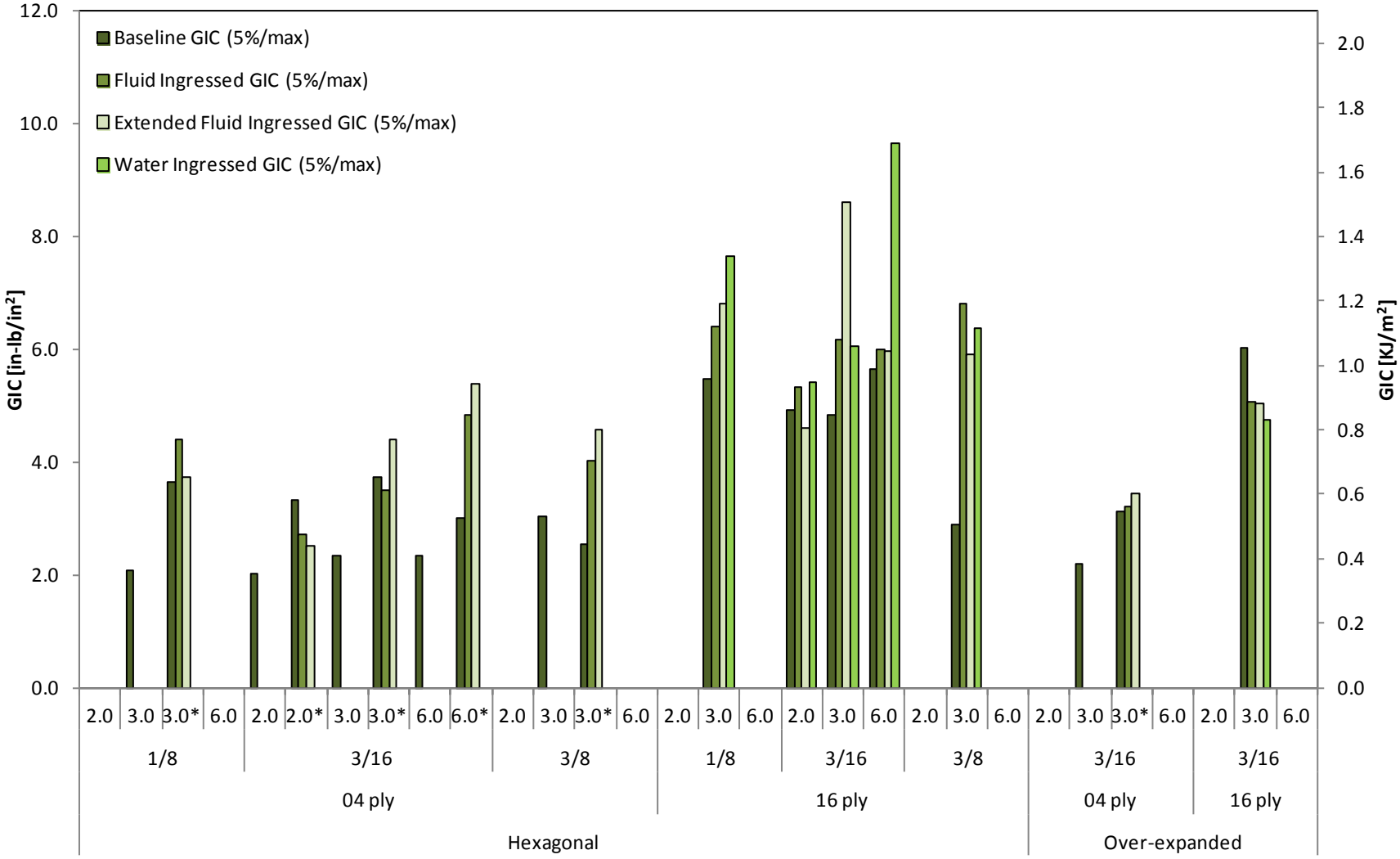

Figure 25. GIC (5%/max) master summary (* a_o = prescribed crack length of 1″)

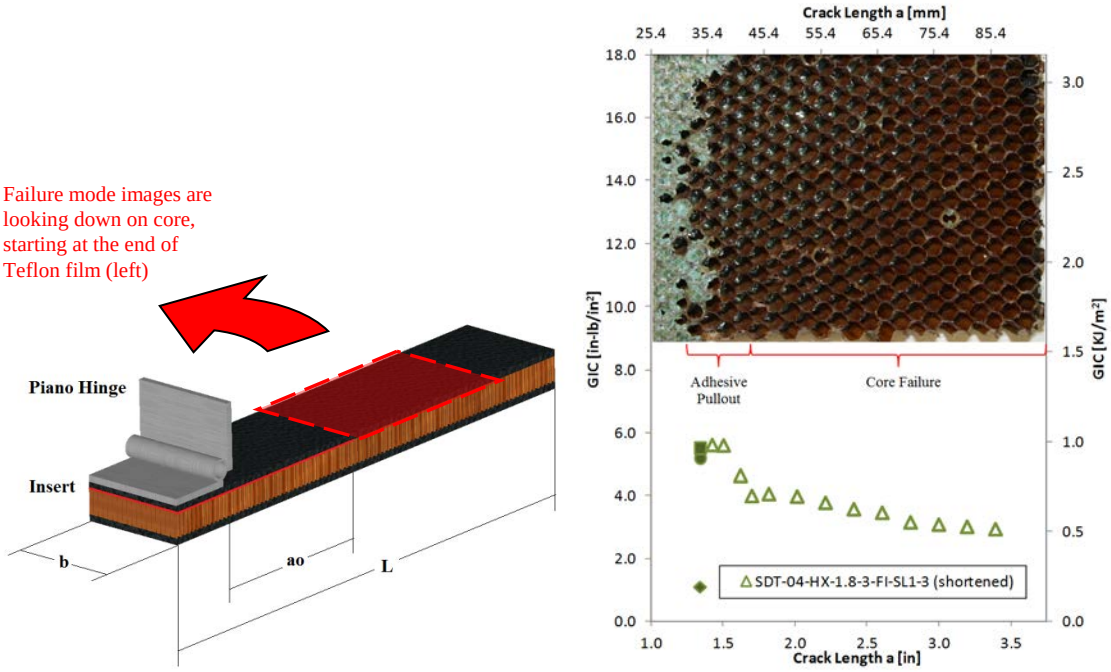

Figure 26. Failure mode and resistance curve

3.1 EFFECTS OF FACESHEET THICKNESS

Facesheet thickness was one of the more prominent variables and had a significant effect on GIC. It is important to note that, theoretically, facesheet thickness should have no influence on fracture toughness because the load and displacements are coupled. However, this assumes that the facesheet is acting as an Euler-Bernoulli beam and, therefore, has small deflections, behaves elastically, and is perfectly built-in. These assumptions were violated for specimens with thin facesheets. These specimens experienced large deflections, which were accounted for by the correction factor *F* that artificially shortens the moment arm. Additionally, specimens with thin facesheets had nonlinear load-displacement curves. This material nonlinearity was not corrected for (which has a large impact on fracture toughness) but could be reduced by changing the specimens' initial geometry (i.e., shortening the prescribed crack length). However, 2.5″ specimens were used in this analysis to keep all other variables constant. An explicit analysis of the change in initial crack length is discussed in section 3.6. Lastly, the facesheet was not perfectly built-in and allowed for small rotations at the crack tip. This deformation changed with facesheet thickness but was accounted for with the Δa correction factor. Because of the difference in the bending stiffness of different facesheets, 4-ply facesheet specimens resulted in large crack tip opening angles, and the 16-ply facesheets had small crack tip opening angles (see figure 27). This resulted in changes in stress distribution and failure modes. By changing the facesheet thickness, the material system's failure mode changed, resulting in substantial differences in fracture toughness.

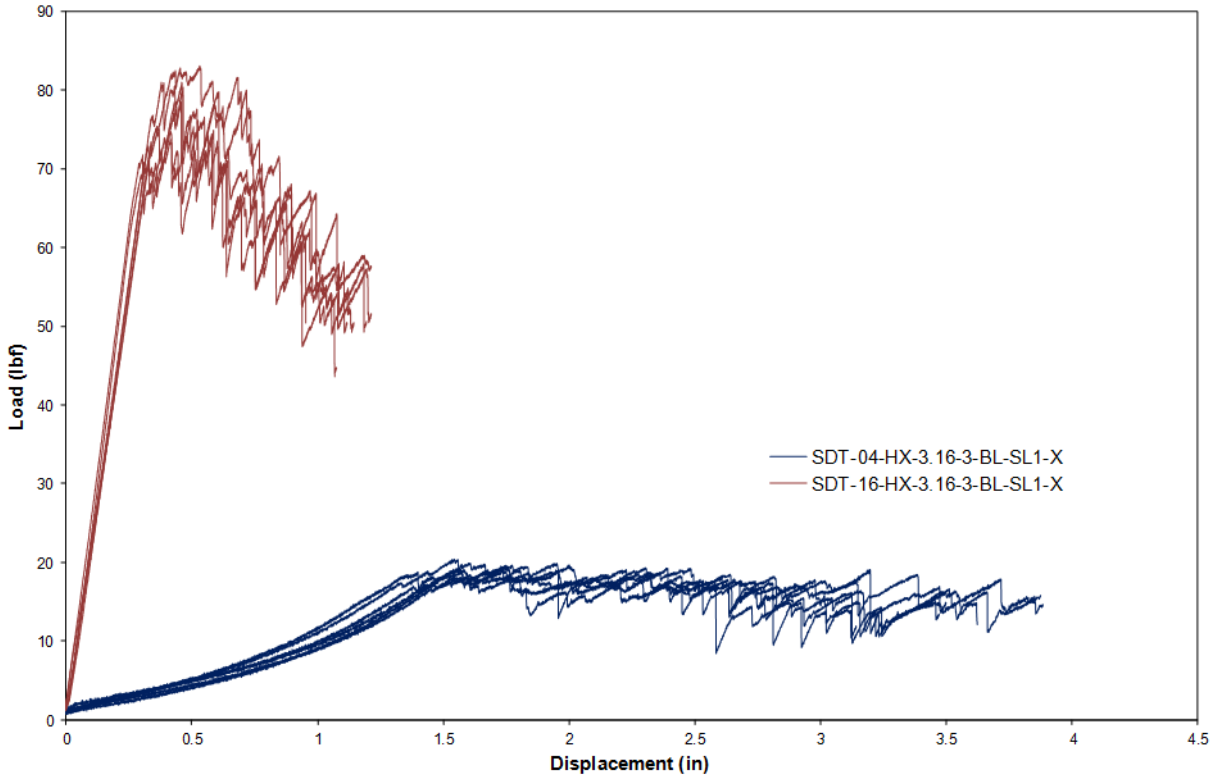

Figure 27. Effect of facesheet thickness on load vs. displacement curves of HRH-10-3/16-3.0 baseline specimens

Figure 28 illustrates how facesheet thickness relates to core type. When examining the thin facesheets, there seemed to be little effect because of core type; however, as the facesheet thickness increased, core type seemed to play a more pivotal role in fracture toughness. Figure 29 shows how facesheet thickness relates to cell size. Analysis revealed an interesting relationship exhibiting a reversal of how influential cell size is to fracture toughness. This is primarily because of the change in failure modes; as the cell size increased, the failure mode of thin facesheets changed from core to adhesive pullout, whereas it changed from mostly pullout to mostly cohesive for thick facesheets. Thick (16-ply) facesheets had increased bending stiffness compared with thin (4-ply) facesheets that resulted in small crack opening angles, thereby changing the crack tip stress distribution. This resulted in a change in failure modes and reversal of fracture toughness values. Figure 30 demonstrates how facesheet thickness relates to core density, which appears to have minimal effect.

For most of the specimen configurations, 16-ply facesheet specimens indicated higher GIC values; however, some of the specimen configurations had slightly rising or falling resistance curves (see figure 31), which can be attributed to changes in failure mode and an increase in material nonlinearity. Additionally, the failure mode at the point where the 5%/max offset value was determined also changed with respect to facesheet thickness in a few specimen configurations. Thick (16-ply) facesheets had increased bending stiffness that resulted in small crack opening angles, thereby changing the crack tip stress distribution. As the cell size increased for the 4-ply (3 pcf) specimens, the failure mode changed from core to pullout,

whereas it changed from mostly pullout to mostly adhesion failure for the 16-ply specimens. This resulted in reversal of fracture toughness values.

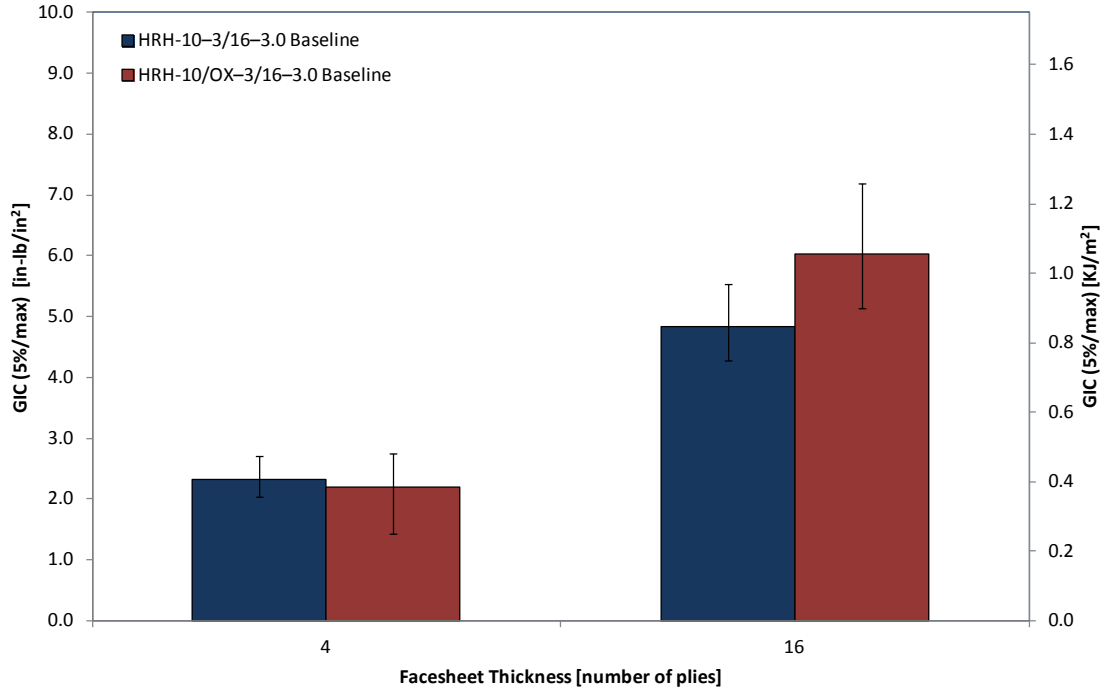

Figure 28. Effect of facesheet thickness with respect to core type

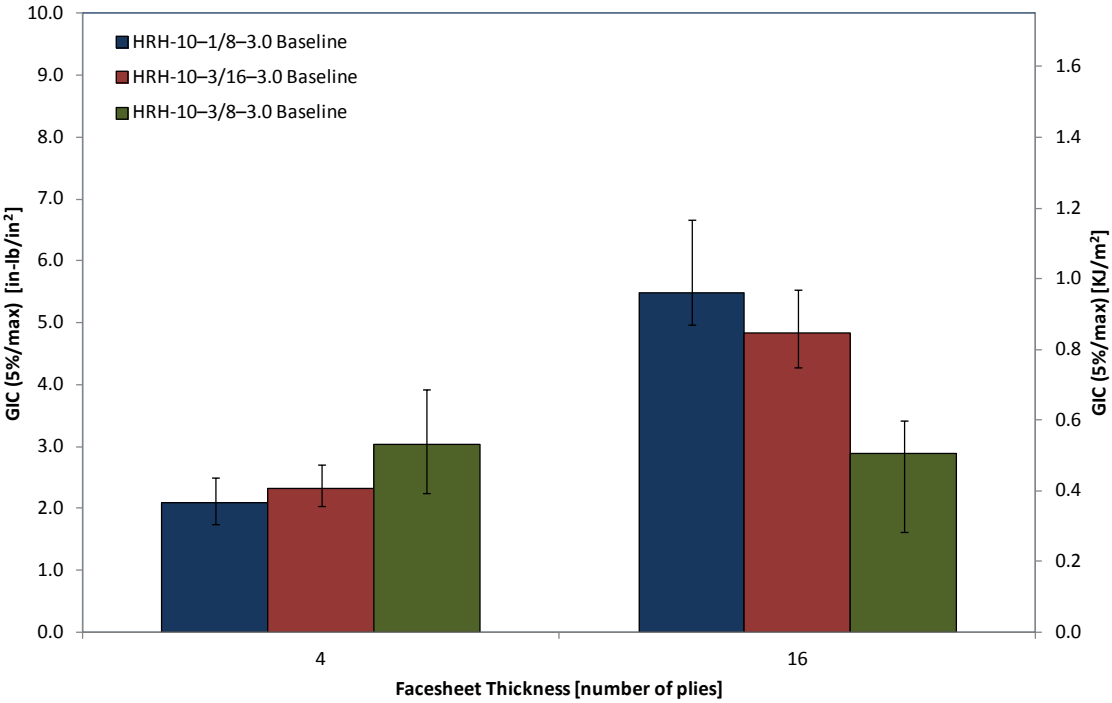

Figure 29. Effect of facesheet thickness with respect to cell size

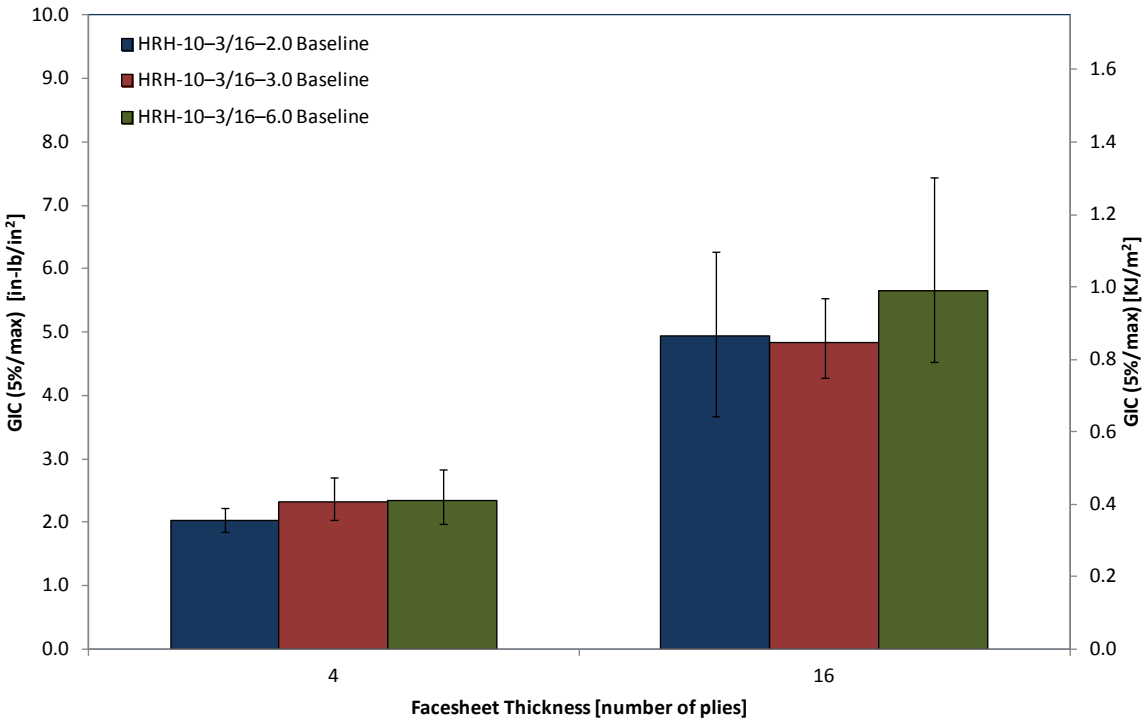

Figure 30. Effect of facesheet thickness with respect to core density

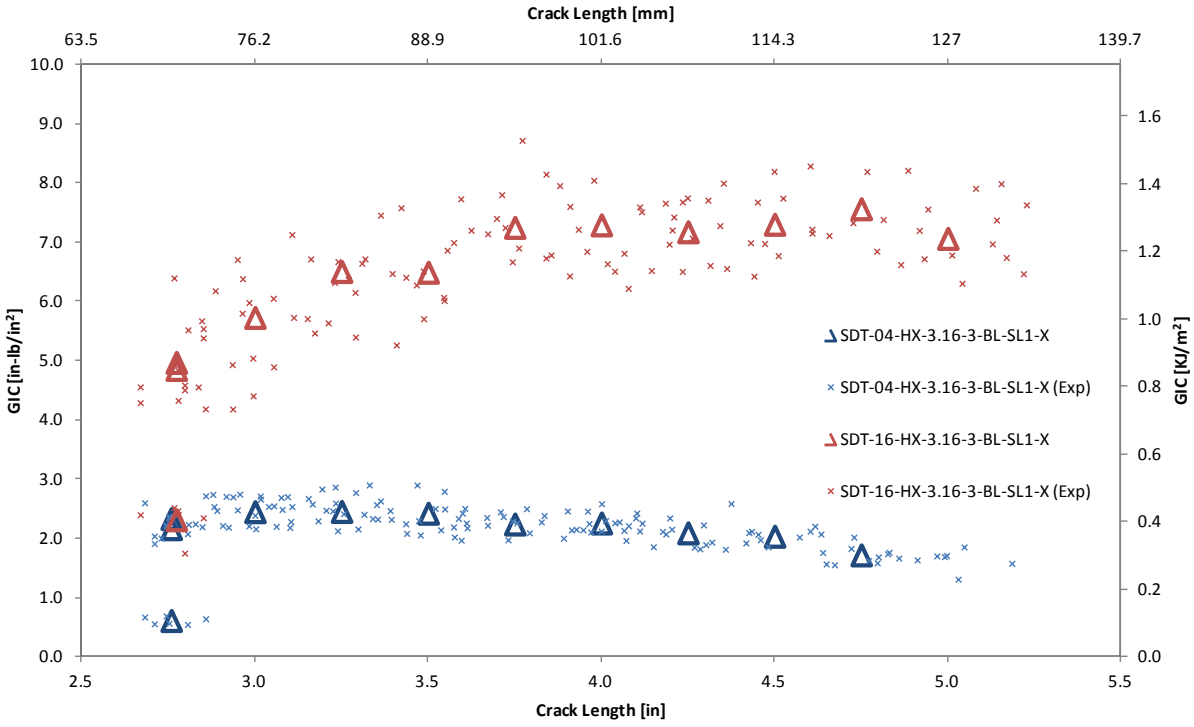

Figure 31. Effect of facesheet thickness on resistance curves of HRH-10-3/16-3.0 baseline specimens

3.2 EFFECTS OF CORE TYPE

Another important variable that could play a role in fracture toughness is core type. Both hexagonal and over-expanded core types were investigated.

Figure 32 illustrates how core type relates to 4-ply specimens, at both initial crack length and each environmental condition. A slight change in fracture toughness was exhibited and became more pronounced for the shortened specimens and even more so in the extended fluid-ingressed specimens. Figure 33 represents the 16-ply specimens, which exhibited a significant impact on fracture toughness, especially in the extended fluid-ingressed specimens. It is important to note that the HX was slightly more fracture resistant than the over-expanded core.

Fracture toughness was found to be higher throughout the resistance curve for the HX (see figure 34). The failure mode for the HX was primarily cohesive or PO in the baseline and core failure after conditioning, compared with the over-expanded core, which was predominately core failure regardless of conditioning. When looking at the load-displacement curves, load drops are often found in the HX, representing rapid crack growth and arrest, whereas the over-expanded core was smoother, representing slow stable growth.

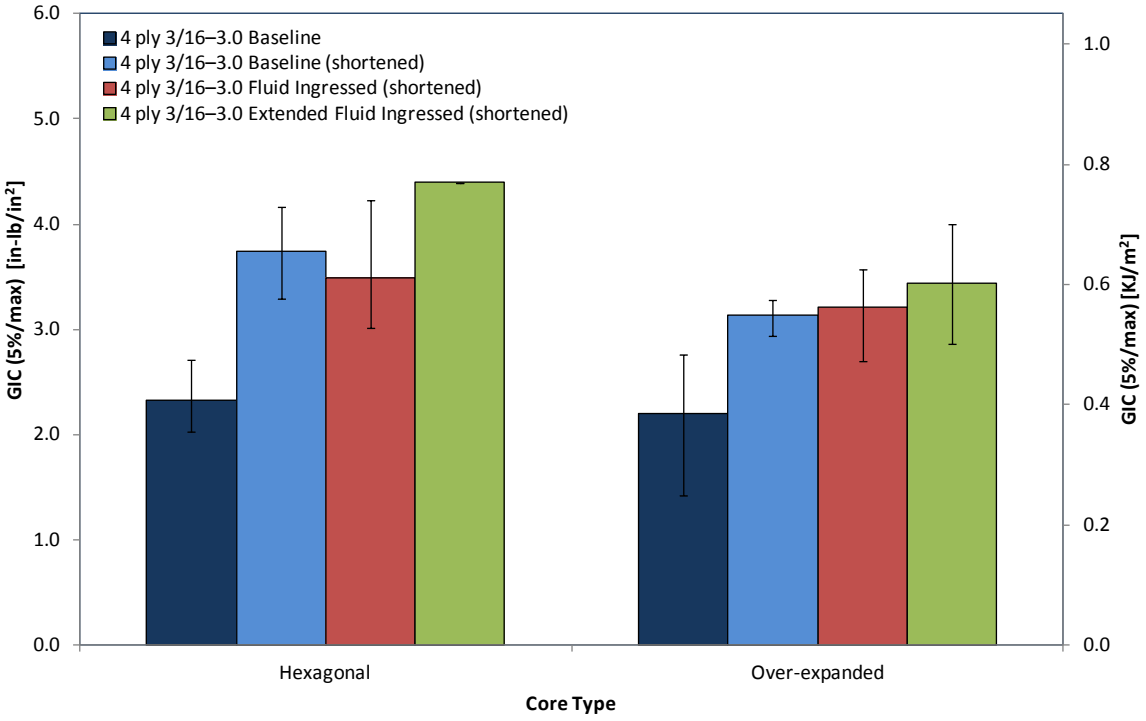

Figure 32. Effects of core type with respect to environmental conditioning and a_o (4 ply)

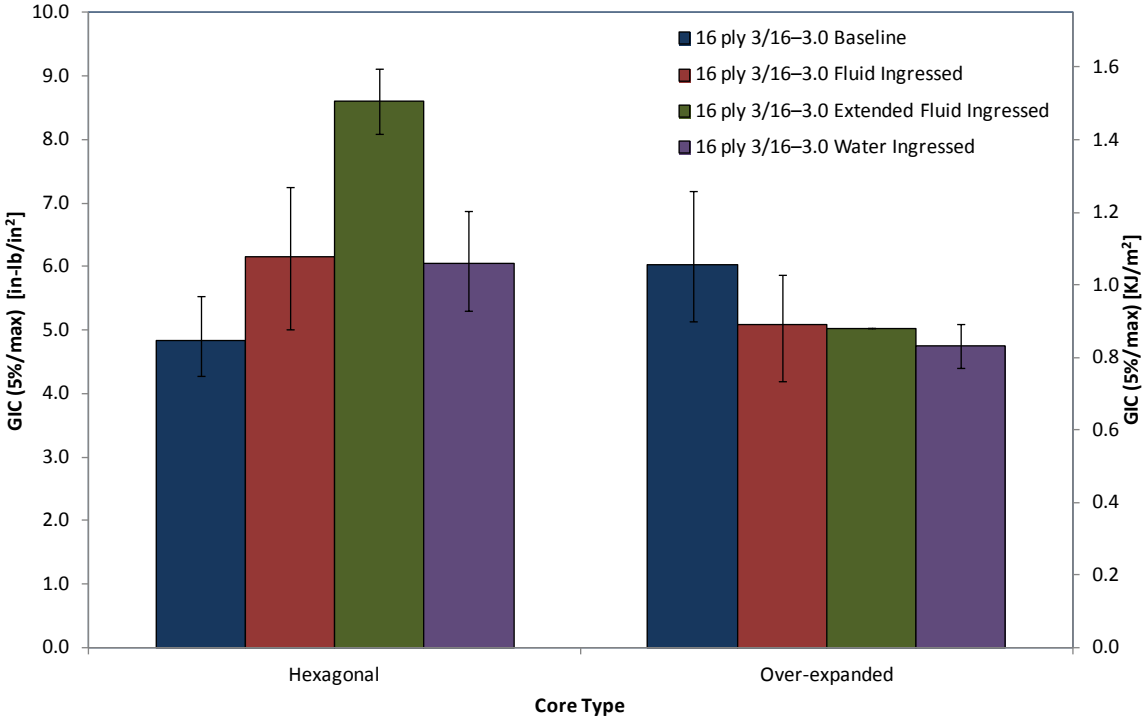

Figure 33. Effects of core type with respect to environmental conditioning (16 ply)

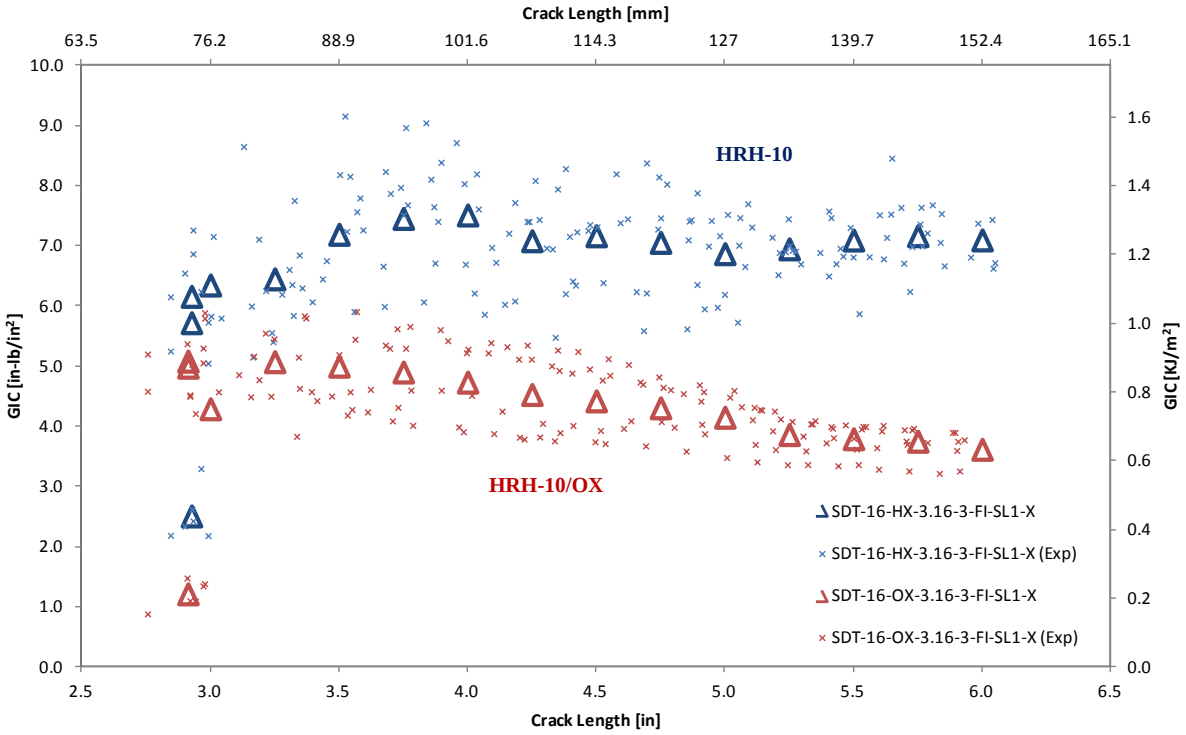

Figure 34. Resistance curves of HRH-10 vs. HRH-10\OX among 16-ply 3/16–3.0 fluid-ingressed specimens

3.3 EFFECTS OF CELL SIZE

Three cell sizes were analyzed: 1/8″, 3/16″, and 3/8″. Figure 35 shows example resistance curves for 16-ply baseline specimens.

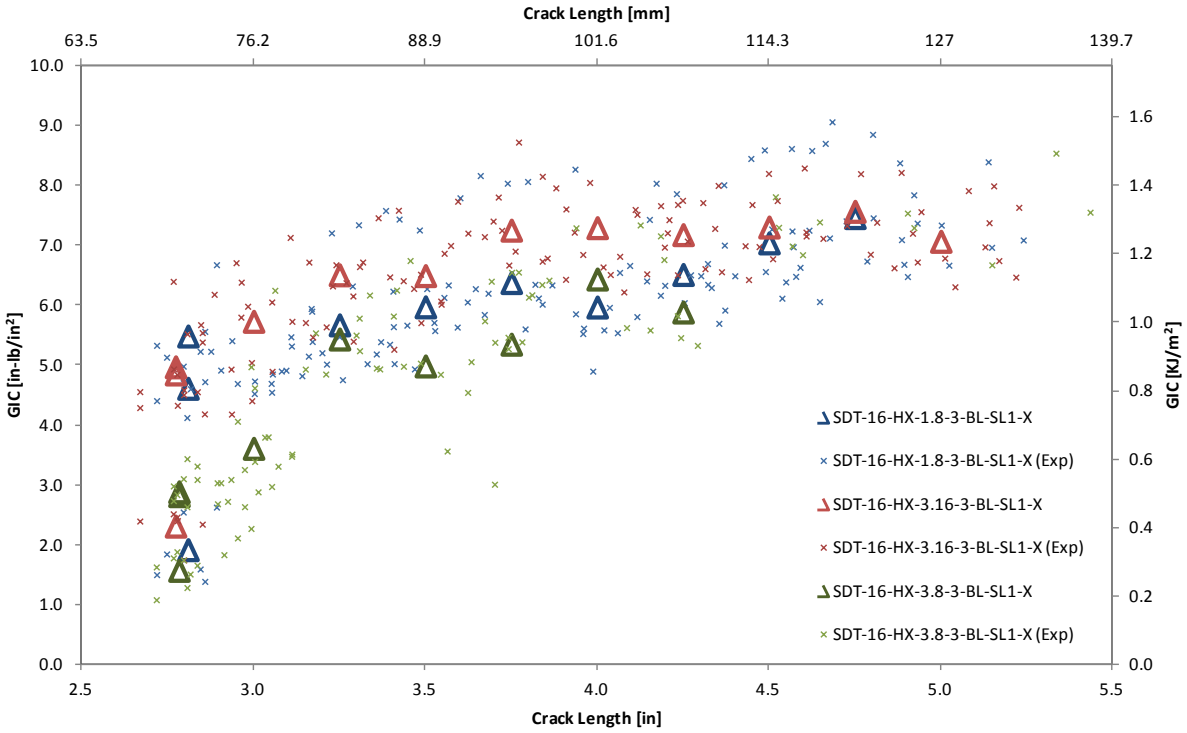

Figure 35. Resistance curves of 16-ply HRH-10–3.0 baseline specimens

Figure 36 illustrates how cell size played a role in 4-ply specimens with respect to initial crack length and environmental condition. Figure 37 represents 16-ply specimens. Because of coupling effects of different sandwich parameters (i.e., cell size, initial geometry, and environmental condition), no clear patterns are observed.

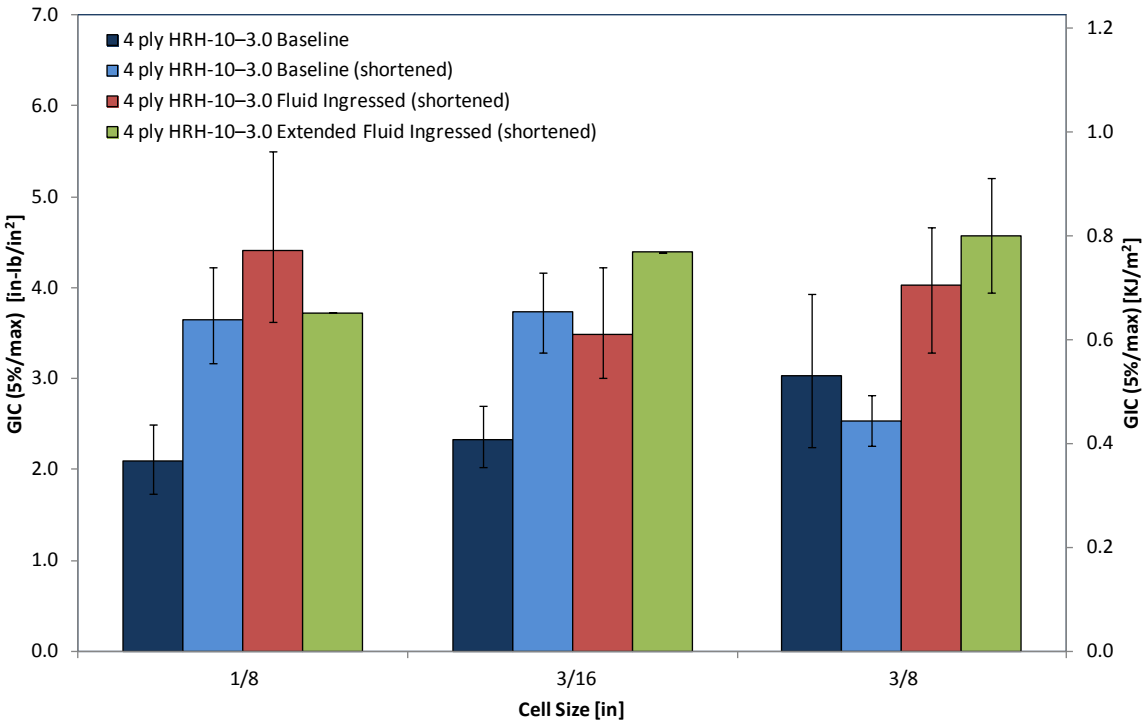

Figure 36. Effects of cell size with respect to a_o and environmental conditioning (4 ply)

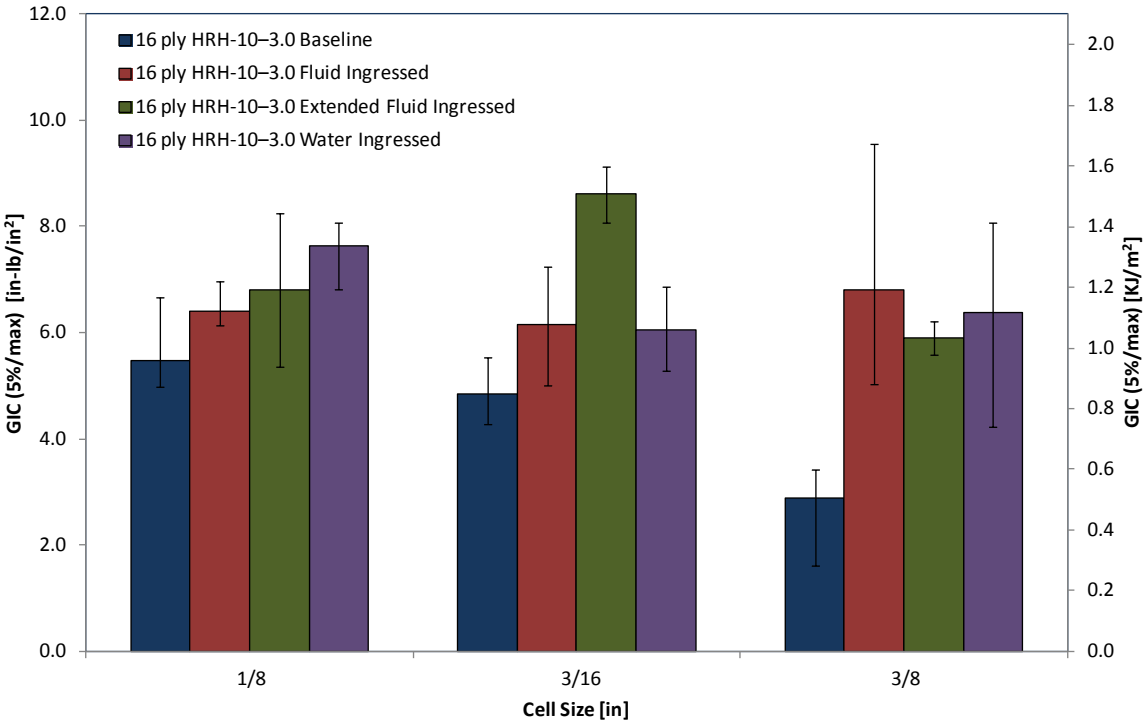

Figure 37. Effects of cell size with respect to environmental conditioning (16 ply)

When investigating the resistance curve, no discernible pattern was found correlating the exact effects of differentiating cell size, which could be due to the coupling of changing initial crack length and environmental conditions, or the changing failure modes between specimen configurations. When analyzing the failure modes, a general assessment could be made that the 1/8″ cell size failed primarily in the core for thin facesheets and in the adhesive for thick facesheets (cohesive failure). The 3/16″ cell size failed in pullout for thin facesheet specimens and in the adhesive, or in the core for thick facesheets. The 3/8″ cell size failed in pullout for thin facesheet specimens, whereas a combination of pullout and cohesive occurred for thick specimens. An additional observation of the load-displacement curve indicates that as the cell size grew, the load drops became larger and more evident, resulting in rapid crack growth and arrest versus a more stable crack growth found in smaller cell sizes (figure 38).

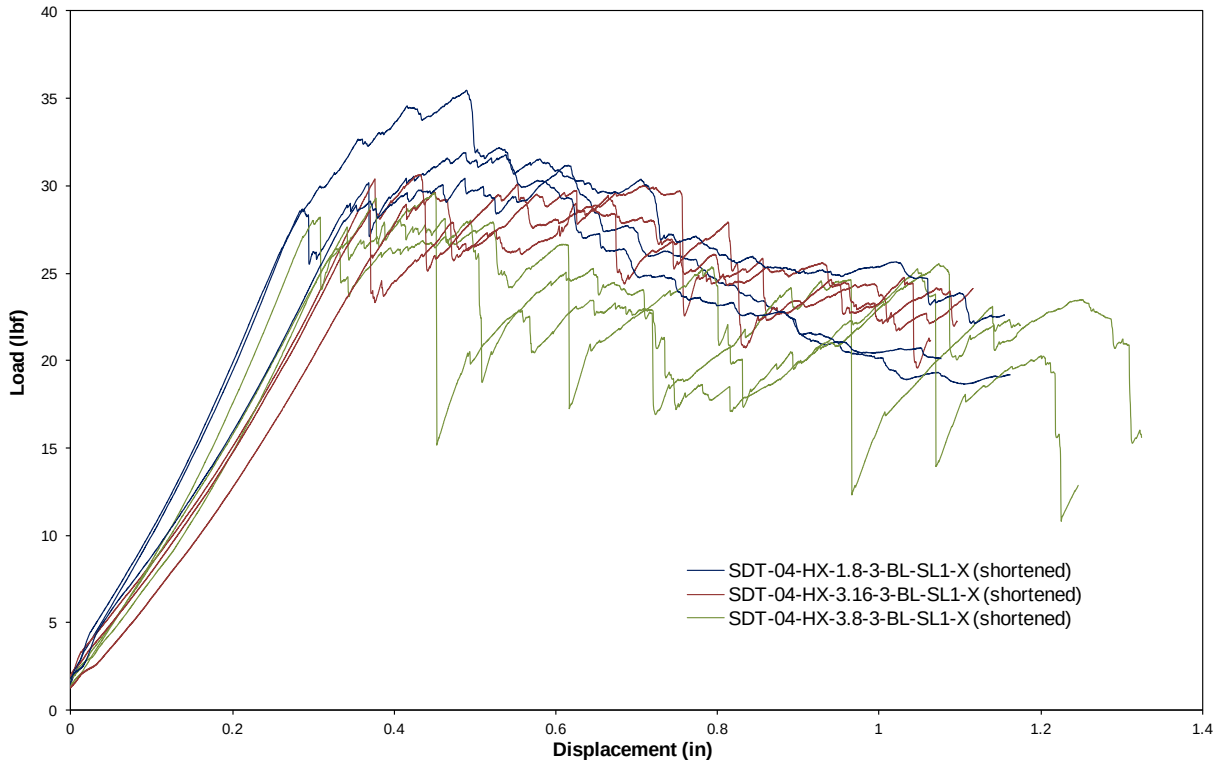

Figure 38. Load vs. displacement curves of shortened 4-ply HRH-10–3.0 baseline specimens

3.4 EFFECTS OF CORE DENSITY

Core density had a similar effect to cell size on fracture toughness. One reason could be the adhesive fillets that formed during specimen fabrication. These fillets artificially built up the cell walls, thereby making core density less significant. The initial disbond was produced using Teflon separator film placed above the core (bag side). Therefore, the side with the prescribed crack was the top side and, as the specimens were cured, gravity led to substantial fillet formation. A study was conducted with the disbond being built on the tool side with the results in volume III of this report. Additionally, as the core density changed, so did the paper thickness

within the core, affecting the fracture toughness of the core. Future analysis needs to be conducted to establish the significance of paper thickness.

Figure 39 illustrates how core density affected fracture toughness with respect to initial crack length and environmental conditioning in 4-ply facesheet specimens. Similarly, figure 40 shows the results for the 16-ply facesheet specimens.

Resistance curves for the 4-ply facesheet specimens did not seem to follow a pattern; however, when investigating the 16-ply facesheet specimens, the 2 pcf core seemed to fall below the other two cell densities (see figure 41), and the failure modes also varied. Among 4-ply facesheet specimens, the 2 pcf core had primarily core failure with some pullout; the 3-pound-per-cubic-foot core had pullout with some core failure; and the 6 pcf core had mostly pullout. When investigating 16-ply facesheet specimens, the 2 pcf core experienced predominately core failure, whereas the 3 pcf core was a mixture of core and cohesion, and the 6 pcf core was a mixture of adhesive/cohesion and PO. Lastly, when analyzing the load-displacement plots, the 2 pcf core was relatively stable with a slowly falling curve, whereas the 3 pcf core had small load drops, indicating rapid crack growth and arrest, and the 6 pcf core experienced significant load drops, as shown in figure 42.

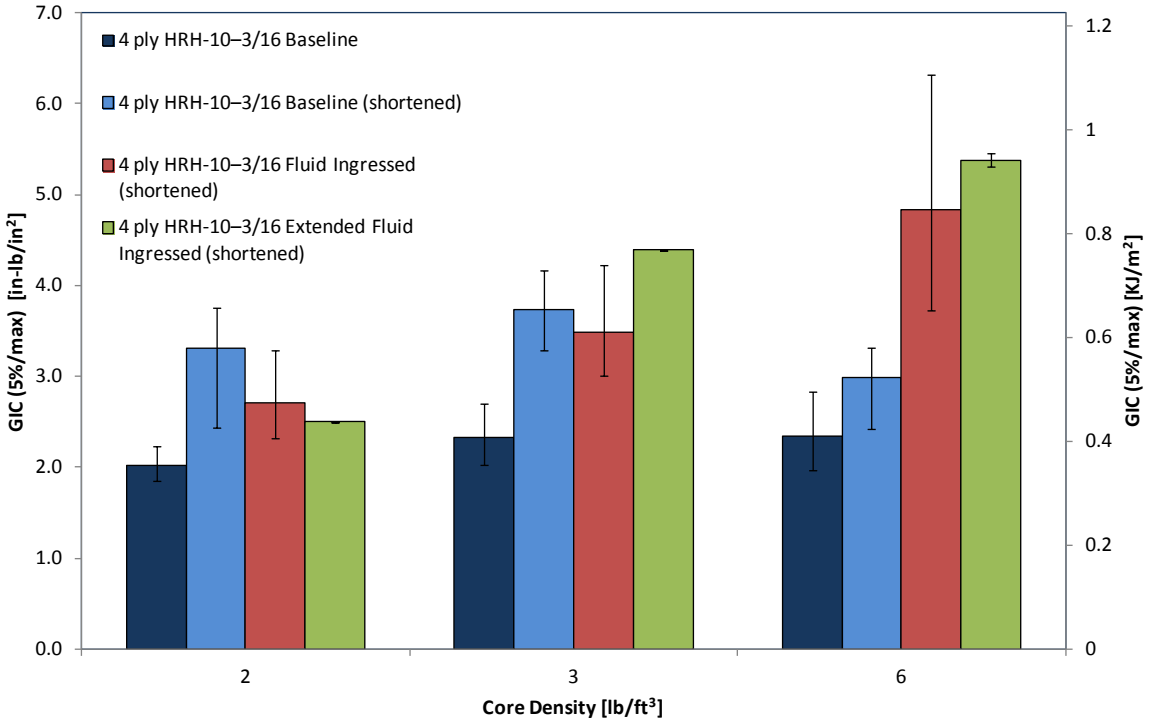

Figure 39. Effects of core density with respect to a_o and environmental conditioning (4 ply)

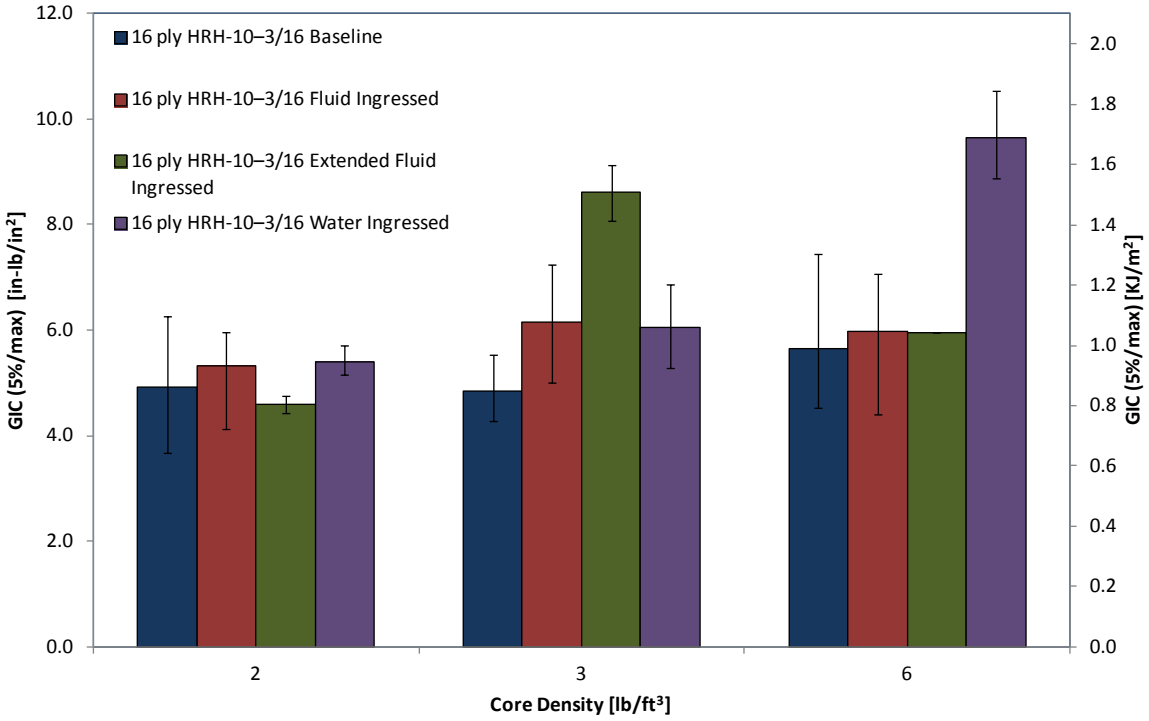

Figure 40. Effects of core density with respect to environmental conditioning (16 ply)

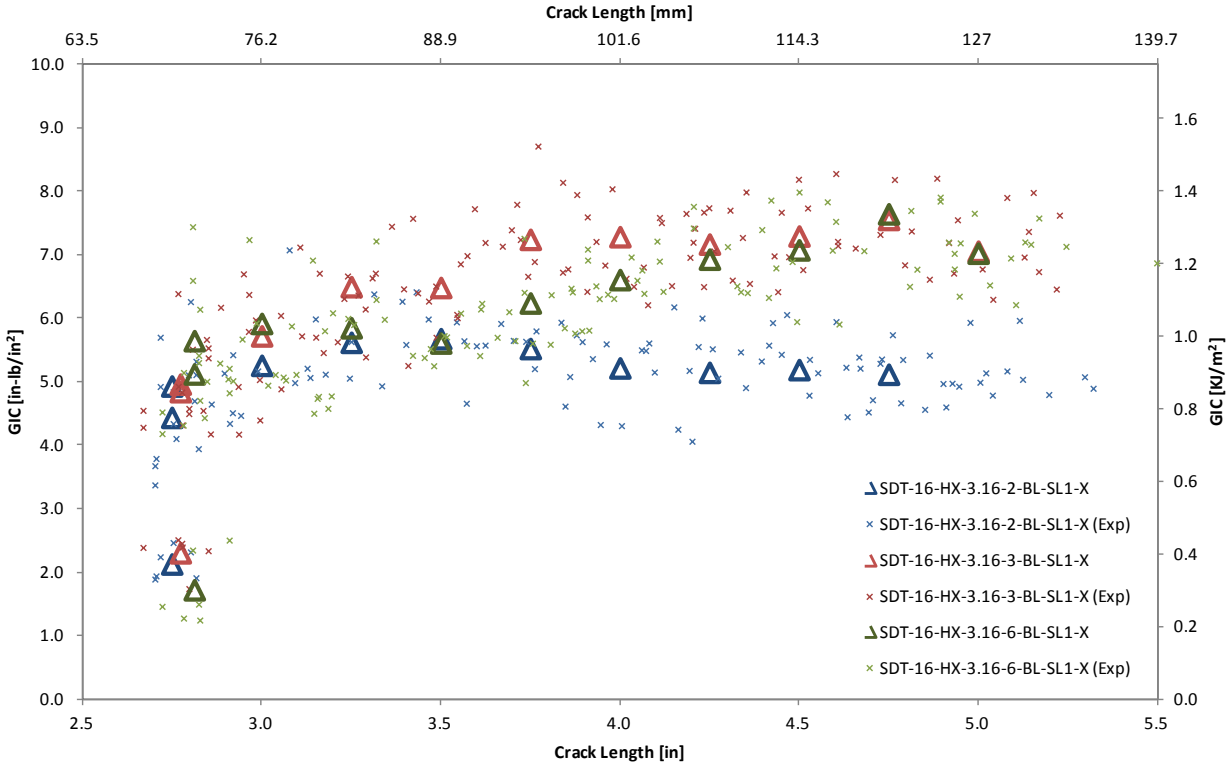

Figure 41. Resistance curves of 16-ply HRH-10–3/16 baseline specimens

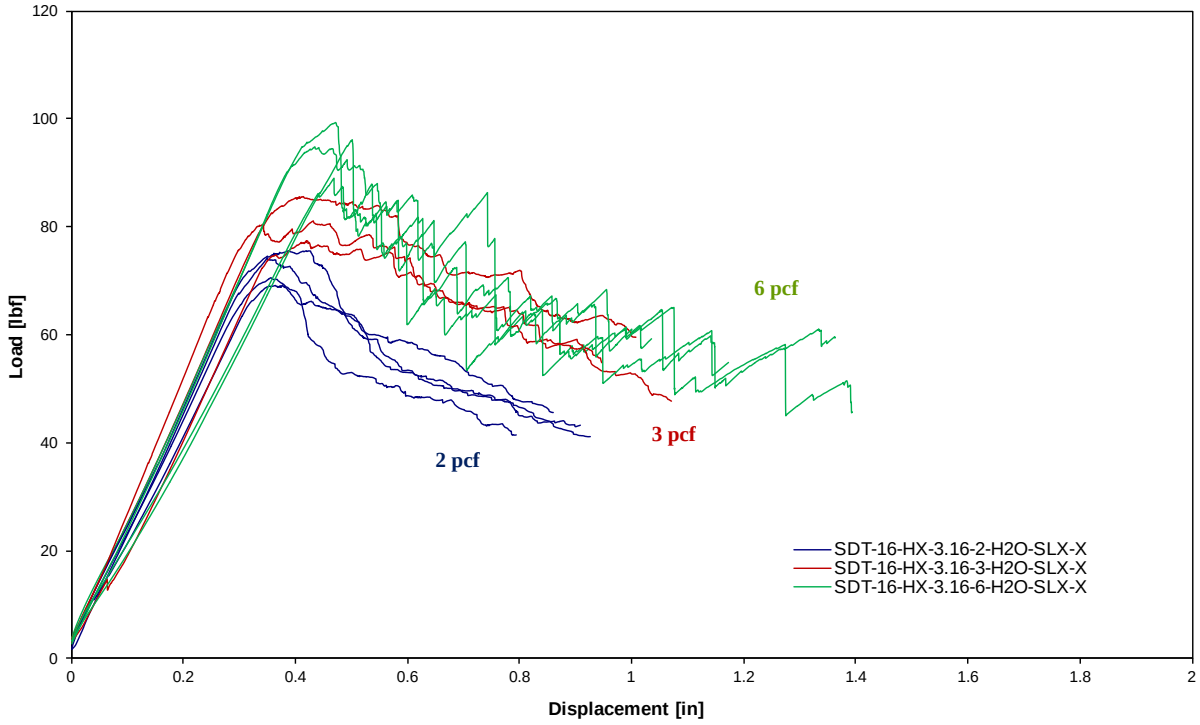

Figure 42. Load vs. displacement curves for shortened 16-ply HRH-10–3/16 water-ingressed specimens

3.5 EFFECTS OF ENVIRONMENTAL CONDITIONING

Environmental conditioning played a significant role on fracture toughness for the configuration with 16-ply facesheets. Ingressing the specimens in an acidic Skydrol/water solution had an effect on material stiffness and failure modes, which in turn affected the GIC. Details of effects of environmental conditioning on GIC are included in appendix F.5.

Figures 43–45 show results for 4-ply specimens with respect to core type, cell size, and core density, respectively. When analyzing core type, environmental conditioning seemed to have little effect on fracture toughness. No clear trend can be established when considering how fluid ingression affects cell size. However, when considering the effect of core density on environmental conditioning, the 6 pcf core's fracture toughness increased (see figure 45); conversely, fracture toughness decreased in the 2 pcf core. This is unexplainable because all failures here were in the core. Figures 46–48 represent 16-ply specimens with respect to core type, cell size, and core density, respectively. The failure for the 16-ply specimens was adhesive resulting in higher facture toughness. Core type played a significant role because, as a result of fluid ingression, the GIC drastically increased for one core and fell for the other. When investigating the effects of fluid ingression with respect to cell size, it became evident that as cell size increased, so did fracture toughness. However, when considering core density, little effect was found except for the 3 pcf core. Figure 49 shows a comparison of the resistance curves for HRH-10–3/16–6.0 specimens conditioned with Skydrol and water. This figure shows that

water-ingressed specimens for this specimen configuration had significantly high fracture toughness (5%/max). In general, fluid-ingressed specimens had higher fracture toughness values compared with corresponding baseline configurations.

The resistance curves for most material systems would converge as the crack grows. Primary differences in the resistance curves can be found in the initial region, where the recorded values were determined (see figures 49 and 50). This could be due to the change in stiffness, the increased load-carrying capability, or the impact of the varying failure modes. When considering failure modes, it becomes evident that, initially, they varied in the recordable region (i.e., nonlinear, visual, and 5% offset or max load); however, when considering the remainder of the specimen, the failure modes became much more similar, except for the hexagonal, 3/16″, 3 pcf core. When considering the 4-ply specimens for some specimen configurations, the stiffness increased, whereas in others, it decreased; therefore, further study needs to take place by considering the elastic-plastic stress state of the crack tip after fluid ingression. Among the 16-ply specimens, however, the fluid-ingressed specimens always experienced a reduction in stiffness because the failure mode was adhesive, not core (see figure 51).

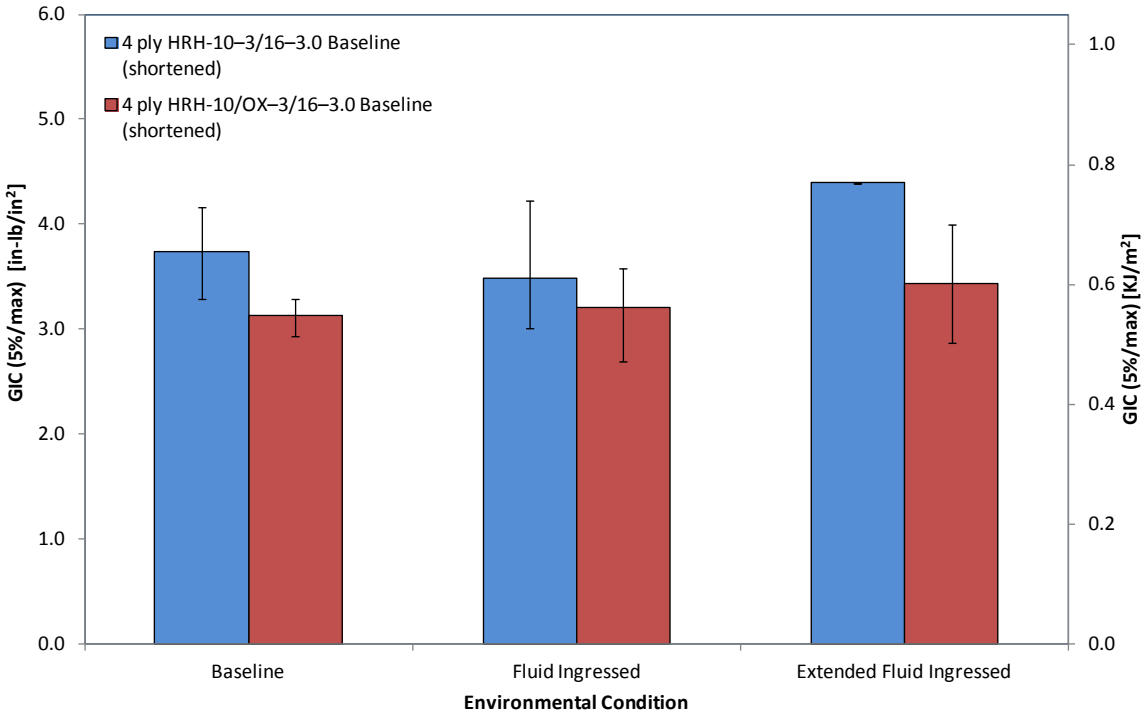

Figure 43. Effects of environmental conditioning with respect to core type (4 ply)

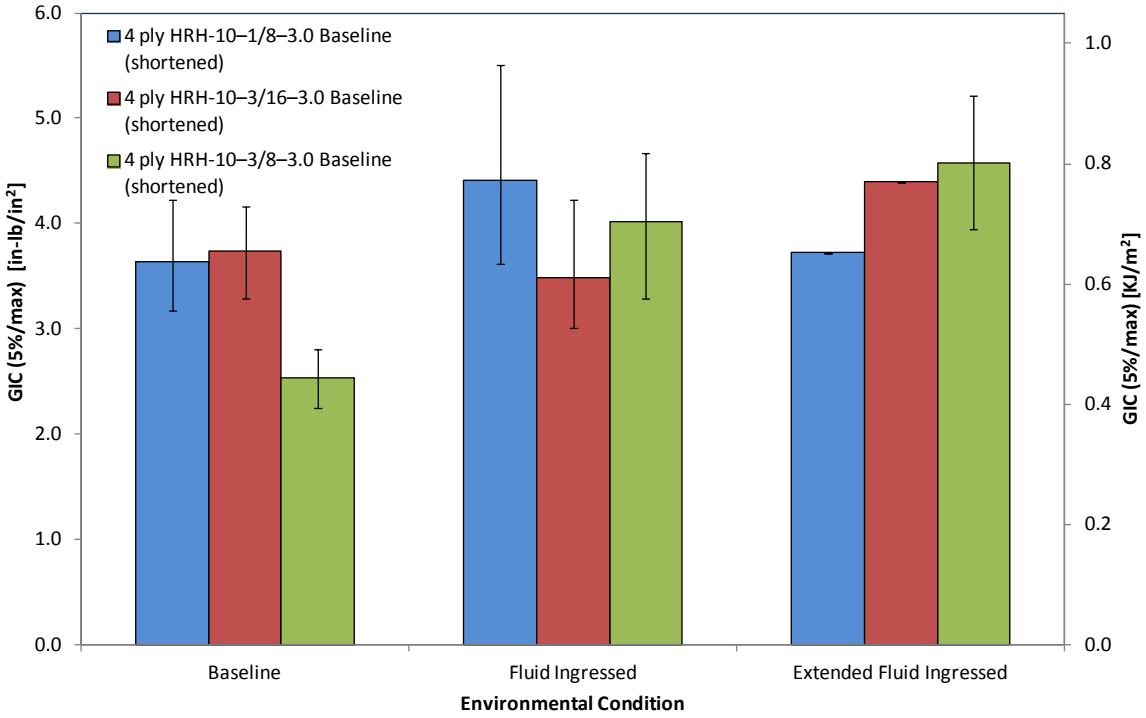

Figure 44. Effects of environmental conditioning with respect to cell size (4 ply)

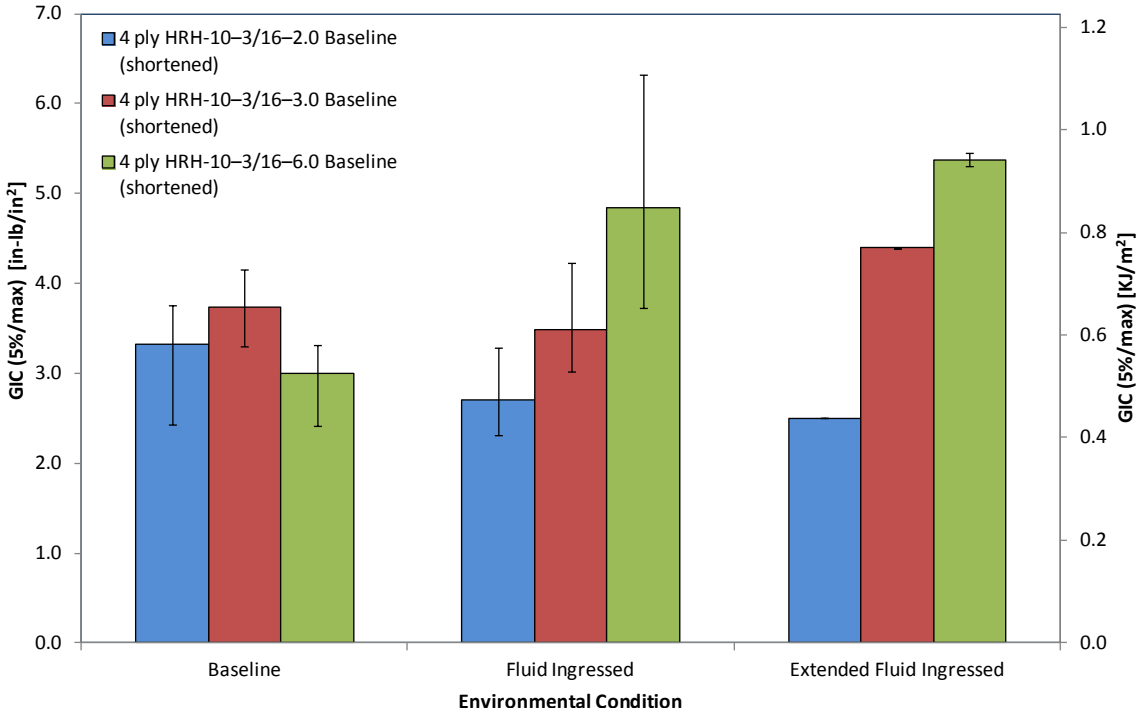

Figure 45. Effects of environmental conditioning with respect to core density (4 ply)

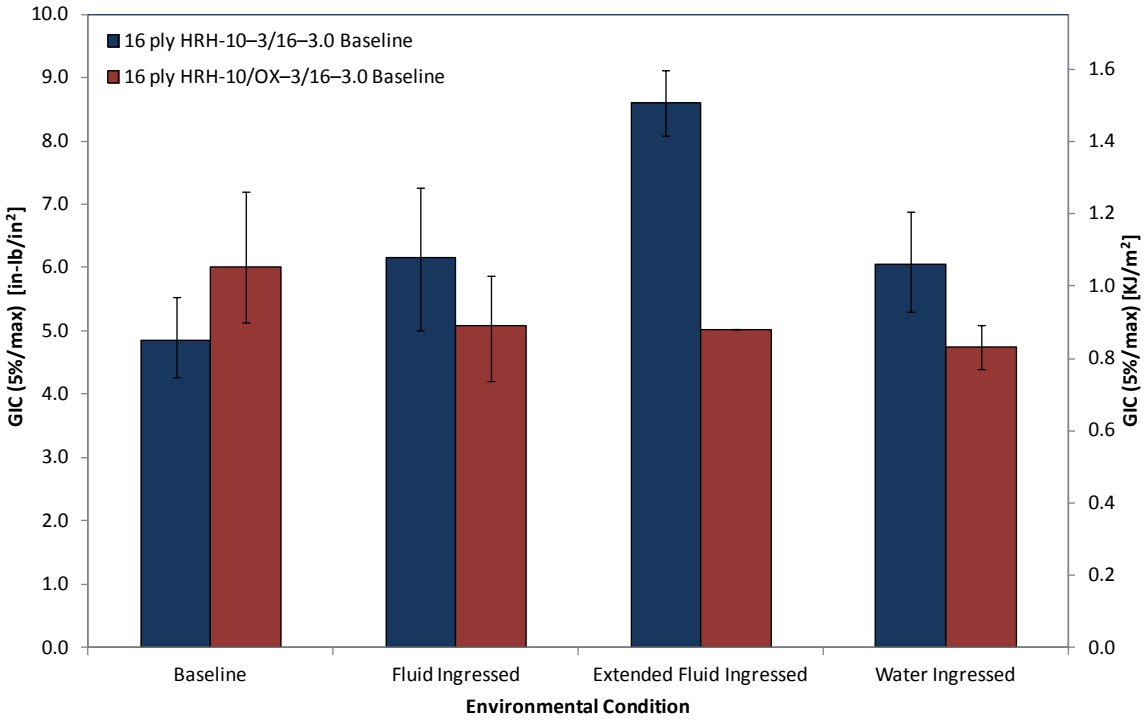

Figure 46. Effects of environmental conditioning with respect to core type (16 ply)

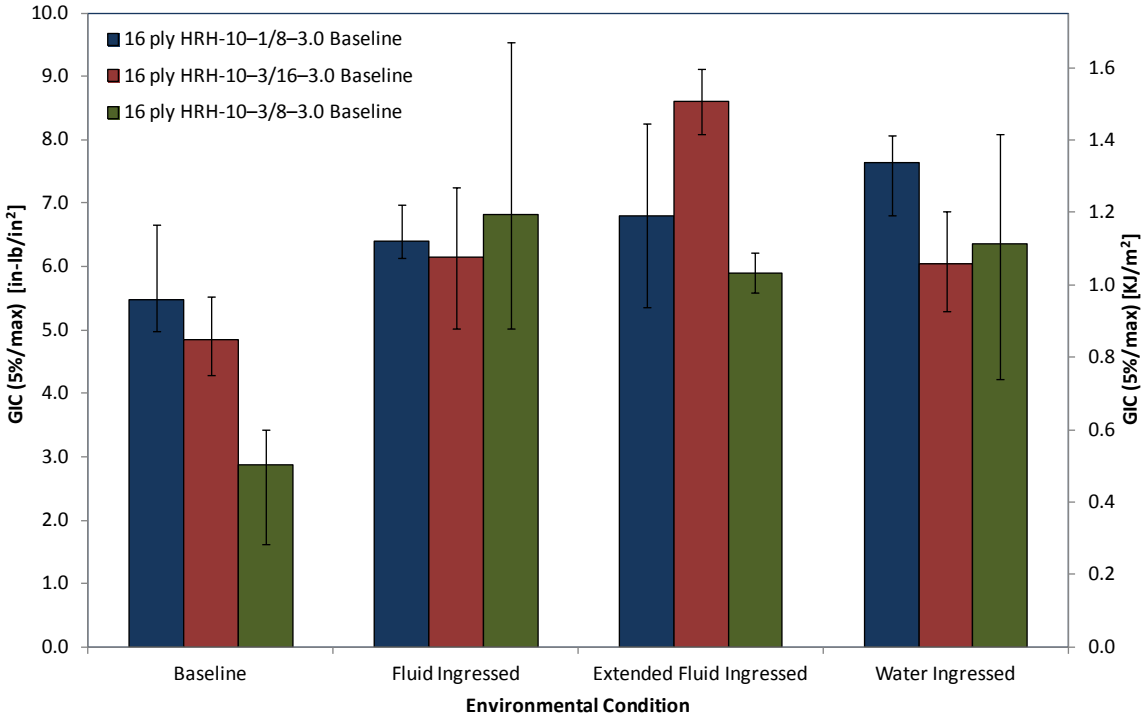

Figure 47. Effects of environmental conditioning with respect to cell size (16 ply)

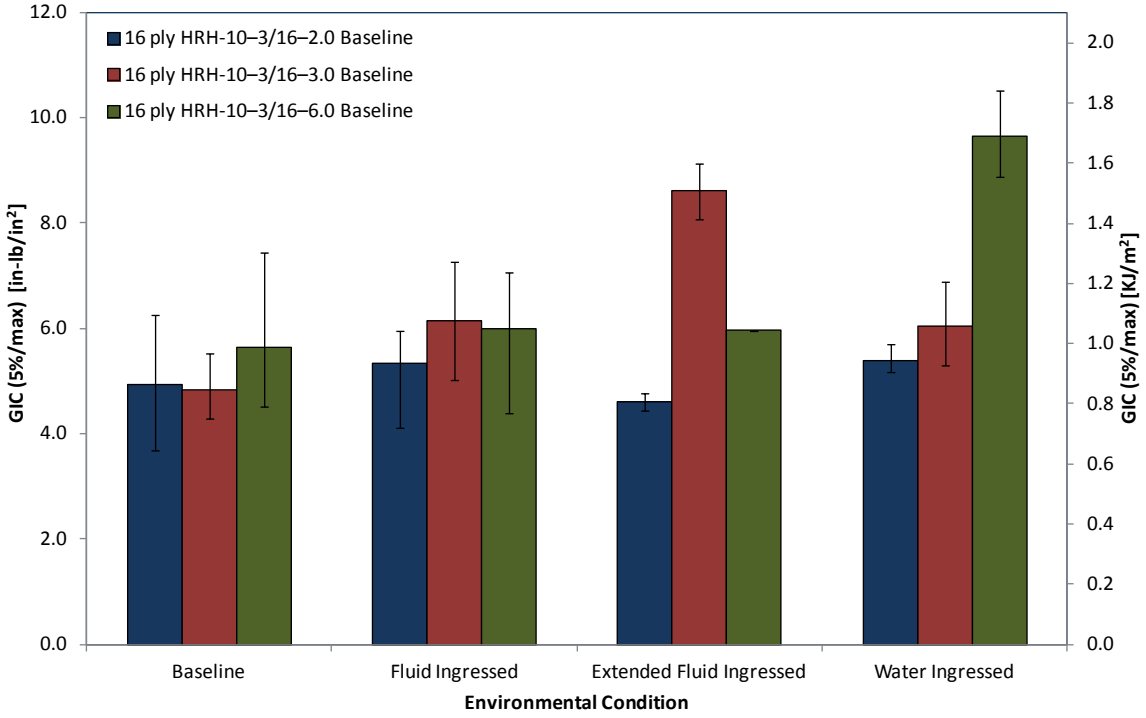

Figure 48. Effects of environmental conditioning with respect to core density (16 ply)

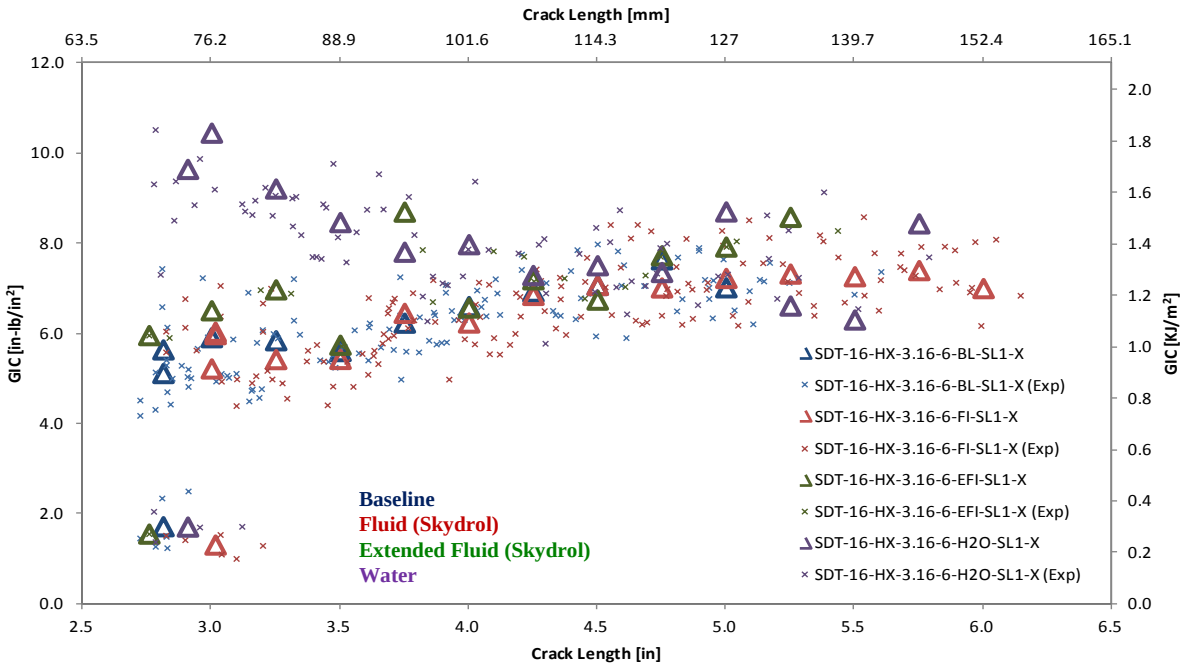

Figure 49. Effects of fluid ingression on resistance curves of 16-ply HRH-10–3/16–6.0 specimens

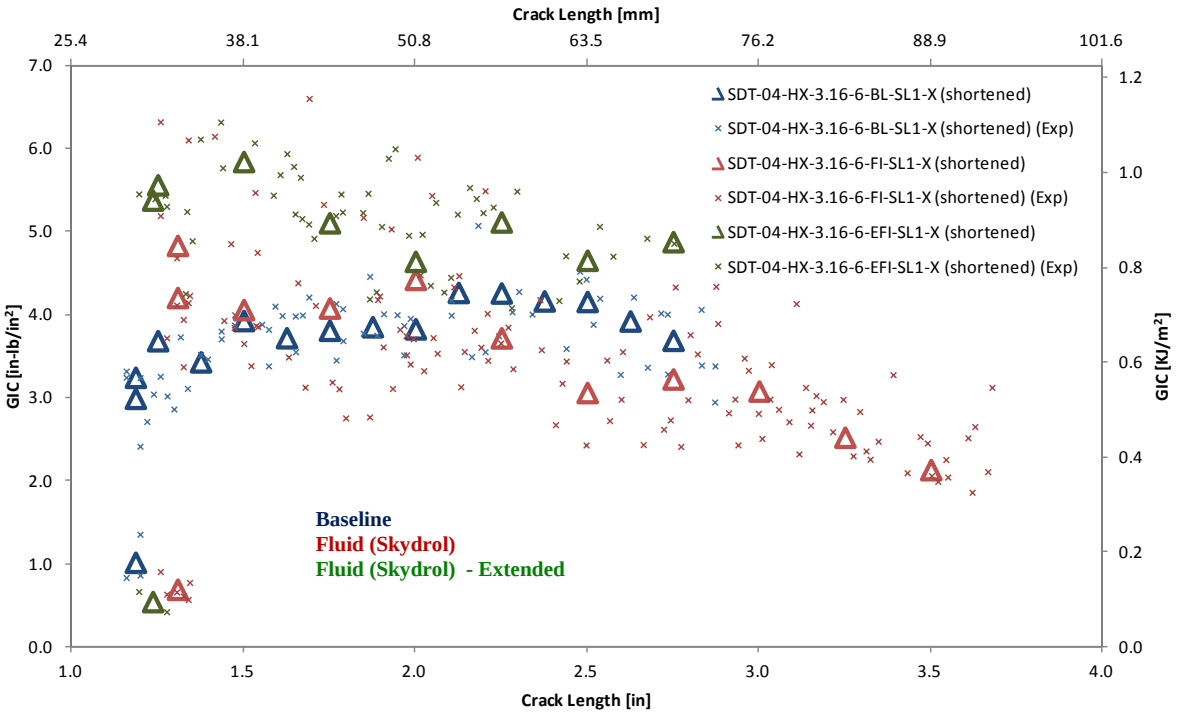

Figure 50. Effects of fluid ingression on resistance curves of 4-ply HRH-10–3/16–6.0 specimens

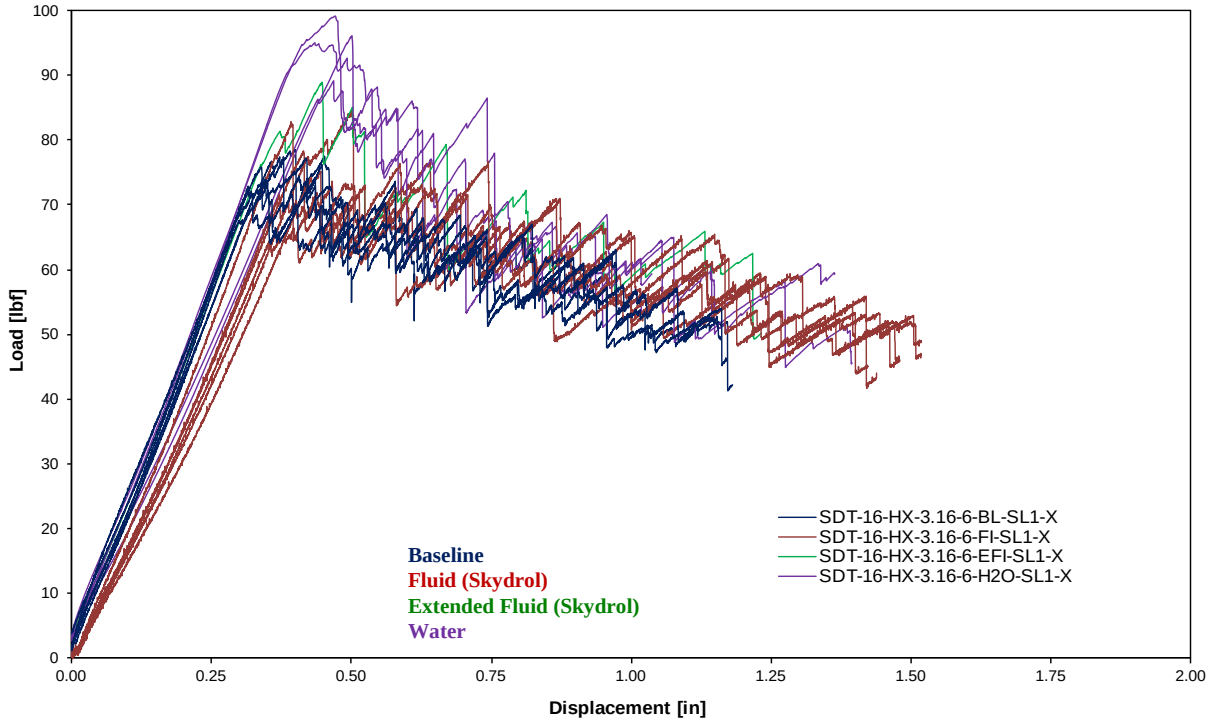

Figure 51. Load vs. displacement curves of 16-ply HRH-10–3/16–6.0 specimens

3.6 EFFECTS OF INITIAL CRACK LENGTH

The length of the initial crack played a critical role in determining fracture toughness. This was because, among the 4-ply specimens, a large prescribed crack (2.5″) resulted in large displacement and geometric nonlinearity. Correction factors were in place to account for these anomalies; however, failure modes and other issues still resulted in significant differences in fracture toughness.

Figures 52–54 show that the shorter prescribed crack length had significantly higher fracture toughness, except for one instance—the 4-ply, hexagonal, 3/4″, 3 pcf specimens.

The resistance curves for the 1″ and 2.5″ prescribed crack length specimens are continuous and could be represented as a single curve (see figure 55). It seems rational that the curves should be continuous and should correspond to a single specimen, starting with a 1″ prescribed crack length and growing through the range of the 2.5″ prescribed crack length specimens. The failure mode seems fairly consistent between the two prescribed crack length geometries, with the shortened specimens occasionally having slightly more core failure. The load-displacement curves also appear to be continuous, for the same reasons as stated previously with significant displacements for longer crack lengths (see figure 56).

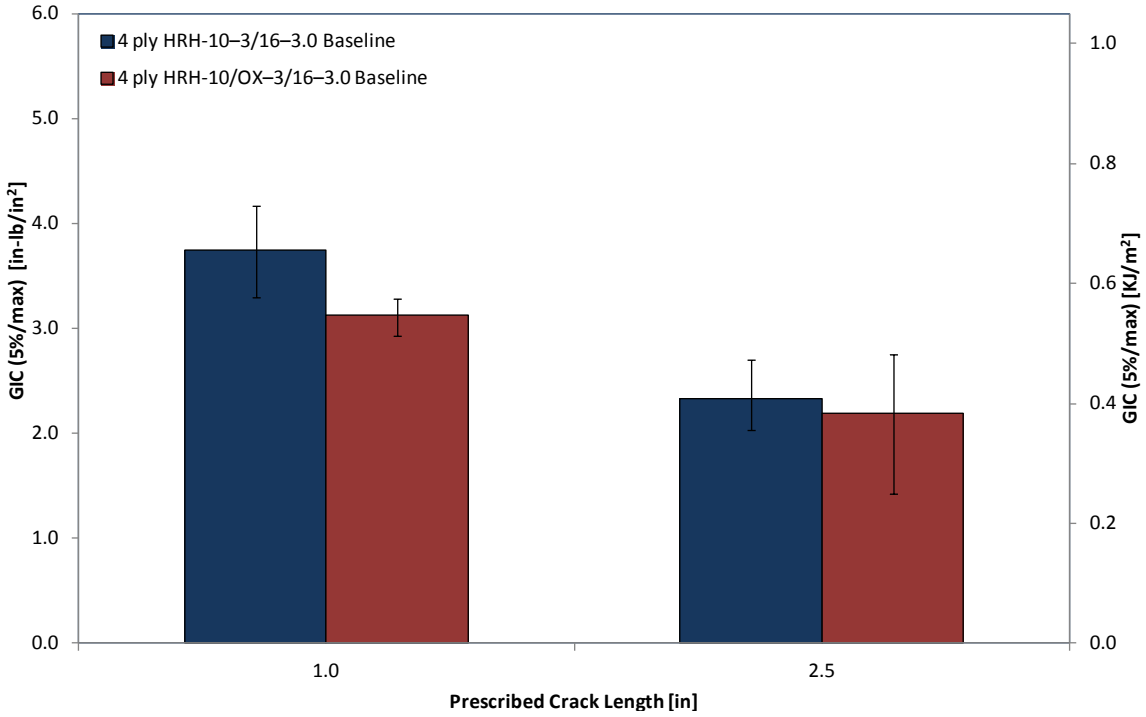

Figure 52. Effects of a_o with respect to core type (4 ply)

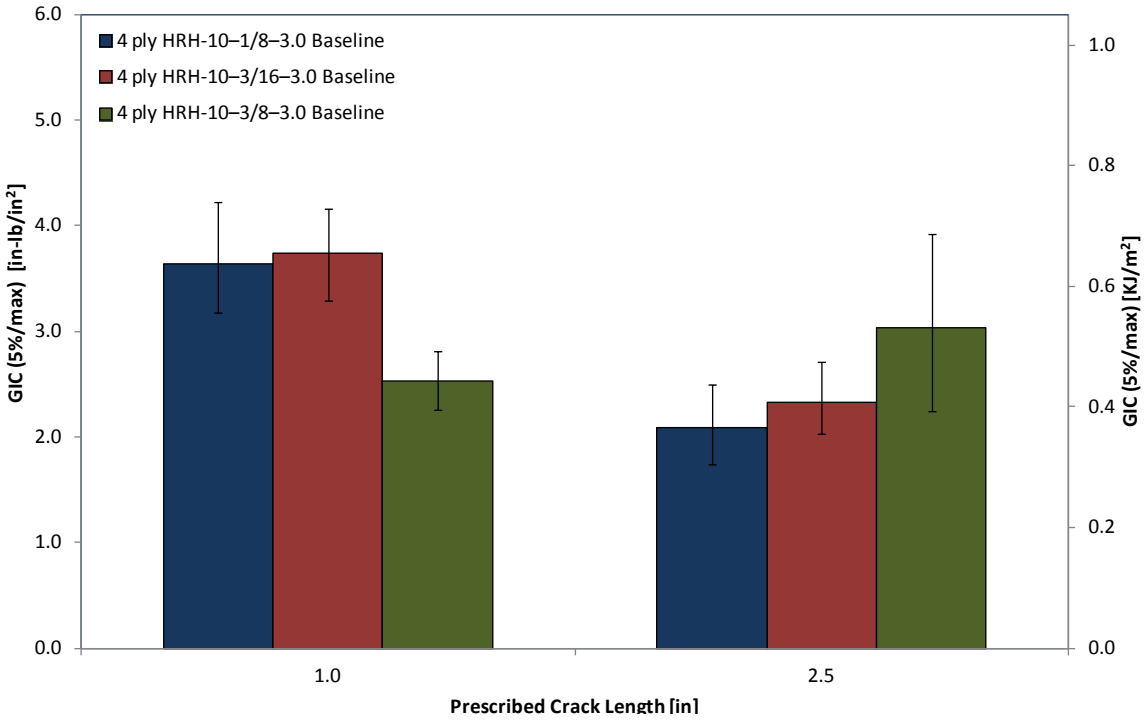

Figure 53. Effects of a_o with respect to cell size (4 ply)

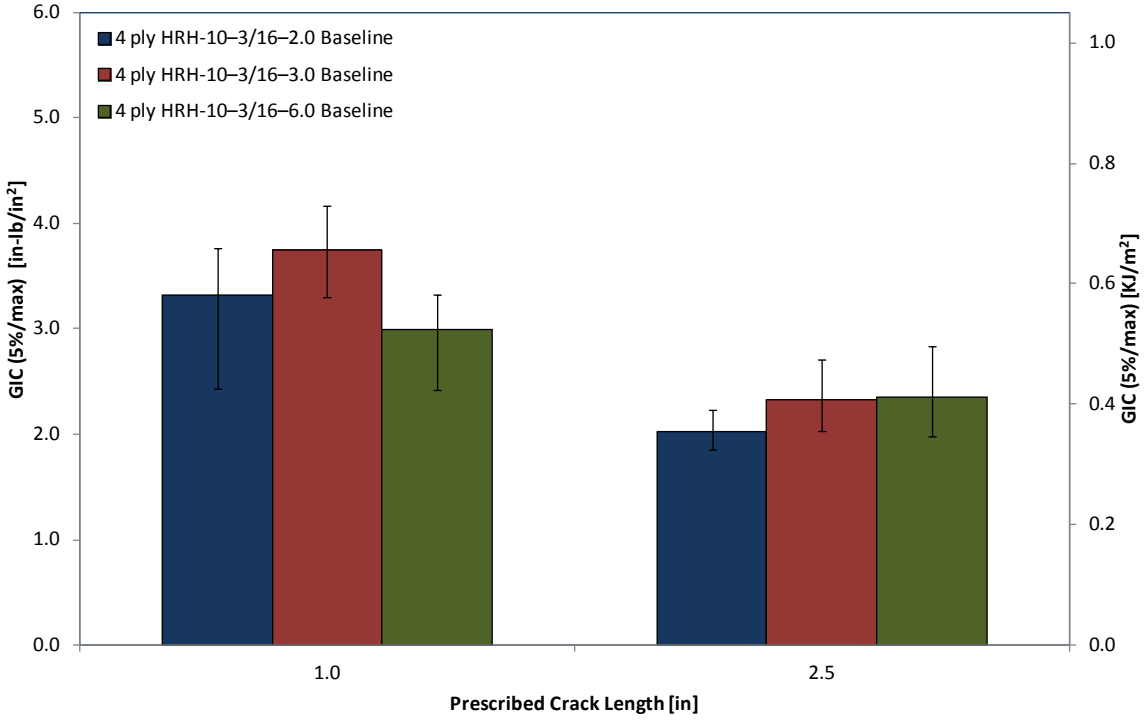

Figure 54. Effects of a_o with respect to core density (16 ply)

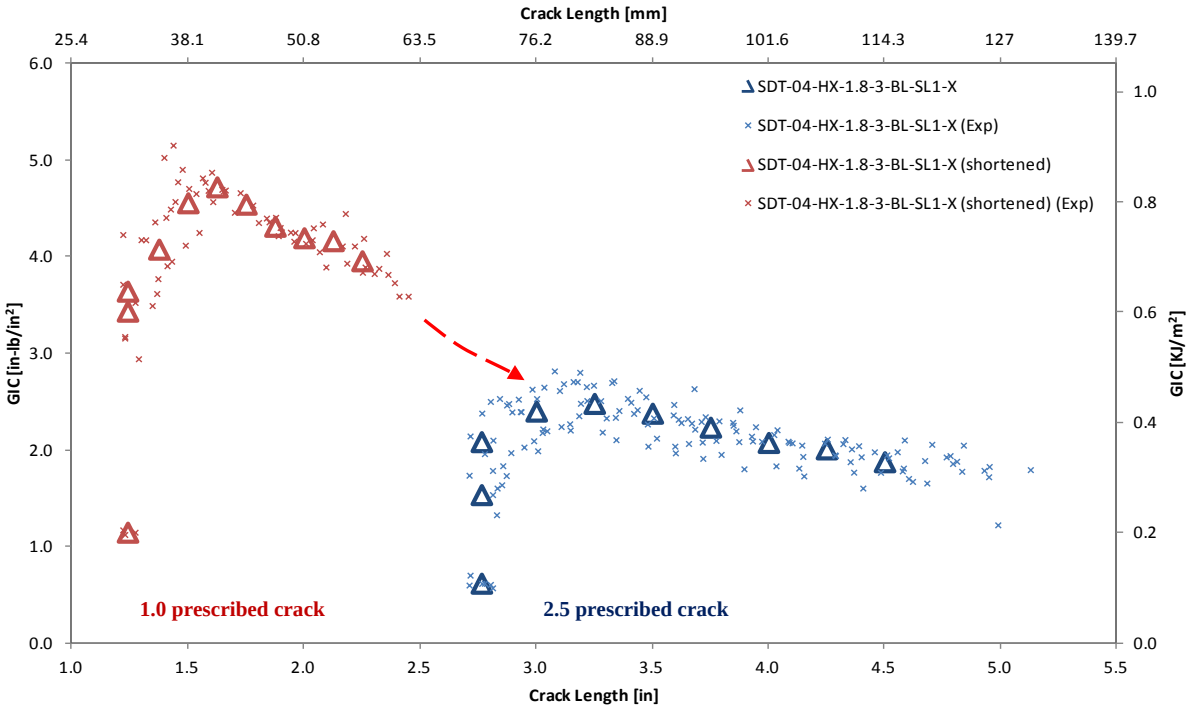

Figure 55. Resistance curves of 4-ply HRH-10–1/8–3.0 baseline specimens

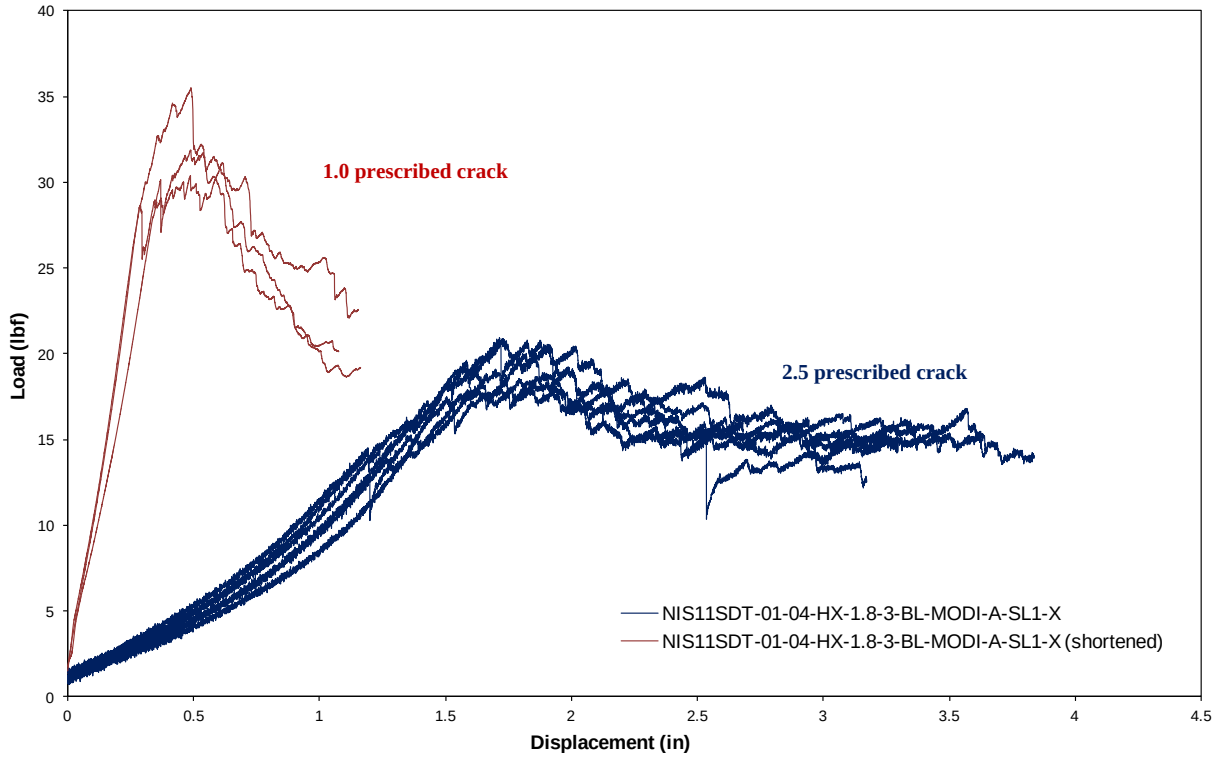

Figure 56. Load vs. displacement curves of 4-ply HRH-10–1/8–3.0 baseline specimens

3.7 SUMMARY OF FAILURE MODES FOR SCB SANDWICH TEST SPECIMENS

Fracture toughness was strongly dependent on failure mode and in distinguishing the behavior of the resistance curves. The failure modes are shown in figures 57–68. No single rule holds true for every geometry, fluid ingression, or material system because the variables are interrelated. However, two patterns were observed.

First, changes in the failure mode substantially impacted data scatter and the coefficient of variation. Core failure resulted in the smallest scatter and coefficient of variation, whereas PO had the largest scatter and coefficient of variation, with adhesion failure somewhere in between. This was because of the mechanisms behind the failure, which are best shown in the load-displacement curves. Core failure had a relatively smooth load-displacement curve with very small or no load drops (i.e., a small change in energy), indicating stable crack growth that was slow and continuous, whereas PO had very large load drops (i.e., a large change in energy), indicating abrupt crack growth and arrest. Adhesion failure fell somewhere in between.

Second, changes in the failure mode also impacted fracture toughness. For example, PO nearly always resulted in a higher GIC than adhesion failure. Core failure, however, depended on core type, cell size, and core density, relative to how much energy would be required to force the crack to occur in the core as opposed to the interface.

Note: In figures 57 and 68, the prescribed crack tip occurs at the far-left edge, with the resulting crack propagation moving to the right.

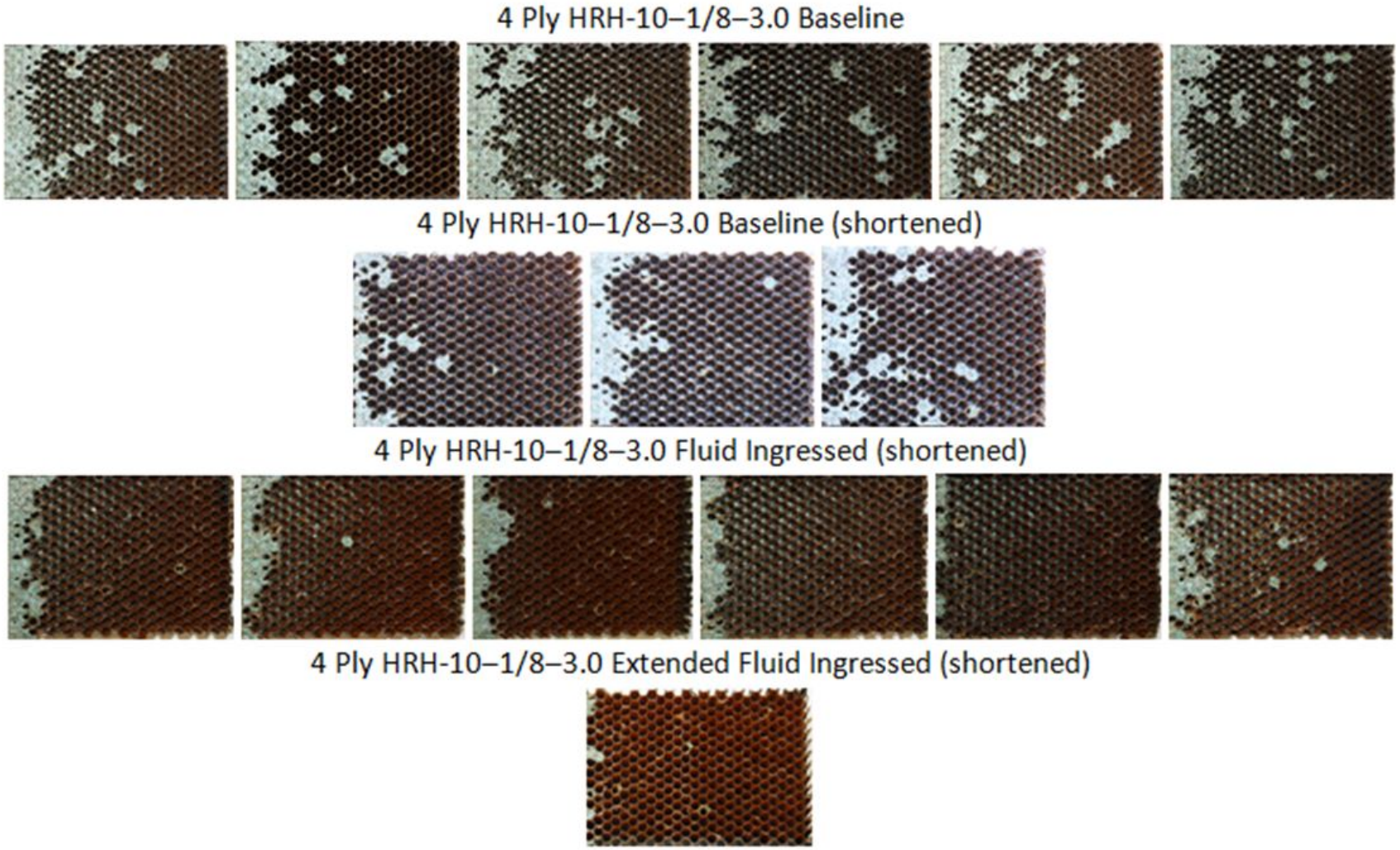

Figure 57. Failure modes of HRH-10–1/8–3.0 thin specimens (4 ply)

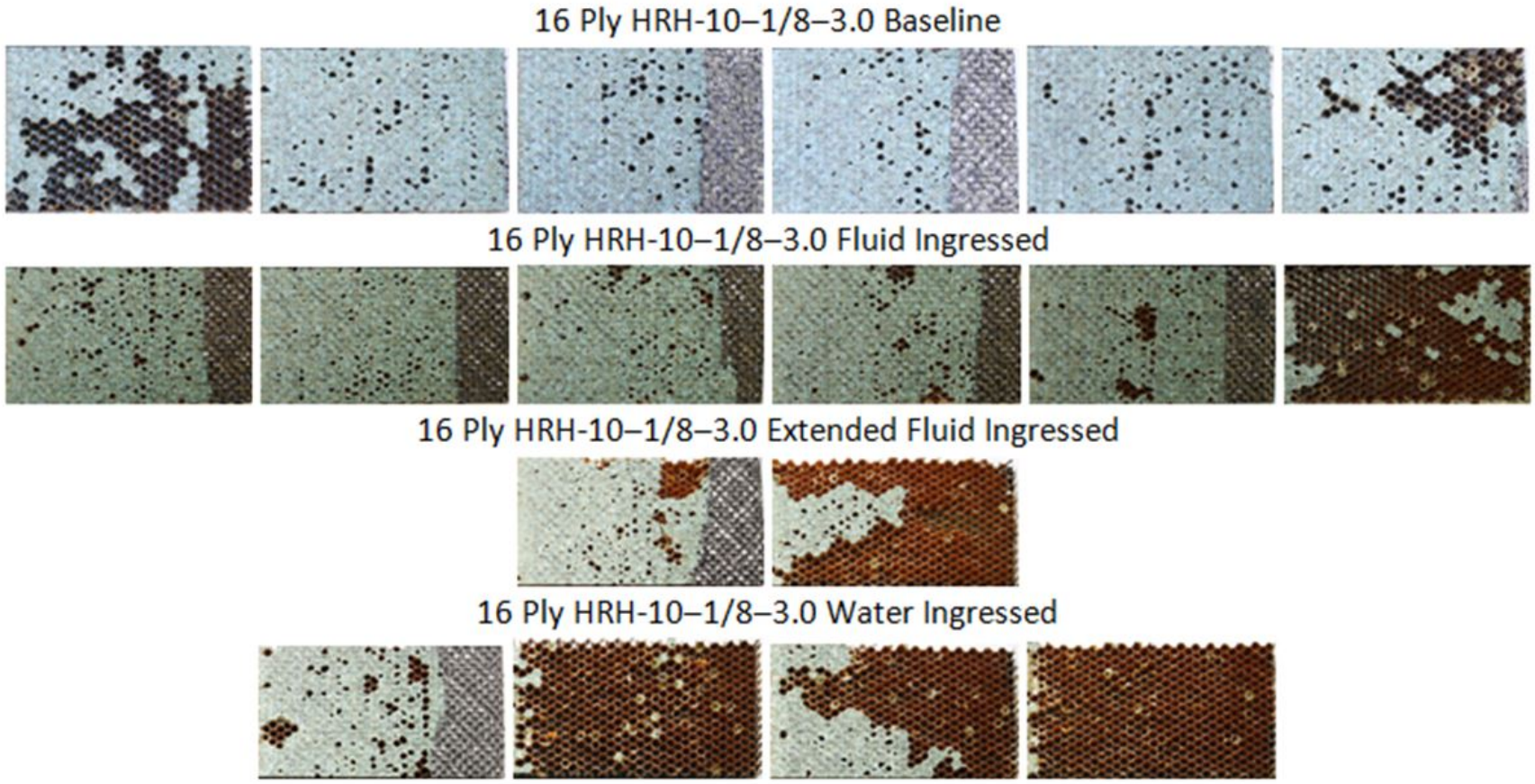

Figure 58. Failure modes of HRH-10–1/8–3.0 thick specimens (16 ply)

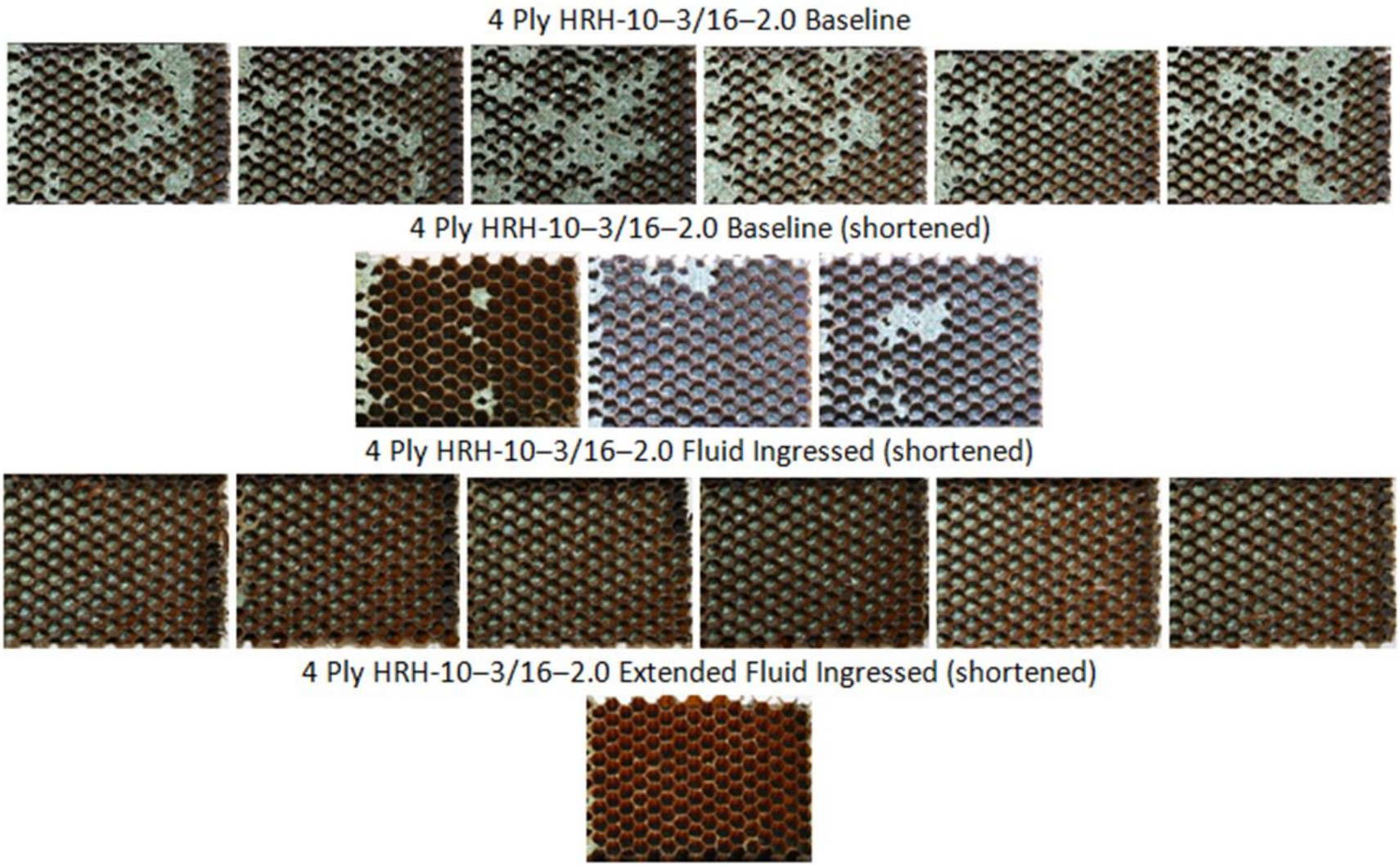

Figure 59. Failure modes of HRH-10–3/16–2.0 thin specimens (4 ply)

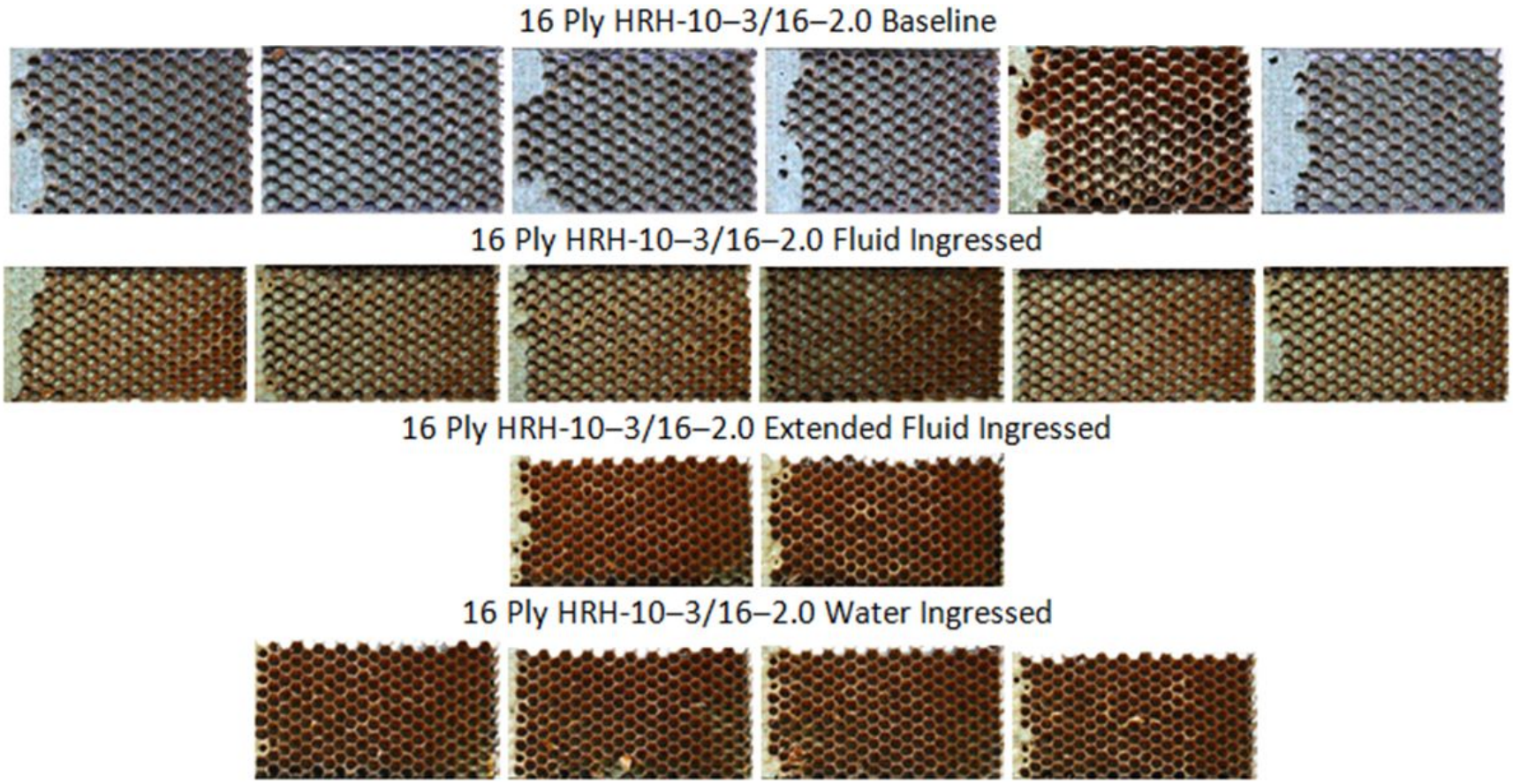

Figure 60. Failure modes of HRH-10–3/16–2.0 thick specimens (16 ply)

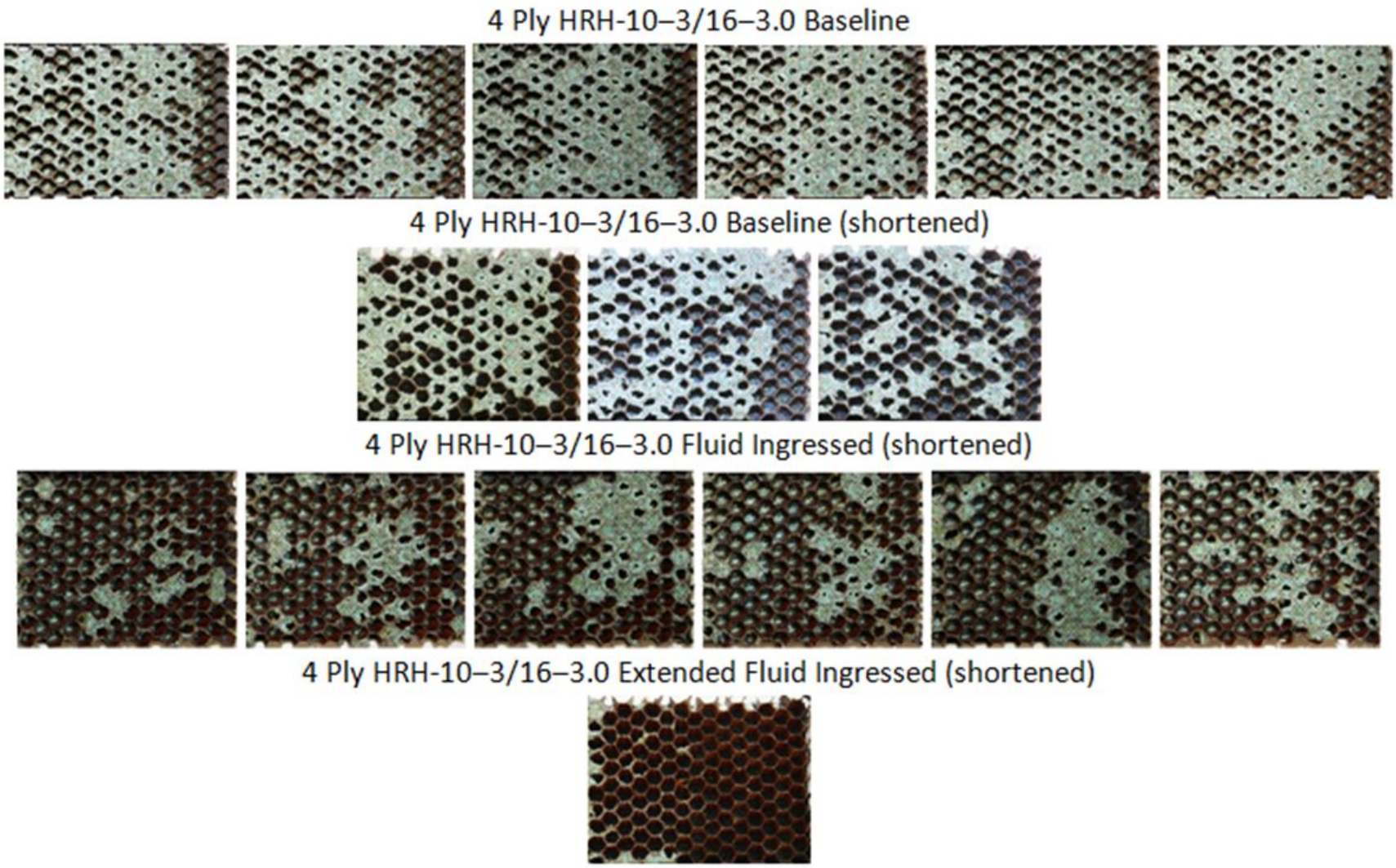

Figure 61. Failure modes of HRH-10–3/16–3.0 thin specimens (4 ply)

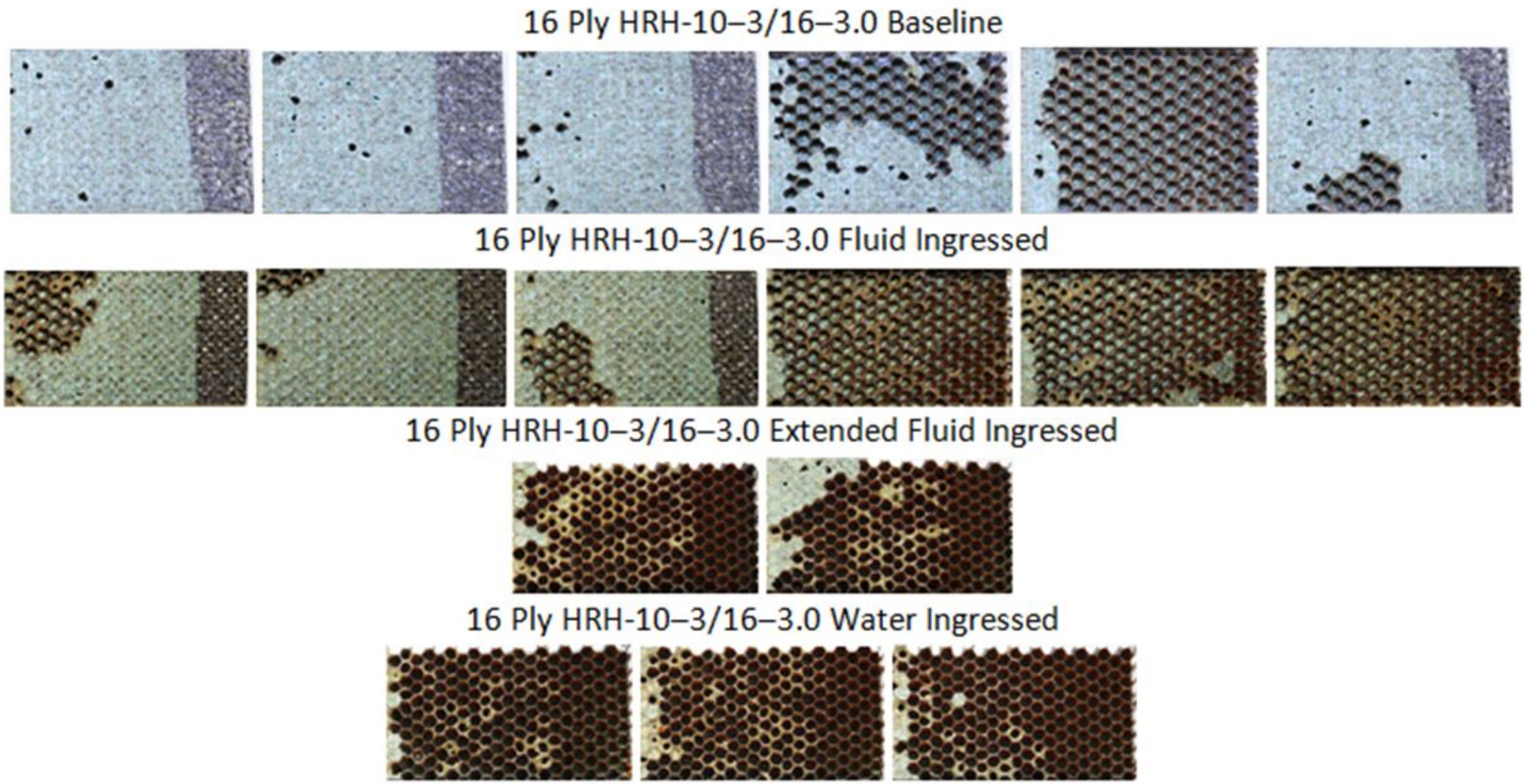

Figure 62. Failure modes of HRH-10–3/16–3.0 thick specimens (16 ply)

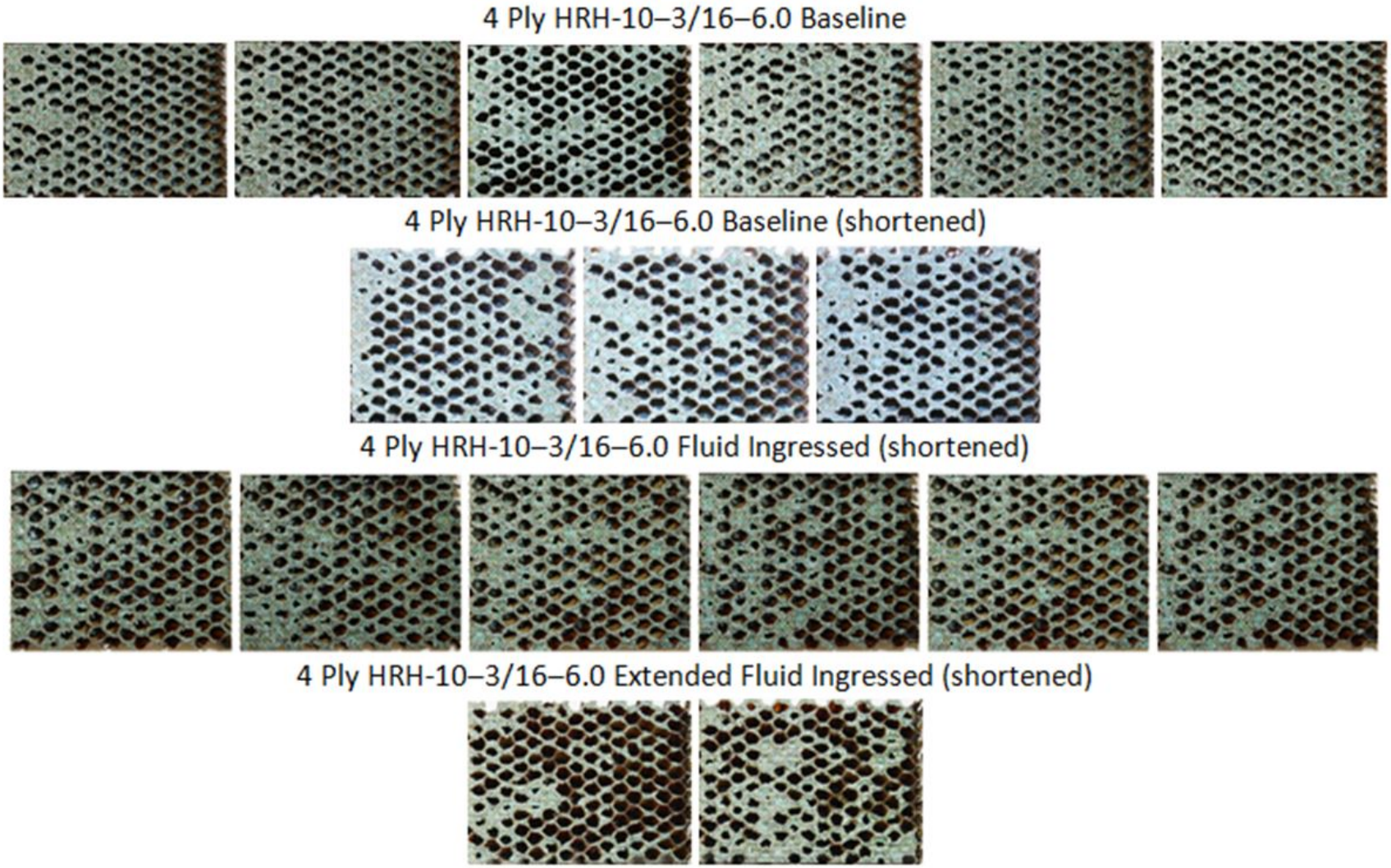

Figure 63. Failure modes of HRH-10–3/16–6.0 thin specimens (4-ply)

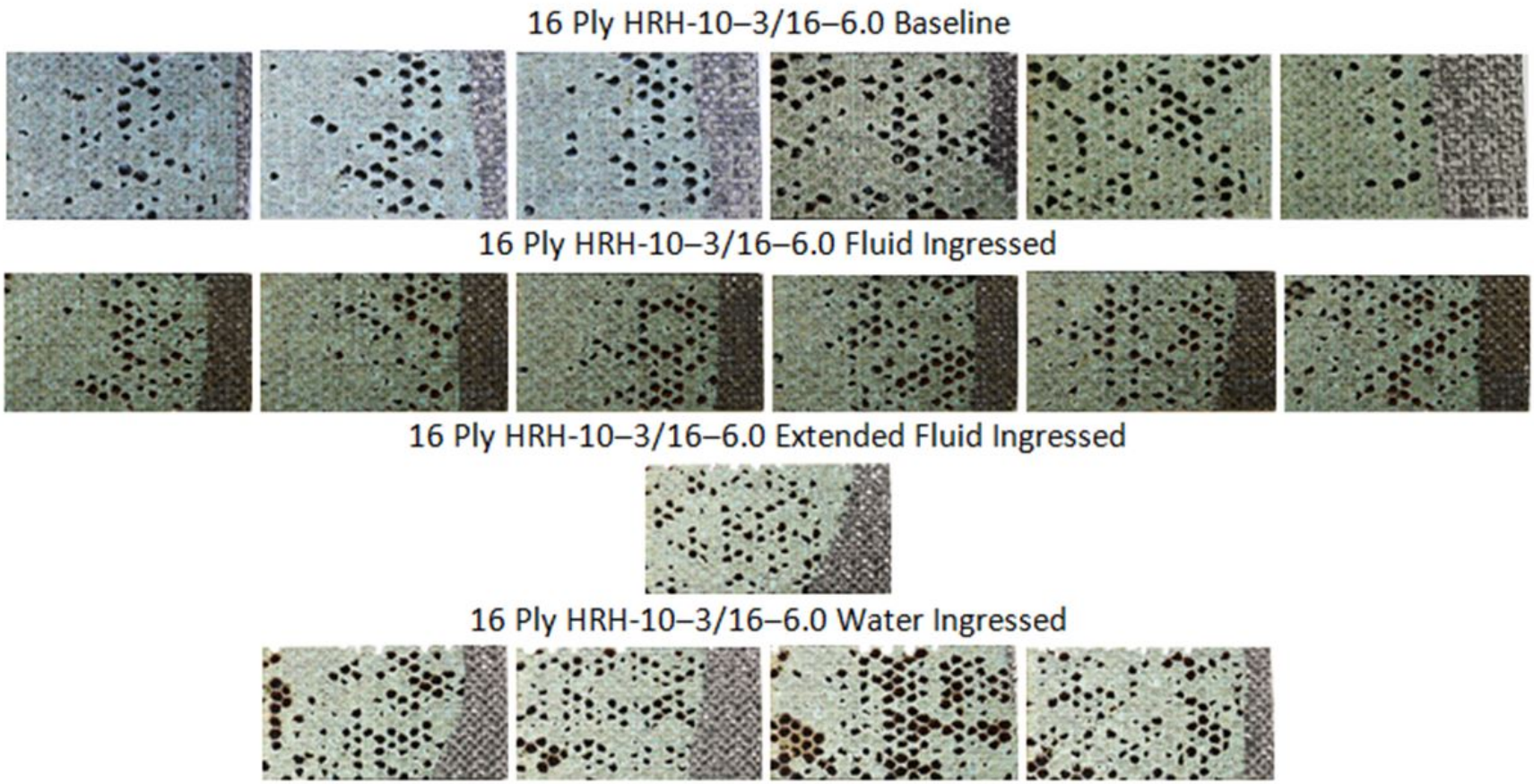

Figure 64. Failure modes of HRH-10–3/16–6.0 thick specimens (16 ply)

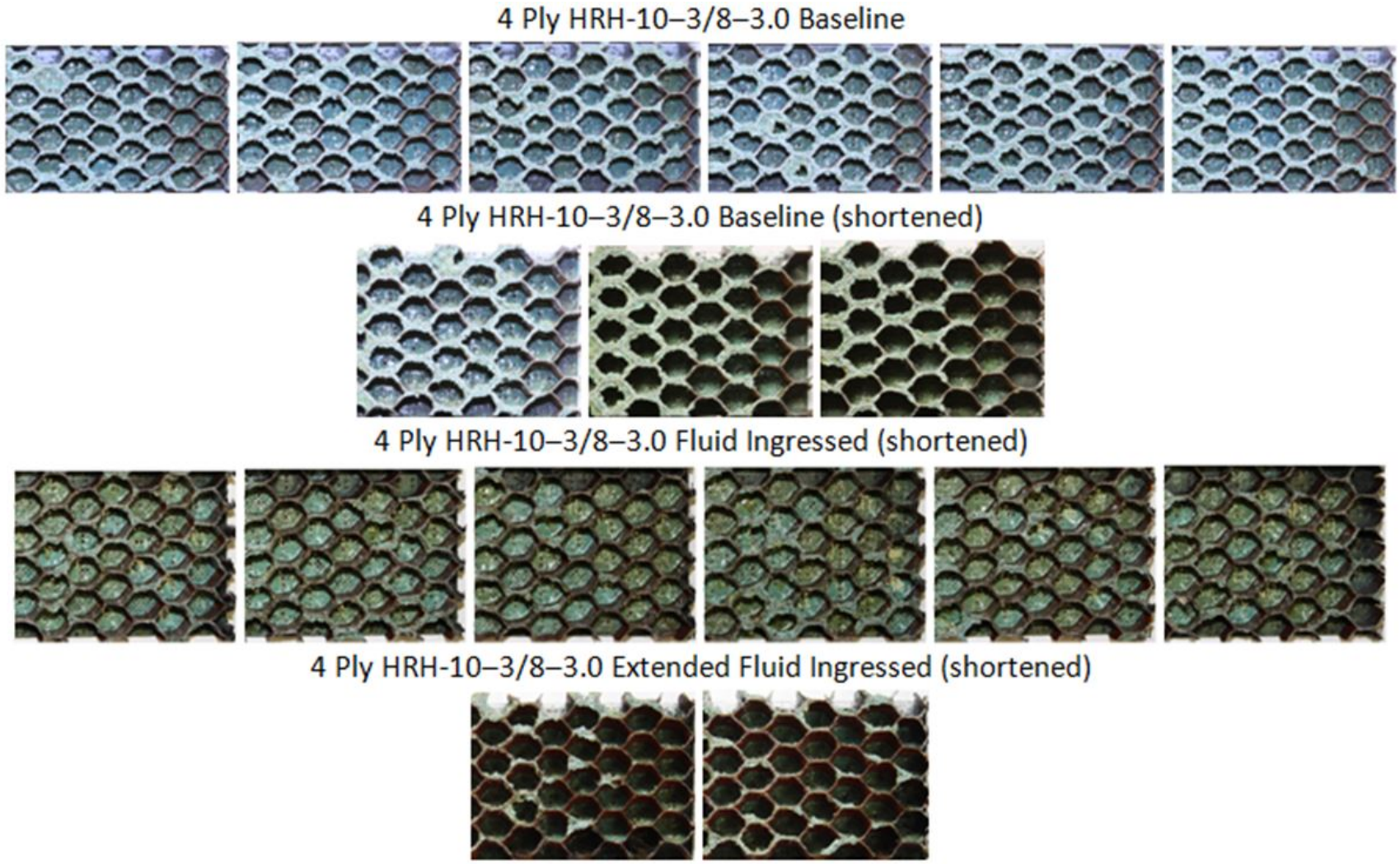

Figure 65. Failure modes of HRH-10–3/8–3.0 thin specimens (4 ply)

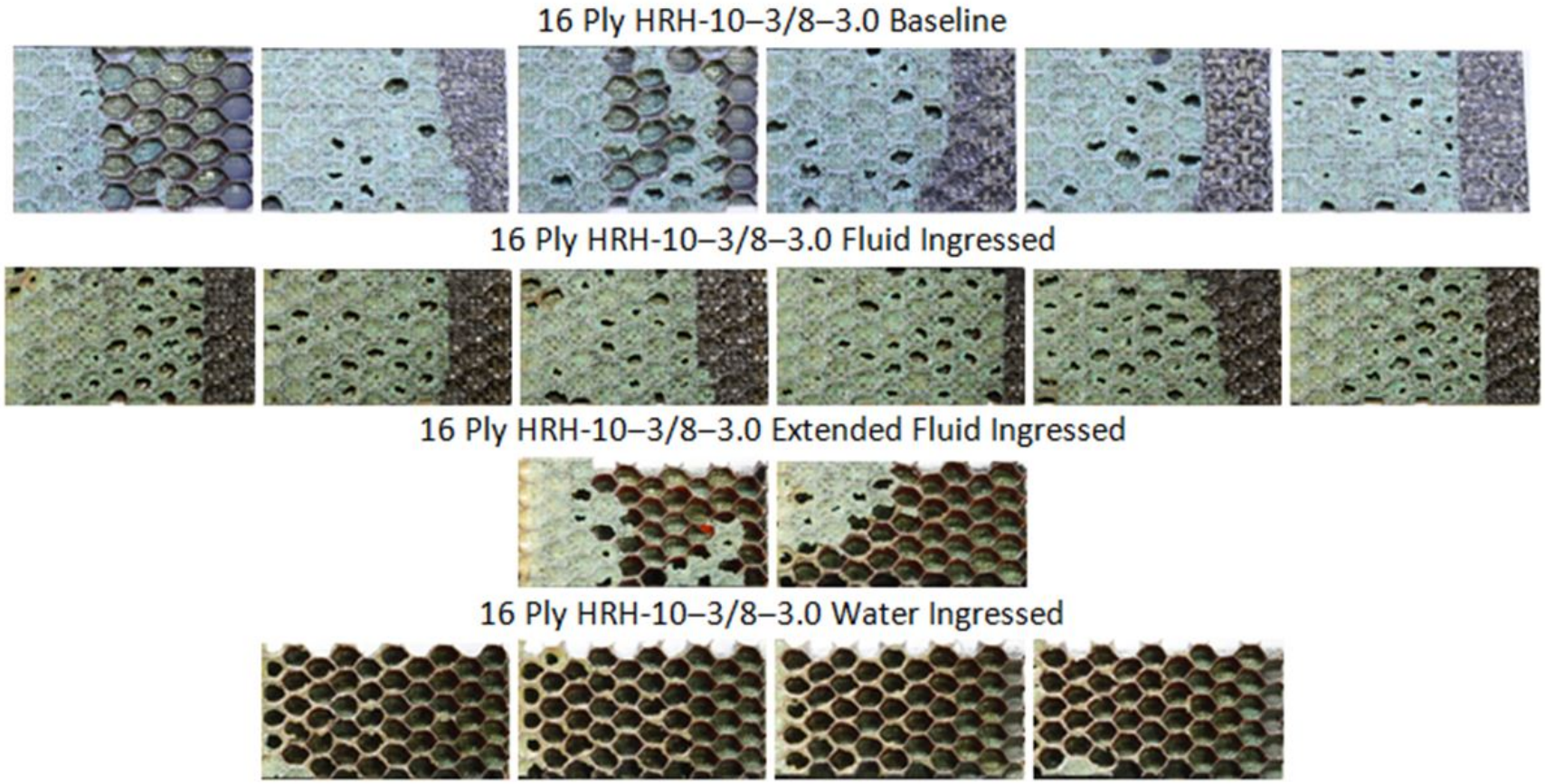

Figure 66. Failure modes of HRH-10–3/8–3.0 thick specimens (16 ply)

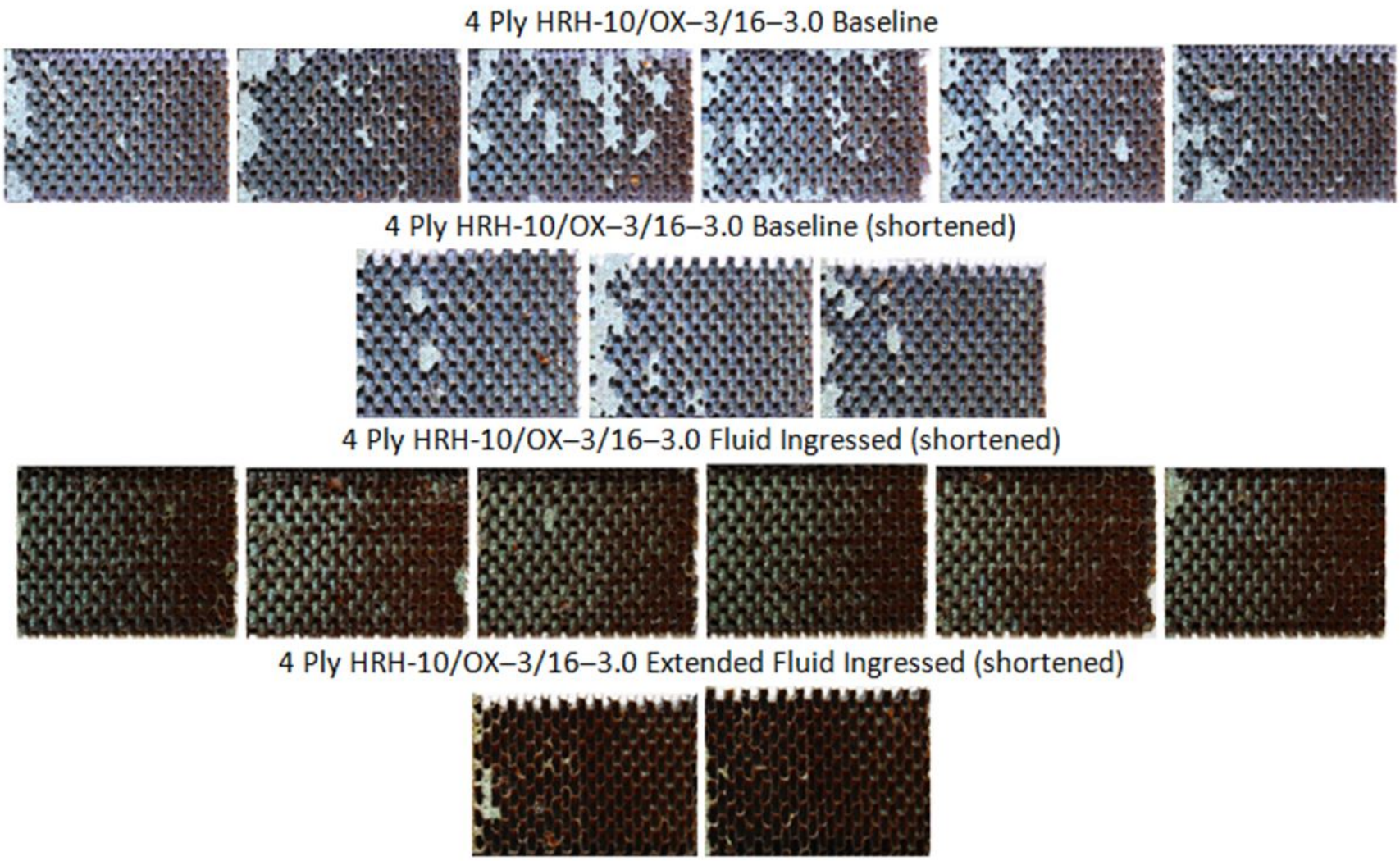

Figure 67. Failure modes of HRH-10/OX–3/16–3.0 thin specimens (4 ply)

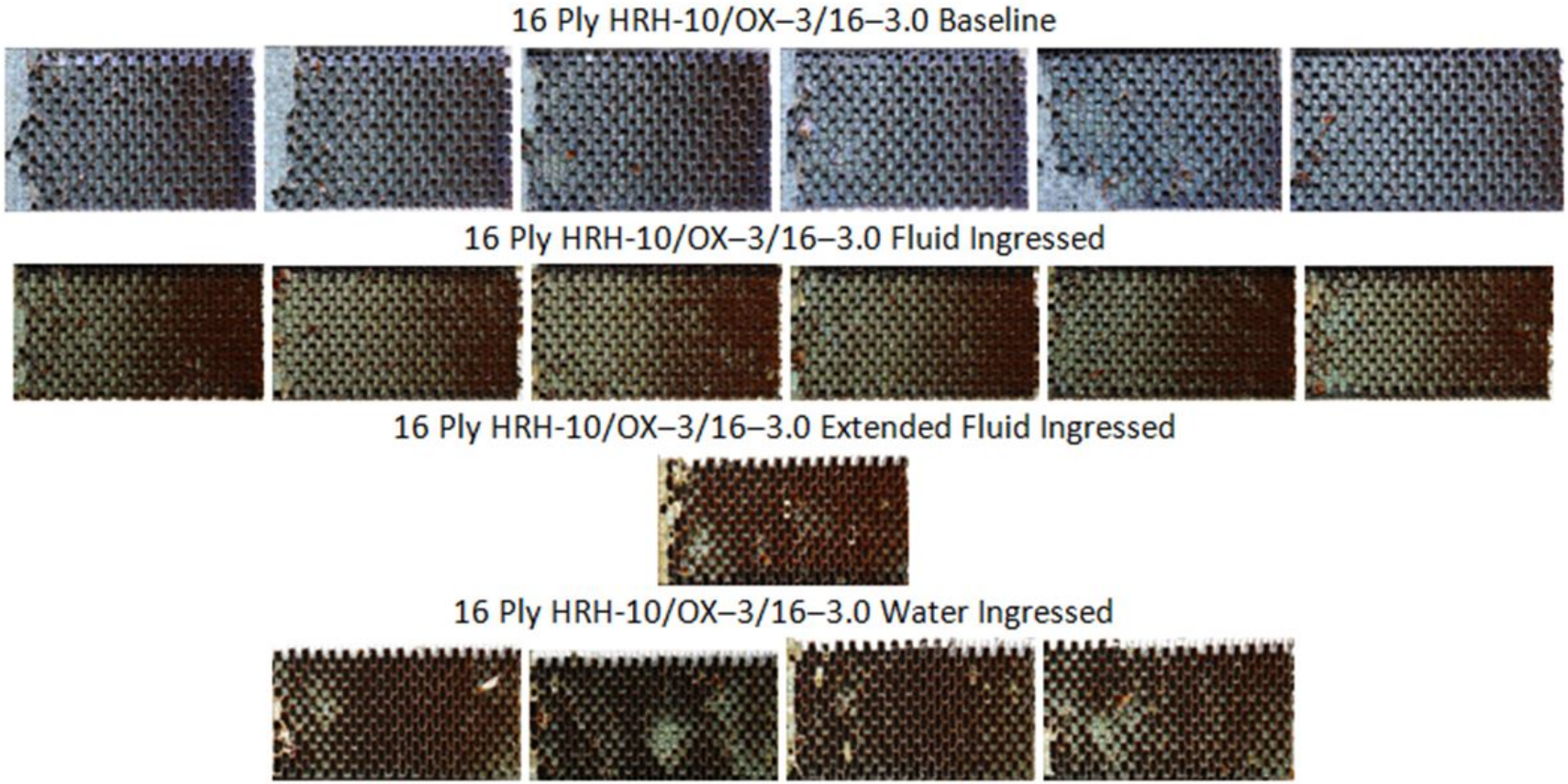

Figure 68. Failure modes of HRH-10/OX–3/16–3.0 thick specimens (16 ply)

4. CONCLUSION AND RECOMMENDATIONS

A research program was conducted on the effects of various sandwich configurations including fluid ingression on fracture toughness of composite sandwich. The SCB specimens were found to be most suitable for determining the Mode I fracture toughness (GIC) of composite sandwich specimens based on the preliminary DCB and SCB tests. The SCB test fixture with a traveling stage prevented mixed-mode mechanics and kinking. Failure modes were complex and often a mixture of the primary crack propagation modes identified in this report. This contributed to the significant data scatter observed in the preliminary test data. The immaturity of the test procedure and the variation in the initial flaws could also have contributed to the data scatter. Note that the SCB test configuration does not directly relate to the damage growth phenomenon in a sandwich structure because the realistic damage is often a mixed-mode fracture, but it provided a set of comparative data for identifying the effects of different core parameters on Mode I damage growth. Also, these data will be useful in analytical models for predicting the growth phenomenon. This research will be expanded to larger and more-realistic specimen configurations representing aircraft structures undergoing GAG cycles.

The impact of several key sandwich parameters on GIC and propagation values was analyzed in detail. These were: a) facesheet thickness; b) core type; c) cell size; d) core density; e) environmental conditioning; and f) prescribed crack length. It is important to note that several other variables can contribute to GIC, such as ribbon direction, fabrication technique, and prescribed crack location with respect to cell walls, etc. These variables are studied in Volume III of this report. Therefore, the discussion and conclusions here are solely based on the results included in this volume.

Theoretically, facesheet thickness should have no influence on fracture toughness. However, large deflection, material nonlinearity, and changing failure modes resulted in facesheet thickness playing a predominant role in GIC among various sandwich configurations. Typically, the thicker the facesheet, the larger the fracture toughness, regardless of core type, cell size, or cell density whether considering the recorded values (i.e., NL, visual onset of crack growth, or 5%) or crack propagation values.

Except for extended fluid ingression specimens for HX, core type had no effect on GIC. When examining the entire resistance curve, it was found that the HX was somewhat more fracture-resistant than the OX. Additionally, the failure modes between the two core types varied significantly. The failure mode for the HX was adhesive or pullout whereas the failure mode for the OX was core failure.

Cell size played a minimal role in determining fracture toughness. However, cell fillets and paper thickness may have also contributed to how cell size influenced fracture toughness. The 1/8″ core resulted in primarily core and adhesion failure, whereas the 3/16″ core resulted in primarily adhesive and PO. The 3/8″ core resulted primarily in PO. Cell size also affected the load-displacement curves (i.e., larger load drops—and crack arrest—as the cell size increased).

Core density had a small impact on fracture toughness. This is because of the fillets and how they artificially thicken cell walls and potentially paper thickness. Failure mode was influenced by core density moving from core to PO as density increased. Core density also affected the

load-displacement curves (i.e., larger load drops—and crack arrest—as the core density increased).

Fluid ingression using an acidic Skydrol/water mixture had a significant impact on both the bond line (acid degradation) and the core (moisture absorption), which resulted in greater fracture toughness. Crack tip softening due to moisture absorption and the weakened adhesive played a key role in damage growth, especially at the initial region of the resistance curve. When considering the entire resistance curve, it can be observed that resistance curves typically converge among the various environmental conditions.

The prescribed crack length played a role in determining fracture toughness. Large prescribed crack lengths led to significantly larger displacements and nonlinear behavior in thin facesheet specimens. Once the correction factors were applied, it was observed that the shortened, 1″ specimens had significantly higher fracture toughness than the 2.5″ specimens, regardless of core type, cell size, or core density. Additionally, both resistance curves and load-displacement curves (which were superimposed) appeared to be continuous for any given sandwich configuration.

Changes in failure mode substantially impacted data scatter (coefficient of variation). Core failure, compared with adhesion failure, resulted in the least scatter. PO resulted in the highest scatter. This was because of the mechanisms behind the failure (i.e., stable [core] versus semi-stable [pullout] crack growth). Changes in failure mode also impacted fracture toughness, with PO resulting in higher GIC than adhesion failure. However, core failure depended on the core type, cell size, and cell density—paper thickness also played a key role.

This study was further extended to evaluate the damage growth rate under cyclic loading for similar parameters discussed in this paper and are reported in Volume II of the report. Furthermore, several other key parameters, such as effects of ribbon direction, fabrication procedures, and crack starter location, were studied in a supplemental test matrix and reported in Volume III of this report.

5. REFERENCES

1. Seneviratne, W., Tomblin, J., & Gunawardana, S. (2007). Experimental Fracture Mechanics for Adhesive Joint Design. *International Conference on Computational & Experimental Engineering and Sciences (ICCES)*, *4*(2), 81–86.

2. Anderson, T.L. (1994). Fracture mechanics: fundamentals and applications, 2nd edition. Boca Raton, FL: CRC Press.

3. Smith, B. L. (2010). Mechanics of damage tolerance: residual strength, fracture crack propagation and damage tolerance evaluation [Class note packet]. Wichita State University, Wichita, KS.

4. Aviles, F., & Carlsson, L. A. (2008). Analysis of the sandwich DCB specimen for debond characterization. *Engineering Fracture Mechanics*, *75*(2), 153–168.

5. Li, X., & Carlsson, L. A. (2000). Elastic foundation analysis of tilted sandwich debond (TSD) specimen. *Journal of Sandwich Structures and Materials, 2*(1), 3–32.

6. Shivakumar, K., Chen, H., & Smith, S. A. (2005). An evaluation of data reduction methods for opening mode fracture toughness of sandwich panels. *Journal of Sandwich Structures and Materials, 7*(1), 77–90.

7. Seneviratne, W., & Tomblin, J. (2011). *Damage growth in fluid-ingressed sandwich structures.* Proceedings from the 1st Technical Workshop for Safety Management Initiative for Sandwich Disbond Growth, Hampton, VA.

8. Cantwell, W. J., & Davies, P. (1994). A Test technique for assessing core-skin adhesion in composite sandwich structures. *Journal of Material Science Letters, 13(*3), 203–205.

9. Cantwell, W. J., & Davies, P. (1996). A study of skin-core adhesion in glass fiber reinforced sandwich materials. *Applied Composite Materials, 3*(6), 407–420.

10. Ratcliffe, J. G. (2010, January, 01). Sizing single cantilever beam specimens for characterizing facesheet/core peel debonding in sandwich structure, NASA/TP-2010-216169. Retrieved from http://ntrs.nasa.gov/search.jsp?R=20100003052.

11. Boresi, A. P., & Schmidt, R. J. (2003). Linear Stress-Strain-Temperature Relations. *Advanced Mechanics of Materials, 6th edition*, (pp. 3–4, 79–90, and 158–160). Hoboken, NJ: John Wiley & Sons, Inc.

12. Hibbeler, R. C. (2004). Design of beams and shafts & Energy methods. In Beer, F. P., Johnston, E. R., DeWolf, J. T., & Mazurek, D. F. (Eds.), *Mechanics of materials, 6th edition* (585–592 & 725–740), Upper Saddle River, NJ: Pearson Prentice Hall.

13. Williams, J. G. (1987). Large displacement and end block effects in 'DCB' interlaminar test in modes I and II. *Journal of Composite Materials, 21*(4), 330–347.

APPENDIX A—SKYDROL/WATER FLUID INGRESSION PROCEDURE

The adhesive used to bond the facesheet to the core can break down when exposed to certain chemicals, such as phosphoric acid. Given enough time, water and hydraulic fluid can produce a byproduct of weak phosphoric acid when combined. With the amount of hydraulic fluid and water on aircraft, it is vital to determine their effect on sandwich composites that have been ingressed in this volatile amalgam.

Before fluid ingression can begin, it is paramount to create a mixture with an acceptable amount of acidity. To produce a viable solution, water and Skydrol® are mixed in a 50:50 ratio, placed in an elevated temperature of 160 °F, agitated for 2 weeks, then placed at room temperature. The elevated temperature acts as a catalyst and accelerates the production of phosphoric acid. The solution is now at a pH of approximately 3–4, and the specimens can be conditioned. The acidity of these solutions for the entire duration can be seen in figure A-1.

Fluid-ingression specimens were conditioned for 45 days and then immediately tested. The length of conditioning was determined empirically. The extended fluid-ingression specimens were tested for 165 days. The length of conditioning was determined based on scheduling.

The water-ingression specimens were placed in deionized water for 45 days.

A.1 PROCEDURE

A.1.1 SCOPE

- This test procedure covers the proper methodology for creating an amalgam of Skydrol and water. The mixture should become a mild acid and is typically used to degrade adhesives.
- The temperature shall be measured in degrees Fahrenheit (F), and acidity shall be measured in pH, both regarded as standard.
- This test procedure does not address all (if any) safety and health concerns associated with the use of this test procedure. The user(s) of this standard must establish appropriate safety and health procedures, and determine the applicable regulations associated with such concerns.

A.1.2 APPLICABLE STUDIES

Skydrol/water round-robin testing was performed in the National Institute for Aviation Research at Wichita State University

A.1.3. SIGNIFICANCE OF USE

Both Skydrol and water can be found within an aircraft—Skydrol as a hydraulic oil and water from condensation—and when mixed, they produce a mild acid that can erode adhesives within sandwich materials and bonded joints. This test method provides a consistent and repeatable approach for producing an acidic mixture composed of Skydrol and water.

A.1.4 APPARATUS

- Conditioning chamber capable of maintaining 160 °F ± 5 °F
- Airtight container that is both acid resistant and temperature rated
- Litmus paper capable of attaining a solution acidity of 1–9 pH

A.1.5 TEST SPECIMEN

The test specimen is a solution that consists of 50% Skydrol and 50% tap water by volume.

A.1.6 EXPERIMENTAL PROCEDURE

- Mix the needed amount of 50% Skydrol and 50% water solution in the airtight container.
- Place the container inside the conditioning camber at 160 °F for 14 days, mixing thoroughly once a day.
- Remove the container from the conditioning camber and let sit at room temperature until cooled.
- Ensure the solution is now at a pH of 3–4.

A.1.7 DATA REDUCTION

Litmus paper is used for monitoring acidity. The results of the acidity monitoring are shown in Figure A-1.

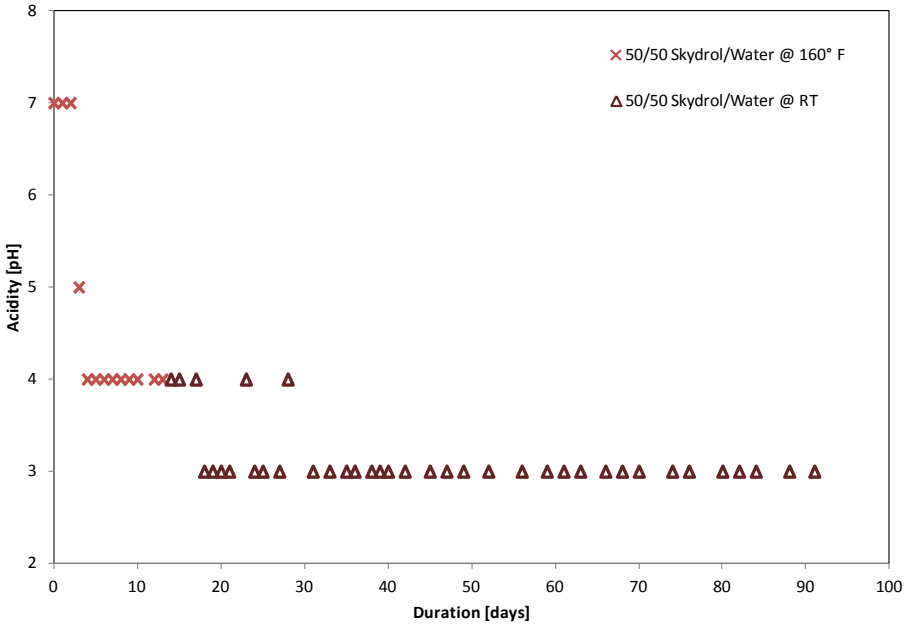

Figure A-1. Sample acidity plot for which solution is kept at constant temperature of 160 °F for 14 days and then at room temperature

APPENDIX B—STATIC RESULTS FOR THIN FACESHEET (4-PLY) AND HRH-10 HEXAGONAL CORES TESTED AS SINGLE-CANTILEVER BEAMS

Note that 4-ply material systems were tested with two prescribed crack lengths. Six baseline specimens were tested with a 2.5″ prescribed crack, and three baseline specimens were tested with a 1″ prescribed crack, referred to as “shortened.” The fluid-ingressed and extended fluid-ingressed specimens were all tested with a 1″ prescribed crack, still referred to as “shortened.”

B.1 HRH–10–1/8–3.0 DATA

B.1.1 HRH-10–1/8–3.0 BASELINE DATA

B.1.1.1 HRH-10–1/8–3.0 Baseline Data (2.5″ Prescribed Crack)

Table B-1. Test summary for HRH-10–1/8–3.0 baseline (2.5″ prescribed crack) pre-crack

Specimen	GIC (in-lb/in^2)			GIC (KJ/m^2)			Failure Mode
	NL	VIS	5%/ max	NL	VIS	5%/ max	
SDT-04-HX-1.8-3-BL-SL1-1	1.215	-	3.308	0.213	-	0.579	Primarily A with occasional PO and a small pocket of C
SDT-04-HX-1.8-3-BL-SL1-2	1.352	-	2.683	0.237	-	0.470	Primarily A with occasional PO
SDT-04-HX-1.8-3-BL-SL1-3	1.369	-	2.579	0.240	-	0.452	Primarily A with occasional PO transitioning to C
SDT-04-HX-1.8-3-BL-SL1-4	0.990	-	2.769	0.173	-	0.485	Primarily A with a couple cells in PO
SDT-04-HX-1.8-3-BL-SL1-5	1.439	-	2.918	0.252	-	0.511	Primarily A with a couple cells in PO
SDT-04-HX-1.8-3-BL-SL1-6	1.398	-	3.368	0.245	-	0.590	Primarily in A with a couple cells in PO and C
AVERAGE GIC	1.294	-	2.937	0.227	-	0.514	
STANDARD DEVIATION	0.167	-	0.330	0.029	-	0.058	
COEFFICIENT OF VARIATION (%)	12.905	-	11.237	12.905	-	11.237	

GIC = Mode I fracture toughness; NL = nonlinear onset of crack growth; VIS = visual onset of crack growth

Table B-2. Test summary HRH-10–1/8–3.0 baseline (2.5″ prescribed crack)

Specimen	GIC (in-lb/in^2)			GIC (KJ/m^2)			Failure Mode
	NL	VIS	5%/ max	NL	VIS	5%/ max	
SDT-04-HX-1.8-3-BL-SL1-1	0.609	-	2.503	0.107	-	0.438	Mix of A, PO, and C, quickly transitioning to C, then a few pockets of A and PO
SDT-04-HX-1.8-3-BL-SL1-2	0.619	-	2.382	0.108	-	0.417	Mix of A, PO, and C, quickly transitioning to C, then multiple cells of A
SDT-04-HX-1.8-3-BL-SL1-3	0.621	-	1.962	0.109	-	0.344	Mix of A, PO, and C, quickly transitioning to C, then multiple cells of A
SDT-04-HX-1.8-3-BL-SL1-4	0.602	-	1.739	0.105	-	0.305	Mix of A, PO, and C, transitioning to C, then multiple cells of A
SDT-04-HX-1.8-3-BL-SL1-5	0.705	-	2.145	0.123	-	0.376	Mix of A, PO, and C, transitioning to C, then multiple cells of A
SDT-04-HX-1.8-3-BL-SL1-6	0.573	1.538	1.788	0.100	0.269	0.313	Mix of A, PO, and C, transitioning to C, then multiple cells of A and PO
AVERAGE GIC	0.622	1.538	2.086	0.109	0.269	0.365	
STANDARD DEVIATION	0.044	-	0.313	0.008	-	0.055	
COEFFICIENT OF VARIATION (%)	7.115	-	14.993	7.115	-	14.993	

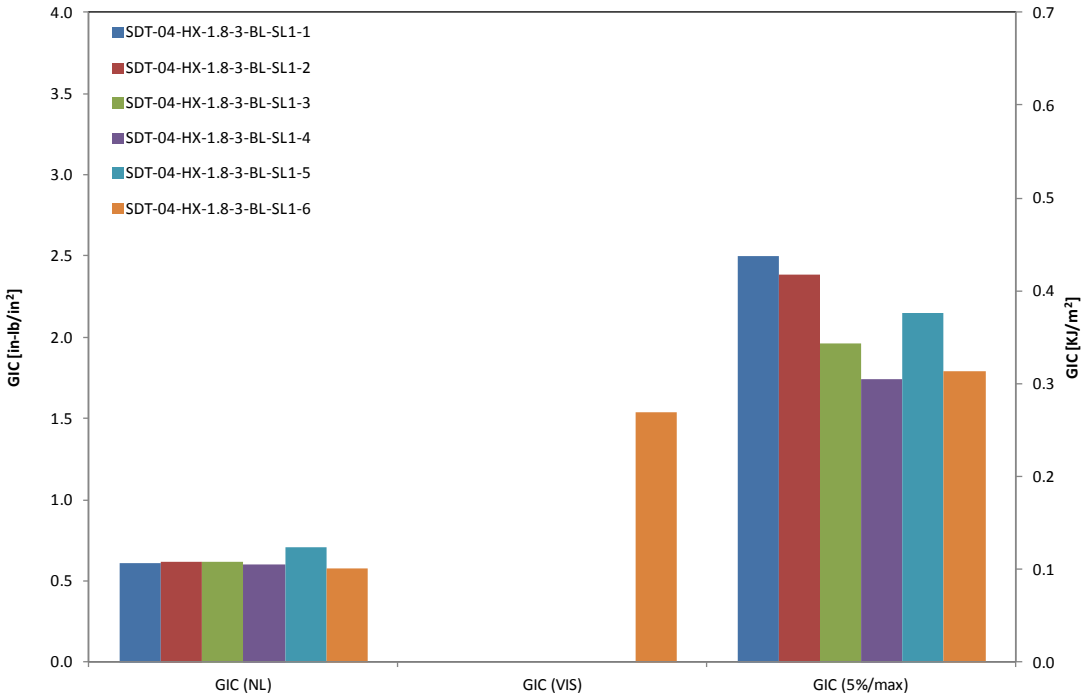

Figure B-1. GIC for HRH-10–1/8–3.0 baseline (2.5″ prescribed crack)

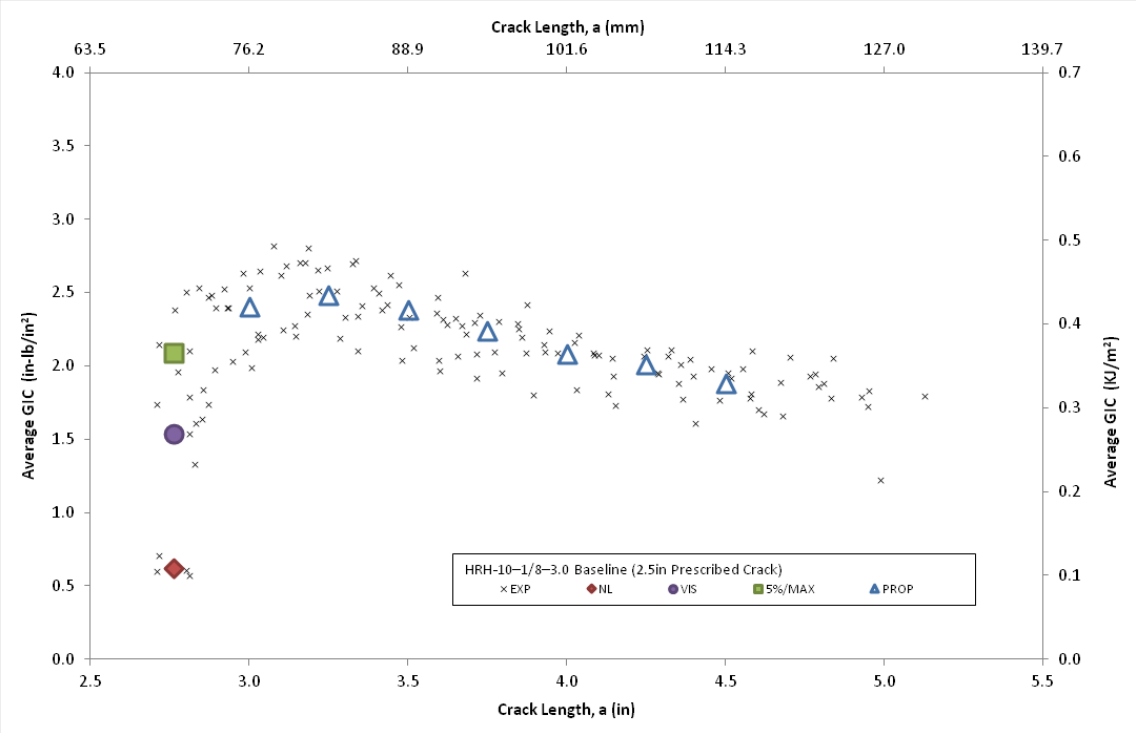

Figure B-2. Resistance curve for HRH-10–1/8–3.0 baseline (2.5″ prescribed crack)

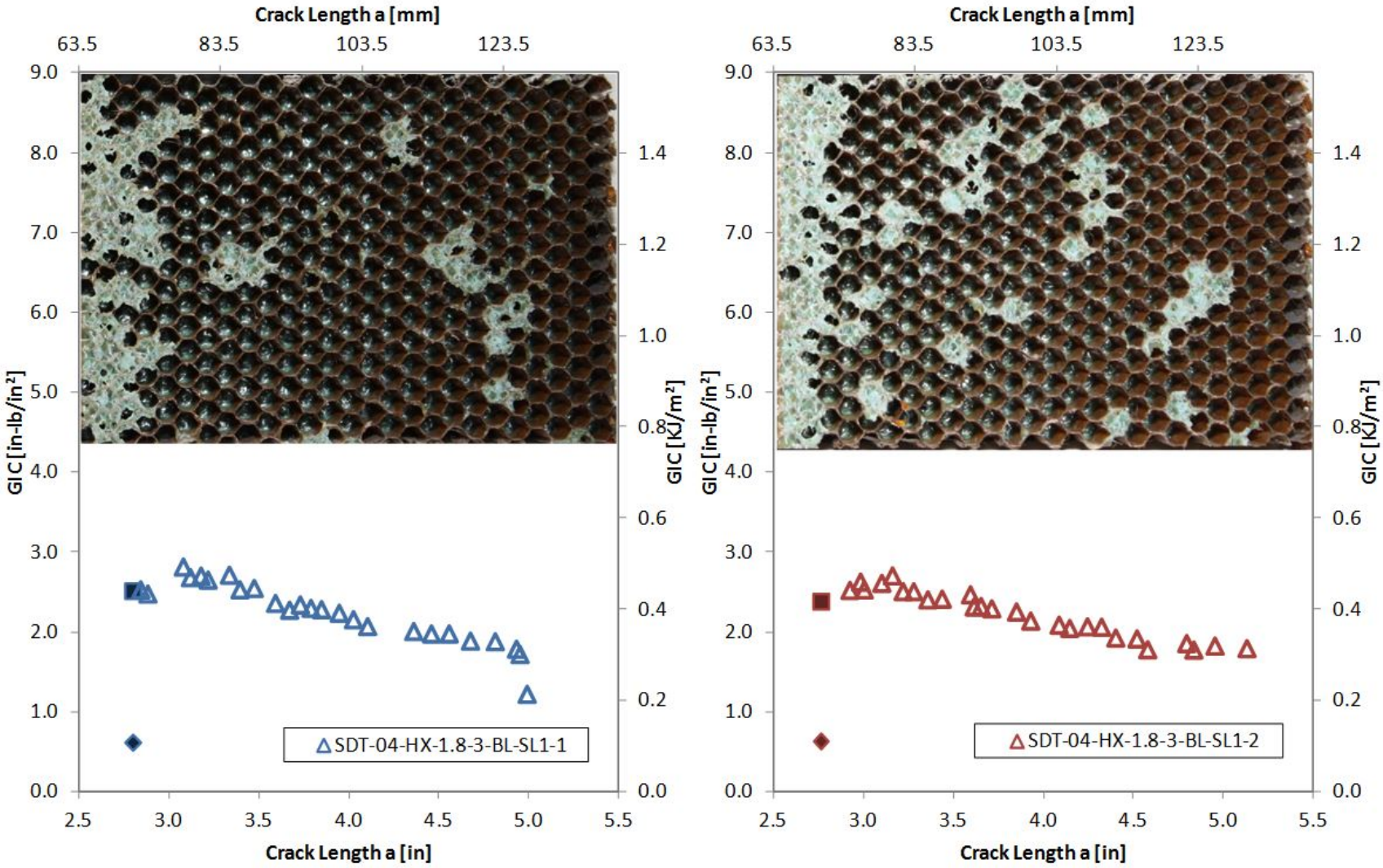

Figure B-3. Failure mode and resistance curve for SDT-04-HX-1.8-3-BL-SL1-X #1 and #2

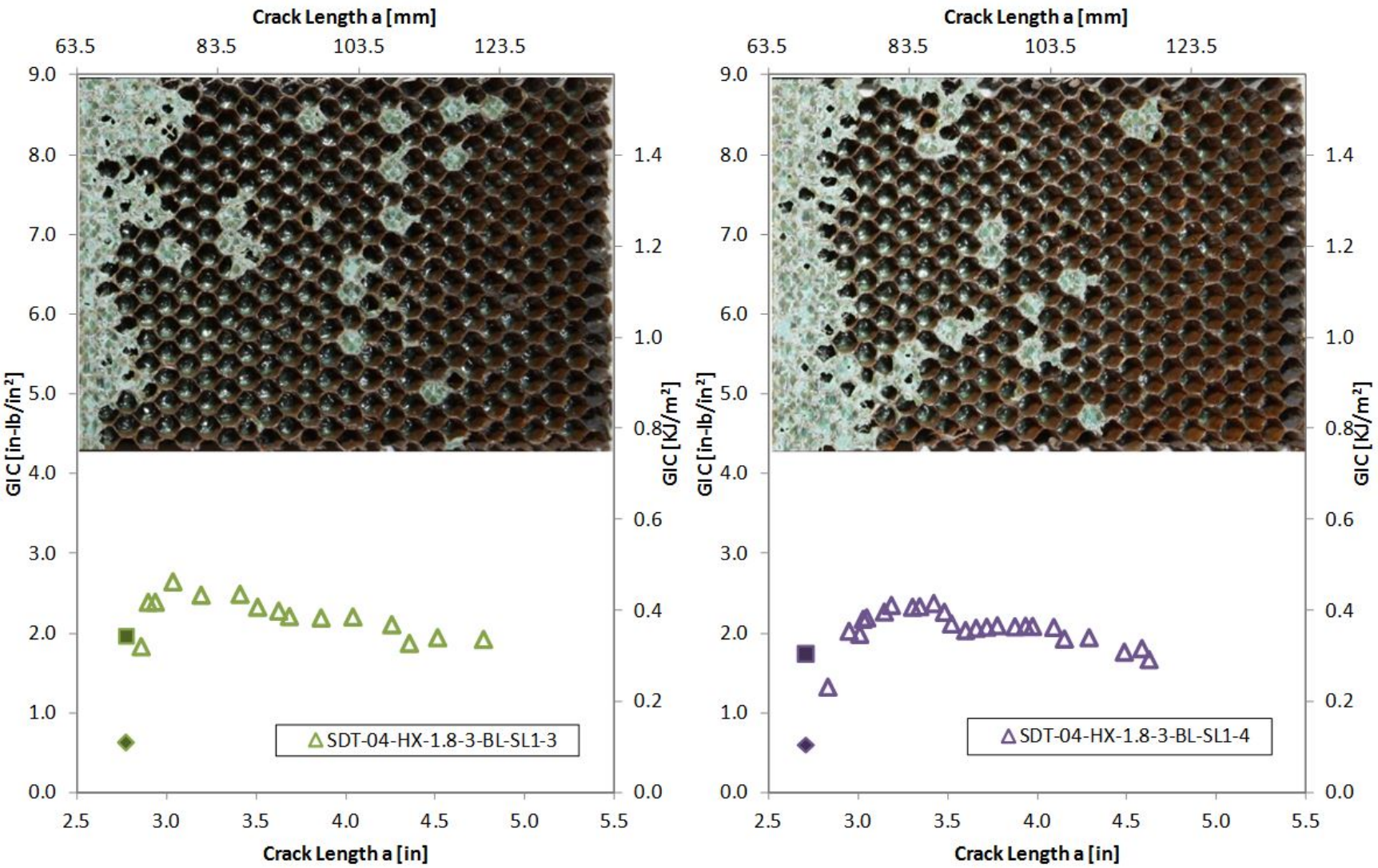

Figure B-4. Failure mode and resistance curve for SDT-04-HX-1.8-3-BL-SL1-X #3 and #4

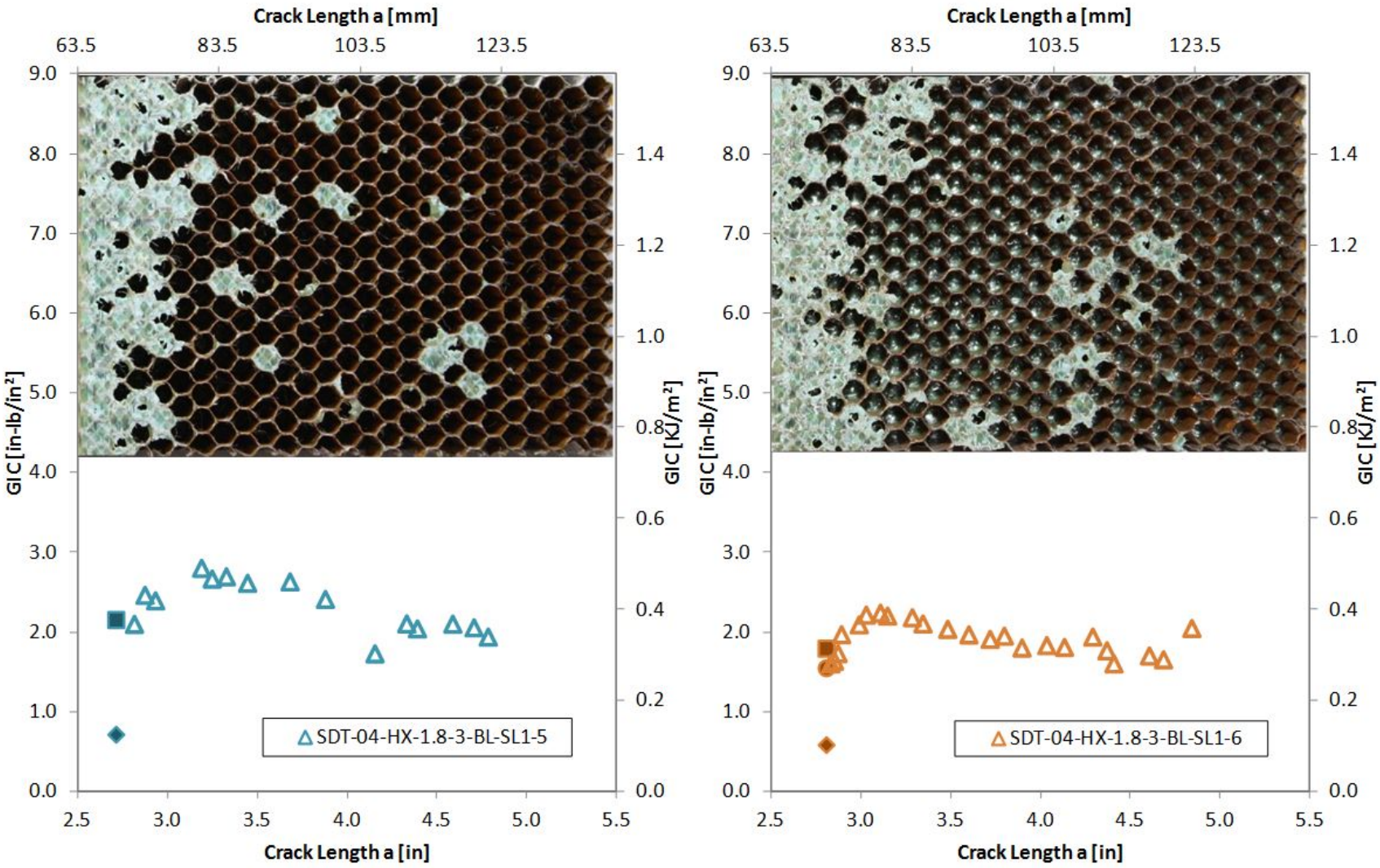

Figure B-5. Failure mode and resistance curve for SDT-04-HX-1.8-3-BL-SL1-X #5 and #6

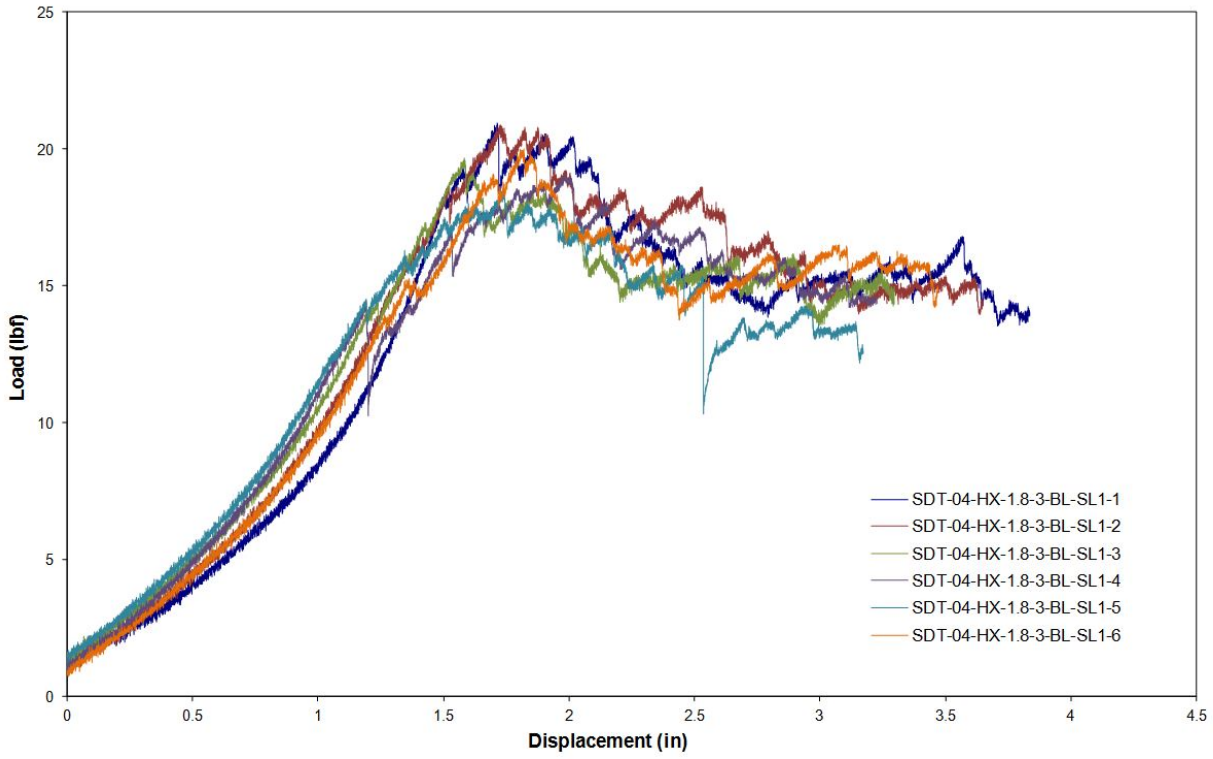

Figure B-6. Load vs. displacement curve for HRH-10–1/8–3.0 baseline (2.5″ prescribed crack)

B.1.1.2 HRH-10–1/8–3.0 Baseline Data (1.0″ Prescribed Crack—Shortened)

Table B-3. Test summary for HRH-10–1/8–3.0 baseline (1″ prescribed crack—shortened) pre-crack

Specimen	GIC (in-lb/in^2)			GIC (KJ/m^2)			Failure Mode
	NL	VIS	5%/ max	NL	VIS	5%/ max	
SDT-04-HX-1.8-3-BL-SL1-7 (shortened)	2.635	-	3.158	0.461	-	0.553	Primarily A, occasionally PO
SDT-04-HX-1.8-3-BL-SL1-8 (shortened)	2.614	-	3.129	0.458	-	0.548	Mix of A and PO, couple cells in C
SDT-04-HX-1.8-3-BL-SLX-7 (shortened)	2.377	-	3.314	0.416	-	0.580	Mix of A and PO, ending in C
AVERAGE GIC	2.542	-	3.200	0.445	-	0.560	
STANDARD DEVIATION	0.009	-	0.031	0.025	-	0.017	
COEFFICIENT OF VARIATION (%)	5.632	-	3.119	5.632	-	3.119	

Table B-4. Test summary for HRH-10–1/8–3.0 baseline (1″ prescribed crack—shortened)

Specimen	GIC (in-lb/in^2)			GIC (KJ/m^2)			Failure Mode
	NL	VIS	5%/ max	NL	VIS	5%/ max	
SDT-04-HX-1.8-3-BL-SL1-7 (shortened)	1.125	3.158	3.174	0.197	0.553	0.556	Primarily C, after quick transition from A to PO
SDT-04-HX-1.8-3-BL-SL1-8 (shortened)	1.174	3.715	4.230	0.206	0.651	0.741	Primarily C, after quick transition from A and PO, with occasional pockets of A and PO
SDT-04-HX-1.8-3-BL-SLX-7 (shortened)	1.149	-	3.527	0.201	-	0.618	Primarily C, with occasional pockets of A and PO
AVERAGE GIC	1.149	3.437	3.644	0.201	0.602	0.638	
STANDARD DEVIATION	0.009	-	0.031	0.004	0.069	0.094	
COEFFICIENT OF VARIATION (%)	2.103	11.459	14.746	2.103	11.459	14.746	

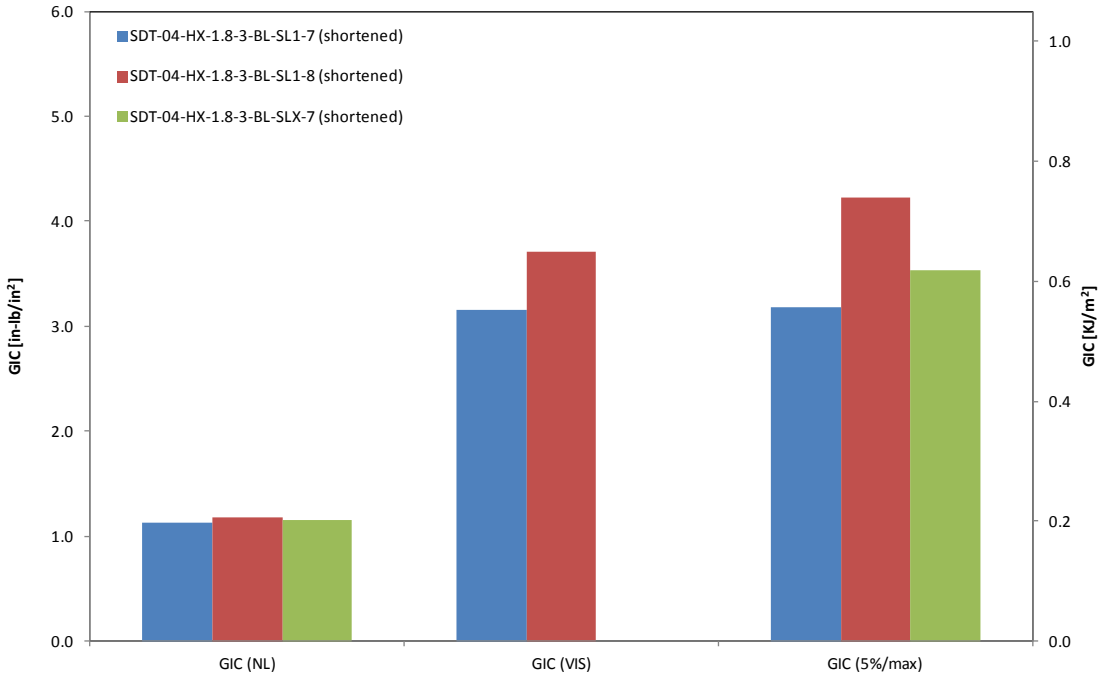

Figure B-7. GIC for HRH-10–1/8–3.0 baseline (1″ prescribed crack—shortened)

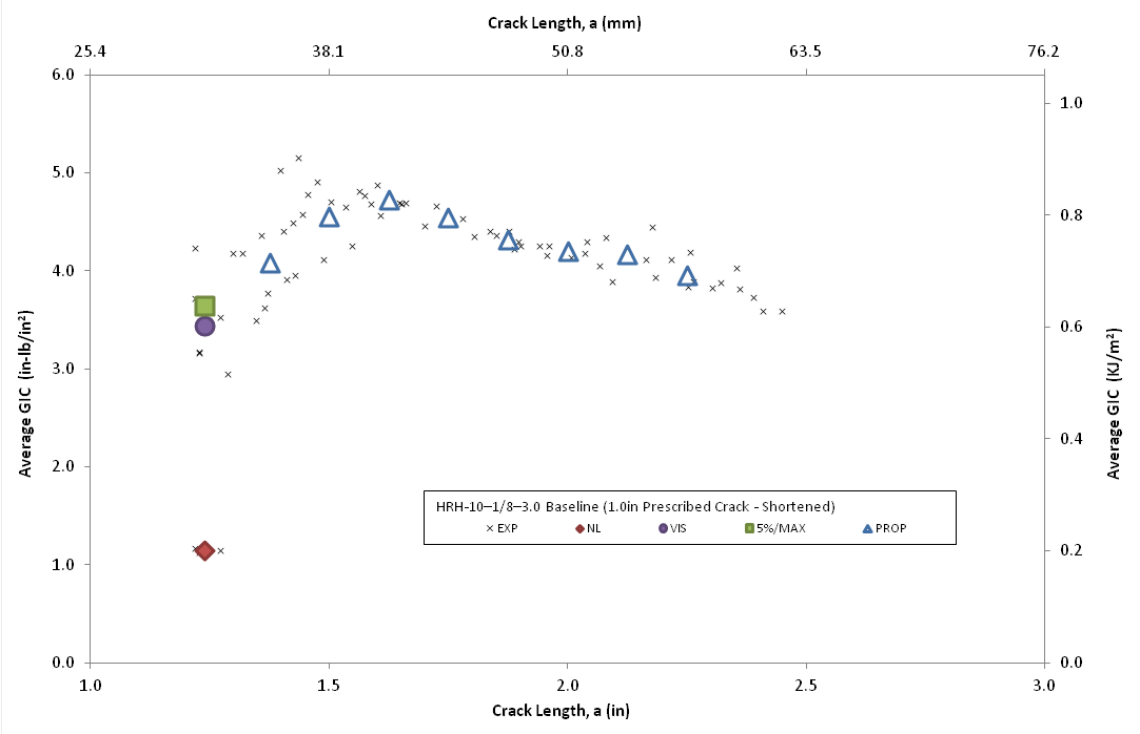

Figure B-8. Resistance curve for HRH-10–1/8–3.0 baseline (1″ prescribed crack—shortened)

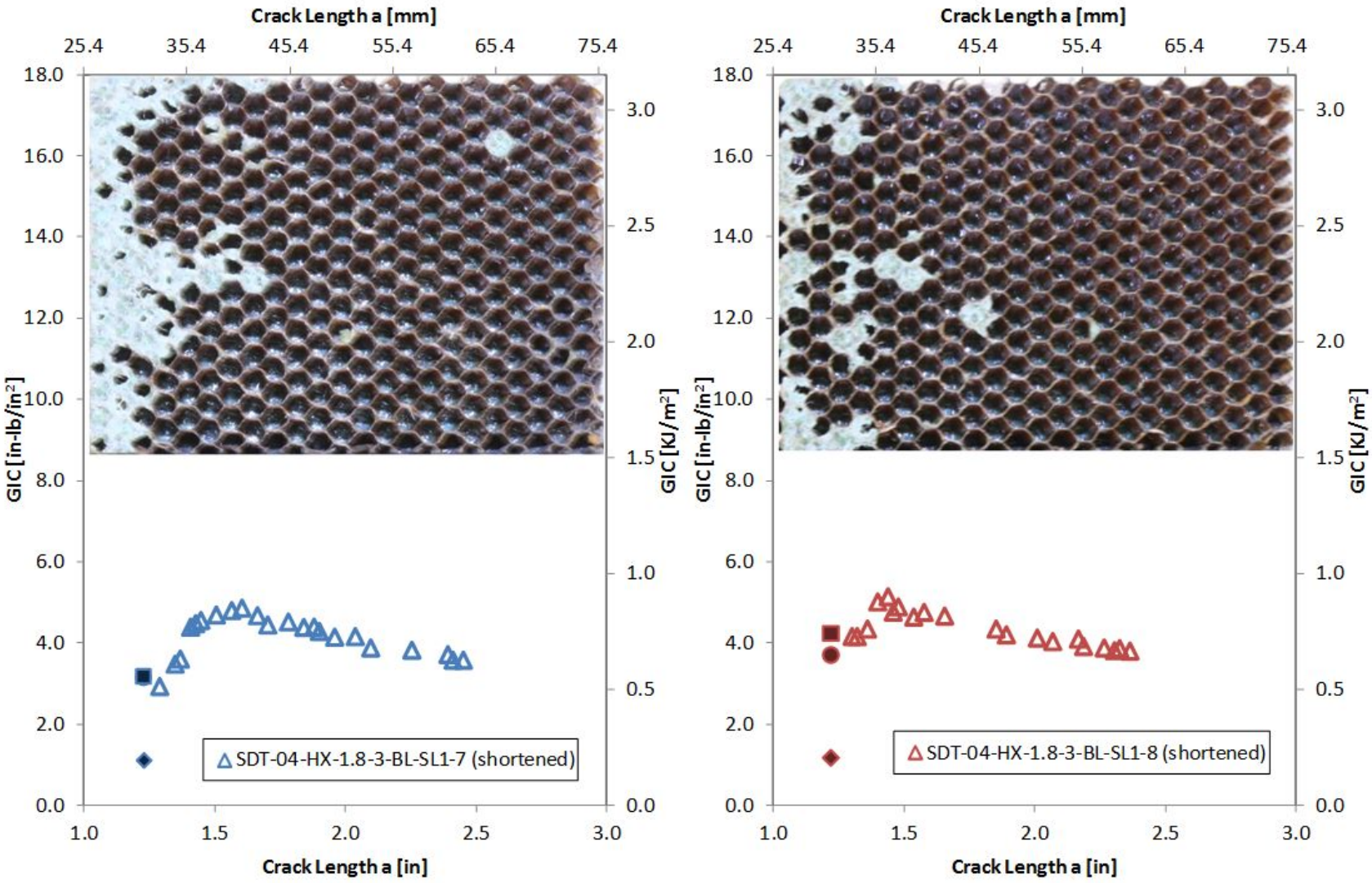

Figure B-9. Failure mode and resistance curve for SDT-04-HX-1.8-3-BL-SL1-X (shortened) #7 and #8

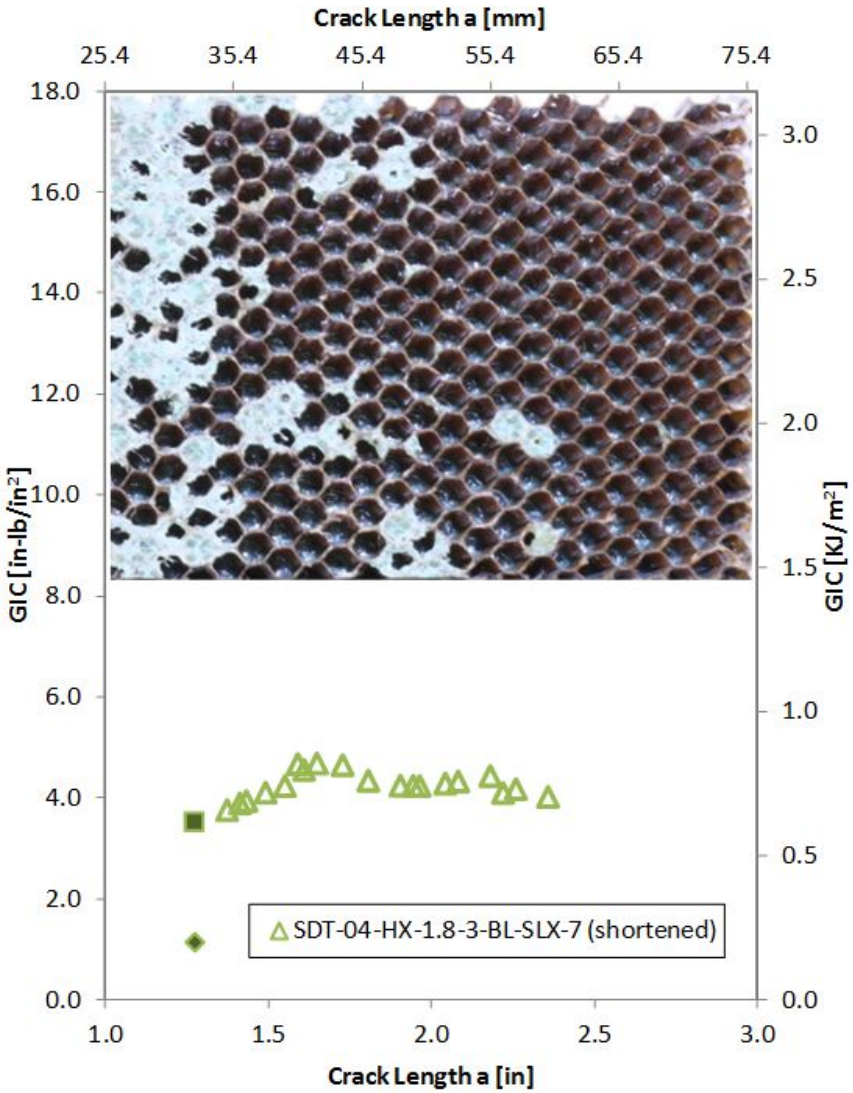

Figure B-10. Failure mode and resistance curve for SDT-04-HX-1.8-3-BL-SLX-X (shortened) #7

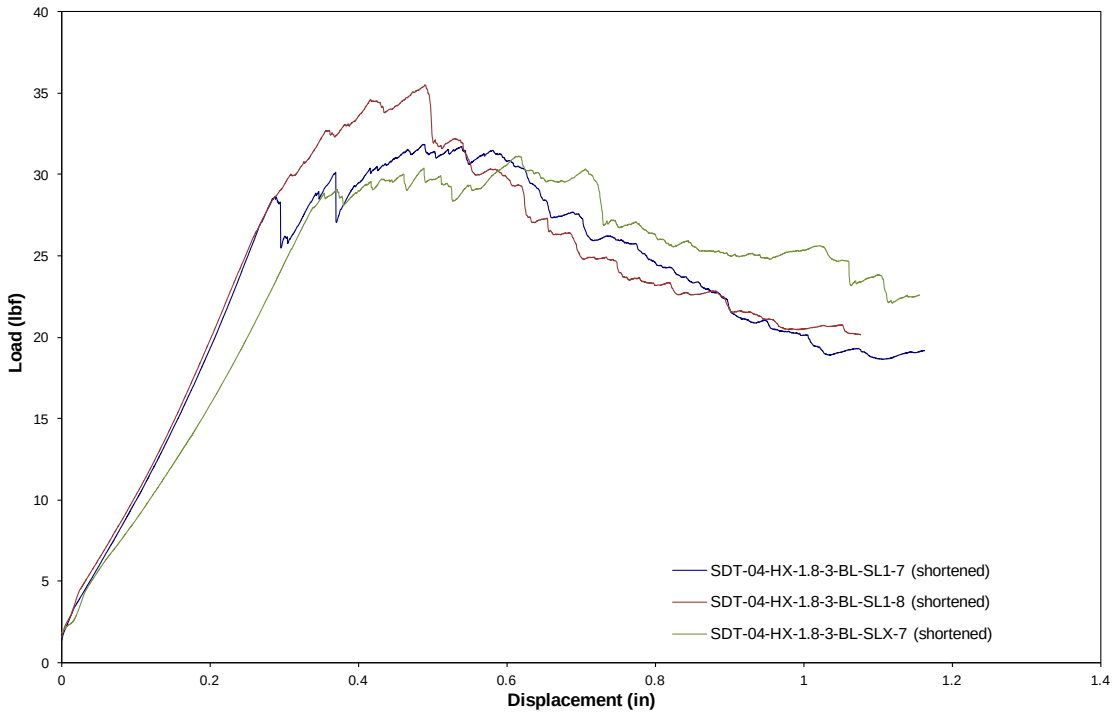

Figure B-11. Load vs. displacement curve for HRH-10–1/8–3.0 baseline (1.0″ prescribed crack—shortened)

B.1.2 HRH-10–1/8–3.0 FLUID-INGRESSED DATA

Table B-5. Test Summary for HRH-10–1/8–3.0 fluid ingressed (1.0″ prescribed crack—shortened) pre-crack

Specimen	GIC (in-lb/in^2)			GIC (KJ/m^2)			Failure Mode
	NL	VIS	5%/ max	NL	VIS	5%/ max	
SDT-04-HX-1.8-3-FI-SL1-1 (shortened)	1.518	-	3.457	0.266	-	0.605	First row in A with a few cells in C, second row in C
SDT-04-HX-1.8-3-FI-SL1-2 (shortened)	2.090	-	2.539	0.366	-	0.445	Primarily in A, couple cells in PO and C
SDT-04-HX-1.8-3-FI-SL1-3 (shortened)	1.723	-	5.400	0.302	-	0.946	First two rows primarily in A with a couple of cells in PO; third row a mix of A and PO
SDT-04-HX-1.8-3-FI-SL1-4 (shortened)	1.304	-	5.490	0.228	-	0.961	Primarily in A with a few cells in C and a cell in PO
SDT-04-HX-1.8-3-FI-SL1-5 (shortened)	1.010	-	1.839	0.177	-	0.322	Primarily in A
SDT-04-HX-1.8-3-FI-SL1-6 (shortened)	1.085	-	1.824	0.190	-	0.319	First two rows primarily in A with a couple of cells in PO and C
AVERAGE GIC	1.455	-	3.425	0.255	-	0.600	
STANDARD DEVIATION	0.409	-	1.675	0.072	-	0.293	
COEFFICIENT OF VARIATION (%)	28.102	-	48.913	28.102	-	48.913	

Table B-6. Test summary for HRH-10–1/8–3.0 fluid ingressed (1″ prescribed crack—shortened)

Specimen	GIC (in-lb/in^2)			GIC (KJ/m^2)			Failure Mode
	NL	VIS	5%/ max	NL	VIS	5%/ max	
SDT-04-HX-1.8-3-FI-SL1-1 (shortened)	0.921	-	3.624	0.161	-	0.635	Primarily in C
SDT-04-HX-1.8-3-FI-SL1-2 (shortened)	1.011	4.200	4.249	0.177	0.735	0.744	Initially a mix of A, PO, and C, then quickly transitioning to C
SDT-04-HX-1.8-3-FI-SL1-3 (shortened)	1.084	5.177	5.506	0.190	0.907	0.964	First row a mix of A and C, then primarily in C
SDT-04-HX-1.8-3-FI-SL1-4 (shortened)	1.286	4.754	4.770	0.225	0.833	0.835	First two rows a mix of A and C with a couple of cells in PO, then primarily in C with a cell in A
SDT-04-HX-1.8-3-FI-SL1-5 (shortened)	0.854	-	3.807	0.149	-	0.667	First row a mix of A and C, next three rows primarily in C with a pocket of A, then primarily in C
SDT-04-HX-1.8-3-FI-SL1-6 (shortened)	0.870	-	4.486	0.152	-	0.786	First row a mix of A and C with a couple of cells in PO, then primarily in C
AVERAGE GIC	1.004	4.710	4.407	0.176	0.825	0.772	
STANDARD DEVIATION	0.163	0.490	0.685	0.029	0.086	0.120	
COEFFICIENT OF VARIATION (%)	16.270	10.403	15.540	16.270	10.403	15.540	

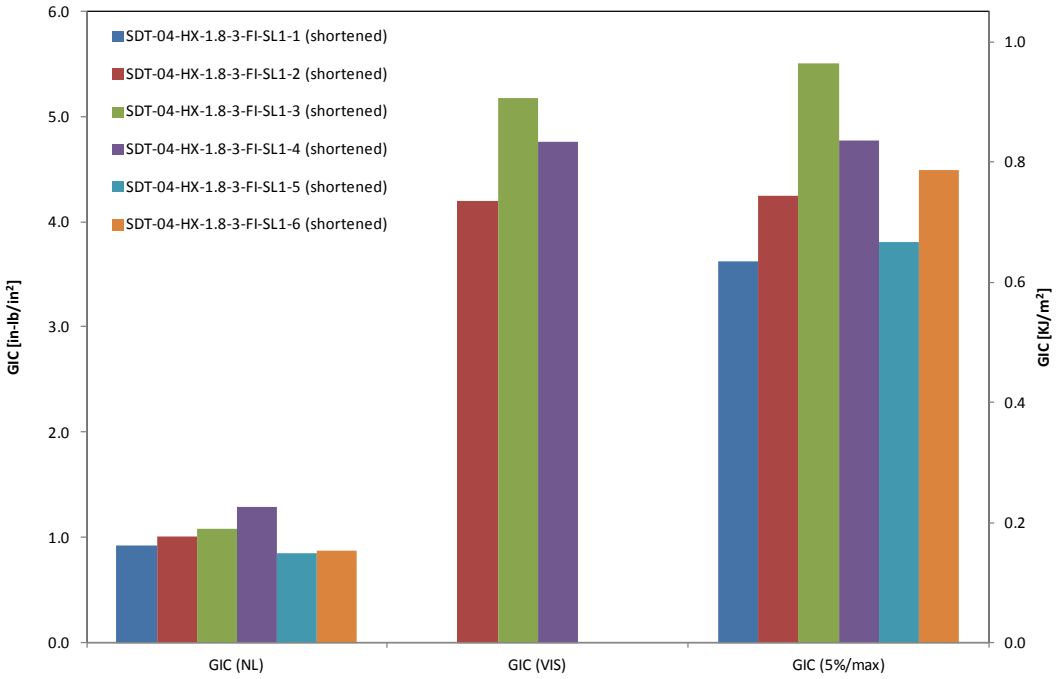

Figure B-12. GIC for HRH-10–1/8–3.0 fluid-ingressed (1″ prescribed crack—shortened)

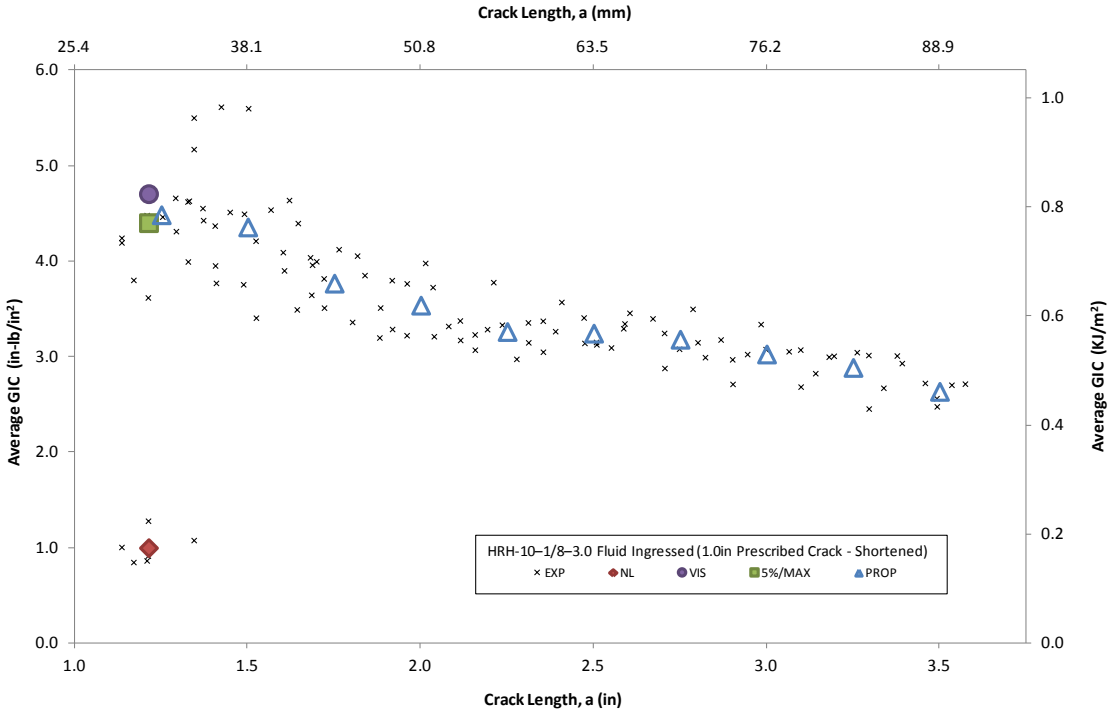

Figure B-13. Resistance curve for HRH-10–1/8–3.0 fluid-ingressed (1″ prescribed crack—shortened)

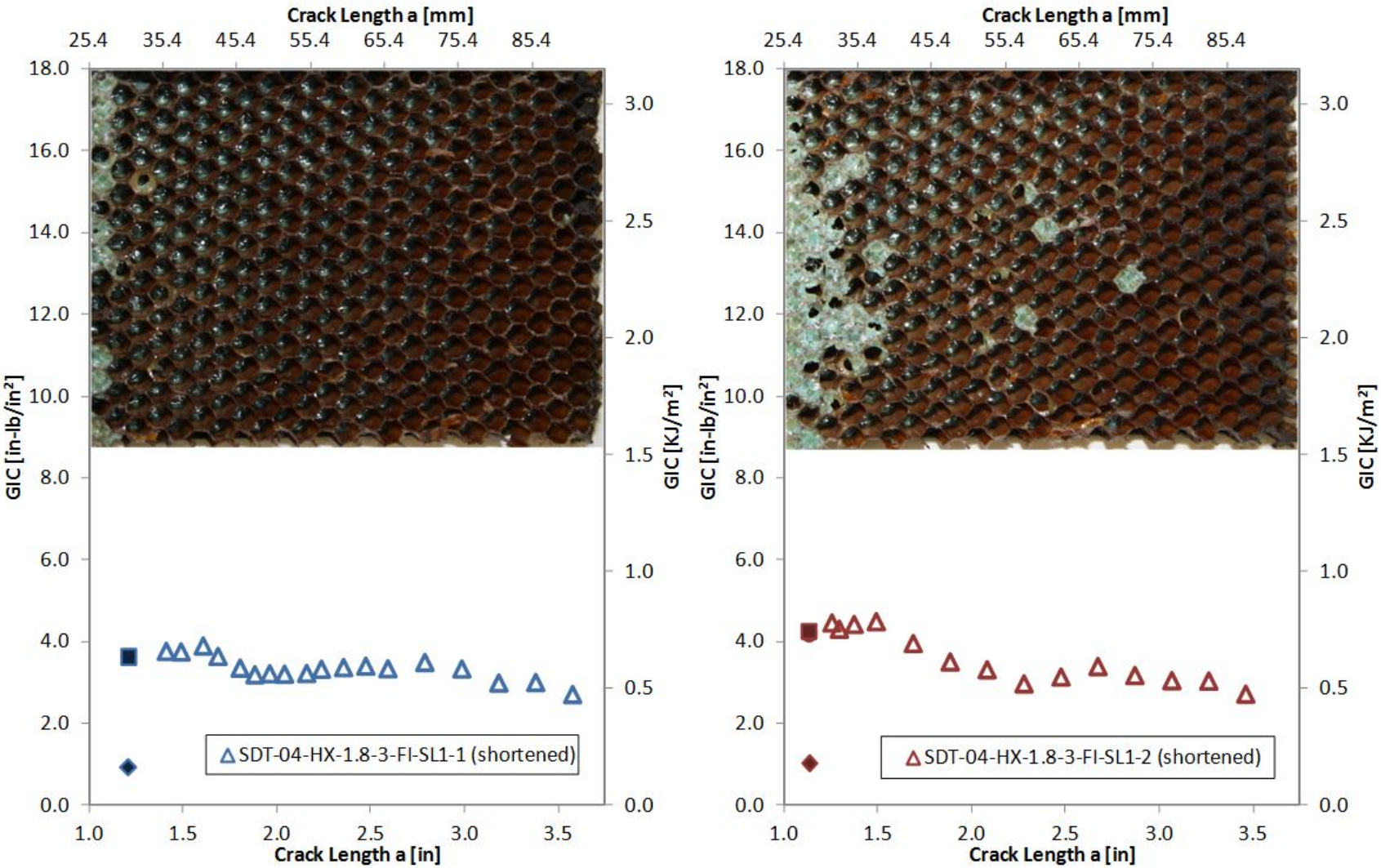

Figure B-14. Failure mode and resistance curve for SDT-04-HX-1.8-3-FI-SL1-X (shortened) #1 and #2

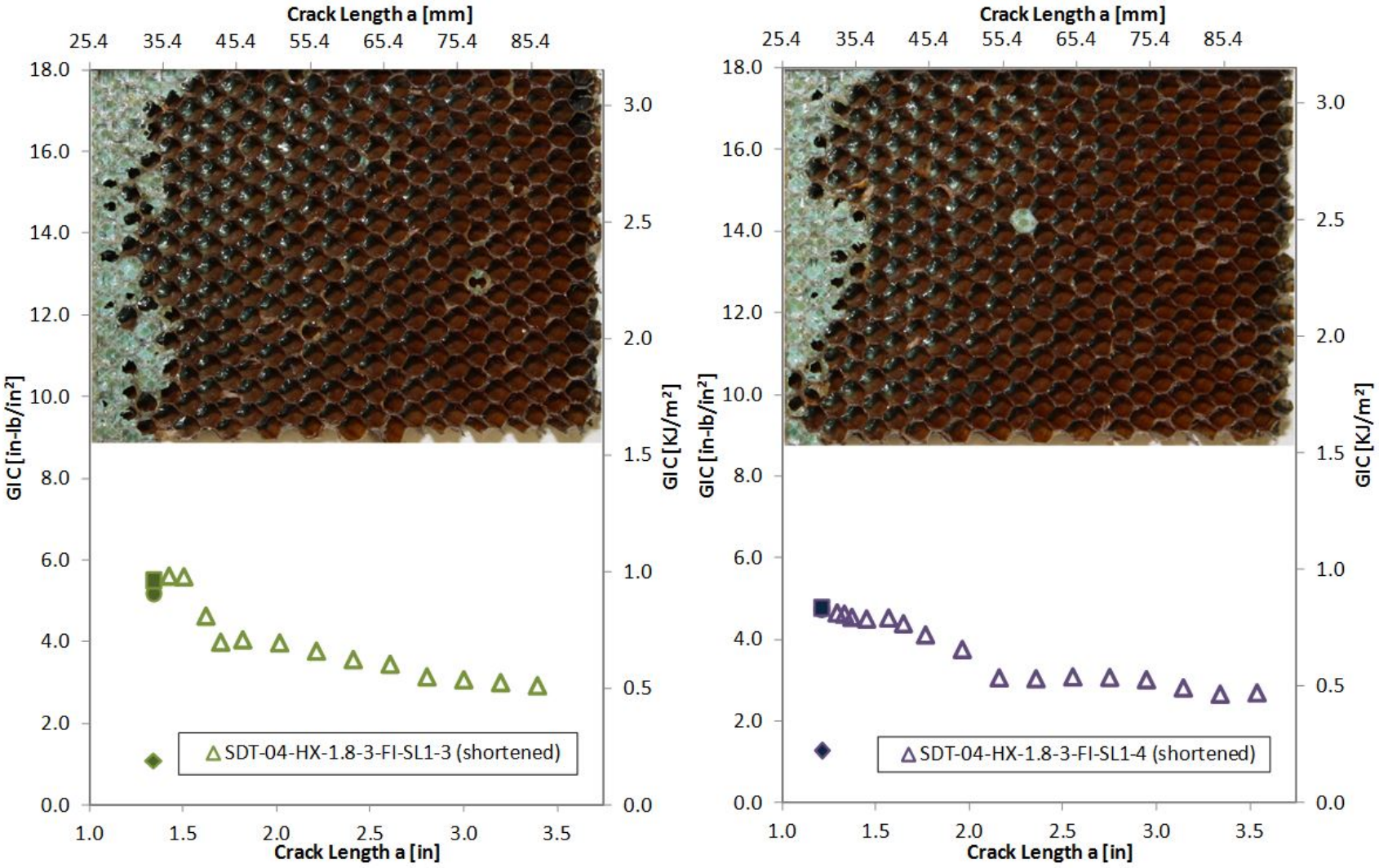

Figure B-15. Failure mode and resistance curve for SDT-04-HX-1.8-3-FI-SL1-X (shortened) #3 and #4

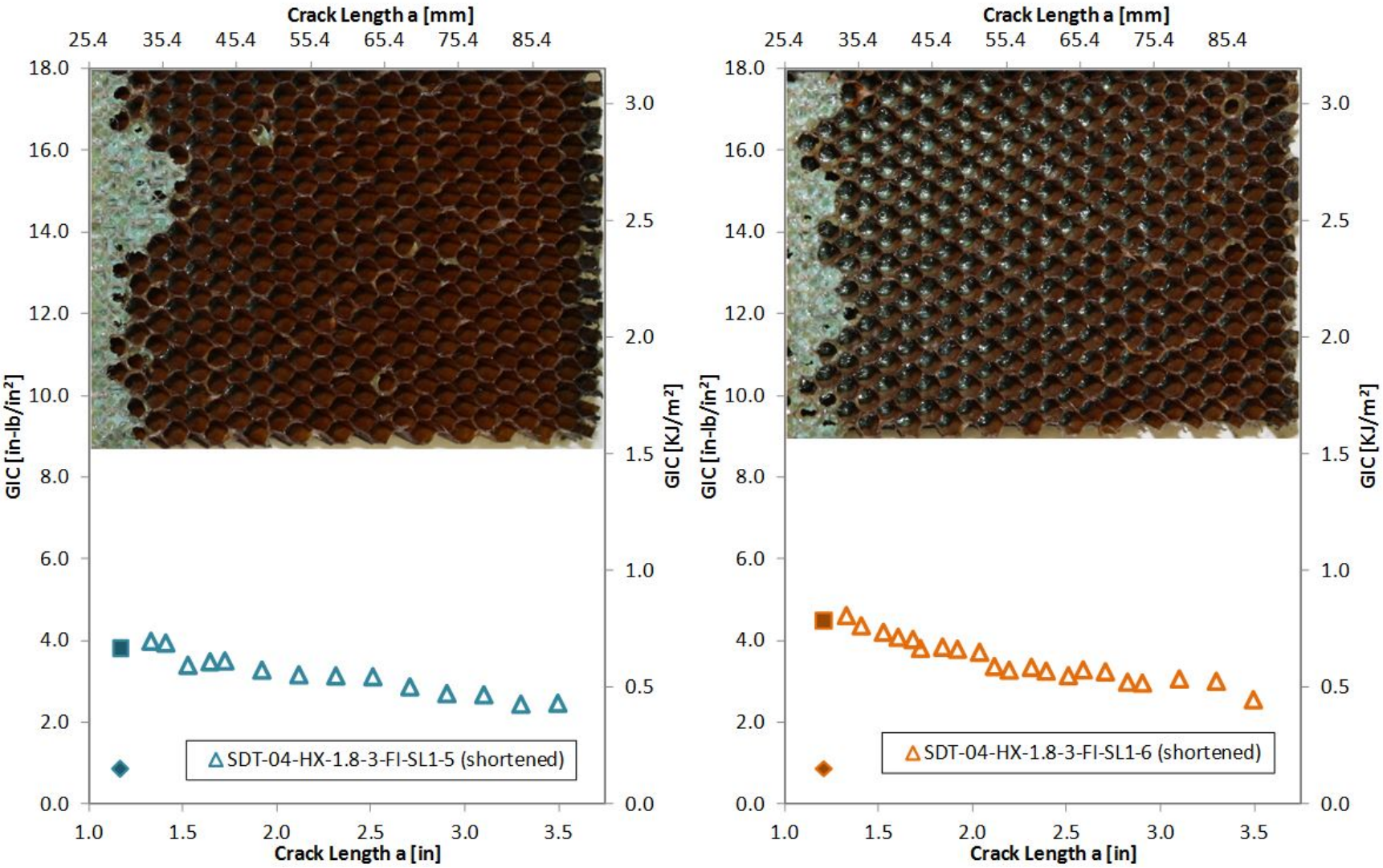

Figure B-16. Failure mode and resistance curve for NIS11SDT-01-04-HX-1.8-3-FI -OD1-A-SL1-X (shortened) #5 and #6

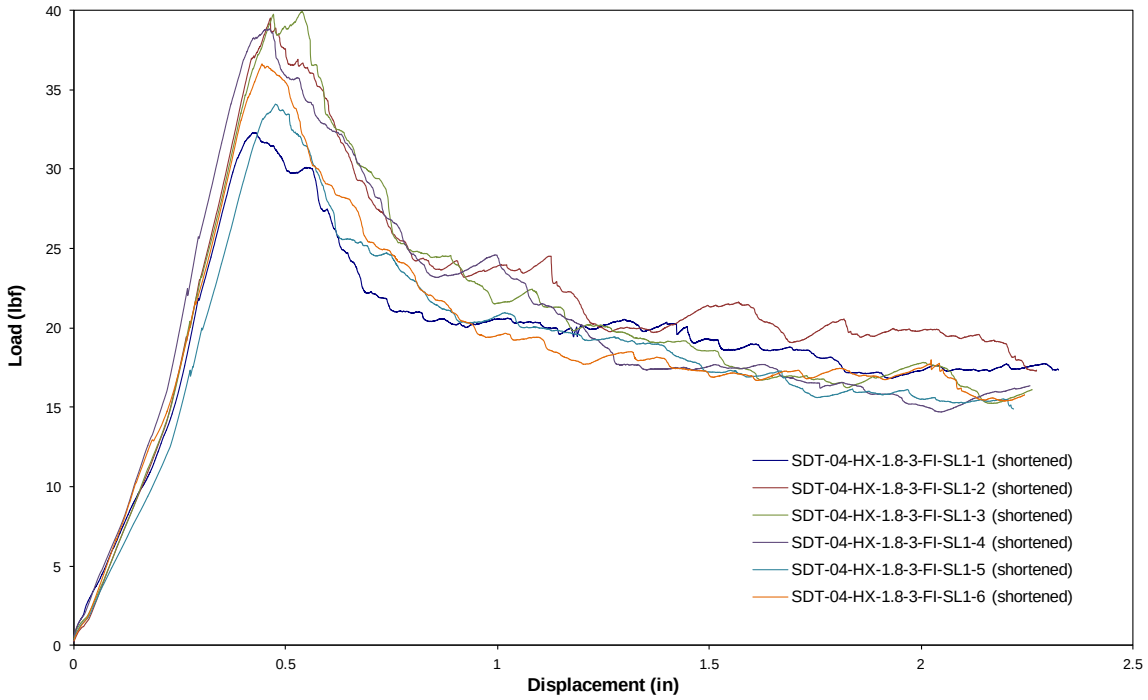

Figure B-17. Load vs. displacement curve for HRH-10–1/8–3.0 fluid-ingressed (1″ prescribed crack—shortened)

B.1.3 HRH-10–1/8–3.0 EXTENDED FLUID-INGRESSED DATA

Table B-7. Test summary for HRH-10–1/8–3.0 extended fluid-ingressed (1″ prescribed crack—shortened) pre-crack

Specimen	GIC (in-lb/in^2)			GIC (KJ/m^2)			Failure Mode
	NL	VIS	5%/ max	NL	VIS	5%/ max	
SDT-04-HX-1.8-3-EFI-SL1-7 (shortened)	-	-	-	-			
SDT-04-HX-1.8-3-EFI-SL1-8 (shortened)	2.136	-	4.135	0.374	-	0.724	First row primarily C with a few rows in A, second row in C with one cell in A
AVERAGE GIC	2.136	-	4.135	0.374	-	0.724	
STANDARD DEVIATION	-	-	-	-	-	-	
COEFFICIENT OF VARIATION (%)	-	-	-	-	-	-	

Table B-8. Test summary for HRH-10–1/8–3.0 extended fluid-ingressed (1″ prescribed crack—shortened)

Specimen	GIC (in-lb/in^2)			GIC (KJ/m^2)			Failure Mode
	NL	VIS	5%/ max	NL	VIS	5%/ max	
SDT-04-HX-1.8-3-EFI-SL1-7 (shortened)	-	-	-	-	-	-	
SDT-04-HX-1.8-3-EFI-SL1-8 (shortened)	0.422	-	3.725	0.074	-	0.652	Primarily in C
AVERAGE GIC	0.422	-	3.725	0.074	-	0.652	
STANDARD DEVIATION	-	-	-	-	-	-	
COEFFICIENT OF VARIATION (%)	-	-	-	-	-	-	

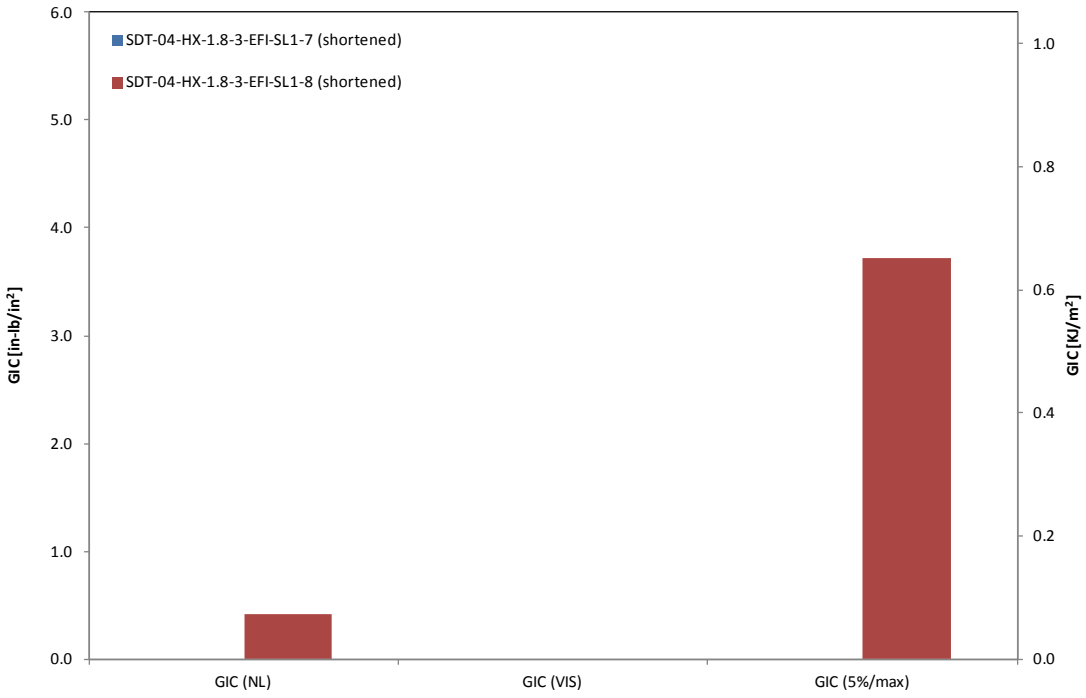

Figure B-18. GIC for HRH-10–1/8–3.0 extended fluid ingressed (1″ prescribed crack—shortened)

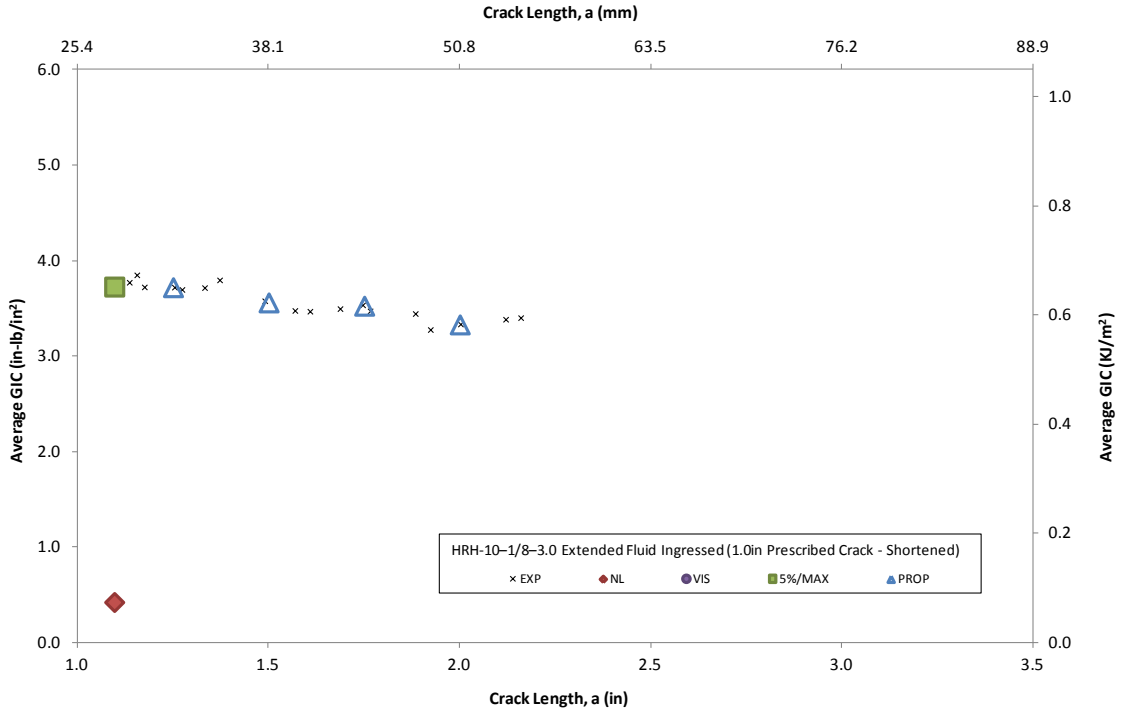

Figure B-19. Resistance curve for HRH-10–1/8–3.0 extended fluid ingressed (1″ prescribed crack—shortened)

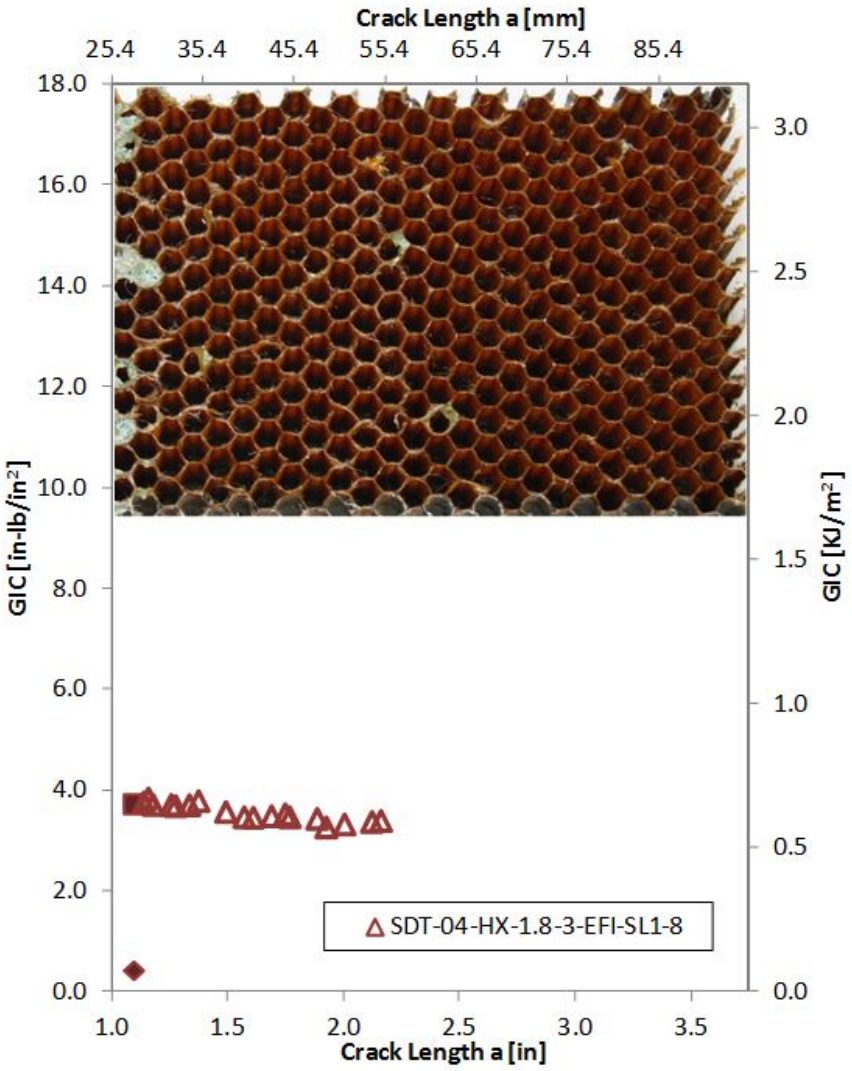

Figure B-20. Failure mode and resistance curve for SDT-04-HX-1.8-3-EFI-SL1-X (shortened) #8

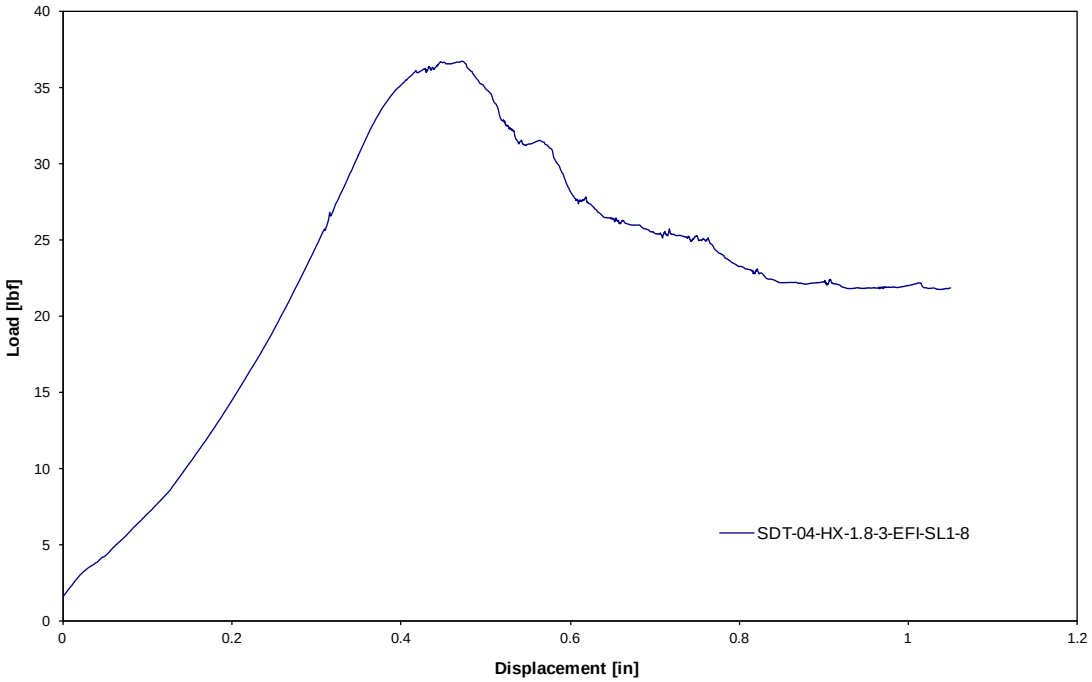

Figure B-21. Load vs. displacement curve for HRH-10–1/8–3.0 extended fluid ingressed (1″ prescribed crack—shortened)

B.2 HRH-10–3/16–2.0 DATA

B.2.1 HRH-10–3/16–2.0 BASELINE DATA

B.2.1.1 HRH-10–3/16–2.0 Baseline Data (2.5″ Prescribed Crack)

Table B-9. Test summary for HRH-10–3/16–2.0 baseline (2.5″ prescribed crack) pre-crack

Specimen	GIC (in-lb/in^2)			GIC (KJ/m^2)			Failure Mode
	NL	VIS	5%/max	NL	VIS	5%/max	
SDT-04-HX-3.16-2-BL-SL1-1	0.874	-	3.280	0.153	-	0.574	First row primarily PO with a couple of cells in A; second row primarily in C with a couple of cells in A and PO
SDT-04-HX-3.16-2-BL-SL1-2	0.963	-	3.494	0.169	-	0.612	Mix of A and PO with a couple of cells in C
SDT-04-HX-3.16-2-BL-SL1-3	0.892	-	2.654	0.156	-	0.465	Mix of A, PO, and C
SDT-04-HX-3.16-2-BL-SL1-4	1.048	-	3.365	0.184	-	0.589	First row primarily PO with a cell in A; second row primarily in C with a few cells in PO
SDT-04-HX-3.16-2-BL-SL1-5	0.894	-	3.598	0.157	-	0.630	First row primarily PO; second row primarily in C with a few cells in PO
SDT-04-HX-3.16-2-BL-SL1-6	0.904	-	3.140	0.158	-	0.550	First row primarily PO; second row primarily in C with a few cells in PO
AVERAGE GIC	0.929	-	3.255	0.163	-	0.570	
STANDARD DEVIATION	0.066	-	0.335	0.012	-	0.059	
COEFFICIENT OF VARIATION (%)	7.072	-	10.297	7.072	-	10.297	

Table B-10. Test summary for HRH-10–3/16–2.0 baseline (2.5″ prescribed crack)

Specimen	GIC (in-lb/in^2)			GIC (KJ/m^2)			Failure Mode
	NL	VIS	5%/ max	NL	VIS	5%/ max	
SDT-04-HX-3.16-2-BL-SL1-1	0.603	1.782	2.067	0.106	0.312	0.362	Primarily in C with a couple small pockets of A and PO
SDT-04-HX-3.16-2-BL-SL1-2	0.585	-	1.872	0.102	-	0.328	Primarily in C with pockets of A and PO
SDT-04-HX-3.16-2-BL-SL1-3	0.655	-	1.917	0.115	-	0.336	Primarily in C with small pockets of A and PO, then a mix of A, PO, and C
SDT-04-HX-3.16-2-BL-SL1-4	0.602	-	2.230	0.105	-	0.390	Primarily in C with a pocket of A and PO, then a mix of PO and C
SDT-04-HX-3.16-2-BL-SL1-5	0.597	2.108	2.175	0.105	0.369	0.381	Primarily in C with a pocket of A and PO, then a mix of PO and C
SDT-04-HX-3.16-2-BL-SL1-6	0.588	-	1.858	0.103	-	0.325	Primarily C, then quickly transitioning to a mix of A, PO, and C
AVERAGE GIC	0.605	1.945	2.020	0.106	0.341	0.354	
STANDARD DEVIATION	0.026	0.231	0.161	0.004	0.040	0.028	
COEFFICIENT OF VARIATION (%)	8.623	11.868	7.947	4.241	11.868	7.947	

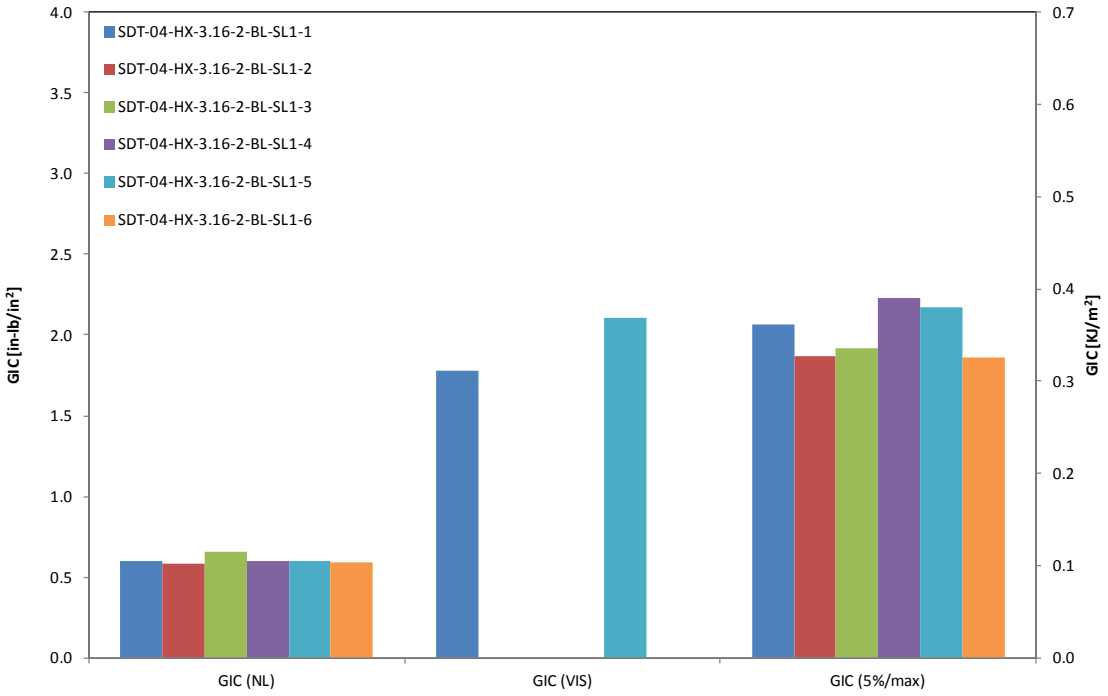

Figure B-22. GIC for HRH-10–3/16–2.0 baseline (2.5″ prescribed crack)

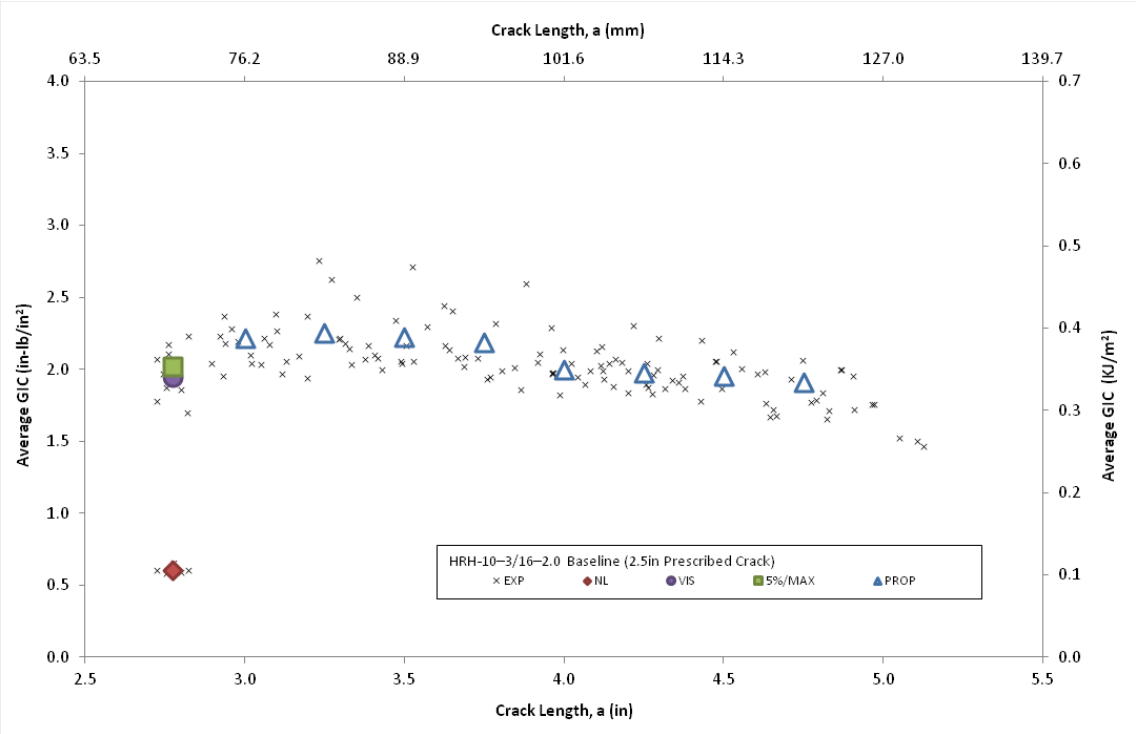

Figure B-23. Resistance curve for HRH-10–3/16–2.0 baseline (2.5″ prescribed crack)

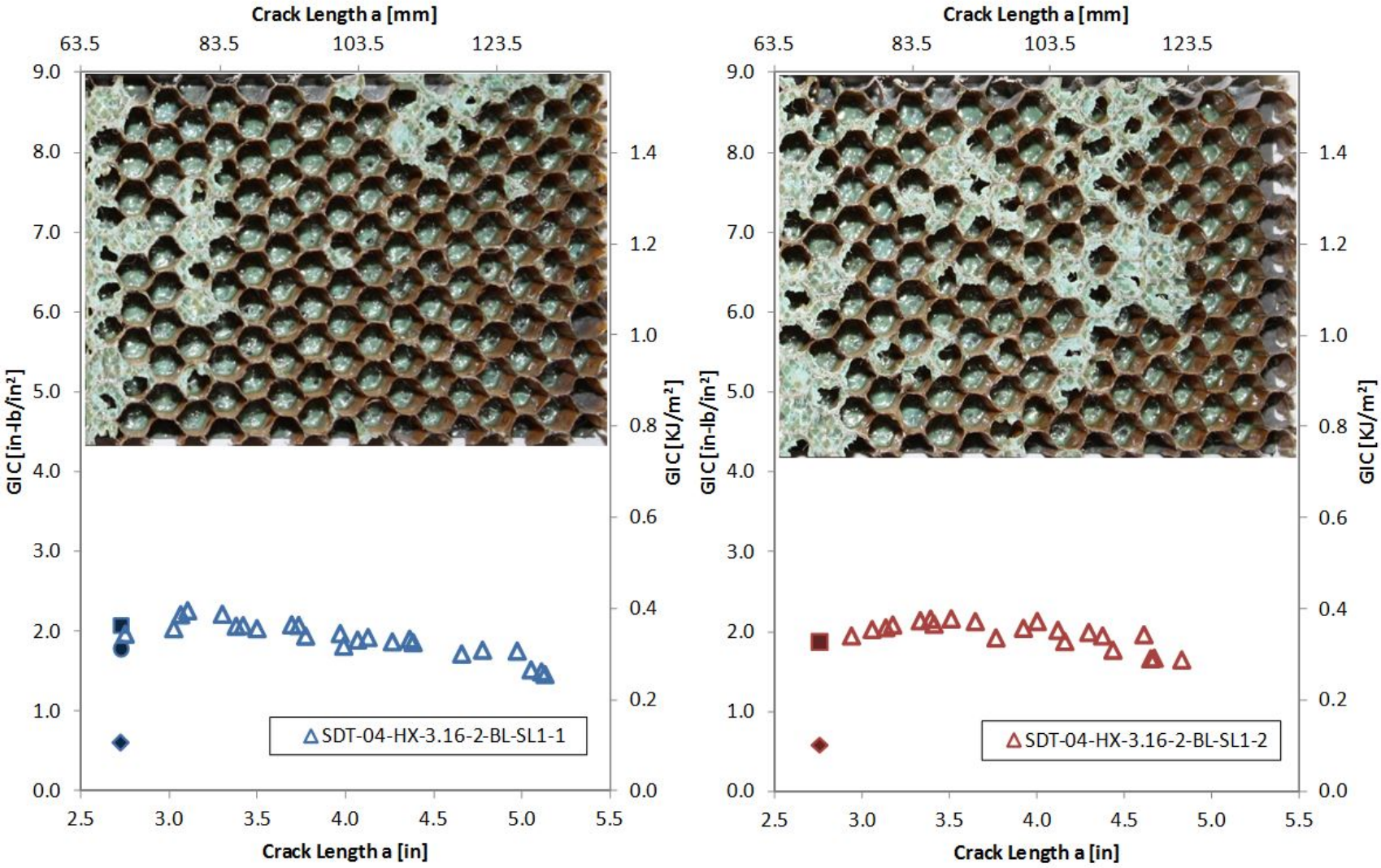

Figure B-24. Failure mode and resistance curve for SDT-04-HX-3.16-2-BL -SL1-X #1 and #2

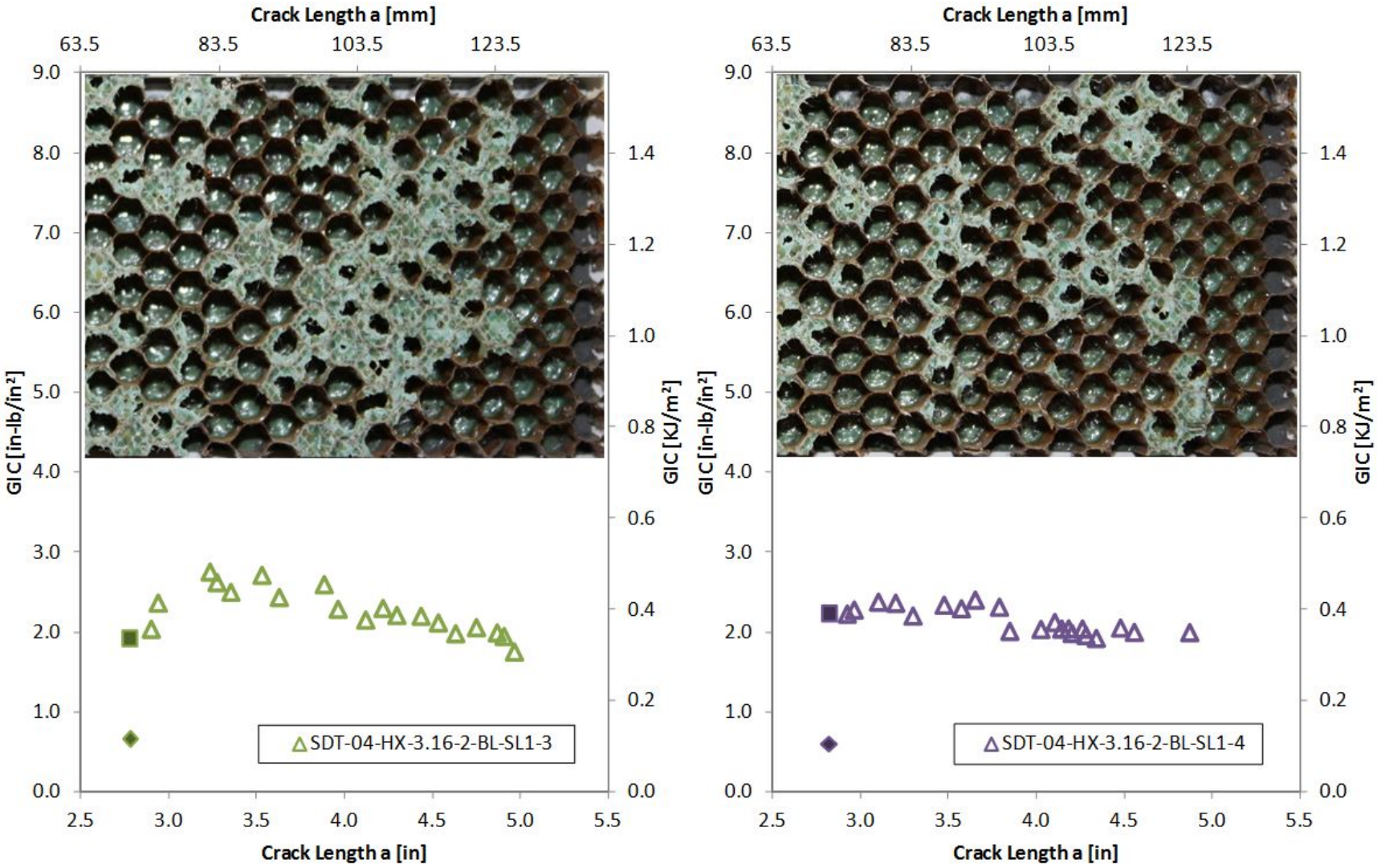

Figure B-25. Failure mode and resistance curve for SDT-04-HX-3.16-2-BL -SL1-X #3 and #4

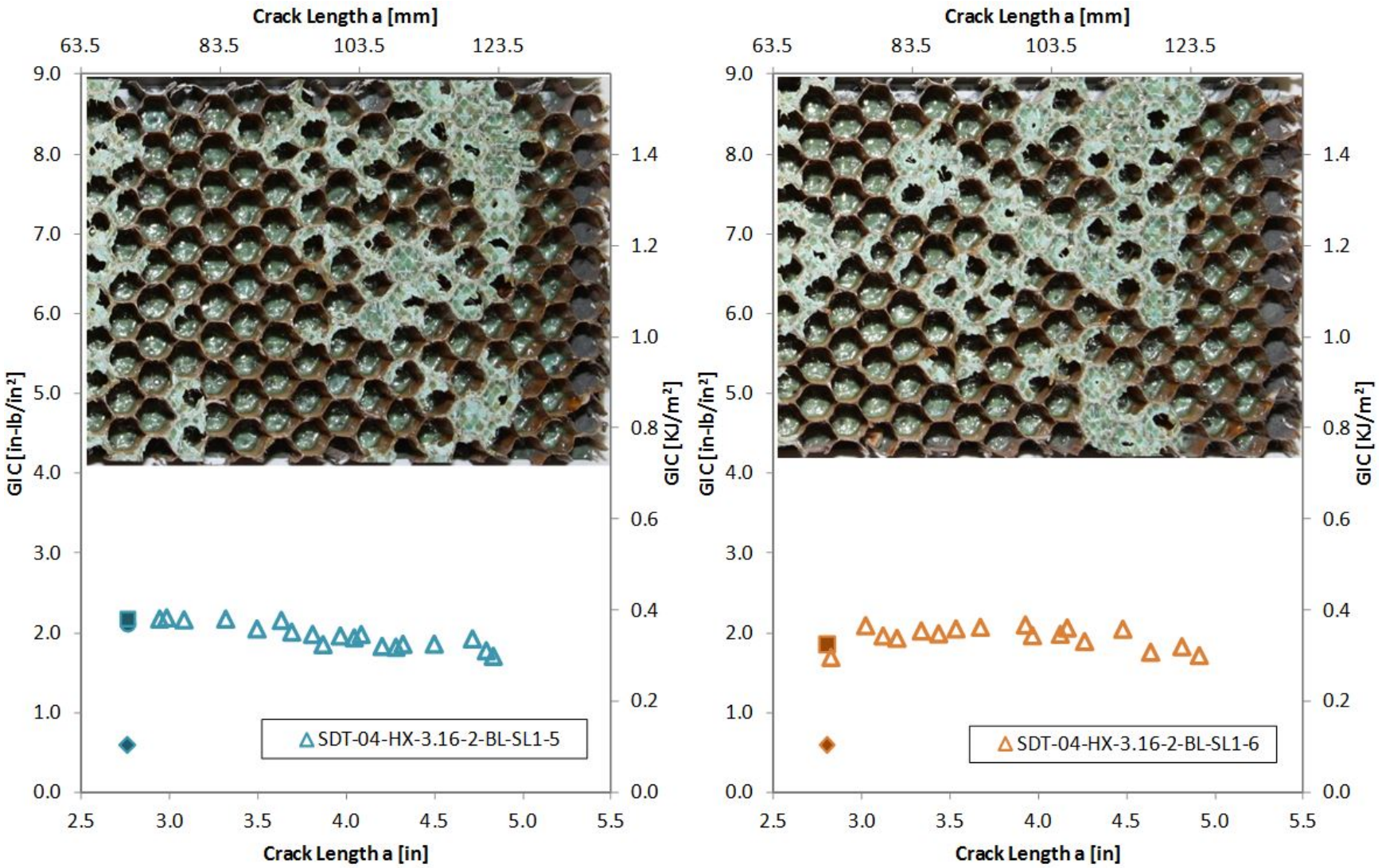

Figure B-26. Failure mode and resistance curve for SDT-04-HX-3.16-2-BL -SL1-X #5 and #6

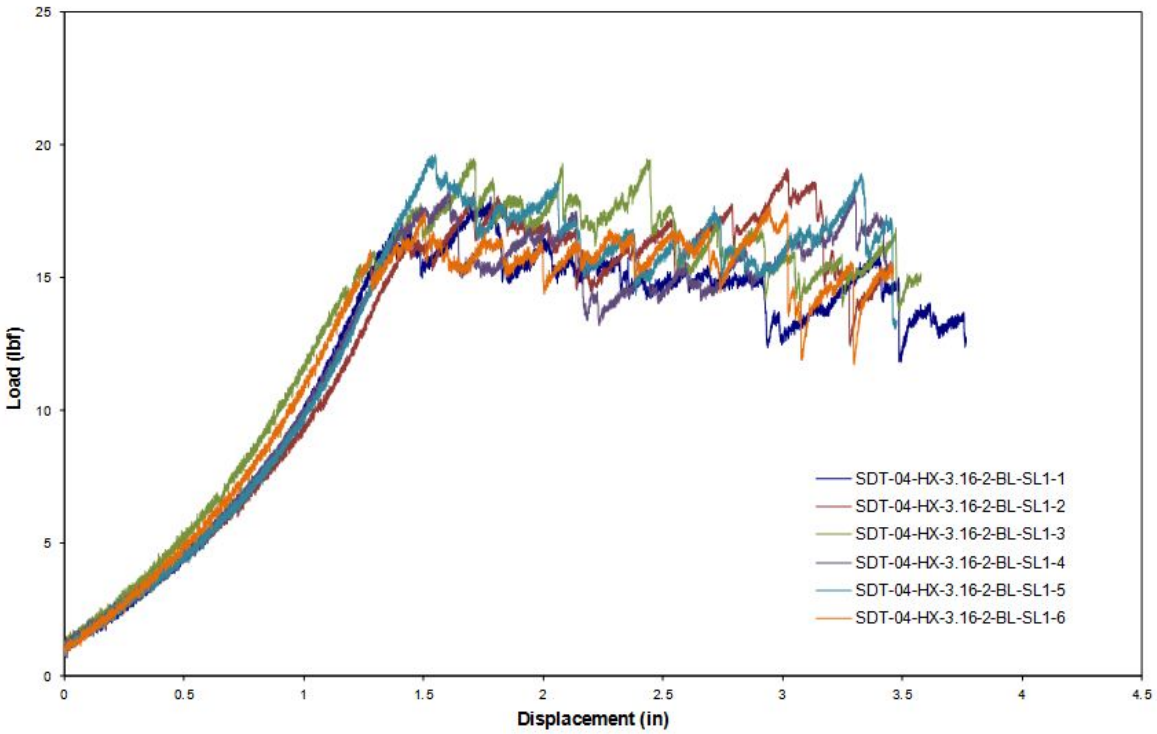

Figure B-27. Load vs. displacement curve for HRH-10–3/16–2.0 baseline (2.5″ prescribed crack)

B.2.1.2. HRH-10–3/16-2.0 Baseline Data (1″ Prescribed Crack—Shortened)

Table B-11. Test summary for HRH-10–3/16-2.0 baseline (1″ prescribed crack—shortened) pre-crack

Specimen	GIC (in-lb/in^2)			GIC (KJ/m^2)			Failure Mode
	NL	VIS	5%/max	NL	VIS	5%/max	
SDT-04-HX-3.16-2-BL-SL1-7 (shortened)	1.974	-	4.362	0.346	-	0.764	First row of cells PO, then C
SDT-04-HX-3.16-2-BL-SL1-8 (shortened)	1.844	-	2.145	0.323	-	0.376	First row of cells PO, then C
SDT-04-HX-3.16-2-BL-SLX-7 (shortened)	1.866	-	3.982	0.327	-	0.697	First row of cells PO, then C
AVERAGE GIC	1.895	-	3.496	0.332	-	0.612	
STANDARD DEVIATION	0.009	-	0.031	0.012	-	0.208	
COEFFICIENT OF VARIATION (%)	3.653	-	33.918	3.653	-	33.918	

Table B-12. Test summary for HRH-10–3/16-2.0 baseline (1″ prescribed crack—shortened)

Specimen	GIC (in-lb/in^2)			GIC (KJ/m^2)			Failure Mode
	NL	VIS	5%/ max	NL	VIS	5%/ max	
SDT-04-HX-3.16-2-BL-SL1-7 (shortened)	1.163	-	3.759	0.204	-	0.658	Primarily C with occasional pockets of A and PO
SDT-04-HX-3.16-2-BL-SL1-8 (shortened)	0.961	-	2.434	0.168	-	0.426	Primarily C with occasional pockets of A and PO
SDT-04-HX-3.16-2-BL-SLX-7 (shortened)	1.076	-	3.758	0.188	-	0.658	Primarily C with occasional pockets of A and PO
AVERAGE GIC	1.067	-	3.317	0.187	-	0.581	
STANDARD DEVIATION	0.009	-	0.031	0.018	-	0.134	
COEFFICIENT OF VARIATION (%)	9.516	-	23.047	9.516	-	23.047	

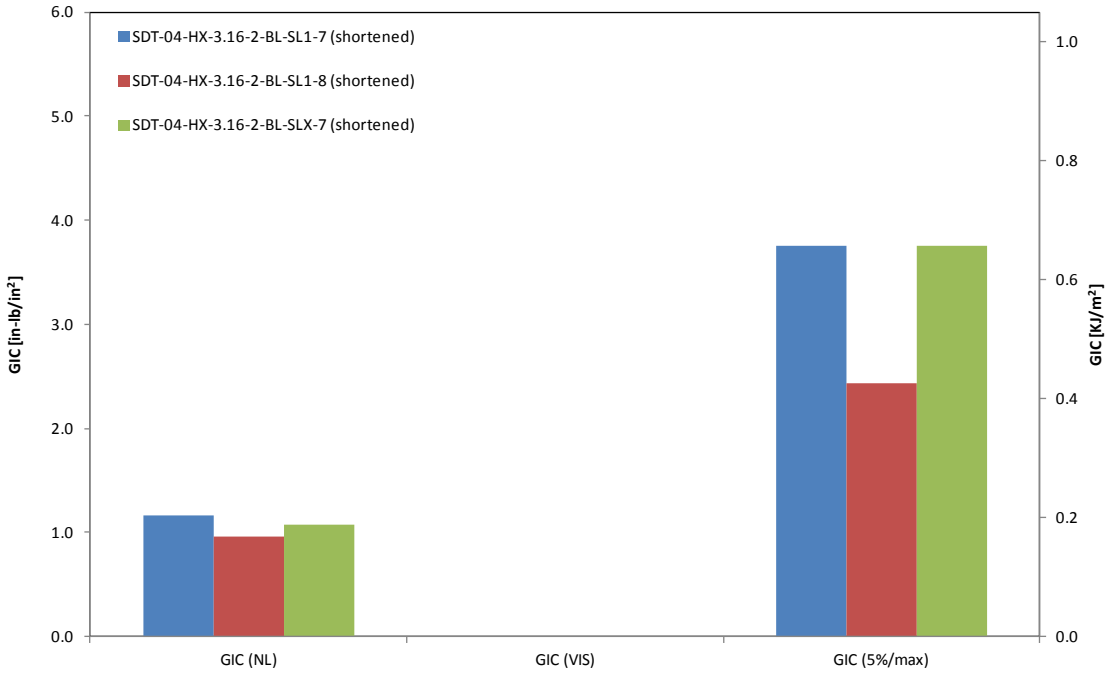

Figure B-28. GIC for HRH-10–3/16-2.0 baseline (1″ prescribed crack—shortened)

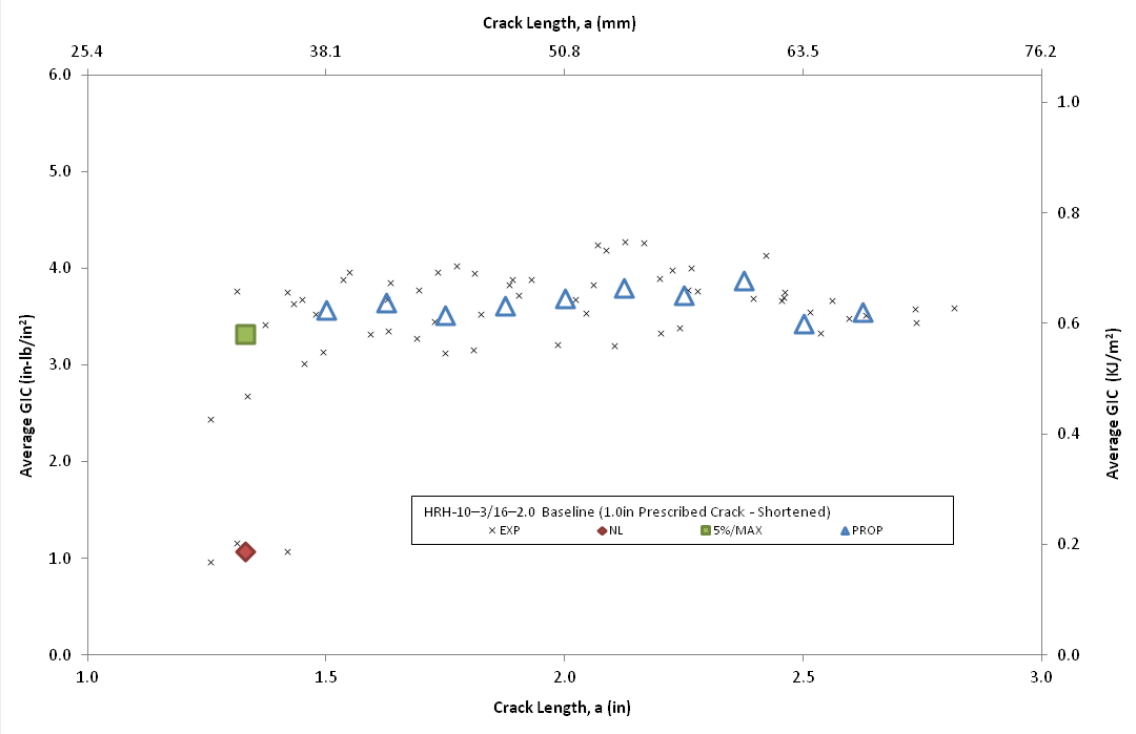

Figure B-29. Resistance curve for HRH-10–3/16-2.0 baseline (1″ prescribed crack—shortened)

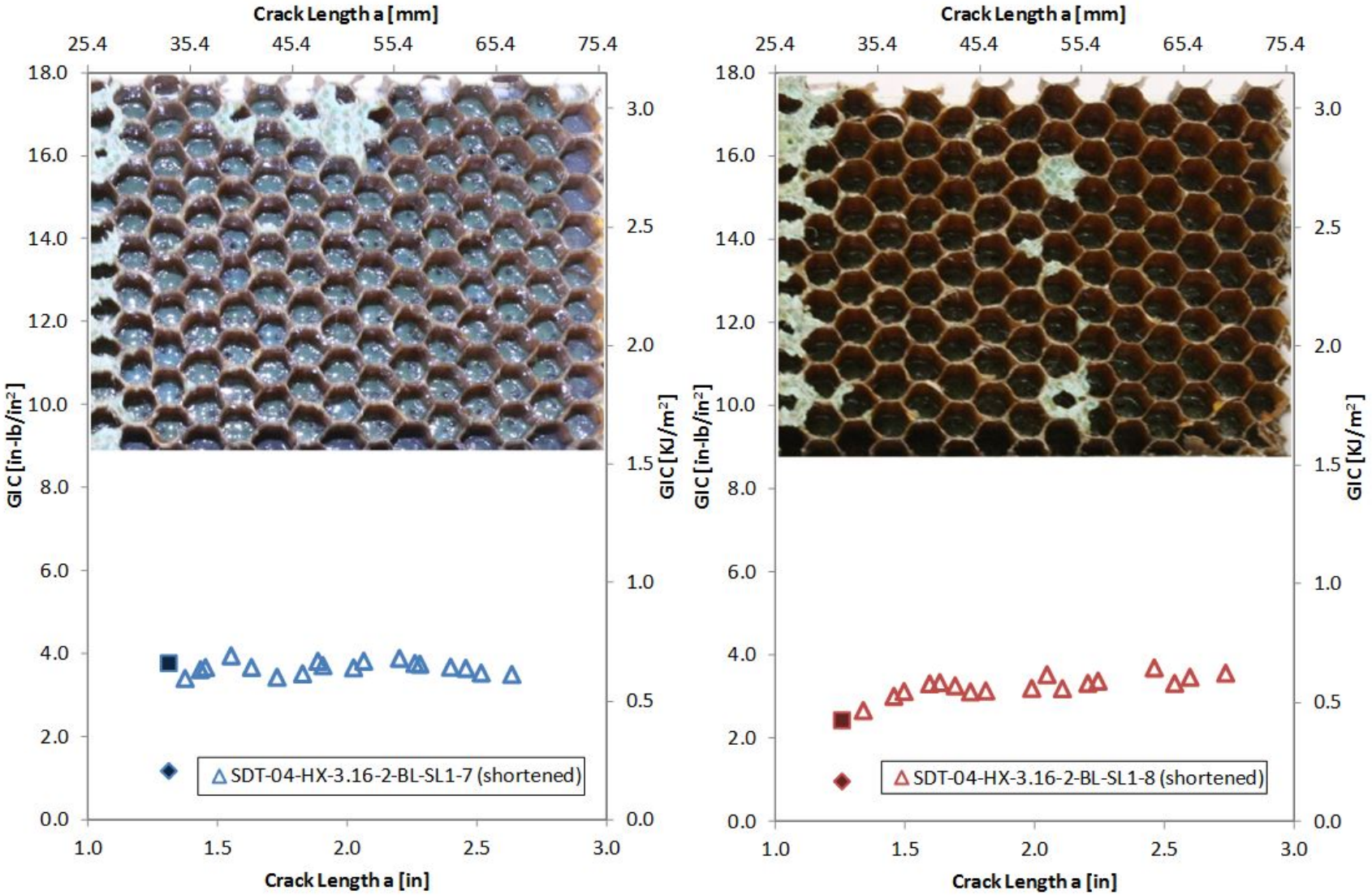

Figure B-30. Failure mode and resistance curve for SDT-04-HX-3.16-2-BL -SL1-X (shortened) #7 and #8

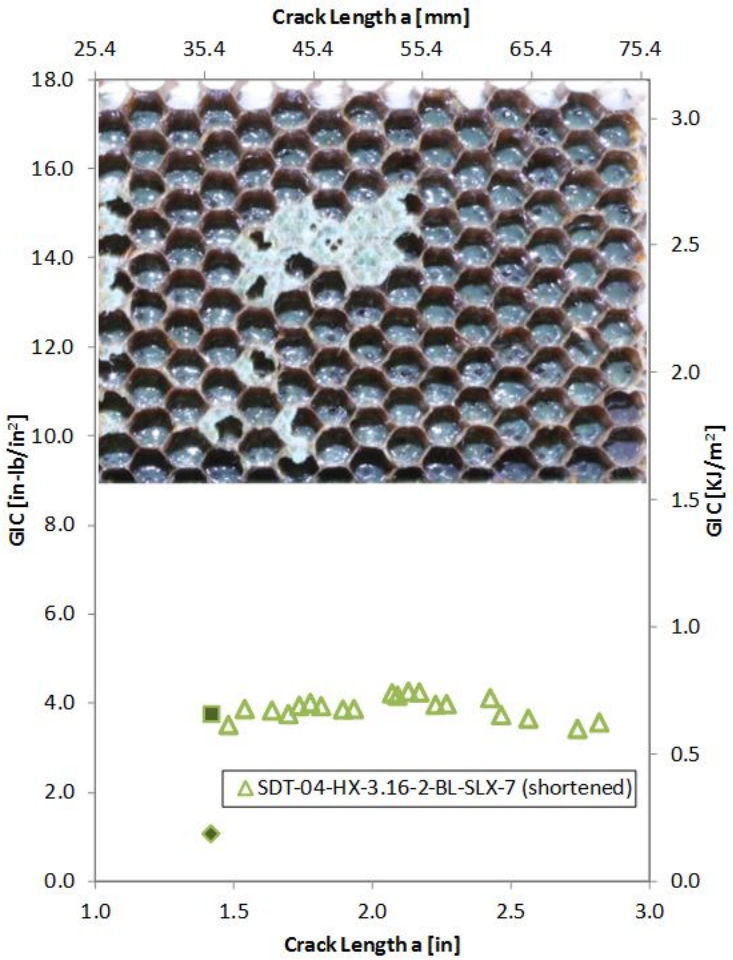

Figure B-31. Failure mode and resistance curve for SDT-04-HX-3.16-2-BL-SLX-X (shortened) #7

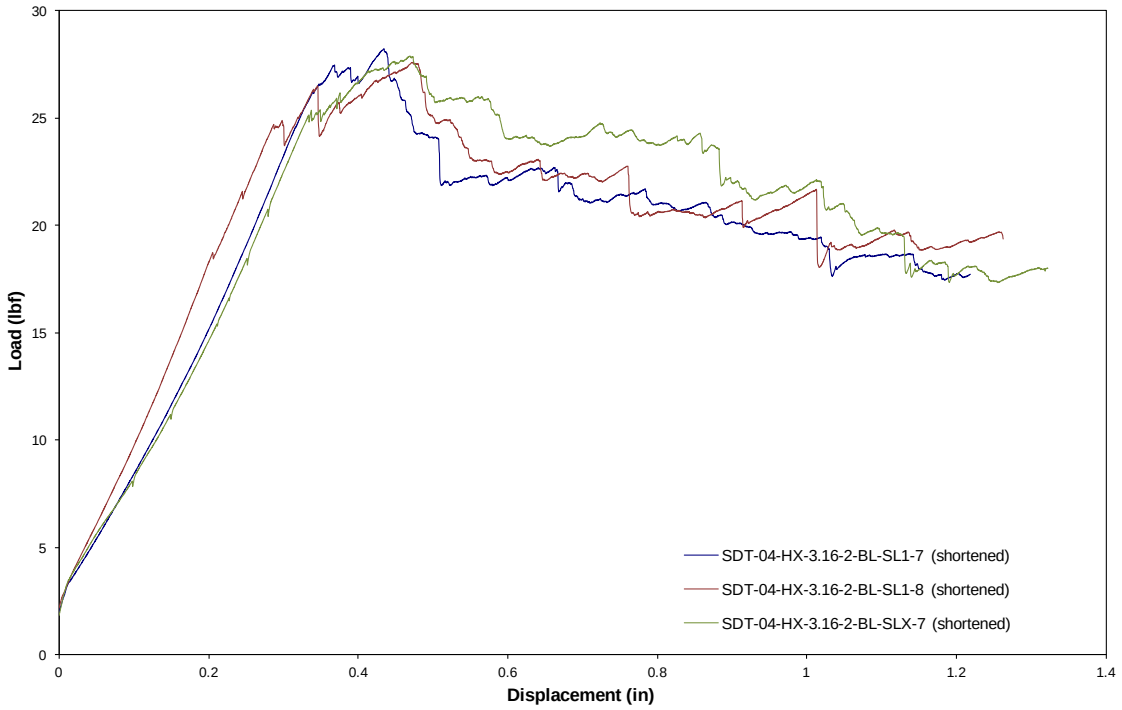

Figure B-32. Load vs. displacement curve for HRH-10–3/16-2.0 baseline (1″ prescribed crack—shortened)

B.2.2. HRH-10–3/16–2.0 FLUID-INGRESSED DATA

Table B-13. test summary for HRH-10–3/16–2.0 fluid ingressed (1″ prescribed crack—shortened) pre-crack

Specimen	GIC (in-lb/in^2)			GIC (KJ/m^2)			Failure Mode
	NL	VIS	5%/ max	NL	VIS	5%/ max	
SDT-04-HX-3.16-2-FI-SL1-1 (shortened)	0.331	-	0.736	0.058	-	0.129	Primarily in C
SDT-04-HX-3.16-2-FI-SL1-2 (shortened)	1.581	-	3.662	0.277	-	0.641	Primarily in C
SDT-04-HX-3.16-2-FI-SL1-3 (shortened)	0.355	-	0.592	0.062	-	0.104	Primarily in C
SDT-04-HX-3.16-2-FI-SL1-4 (shortened)	0.359	-	0.505	0.063	-	0.088	Primarily in C
SDT-04-HX-3.16-2-FI-SL1-5 (shortened)	1.238	-	2.210	0.217	-	0.387	Primarily in C
SDT-04-HX-3.16-2-FI-SL1-6 (shortened)	1.610	-	2.918	0.282	-	0.511	Primarily in C
AVERAGE GIC	0.912	-	1.771	0.160	-	0.310	
STANDARD DEVIATION	0.632	-	1.353	0.111	-	0.237	
COEFFICIENT OF VARIATION (%)	69.234	-	76.396	69.234	-	76.396	

Table B-14. Test summary for HRH-10–3/16–2.0 fluid ingressed (1″ prescribed crack—shortened)

Specimen	GIC (in-lb/in^2)			GIC (KJ/m^2)			Failure Mode
	NL	VIS	5%/ max	NL	VIS	5%/ max	
SDT-04-HX-3.16-2-FI-SL1-1 (shortened)	1.185	-	2.685	0.207	-	0.470	Primarily in C
SDT-04-HX-3.16-2-FI-SL1-2 (shortened)	0.697	2.539	2.679	0.122	0.445	0.469	Primarily in C
SDT-04-HX-3.16-2-FI-SL1-3 (shortened)	0.865	-	2.817	0.151	-	0.493	Primarily in C
SDT-04-HX-3.16-2-FI-SL1-4 (shortened)	0.699	-	2.460	0.122	-	0.431	Primarily in C
SDT-04-HX-3.16-2-FI-SL1-5 (shortened)	0.704	-	2.320	0.123	-	0.406	Primarily in C
SDT-04-HX-3.16-2-FI-SL1-6 (shortened)	1.131	3.128	3.282	0.198	0.548	0.575	Primarily in C
AVERAGE GIC	0.880	2.834	2.707	0.154	0.496	0.474	
STANDARD DEVIATION	0.225	0.417	0.333	0.039	0.073	0.058	
COEFFICIENT OF VARIATION (%)	25.557	14.717	12.301	25.557	14.717	12.301	

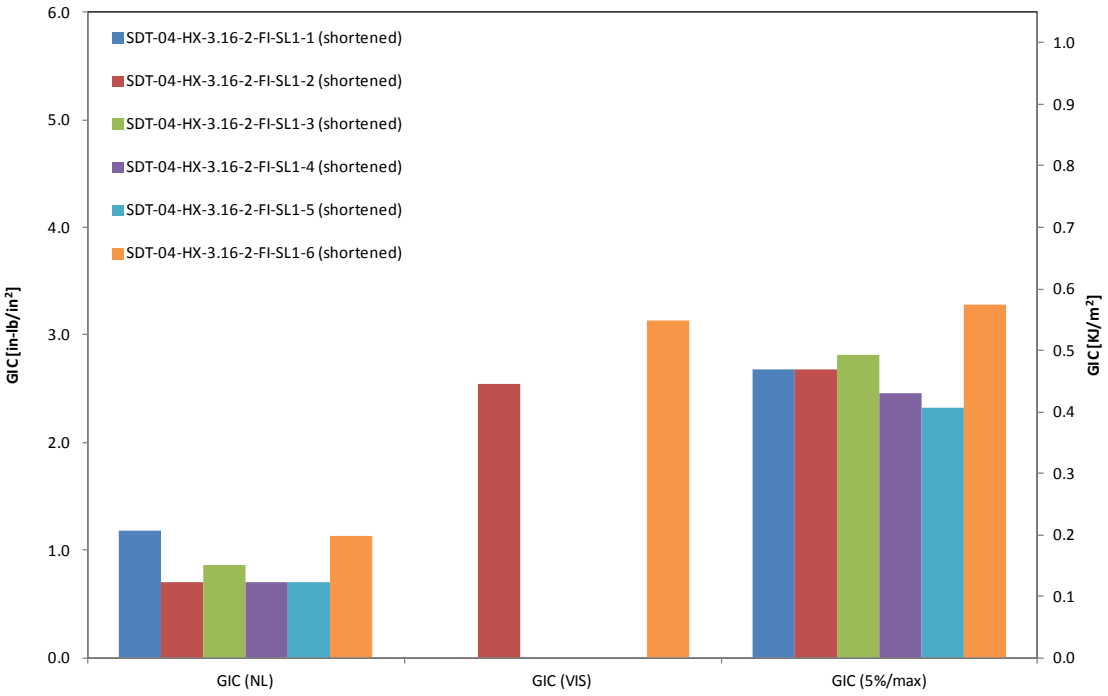

Figure B-33. GIC for HRH-10–3/16–2.0 fluid-ingressed (1″ prescribed crack—shortened)

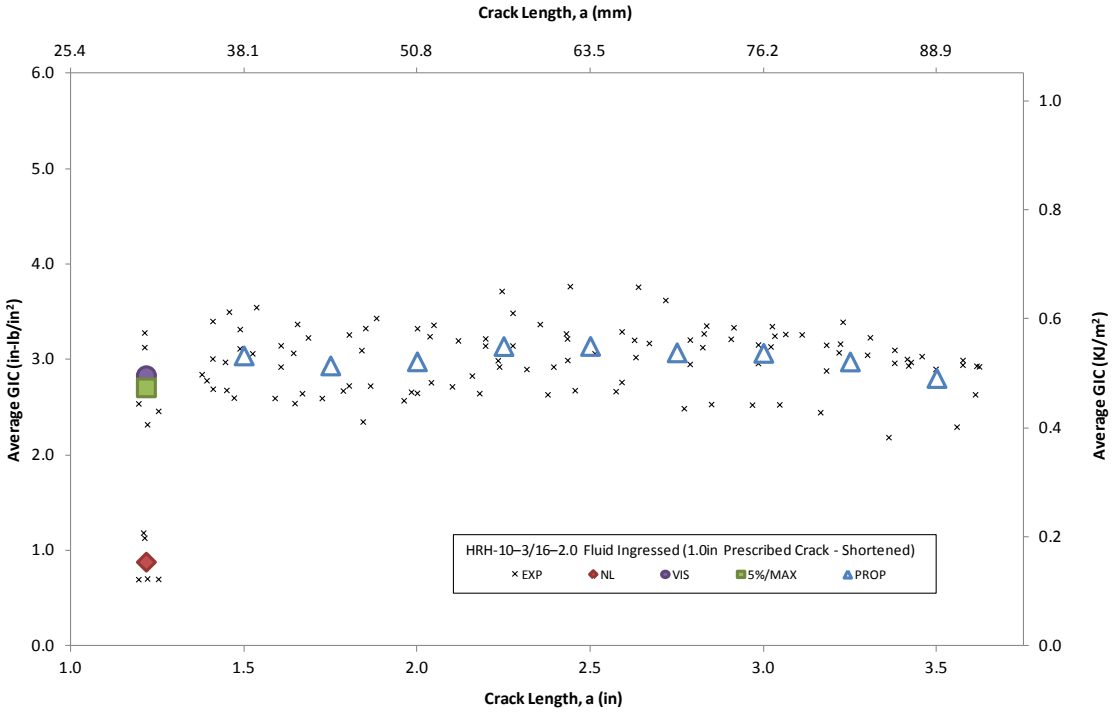

Figure B-34. Resistance curve for HRH-10–3/16–2.0 fluid-ingressed (1″ prescribed crack—shortened)

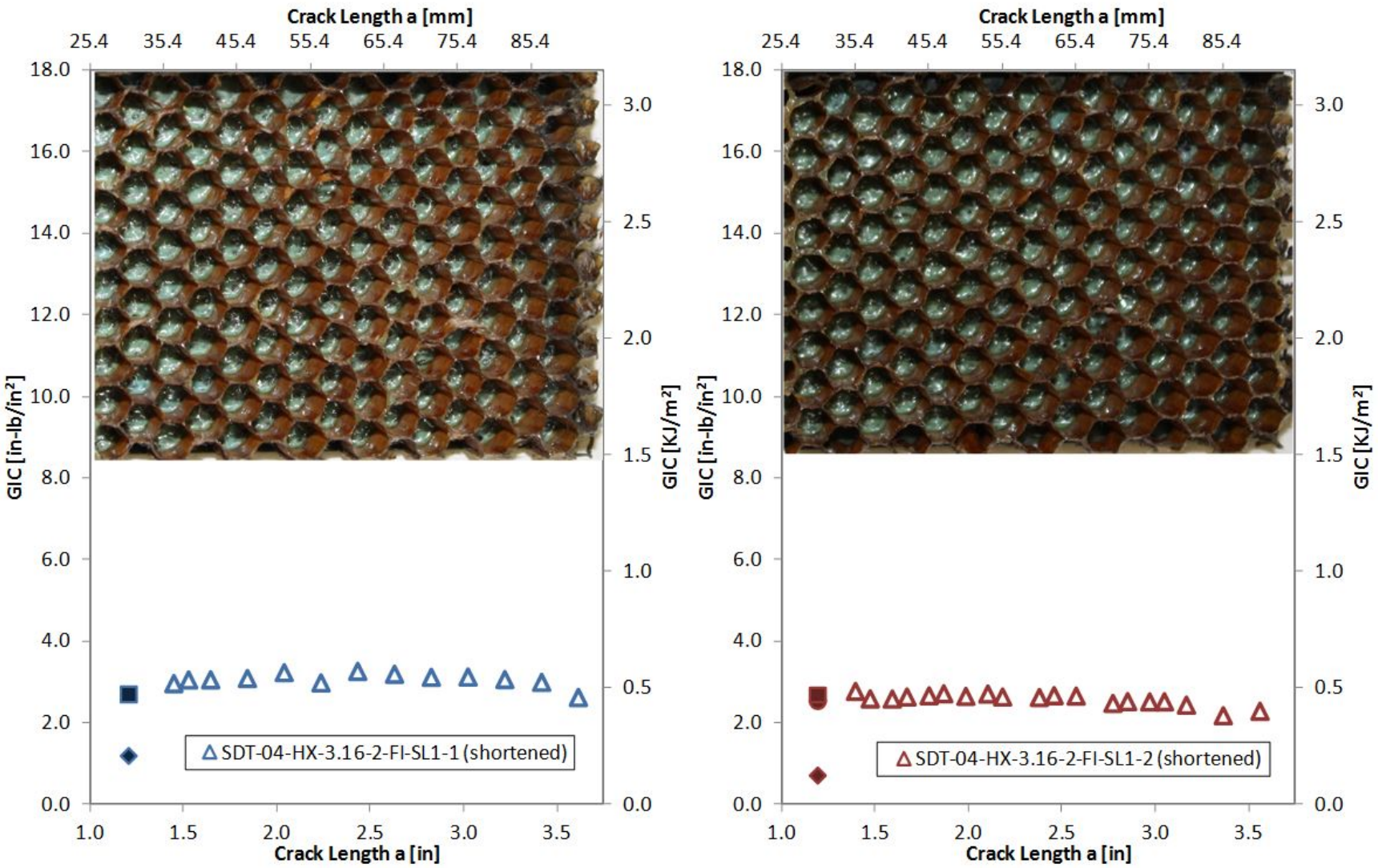

Figure B-35. Failure mode and resistance curve for SDT-04-HX-3.16-2-FI-SL1-X (shortened) #1 and #2

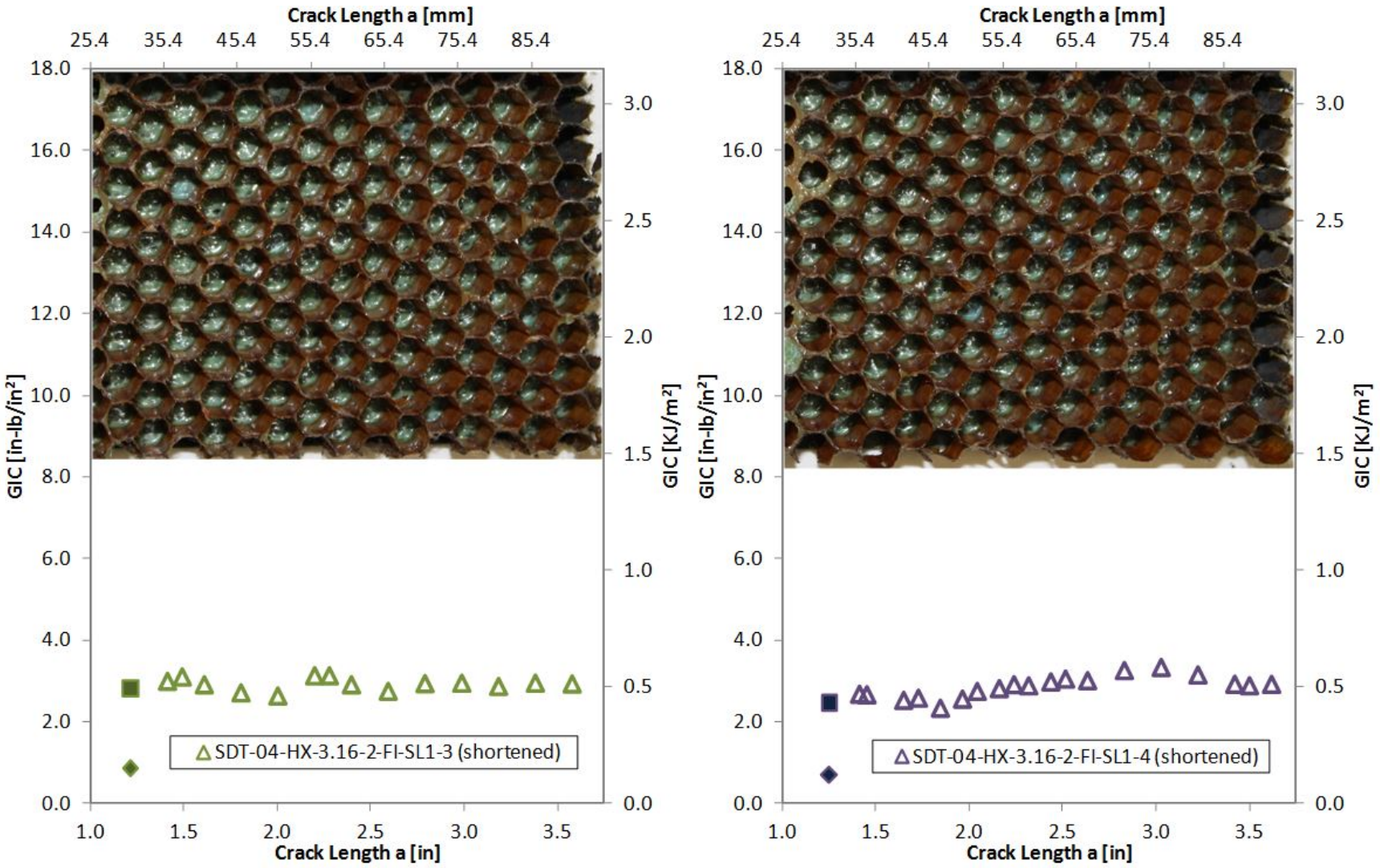

Figure B-36. Failure mode and resistance curve for SDT-04-HX-3.16-2-FI-SL1-X (shortened) #3 and #4

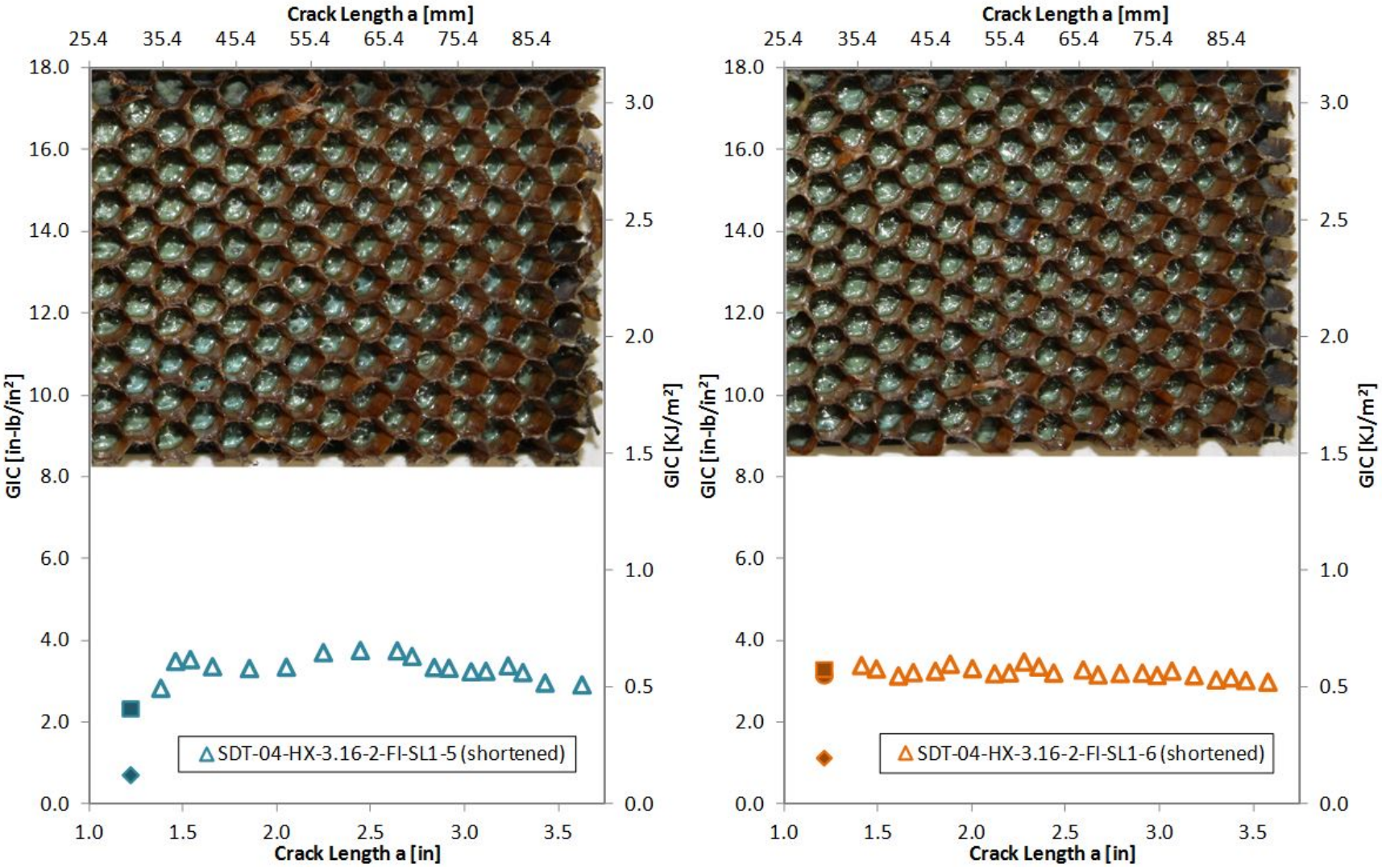

Figure B-37. Failure mode and resistance curve for SDT-04-HX-3.16-2-FI-SL1-X (shortened) #5 and #6

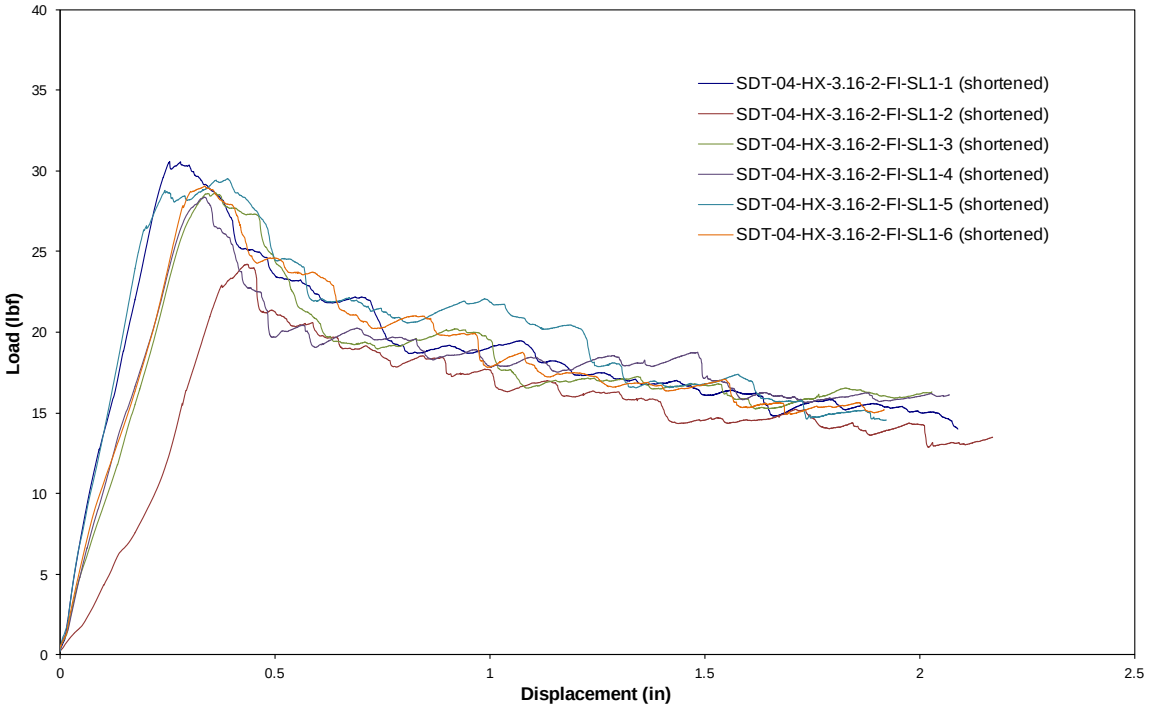

Figure B-38. Load vs. displacement curve for HRH-10–3/16–2.0 fluid-ingressed (1″prescribed crack—shortened)

B.2.3 HRH-10–3/16–2.0 EXTENDED FLUID-INGRESSED DATA

Table B-15. Test summary for HRH-10–3/16–2.0 extended fluid ingressed (1″ prescribed crack—shortened) pre-crack

Specimen	GIC (in-lb/in^2)			GIC (KJ/m^2)			Failure Mode
	NL	VIS	5%/max	NL	VIS	5%/max	
SDT-04-HX-3.16-2-EFI-SL1-7 (shortened)	-	-	-	-	-	-	
SDT-04-HX-3.16-2-EFI-SL1-8 (shortened)	1.018	-	4.691	0.178	-	0.821	Primarily in C
AVERAGE GIC	1.018	-	4.691	0.178	-	0.821	
STANDARD DEVIATION	-	-	-	-	-	-	
COEFFICIENT OF VARIATION (%)	-	-	-	-	-	-	

Table B-16. Test summary for HRH-10–3/16–2.0 extended fluid ingressed (1″ prescribed crack—shortened)

Specimen	GIC (in-lb/in^2)			GIC (KJ/m^2)			Failure Mode
	NL	VIS	5%/max	NL	VIS	5%/max	
SDT-04-HX-3.16-2-EFI-SL1-7 (shortened)	-	-	-	-	-	-	
SDT-04-HX-3.16-2-EFI-SL1-8 (shortened)	1.064	-	2.499	0.186	-	0.438	Primarily in C
AVERAGE GIC	1.064	-	2.499	0.186	-	0.438	
STANDARD DEVIATION	-	-	-	-	-	-	
COEFFICIENT OF VARIATION (%)	-	-	-	-	-	-	

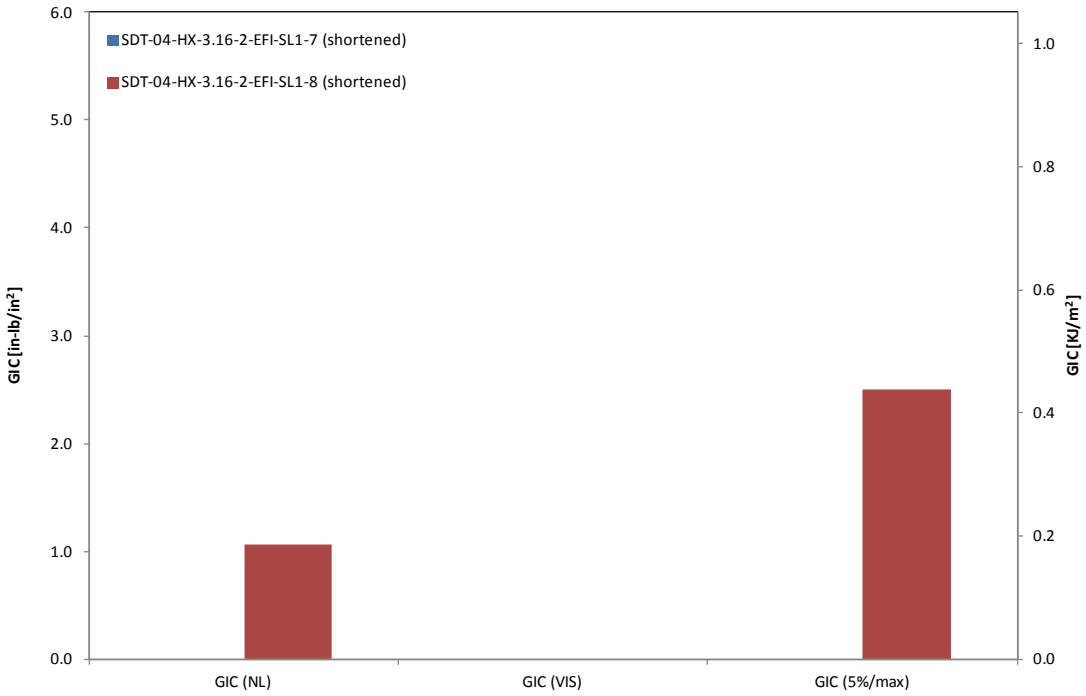

Figure B-39. GIC for HRH-10–3/16–2.0 extended fluid ingressed (1″ prescribed crack—shortened)

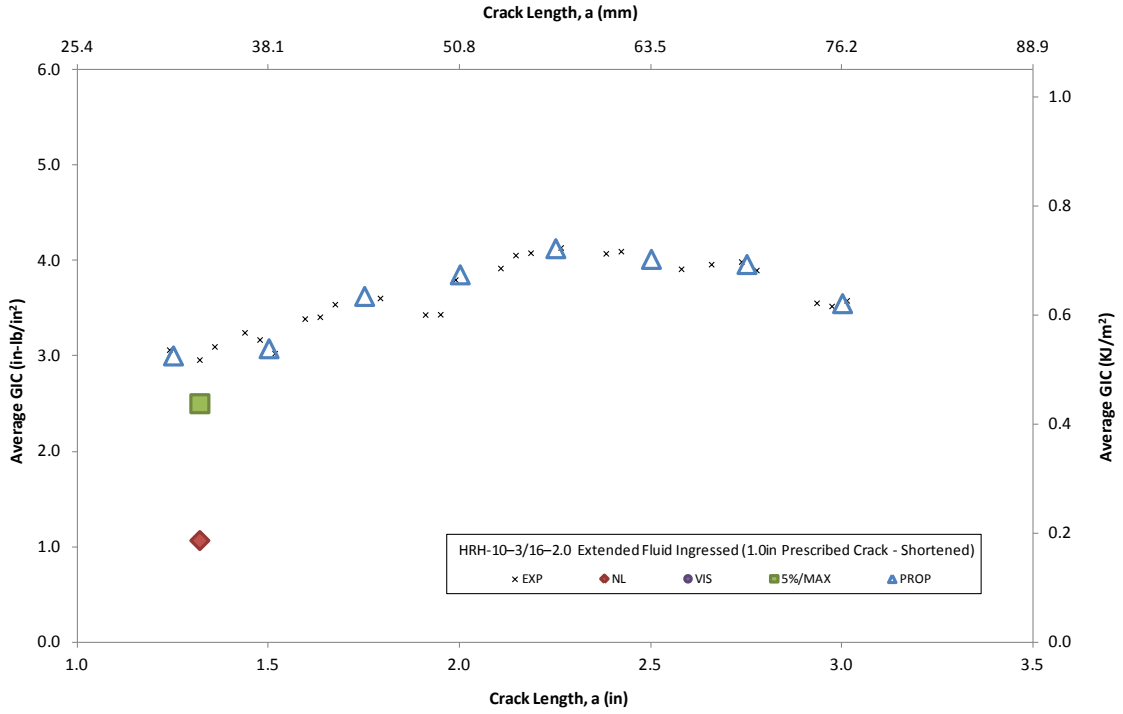

Figure B-40. Resistance curve for HRH-10–3/16–2.0 extended fluid ingressed (1″ prescribed crack—shortened)

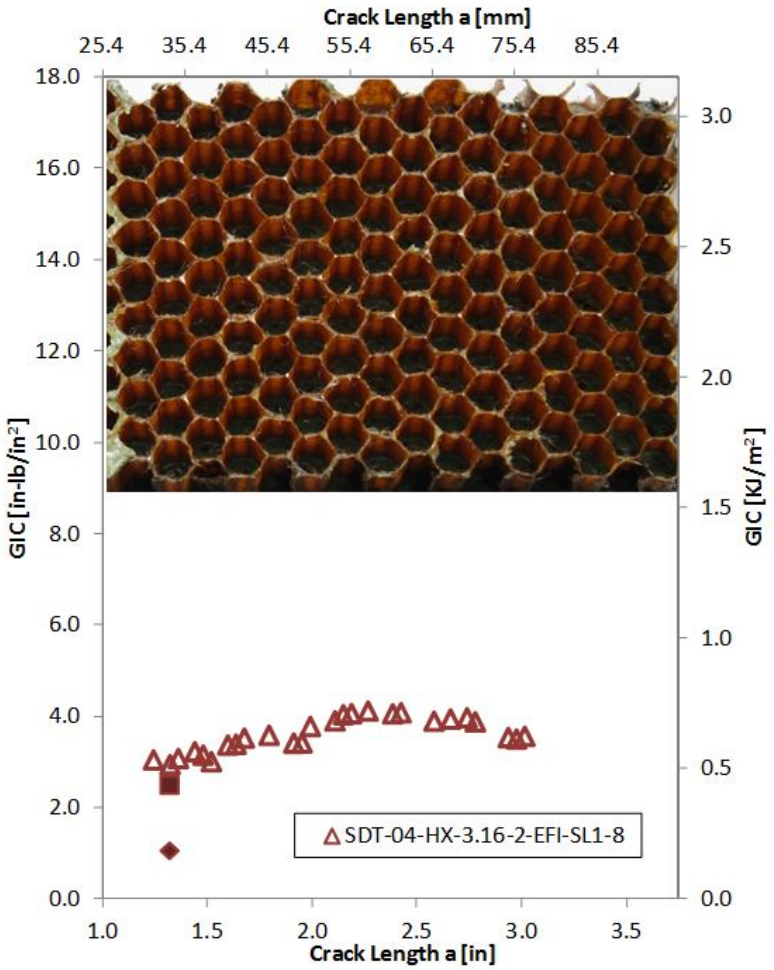

Figure B-41. Failure mode and resistance curve for SDT-04-HX-3.16-2-EFI-SL1-X (shortened) #8

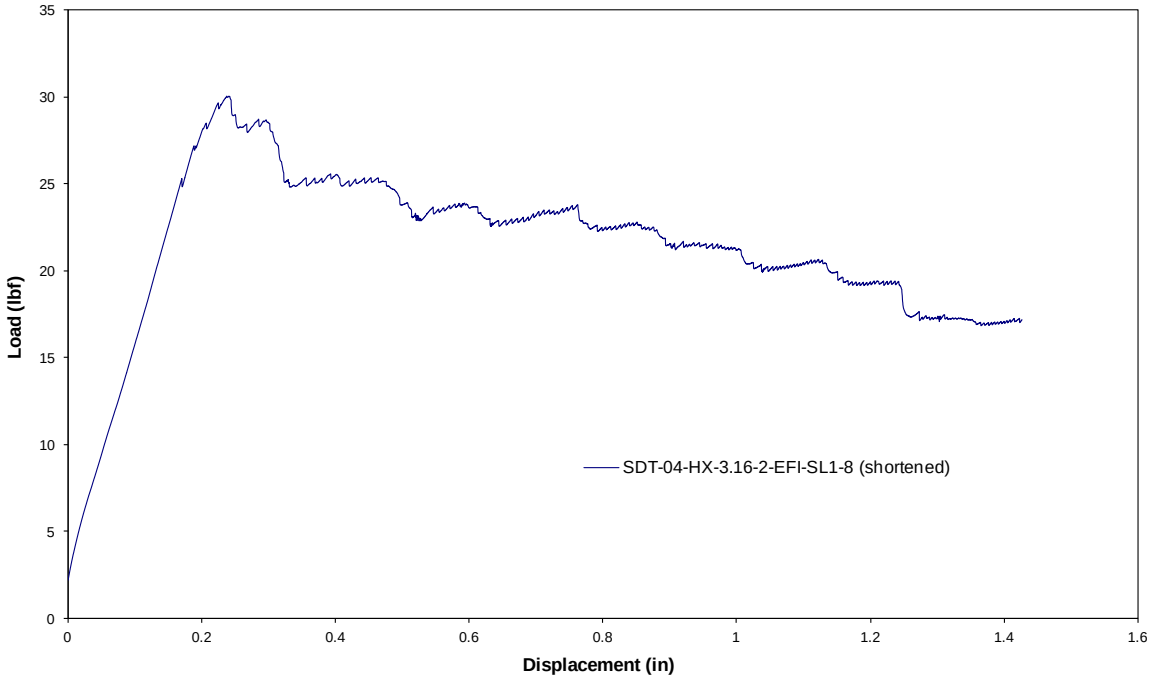

Figure B-42. Load vs. displacement curve for HRH-10–3/16–2.0 extended fluid ingressed (1″ prescribed crack—shortened)

B.3 HRH-10–3/16–3.0 DATA

B.3.1 HRH-10–3/16–3.0 BASELINE DATA

B.3.1.1 HRH-10–3/16–3.0 Baseline Data (2.5″ Prescribed Crack)

Table B-17. Test summary for HRH-10–3/16–3.0 baseline (2.5″ prescribed crack) pre-crack

Specimen	GIC (in-lb/in^2)			GIC (KJ/m^2)			Failure Mode
	NL	VIS	5%/max	NL	VIS	5%/max	
SDT-04-HX-3.16-3-BL-SL1-1	1.171	-	3.651	0.205	-	0.639	Primarily PO with a couple of cells in A and C
SDT-04-HX-3.16-3-BL-SL1-2	0.737	-	3.615	0.129	-	0.633	Primarily PO with a couple of cells in A
SDT-04-HX-3.16-3-BL-SL1-3	0.536	-	3.482	0.094	-	0.610	Primarily PO with a couple of cells in A
SDT-04-HX-3.16-3-BL-SL1-4	1.124	-	3.532	0.197	-	0.619	Primarily PO with a couple of cells in A
SDT-04-HX-3.16-3-BL-SL1-5	1.179	-	3.590	0.207	-	0.629	Primarily PO with a couple of cells in A
SDT-04-HX-3.16-3-BL-SL1-6	0.954	-	3.885	0.167	-	0.680	Primarily PO with several cells in A
AVERAGE GIC	0.950	-	3.626	0.166	-	0.635	
STANDARD DEVIATION	0.264	-	0.140	0.046	-	0.025	
COEFFICIENT OF VARIATION (%)	27.769	-	3.871	27.769	-	3.871	

Table B-18. Test summary for HRH-10–3/16–3.0 baseline (2.5″ prescribed crack)

Specimen	GIC (in-lb/in^2)			GIC (KJ/m^2)			Failure Mode
	NL	VIS	5%/ max	NL	VIS	5%/ max	
SDT-04-HX-3.16-3-BL-SL1-1	0.538	-	2.068	0.094	-	0.362	Primarily PO with a pocket of C, then a mix of A and PO
SDT-04-HX-3.16-3-BL-SL1-2	0.683	2.193	2.217	0.120	0.384	0.388	Primarily PO with a pocket of C, then a mix of A and PO
SDT-04-HX-3.16-3-BL-SL1-3	0.557	2.364	2.334	0.098	0.414	0.409	Mix of A, PO, and C, then mix of A and PO
SDT-04-HX-3.16-3-BL-SL1-4	0.548	1.903	2.030	0.096	0.333	0.355	Mix of A and PO with pockets of C
SDT-04-HX-3.16-3-BL-SL1-5	0.633	-	2.708	0.111	-	0.474	Primarily PO with a pocket of C, then a mix of A and PO
SDT-04-HX-3.16-3-BL-SL1-6	0.662	-	2.591	0.116	-	0.454	Mix of A, PO, and C, then mix of A and PO
AVERAGE GIC	0.604	2.153	2.325	0.106	0.377	0.407	
STANDARD DEVIATION	0.064	0.233	0.277	0.011	0.041	0.048	
COEFFICIENT OF VARIATION (%)	10.536	10.830	11.901	10.536	10.830	11.901	

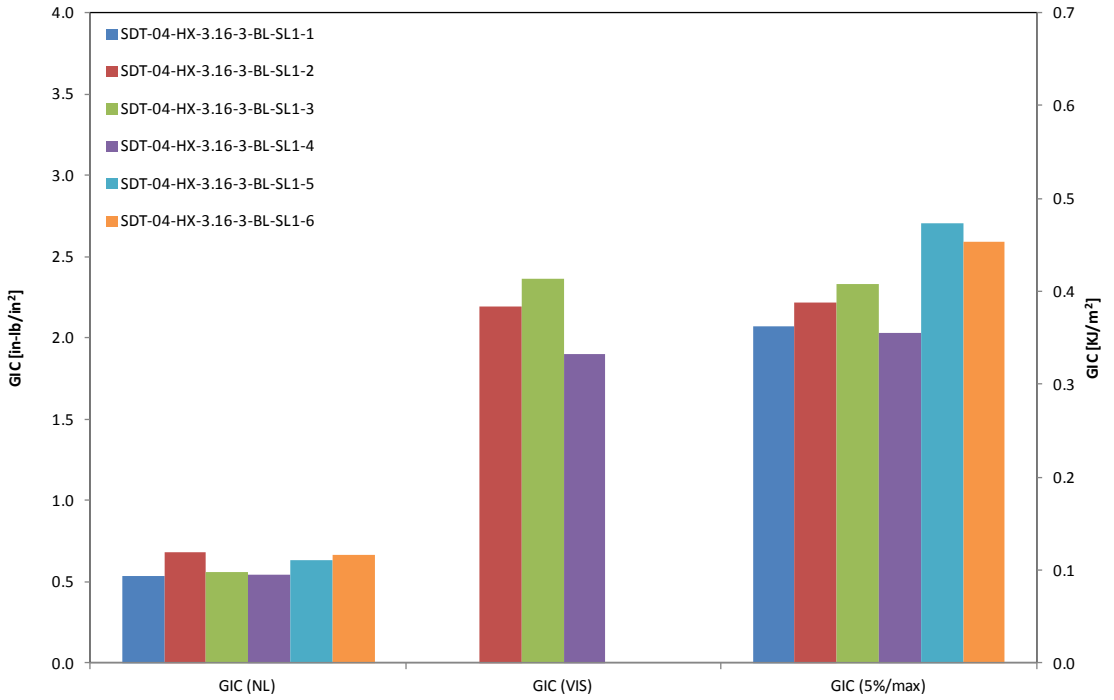

Figure B-43. GIC for HRH-10–3/16–3.0 baseline (2.5″ prescribed crack)

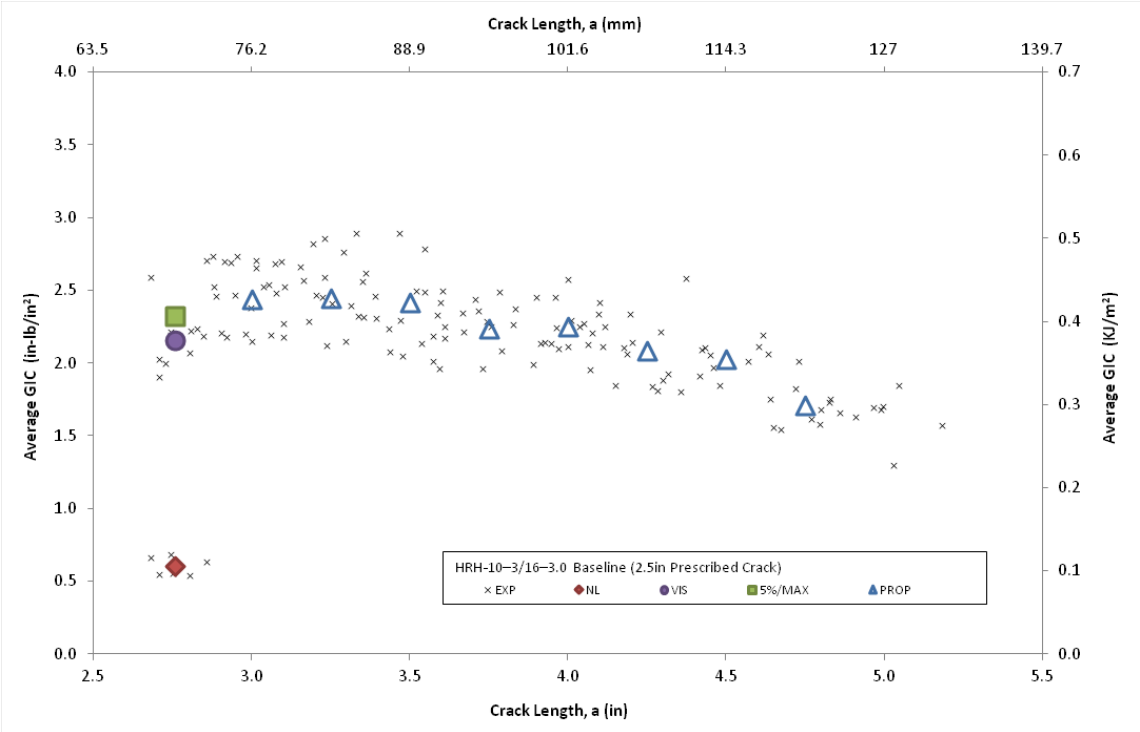

Figure B-44. Resistance curve for HRH-10–3/16–3.0 baseline (2.5″ prescribed crack)

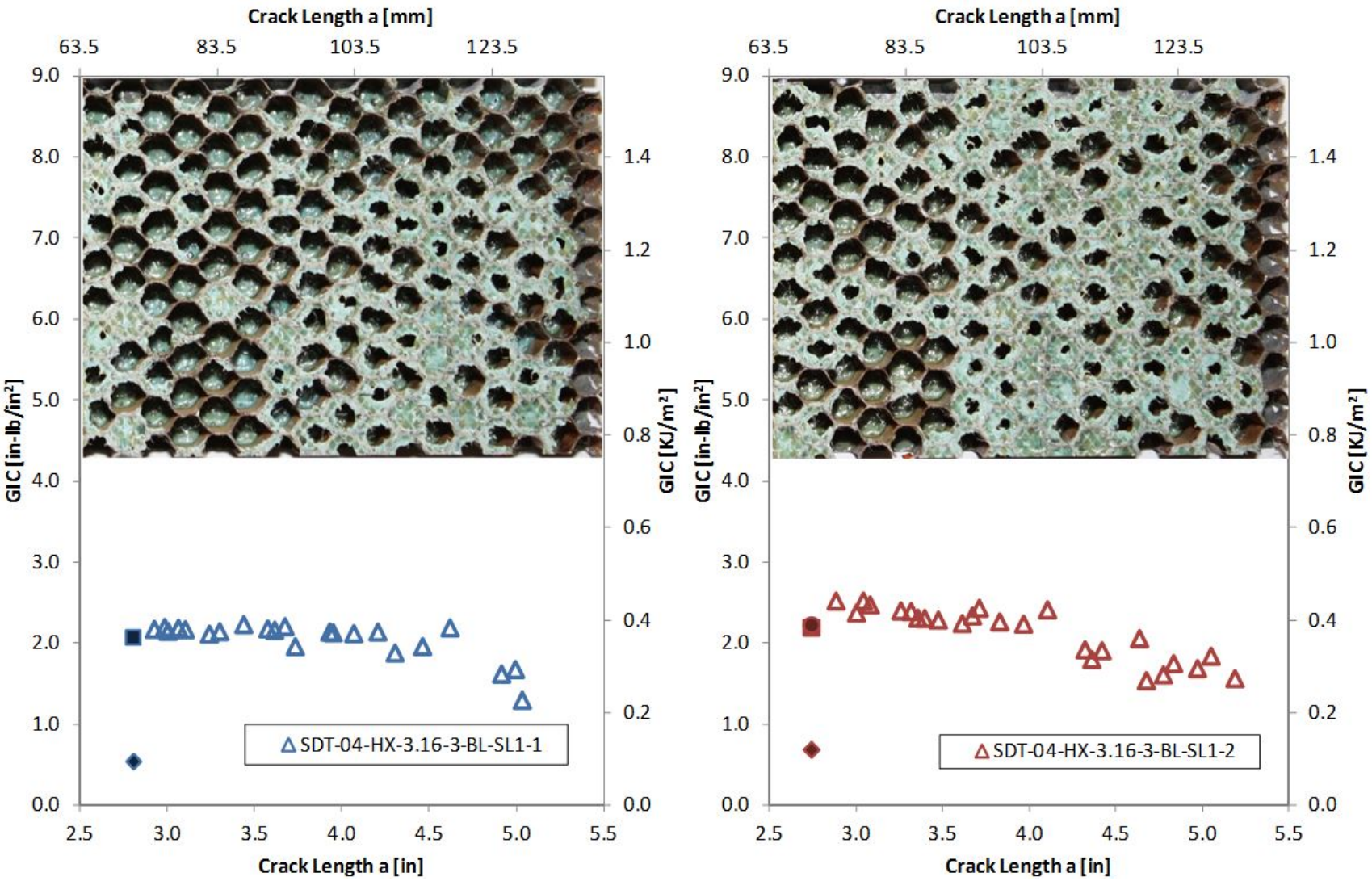

Figure B-45. Failure mode and resistance curve for SDT-04-HX-3.16-3-BL-SL1-X #1 and #2

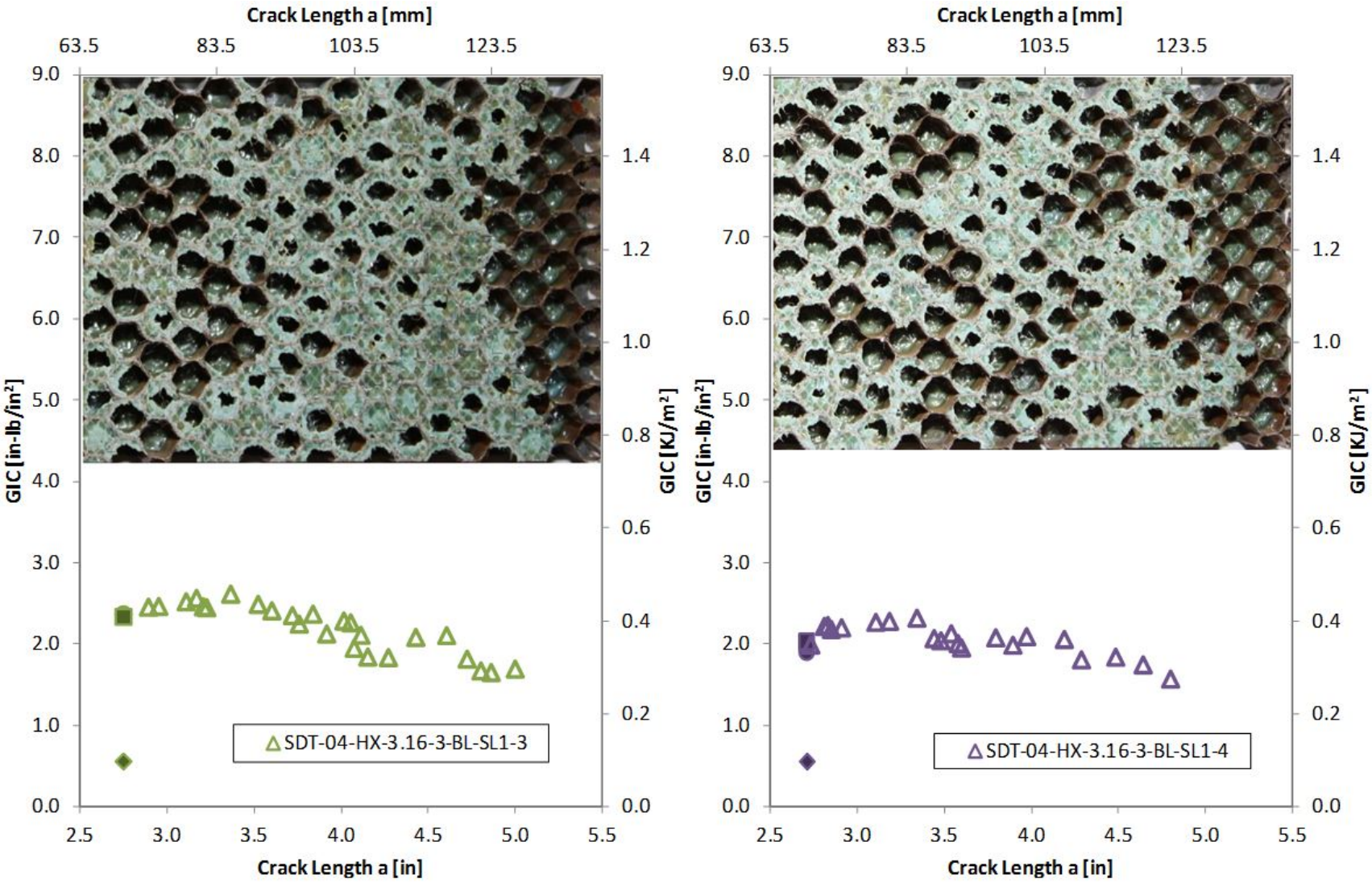

Figure B-46. Failure mode and resistance curve for SDT-04-HX-3.16-3-BL-SL1-X #3 and #4

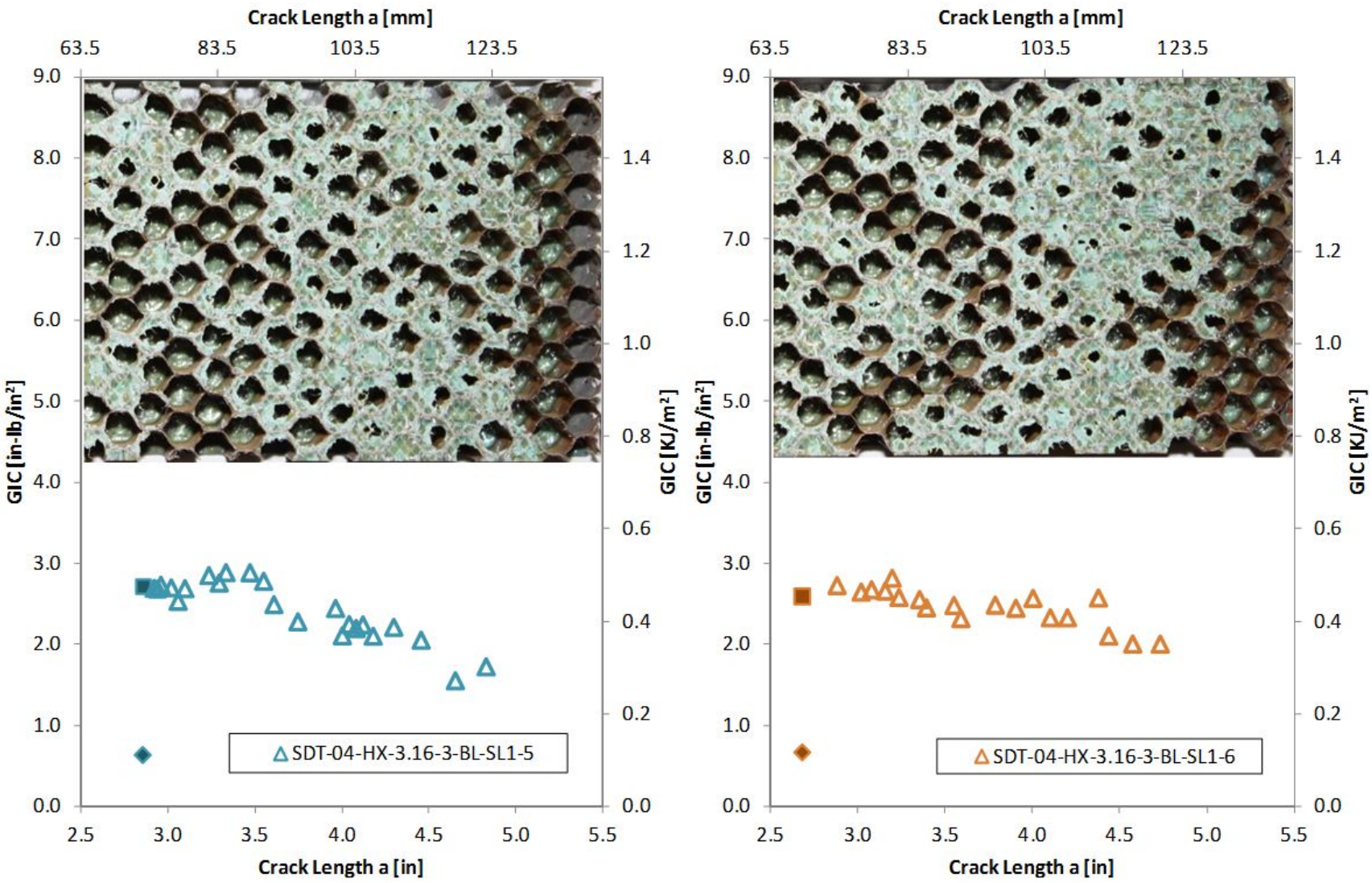

Figure B-47. Failure mode and resistance curve for SDT-04-HX-3.16-3-BL-SL1-X #5 and #6

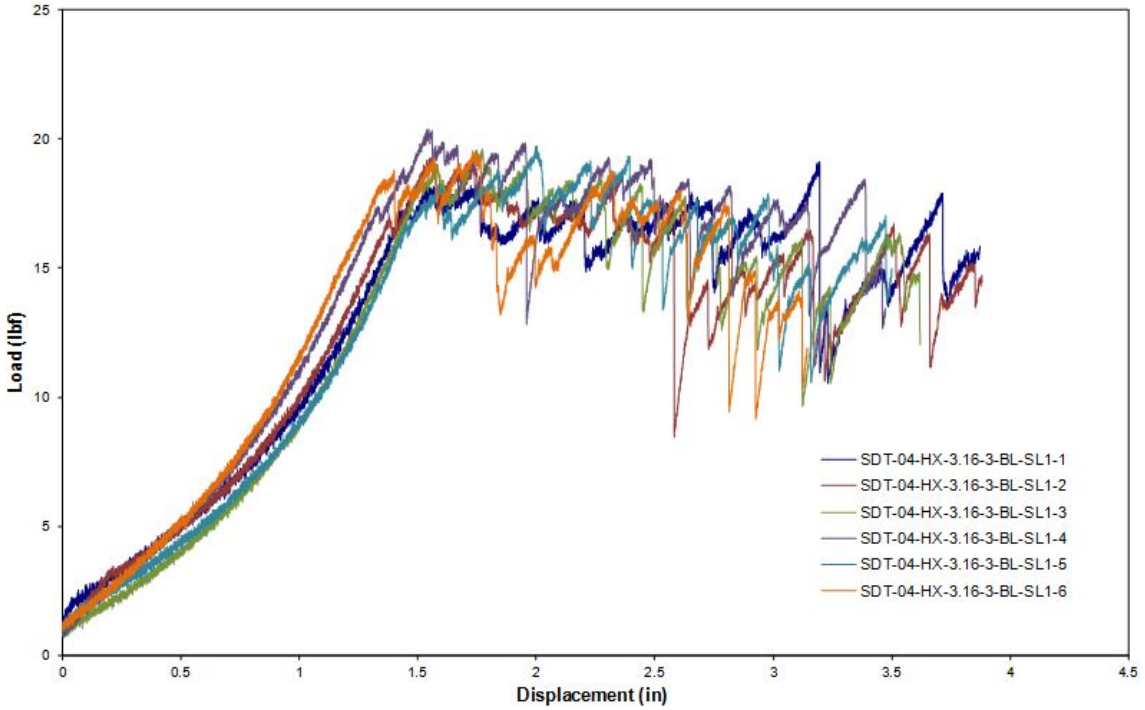

Figure B-48. Load vs. displacement curve for HRH-10–3/16–3.0 baseline (2.5″ prescribed crack)

B.3.1.2. HRH-10–3/16–3.0 Baseline Data (1″ Prescribed Crack—Shortened)

Table B-19. Test summary for HRH-10–3/16–3.0 baseline (1″ prescribed crack—shortened) pre-crack

Specimen	GIC (in-lb/in^2)			GIC (KJ/m^2)			Failure Mode
	NL	VIS	5%/ max	NL	VIS	5%/ max	
SDT-04-HX-3.16-3-BL-SL1-7 (shortened)	2.361	-	3.386	0.413	-	0.593	Primarily PO with a couple of cells in A
SDT-04-HX-3.16-3-BL-SL1-8 (shortened)	1.706	-	2.461	0.299	-	0.431	Mix of A and PO
SDT-04-HX-3.16-3-BL-SLX-7 (shortened)	0.749	-	1.183	0.131	-	0.207	First row of cells in PO; second row a mix of PO and C
AVERAGE GIC	1.605	-	2.343	0.281	-	0.410	
STANDARD DEVIATION	0.009	-	0.031	0.142	-	0.194	
COEFFICIENT OF VARIATION (%)	50.492	-	47.209	50.492	-	47.209	

Table B-20. Test summary for HRH-10–3/16–3.0 baseline (1″ prescribed crack—shortened)

Specimen	GIC (in-lb/in^2)			GIC (KJ/m^2)			Failure Mode
	NL	VIS	5%/ max	NL	VIS	5%/ max	
SDT-04-HX-3.16-3-BL-SL1-7 (shortened)	1.514	-	4.162	0.265	-	0.729	Primarily PO with some mix in PO and A; occasional pockets of C
SDT-04-HX-3.16-3-BL-SL1-8 (shortened)	1.200	-	3.294	0.210	-	0.577	Primarily PO with occasional pockets of C
SDT-04-HX-3.16-3-BL-SLX-7 (shortened)	1.372	3.058	3.763	0.240	0.536	0.659	Mix of A, PO, and C
AVERAGE GIC	1.362	3.058	3.740	0.239	0.536	0.655	
STANDARD DEVIATION	0.009	-	0.031	0.028	-	0.076	
COEFFICIENT OF VARIATION (%)	11.560	-	11.622	11.560	-	11.622	

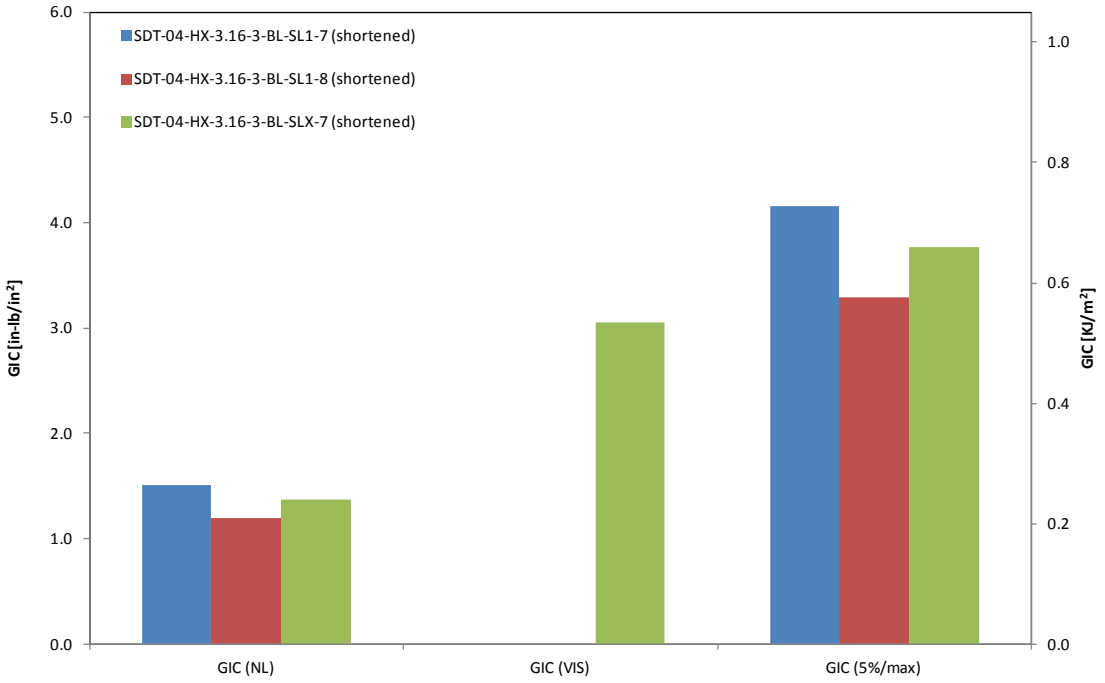

Figure B-49. GIC for HRH-10–3/16–3.0 baseline (1″ prescribed crack—shortened)

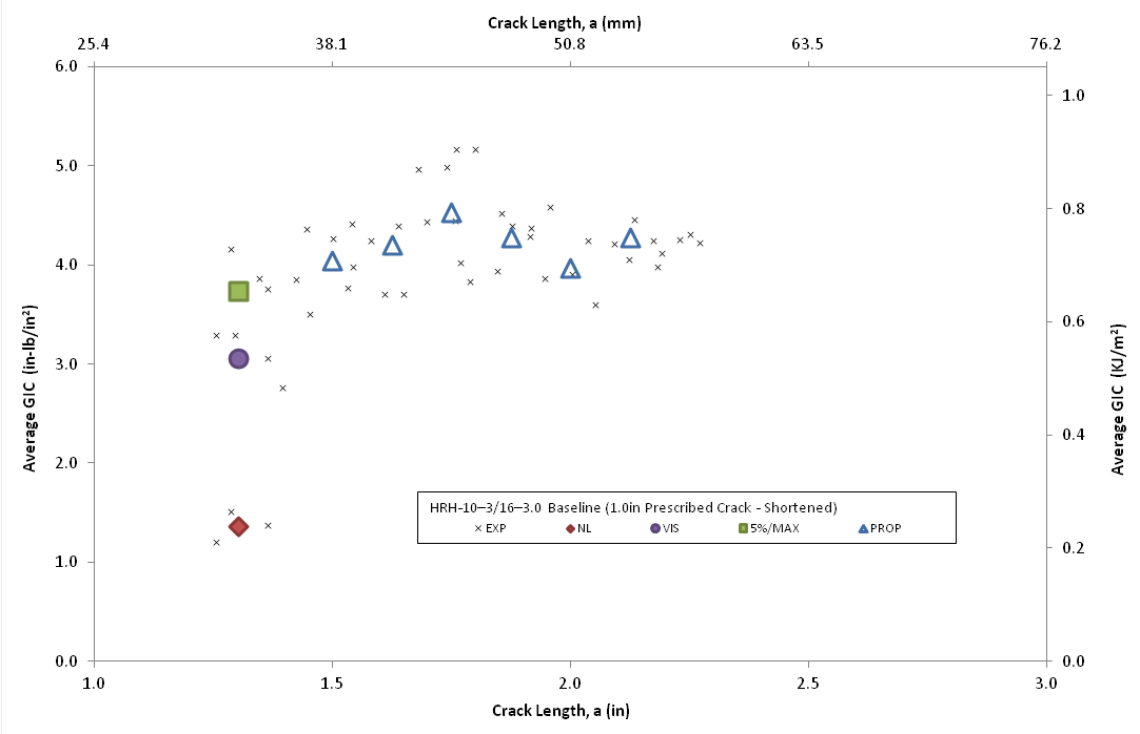

Figure B-50. Resistance curve for HRH-10–3/16–3.0 baseline (1″ prescribed crack—shortened)

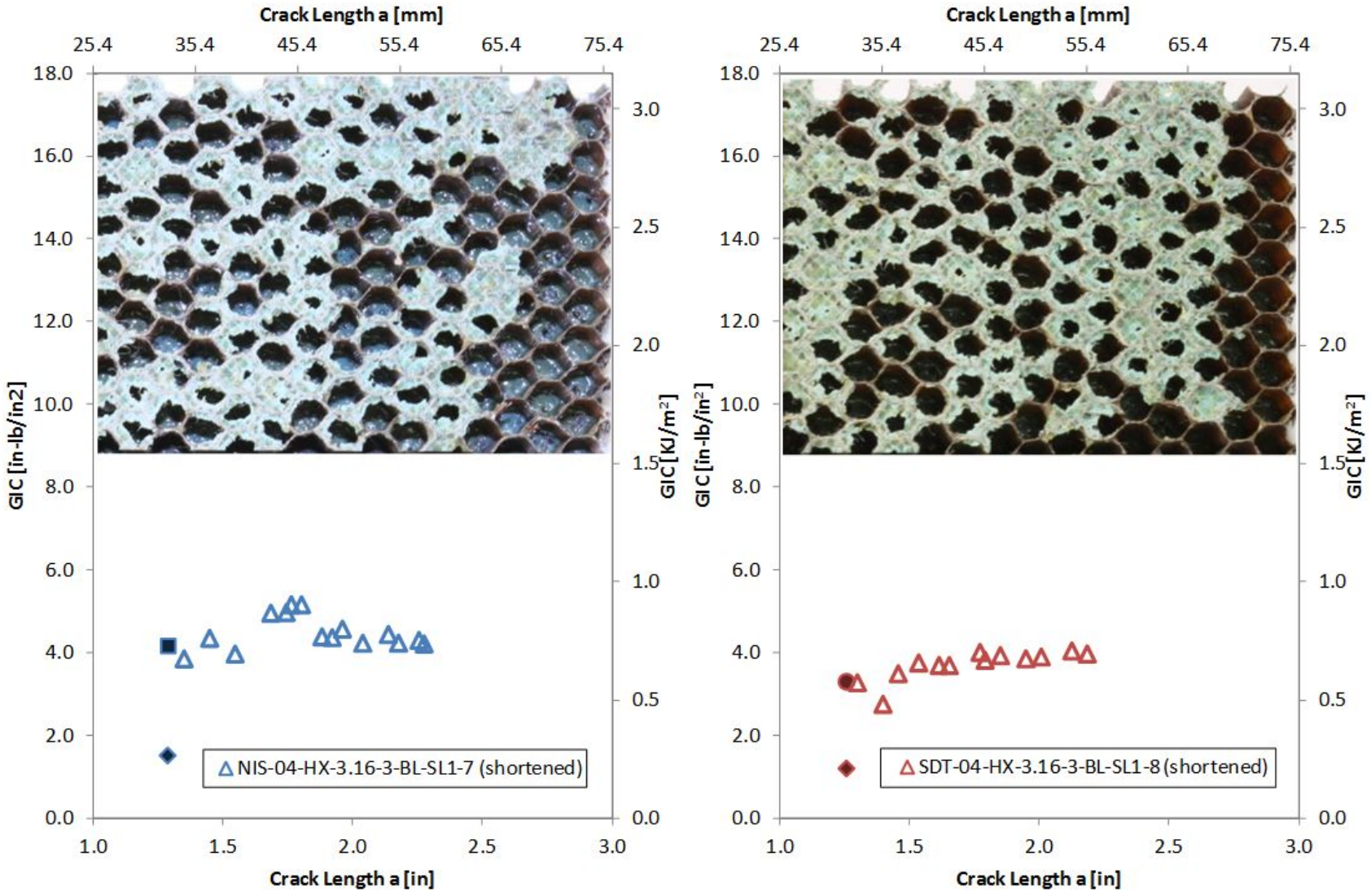

Figure B-51. Failure mode and resistance curve for SDT-04-HX-3.16-3-BL-SL1-X (shortened) #7 and #8

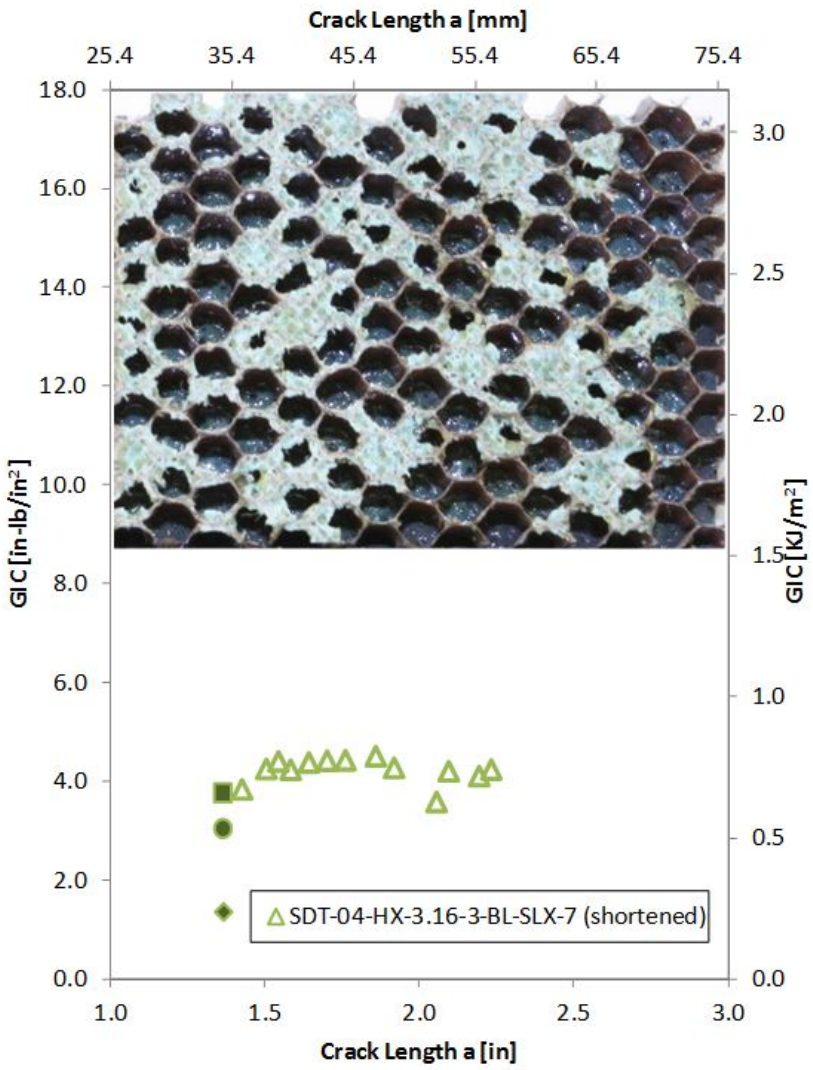

Figure B-52. Failure mode and resistance curve for SDT-04-HX-3.16-3-BL-SLX-X (shortened) #7

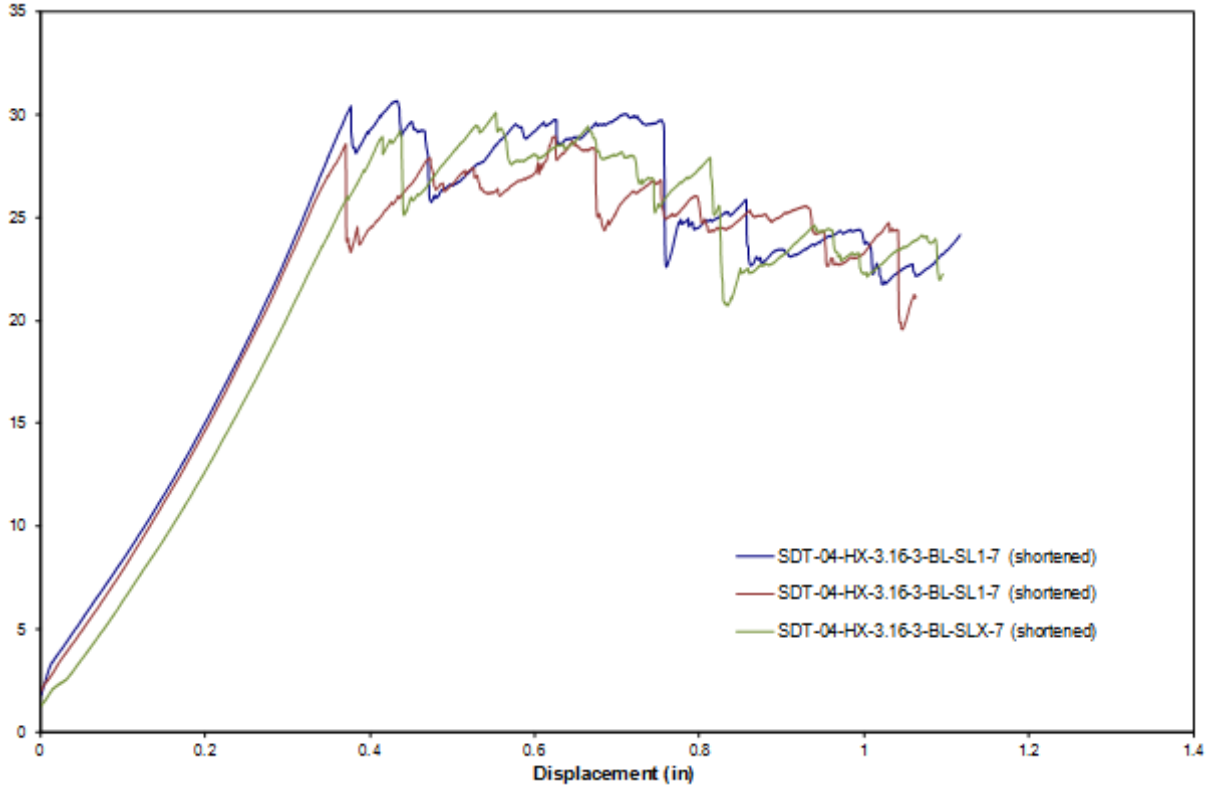

Figure B-53. Load vs. displacement curve for HRH-10–3/16–3.0 baseline (1″ prescribed crack—shortened)

B.3.2 HRH-10–3/16–3.0 FLUID-INGRESSED DATA

Table B-21. Test summary for HRH-10–3/16–3.0 fluid ingressed (1″ prescribed crack—shortened) pre-crack

Specimen	GIC (in-lb/in^2)			GIC (KJ/m^2)			Failure Mode
	NL	VIS	5%/ max	NL	VIS	5%/ max	
SDT-04-HX-3.16-3-FI-SL1-1 (shortened)	2.070	-	3.032	0.363	-	0.531	Primarily in C with two cells in A
SDT-04-HX-3.16-3-FI-SL1-2 (shortened)	1.168	-	2.224	0.205	-	0.389	Primarily in C with two cells in A
SDT-04-HX-3.16-3-FI-SL1-4 (shortened)	0.817	-	1.349	0.143	-	0.236	Primarily in C with a few cells in A and PO
SDT-04-HX-3.16-3-FI-SL1-5 (shortened)	1.038	-	1.872	0.182	-	0.328	Primarily in C with a few cells in A and PO
SDT-04-HX-3.16-3-FI-SL1-6 (shortened)	0.572	-	0.757	0.100	-	0.133	First row a mix of A, PO, and C, second row primarily in C with a couple cells in PO
SDT-04-HX-3.16-3-FI-SL1-7 (shortened)	0.314	-	0.567	0.055	-	0.099	Primarily in C
AVERAGE GIC	0.997	-	1.634	0.175	-	0.286	
STANDARD DEVIATION	0.610	-	0.933	0.107	-	0.163	
COEFFICIENT OF VARIATION (%)	61.234	-	57.087	61.234	-	57.087	

Table B-22. Test summary for HRH-10–3/16–3.0 fluid ingressed (1″ prescribed crack—shortened)

Specimen	GIC (in-lb/in^2)			GIC (KJ/m^2)			Failure Mode
	NL	VIS	5%/ max	NL	VIS	5%/ max	
SDT-04-HX-3.16-3-FI-SL1-1 (shortened)	1.395	-	3.308	0.244	-	0.579	Primarily in C with several scattered cells in A and PO
SDT-04-HX-3.16-3-FI-SL1-2 (shortened)	0.869	-	3.044	0.152	-	0.533	Primarily in C with several scattered cells in A and PO
SDT-04-HX-3.16-3-FI-SL1-4 (shortened)	0.965	-	3.015	0.169	-	0.528	First several rows primarily in C with a couple cells in A or PO, then transitions to a mix of A, PO, and C
SDT-04-HX-3.16-3-FI-SL1-5 (shortened)	1.034	-	3.683	0.181	-	0.645	First several rows primarily in C with a couple cells in A, then transitions to a mix of PO and C with a few cells in A
SDT-04-HX-3.16-3-FI-SL1-6 (shortened)	0.786	3.590	3.667	0.138	0.629	0.642	First several rows primarily in C with a couple cells in A or PO, then transitions to a mix of A and PO with a few cells in C
SDT-04-HX-3.16-3-FI-SL1-7 (shortened)	0.826	-	4.230	0.145	-	0.741	First several rows primarily in C with a couple cells in A or PO, then transitions to a mix of A, PO, and C
AVERAGE GIC	0.979	3.590	3.491	0.171	0.629	0.611	
STANDARD DEVIATION	0.223	-	0.463	0.039	-	0.081	
COEFFICIENT OF VARIATION (%)	22.786	-	13.268	22.786	-	13.268	

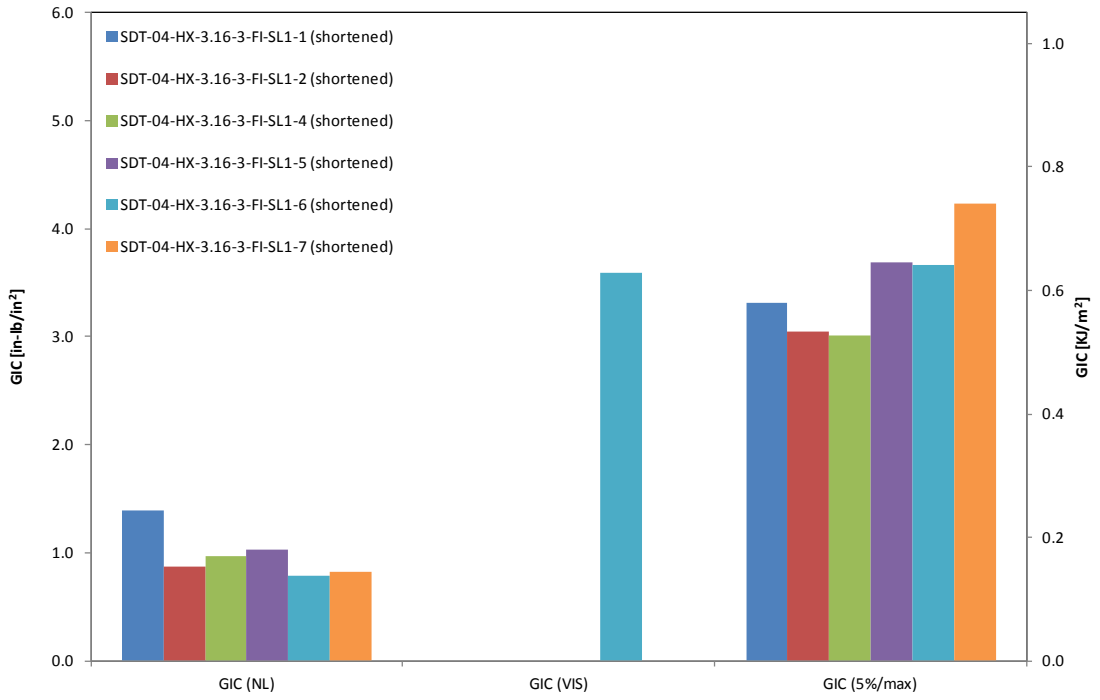

Figure B-54. GIC for HRH-10–3/16–3.0 fluid ingressed (1″ prescribed crack—shortened)

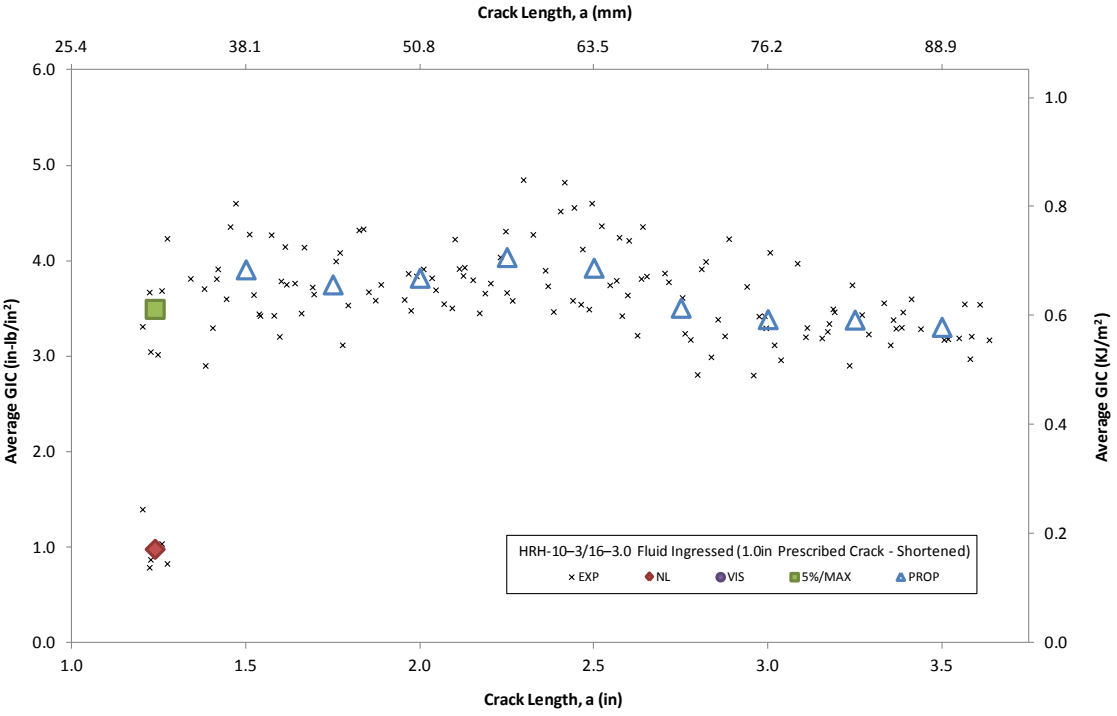

Figure B-55. Resistance curve for HRH-10–3/16–3.0 fluid ingressed (1.0″ prescribed crack—shortened)

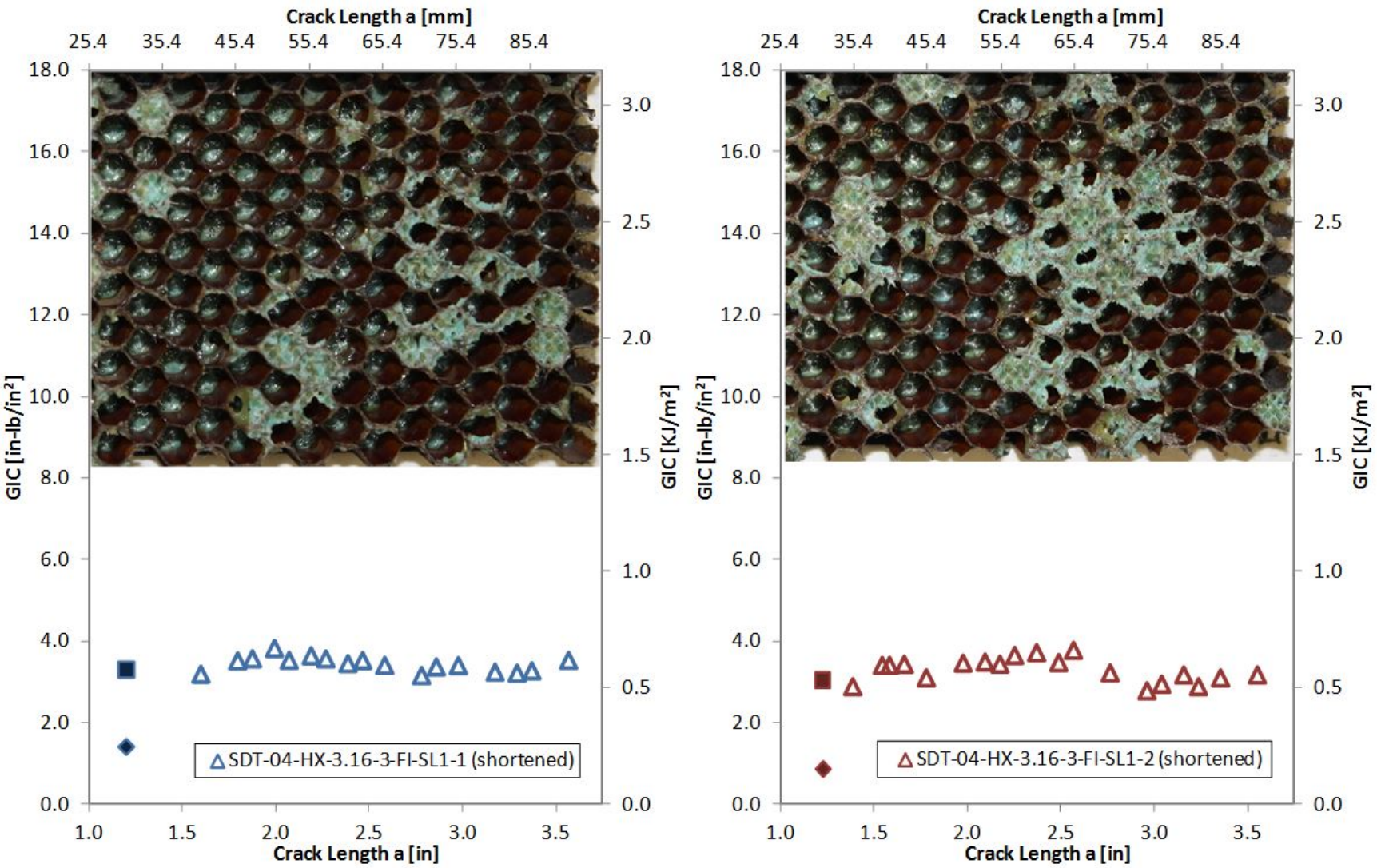

Figure B-56. Failure mode and resistance curve for SDT-04-HX-3.16-3-FI-SL1-X (shortened) #1 and #2

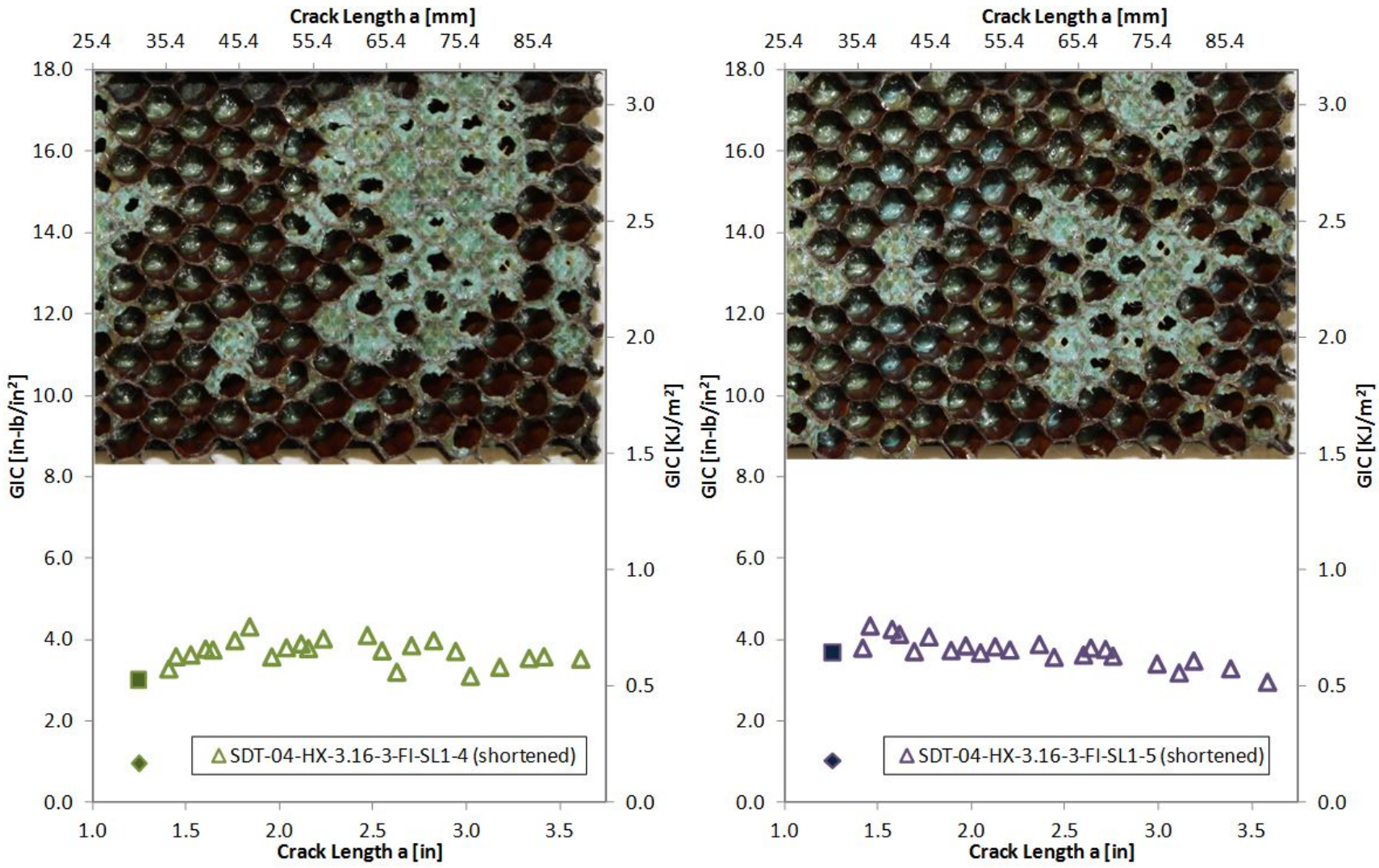

Figure B-57. Failure mode and resistance curve for SDT-04-HX-3.16-3-FI-SL1-X (shortened) #4 and #5

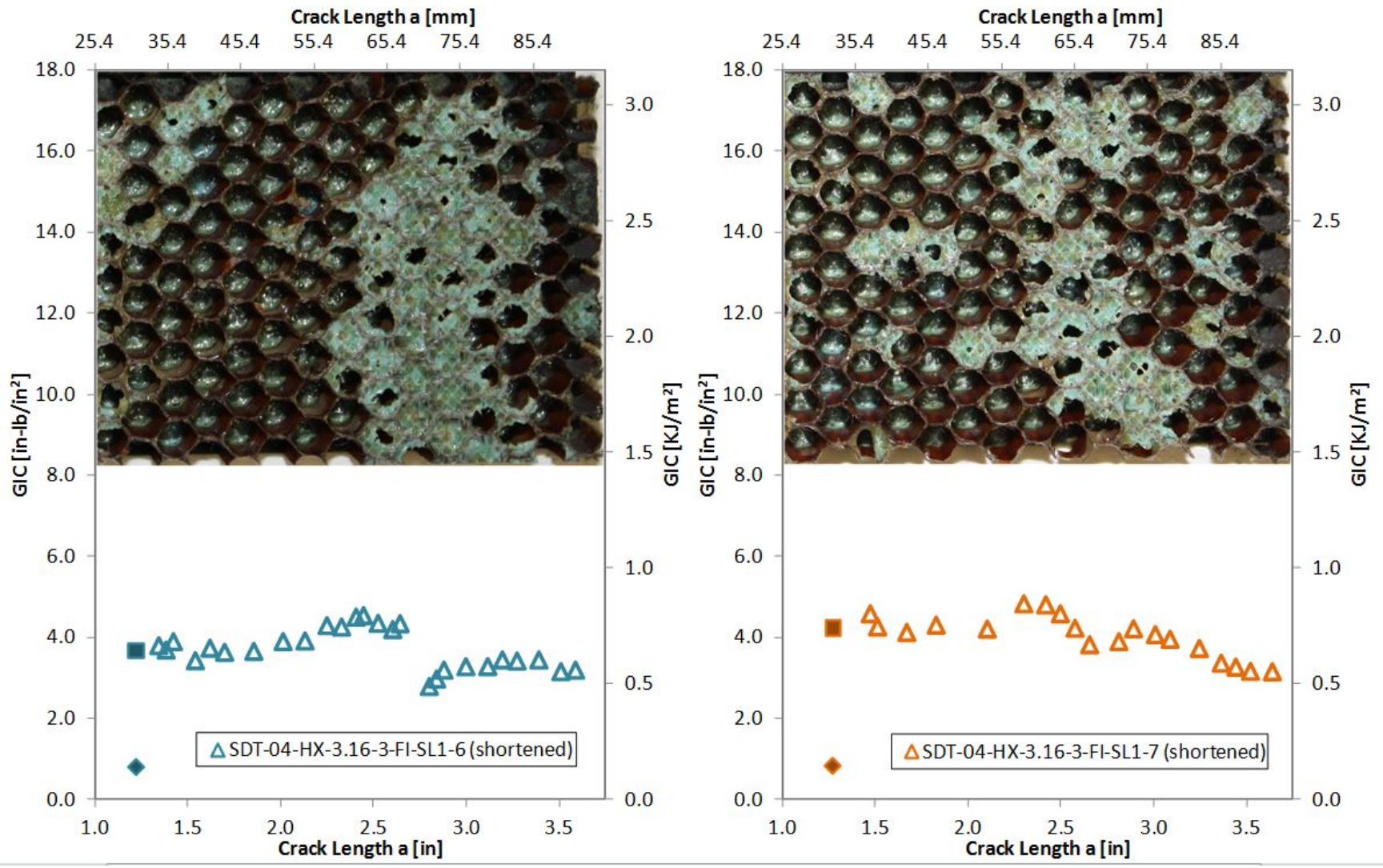

Figure B-58. Failure mode and resistance curve for SDT-04-HX-3.16-3-FI-SL1-X (shortened) #6 and #7

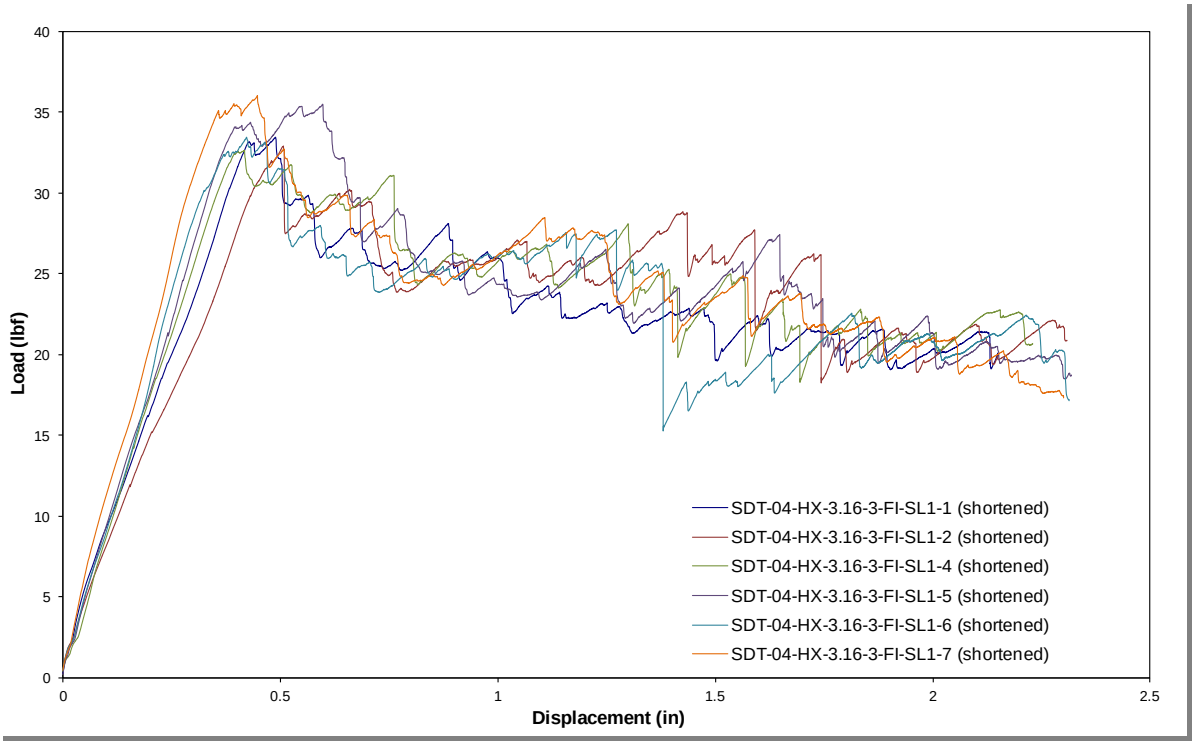

Figure B-59. Load vs. displacement curve for HRH-10–3/16–3.0 fluid ingressed (1″ prescribed crack—shortened)

B.3.3 HRH-10–3/16–3.0 EXTENDED FLUID-INGRESSED DATA

Table B-23. Test summary for HRH-10–3/16–3.0 extended fluid-ingressed (1″ prescribed crack—shortened) pre-crack

Specimen	GIC (in-lb/in^2)			GIC (KJ/m^2)			Failure Mode
	NL	VIS	5%/ max	NL	VIS	5%/ max	
SDT-04-HX-3.16-3-EFI-SL1-7 (shortened)	-	-	-	-	-	-	
SDT-04-HX-3.16-3-EFI-SL1-8 (shortened)	0.757	-	1.607	0.133	-	0.282	First row a mix of PO and C; second row in C
AVERAGE GIC	0.757	-	1.607	0.133	-	0.282	
STANDARD DEVIATION	-	-	-	-	-	-	
COEFFICIENT OF VARIATION (%)	-	-	-	-	-	-	

Table B-24. Test summary for HRH-10–3/16–3.0 extended fluid ingressed (1″ prescribed crack—shortened)

Specimen	GIC (in-lb/in^2)			GIC (KJ/m^2)			Failure Mode
	NL	VIS	5%/ max	NL	VIS	5%/ max	
SDT-04-HX-3.16-3-EFI-SL1-7 (shortened)	-	-	-	-	-	-	
SDT-04-HX-3.16-3-EFI-SL1-8 (shortened)	0.994	-	4.393	0.174	-	0.769	Primarily in C with a couple of cells in A
AVERAGE GIC	0.994	-	4.393	0.174	-	0.769	
STANDARD DEVIATION	-	-	-	-	-	-	
COEFFICIENT OF VARIATION (%)	-	-	-	-	-	-	

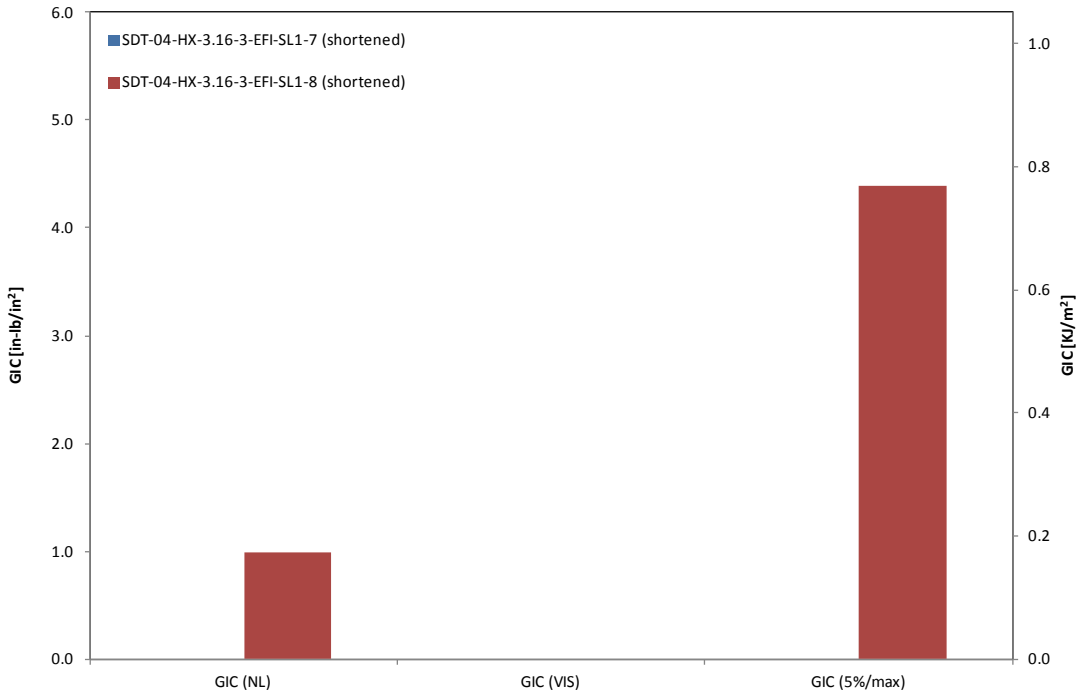

Figure B-60. GIC for HRH-10–3/16–3.0 extended fluid ingressed (1″ prescribed crack—shortened)

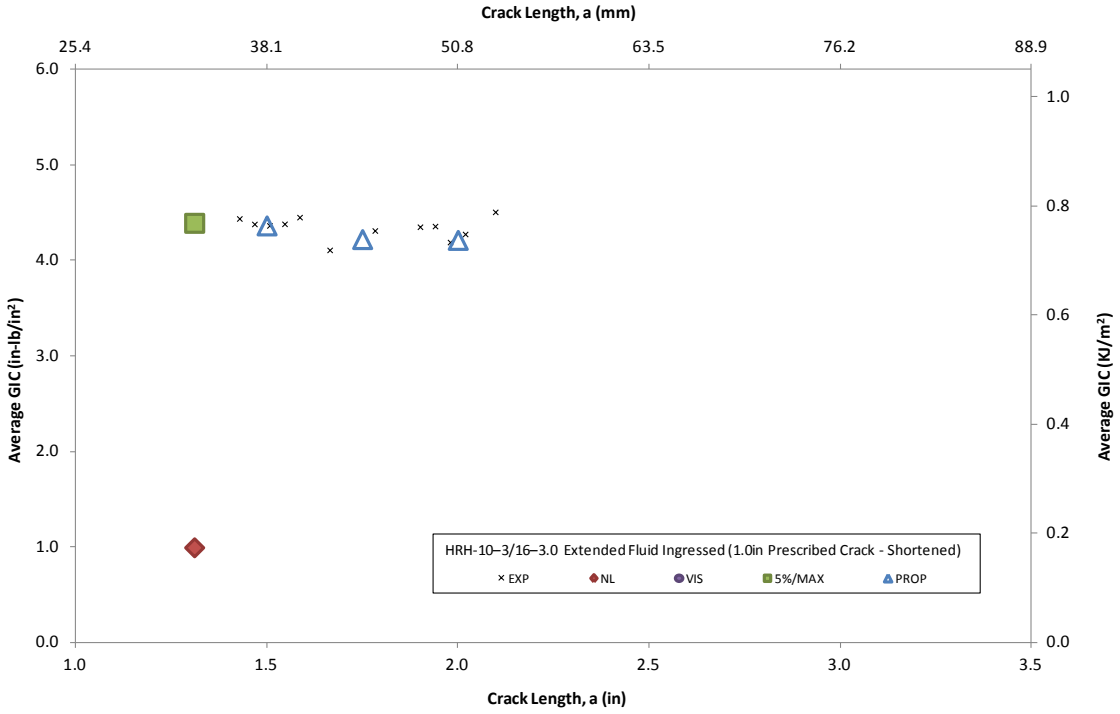

Figure B-61. Resistance curve for HRH-10–3/16–3.0 extended fluid ingressed (1″ prescribed crack—shortened)

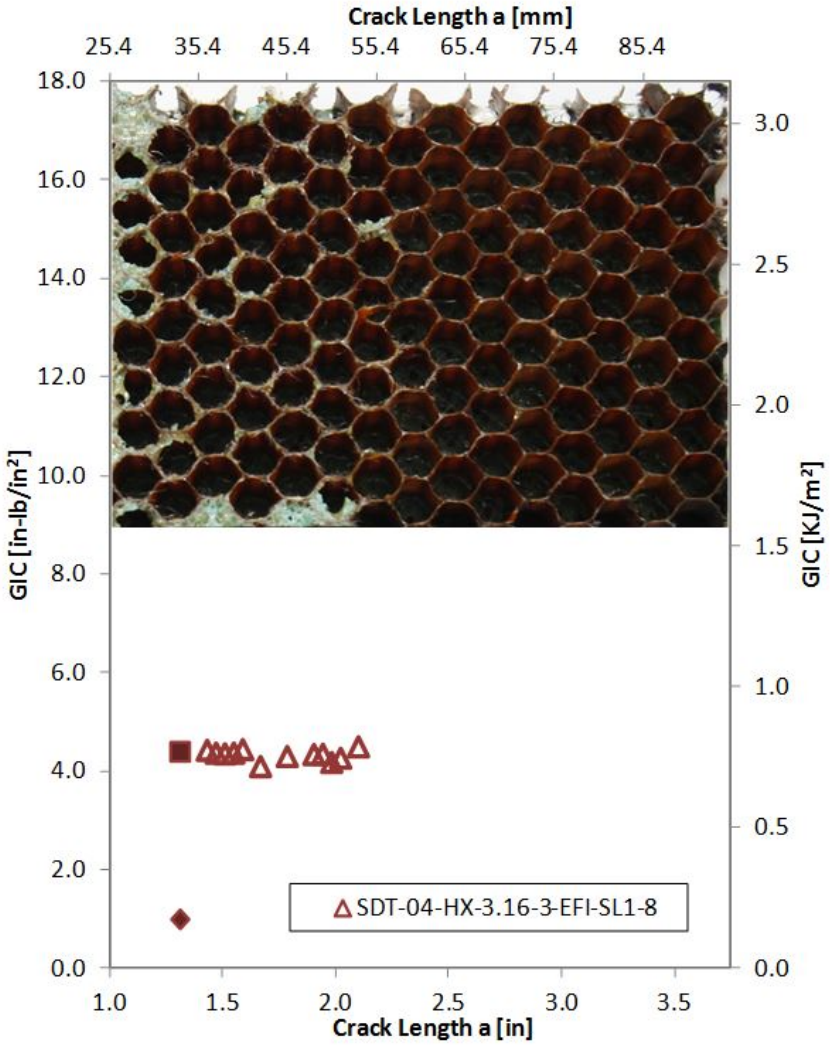

Figure B-62. Failure mode and resistance curve for SDT-04-HX-3.16-3-EFI-SL1-X (shortened) #8

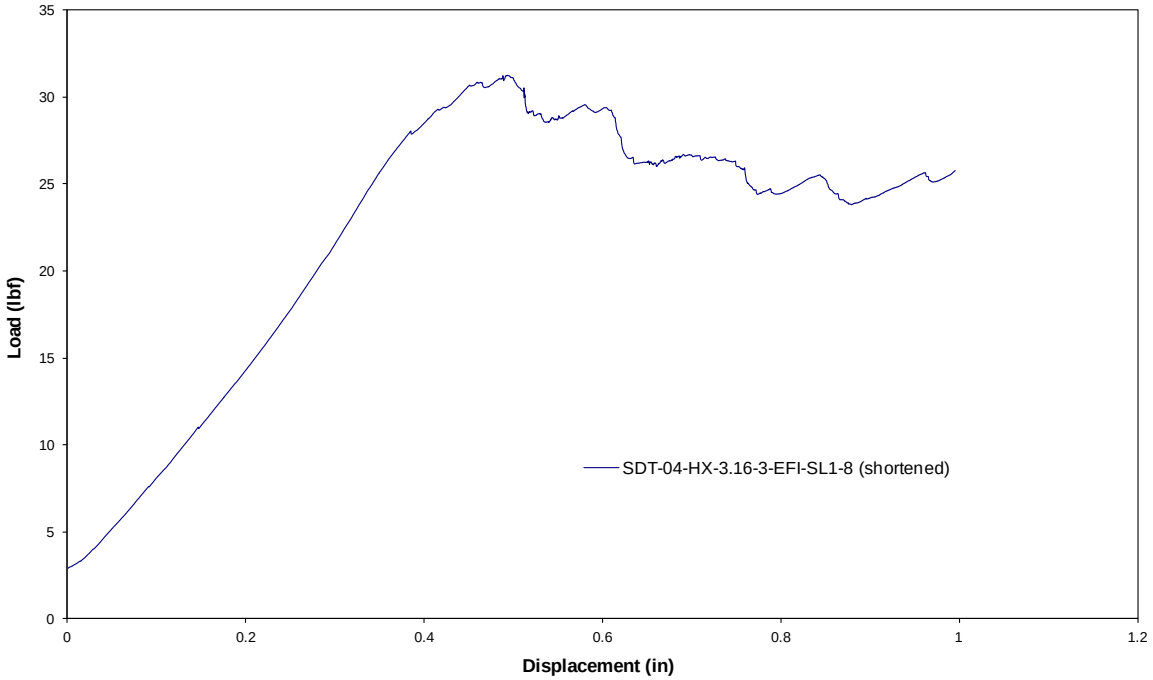

Figure B-63. Load vs. displacement curve for HRH-10–3/16–3.0 extended fluid ingressed (1″ prescribed crack—shortened)

B.4 HRH-10–3/16–6.0 DATA

B.4.1 HRH-10–3/16–6.0 BASELINE DATA

B.4.1.1 HRH-10–3/16–6.0 Baseline Data (2.5″ Prescribed Crack)

Table B-25. Test summary for HRH-10–3/16–6.0 baseline (2″ prescribed crack) pre-crack

Specimen	GIC (in-lb/in^2)			GIC (KJ/m^2)			Failure Mode
	NL	VIS	5%/ max	NL	VIS	5%/ max	
SDT-04-HX-3.16-6-BL-SL1-1	1.362	-	3.391	0.239	-	0.594	Primarily in PO with several cells in A
SDT-04-HX-3.16-6-BL-SL1-2	1.277	-	3.957	0.224	-	0.693	Primarily in PO with several cells in A
SDT-04-HX-3.16-6-BL-SL1-3	1.446	-	3.546	0.253	-	0.621	Primarily in PO with several cells in A
SDT-04-HX-3.16-6-BL-SL1-4	1.279	-	3.446	0.224	-	0.603	Primarily in PO with multiple cells in A
SDT-04-HX-3.16-6-BL-SL1-5	1.346	-	3.333	0.236	-	0.584	Primarily in PO with multiple cells in A
SDT-04-HX-3.16-6-BL-SL1-6	1.450	-	3.371	0.254	-	0.590	Primarily in PO with several cells in A
AVERAGE GIC	1.360	-	3.507	0.238	-	0.614	
STANDARD DEVIATION	0.076	-	0.232	0.013	-	0.041	
COEFFICIENT OF VARIATION (%)	5.601	-	6.621	5.601	-	6.621	

Table B-26. Test summary for HRH-10–3/16–6.0 baseline (2.5″ prescribed crack)

Specimen	GIC (in-lb/in^2)			GIC (KJ/m^2)			Failure Mode
	NL	VIS	5%/ max	NL	VIS	5%/ max	
SDT-04-HX-3.16-6-BL-SL1-1	0.456	1.558	2.071	0.080	0.273	0.363	Mix of A and PO
SDT-04-HX-3.16-6-BL-SL1-2	0.646	-	2.524	0.113	-	0.442	Mix of A and PO
SDT-04-HX-3.16-6-BL-SL1-3	0.585	-	2.349	0.102	-	0.411	Primarily PO with several cells in A
SDT-04-HX-3.16-6-BL-SL1-4	0.524	1.632	1.976	0.092	0.286	0.346	Primarily PO with several cells in A
SDT-04-HX-3.16-6-BL-SL1-5	0.676	2.305	2.343	0.118	0.404	0.410	Primarily PO with several cells in A
SDT-04-HX-3.16-6-BL-SL1-6	0.689	2.555	2.835	0.121	0.447	0.496	Primarily PO with several cells in A
AVERAGE GIC	0.596	2.012	2.349	0.104	0.352	0.411	
STANDARD DEVIATION	0.092	0.494	0.285	0.016	0.086	0.050	
COEFFICIENT OF VARIATION (%)	14.218	24.539	12.123	15.407	24.539	12.123	

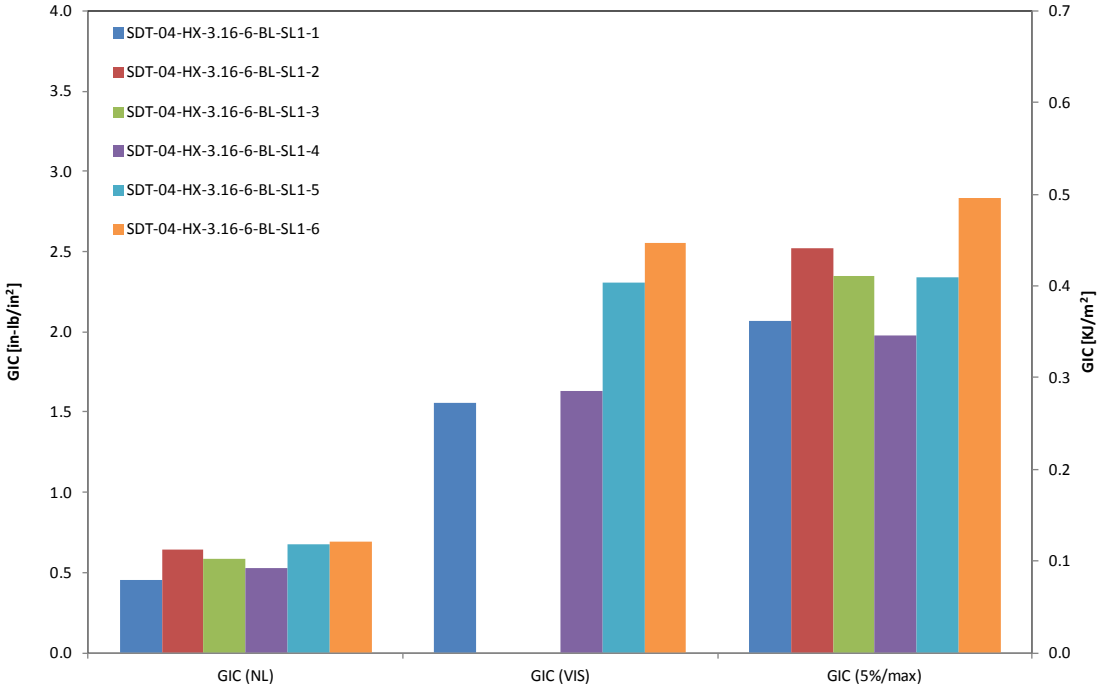

Figure B-64. GIC for HRH-10–3/16–6.0 baseline (2.5″ prescribed crack)

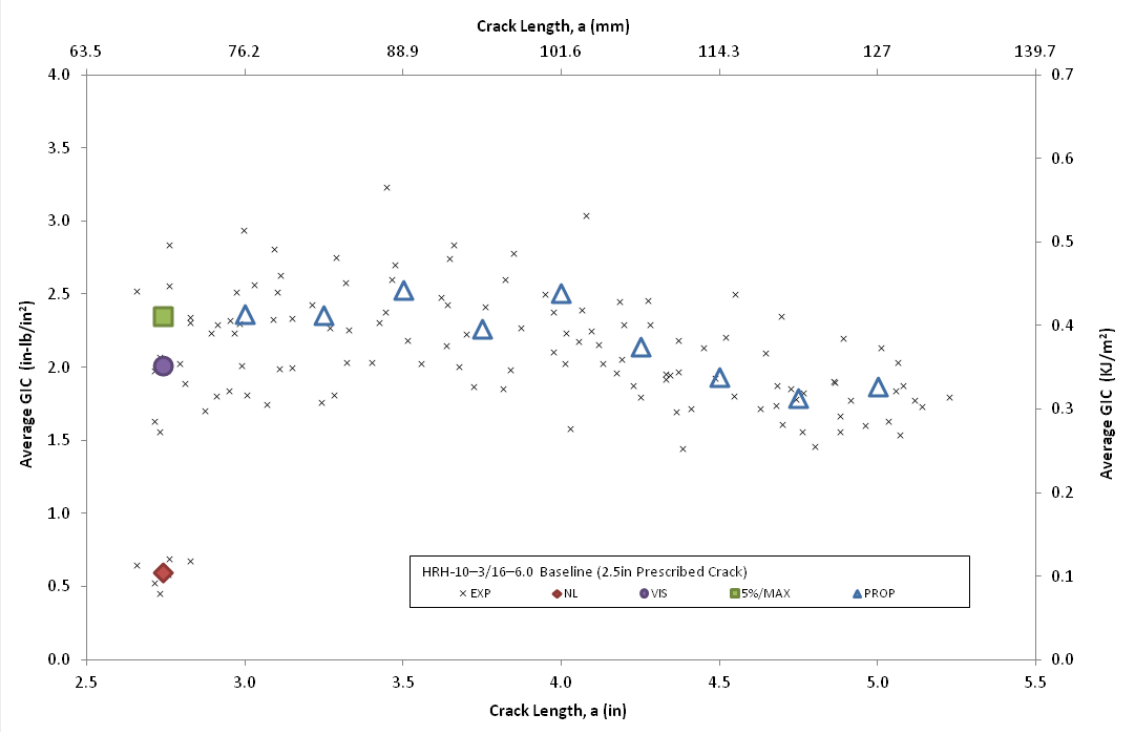

Figure B-65. Resistance curve for HRH-10–3/16–6.0 baseline (2.5″ prescribed crack)

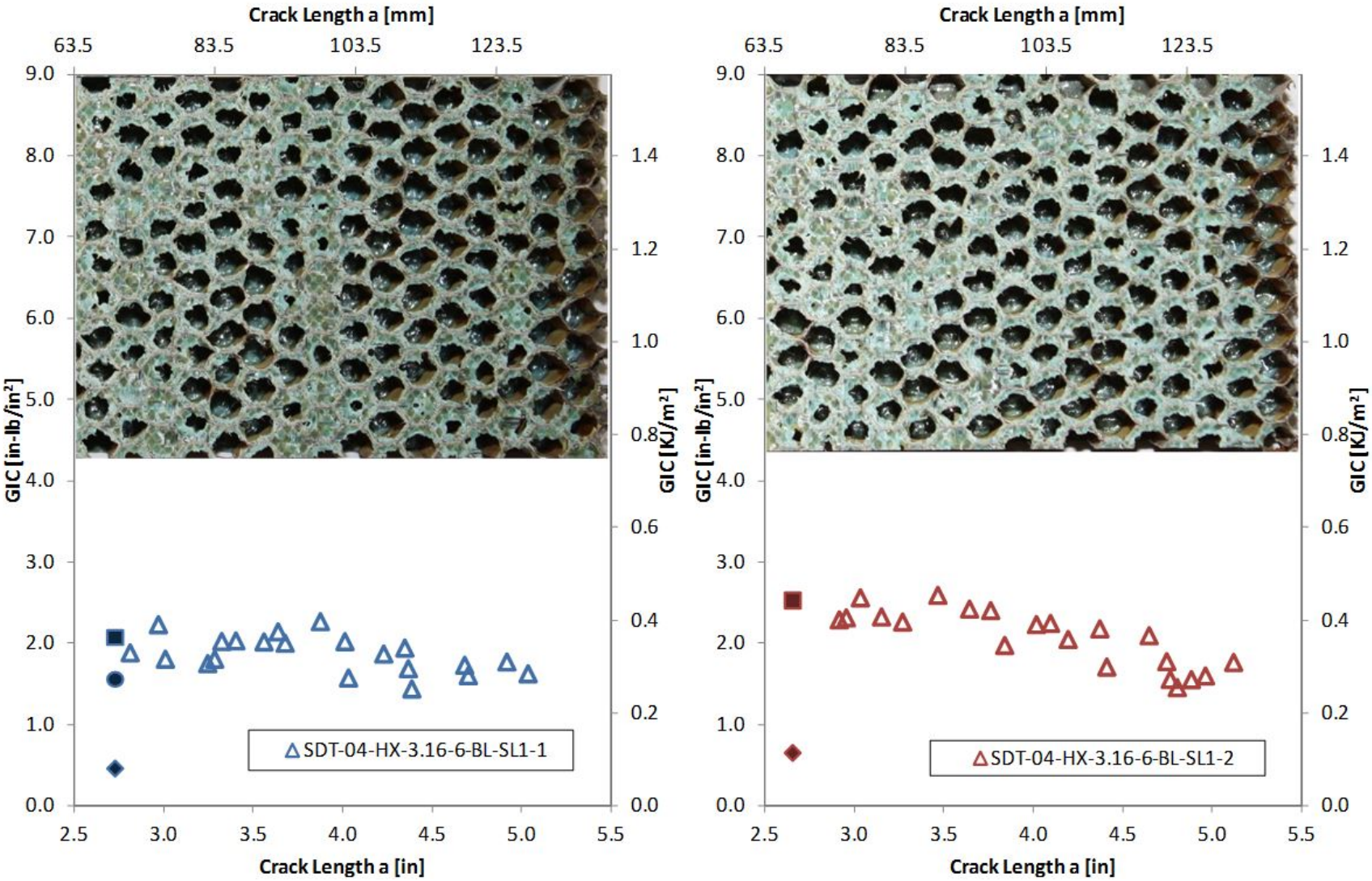

Figure B-66. Failure mode and resistance curve for SDT-04-HX-3.16-6-BL-SL1-X #1 and #2

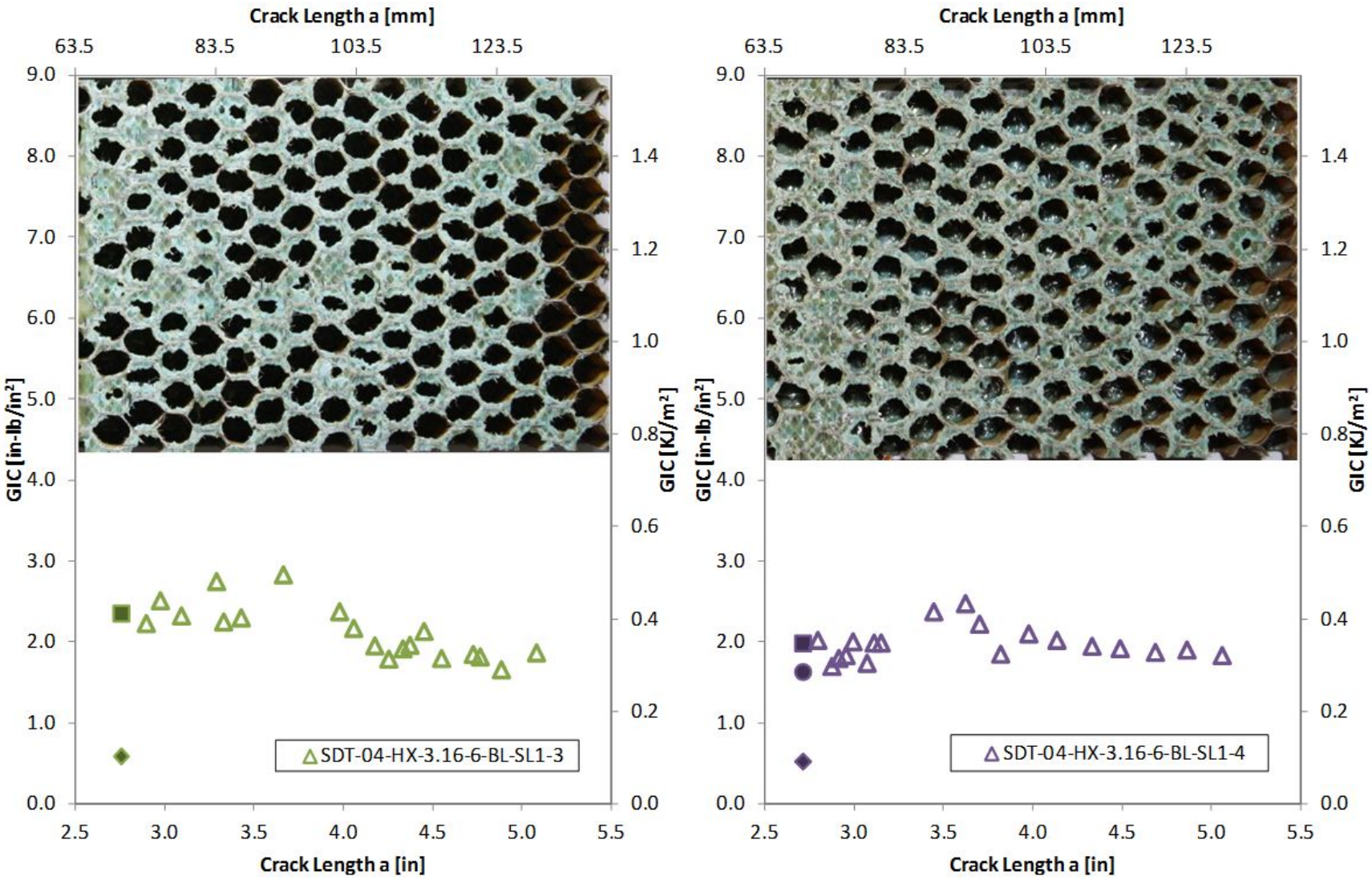

Figure B-67. Failure mode and resistance curve for SDT-04-HX-3.16-6-BL-SL1-X #3 and #4

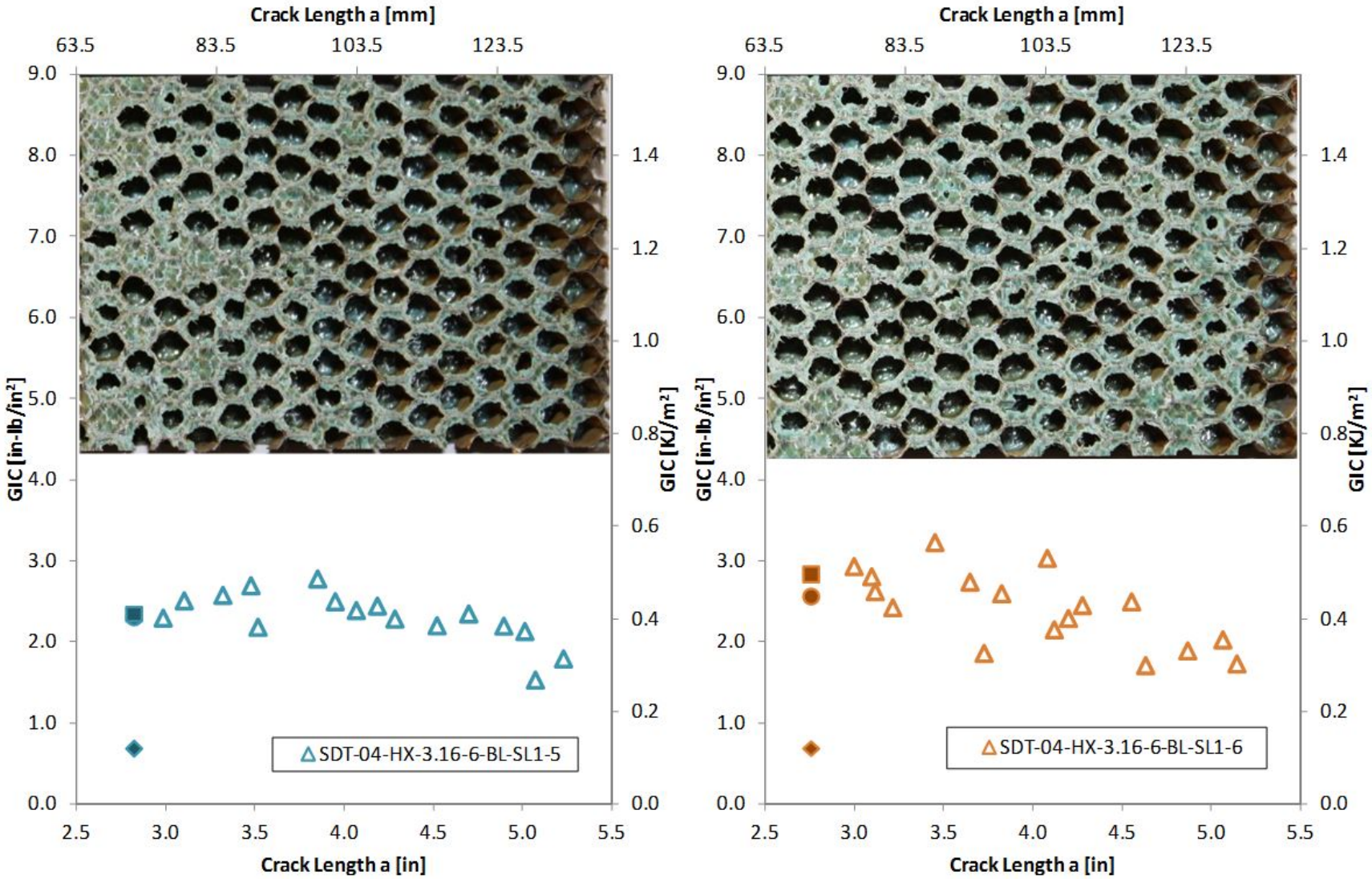

Figure B-68. Failure mode and resistance curve for SDT-04-HX-3.16-6-BL-SL1-X #5 and #6

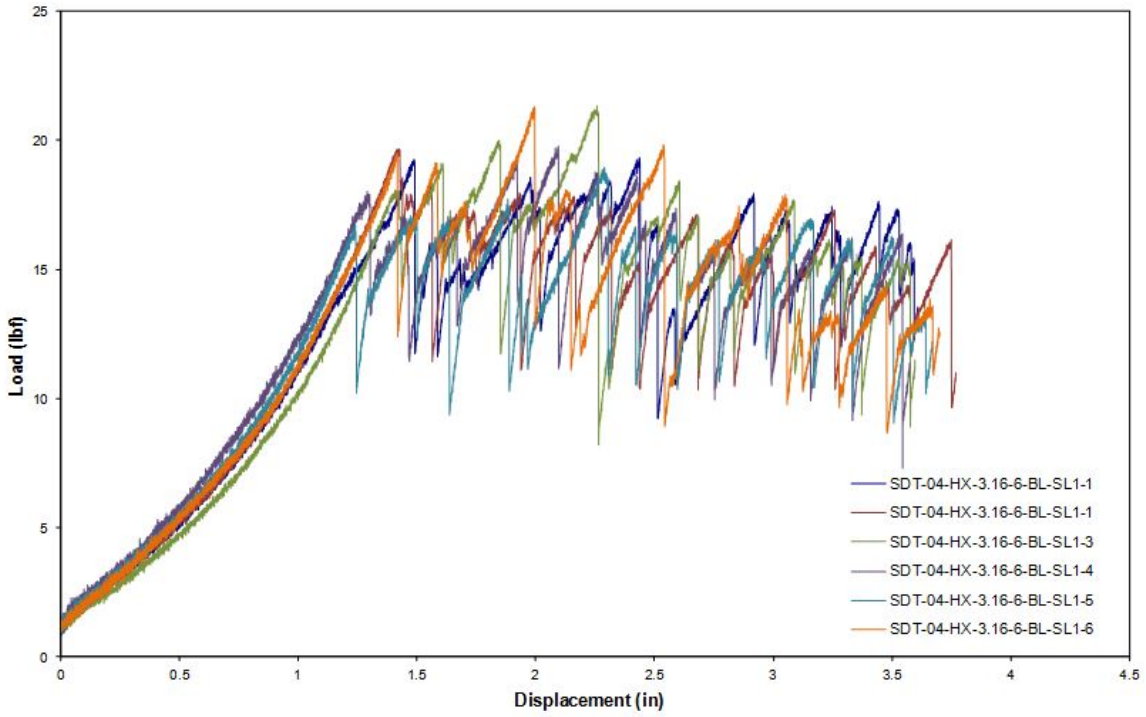

Figure B-69. Load vs. displacement curve for HRH-10–3/16–6.0 baseline (2.5″ prescribed crack)

B.4.1.2 HRH-10–3/16–6.0 Baseline Data (1″ Prescribed Crack—Shortened)

Table B-27. Test summary for HRH-10–3/16–6.0 baseline (1″ prescribed crack—shortened) pre-crack

Specimen	GIC (in-lb/in^2)			GIC (KJ/m^2)			Failure Mode
	NL	VIS	5%/ max	NL	VIS	5%/ max	
SDT-04-HX-3.16-6-BL-SL1-7 (shortened)	2.012	-	3.260	0.352	-	0.571	First row primarily A with a couple of cells in PO; second row a mix of A and PO
SDT-04-HX-3.16-6-BL-SL1-8 (shortened)	2.263	-	3.588	0.396	0.503	0.628	First row primarily in A with a couple of cells in PO; second row in PO
SDT-04-HX-3.16-6-BL-SLX-7 (shortened)	2.625	-	4.622	0.460	-	0.809	Mix of A and PO
AVERAGE GIC	2.300	-	3.823	0.403	-	0.670	
STANDARD DEVIATION	0.009	-	0.031	0.054	-	0.124	
COEFFICIENT OF VARIATION (%)	13.404	-	18.595	13.404	-	18.595	

Table B-28. Test summary for HRH-10–3/16–6.0 baseline (1″ prescribed crack—shortened)

Specimen	GIC (in-lb/in^2)			GIC (KJ/m^2)			Failure Mode
	NL	VIS	5%/max	NL	VIS	5%/max	
SDT-04-HX-3.16-6-BL-SL1-7 (shortened)	1.357	-	2.417	0.238	-	0.423	Primarily in PO with occasional pockets of A
SDT-04-HX-3.16-6-BL-SL1-8 (shortened)	0.865	-	3.242	0.152	-	0.568	Primarily PO
SDT-04-HX-3.16-6-BL-SLX-7 (shortened)	0.836	3.246	3.321	0.146	0.568	0.582	Primarily PO with a couple cells in A
AVERAGE GIC	1.020	3.246	2.993	0.179	0.568	0.524	
STANDARD DEVIATION	0.009	-	0.031	0.051	-	0.088	
COEFFICIENT OF VARIATION (%)	28.717	-	16.727	28.717	-	16.727	

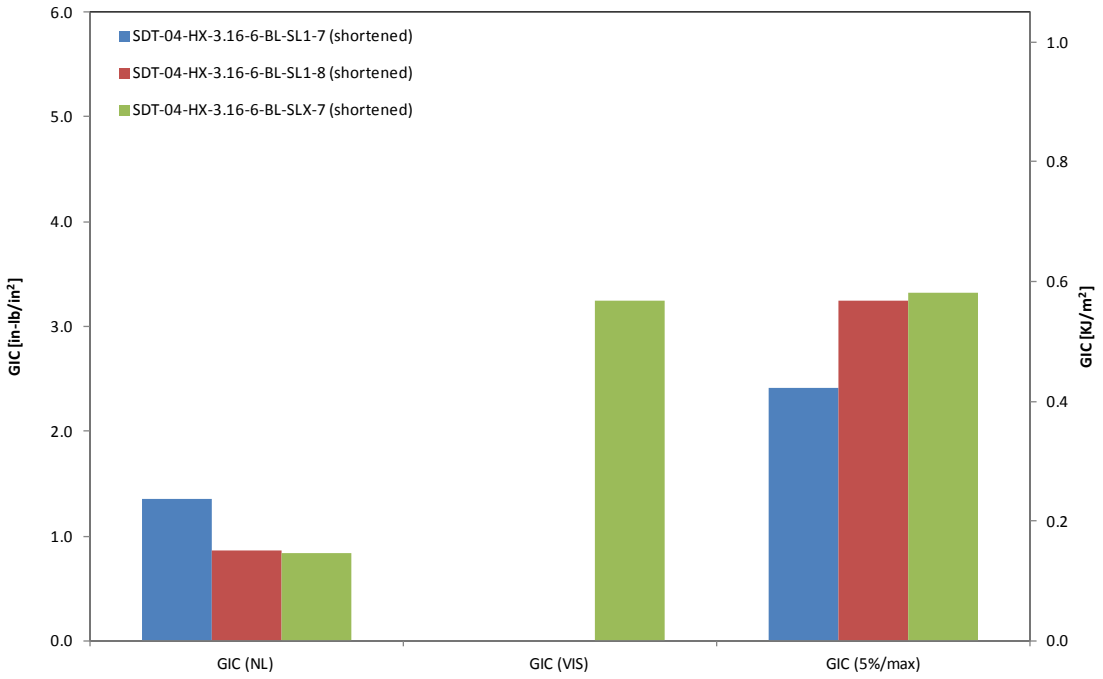

Figure B-70. GIC for HRH-10–3/16–6.0 baseline (1″ prescribed crack—shortened)

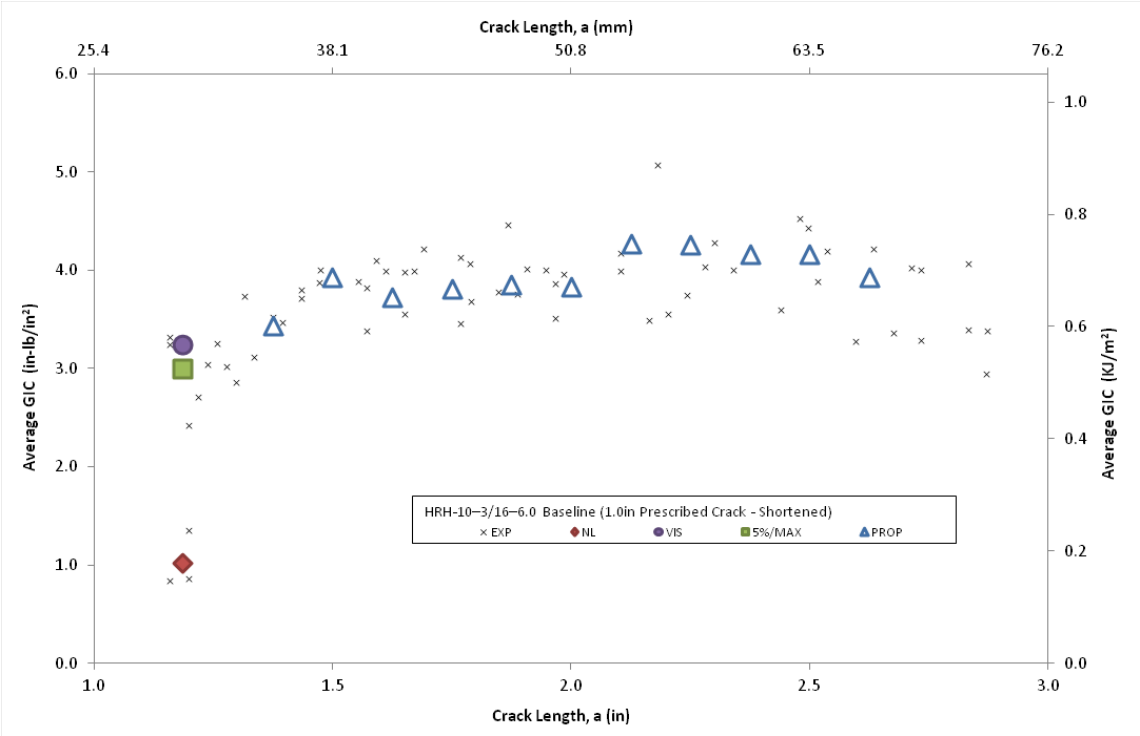

Figure B-71. Resistance curve for HRH-10–3/16–6.0 baseline (1″ prescribed crack—shortened)

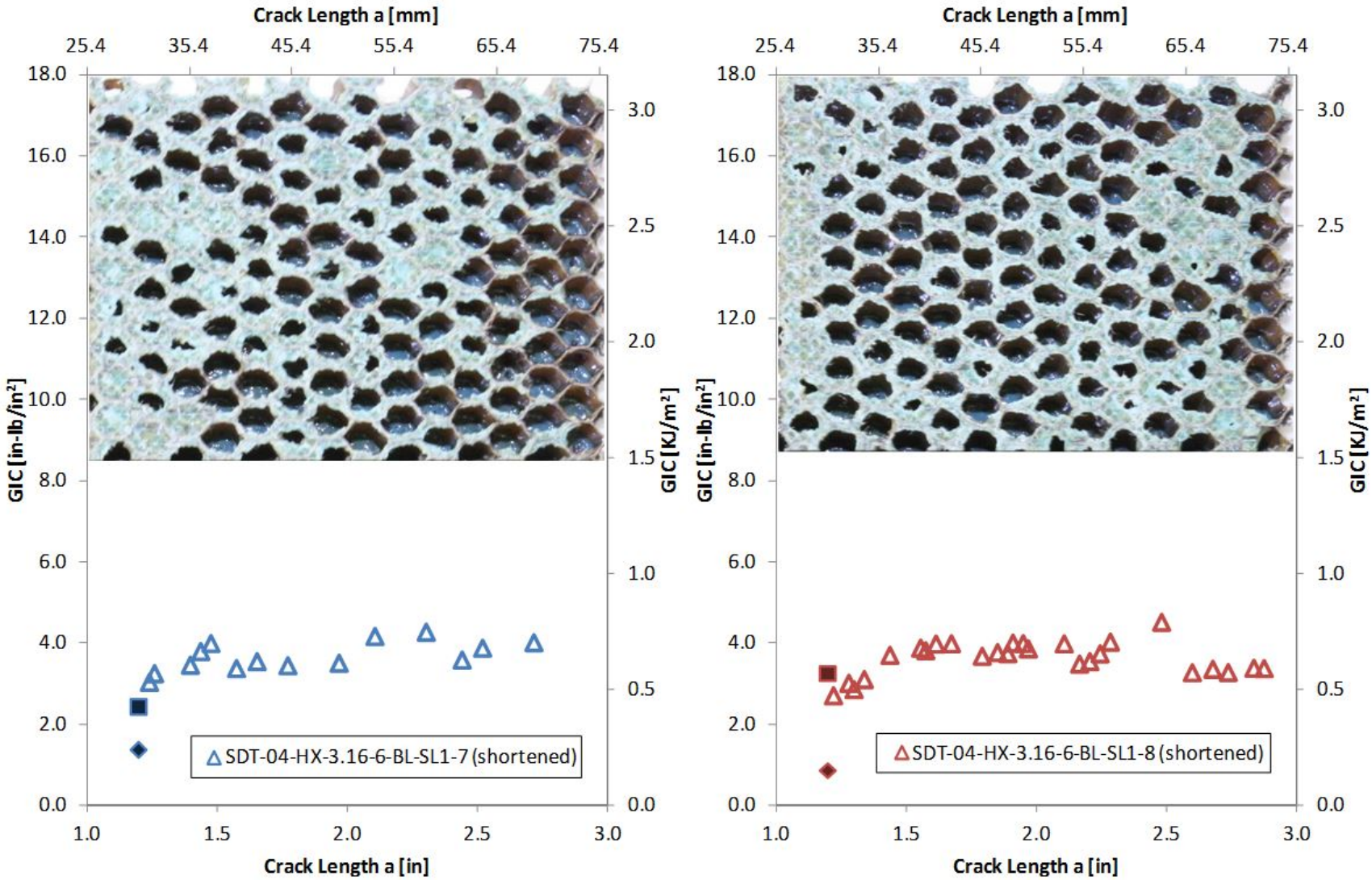

Figure B-72. Failure mode and resistance curve for SDT-04-HX-3.16-6-BL-SL1-X (shortened) #6 and #7

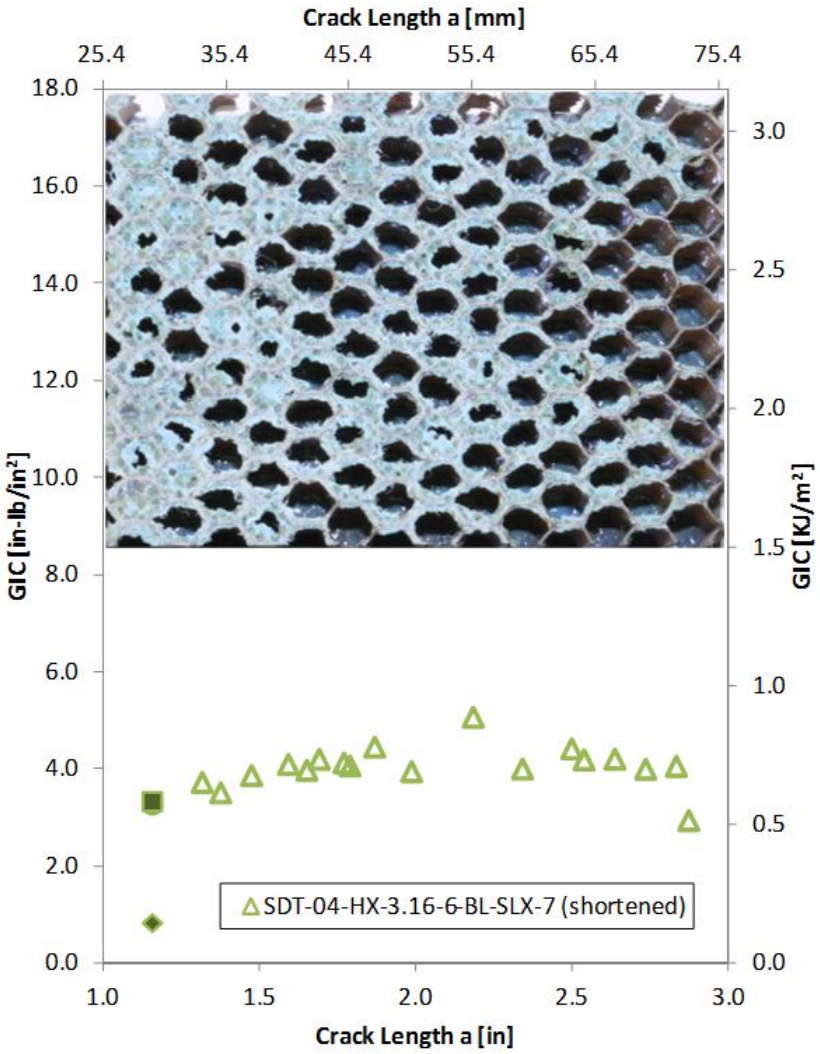

Figure B-73. Failure mode and resistance curve for SDT-04-HX-3.16-6-BL-SLX-X (shortened) #7

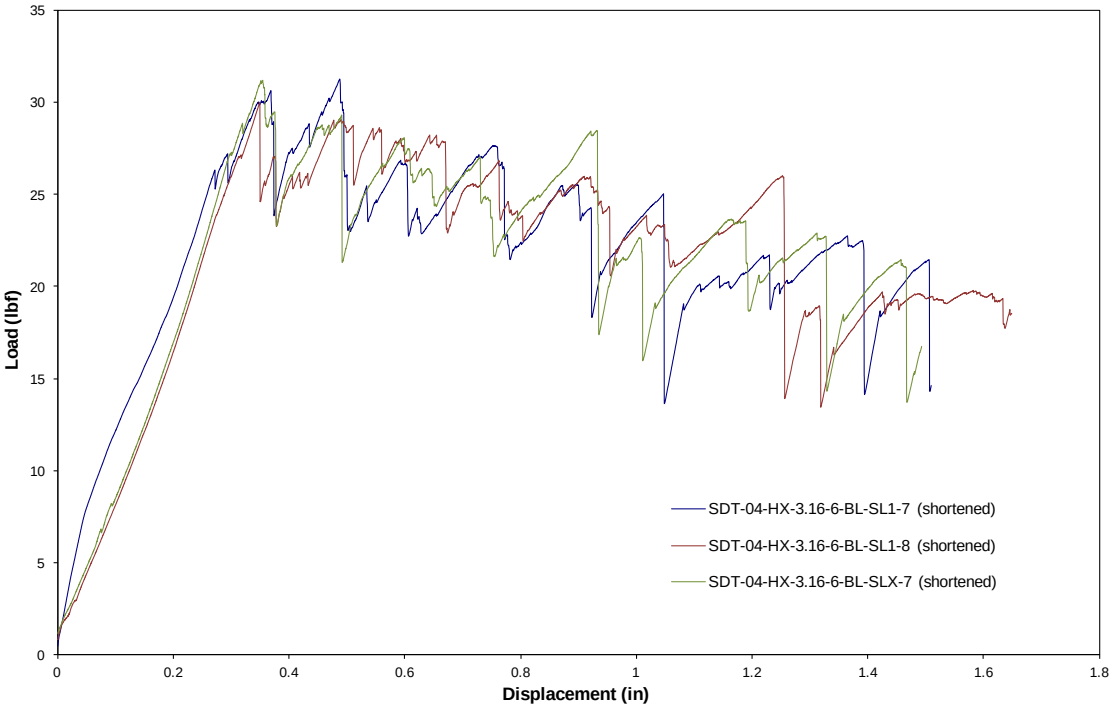

Figure B-74. Load vs. displacement curve for HRH-10–3/16–6.0 baseline (1″ prescribed crack—shortened)

B.4.2. HRH-10–3/16–6.0 FLUID-INGRESSED DATA

Table B-29. Test summary for HRH-10–3/16–6.0 fluid ingressed (1″ prescribed crack—shortened) pre-crack

Specimen	GIC (in-lb/in^2)			GIC (KJ/m^2)			Failure Mode
	NL	VIS	5%/ max	NL	VIS	5%/ max	
SDT-04-HX-3.16-6-FI-SL1-1 (shortened)	1.445	-	3.453	0.253	-	0.605	Primarily in PO with several cells in A
SDT-04-HX-3.16-6-FI-SL1-2 (shortened)	0.992	-	4.507	0.174	-	0.789	Primarily in PO with a couple of cells in A
SDT-04-HX-3.16-6-FI-SL1-3 (shortened)	1.618	-	4.195	0.283	-	0.735	Primarily in PO with several cells in A
SDT-04-HX-3.16-6-FI-SL1-4 (shortened)	1.152	-	4.994	0.202	-	0.875	Primarily in PO with a couple of cells in A
SDT-04-HX-3.16-6-FI-SL1-5 (shortened)	1.503	-	5.252	0.263	-	0.920	Primarily in PO with a few cells in A
SDT-04-HX-3.16-6-FI-SL1-6 (shortened)	1.683	-	6.170	0.295	-	1.081	Primarily in PO with several cells in A
AVERAGE GIC	1.399	-	4.762	0.245	-	0.834	
STANDARD DEVIATION	0.272	-	0.936	0.048	-	0.164	
COEFFICIENT OF VARIATION (%)	19.417	-	19.650	19.417	-	19.650	

Table B-30. Test summary for HRH-10–3/16–6.0 fluid ingressed (1″ prescribed crack—shortened)

Specimen	GIC (in-lb/in^2)			GIC (KJ/m^2)			Failure Mode
	NL	VIS	5%/ max	NL	VIS	5%/ max	
SDT-04-HX-3.16-6-FI-SL1-1 (shortened)	0.663	4.116	4.684	0.116	0.721	0.820	Primarily in PO with a few cells in A
SDT-04-HX-3.16-6-FI-SL1-2 (shortened)	0.908	5.192	6.321	0.159	0.909	1.107	Primarily in PO
SDT-04-HX-3.16-6-FI-SL1-3 (shortened)	0.614	3.373	3.942	0.107	0.591	0.690	Primarily in PO with a few cells in A
SDT-04-HX-3.16-6-FI-SL1-4 (shortened)	0.636	-	3.721	0.111	-	0.652	Primarily in PO with a few cells in A
SDT-04-HX-3.16-6-FI-SL1-5 (shortened)	0.777	-	4.231	0.136	-	0.741	Primarily in PO with a few cells in A
SDT-04-HX-3.16-6-FI-SL1-6 (shortened)	0.572	4.144	6.103	0.100	0.726	1.069	Primarily in PO with a few cells in A
AVERAGE GIC	0.695	4.206	4.834	0.122	0.737	0.847	
STANDARD DEVIATION	0.125	0.748	1.117	0.022	0.131	0.196	
COEFFICIENT OF VARIATION (%)	18.020	17.784	23.114	18.020	17.784	23.114	

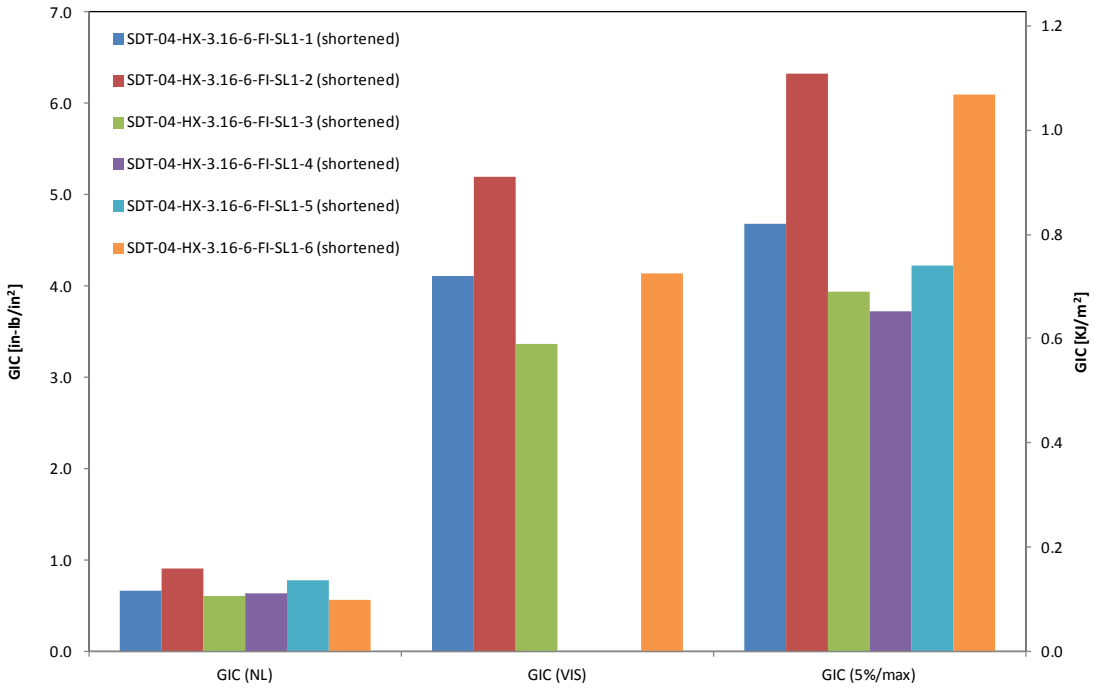

Figure B-75. GIC for HRH-10–3/16–6.0 fluid ingressed (1″ prescribed crack—shortened)

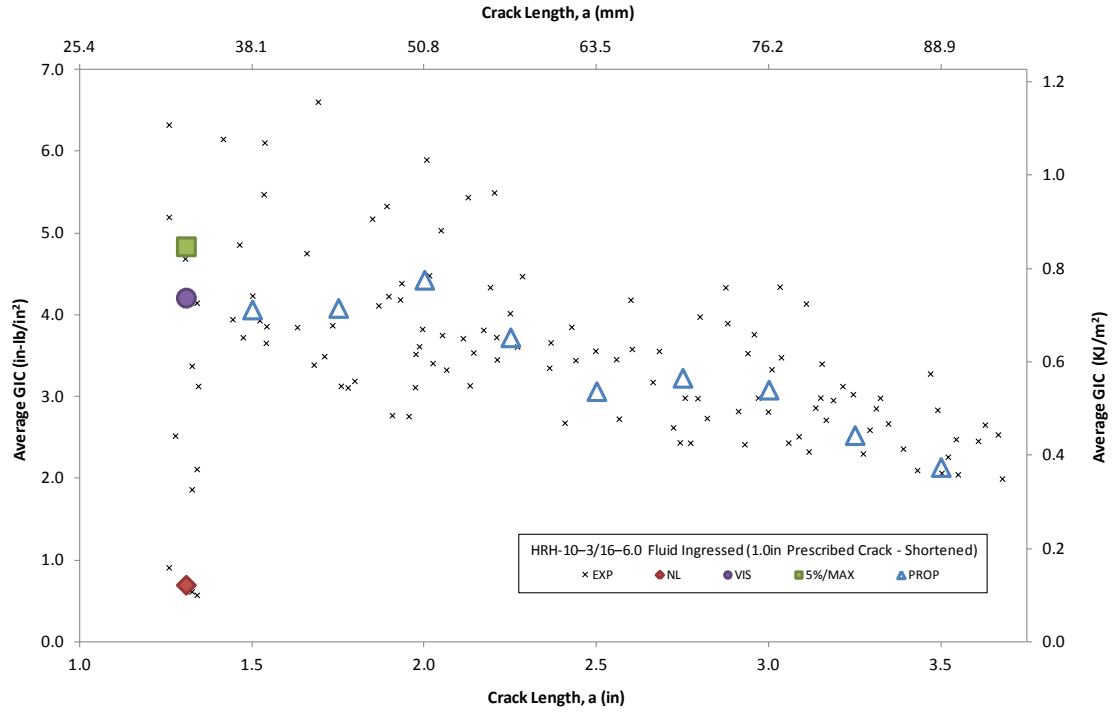

Figure B-76. Resistance curve for HRH-10–3/16–6.0 fluid ingressed (1″ prescribed crack—shortened)

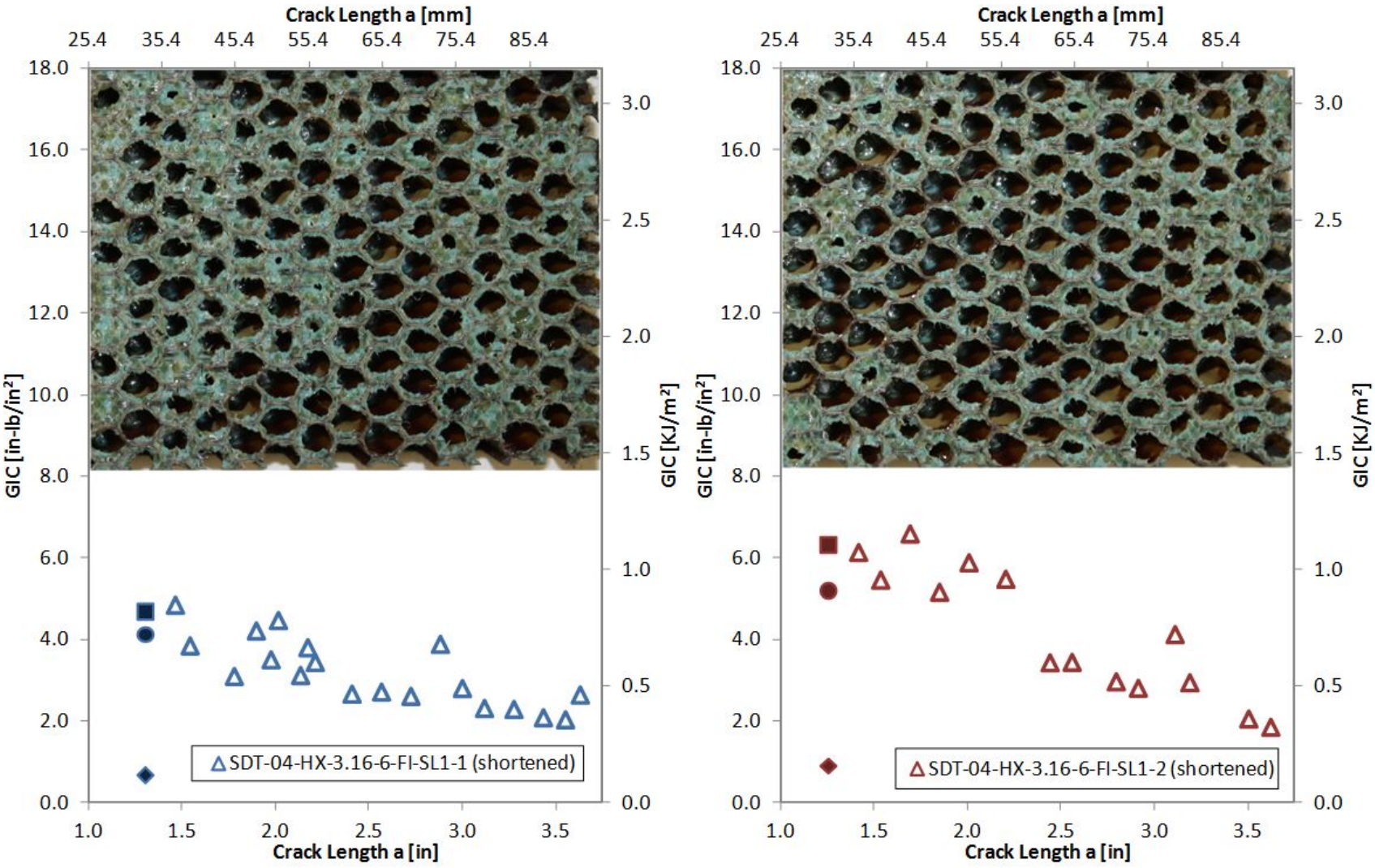

Figure B-77. Failure mode and resistance curve for SDT-04-HX-3.16-6-FI -SL1-X (shortened) #1 and #2

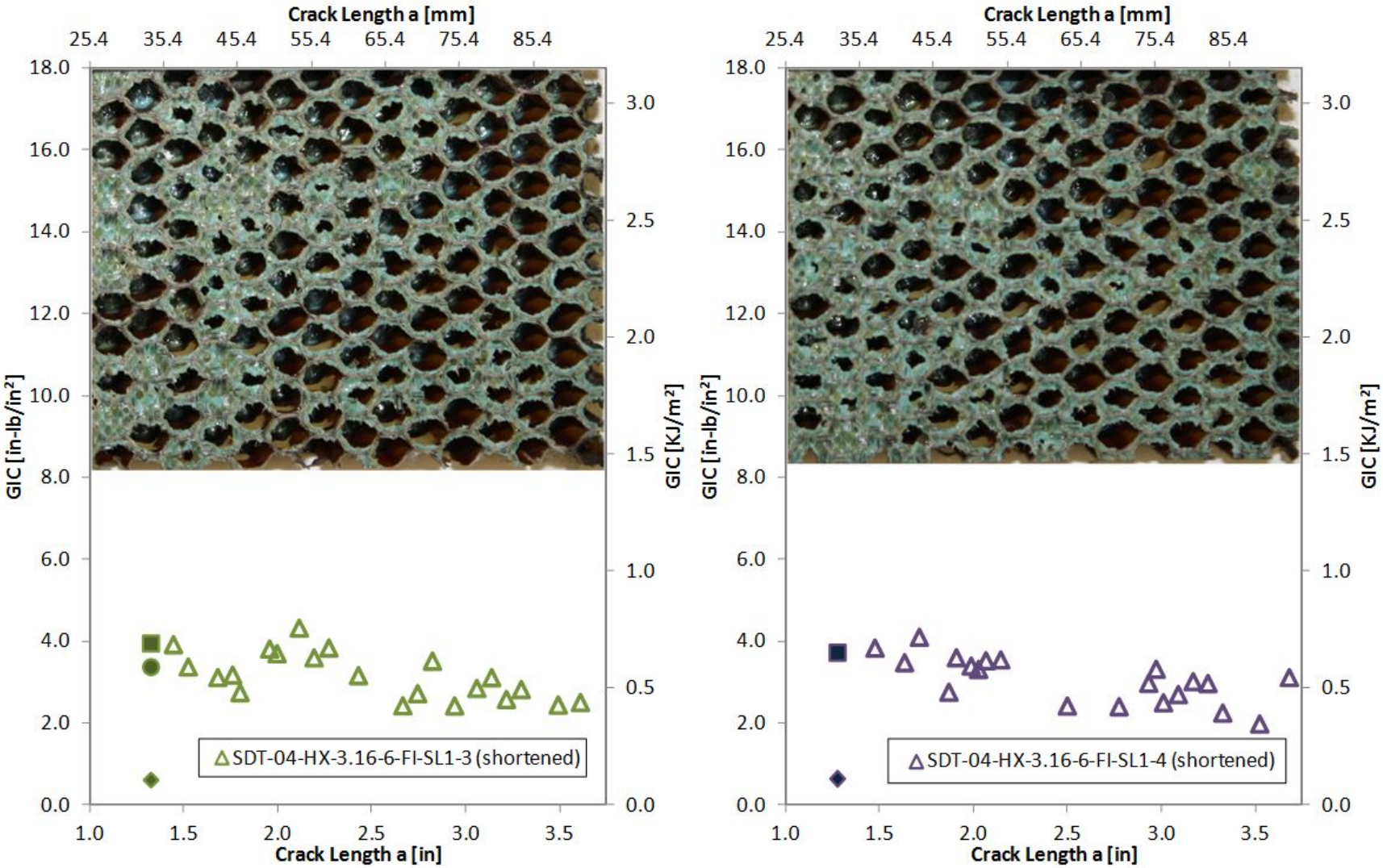

Figure B-78. Failure mode and resistance curve for SDT-04-HX-3.16-6-FI -SL1-X (shortened) #3 and #4

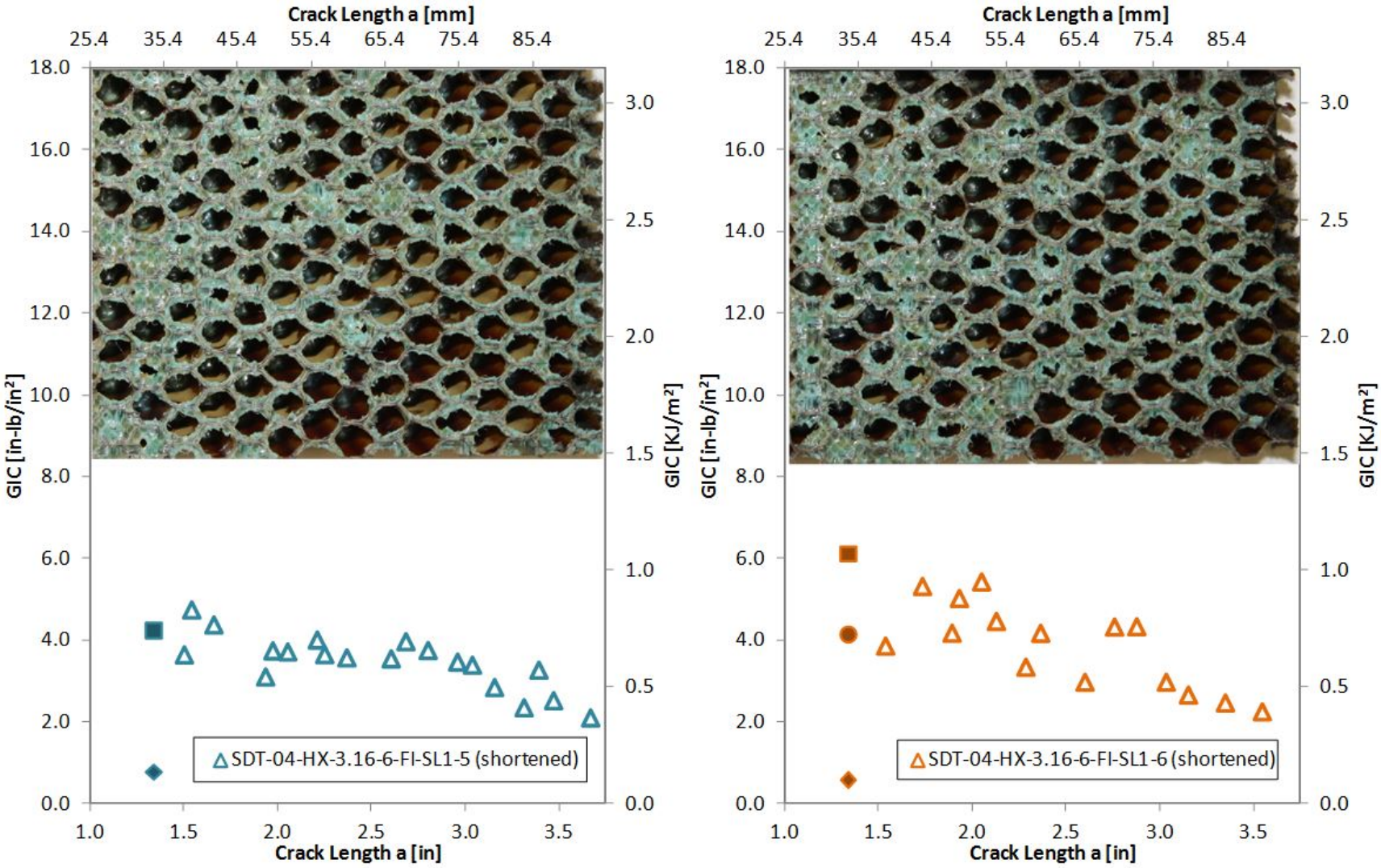

Figure B-79. Failure mode and resistance curve for SDT-04-HX-3.16-6-FI -SL1-X (shortened) #5 and #6

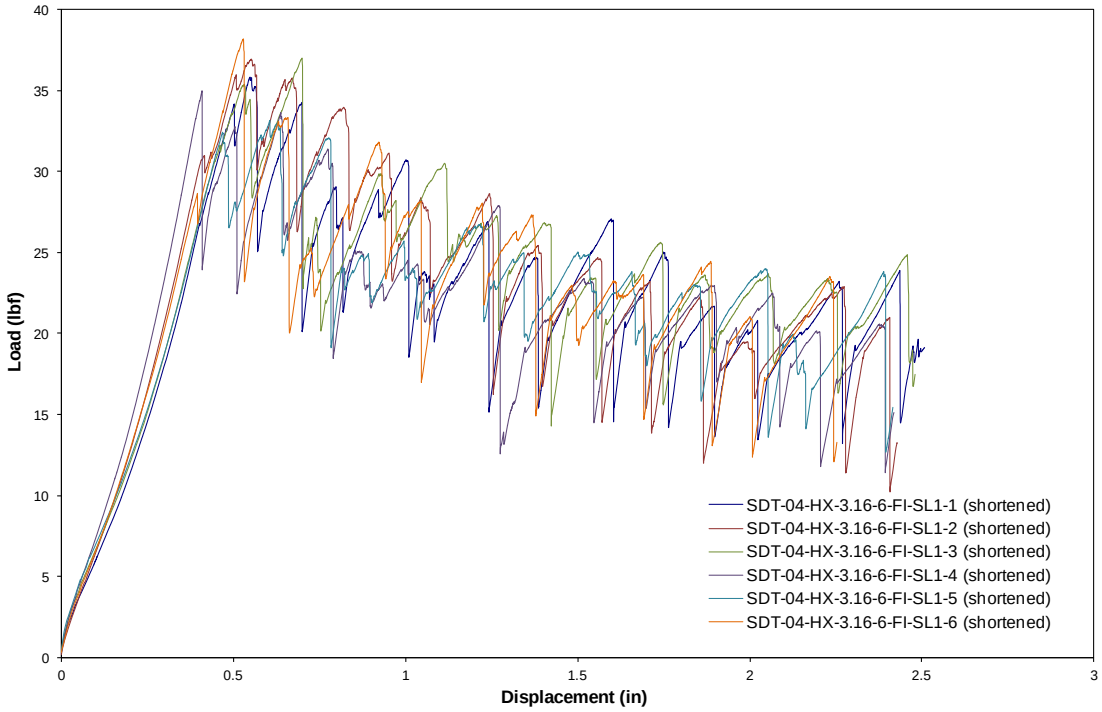

Figure B-80. Load vs. displacement curve for HRH-10–3/16–6.0 fluid ingressed (1″ prescribed crack—shortened)

B.4.3 HRH-10–3/16–6.0 EXTENDED FLUID-INGRESSED DATA

Table B-31. Test summary for HRH-10–3/16–6.0 extended fluid ingressed (1″ prescribed crack—shortened) pre-crack

Specimen	GIC (in-lb/in^2)			GIC (KJ/m^2)			Failure Mode
	NL	VIS	5%/max	NL	VIS	5%/max	
SDT-04-HX-3.16-6-EFI-SL1-7 (shortened)	1.778	-	3.237	0.311	-	0.567	Primarily in PO
SDT-04-HX-3.16-6-EFI-SL1-8 (shortened)	1.301	-	3.800	0.228	-	0.665	Primarily in PO
AVERAGE GIC	1.540	-	3.518	0.270	-	0.616	
STANDARD DEVIATION	0.337	-	0.398	0.059	-	0.070	
COEFFICIENT OF VARIATION (%)	21.882	-	11.310	21.882	-	11.310	

Table B-32. Test summary for HRH-10–3/16–6.0 extended fluid ingressed (1″ prescribed crack—shortened)

Specimen	GIC (in-lb/in^2)			GIC (KJ/m^2)			Failure Mode
	NL	VIS	5%/ max	NL	VIS	5%/ max	
SDT-04-HX-3.16-6-EFI-SL1-7 (shortened)	0.668	-	5.454	0.117	-	0.955	Primarily in PO
SDT-04-HX-3.16-6-EFI-SL1-8 (shortened)	0.425	-	5.304	0.074	-	0.929	Primarily in PO
AVERAGE GIC	0.547	-	5.379	0.096	-	0.942	
STANDARD DEVIATION	0.172	-	0.106	0.030	-	0.019	
COEFFICIENT OF VARIATION (%)	31.497	-	1.968	31.497	-	1.968	

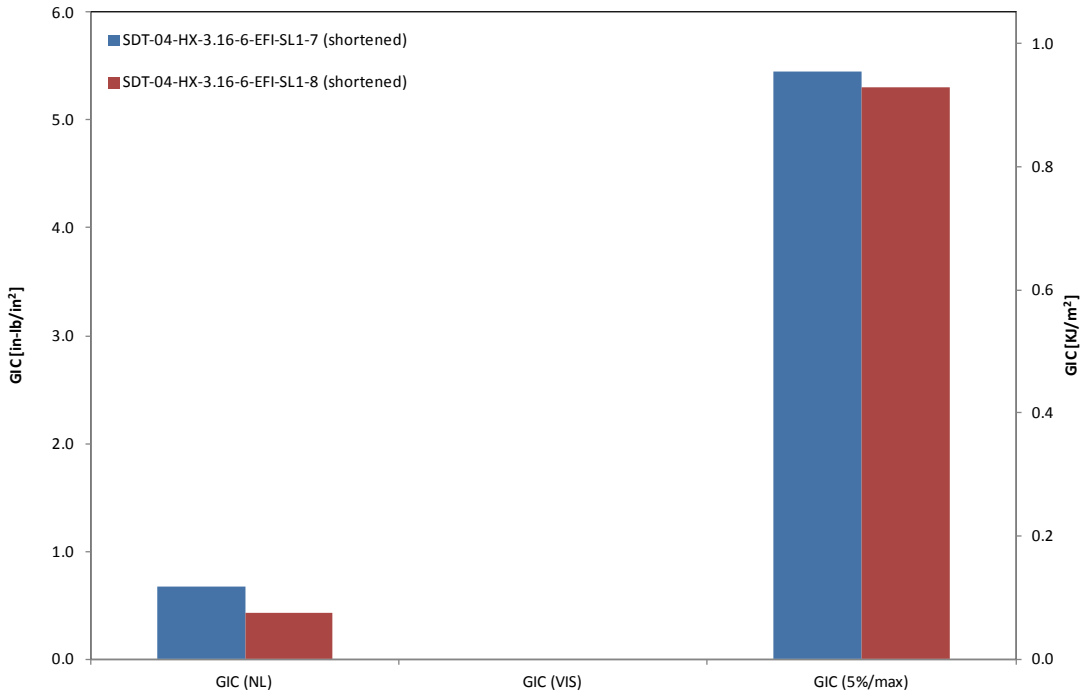

Figure B-81. GIC for HRH-10–3/16–6.0 extended fluid ingressed (1″ prescribed crack—shortened)

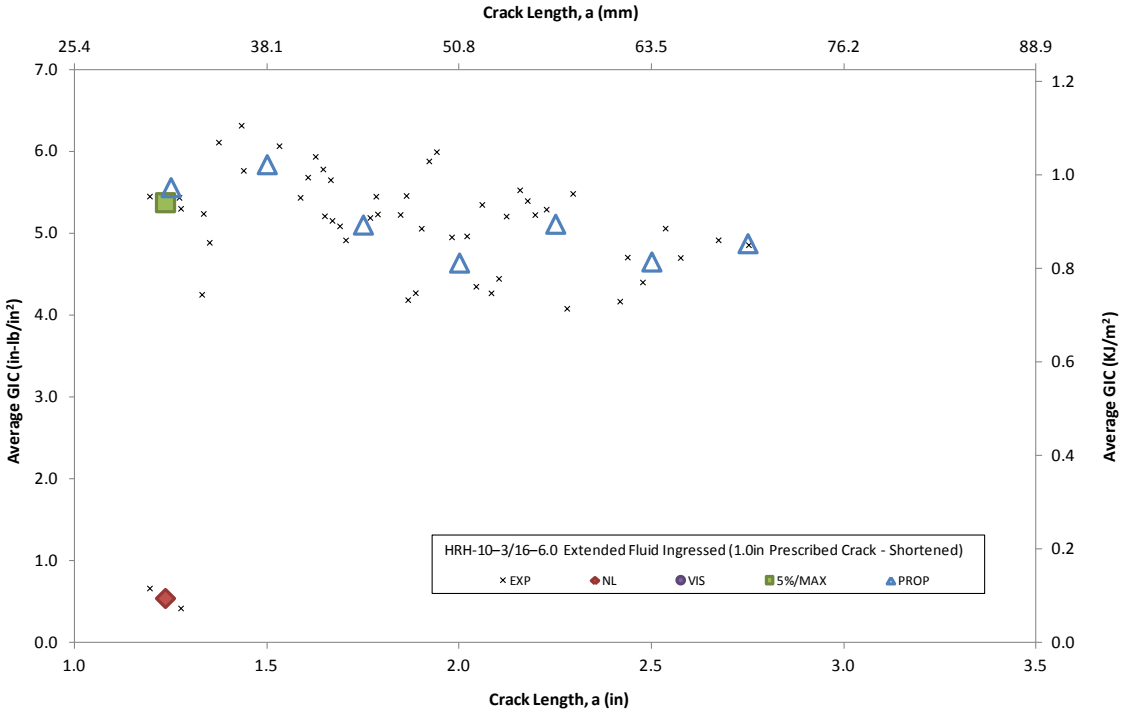

Figure B-82. Resistance curve for HRH-10–3/16–6.0 extended fluid ingressed (1″ prescribed crack—shortened)

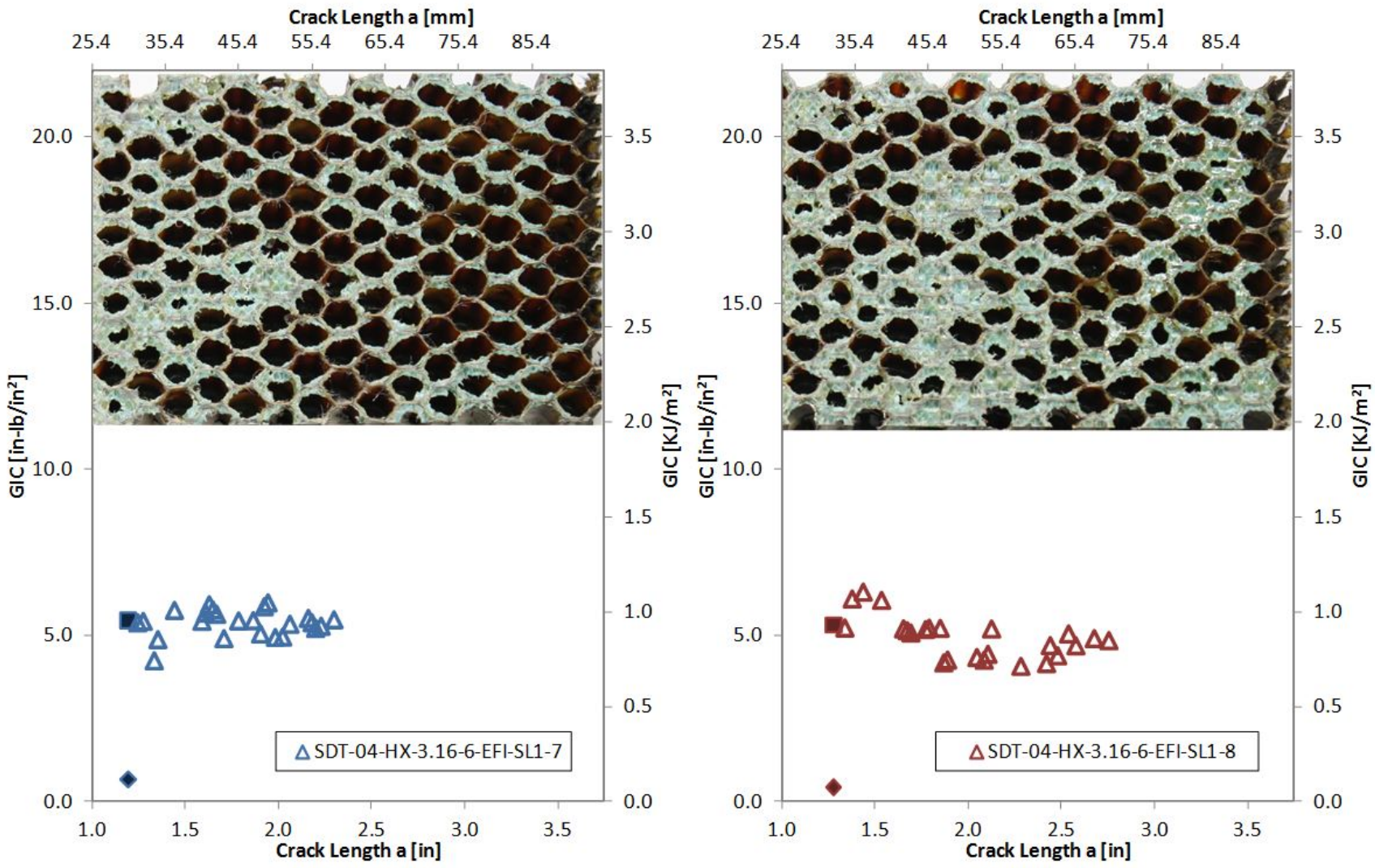

Figure B-83. Failure mode and resistance curve for SDT-04-HX-3.16-6-EFI-SL1-X (shortened) #7 and #8

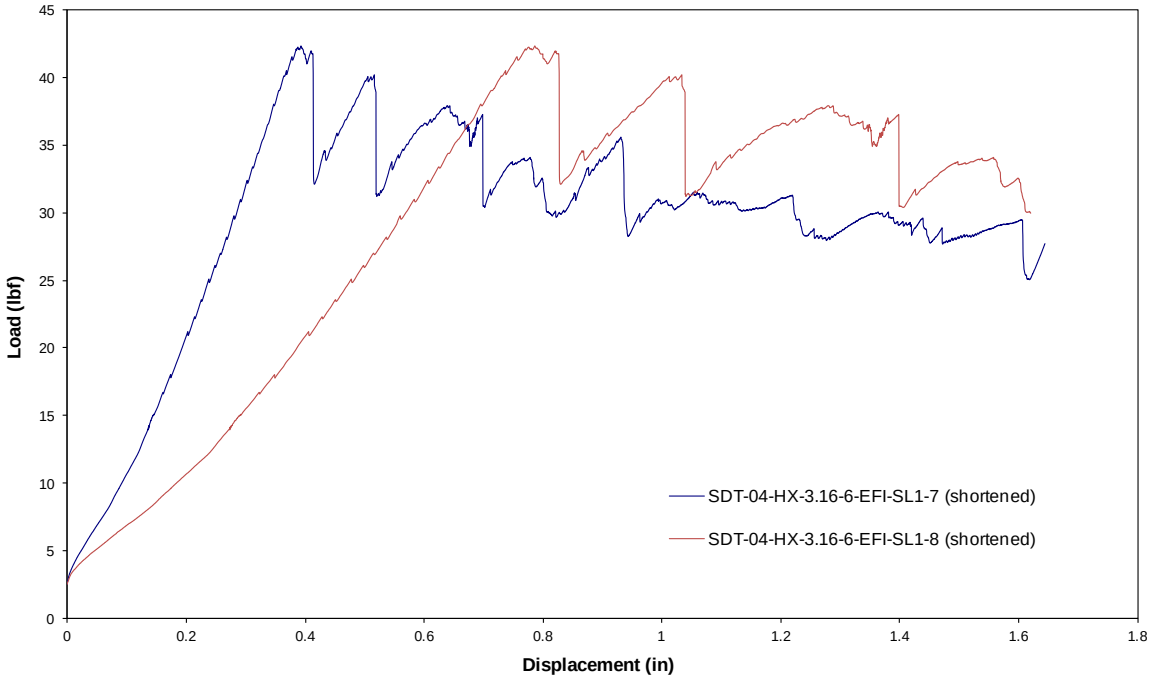

Figure B-84. Load vs. displacement curve for HRH-10–3/16–6.0 extended fluid ingressed (1″ prescribed crack—shortened)

B.5 HRH-10–3/8–3.0 DATA

B.5.1 HRH-10–3/8–3.0 BASELINE DATA

B.5.1.1 HRH-10–3/8–3.0 Baseline Data (2.5″ Prescribed Crack)

Table B-33. Test summary for HRH-10–3/8–3.0 baseline (2.5″ prescribed crack) pre-crack

Specimen	GIC (in-lb/in^2)			GIC (KJ/m^2)			Failure Mode
	NL	VIS	5%/ max	NL	VIS	5%/ max	
SDT-04-HX-3.8-3-BL-SL1-1	0.940	-	3.081	0.165	-	0.539	Primarily PO
SDT-04-HX-3.8-3-BL-SL1-2	1.118	-	3.336	0.196	-	0.584	Primarily PO
SDT-04-HX-3.8-3-BL-SL1-3	1.315	-	3.350	0.230	-	0.587	Primarily PO
SDT-04-HX-3.8-3-BL-SL1-4	0.983	-	2.909	0.172	-	0.510	Primarily PO
SDT-04-HX-3.8-3-BL-SL1-5	1.392	-	2.313	0.244	-	0.405	Primarily PO
SDT-04-HX-3.8-3-BL-SL1-6	1.601	-	2.236	0.280	-	0.392	Primarily PO
AVERAGE GIC	1.225	-	2.871	0.215	-	0.503	
STANDARD DEVIATION	0.256	-	0.491	0.045	-	0.086	
COEFFICIENT OF VARIATION (%)	20.940	-	17.113	20.940	-	17.113	

Table B-34. Test summary for HRH-10–3/8–3.0 baseline (2.5″ prescribed crack)

Specimen	GIC (in-lb/in^2)			GIC (KJ/m^2)			Failure Mode
	NL	VIS	5%/ max	NL	VIS	5%/ max	
SDT-04-HX-3.8-3-BL-SL1-1	0.868	-	2.445	0.152	-	0.428	Primarily PO
SDT-04-HX-3.8-3-BL-SL1-2	0.737	-	3.016	0.129	-	0.528	Primarily PO
SDT-04-HX-3.8-3-BL-SL1-3	0.854	-	3.927	0.150	-	0.688	Primarily PO
SDT-04-HX-3.8-3-BL-SL1-4	0.893	3.149	3.512	0.156	0.551	0.615	Primarily PO with a couple of cells in C on edges
SDT-04-HX-3.8-3-BL-SL1-5	0.812	-	3.031	0.142	-	0.531	Primarily PO with one cell in A
SDT-04-HX-3.8-3-BL-SL1-6	0.567	-	2.251	0.099	-	0.394	Primarily PO
AVERAGE GIC	0.788	3.149	3.030	0.138	0.551	0.531	
STANDARD DEVIATION	0.122	-	0.630	0.021	-	0.110	
COEFFICIENT OF VARIATION (%)	15.420	-	20.802	15.420	-	20.802	

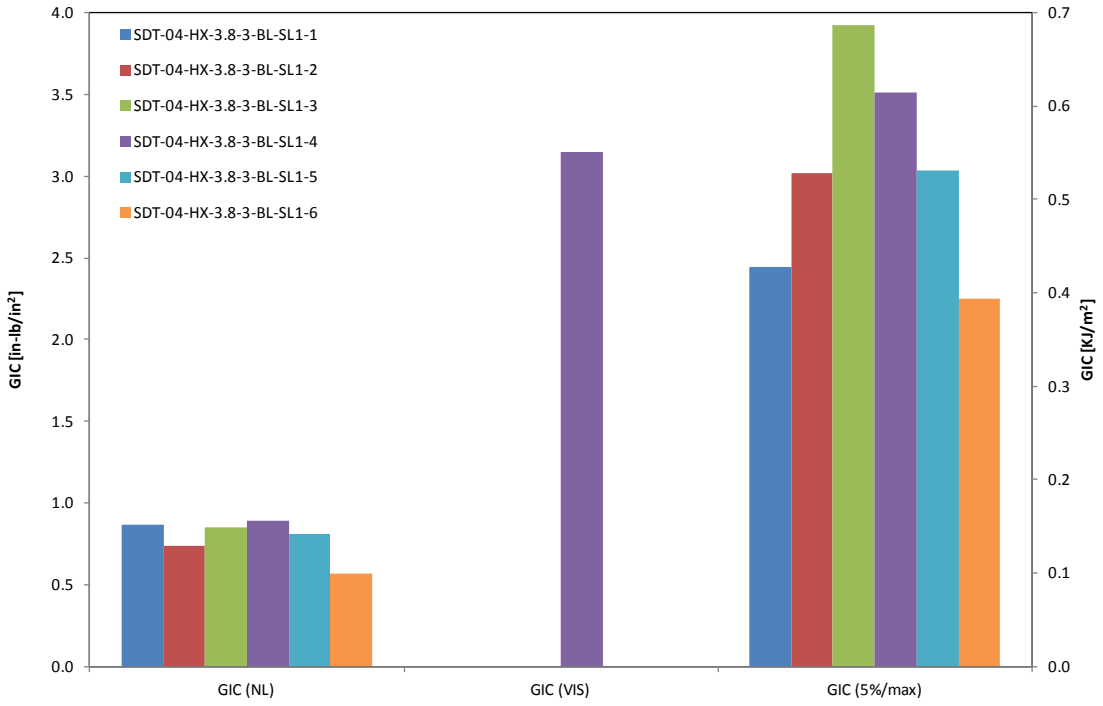

Figure B-85. GIC for HRH-10–3/8–3.0 baseline (2.5″ prescribed crack)

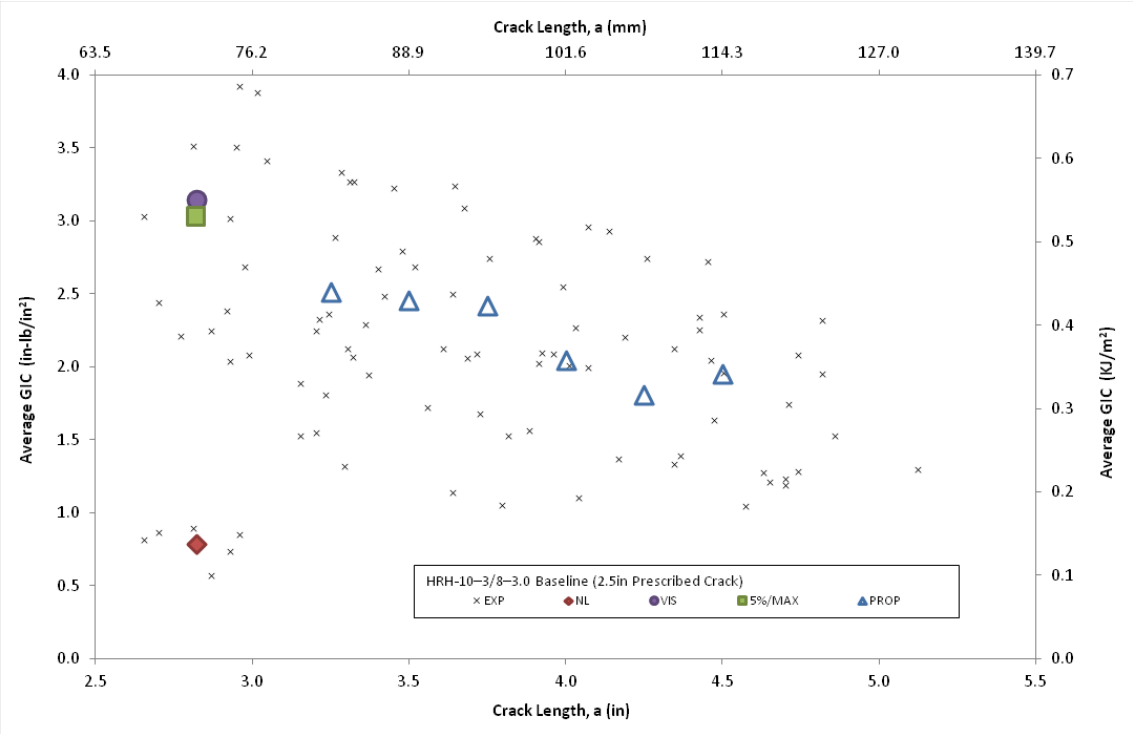

Figure B-86. Resistance curve for HRH-10–3/8–3.0 baseline (2.5″ prescribed crack)

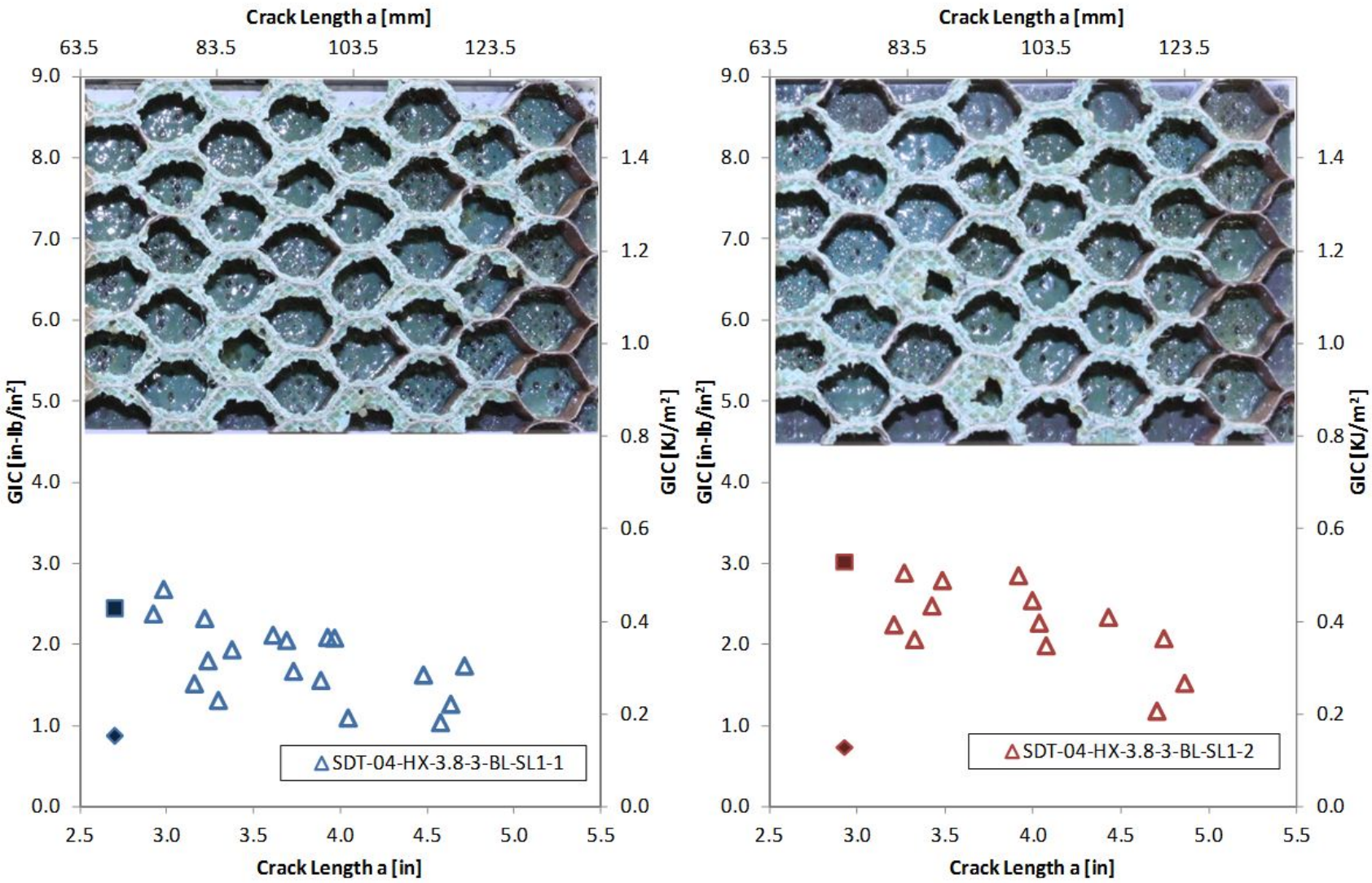

Figure B-87. Failure mode and resistance curve for SDT-04-HX-3.8-3-BL-SL1-X #1 and #2

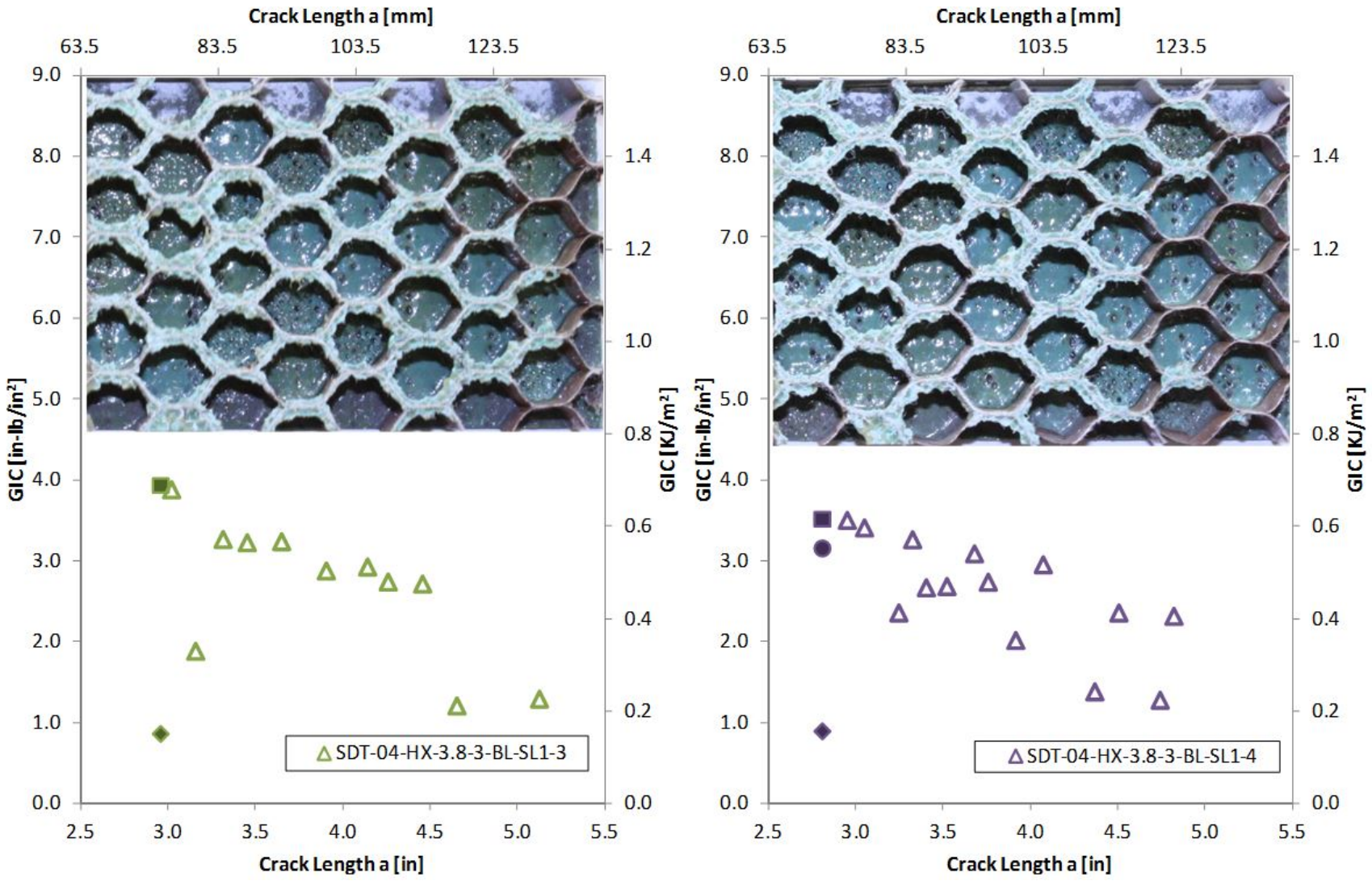

Figure B-88. Failure mode and resistance curve for SDT-04-HX-3.8-3-BL-SL1-X #3 and #4

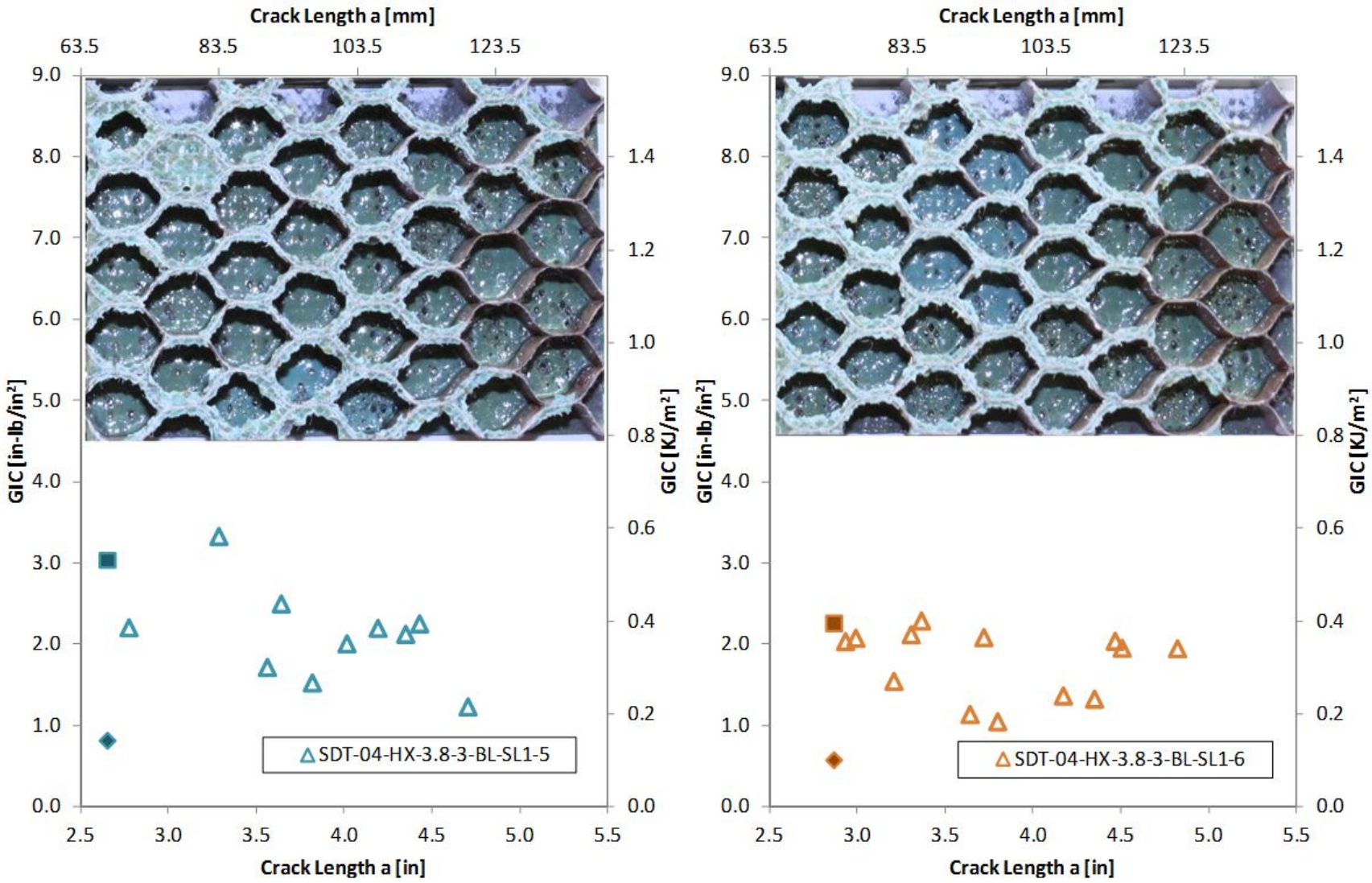

Figure B-89. Failure mode and resistance curve for SDT-04-HX-3.8-3-BL-SL1-X #5 and #6

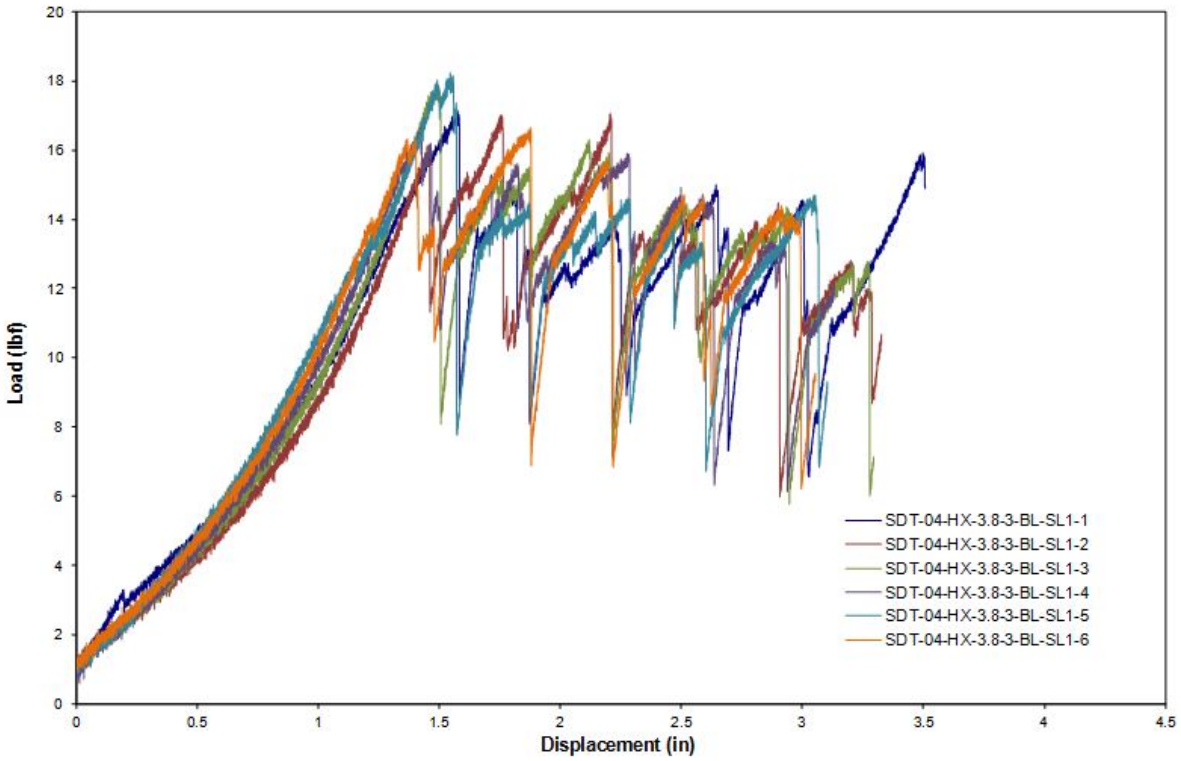

Figure B-90. Load vs. displacement curve for HRH-10–3/8–3.0 baseline (2.5″ prescribed crack)

B.5.1.2 HRH-10–3/8–3.0 Baseline Data (1″ Prescribed Crack—Shortened)

Table B-35. Test summary for HRH-10–3/8–3.0 baseline (1″ prescribed crack—shortened) pre-crack

Specimen	GIC (in-lb/in^2)			GIC (KJ/m^2)			Failure Mode
	NL	VIS	5%/ max	NL	VIS	5%/ max	
SDT-04-HX-3.8-3-BL-SL1-7 (shortened)	2.047	-	2.573	0.359	-	0.451	Primarily PO
SDT-04-HX-3.8-3-BL-SL1-8 (shortened)	1.779	-	2.827	0.312	-	0.495	Primarily PO
SDT-04-HX-3.8-3-BL-SLX-7 (shortened)	1.449	-	1.927	0.254	-	0.338	Primarily PO
AVERAGE GIC	1.758	-	2.443	0.308	-	0.428	
STANDARD DEVIATION	0.009	-	0.031	0.052	-	0.081	
COEFFICIENT OF VARIATION (%)	17.041	-	18.993	17.041	-	18.993	

Table B-36. Test summary for HRH-10–3/8–3.0 baseline (1″ prescribed crack—shortened)

Specimen	GIC (in-lb/in^2)			GIC (KJ/m^2)			Failure Mode
	NL	VIS	5%/ max	NL	VIS	5%/ max	
SDT-04-HX-3.8-3-BL-SL1-7 (shortened)	0.712	2.062	2.256	0.125	0.361	0.395	Primarily PO
SDT-04-HX-3.8-3-BL-SL1-8 (shortened)	0.877	-	2.812	0.154	-	0.493	Primarily PO
SDT-04-HX-3.8-3-BL-SLX-7 (shortened)	1.014	1.993	2.531	0.178	0.349	0.443	Primarily PO
AVERAGE GIC	0.868	2.028	2.533	0.152	0.355	0.444	
STANDARD DEVIATION	0.009	-	0.031	0.026	0.009	0.049	
COEFFICIENT OF VARIATION (%)	17.439	2.404	10.991	17.439	2.404	10.991	

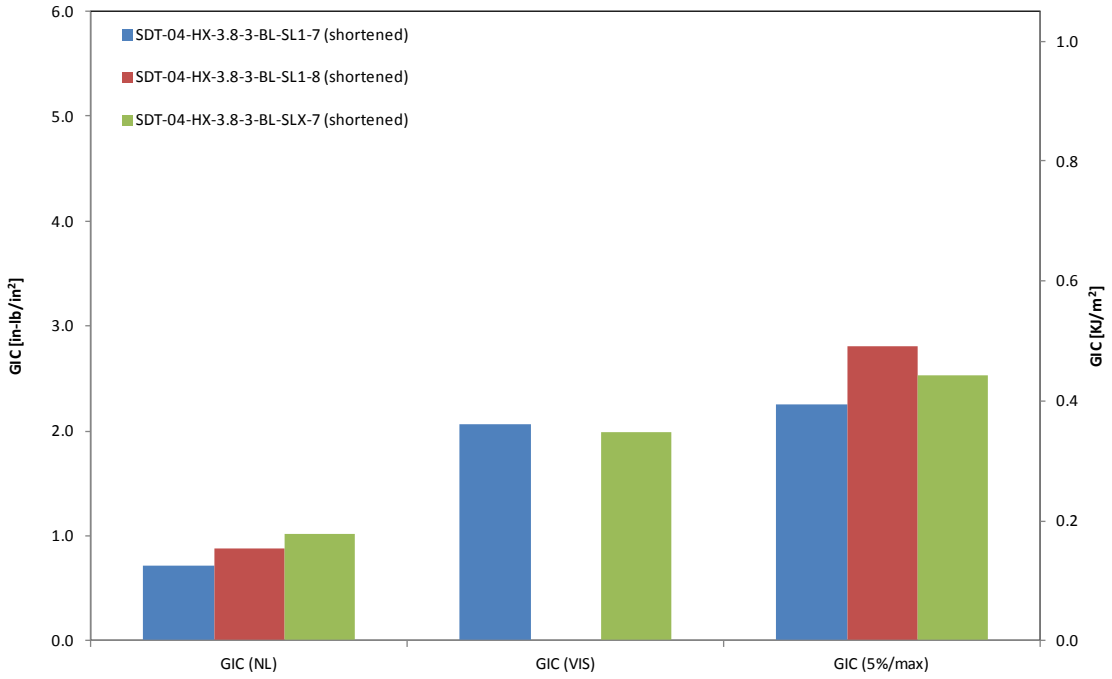

Figure B-91. GIC for HRH-10–3/8–3.0 baseline (1″ prescribed crack—shortened)

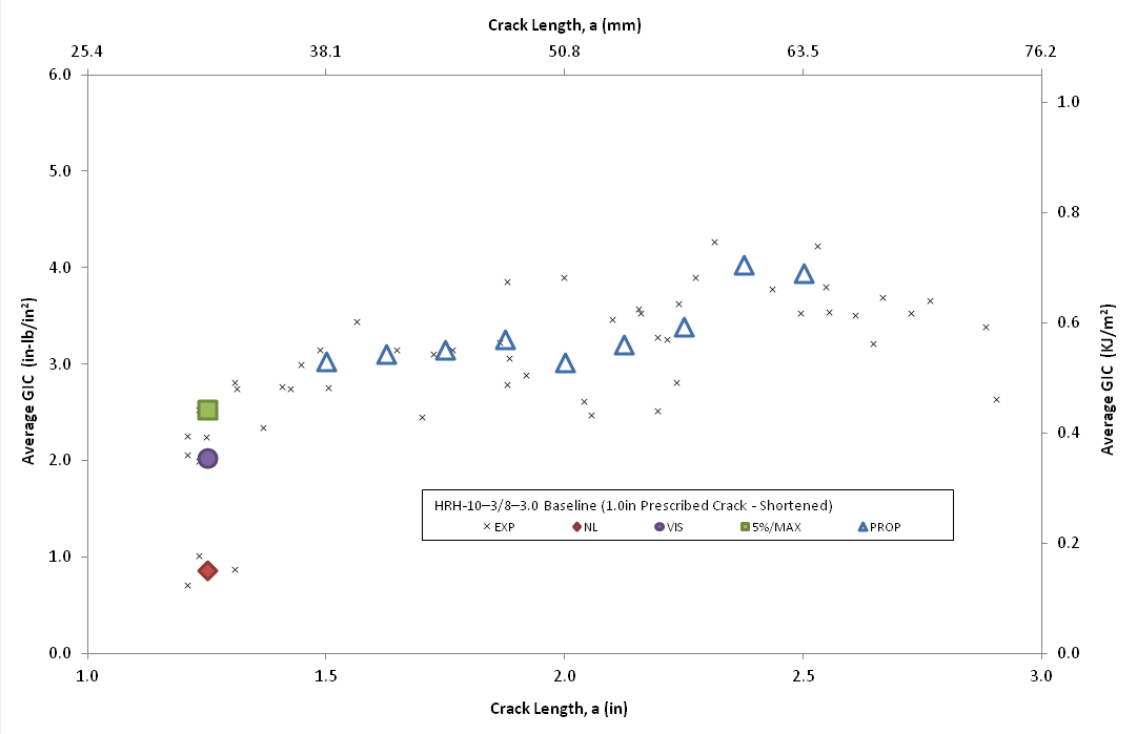

Figure B-92. Resistance curve for HRH-10–3/8–3.0 baseline (1″ prescribed crack—shortened)

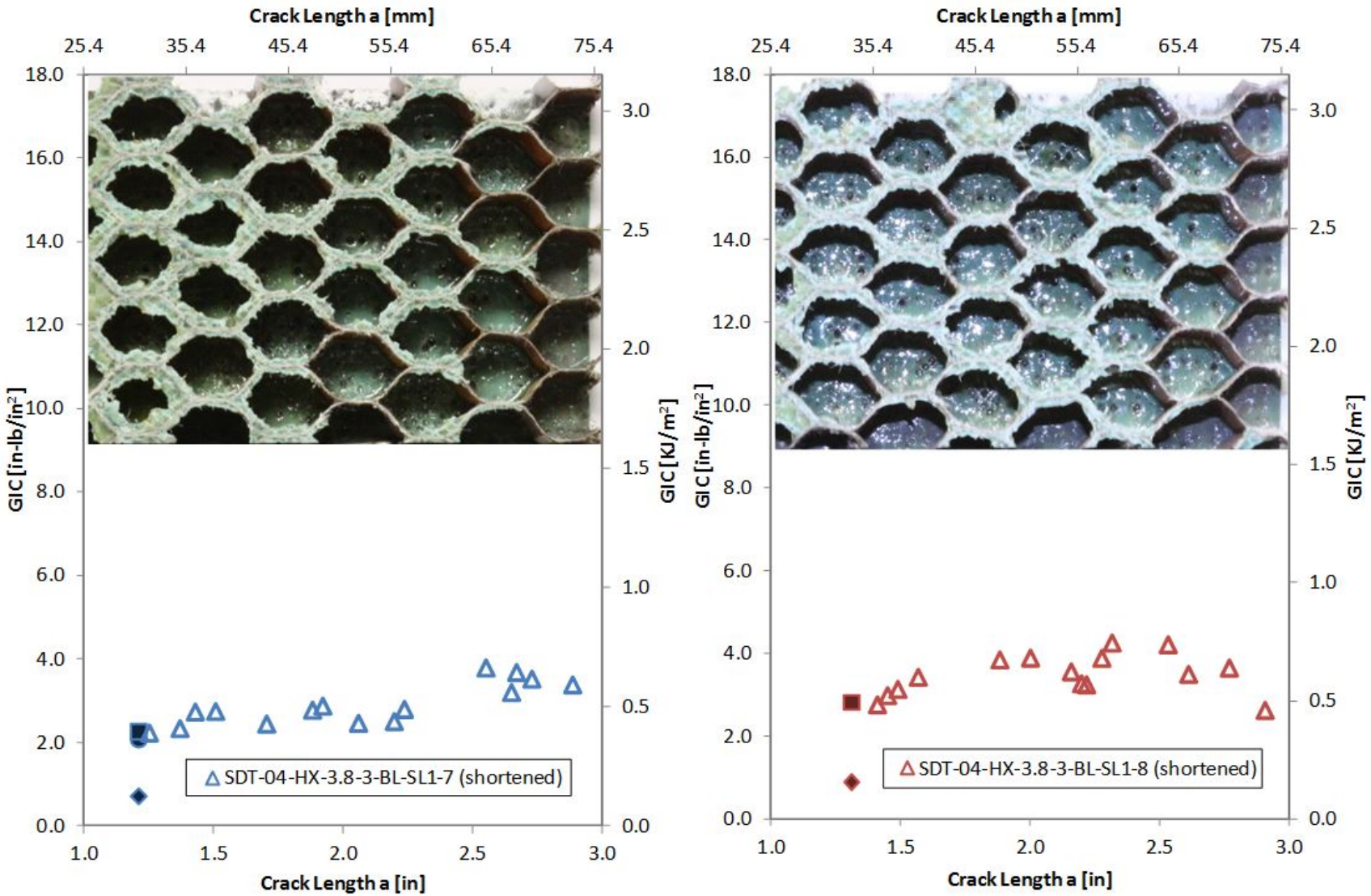

Figure B-93. Failure mode and resistance curve for SDT-04-HX-3.8-3-BL-SL1-X (shortened) #7 and #8

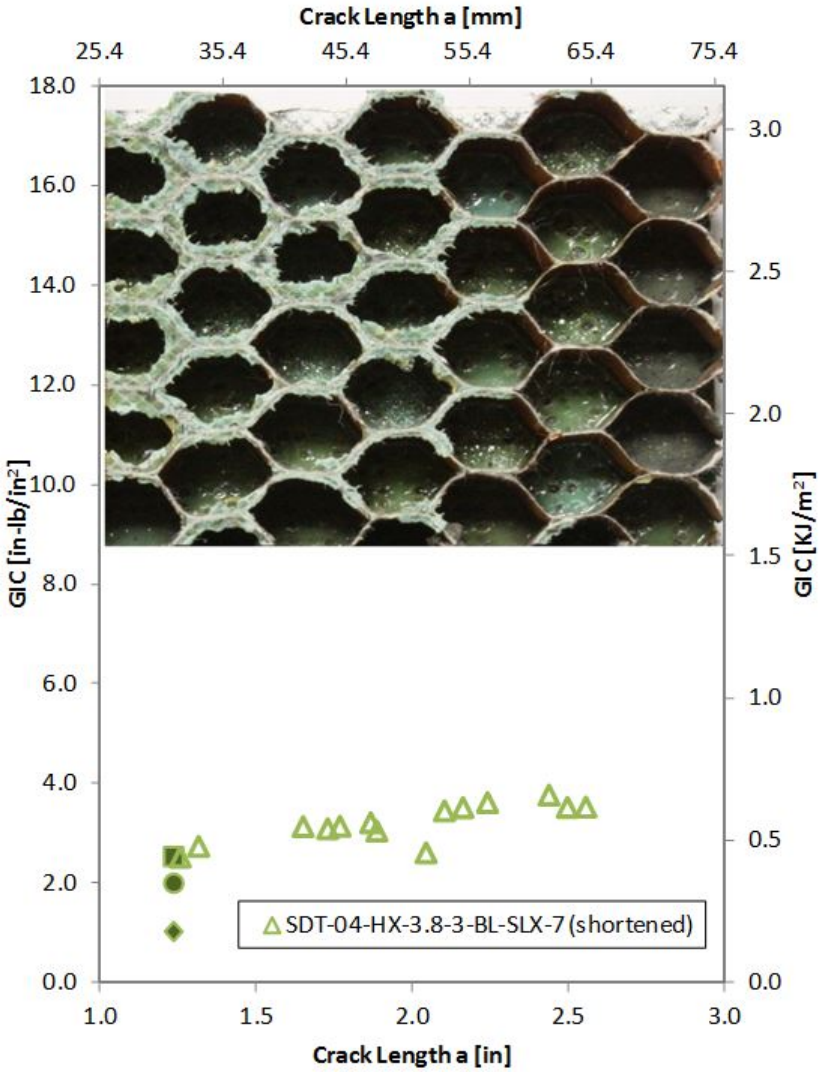

Figure B-94. Failure mode and resistance curve for SDT-04-HX-3.8-3-BL-SLX-X (shortened) #7

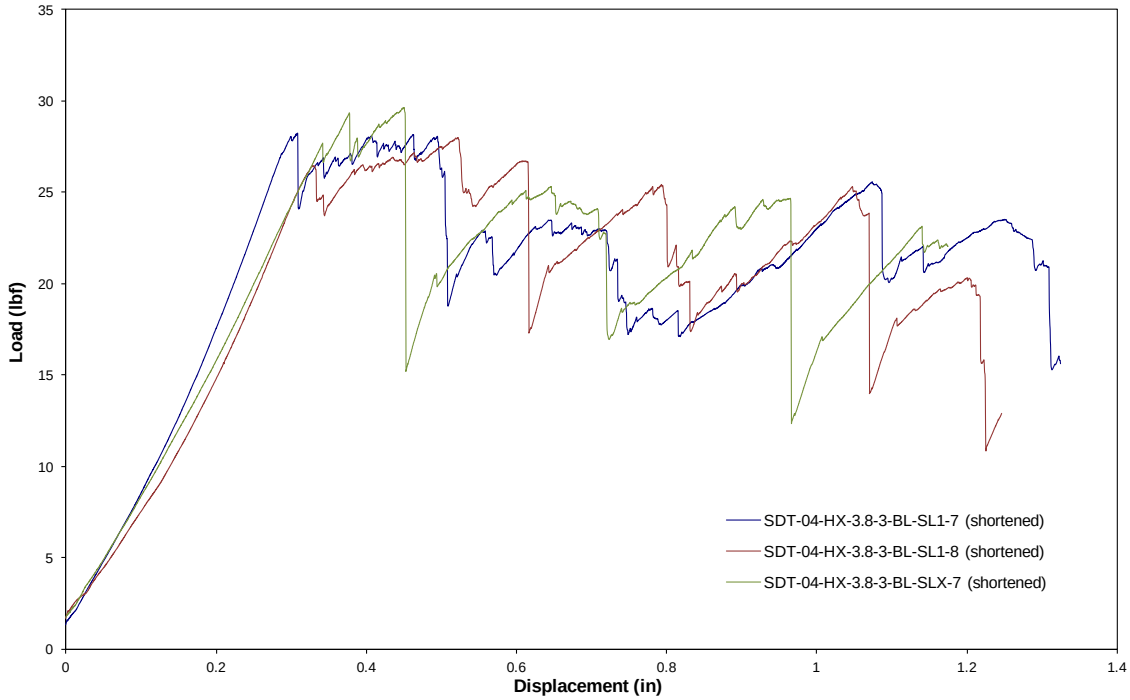

Figure B-95. Load vs. displacement curve for HRH-10–3/8–3.0 baseline (1″ prescribed crack—shortened)

B.5.2 HRH-10–3/8–3.0 FLUID-INGRESSED DATA

Table B-37. Test summary for HRH-10–3/8–3.0 fluid ingressed (1″ prescribed crack—shortened) pre-crack

Specimen	GIC (in-lb/in^2)			GIC (KJ/m^2)			Failure Mode
	NL	VIS	5%/ max	NL	VIS	5%/ max	
SDT-04-HX-3.8-3-FI-SL1-1 (shortened)	0.746	-	1.616	0.131	-	0.283	Mix of PO and C
SDT-04-HX-3.8-3-FI-SL1-2 (shortened)	0.819	-	1.428	0.143	-	0.250	Mix of PO and C
SDT-04-HX-3.8-3-FI-SL1-3 (shortened)	1.142	-	3.132	0.200	-	0.549	Mix of PO and C
SDT-04-HX-3.8-3-FI-SL1-4 (shortened)	0.945	-	3.272	0.165	-	0.573	Mix of PO and C
SDT-04-HX-3.8-3-FI-SL1-5 (shortened)	1.039	-	3.940	0.182	-	0.690	Mix of PO and C
SDT-04-HX-3.8-3-FI-SL1-6 (shortened)	0.885	-	1.335	0.155	-	0.234	Mix of PO and C
AVERAGE GIC	0.929	-	2.454	0.163	-	0.430	
STANDARD DEVIATION	0.145	-	1.126	0.025	-	0.197	
COEFFICIENT OF VARIATION (%)	15.610	-	45.903	15.610	-	45.903	

Table B-38. Test summary for HRH-10–3/8–3.0 fluid ingressed (1″ prescribed crack—shortened)

Specimen	GIC (in-lb/in^2)			GIC (KJ/m^2)			Failure Mode
	NL	VIS	5%/ max	NL	VIS	5%/ max	
SDT-04-HX-3.8-3-FI-SL1-1 (shortened)	0.570	3.794	4.257	0.100	0.664	0.745	Mix of PO and C
SDT-04-HX-3.8-3-FI-SL1-2 (shortened)	0.531	4.550	4.664	0.093	0.797	0.817	Mix of PO and C
SDT-04-HX-3.8-3-FI-SL1-3 (shortened)	0.449	3.723	3.284	0.079	0.652	0.575	Mix of PO and C
SDT-04-HX-3.8-3-FI-SL1-4 (shortened)	0.500	3.467	3.669	0.088	0.607	0.643	Mix of PO and C
SDT-04-HX-3.8-3-FI-SL1-5 (shortened)	0.520	2.889	3.630	0.091	0.506	0.636	Mix of PO and C
SDT-04-HX-3.8-3-FI-SL1-6 (shortened)	0.743	-	4.630	0.130	-	0.811	Mix of PO and C
AVERAGE GIC	0.552	3.685	4.022	0.097	0.645	0.704	
STANDARD DEVIATION	0.102	-	0.576	0.018	0.105	0.101	
COEFFICIENT OF VARIATION (%)	18.404	-	14.326	18.404	16.303	14.326	

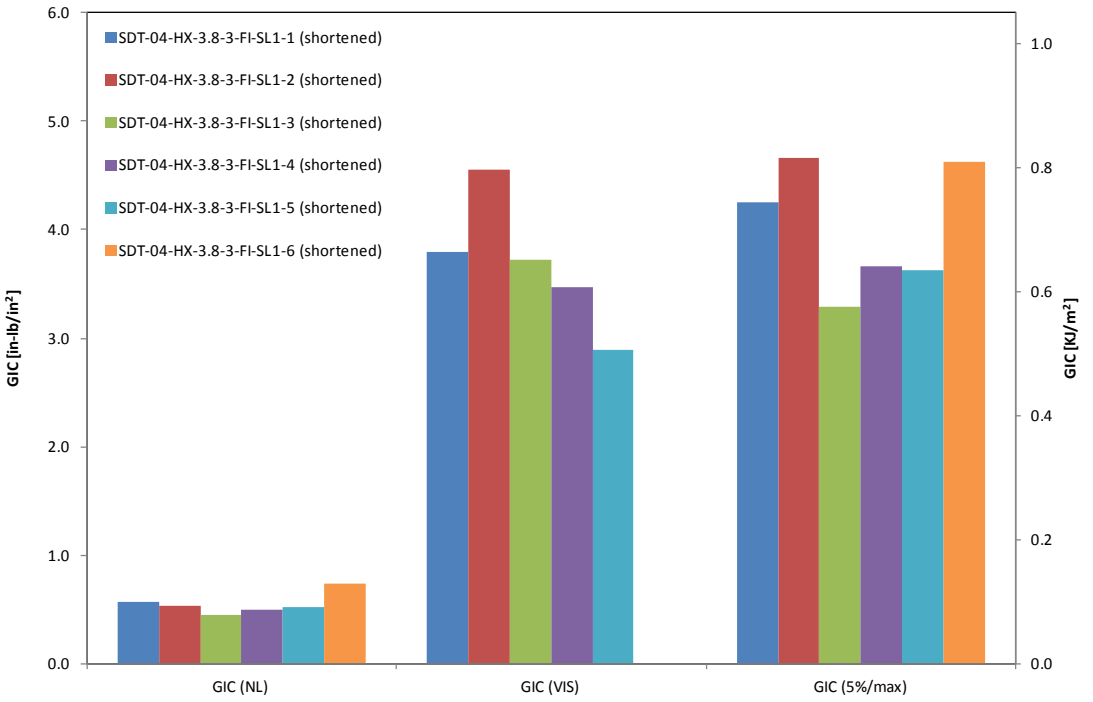

Figure B-96. GIC for HRH-10–3/8–3.0 fluid ingressed (1″ prescribed crack—shortened)

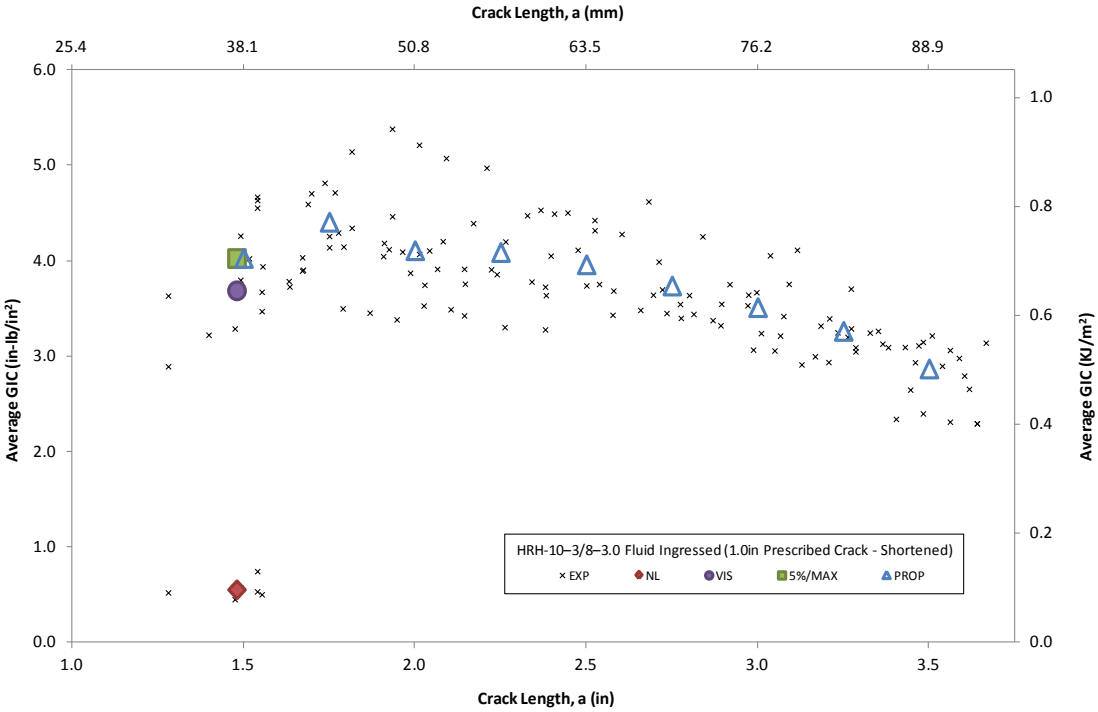

Figure B-97. Resistance curve for HRH-10–3/8–3.0 fluid ingressed (1″ prescribed crack—shortened)

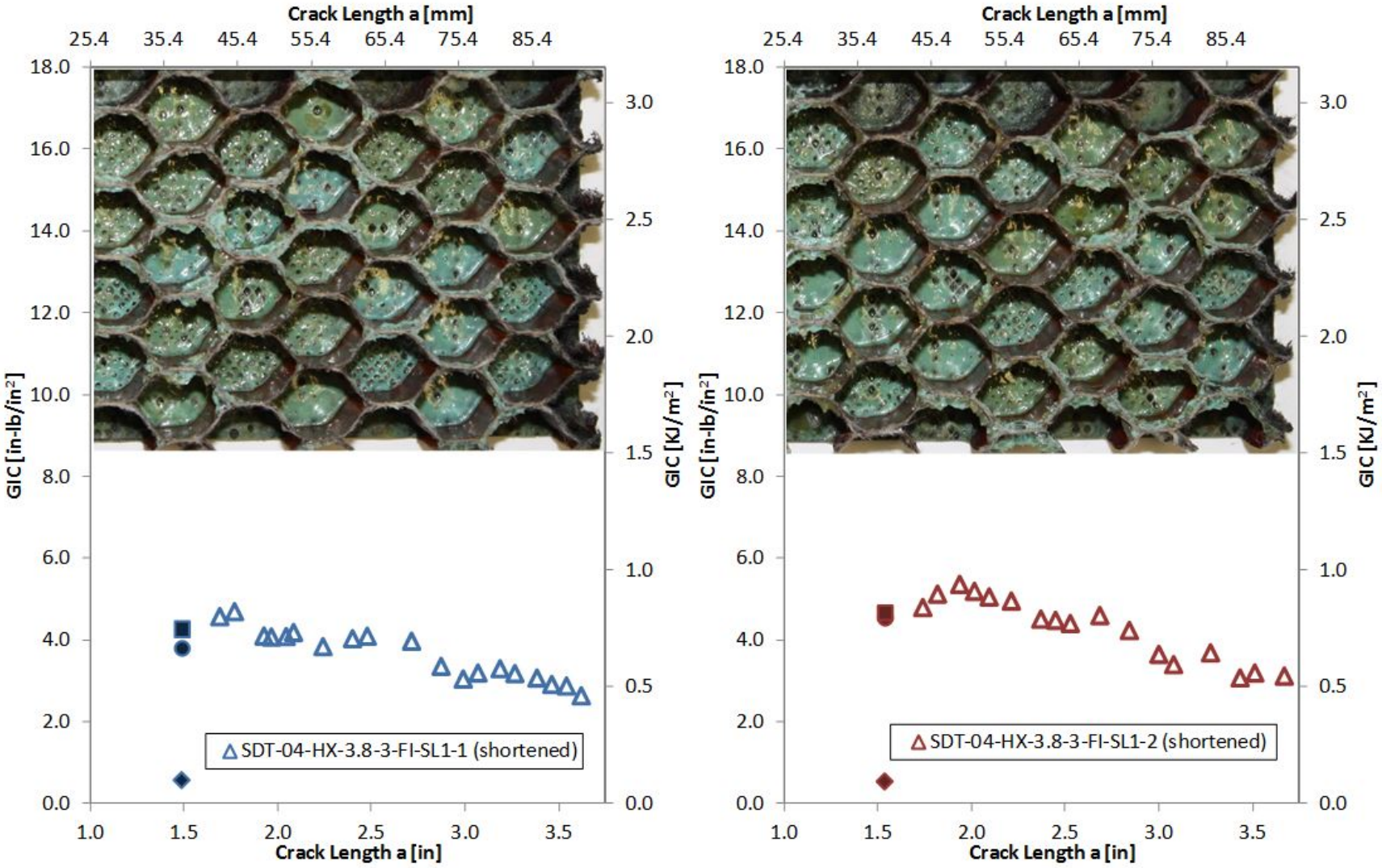

Figure B-98. Failure mode and resistance curve for SDT-04-HX-3.8-3-FI-SL1-X (shortened) #1 and #2

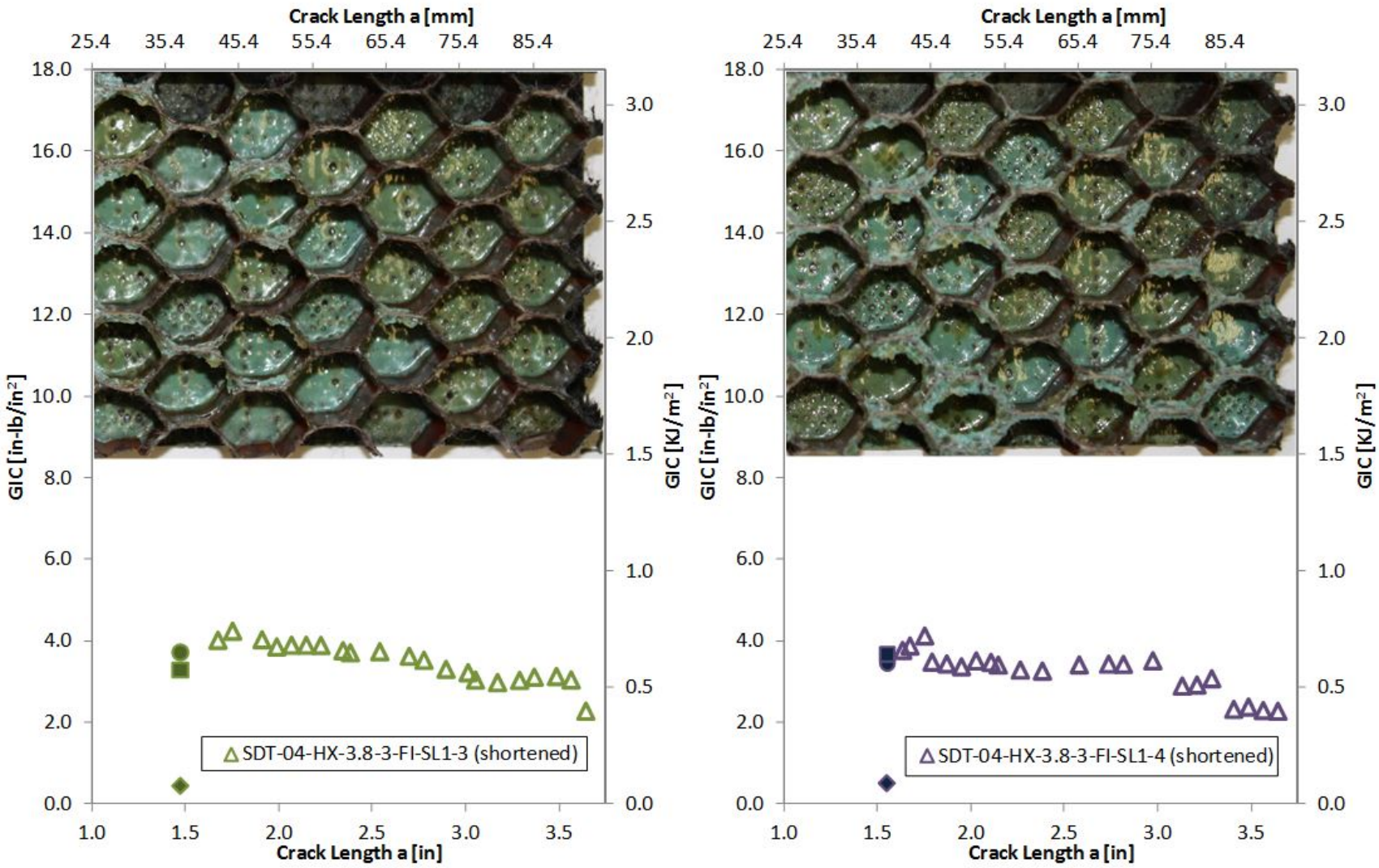

Figure B-99. Failure mode and resistance curve for SDT-04-HX-3.8-3-FI-SL1-X (shortened) #3 and #4

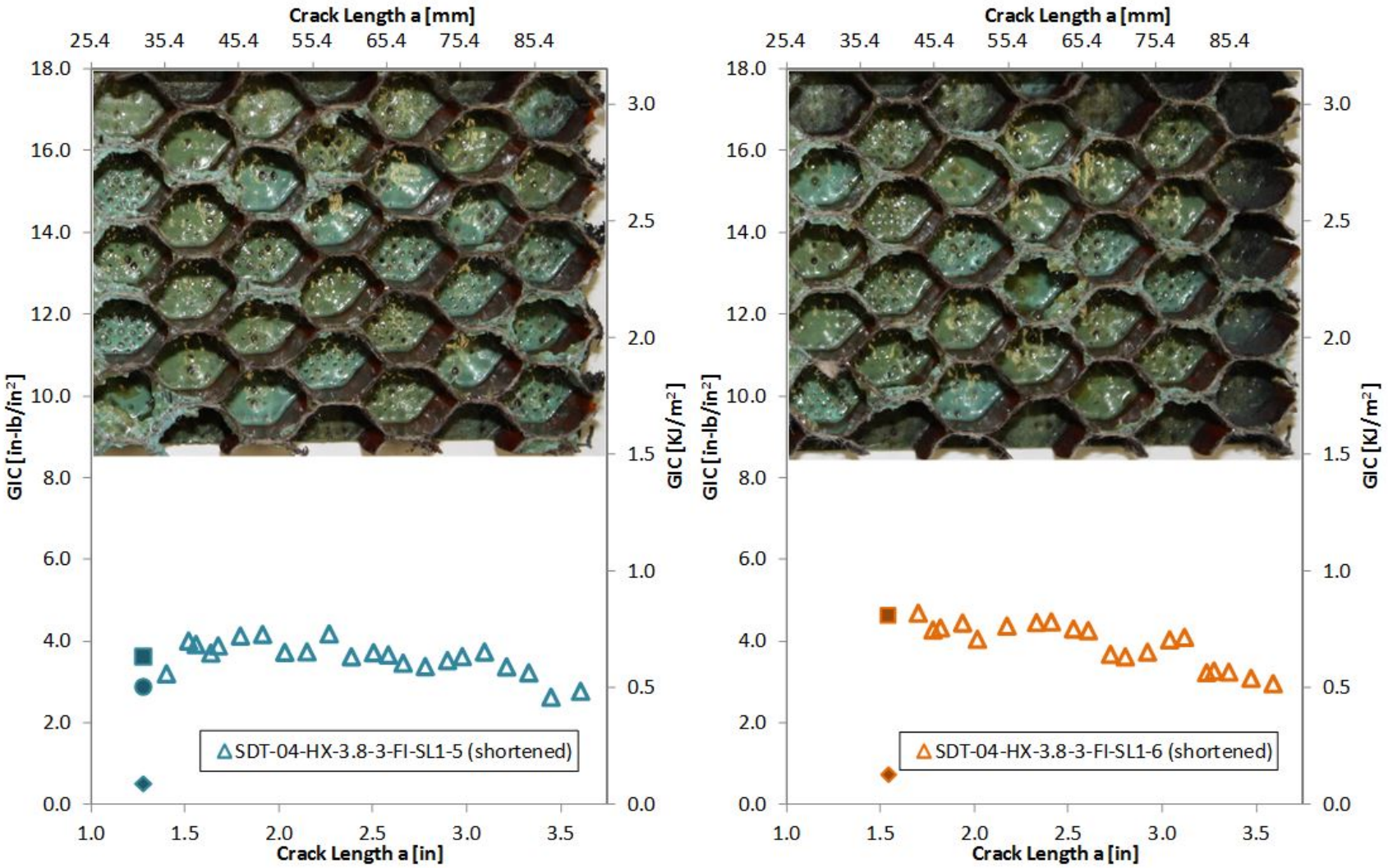

Figure B-100. Failure mode and resistance curve for SDT-04-HX-3.8-3-FI-SL1-X (shortened) #5 and #6

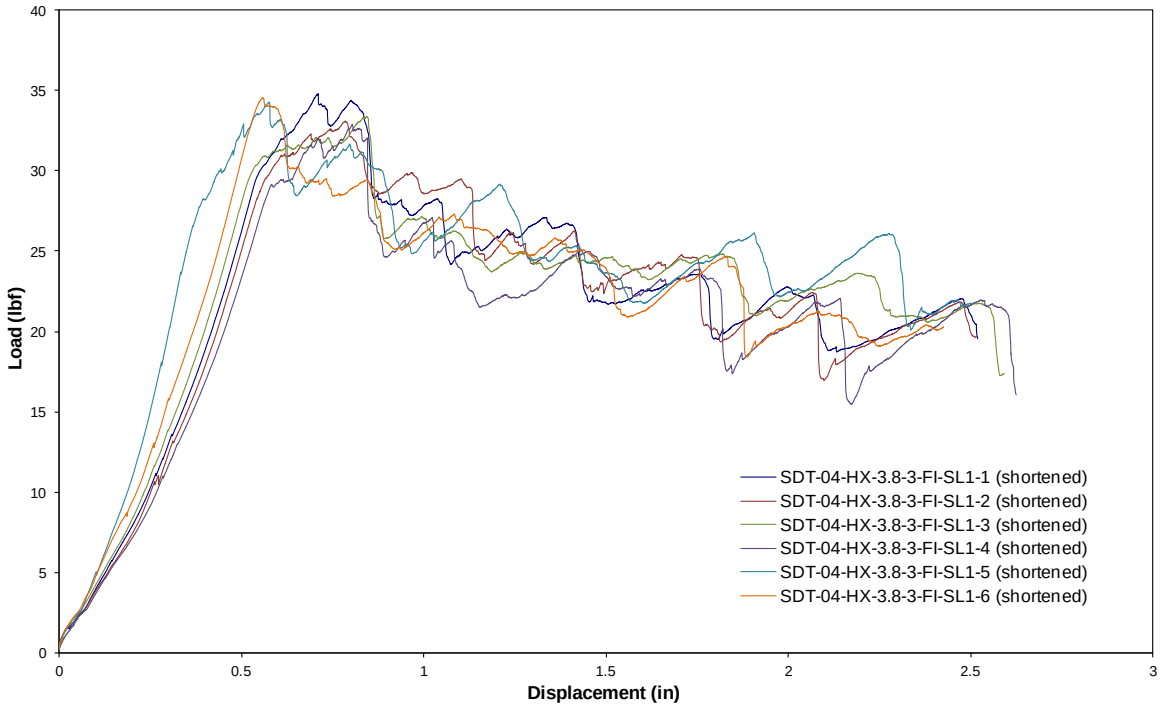

Figure B-101. Load vs. displacement curve for HRH-10–3/8–3.0 fluid ingressed (1″ prescribed crack—shortened)

B.5.3. HRH-10–3/8–3.0 EXTENDED FLUID-INGRESSED DATA

Table B-39. Test summary for HRH-10–3/8–3.0 extended fluid ingressed (1″ prescribed crack—shortened) pre-crack

Specimen	GIC (in-lb/in^2)			GIC (KJ/m^2)			Failure Mode
	NL	VIS	5%/ max	NL	VIS	5%/ max	
SDT-04-HX-3.8-3-EFI-SL1-7 (shortened)	1.028	-	2.200	0.180	-	0.385	Primarily in PO
SDT-04-HX-3.8-3-EFI-SL1-8 (shortened)	0.700	-	4.122	0.123	-	0.722	Primarily in PO
AVERAGE GIC	0.864	-	3.161	0.151	-	0.554	
STANDARD DEVIATION	0.232	-	1.359	0.041	-	0.238	
COEFFICIENT OF VARIATION (%)	26.841	-	42.995	26.841	-	42.995	

Table B-40. Test summary for HRH-10–3/8–3.0 extended fluid ingressed (1″ prescribed crack—shortened)

Specimen	GIC (in-lb/in^2)			GIC (KJ/m^2)			Failure Mode
	NL	VIS	5%/ max	NL	VIS	5%/ max	
SDT-04-HX-3.8-3-EFI-SL1-7 (shortened)	1.061	-	5.212	0.186	-	0.913	Mix of PO and C
SDT-04-HX-3.8-3-EFI-SL1-8 (shortened)	1.027	-	3.943	0.180	-	0.691	Mix of PO and C
AVERAGE GIC	1.044	-	4.578	0.183	-	0.802	
STANDARD DEVIATION	0.024	-	0.898	0.004	-	0.157	
COEFFICIENT OF VARIATION (%)	2.311	-	19.610	2.311	-	19.610	

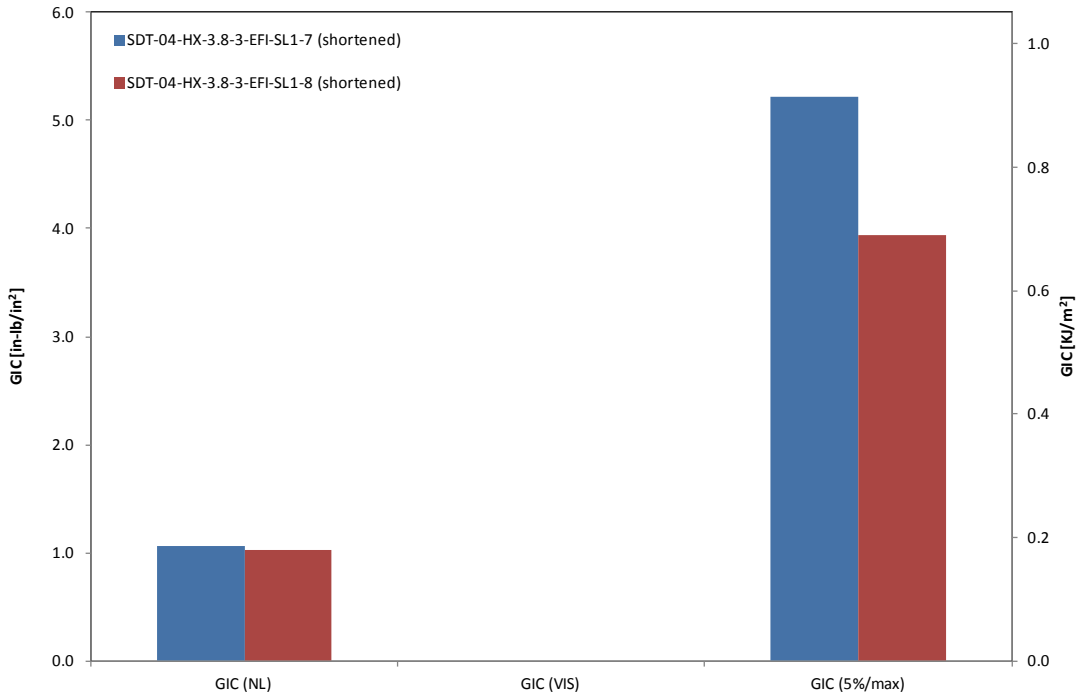

Figure B-102. GIC for HRH-10–3/8–3.0 extended fluid ingressed (1″ prescribed crack—shortened)

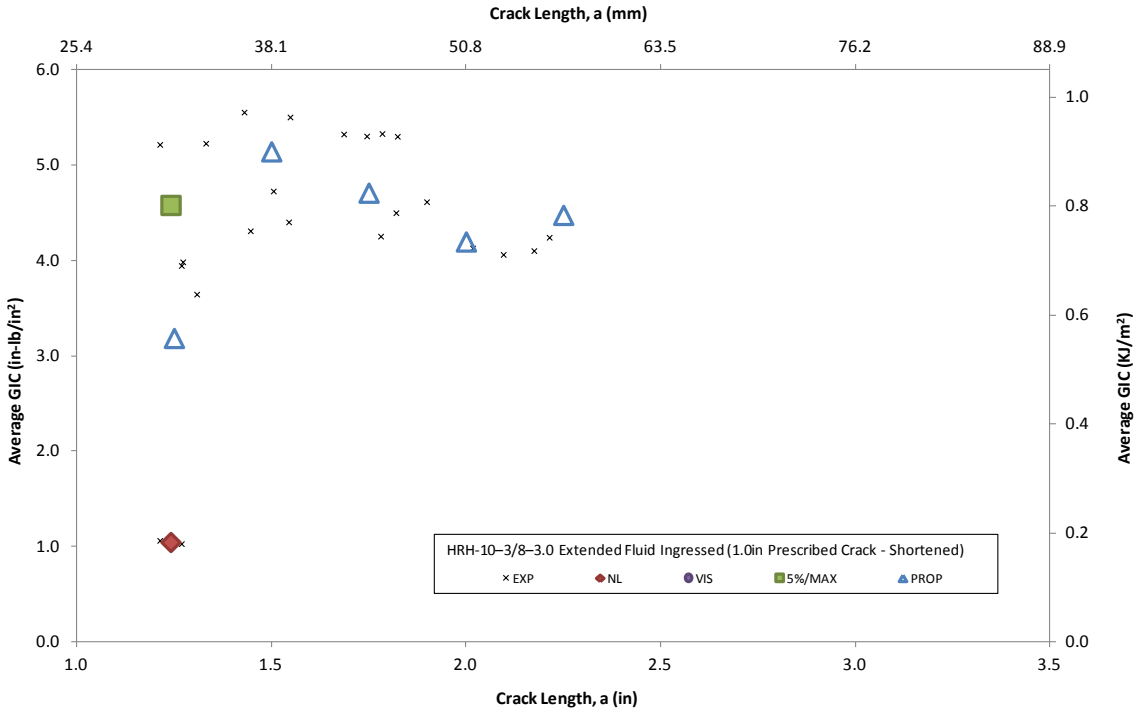

Figure B-103. Resistance curve for HRH-10–3/8–3.0 extended fluid ingressed (1″ prescribed crack—shortened)

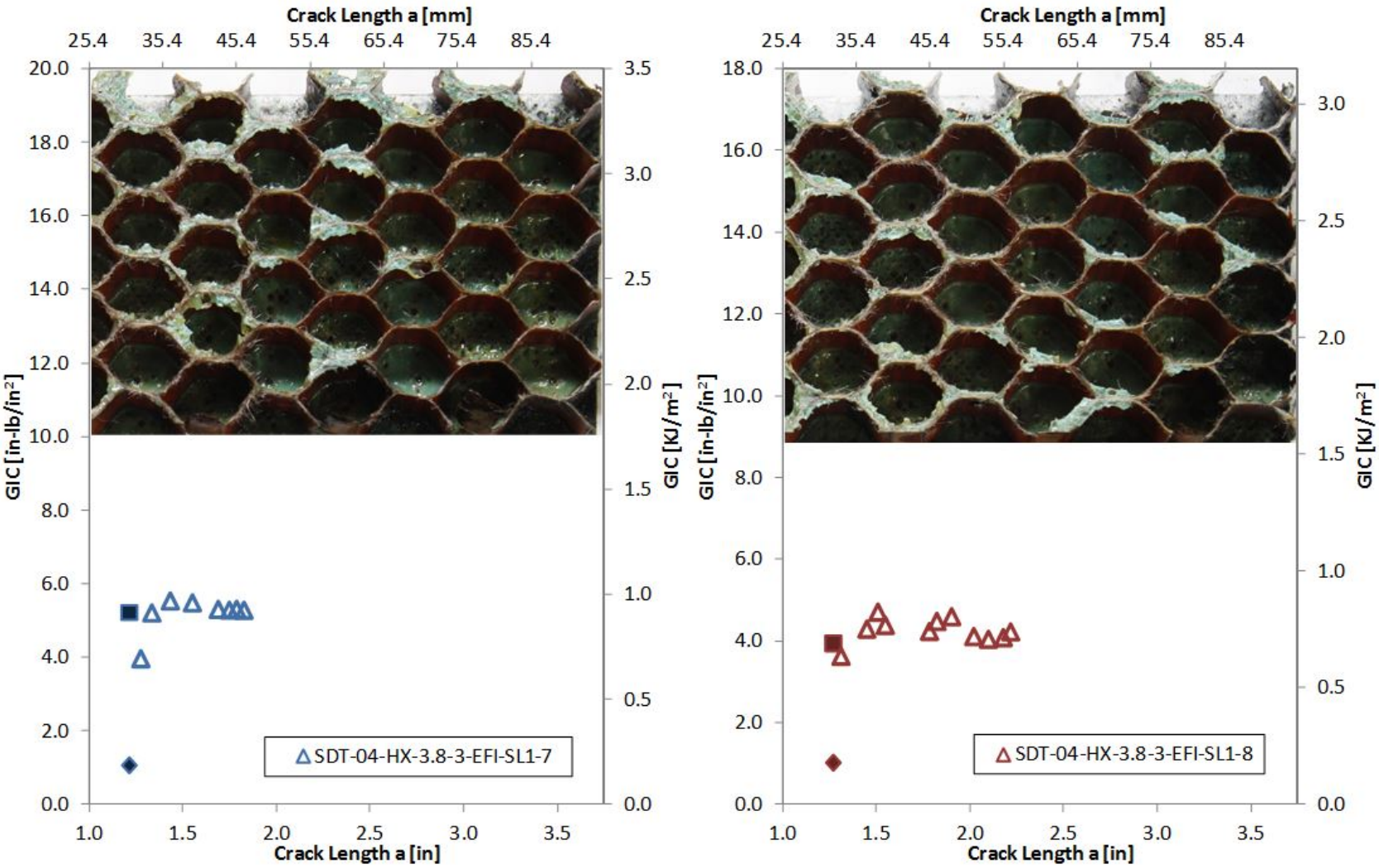

Figure B-104. Failure mode and resistance curve for SDT-04-HX-3.8-3-EFI-SL1-X (shortened) #7 and #8

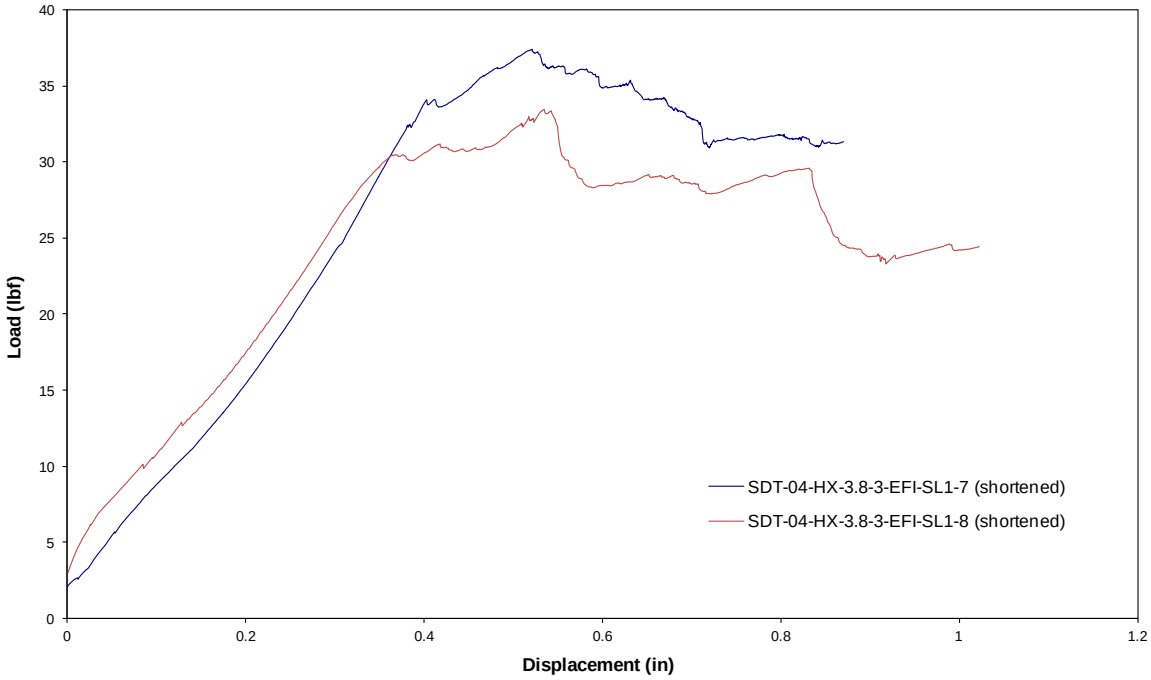

Figure B-105. Load vs. displacement curve for HRH-10–3/8–3.0 extended fluid ingressed (1″ prescribed crack—shortened)

APPENDIX C—STATIC RESULTS FOR THICK FACESHEET (16 PLY) AND HRH-10 HEXAGONAL CORES TESTED AS SINGLE-CANTILEVER BEAMS

Note that 16-ply material systems were tested with one prescribed crack length. The baseline, fluid-ingressed, extended fluid-ingressed, and water-ingressed specimens were all tested with a 2.5″ prescribed crack.

C.1. HRH-10–1/8–3.0 DATA

C.1.1 HRH-10–1/8–3.0 BASELINE DATA

Table C-1. Test summary for HRH-10–1/8–3.0 baseline (2.5″ prescribed crack) precrack

Specimen	GIC (in-lb/in^2)			GIC (KJ/m^2)			Failure Mode
	NL	VIS	5%/max	NL	VIS	5%/max	
SDT-16-HX-1.8-3-BL-SL1-1	1.766	-	2.939	0.309	-	0.515	Primarily A with a couple of cells in C
SDT-16-HX-1.8-3-BL-SL1-2	2.518	-	4.659	0.441	-	0.816	Primarily A with occasional PO
SDT-16-HX-1.8-3-BL-SL1-3	1.842	-	3.778	0.323	-	0.662	Primarily A with last several rows in D
SDT-16-HX-1.8-3-BL-SL1-4	2.015	-	3.413	0.353	-	0.598	Primarily A with last several rows in D
SDT-16-HX-1.8-3-BL-SL1-5	1.525	-	3.227	0.267	0.352	0.565	Primarily A
SDT-16-HX-1.8-3-BL-SL1-6	1.941	-	3.246	0.340	-	0.568	Primarily A
AVERAGE GIC	1.935	2.008	3.544	0.339	0.352	0.621	
STANDARD DEVIATION	0.332	-	0.612	0.058	-	0.107	
COEFFICIENT OF VARIATION (%)	17.171	-	17.263	17.171	-	17.263	

Table C-2. Test summary for HRH-10–1/8–3.0 baseline (2.5″ prescribed crack)

Specimen	GIC (in-lb/in^2)			GIC (KJ/m^2)			Failure Mode
	NL	VIS	5%/max	NL	VIS	5%/max	
SDT-16-HX-1.8-3-BL-SL1-1	2.622	-	6.664	0.459	-	1.167	Mix of A and C with occasional PO and S
SDT-16-HX-1.8-3-BL-SL1-2	1.496	4.397	5.320	0.262	0.770	0.932	Mix of A and PO and S
SDT-16-HX-1.8-3-BL-SL1-3	1.383	4.714	5.553	0.242	0.825	0.972	Primarily A, then a mix of A and PO and S
SDT-16-HX-1.8-3-BL-SL1-4	1.590	-	5.220	0.278	-	0.914	Primarily A, then a mix of A and PO and S
SDT-16-HX-1.8-3-BL-SL1-5	1.841	-	5.122	0.322	-	0.897	Mix of A and PO and S
SDT-16-HX-1.8-3-BL-SL1-6	2.540	4.697	4.972	0.445	0.823	0.871	Primarily a mix of A and PO with a pocket of C, then a mix of A and PO and C and S
AVERAGE GIC	1.912	4.603	5.475	0.335	0.806	0.959	
STANDARD DEVIATION	0.540	0.178	0.614	0.095	0.031	0.108	
COEFFICIENT OF VARIATION (%)	28.259	3.871	11.217	28.259	3.871	11.217	

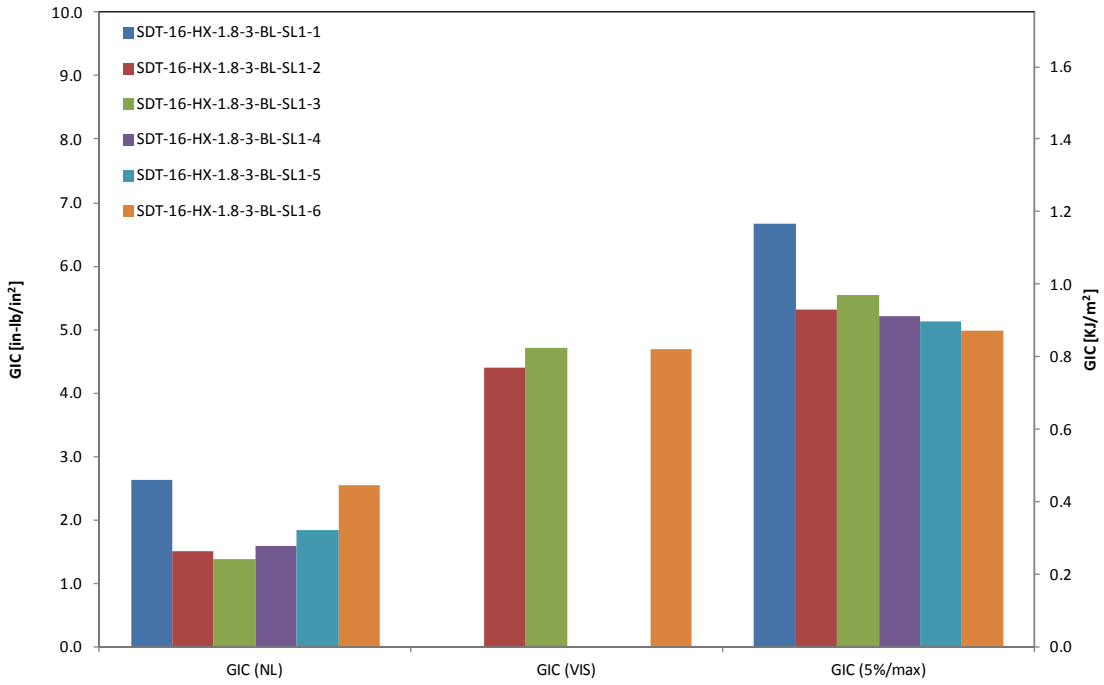

Figure C-1. GIC for HRH-10–1/8–3.0 baseline (2.5″ prescribed crack)

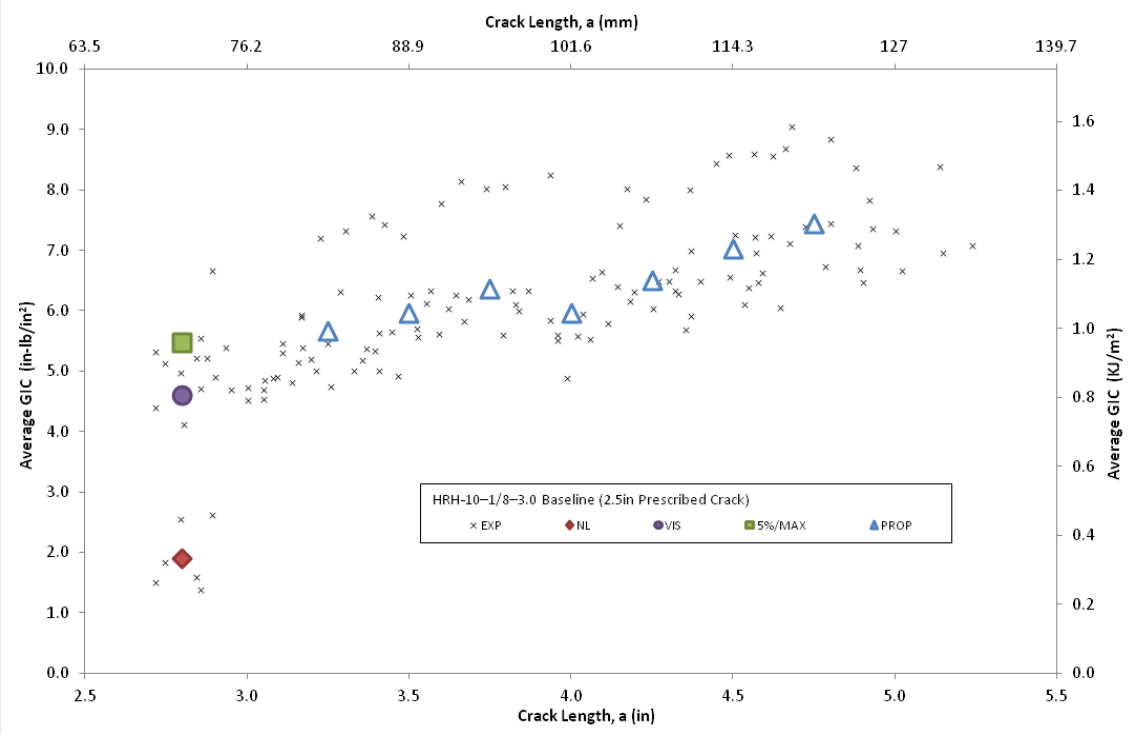

Figure C-2. Resistance curve for HRH-10–1/8–3.0 baseline (2.5″ prescribed crack)

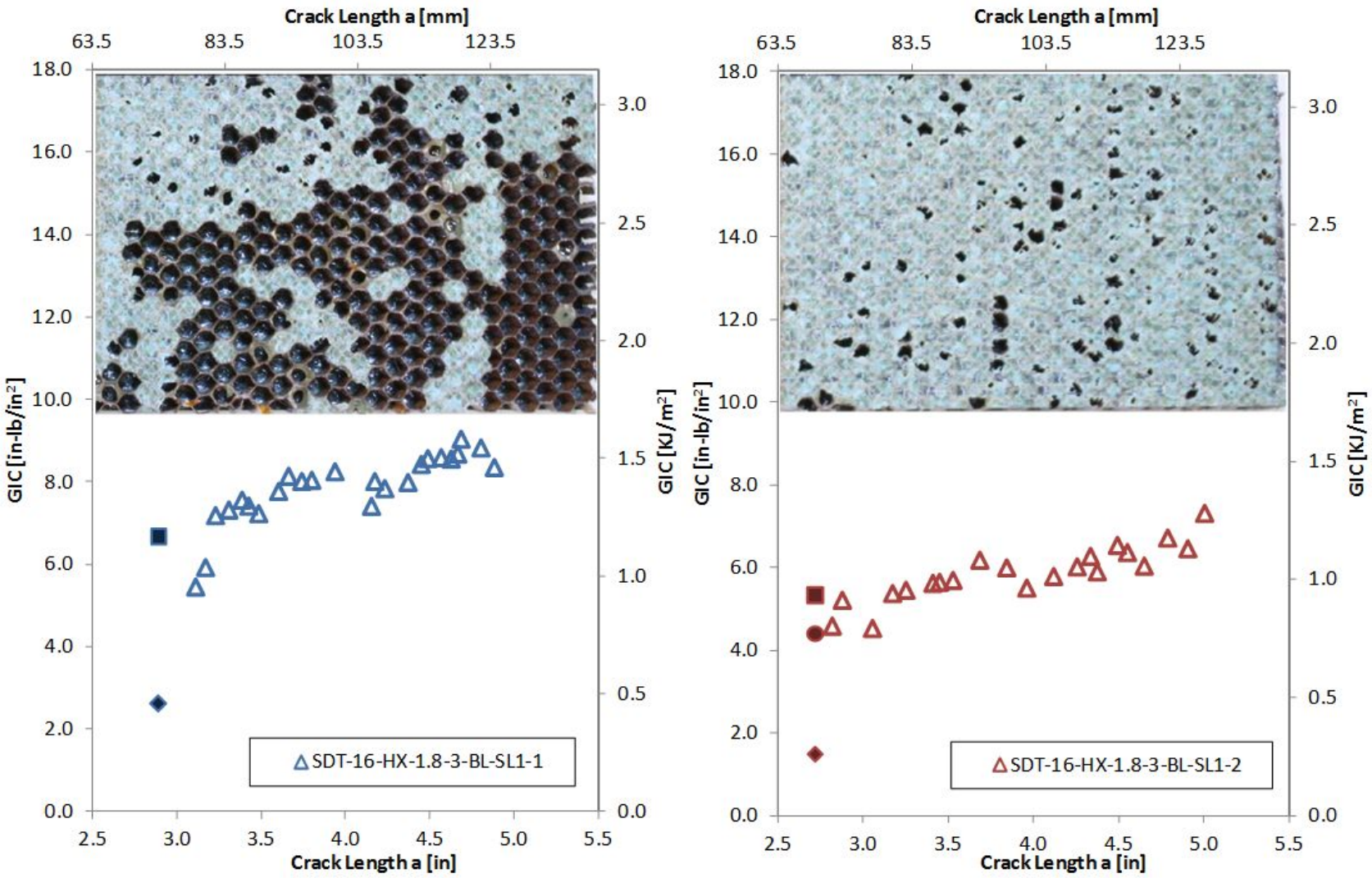

Figure C-3. Failure mode image and resistance curve for SDT-16-HX-1.8-3-BL-SL1-X #1 and #2

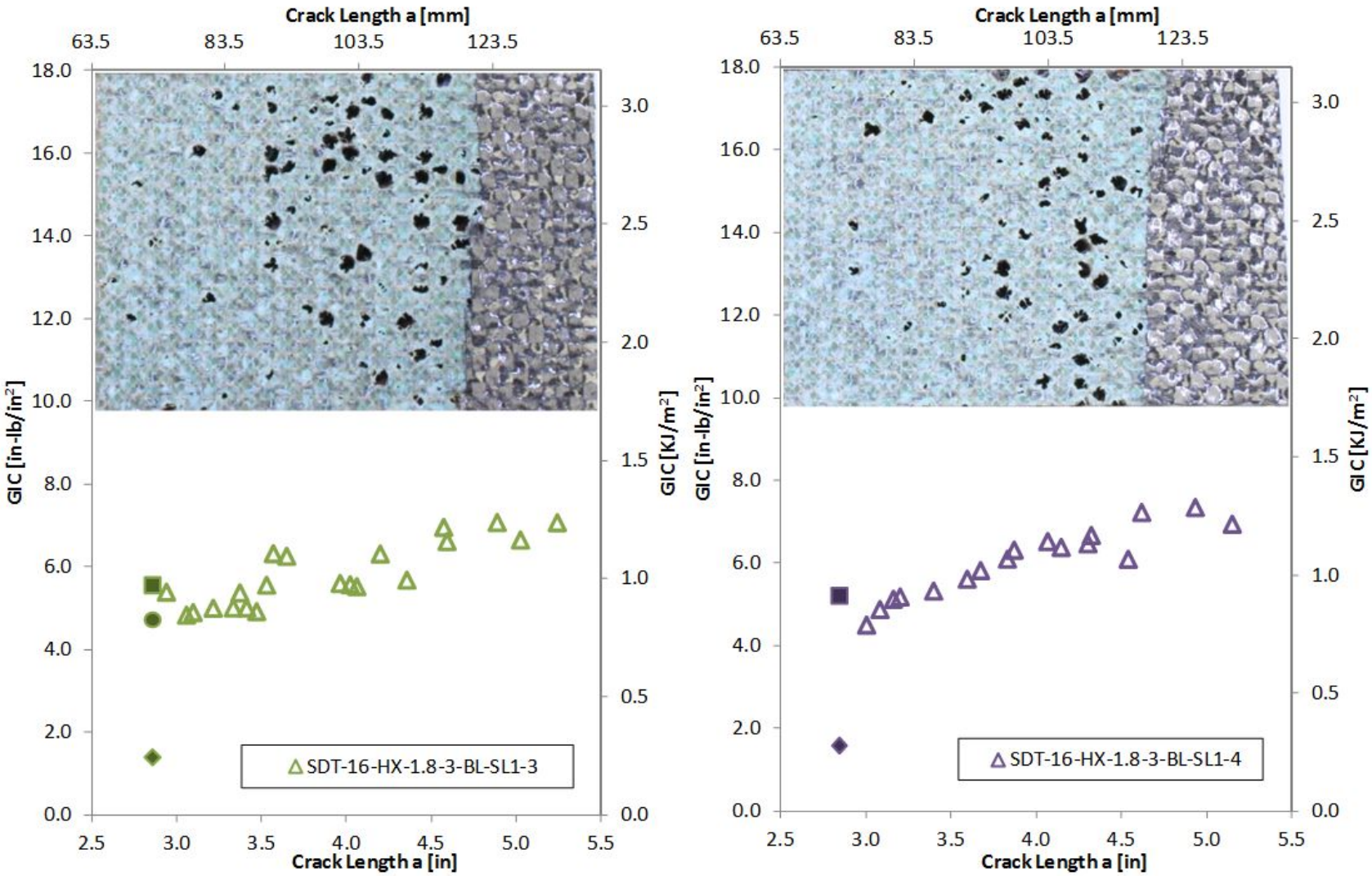

Figure C-4. Failure mode image and resistance curve for SDT-16-HX-1.8-3-BL-SL1-X #3 and #4

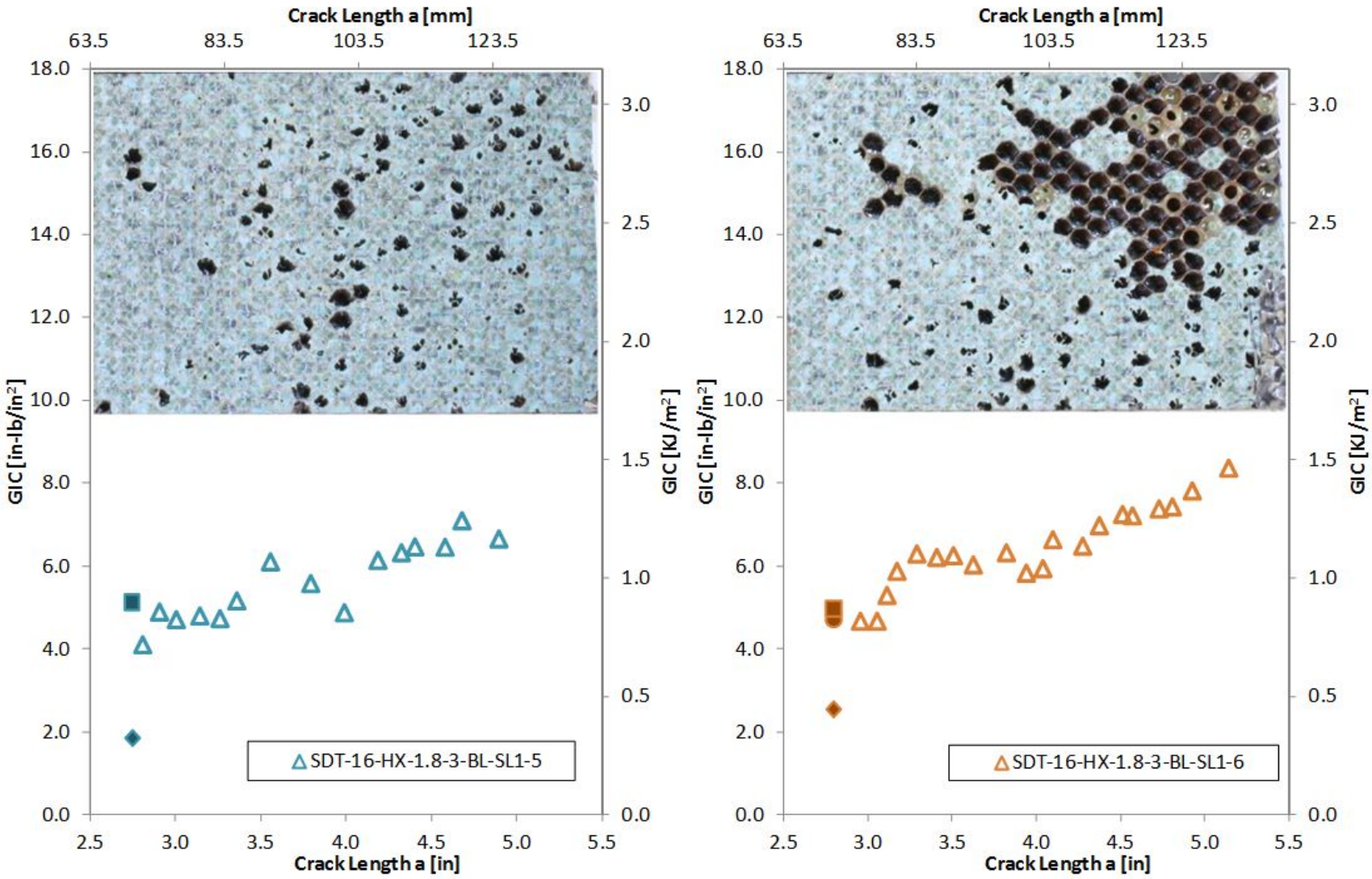

Figure C-5. Failure mode image and resistance curve for SDT-16-HX-1.8-3-BL-SL1-X #5 and #6

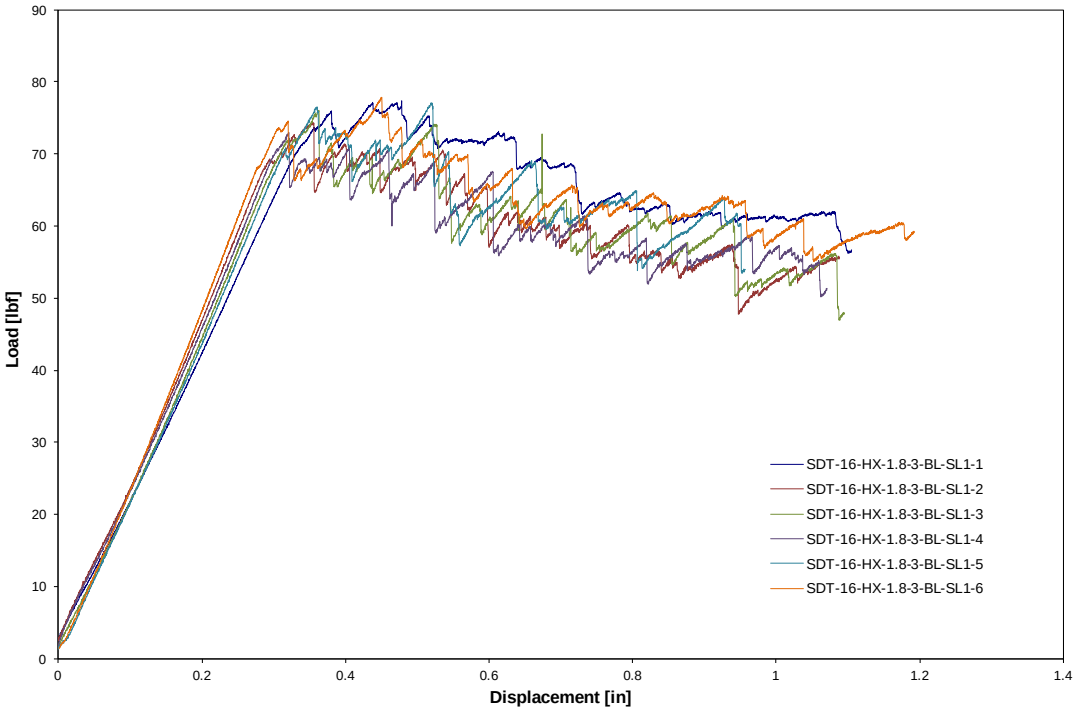

Figure C-6. Load vs. displacement curve for HRH-10–1/8–3.0 baseline (2.5-inch prescribed crack)

C.1.2 HRH-10–1/8–3.0 FLUID-INGRESSED DATA

Table C-3. Test summary for HRH-10–1/8–3.0 fluid ingressed (2.5″ prescribed crack) precrack

Specimen	GIC (in-lb/in^2)			GIC (KJ/m^2)			Failure Mode
	NL	VIS	5%/max	NL	VIS	5%/max	
SDT-16-HX-1.8-3-FI-SL1-1	1.751	-	5.283	0.307	-	0.925	First row primarily in A with several cells in C; next two rows primarily in C with a few cells in A and one cell in PO
SDT-16-HX-1.8-3-FI-SL1-2	1.266	-	3.659	0.222	-	0.641	Primarily in A with several cells in PO
SDT-16-HX-1.8-3-FI-SL1-3	1.515	-	3.503	0.265	-	0.614	Primarily in A with a cell in PO
SDT-16-HX-1.8-3-FI-SL1-4	1.575	-	2.968	0.276	-	0.520	Primarily in A with a few cells in PO
SDT-16-HX-1.8-3-FI-SL1-5	1.789	-	3.550	0.313	-	0.622	Primarily in A with a cell in PO
SDT-16-HX-1.8-3-FI-SL1-6	1.588	-	2.695	0.278	-	0.472	Primarily in A with a few cells in PO
AVERAGE GIC	1.581	-	3.610	0.277	-	0.632	
STANDARD DEVIATION	0.187	-	0.901	0.033	-	0.158	
COEFFICIENT OF VARIATION (%)	11.860	-	24.973	11.860	-	24.973	

Table C-4. Test summary for HRH-10–1/8–3.0 fluid ingressed (2.5″ prescribed crack)

Specimen	GIC (in-lb/in^2)			GIC (KJ/m^2)			Failure Mode
	NL	VIS	5%/max	NL	VIS	5%/max	
SDT-16-HX-1.8-3-FI-SL1-1	1.569	-	6.261	0.275	-	1.096	First two thirds primarily in C with a few cells in A; last third primarily in C with a large pocket of A and a few other cells in A and PO
SDT-16-HX-1.8-3-FI-SL1-2	1.730	-	6.344	0.303	-	1.111	Primarily a mix of A and PO with the last few rows in D
SDT-16-HX-1.8-3-FI-SL1-3	0.732	6.445	6.498	0.128	1.129	1.138	Primarily a mix of A and PO with the last few rows in D
SDT-16-HX-1.8-3-FI-SL1-4	1.354	-	6.135	0.237	-	1.074	Primarily a mix of A and PO with a few cells in C and the last few rows in D
SDT-16-HX-1.8-3-FI-SL1-5	0.738	-	6.151	0.129	-	1.077	Primarily a mix of A and PO with a couple of small pockets in C and last few rows in D
SDT-16-HX-1.8-3-FI-SL1-6	1.080	6.007	6.968	0.189	1.052	1.220	Primarily a mix of A and PO with a couple of small pockets in C and last few rows in D
AVERAGE GIC	1.201	6.226	6.393	0.210	1.090	1.120	
STANDARD DEVIATION	0.421	0.310	0.312	0.074	0.054	0.055	
COEFFICIENT OF VARIATION (%)	35.084	4.977	4.880	35.084	4.977	4.880	

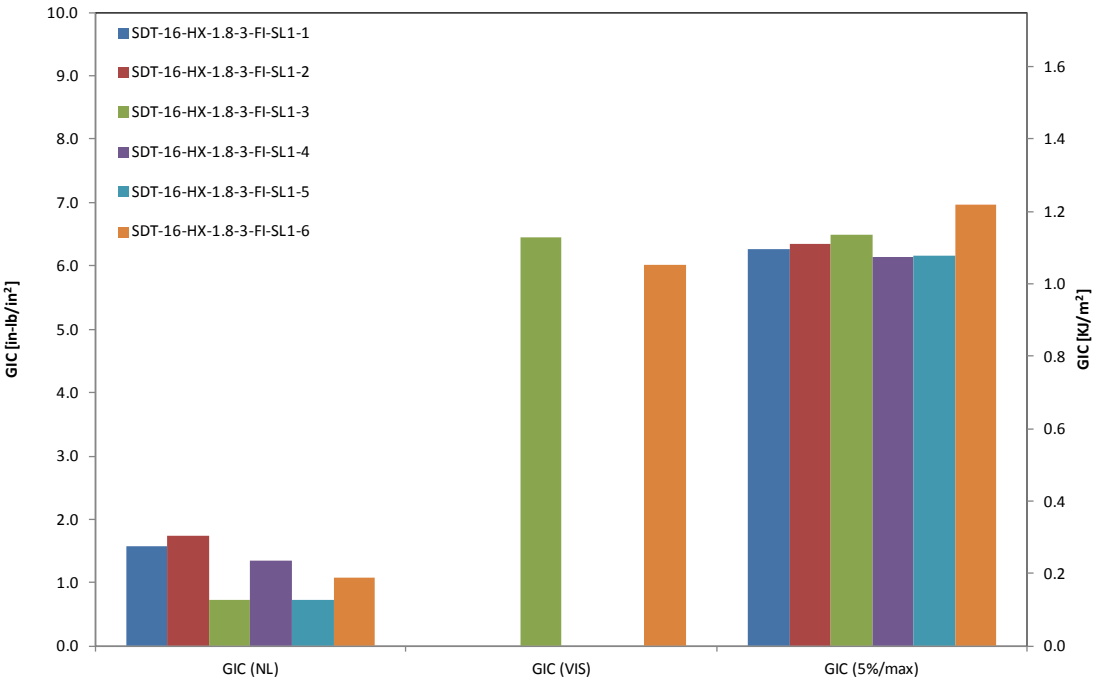

Figure C-7. GIC for HRH-10–1/8–3.0 fluid ingressed (2.5″ prescribed crack)

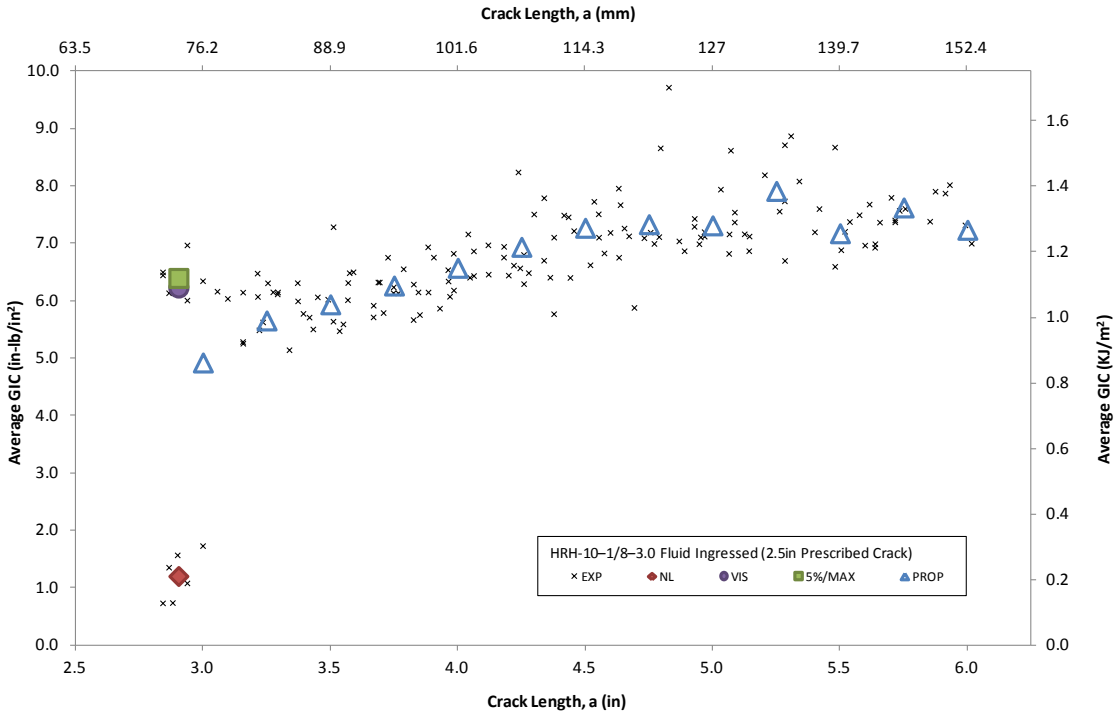

Figure C-8. Resistance curve for HRH-10–1/8–3.0 fluid ingressed (2.5″ prescribed crack)

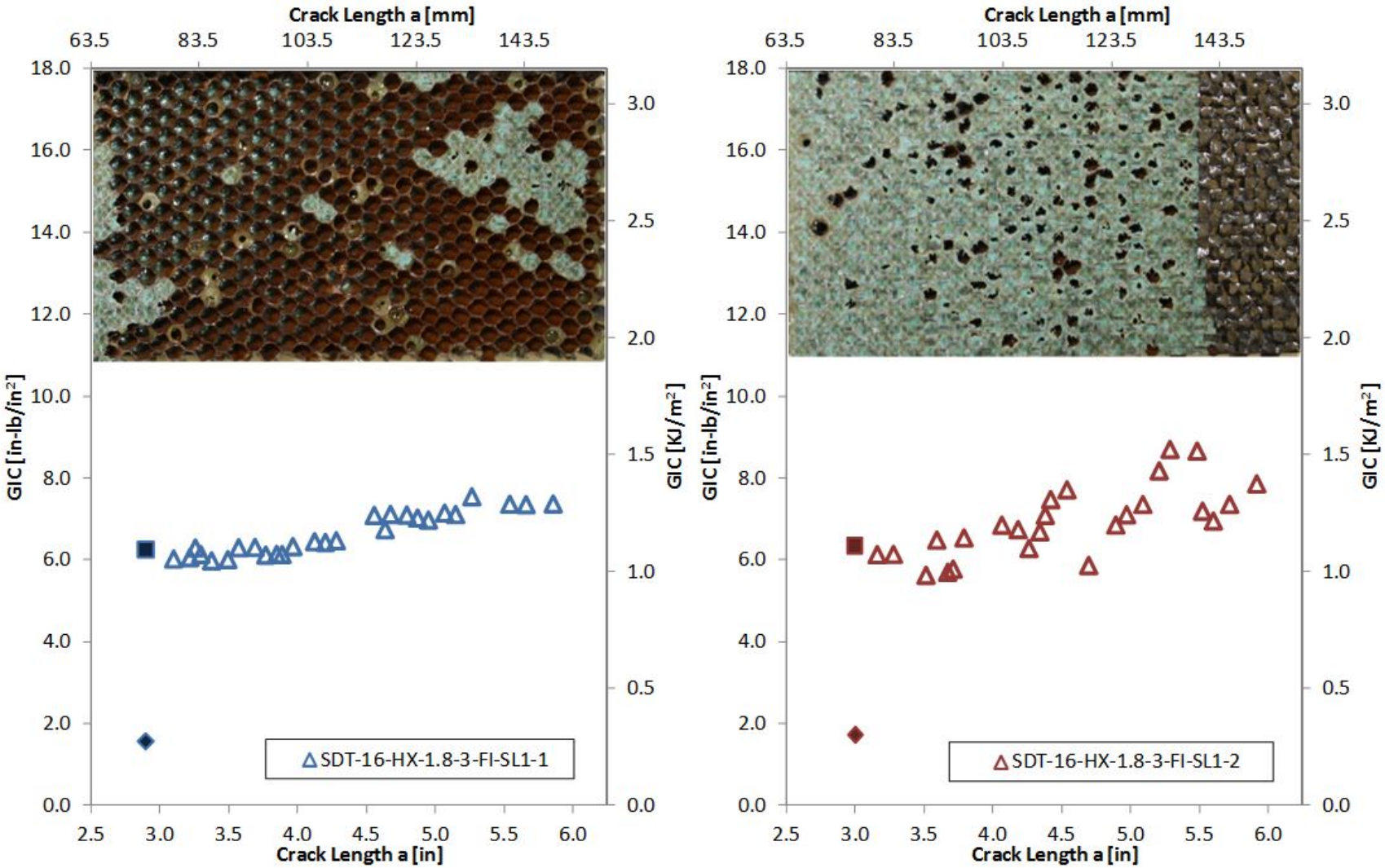

Figure C-9. Failure mode image and resistance curve for SDT-16-HX-1.8-3-FI-SL1-X #1 and #2

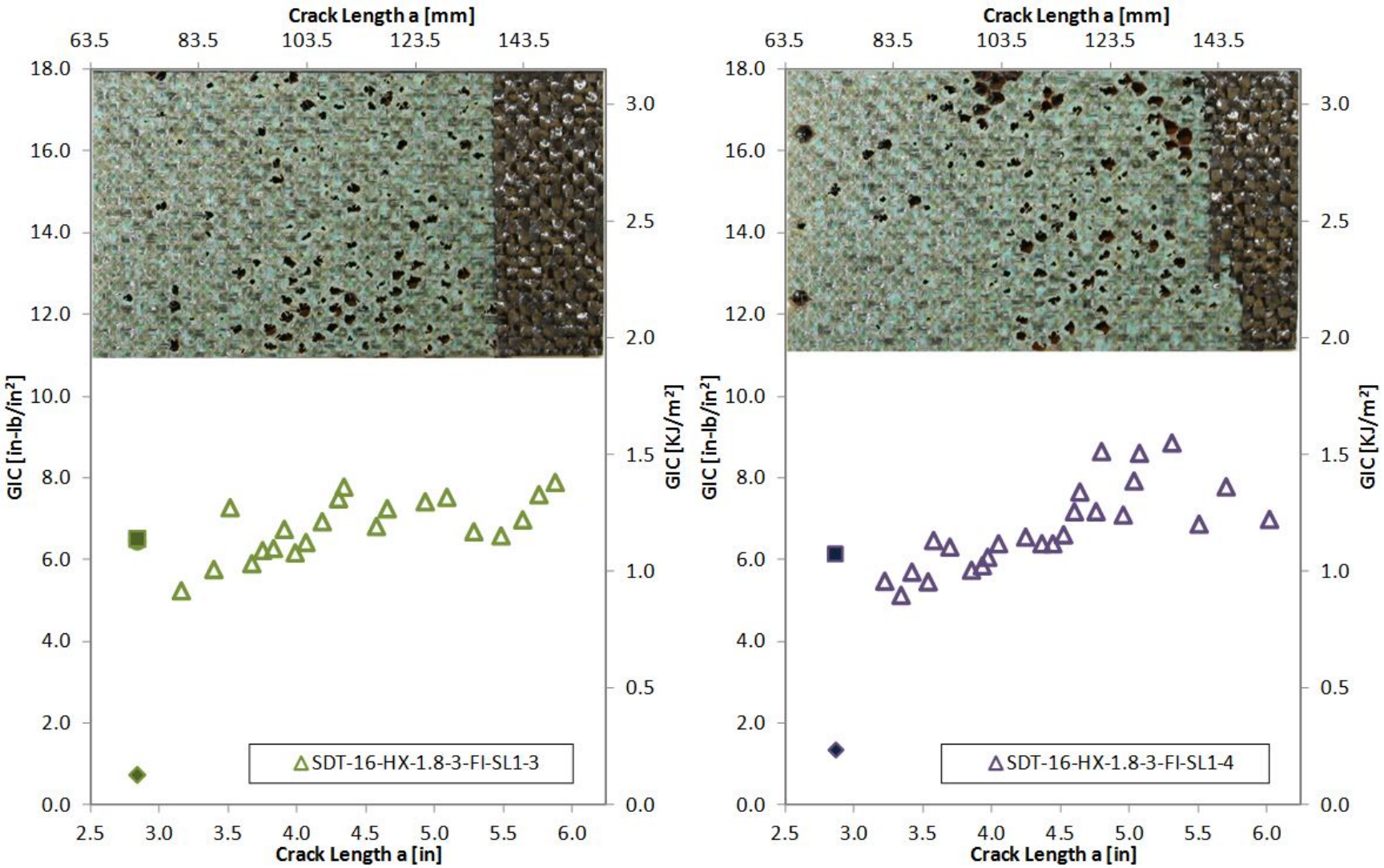

Figure C-10. Failure mode image and resistance curve for SDT-16-HX-1.8-3-FI-SL1-X #3 and #4

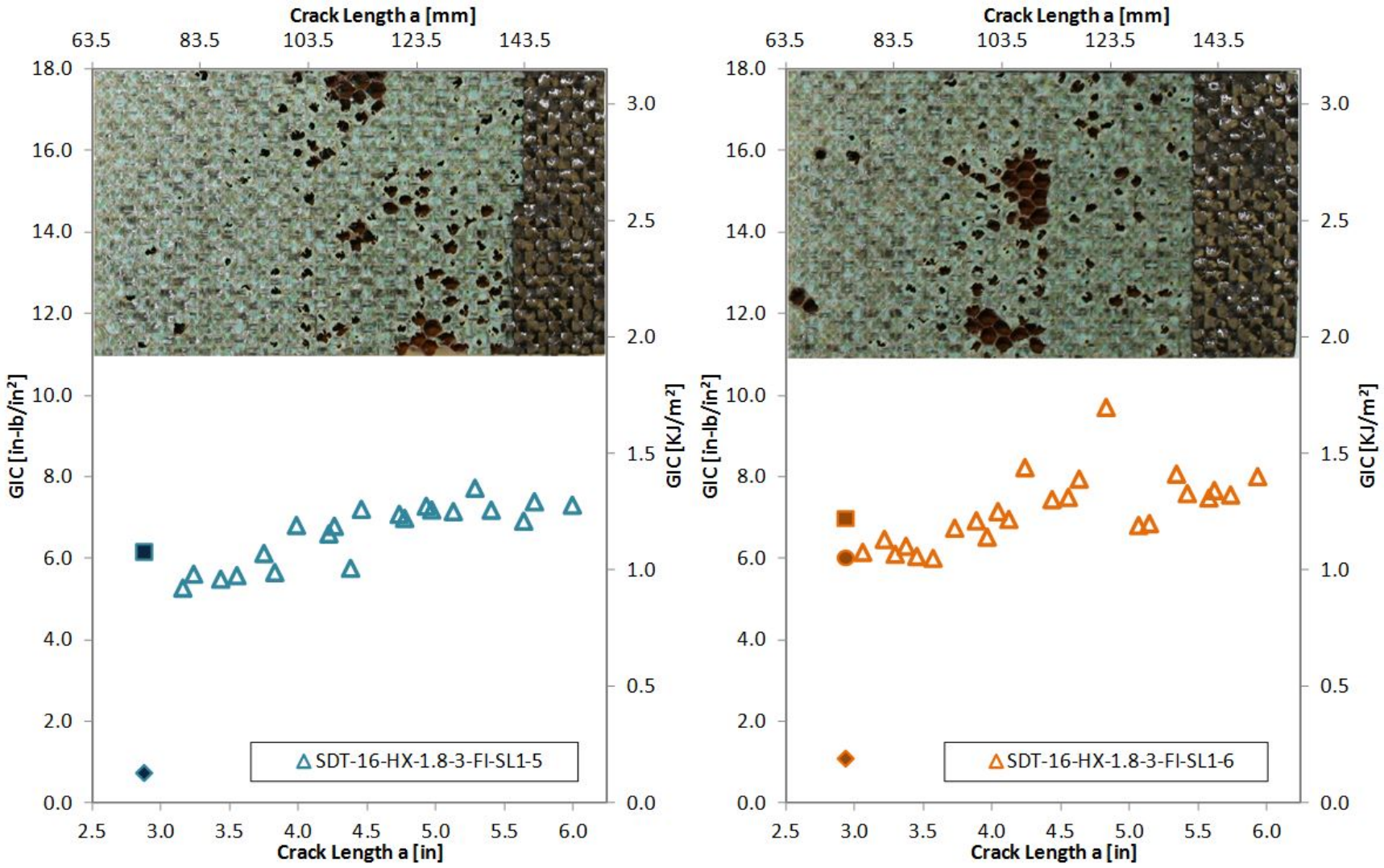

Figure C-11. Failure mode image and resistance curve for SDT-16-HX-1.8-3-FI-SL1-X #5 and #6

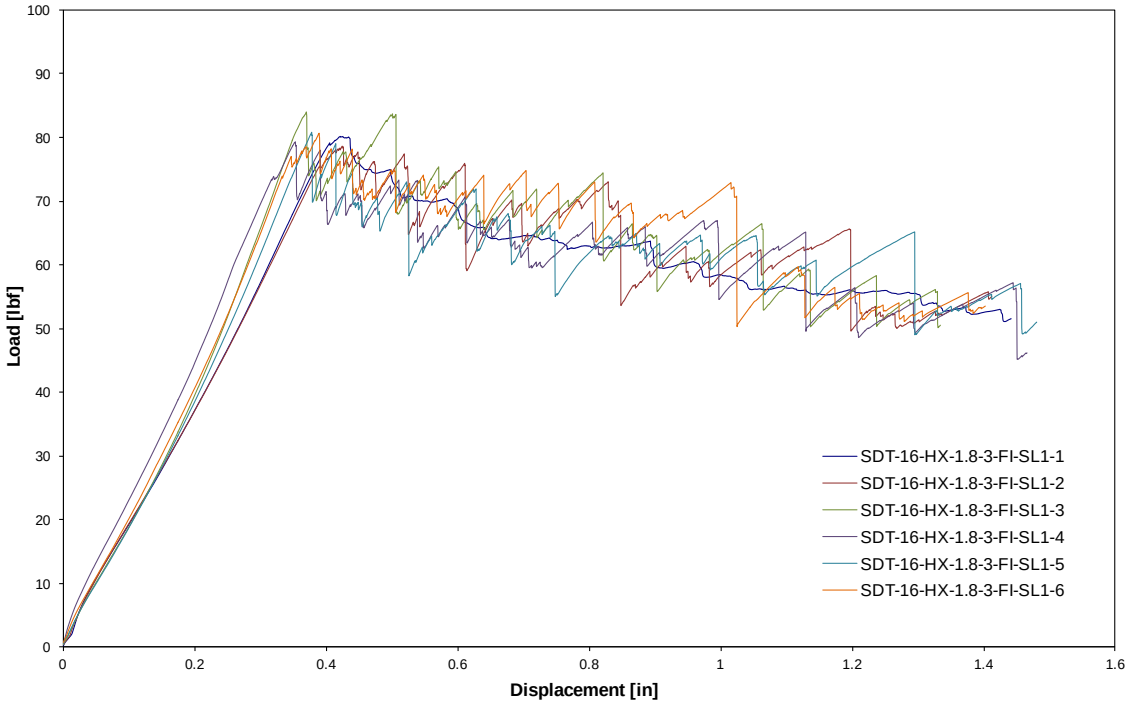

Figure C-12. Load vs. displacement curve for HRH-10–1/8–3.0 fluid ingressed (2.5″ prescribed crack)

C.1.3 HRH-10–1/8–3.0 EXTENDED FLUID-INGRESSED DATA

Table C-5. Test summary for HRH-10–1/8–3.0 extended fluid ingressed (2.5″ prescribed crack) precrack

Specimen	GIC (in-lb/in^2)			GIC (KJ/m^2)			Failure Mode
	NL	VIS	5%/max	NL	VIS	5%/max	
SDT-16-HX-1.8-3-EFI-SL1-7	1.733	-	3.138	0.303	-	0.549	Primarily in A
SDT-16-HX-1.8-3-EFI-SL1-8	2.055	-	3.827	0.360	-	0.670	Primarily in A with several cells in C
AVERAGE GIC	1.894	-	3.482	0.332	-	0.610	
STANDARD DEVIATION	0.228	-	0.487	0.040	-	0.085	
COEFFICIENT OF VARIATION (%)	12.041	-	13.997	12.041	-	13.997	

Table C-6. Test summary for HRH-10–1/8–3.0 extended fluid ingressed (2.5″ prescribed crack)

Specimen	GIC (in-lb/in^2)			GIC (KJ/m^2)			Failure Mode
	NL	VIS	5%/max	NL	VIS	5%/max	
SDT-16-HX-1.8-3-EFI-SL1-7	1.767	-	5.365	0.309	-	0.940	Primarily A, then transitions into a mix of A and PO, then a large pocket of C, lastly S
SDT-16-HX-1.8-3-EFI-SL1-8	2.134	-	8.252	0.374	-	1.445	Mix of A, PO, and C that transitions to C
AVERAGE GIC	1.950	-	6.809	0.342	-	1.192	
STANDARD DEVIATION	0.259	-	2.042	0.045	-	0.358	
COEFFICIENT OF VARIATION (%)	13.303	-	29.985	13.303	-	29.985	

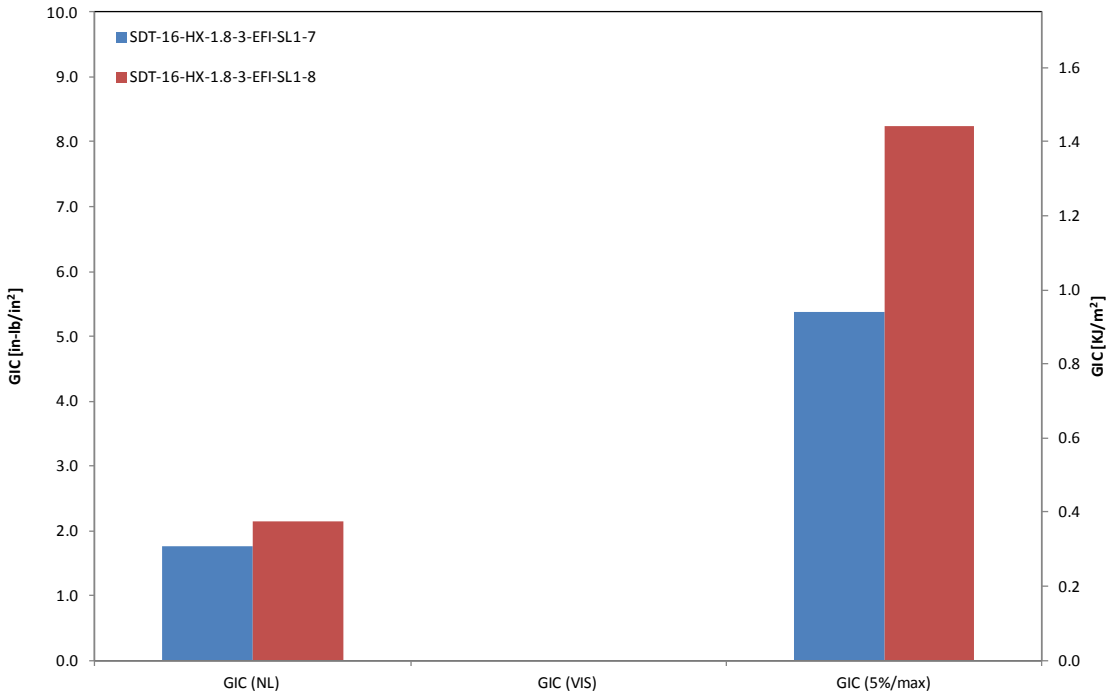

Figure C-13. GIC for HRH-10–1/8–3.0 extended fluid ingressed (2.5″ prescribed crack)

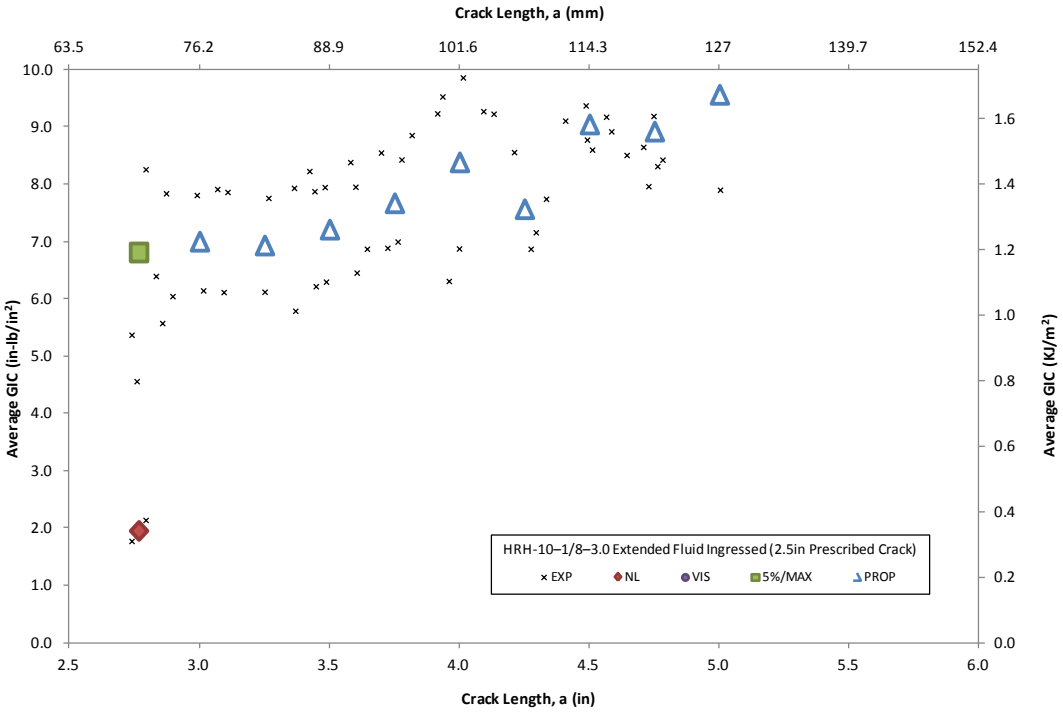

Figure C-14. Resistance curve for HRH-10–1/8–3.0 extended fluid ingressed (2.5″ prescribed crack)

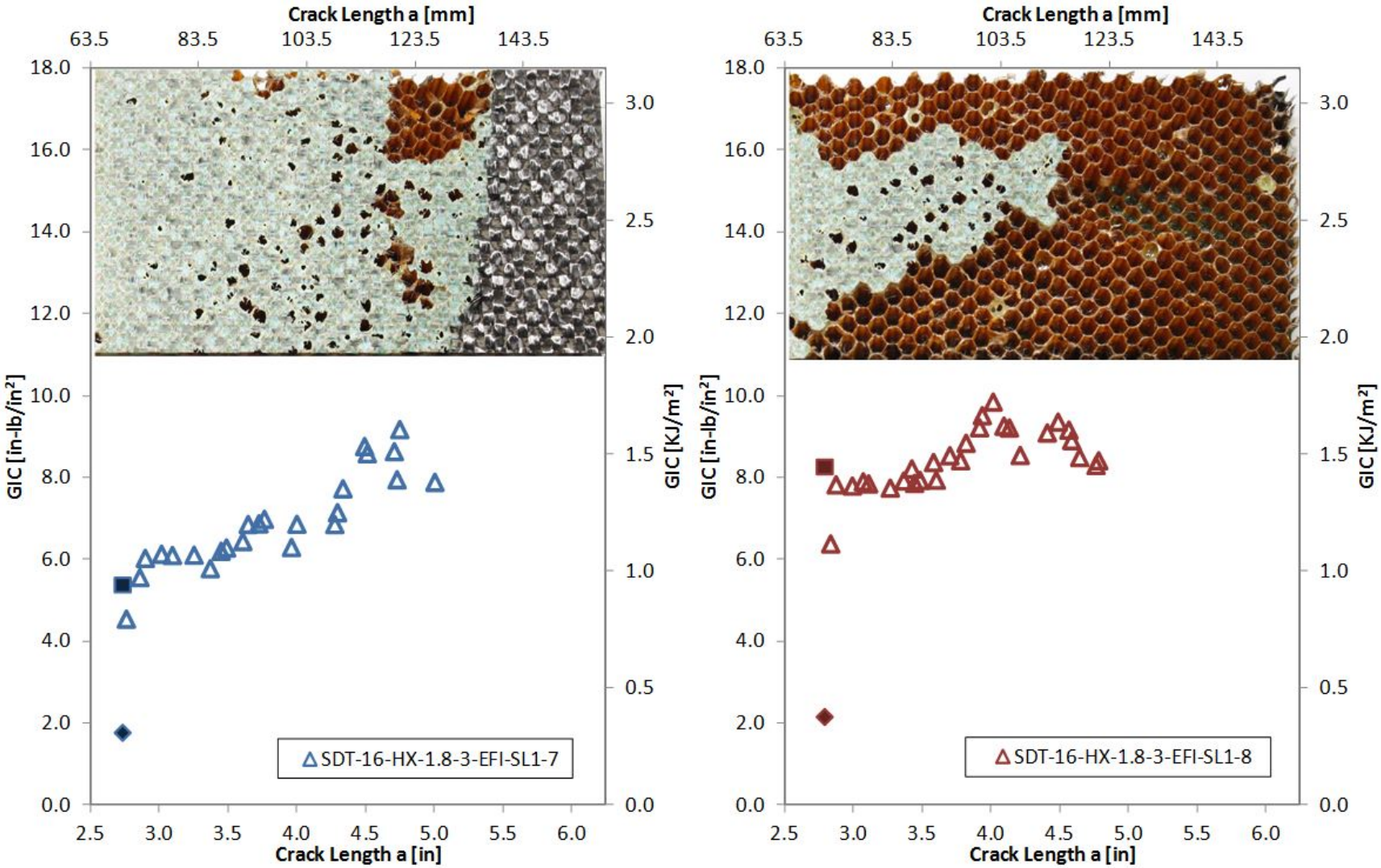

Figure C-15. Failure mode image and resistance curve for SDT-16-HX-1.8-3-EFI-SL1-X #7 and #8

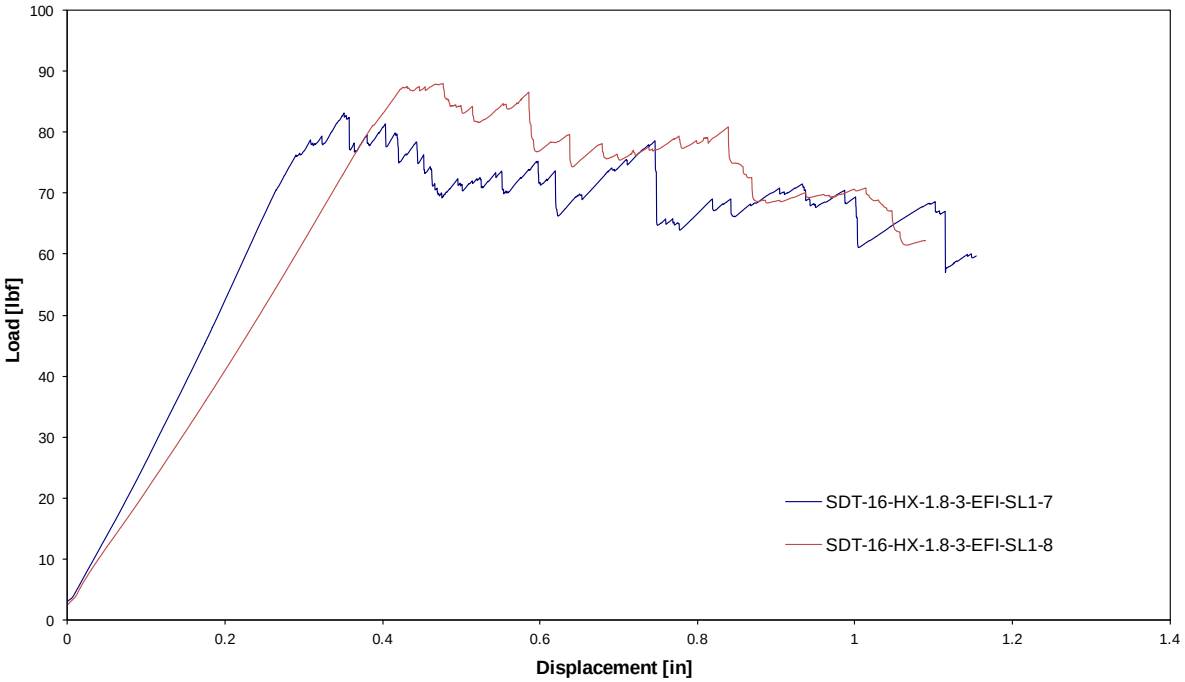

Figure C-16. Load vs. displacement curve for HRH-10–1/8–3.0 extended fluid ingressed (2.5″ prescribed crack)

C.1.4 HRH-10–1/8–3.0 WATER-INGRESSED DATA

Table C-7. Test summary for HRH-10–1/8–3.0 water ingressed (2.5″ prescribed crack) precrack

Specimen	GIC (in-lb/in^2)			GIC (KJ/m^2)			Failure Mode
	NL	VIS	5%/max	NL	VIS	5%/max	
SDT-16-HX-1.8-3-H2O-SL1-7	3.134	-	4.589	0.549	-	0.804	First couple of rows primarily in A with a pocket of C
SDT-16-HX-1.8-3-H2O-SL1-8	3.771	-	5.361	0.660	-	0.939	Mix of A and C
SDT-16-HX-1.8-3-H2O-SLX-7	2.088	-	4.258	0.366	-	0.746	Primarily in A with a couple of cells in C
SDT-16-HX-1.8-3-H2O-SLX-8	2.527	-	4.466	0.443	-	0.782	Mix of A and C
AVERAGE GIC	2.880	-	4.669	0.504	-	0.818	
STANDARD DEVIATION	0.733	-	0.482	0.128	-	0.084	
COEFFICIENT OF VARIATION (%)	25.447	-	10.314	25.447	-	10.314	

Table C-8. Test summary for HRH-10–1/8–3.0 water ingressed (2.5″ prescribed crack)

Specimen	GIC (in-lb/in^2)			GIC (KJ/m^2)			Failure Mode
	NL	VIS	5%/max	NL	VIS	5%/max	
SDT-16-HX-1.8-3-H2O-SL1-7	3.435	-	8.040	0.602	-	1.408	Primarily A with a pocket of C, then a mix of A and PO, then S
SDT-16-HX-1.8-3-H2O-SL1-8	2.381	-	7.611	0.417	-	1.333	Primarily in C with a few cells in A
SDT-16-HX-1.8-3-H2O-SLX-7	3.977	-	8.070	0.697	-	1.413	Mix of A and C, then C
SDT-16-HX-1.8-3-H2O-SLX-8	5.167	-	6.811	0.905	-	1.193	Primarily in C
AVERAGE GIC	3.740	-	7.633	0.655	-	1.337	
STANDARD DEVIATION	1.159	-	0.587	0.203	-	0.103	
COEFFICIENT OF VARIATION (%)	30.993	-	7.687	30.993	-	7.687	

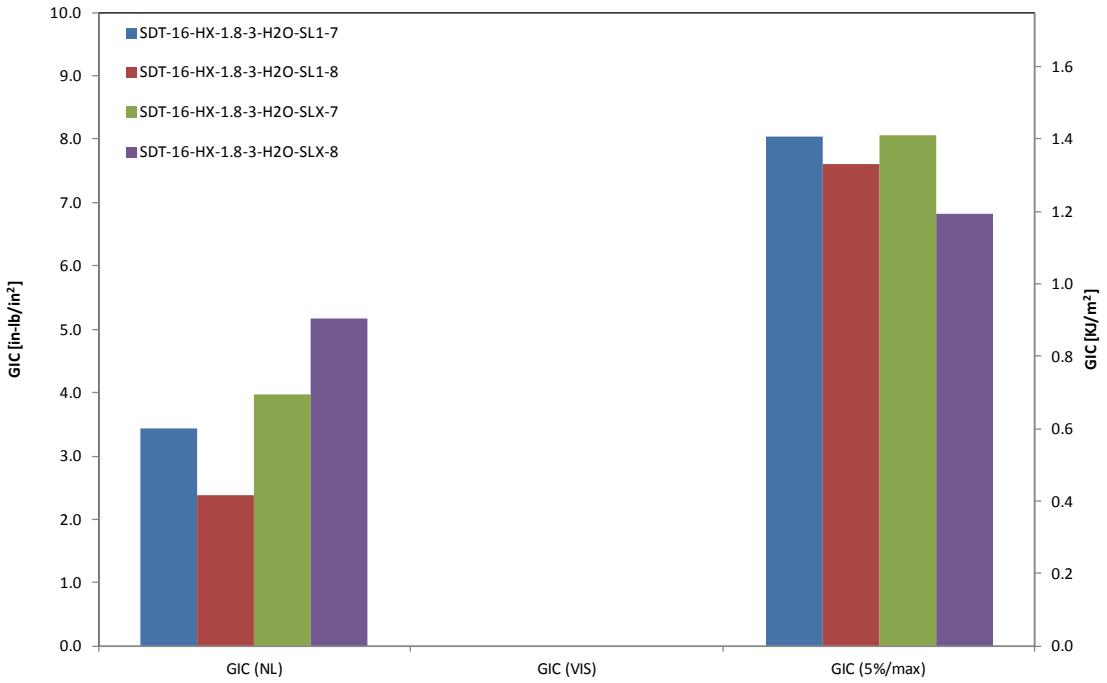

Figure C-17. GIC for HRH-10–1/8–3.0 water ingressed (2.5″ prescribed crack)

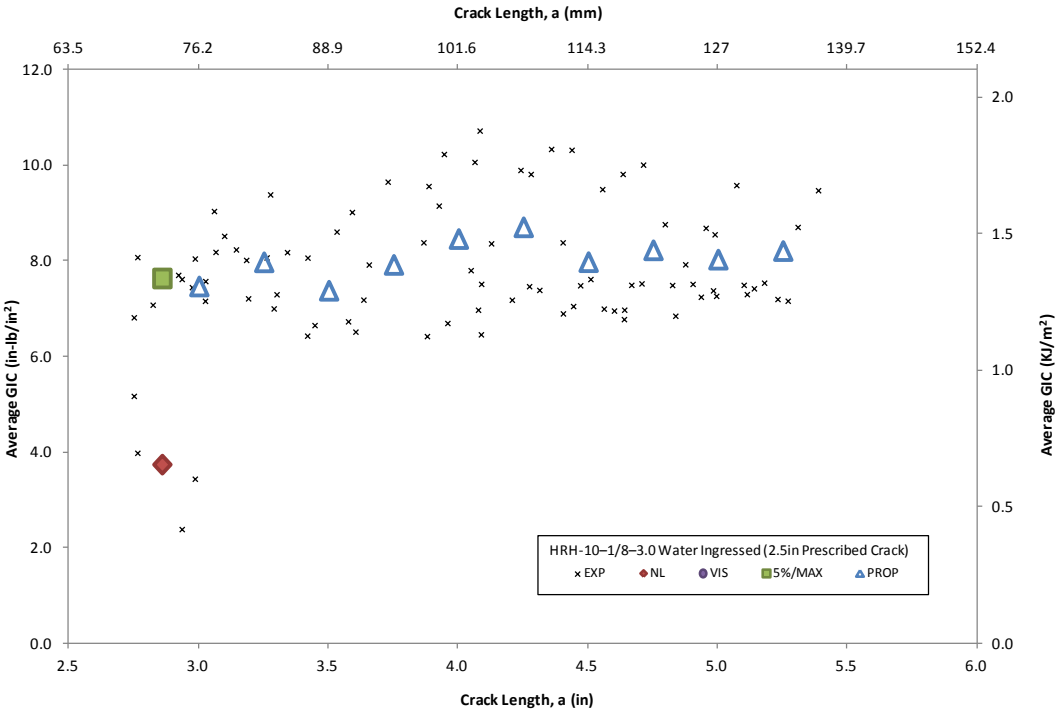

Figure C-18. Resistance curve for HRH-10–1/8–3.0 water ingressed (2.5″ prescribed crack)

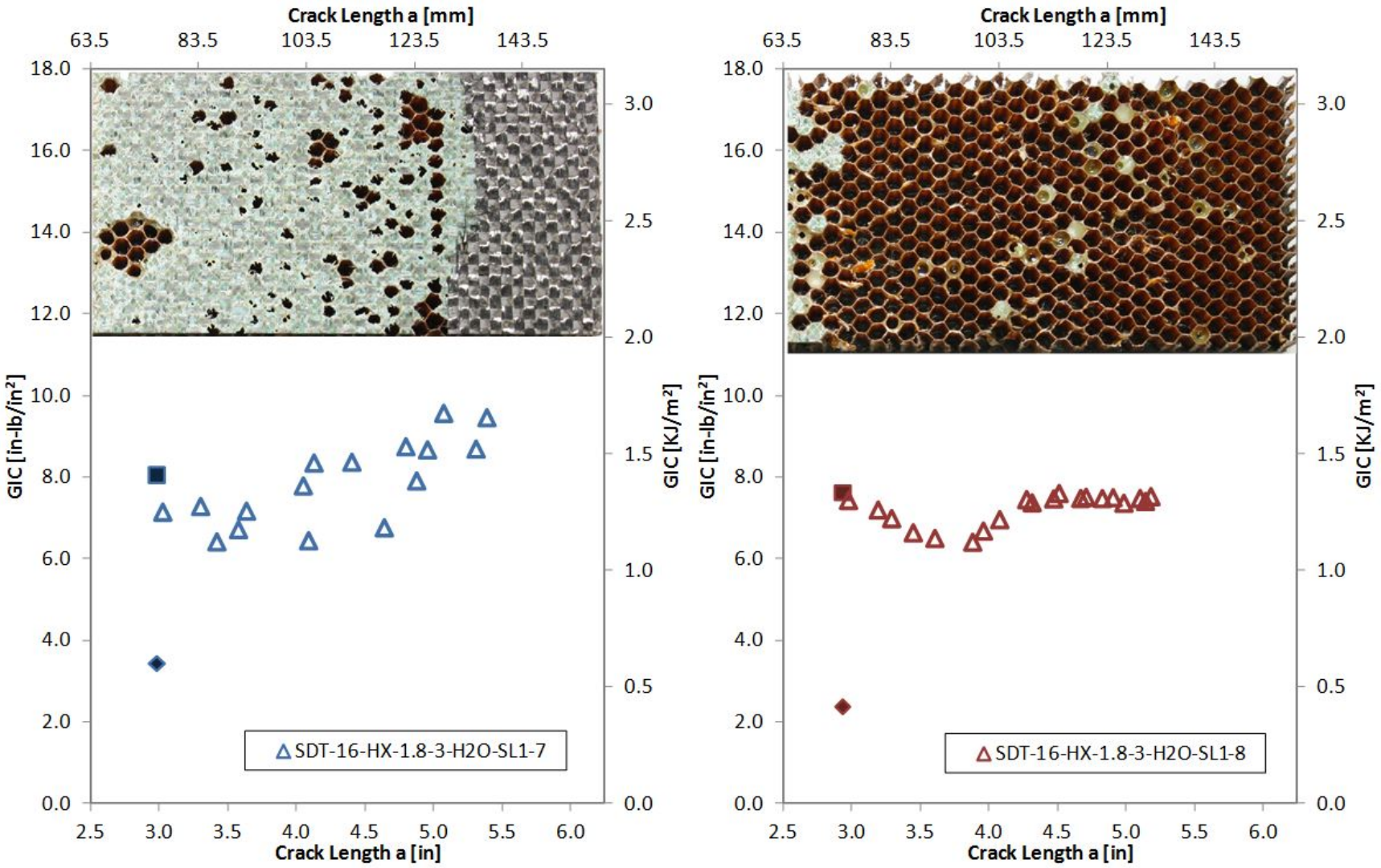

Figure C-19. Failure mode image and resistance curve for SDT-16-HX-1.8-3-H2O-SL1-X #7 and #8

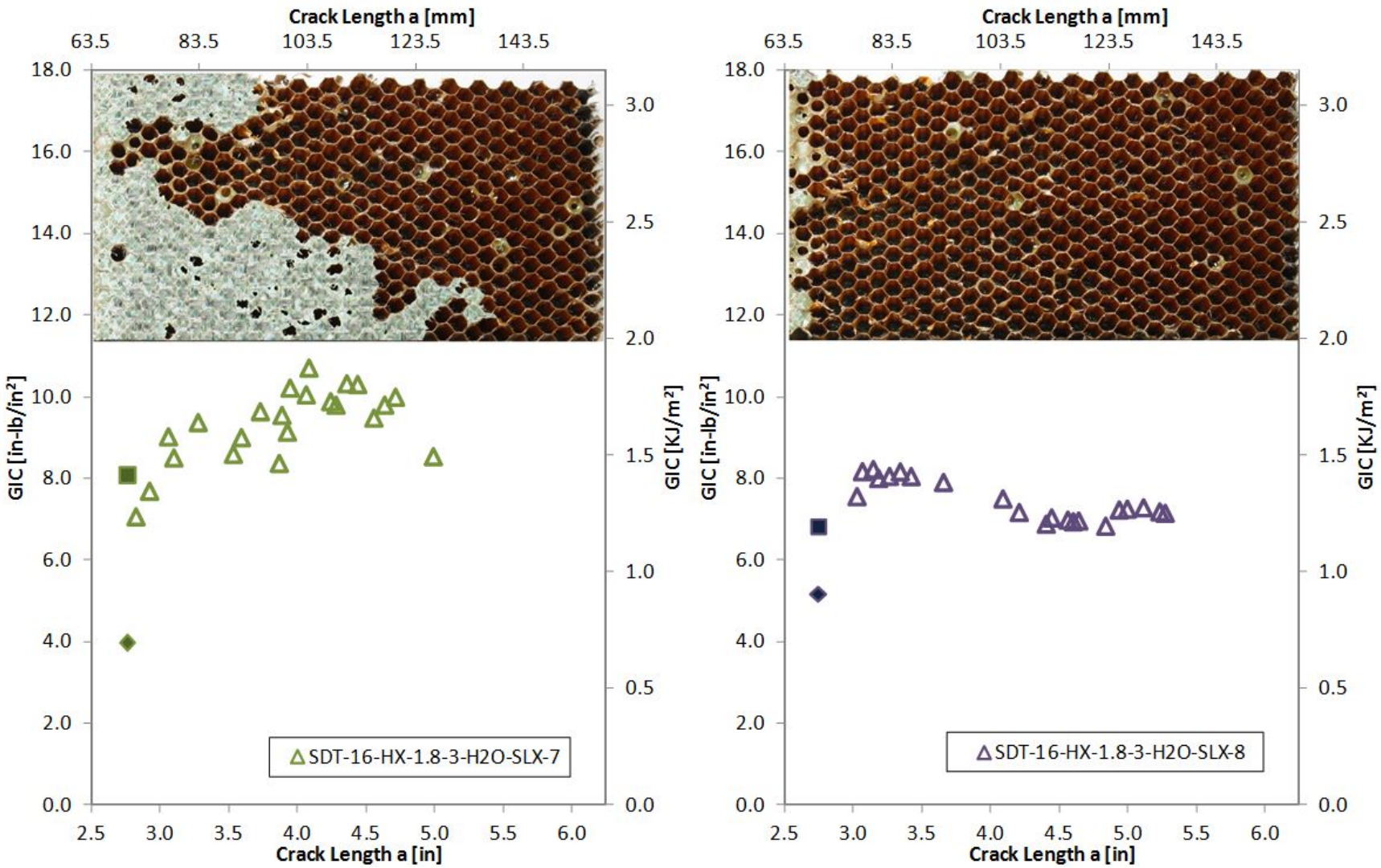

Figure C-20. Failure mode image and resistance curve for SDT-16-HX-1.8-3-H2O-SLX-X #7 and #8

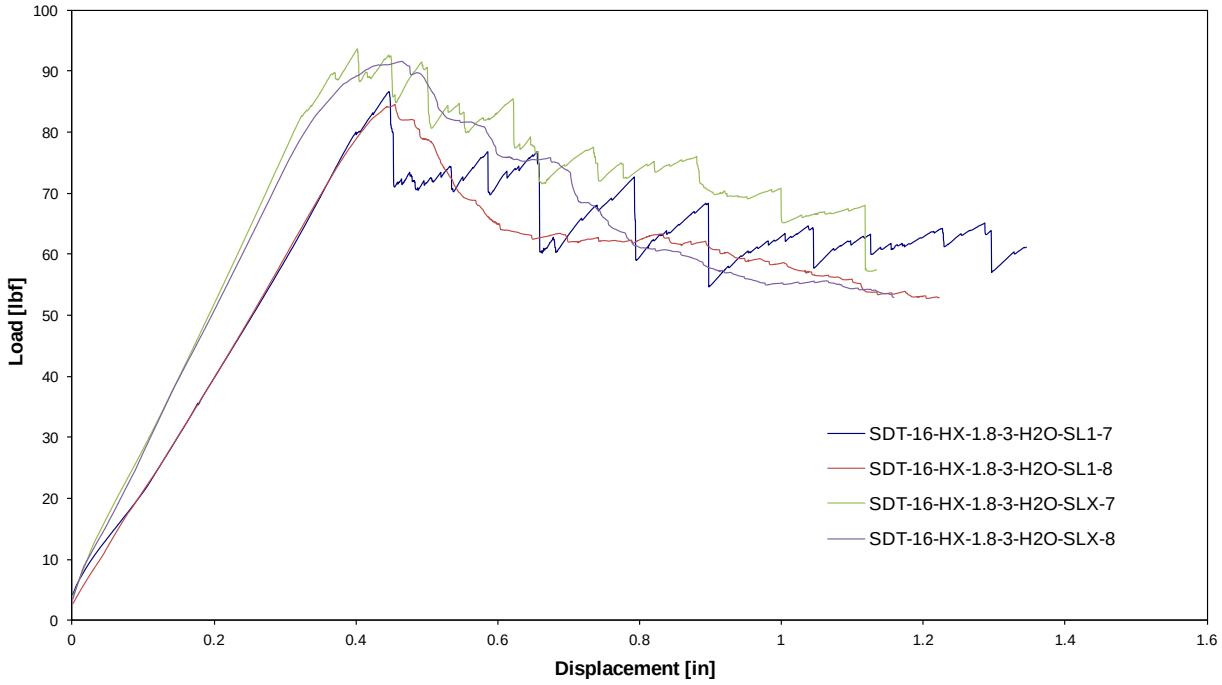

Figure C-21. Load vs. displacement curve for HRH-10–1/8–3.0 water ingressed (2.5″ prescribed crack)

C.2 HRH-10–3/16–2.0 DATA

C.2.1 HRH-10–3/16–2.0 BASELINE DATA

Table C-9. Test summary for HRH-10–3/16–2.0 baseline (2.5″ prescribed crack) precrack

Specimen	GIC (in-lb/in^2)			GIC (KJ/m^2)			Failure Mode
	NL	VIS	5%/max	NL	VIS	5%/max	
SDT-16-HX-3.16-2-BL-SL1-1	1.551	-	3.593	0.272	-	0.629	First row primarily in A with a cell in PO; second row a mix of A and C
SDT-16-HX-3.16-2-BL-SL1-2	1.512	-	3.214	0.265	-	0.563	First row primarily in A; second row a mix of A and PO
SDT-16-HX-3.16-2-BL-SL1-3	1.529	-	2.654	0.268	-	0.465	First row primarily in A; second row a mix of A and C
SDT-16-HX-3.16-2-BL-SL1-4	2.364	-	3.105	0.414	-	0.544	Primarily in C
SDT-16-HX-3.16-2-BL-SL1-5	2.105	-	4.118	0.369	-	0.721	First row primarily in A with a cell in PO; second row a mix of A and C
SDT-16-HX-3.16-2-BL-SL1-6	2.461	-	3.442	0.431	-	0.603	Primarily in A with a couple cells in PO
AVERAGE GIC	1.920	-	3.354	0.336	-	0.587	
STANDARD DEVIATION	0.443	-	0.494	0.078	-	0.087	
COEFFICIENT OF VARIATION (%)	23.055	-	14.731	23.055	-	14.731	

Table C-10. Test summary for HRH-10–3/16–2.0 baseline (2.5″prescribed crack)

Specimen	GIC (in-lb/in^2)			GIC (KJ/m^2)			Failure Mode
	NL	VIS	5%/max	NL	VIS	5%/max	
SDT-16-HX-3.16-2-BL-SL1-1	1.941	-	3.790	0.340	-	0.664	Primarily in C after a quick transition from a mix of A and C
SDT-16-HX-3.16-2-BL-SL1-2	2.466	4.339	4.841	0.432	0.760	0.848	Primarily in C after a quick transition from a mix of A and C
SDT-16-HX-3.16-2-BL-SL1-3	2.319	-	6.260	0.406	-	1.096	Primarily in C after a quick transition from a mix of A and C
SDT-16-HX-3.16-2-BL-SL1-4	1.912	5.111	5.320	0.335	0.895	0.932	Primarily in C
SDT-16-HX-3.16-2-BL-SL1-5	2.242	4.923	5.699	0.393	0.862	0.998	Primarily in C after a quick transition from a mix of A and C
SDT-16-HX-3.16-2-BL-SL1-6	1.891	3.374	3.676	0.331	0.591	0.644	Primarily in C after a quick transition from a mix of A and C
AVERAGE GIC	2.128	4.437	4.931	0.373	0.777	0.864	
STANDARD DEVIATION	0.246	0.781	1.038	0.043	0.137	0.182	
COEFFICIENT OF VARIATION (%)	11.543	17.606	21.061	11.543	17.606	21.061	

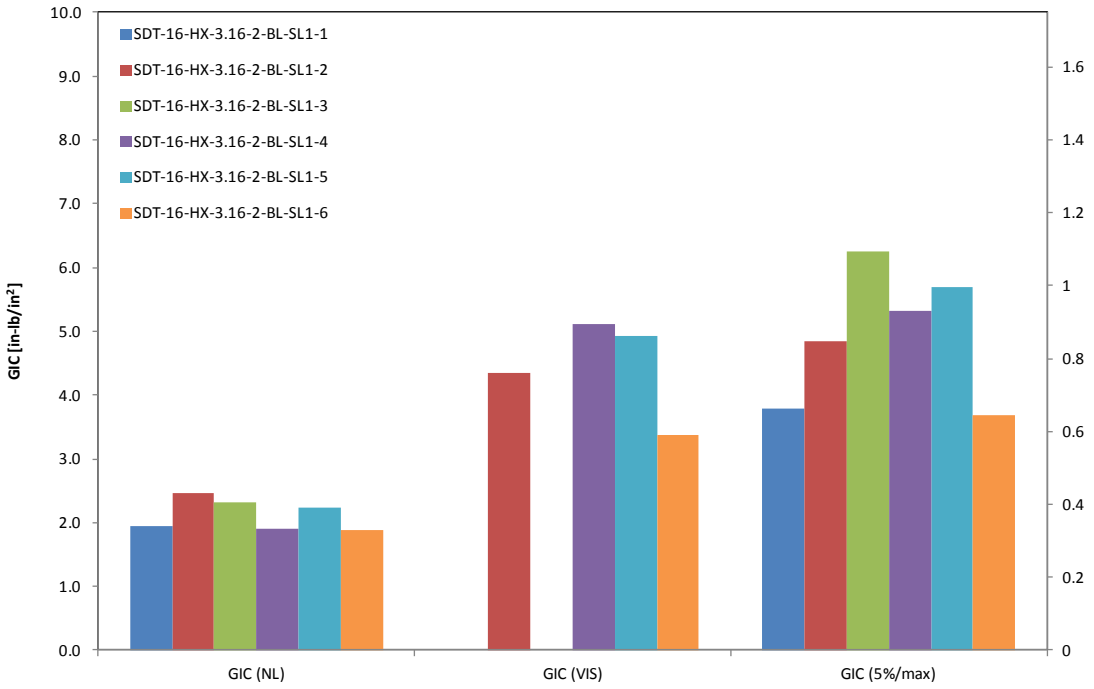

Figure C-22. GIC for HRH-10–3/16–2.0 baseline (2.5″ prescribed crack)

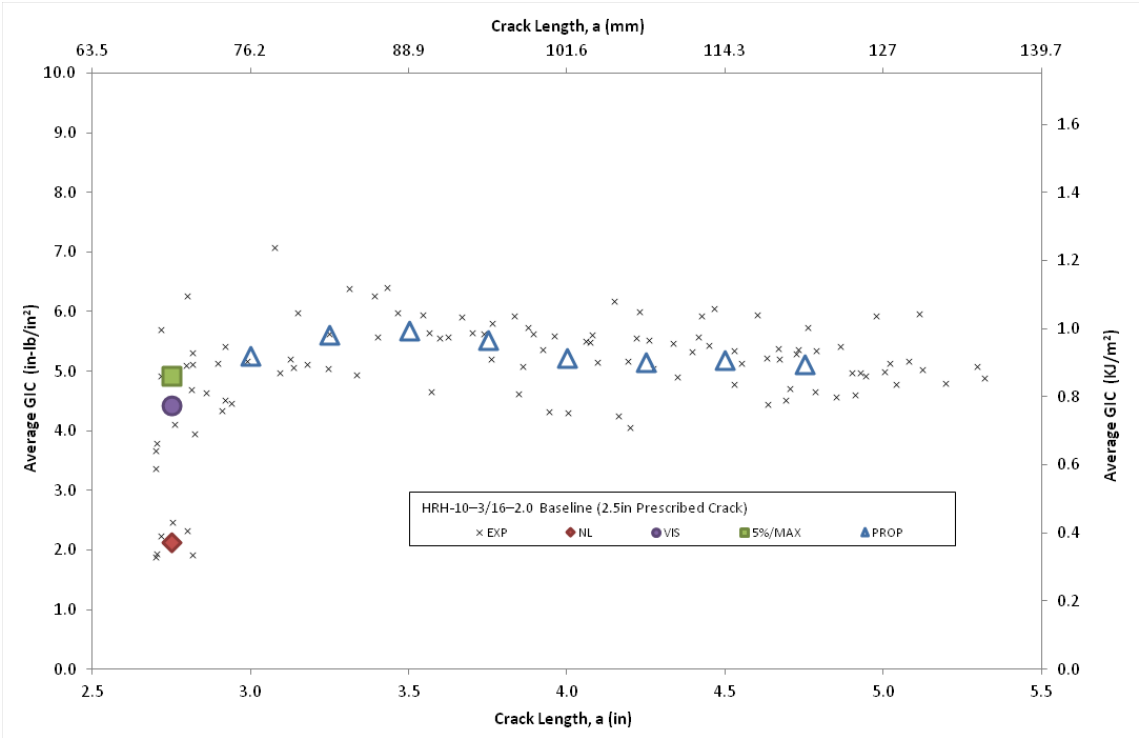

Figure C-23. Resistance curve for HRH-10–3/16–2.0 baseline (2.5″ prescribed crack)

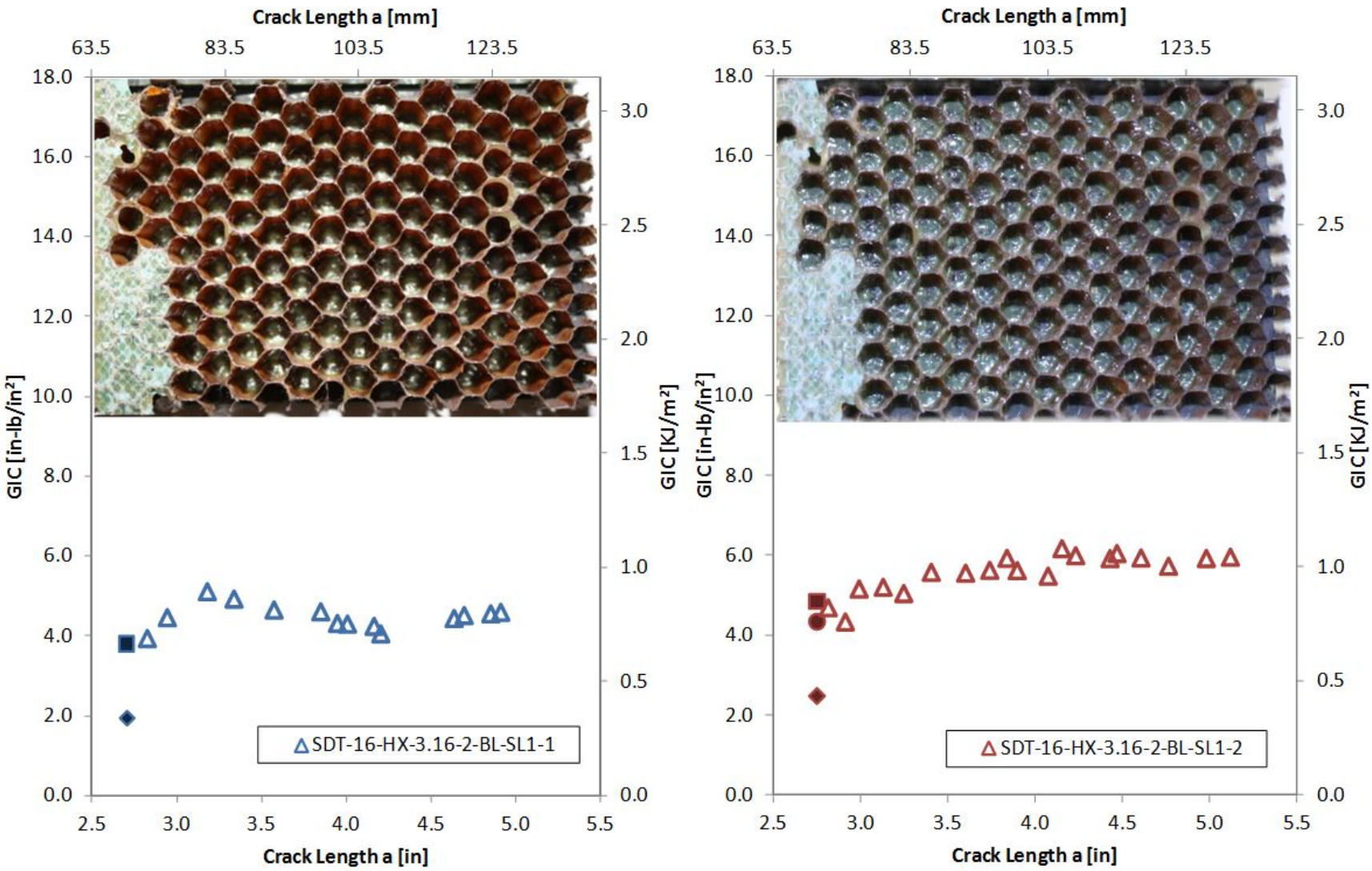

Figure C-24. Failure mode image and resistance curve for SDT-16-HX-3.16-2-BL-SL1-X #1 and #2

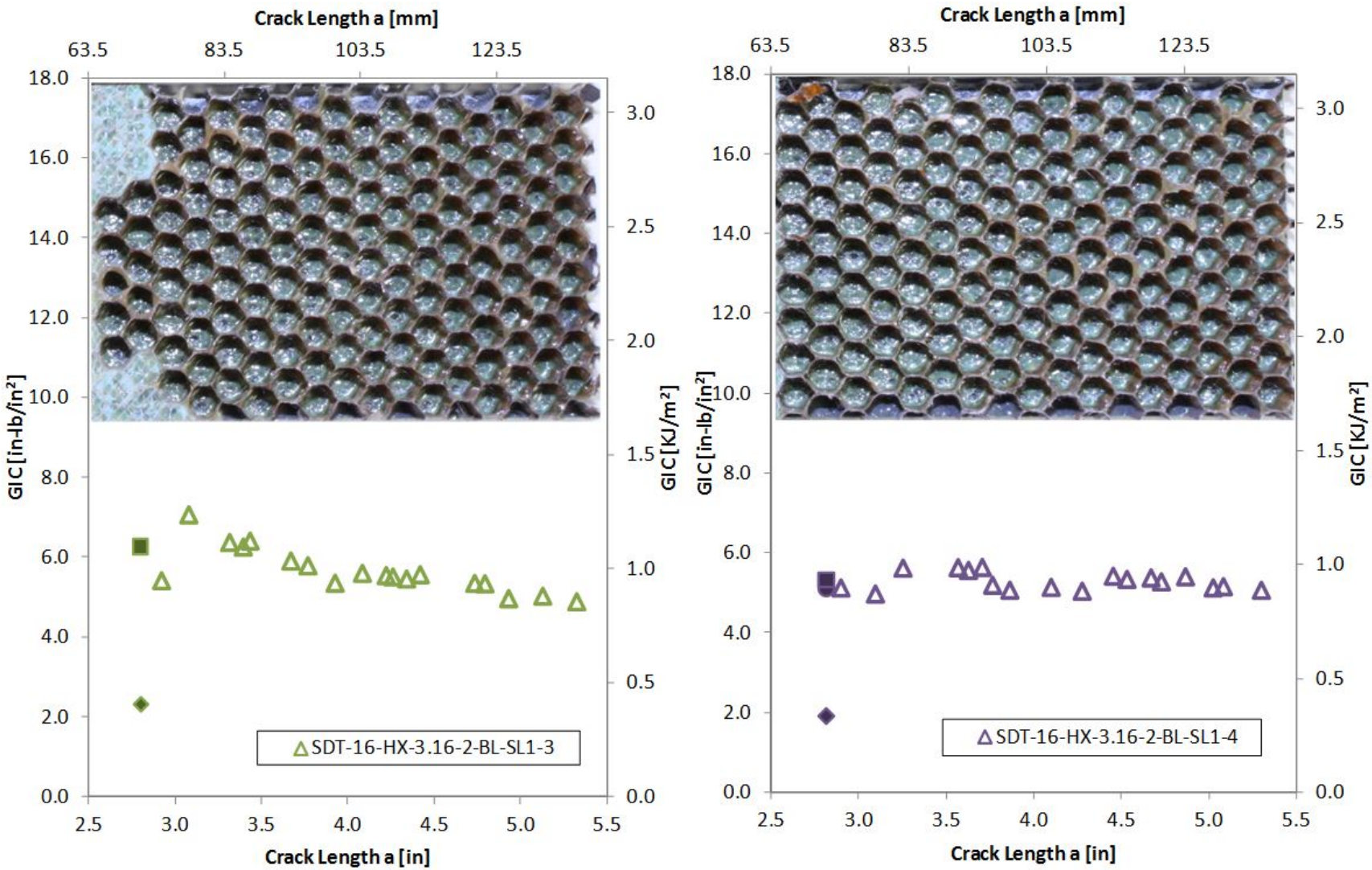

Figure C-25. Failure mode image and resistance curve for SDT-16-HX-3.16-2-BL-SL1-X #3 and #4

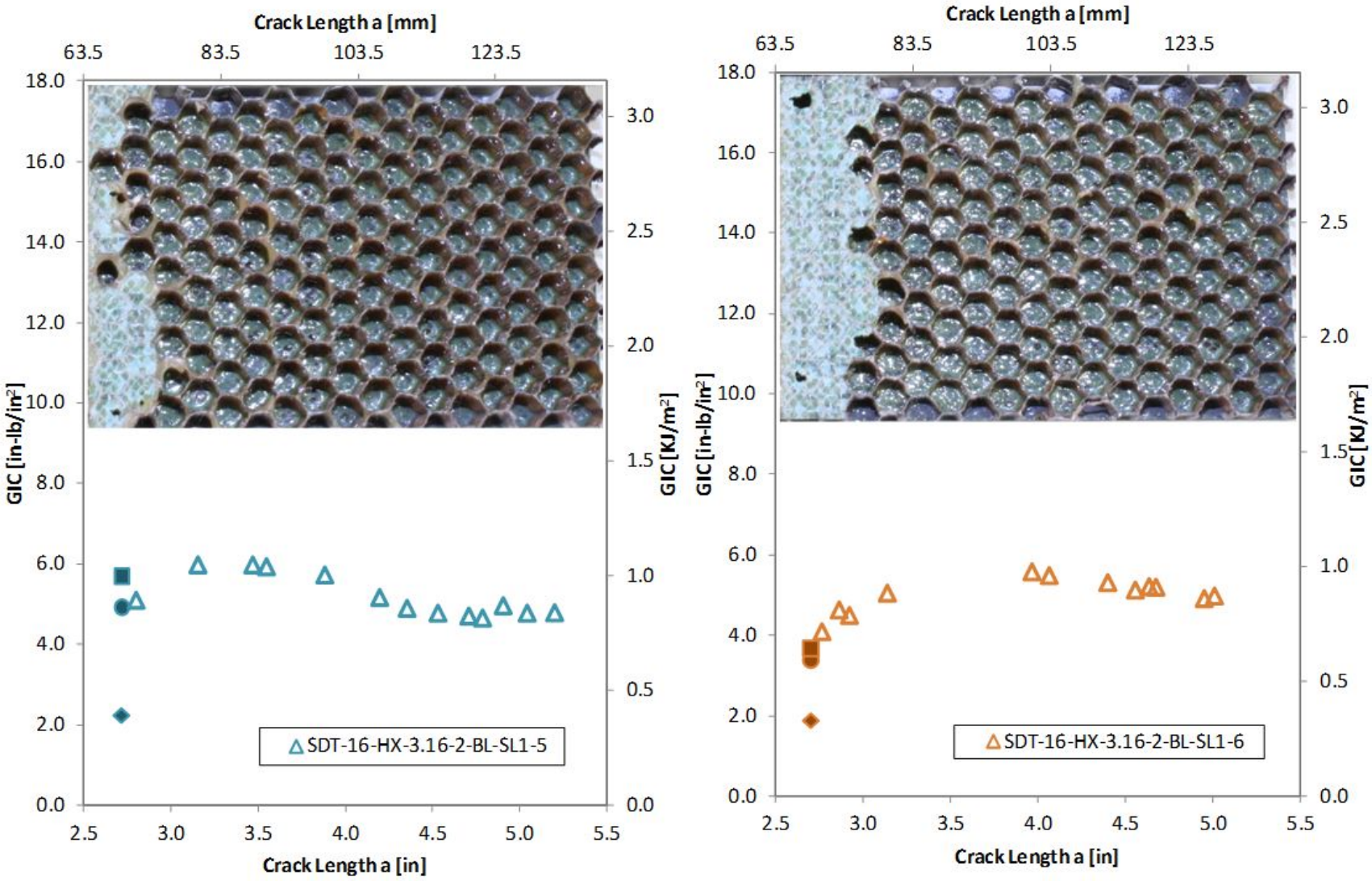

Figure C-26. Failure mode image and resistance curve for SDT-16-HX-3.16-2-BL-SL1-X #5 and #6

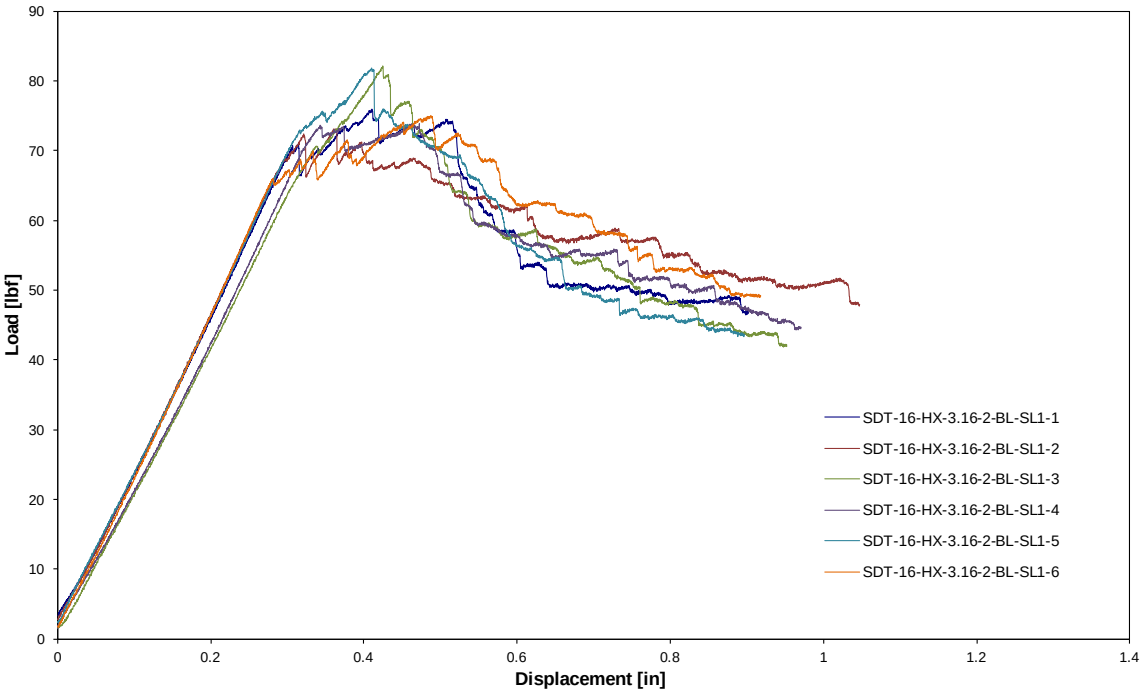

Figure C-27. Load vs. displacement curve for HRH-10–3/16–2.0 baseline (2.5″ prescribed crack)

C.2.2. HRH-10–3/16–2.0 FLUID-INGRESSED DATA

Table C-11. Test summary for HRH-10–3/16–2.0 fluid ingressed (2.5″ prescribed crack) precrack

Specimen	GIC (in-lb/in^2)			GIC (KJ/m^2)			Failure Mode
	NL	VIS	5%/max	NL	VIS	5%/max	
SDT-16-HX-3.16-2-FI-SL1-1	2.245	-	2.927	0.393	0.000	0.513	First row primarily in A, then primarily in C
SDT-16-HX-3.16-2-FI-SL1-2	1.443	-	2.060	0.253	0.000	0.361	First row primarily in A, then primarily in C
SDT-16-HX-3.16-2-FI-SL1-3	2.374	-	2.979	0.416	0.000	0.522	First row primarily in A; second row primarily in A with a few cells in C, then primarily in C
SDT-16-HX-3.16-2-FI-SL1-4	1.596	-	2.502	0.279	0.000	0.438	First row primarily in A, then primarily in C with a cell in A
SDT-16-HX-3.16-2-FI-SL1-5	1.472	-	3.532	0.258	0.000	0.619	First two rows primarily in A; third row a mix of A and C, then primarily C with a couple cells in A
SDT-16-HX-3.16-2-FI-SL1-6	1.447	-	3.113	0.253	0.000	0.545	First row primarily in A, second row primarily in A with a few cells in C, then primarily in C
AVERAGE GIC	1.763	-	2.852	0.309	0.000	0.499	
STANDARD DEVIATION	0.429	-	0.510	0.075	0.000	0.089	
COEFFICIENT OF VARIATION (%)	24.354	-	17.891	24.354	-	17.891	

Table C-12. Test summary for HRH-10–3/16–2.0 fluid ingressed (2.5″ prescribed crack)

Specimen	GIC (in-lb/in^2)			GIC (KJ/m^2)			Failure Mode
	NL	VIS	5%/max	NL	VIS	5%/max	
SDT-16-HX-3.16-2-FI-SL1-1	1.168	4.184	4.490	0.205	0.733	0.786	Primarily in C
SDT-16-HX-3.16-2-FI-SL1-2	1.611	-	5.943	0.282	-	1.041	Primarily in C
SDT-16-HX-3.16-2-FI-SL1-3	2.231	-	5.965	0.391	-	1.045	Primarily in C
SDT-16-HX-3.16-2-FI-SL1-4	0.978	-	4.119	0.171	-	0.721	Primarily in C
SDT-16-HX-3.16-2-FI-SL1-5	1.583	5.501	5.716	0.277	0.963	1.001	First row primarily C with a couple cells in A, then primarily in C
SDT-16-HX-3.16-2-FI-SL1-6	1.826	5.740	5.756	0.320	1.005	1.008	Primarily in C
AVERAGE GIC	1.566	5.142	5.331	0.274	0.900	0.934	
STANDARD DEVIATION	0.451	0.838	0.810	0.079	0.147	0.142	
COEFFICIENT OF VARIATION (%)	28.782	16.292	15.192	28.782	16.292	15.192	

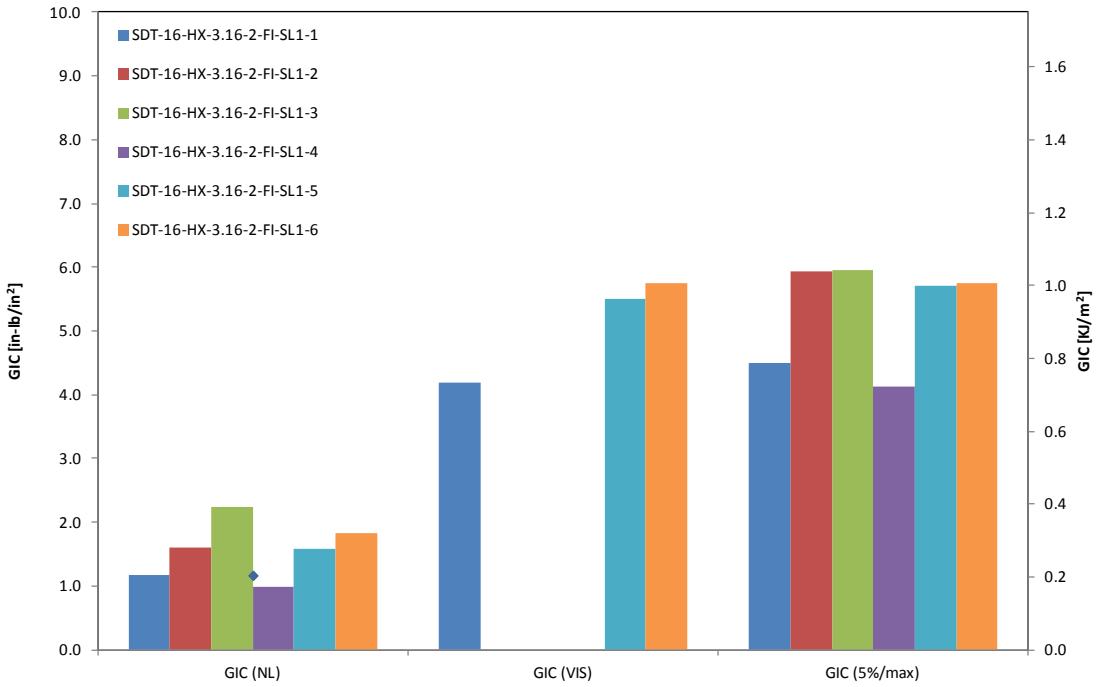

Figure C-28. GIC for HRH-10–3/16–2.0 fluid ingressed (2.5″ prescribed crack)

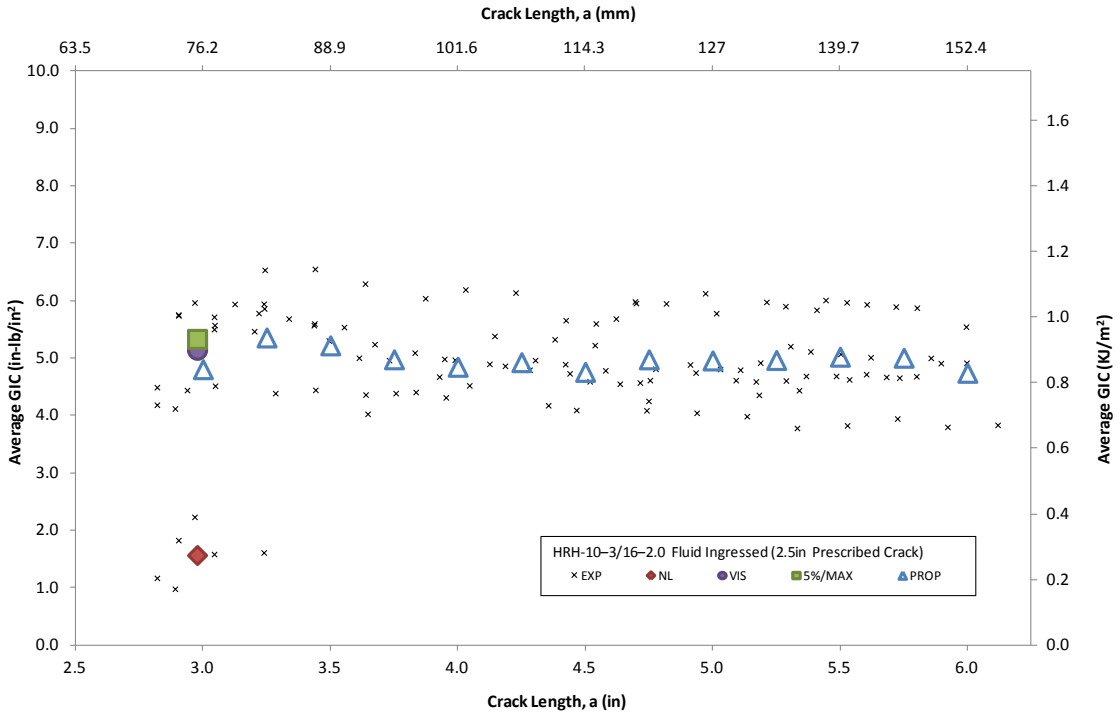

Figure C-29. Resistance curve for HRH-10–3/16–2.0 fluid ingressed (2.5″ prescribed crack)

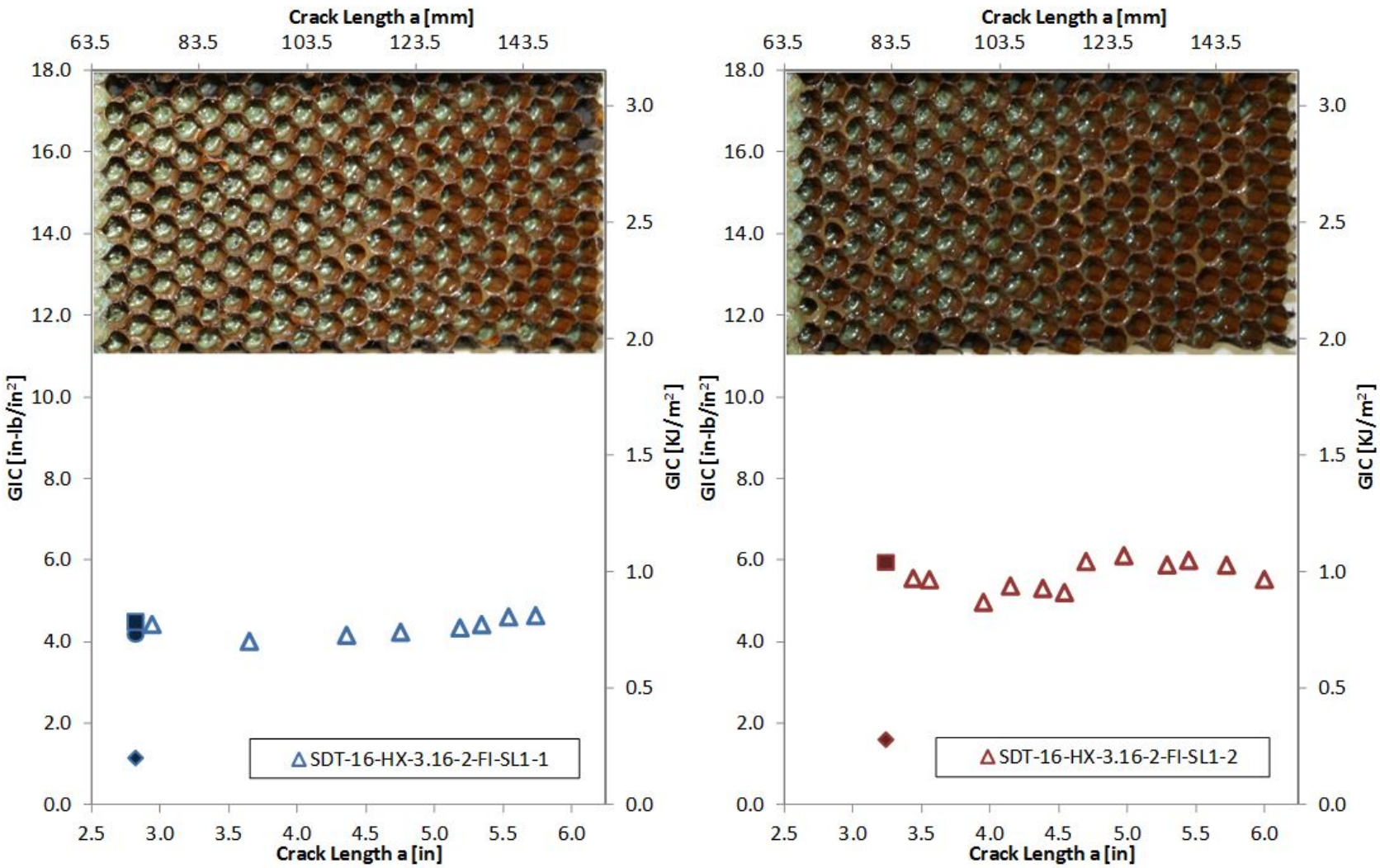

Figure C-30. Failure mode image and resistance curve for SDT-16-HX-3.16-2-FI-SL1-X #1 and #2

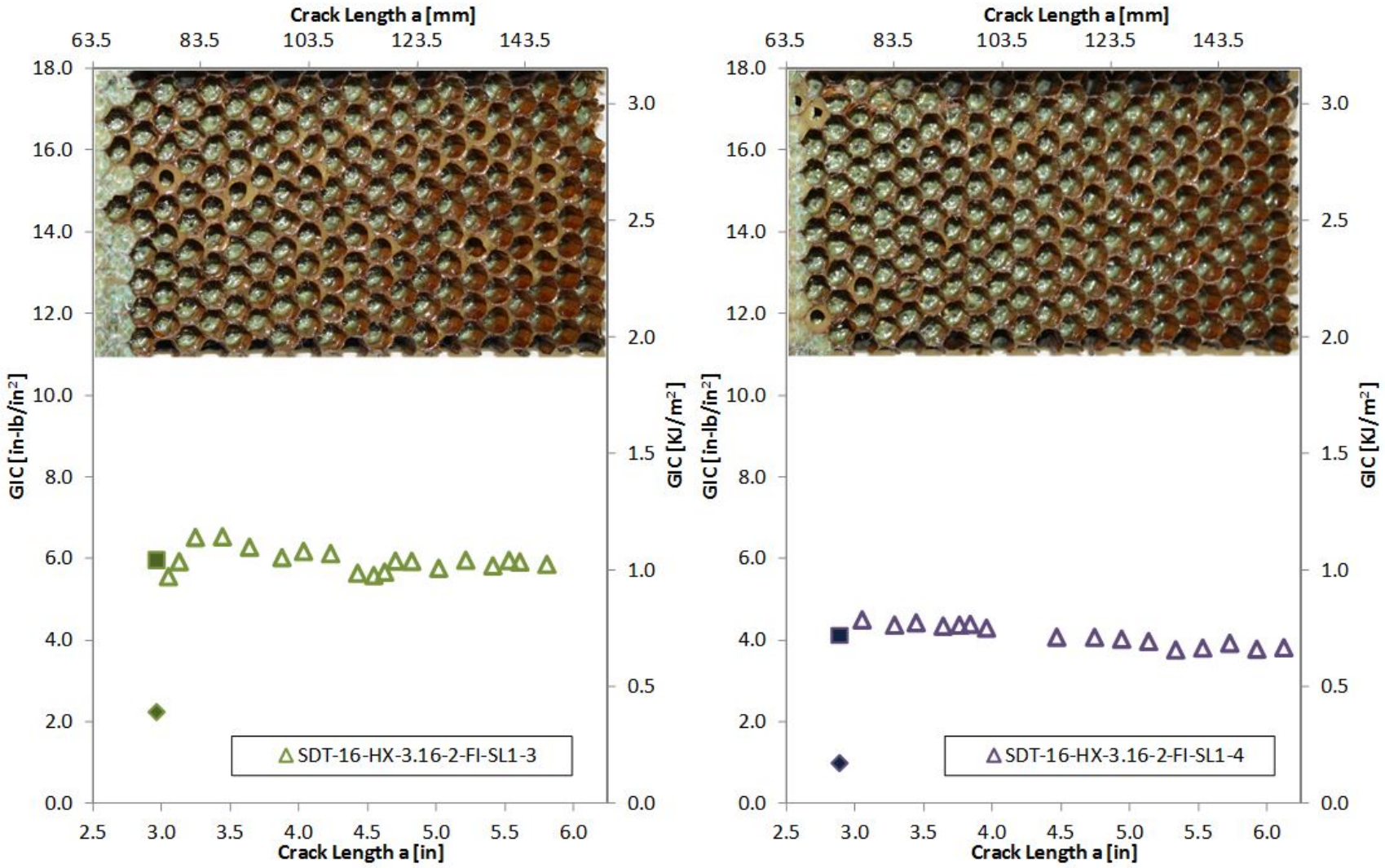

Figure C-31. Failure mode image and resistance curve for SDT-16-HX-3.16-2-FI-SL1-X #3 and #4

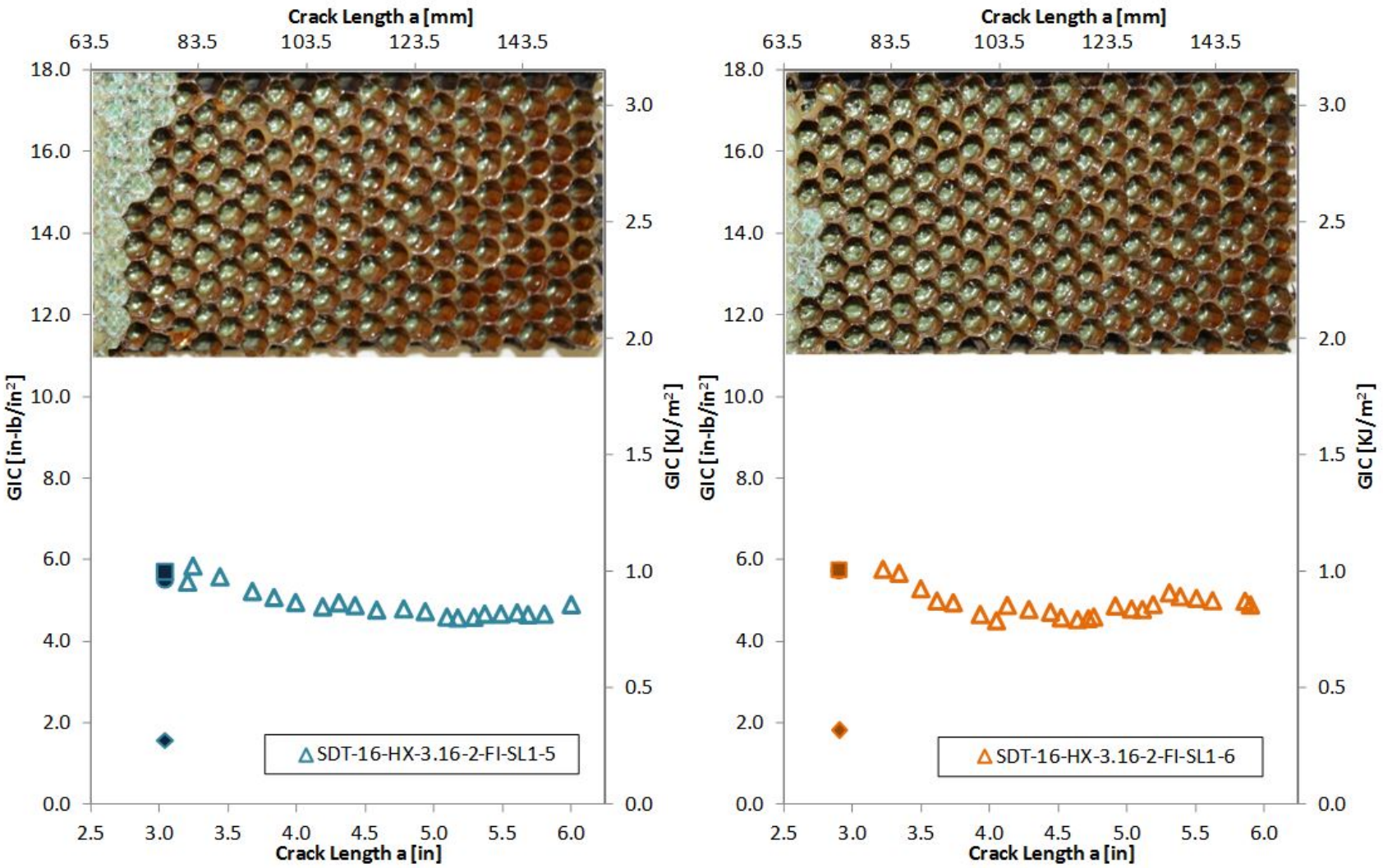

Figure C-32. Failure mode image and resistance curve for SDT-16-HX-3.16-2-FI-SL1-X #5 and #6

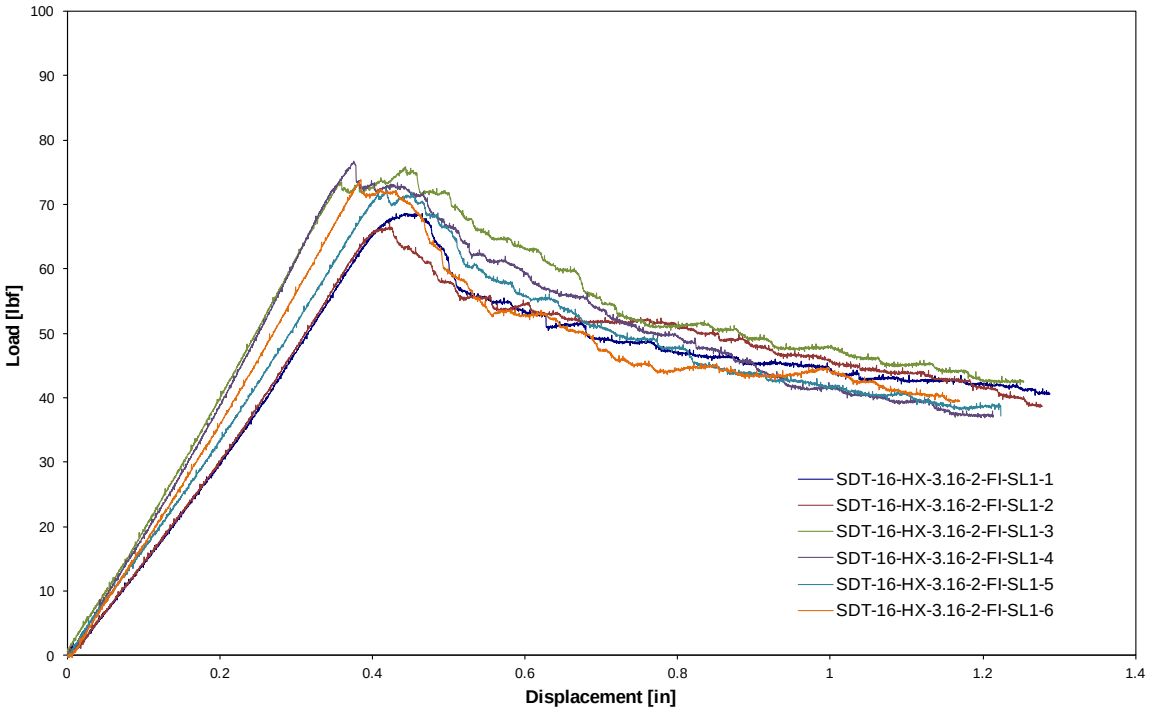

Figure C-33. Load vs. displacement curve for HRH-10–3/16–2.0 fluid ingressed (2.5″ prescribed crack)

C.2.3 HRH-10–3/16–2.0 EXTENDED FLUID-INGRESSED DATA

Table C-13. Test summary for HRH-10–3/16–2.0 extended fluid ingressed (2.5″ prescribed crack) precrack

Specimen	GIC (in-lb/in^2)			GIC (KJ/m^2)			Failure Mode
	NL	VIS	5%/max	NL	VIS	5%/max	
SDT-16-HX-3.16-2-EFI-SL1-7	2.295	-	3.403	0.402	-	0.596	First row A; second row a mix of C and PO
SDT-16-HX-3.16-2-EFI-SL1-8	2.006	-	2.634	0.351	-	0.461	First row A; second row a mix of C and PO
AVERAGE GIC	2.150	-	3.018	0.377	-	0.529	
STANDARD DEVIATION	0.204	-	0.544	0.036	-	0.095	
COEFFICIENT OF VARIATION (%)	9.501	-	18.014	9.501	-	18.014	

Table C-14. Test Summary for HRH-10–3/16–2.0 extended fluid ingressed (2.5″prescribed crack)

Specimen	GIC (in-lb/in^2)			GIC (KJ/m^2)			Failure Mode
	NL	VIS	5%/max	NL	VIS	5%/max	
SDT-16-HX-3.16-2-EFI-SL1-7	2.253	-	4.438	0.395	-	0.777	Primarily in C
SDT-16-HX-3.16-2-EFI-SL1-8	2.388	-	4.759	0.418	-	0.833	Primarily in C
AVERAGE GIC	2.320	-	4.598	0.406	-	0.805	
STANDARD DEVIATION	0.095	-	0.227	0.017	-	0.040	
COEFFICIENT OF VARIATION (%)	4.107	-	4.928	4.107	-	4.928	

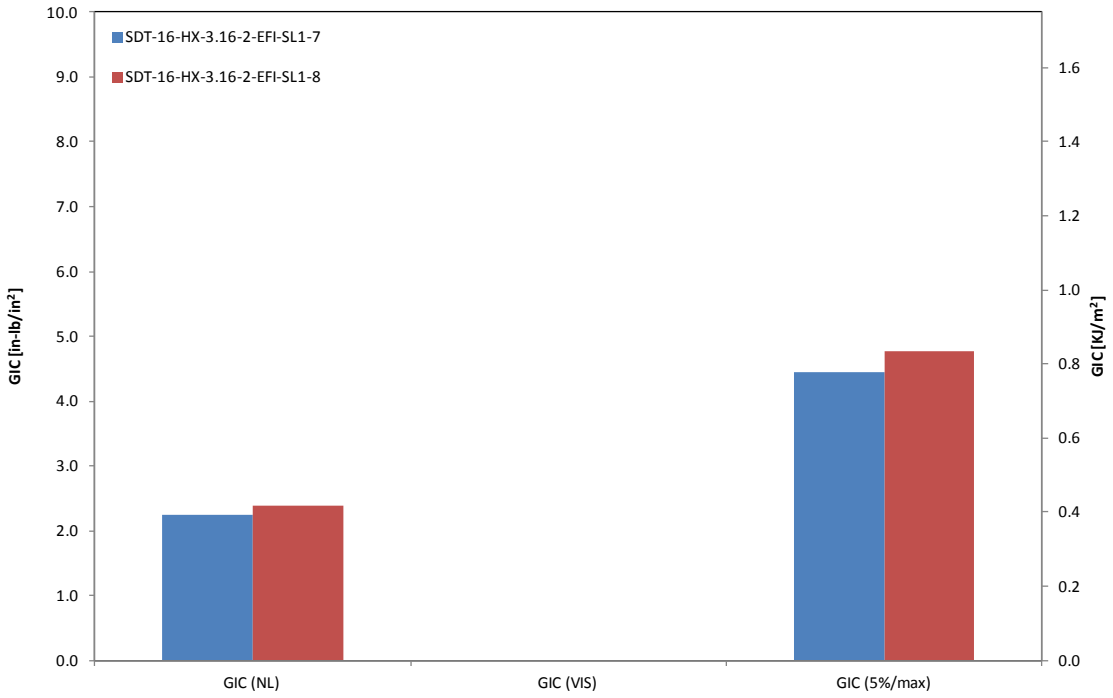

Figure C-34. GIC for HRH-10–3/16–2.0 extended fluid ingressed (2.5″ prescribed crack)

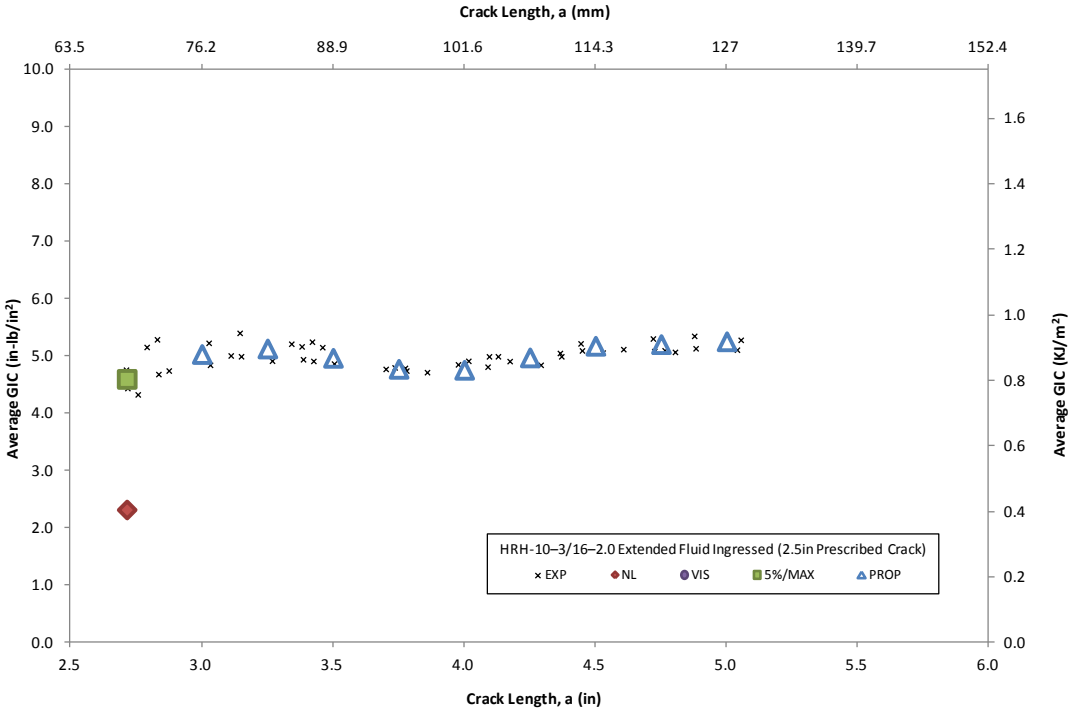

Figure C-35. Resistance curve for HRH-10–3/16–2.0 extended fluid ingressed (2.5″ prescribed crack)

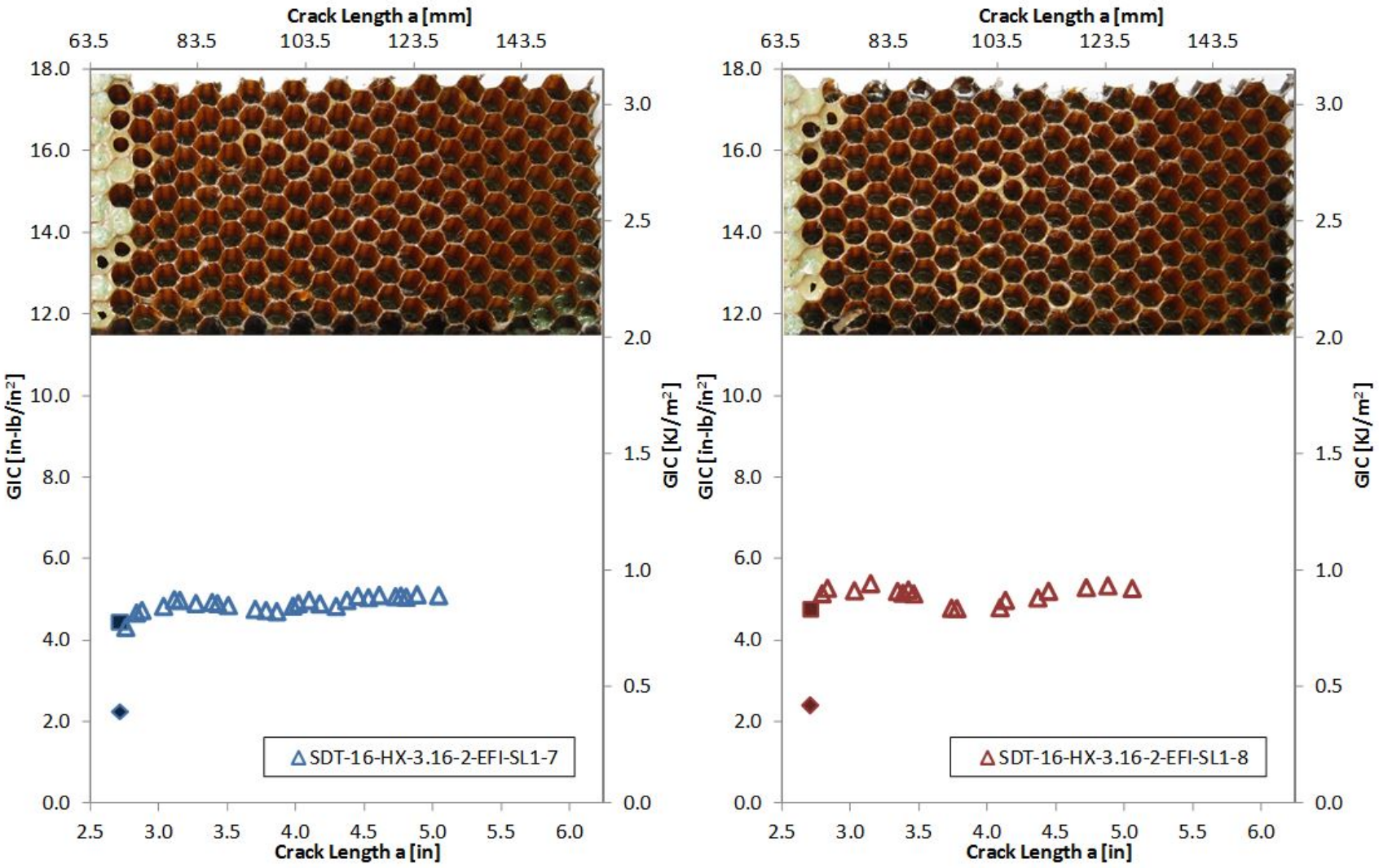

Figure C-36. Failure mode image and resistance curve for SDT-16-HX-3.16-2-EFI-SL1-X #7 and #8

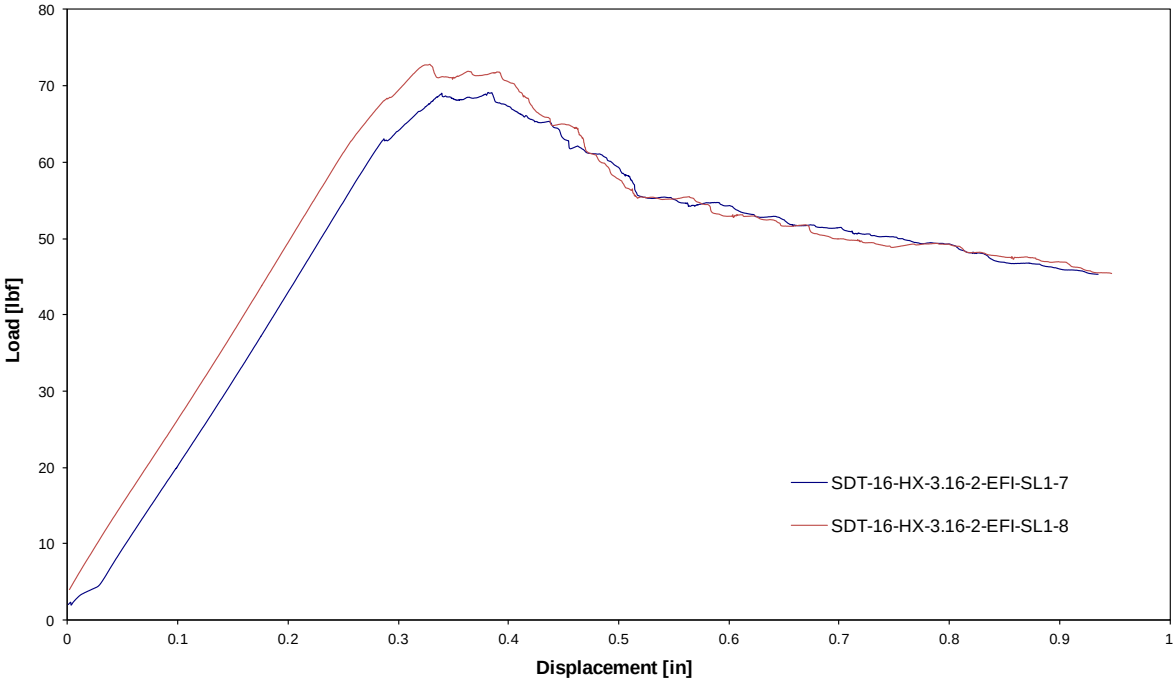

Figure C-37. Load vs. displacement curve for HRH-10–3/16–2.0 extended fluid ingressed (2.5″ prescribed crack)

C.2.4 HRH-10–3/16–2.0 WATER-INGRESSED DATA

Table C-15. Test summary for HRH-10–3/16–2.0 water ingressed (2.5″ prescribed crack) precrack

Specimen	GIC (in-lb/in^2)			GIC (KJ/m^2)			Failure Mode
	NL	VIS	5%/max	NL	VIS	5%/max	
SDT-16-HX-3.16-2-H2O-SL1-7	1.643	-	2.766	0.288	-	0.484	Primarily in C
SDT-16-HX-3.16-2-H2O-SL1-8	1.181	-	1.934	0.207	-	0.339	Primarily in C
SDT-16-HX-3.16-2-H2O-SLX-7	1.657	-	2.803	0.290	-	0.491	Primarily in C
SDT-16-HX-3.16-2-H2O-SLX-8	1.195	-	2.456	0.209	-	0.430	Primarily in C
AVERAGE GIC	1.419	-	2.490	0.248	-	0.436	
STANDARD DEVIATION	0.267	-	0.402	0.047	-	0.070	
COEFFICIENT OF VARIATION (%)	18.818	-	16.143	18.818	-	16.143	

Table C-16. Test summary for HRH-10–3/16–2.0 water ingressed (2.5″ prescribed crack)

Specimen	GIC (in-lb/in^2)			GIC (KJ/m^2)			Failure Mode
	NL	VIS	5%/max	NL	VIS	5%/max	
SDT-16-HX-3.16-2-H2O-SL1-7	1.509	-	5.258	0.264	-	0.921	Primarily in C
SDT-16-HX-3.16-2-H2O-SL1-8	1.829	-	5.467	0.320	-	0.957	Primarily in C
SDT-16-HX-3.16-2-H2O-SLX-7	1.369	-	5.166	0.240	-	0.905	Primarily in C
SDT-16-HX-3.16-2-H2O-SLX-8	1.442	-	5.700	0.252	-	0.998	
AVERAGE GIC	1.537	-	5.398	0.269	-	0.945	
STANDARD DEVIATION	0.203	-	0.238	0.036	-	0.042	
COEFFICIENT OF VARIATION (%)	13.200	-	4.401	13.200	-	4.401	

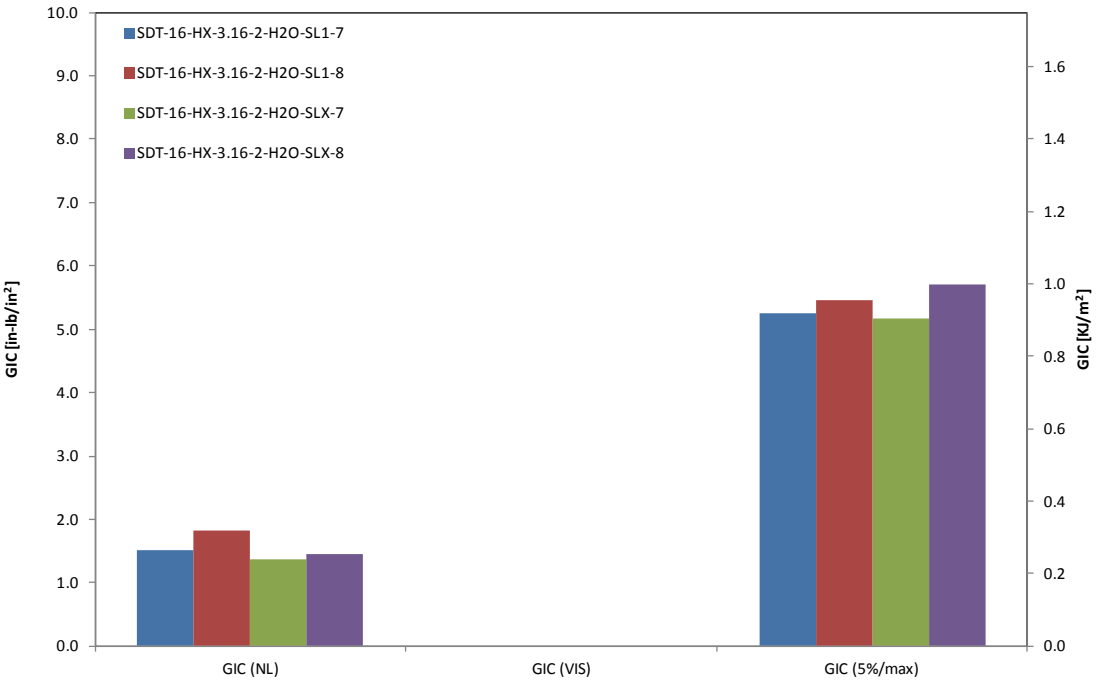

Figure C-38. GIC for HRH-10–3/16–2.0 water ingressed (2.5″ prescribed crack)

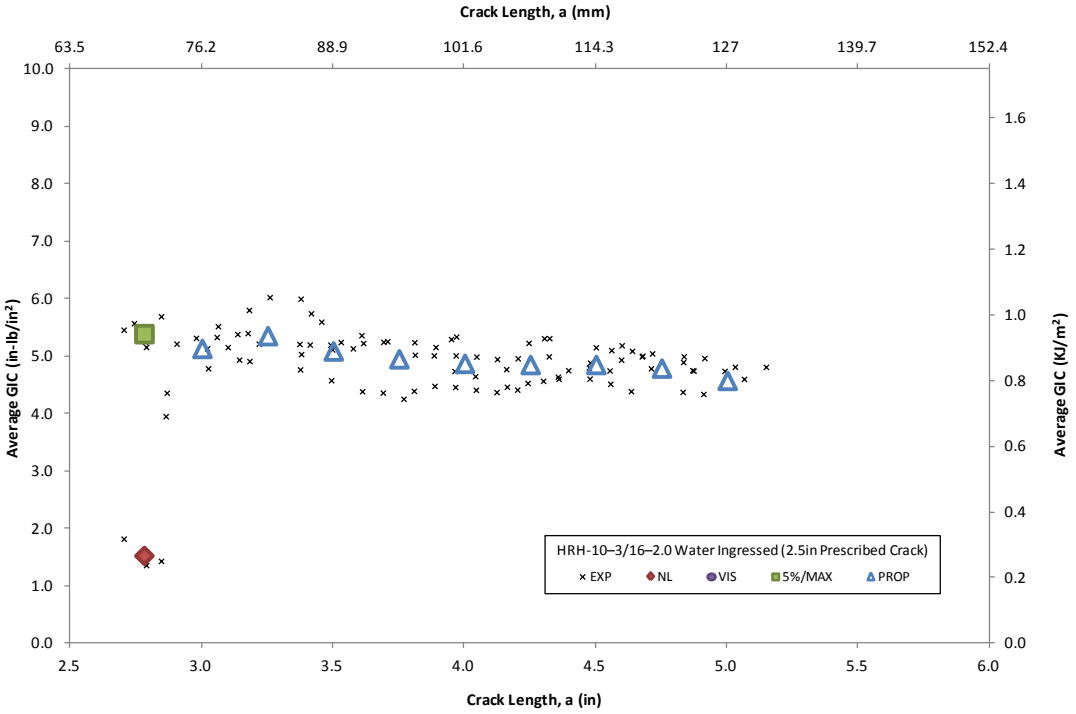

Figure C-39. Resistance curve for HRH-10–3/16–2.0 water ingressed (2.5″ prescribed crack)

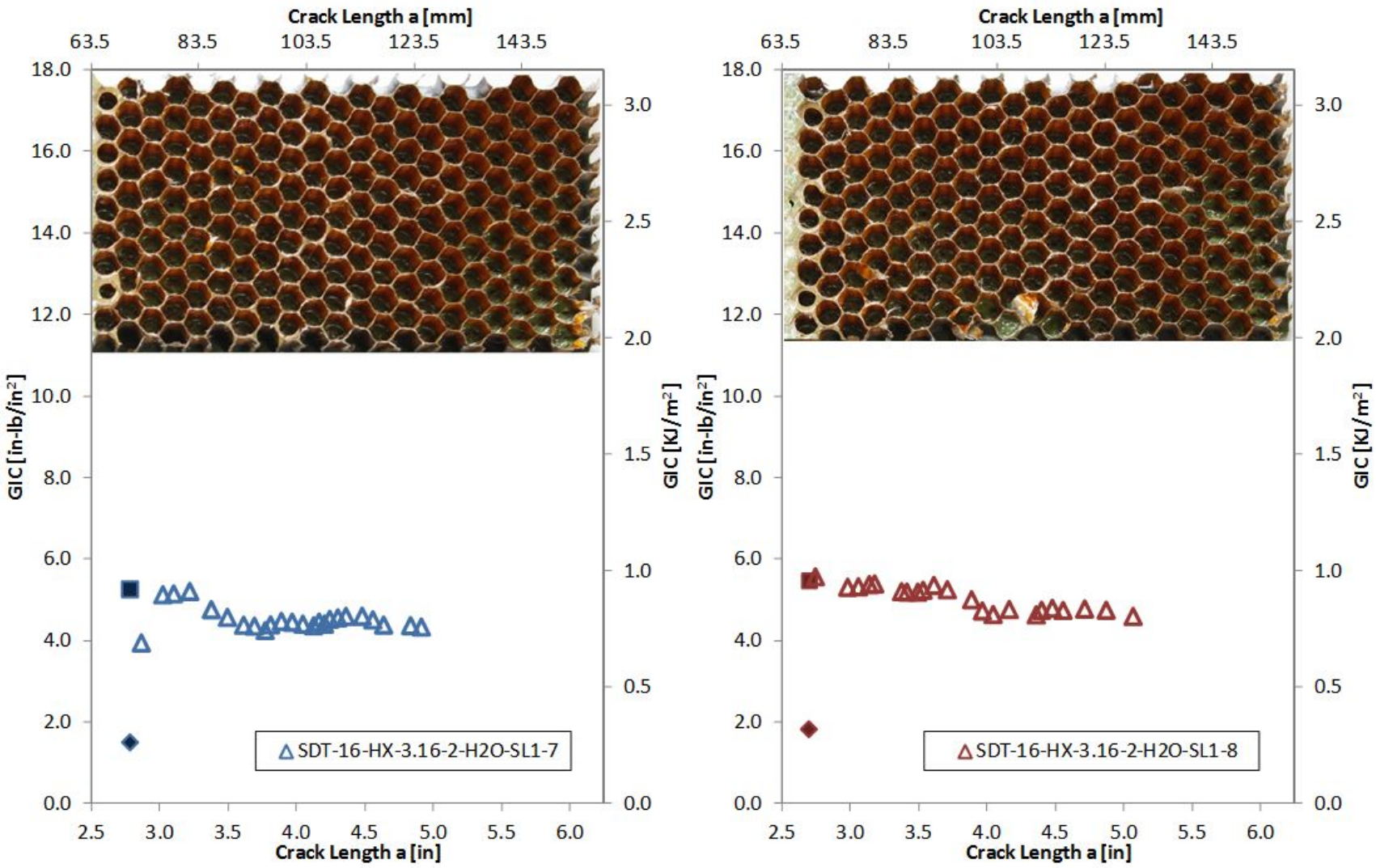

Figure C-40. Failure mode image and resistance curve for SDT-16-HX-3.16-2-H2O-SL1-X #7 and #8

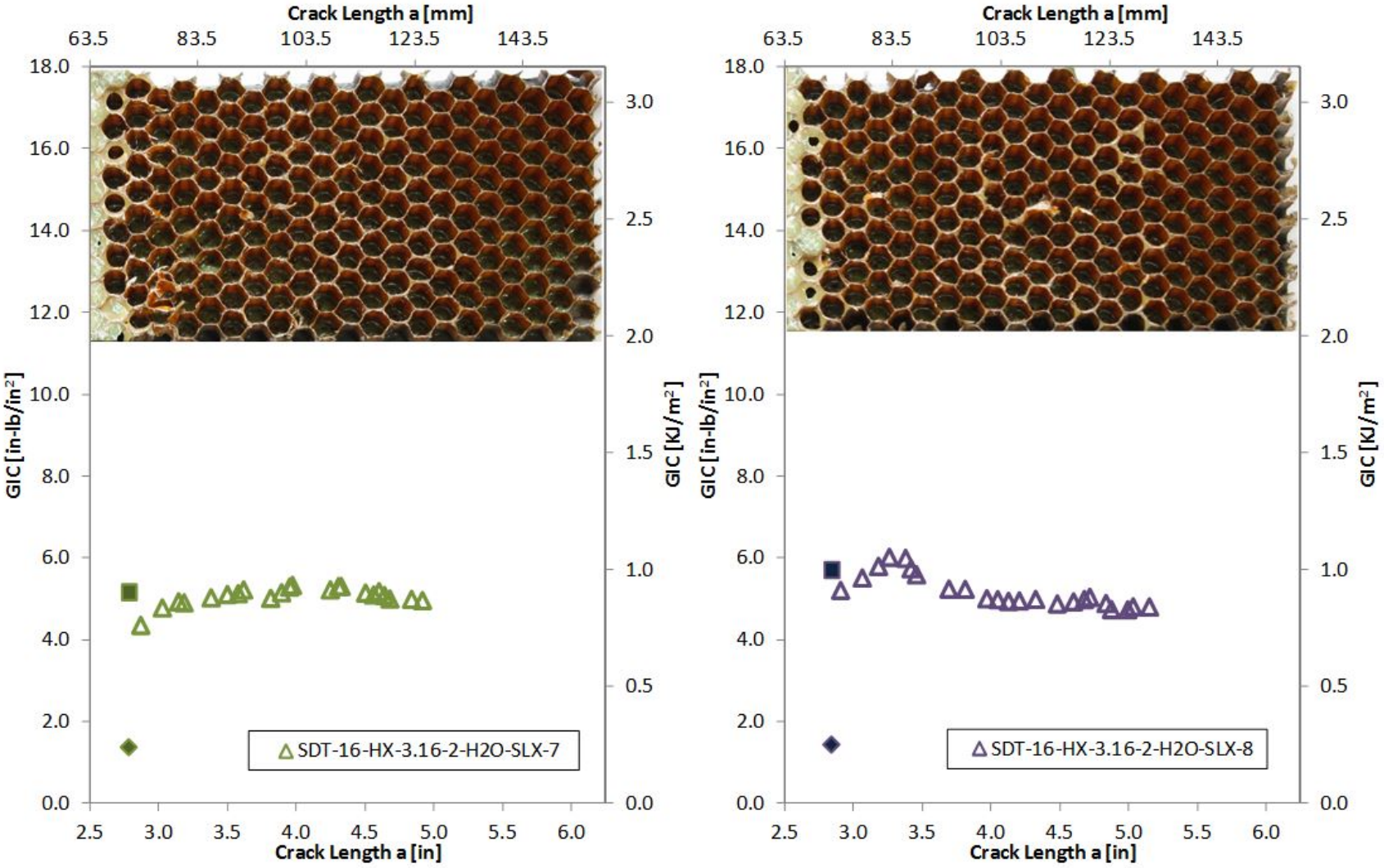

Figure C-41. Failure mode image and resistance curve for SDT-16-HX-3.16-2-H2O-SLX-X #7 and #8

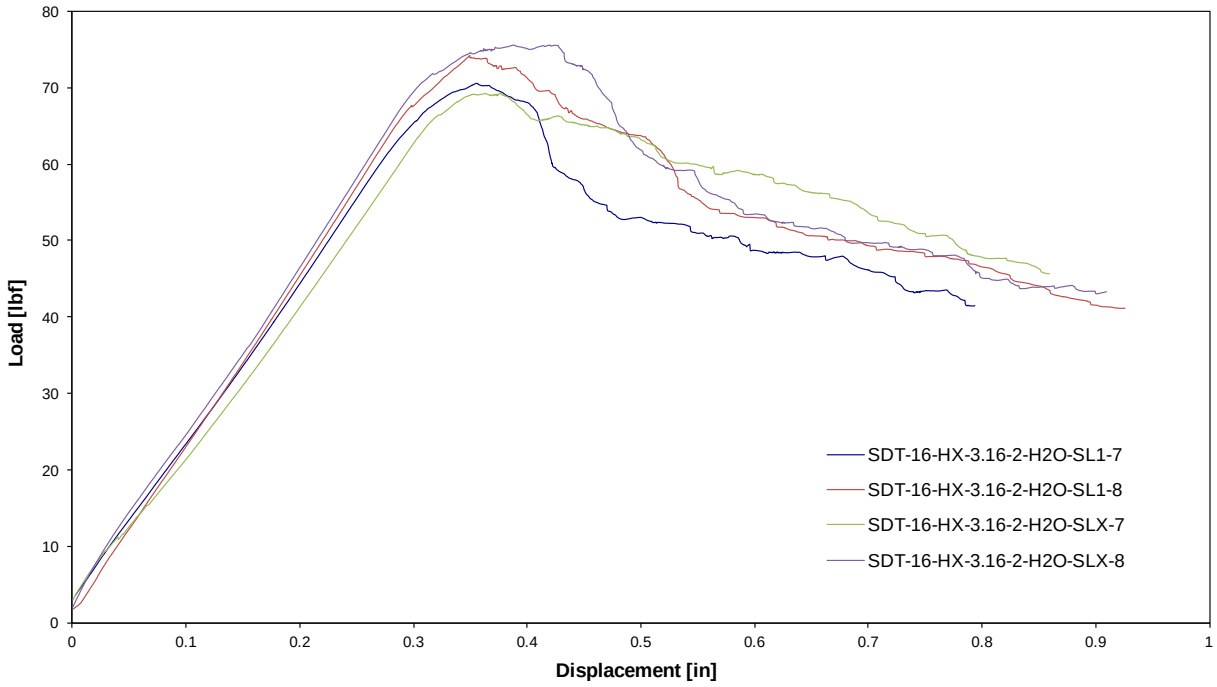

Figure C-42. Load vs. displacement curve for HRH-10–3/16–2.0 water ingressed (2.5″ prescribed crack)

C.3 HRH-10–3/16–3.0 DATA

C.3.1 HRH-10–3/16–3.0 BASELINE DATA

Table C-17. Test summary for HRH-10–3/16–3.0 baseline (2.5″ prescribed crack) precrack

Specimen	GIC (in-lb/in^2)			GIC (KJ/m^2)			Failure Mode
	NL	VIS	5%/max	NL	VIS	5%/max	
SDT-16-HX-3.16-3-BL-SL1-1	1.904	-	3.637	0.333	-	0.637	Mix of A and PO
SDT-16-HX-3.16-3-BL-SL1-2	1.423	-	2.594	0.249	-	0.454	Primarily A with a couple cells in PO
SDT-16-HX-3.16-3-BL-SL1-3	1.484	-	4.131	0.260	-	0.723	Primarily A with a couple cells in PO and a cell in C
SDT-16-HX-3.16-3-BL-SL1-4	1.923	-	3.577	0.337	-	0.626	Primarily A with a couple cells in PO
SDT-16-HX-3.16-3-BL-SL1-5	1.619	-	3.226	0.284	-	0.565	Primarily A with a couple cells in PO
SDT-16-HX-3.16-3-BL-SL1-6	1.716	-	2.962	0.300	-	0.519	Primarily A
AVERAGE GIC	1.678	-	3.354	0.294	-	0.587	
STANDARD DEVIATION	0.209	-	0.544	0.037	-	0.095	
COEFFICIENT OF VARIATION (%)	12.456	-	16.222	12.456	-	16.222	

Table C-18. Test summary for HRH-10–3/16–3.0 baseline (2.5″ prescribed crack)

Specimen	GIC (in-lb/in^2)			GIC (KJ/m^2)			Failure Mode
	NL	VIS	5%/max	NL	VIS	5%/max	
SDT-16-HX-3.16-3-BL-SL1-1	2.337	5.374	5.531	0.409	0.941	0.969	Mix of A and C with occasional PO and S
SDT-16-HX-3.16-3-BL-SL1-2	2.389	4.548	4.281	0.418	0.796	0.750	Primarily A with occasional PO and a couple cells in C and S
SDT-16-HX-3.16-3-BL-SL1-3	2.510	-	5.508	0.440	-	0.965	Primarily A with occasional PO; last few rows in D
SDT-16-HX-3.16-3-BL-SL1-4	2.454	-	4.835	0.430	-	0.847	Primarily A with occasional PO; last few rows in D
SDT-16-HX-3.16-3-BL-SL1-5	2.396	-	4.319	0.420	-	0.756	Primarily A with occasional PO; last few rows in D
SDT-16-HX-3.16-3-BL-SL1-6	1.741	-	4.578	0.305	-	0.802	Primarily in A with occasional PO; large pocket of C in last few rows in D
AVERAGE GIC	2.305	4.961	4.842	0.404	0.869	0.848	
STANDARD DEVIATION	0.282	0.584	0.562	0.049	0.102	0.098	
COEFFICIENT OF VARIATION (%)	12.251	11.776	11.598	12.251	11.776	11.598	

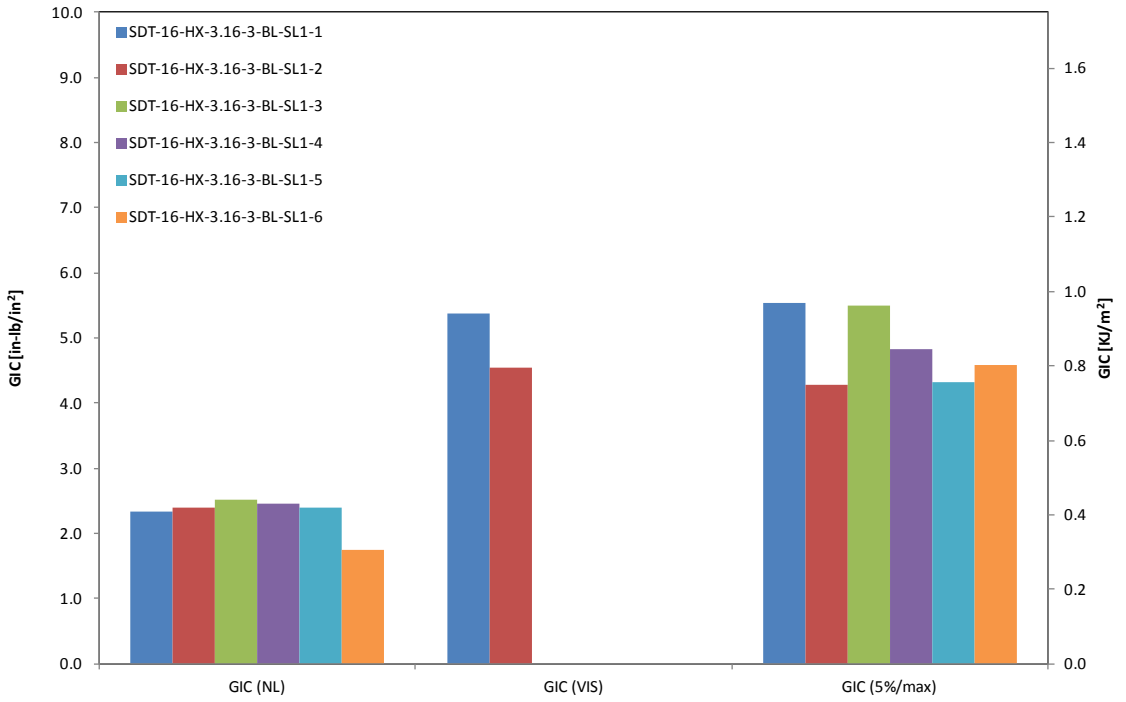

Figure C-43. GIC for HRH-10–3/16–3.0 baseline (2.5″ prescribed crack)

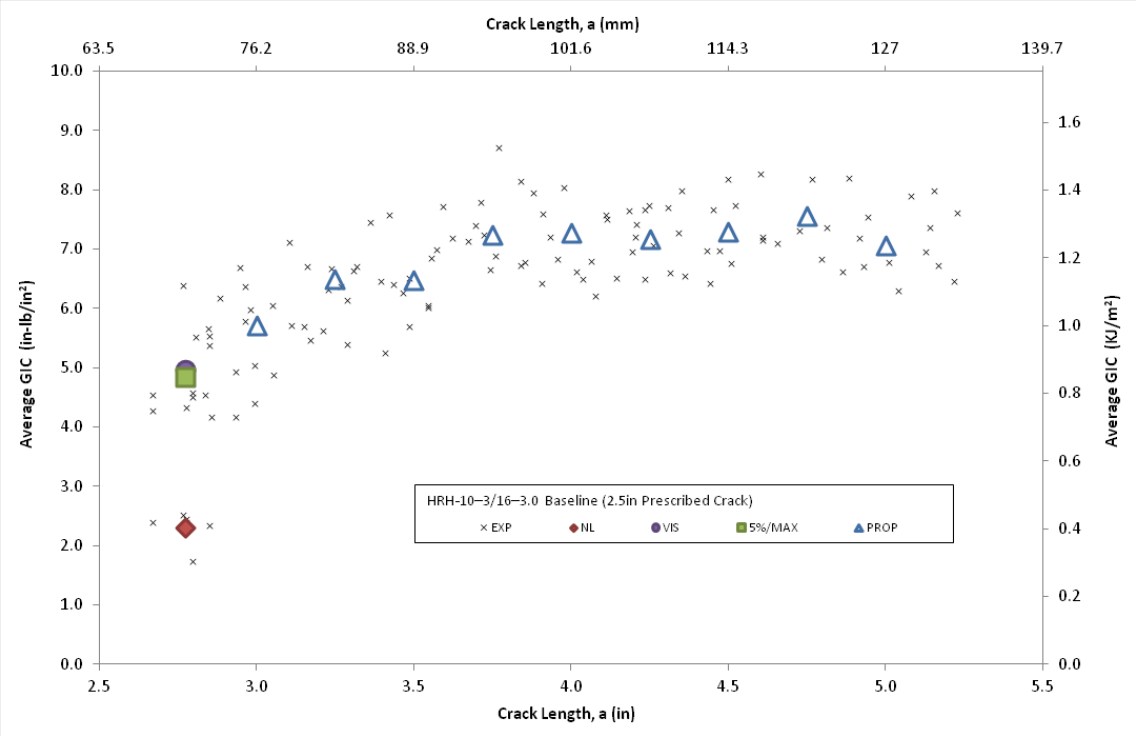

Figure C-44. Resistance curve for HRH-10–3/16–3.0 baseline (2.5″ prescribed crack)

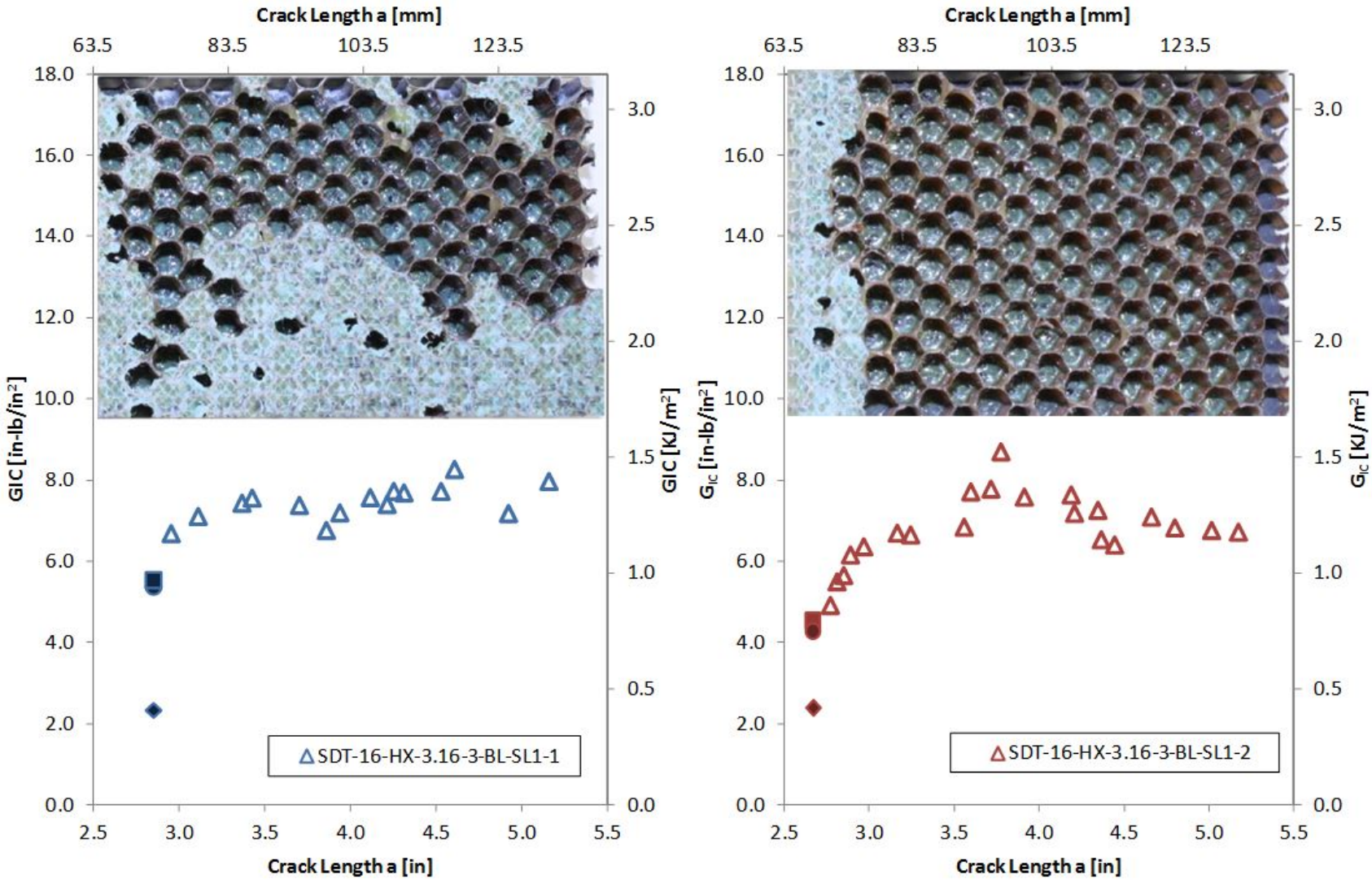

Figure C-45. Failure mode image and resistance curve for SDT-16-HX-3.16-3-BL-SL1-X #1 and #2

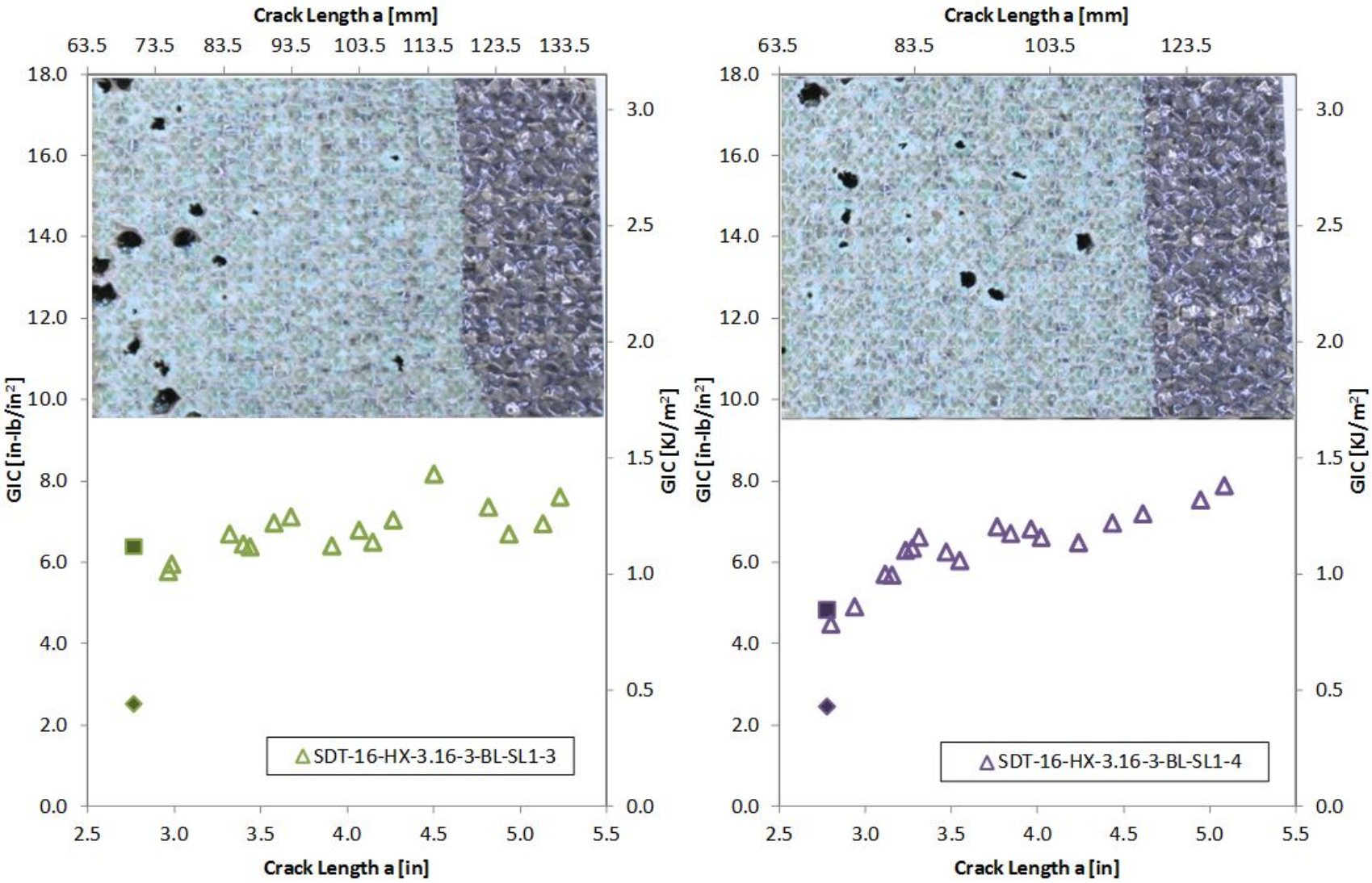

Figure C-46. Failure mode image and resistance curve for SDT-16-HX-3.16-3-BL-SL1-X #3 and #4

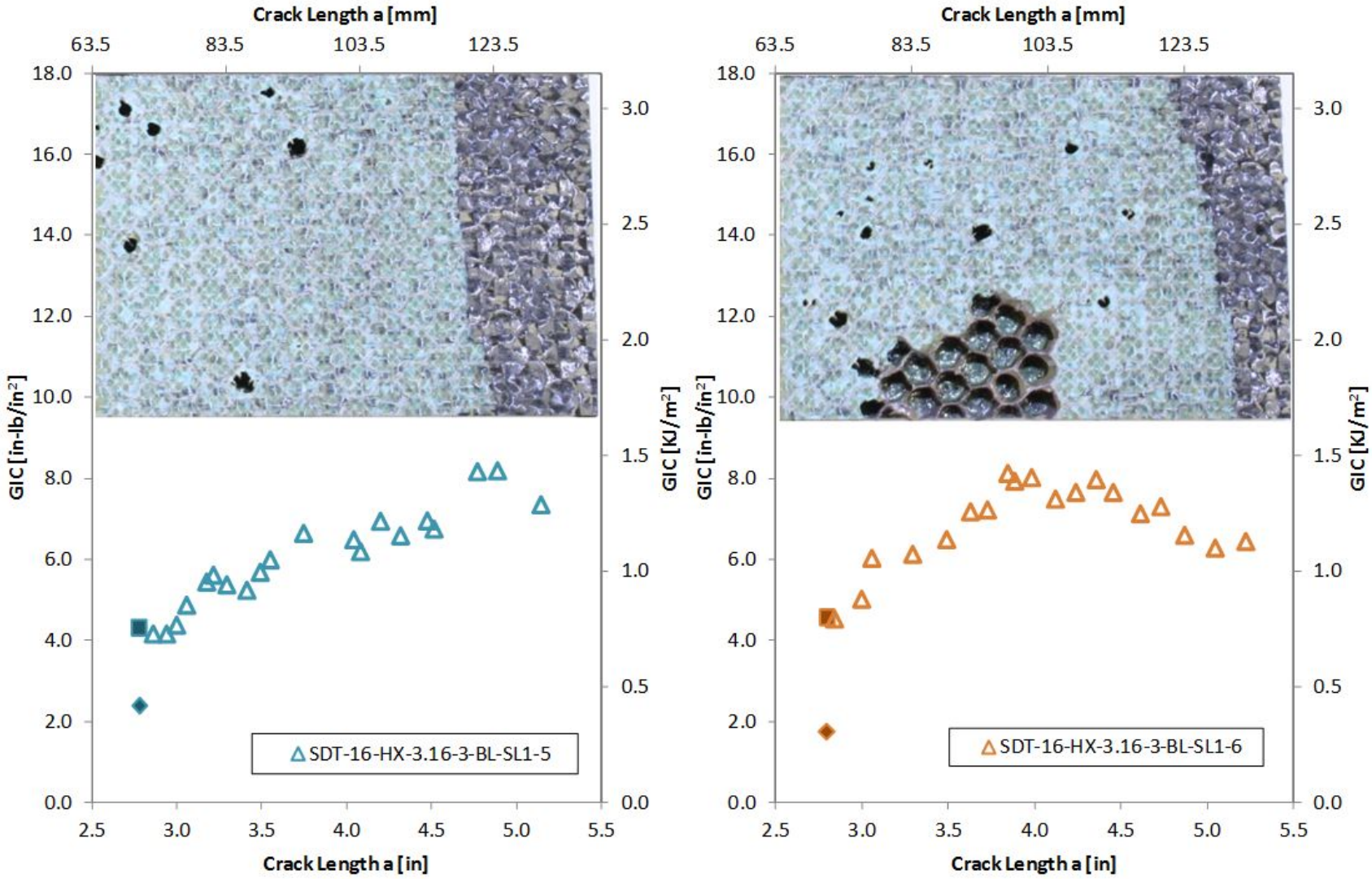

Figure C-47. Failure mode image and resistance curve for SDT-16-HX-3.16-3-BL-SL1-X #5 and #6

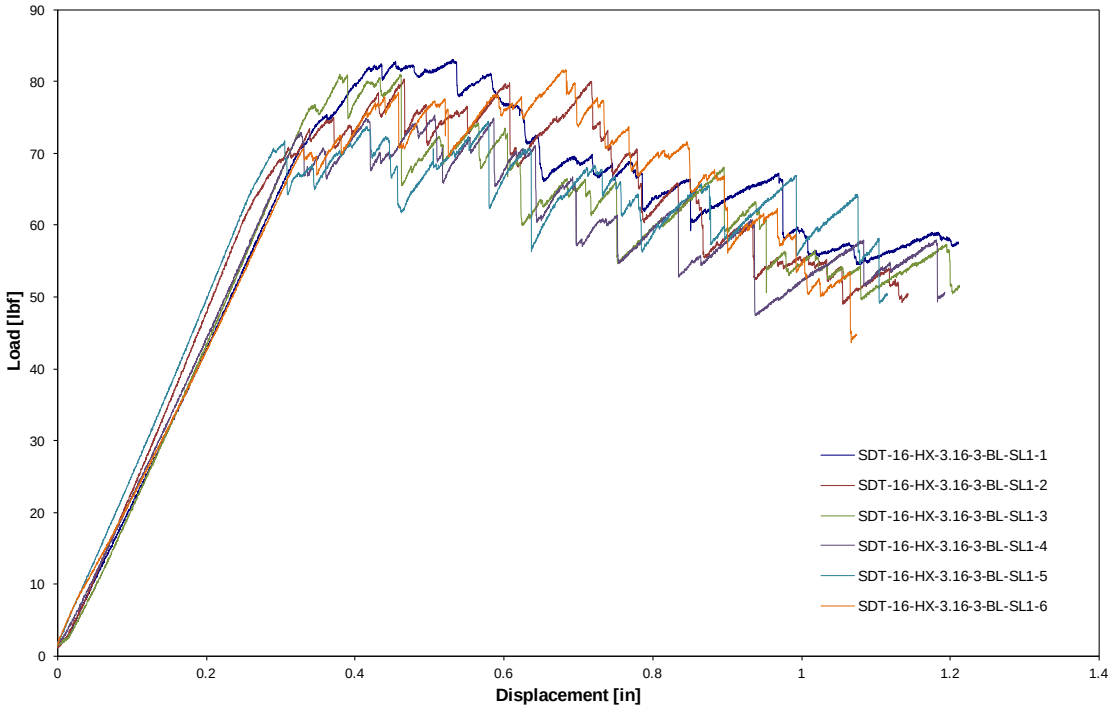

Figure C-48. Load vs. displacement curve for HRH-10–3/16–3.0 baseline (2.5″ prescribed crack)

C.3.2 HRH-10–3/16–3.0 FLUID-INGRESSED DATA

Table C-19. Test summary for HRH-10–3/16–3.0 fluid ingressed (2.5″ prescribed crack) precrack

Specimen	GIC (in-lb/in^2)			GIC (KJ/m^2)			Failure Mode
	NL	VIS	5%/max	NL	VIS	5%/max	
SDT-16-HX-3.16-3-FI-SL1-1	1.585	-	3.368	0.278	-	0.590	First row a mix of A and C, then primarily in C
SDT-16-HX-3.16-3-FI-SL1-2	1.066	-	1.780	0.187	-	0.312	First row primarily in A with a cell in C, second row primarily in C with a few cells in A, then primarily in C
SDT-16-HX-3.16-3-FI-SL1-3	1.642	-	2.477	0.288	-	0.434	First row primarily in A, then primarily in A with a large pocket of C
SDT-16-HX-3.16-3-FI-SL1-4	1.080	-	2.091	0.189	-	0.366	Primarily in A with several cells in C and a cell in PO
SDT-16-HX-3.16-3-FI-SL1-5	1.261	-	2.534	0.221	-	0.444	First row a mix of A, PO, and C, then primarily in C with several cells in A
SDT-16-HX-3.16-3-FI-SL1-6	1.208	-	2.454	0.212	-	0.430	Primarily in C with a few cells in A
AVERAGE GIC	1.307	-	2.451	0.229	-	0.429	
STANDARD DEVIATION	0.249	-	0.534	0.044	-	0.094	
COEFFICIENT OF VARIATION (%)	19.069	-	21.801	19.069	-	21.801	

Table C-20. Test summary for HRH-10–3/16–3.0 fluid ingressed (2.5″ prescribed crack)

Specimen	GIC (in-lb/in^2)			GIC (KJ/m^2)			Failure Mode
	NL	VIS	5%/max	NL	VIS	5%/max	
SDT-16-HX-3.16-3-FI-SL1-1	2.614	-	5.019	0.458	-	0.879	Primarily in C with two small pockets of A
SDT-16-HX-3.16-3-FI-SL1-2	2.331	-	6.537	0.408	-	1.145	Primarily in C
SDT-16-HX-3.16-3-FI-SL1-3	2.419	6.857	7.253	0.424	1.201	1.270	Primarily in A with a large pocket in C, then last few rows in D
SDT-16-HX-3.16-3-FI-SL1-4	2.179	5.242	6.144	0.382	0.918	1.076	Primarily in A with a small pocket of C, then last few rows in D
SDT-16-HX-3.16-3-FI-SL1-5	2.174	5.039	5.721	0.381	0.883	1.002	Initially a mix of A and C, then primarily A with last few rows in D
SDT-16-HX-3.16-3-FI-SL1-6	3.289	-	6.231	0.576	-	1.091	Primarily in C
AVERAGE GIC	2.501	5.713	6.151	0.438	1.000	1.077	
STANDARD DEVIATION	0.420	0.996	0.753	0.073	0.174	0.132	
COEFFICIENT OF VARIATION (%)	16.775	17.440	12.248	16.775	17.440	12.248	

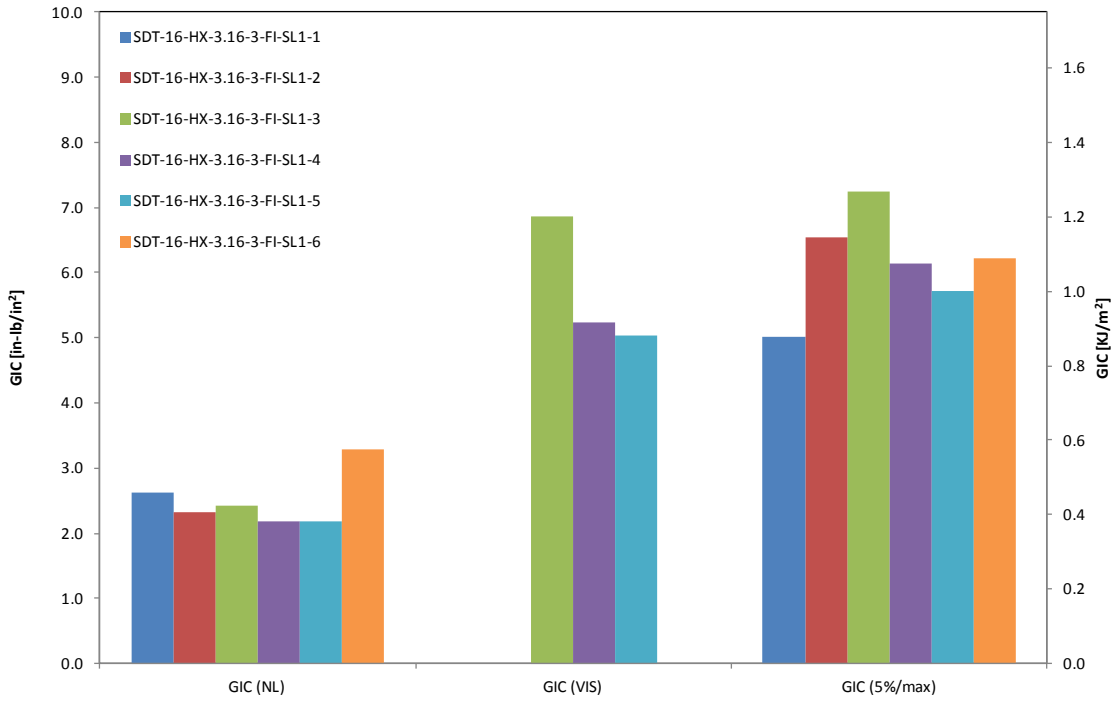

Figure C-49. GIC for HRH-10–3/16–3.0 fluid ingressed (2.5″ prescribed crack)

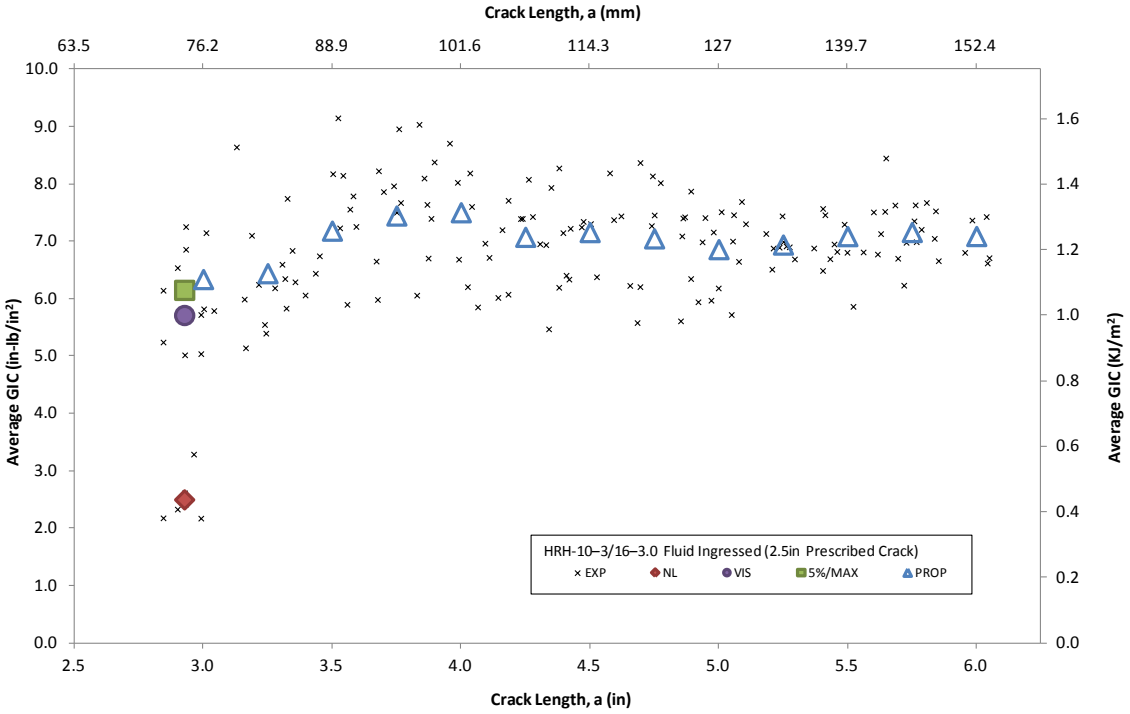

Figure C-50. Resistance curve for HRH-10–3/16–3.0 fluid ingressed (2.5″ prescribed crack)

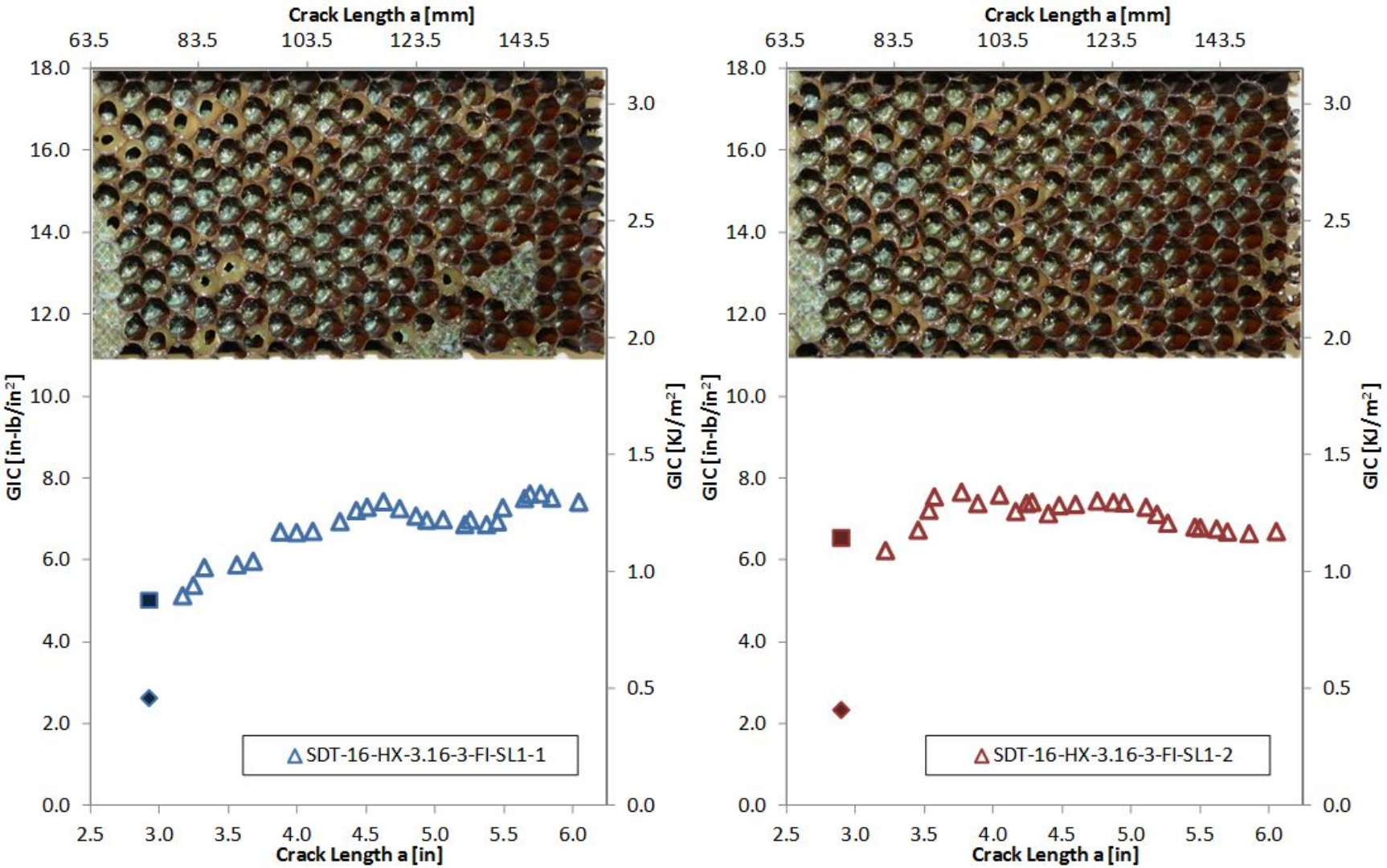

Figure C-51. Failure mode image and resistance curve for SDT-16-HX-3.16-3-FI-SL1-X #1 and #2

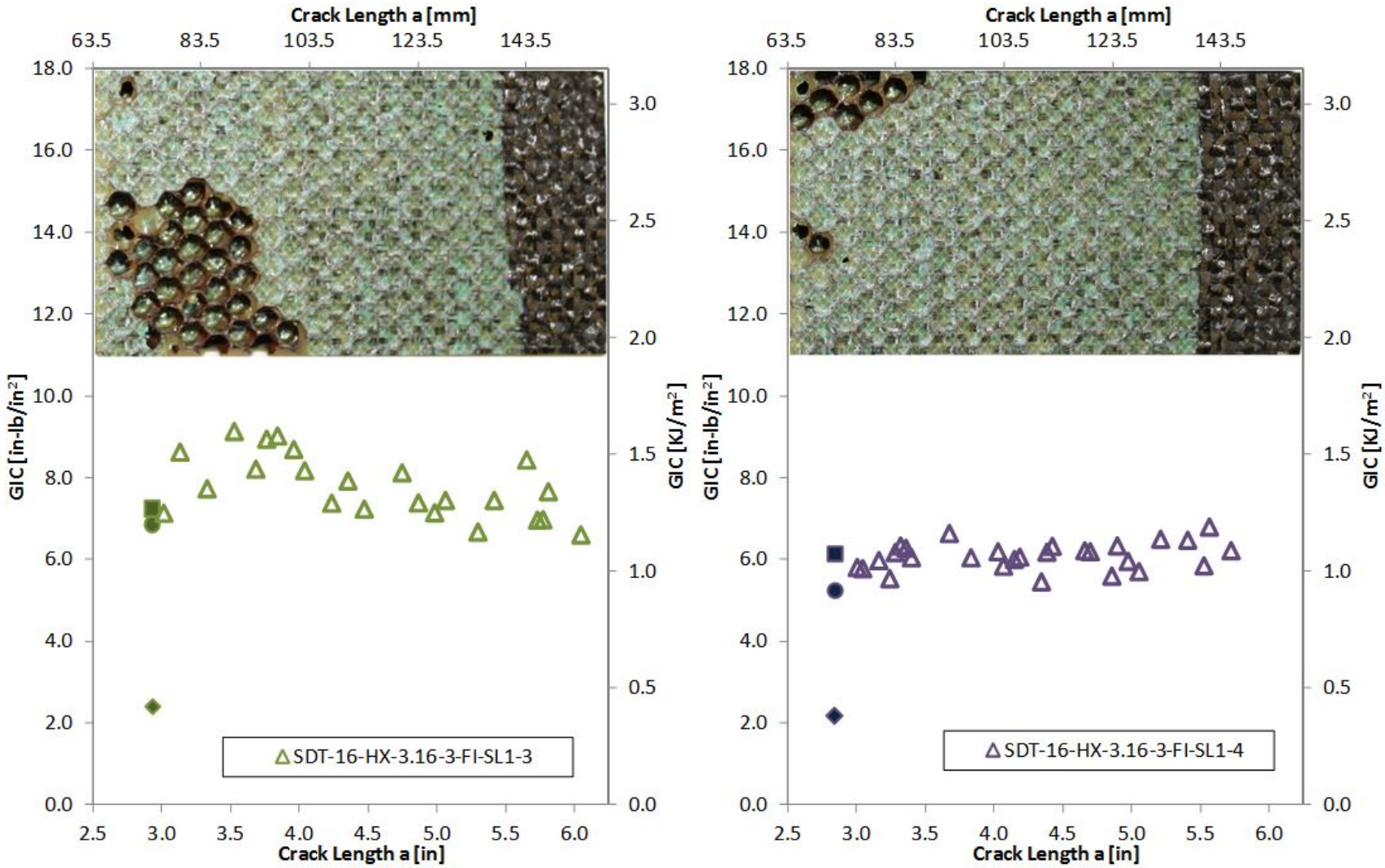

Figure C-52. Failure mode image and resistance curve for SDT-16-HX-3.16-3-FI-SL1-X #3 and #4

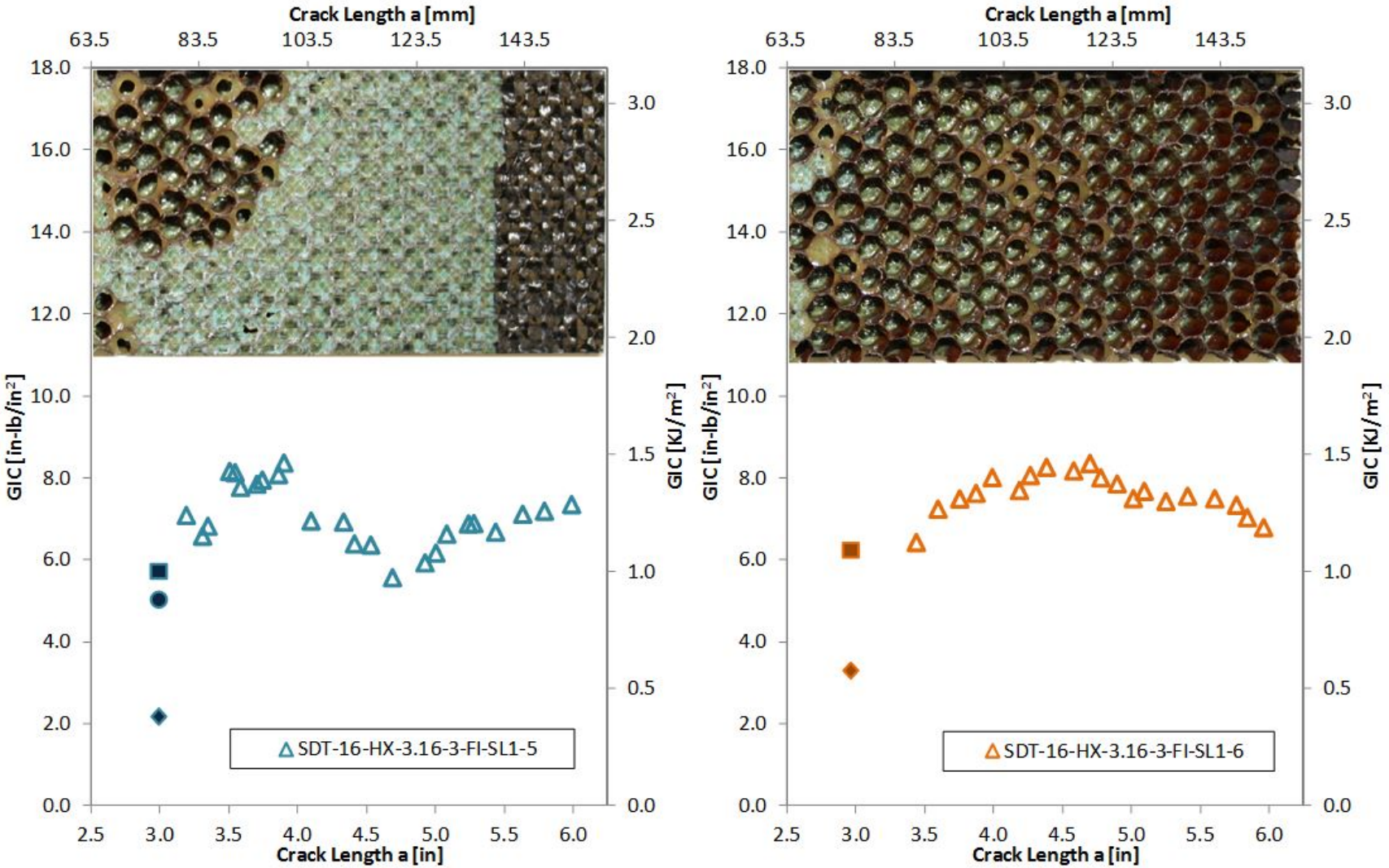

Figure C-53. Failure mode image and resistance curve for SDT-16-HX-3.16-3-FI-SL1-X #5 and #6

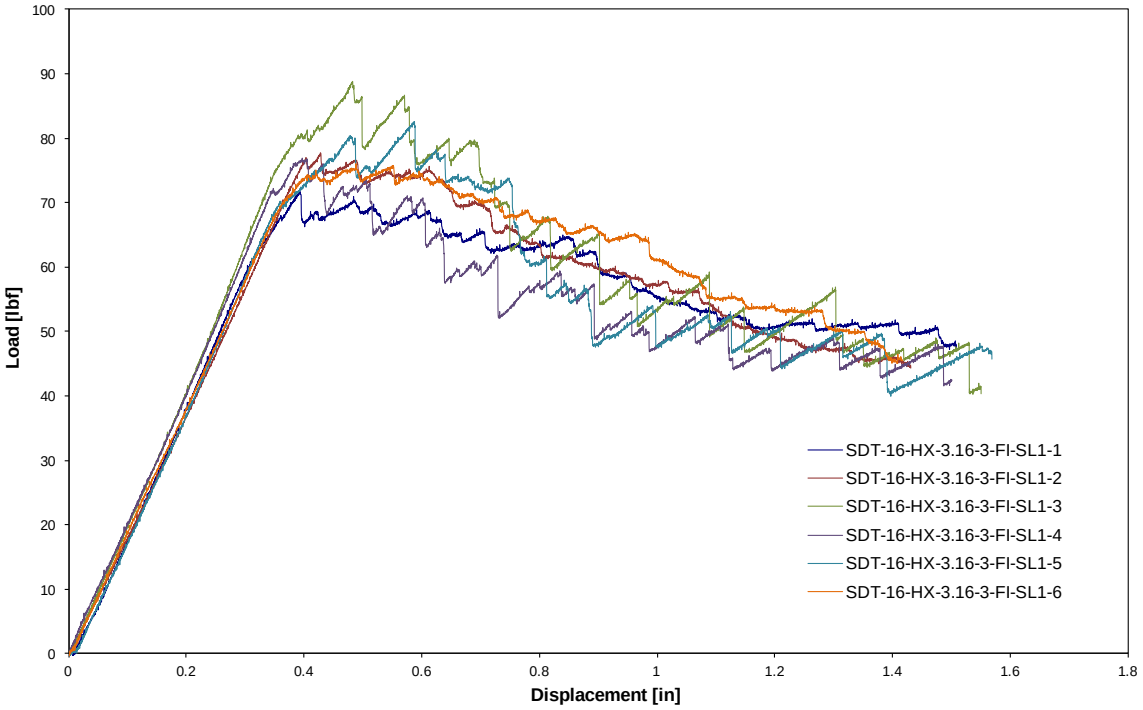

Figure C-54. Load vs. displacement curve for HRH-10–3/16–3.0 fluid ingressed (2.5″ prescribed crack)

C.3.3 HRH-10–3/16–3.0 EXTENDED FLUID-INGRESSED DATA

Table C-21. Test summary for HRH-10–3/16–3.0 extended fluid ingressed (2.5″ prescribed crack) precrack

Specimen	GIC (in-lb/in^2)			GIC (KJ/m^2)			Failure Mode
	NL	VIS	5%/max	NL	VIS	5%/max	
SDT-16-HX-3.16-3-EFI-SL1-7	2.756	-	5.744	0.483	-	1.006	First row a mix of A and C; second row in C with a of couple cells in A
SDT-16-HX-3.16-3-EFI-SL1-8	2.959	-	5.121	0.518	-	0.897	First couple rows in A with a couple of cells in C
AVERAGE GIC	2.858	-	5.432	0.500	-	0.951	
STANDARD DEVIATION	0.144	-	0.441	0.025	-	0.077	
COEFFICIENT OF VARIATION (%)	5.024	-	8.114	5.024	-	8.114	

Table C-22. Test summary for HRH-10–3/16–3.0 extended fluid ingressed (2.5″ prescribed crack)

Specimen	GIC (in-lb/in^2)			GIC (KJ/m^2)			Failure Mode
	NL	VIS	5%/max	NL	VIS	5%/max	
SDT-16-HX-3.16-3-EFI-SL1-7	2.336	-	8.080	0.409	-	1.415	Primarily in C
SDT-16-HX-3.16-3-EFI-SL1-8	2.614	-	9.123	0.458	-	1.598	Mix of A and C that quickly transitions to just C
AVERAGE GIC	2.475	-	8.602	0.433	-	1.506	
STANDARD DEVIATION	0.197	-	0.737	0.034	-	0.129	
COEFFICIENT OF VARIATION (%)	7.957	-	8.573	7.957	-	8.573	

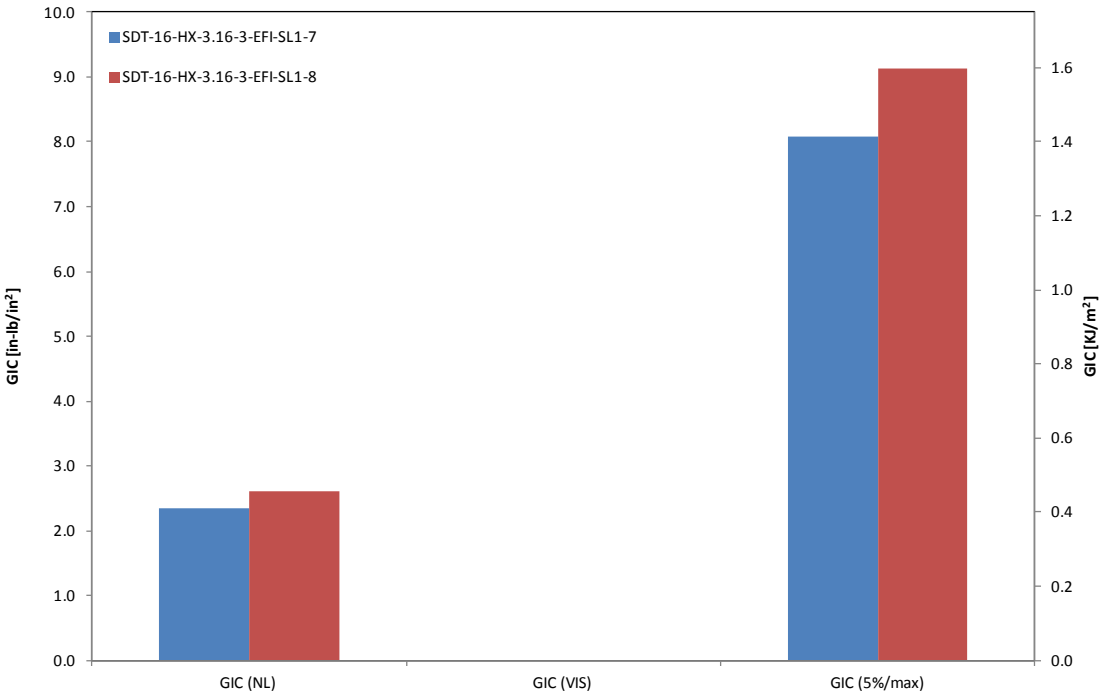

Figure C-55. GIC for HRH-10–3/16–3.0 extended fluid ingressed (2.5″ prescribed crack)

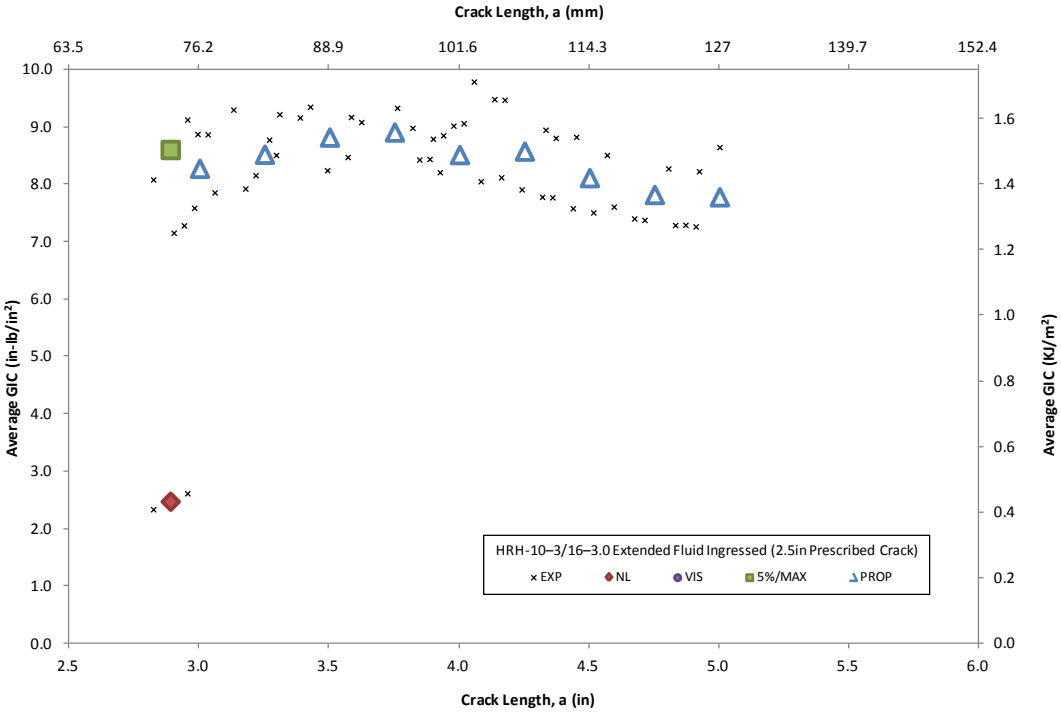

Figure C-56. Resistance curve for HRH-10–3/16–3.0 extended fluid ingressed (2.5″ prescribed crack)

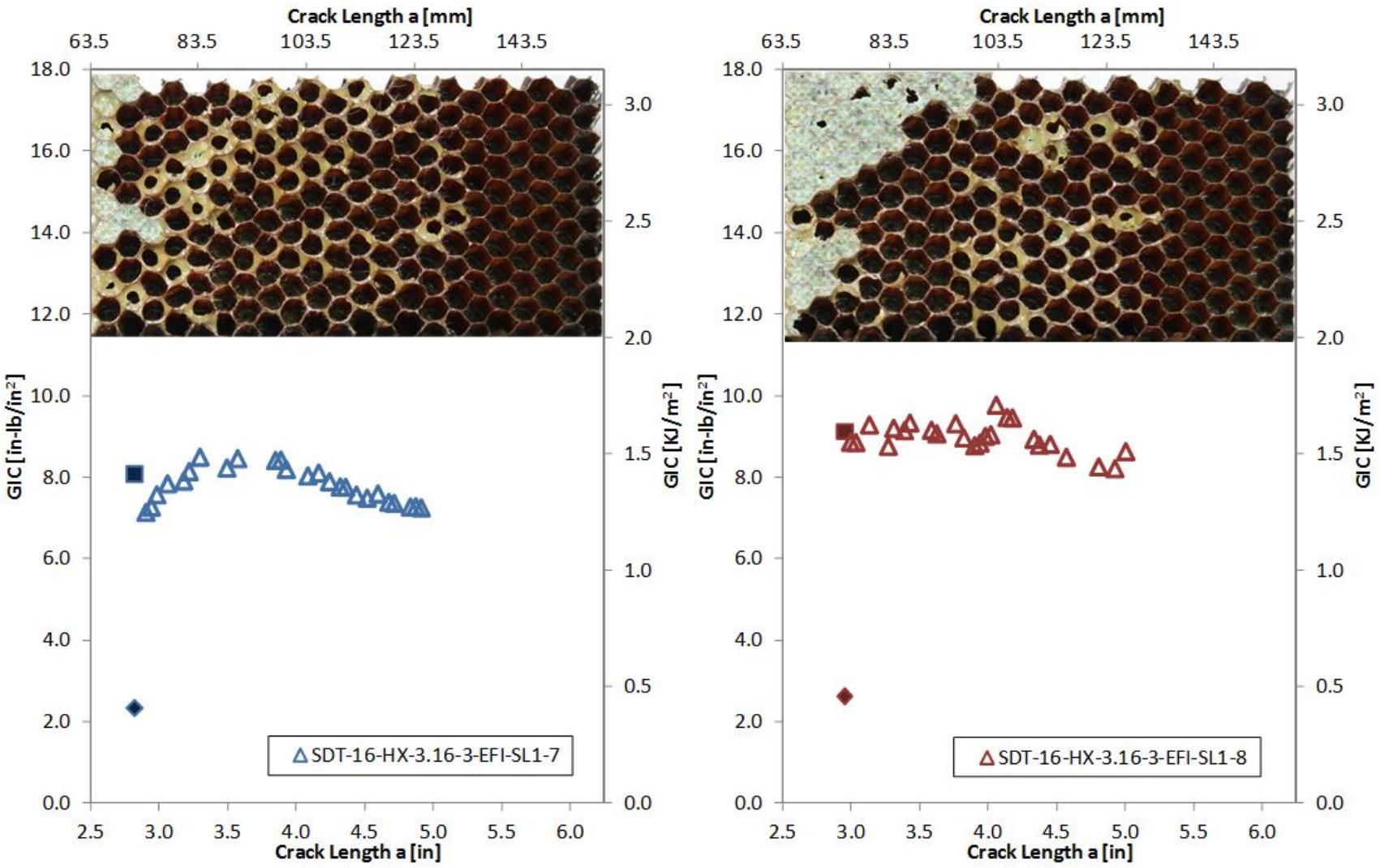

Figure C-57. Failure mode image and resistance curve for SDT-16-HX-3.16-3-EFI-SL1-X #7 and #8

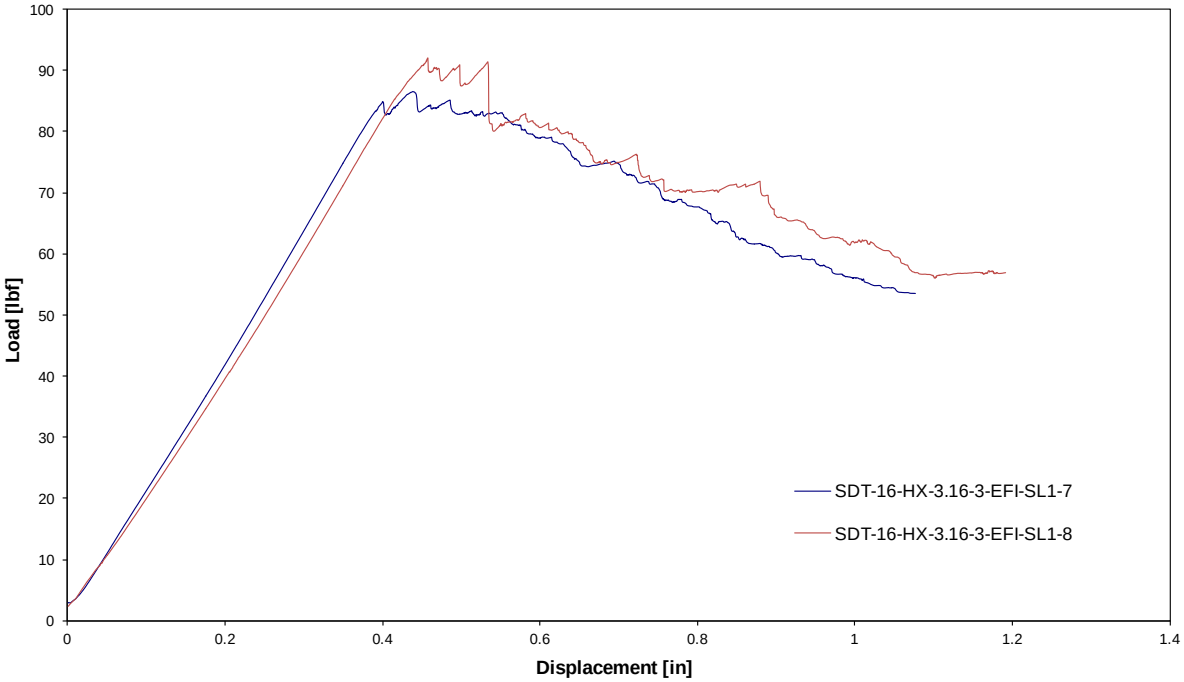

Figure C-58. Load vs. displacement curve for HRH-10–3/16–3.0 extended fluid ingressed (2.5″ prescribed crack)

C.3.4. HRH-10–3/16–3.0 WATER-INGRESSED DATA

Table C-23. Test summary for HRH-10–3/16–3.0 water ingressed (2.5″ prescribed crack) precrack

Specimen	GIC (in-lb/in^2)			GIC (KJ/m^2)			Failure Mode
	NL	VIS	5%/max	NL	VIS	5%/max	
SDT-16-HX-3.16-3-H2O-SL1-7	2.683	-	7.710	0.470	-	1.350	First row a mix of A and C, then C
SDT-16-HX-3.16-3-H2O-SL1-8	-	-	-	-	-	-	
SDT-16-HX-3.16-3-H2O-SLX-7	2.560	-	4.391	0.448	-	0.769	First row a mix of A and C, then C
SDT-16-HX-3.16-3-H2O-SLX -8	3.636	-	5.704	0.637	-	0.999	First row a mix of A and C, then C
AVERAGE GIC	2.959	-	5.935	0.518	-	1.039	
STANDARD DEVIATION	0.589	-	1.672	0.103	-	0.293	
COEFFICIENT OF VARIATION (%)	19.911	-	28.168	19.911	-	28.168	

Table C-24. Test summary for HRH-10–3/16–3.0 water ingressed (2.5″ prescribed crack)

Specimen	GIC (in-lb/in^2)			GIC (KJ/m^2)			Failure Mode
	NL	VIS	5%/max	NL	VIS	5%/max	
SDT-16-HX-3.16-3-H2O-SL1-7	1.771	-	6.879	0.310	-	1.205	Primarily in C
SDT-16-HX-3.16-3-H2O-SL1-8	-	-	-	-	-	-	
SDT-16-HX-3.16-3-H2O-SLX-7	3.978	-	5.974	0.697	-	1.046	Primarily in C
SDT-16-HX-3.16-3-H2O-SLX -8	3.531	-	5.295	0.618	-	0.927	Primarily in C
AVERAGE GIC	3.093	-	6.050	0.542	-	1.059	
STANDARD DEVIATION	1.167	-	0.795	0.204	-	0.139	
COEFFICIENT OF VARIATION (%)	37.721	-	13.138	37.721	-	13.138	

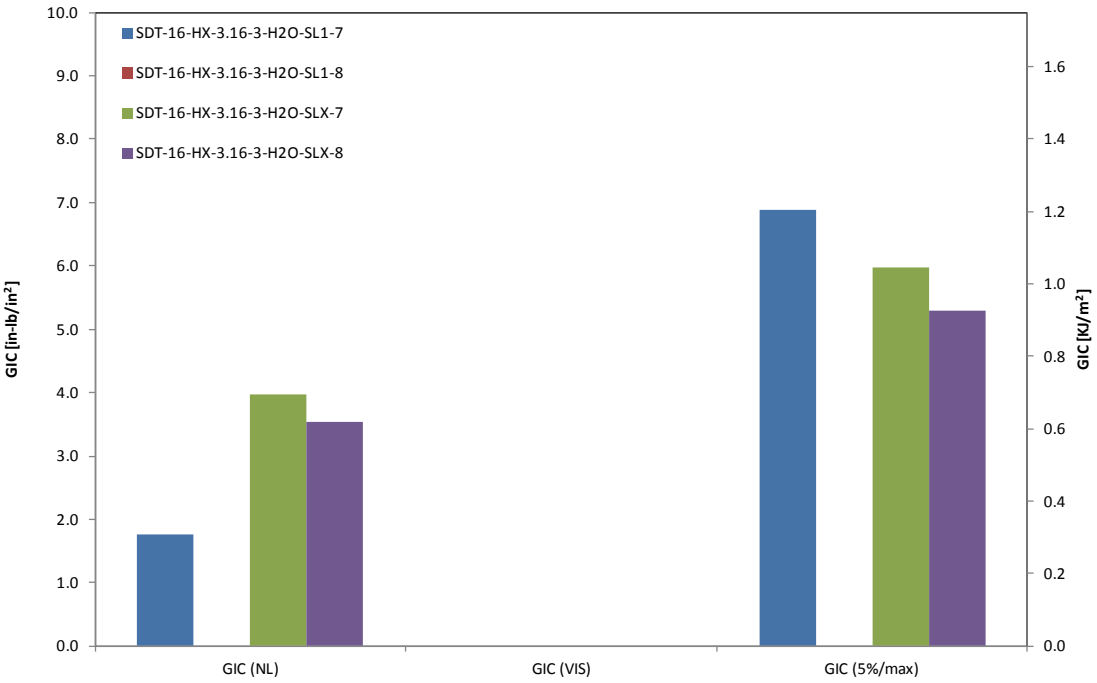

Figure C-59. HRH-10–3/16–3.0 water ingressed (2.5-inch prescribed crack)

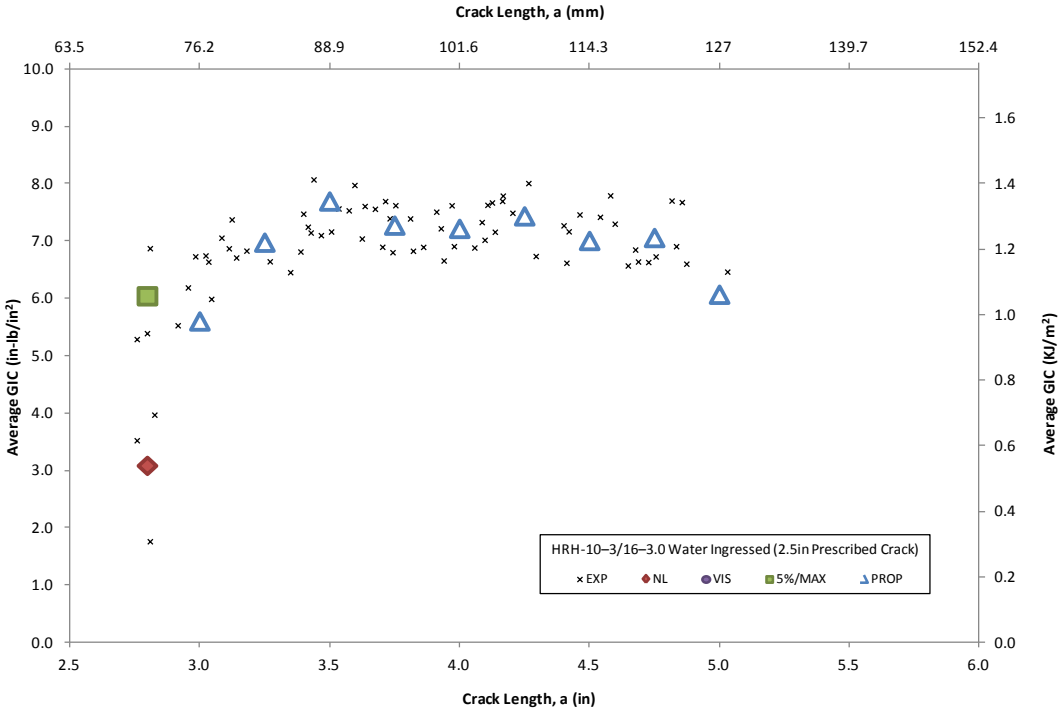

Figure C-60. Resistance curve for HRH-10–3/16–3.0 water ingressed (2.5″ prescribed crack)

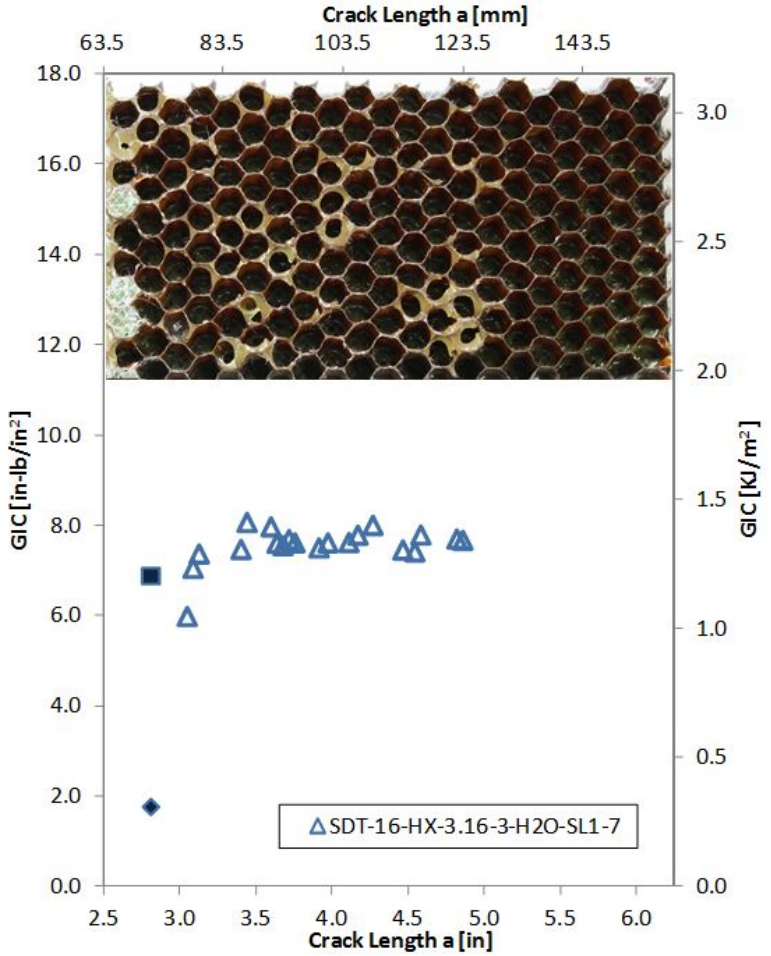

Figure C-61. Failure mode image and resistance curve for SDT-16-HX-3.16-3-H2O-SL1-X #7

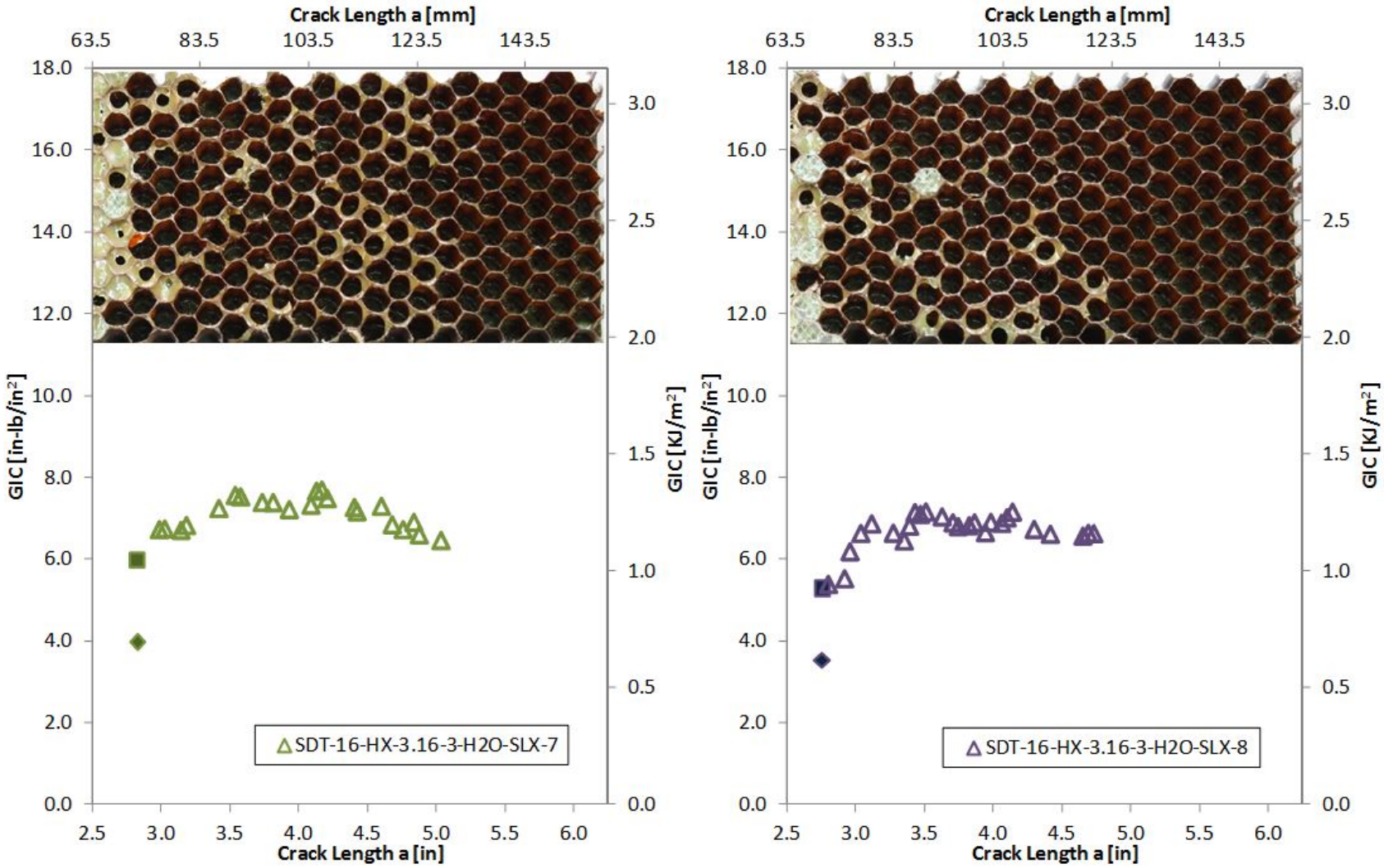

Figure C-62. Failure mode image and resistance curve for SDT-16-HX-3.16-3-H2O-SLX-X #7 and #8

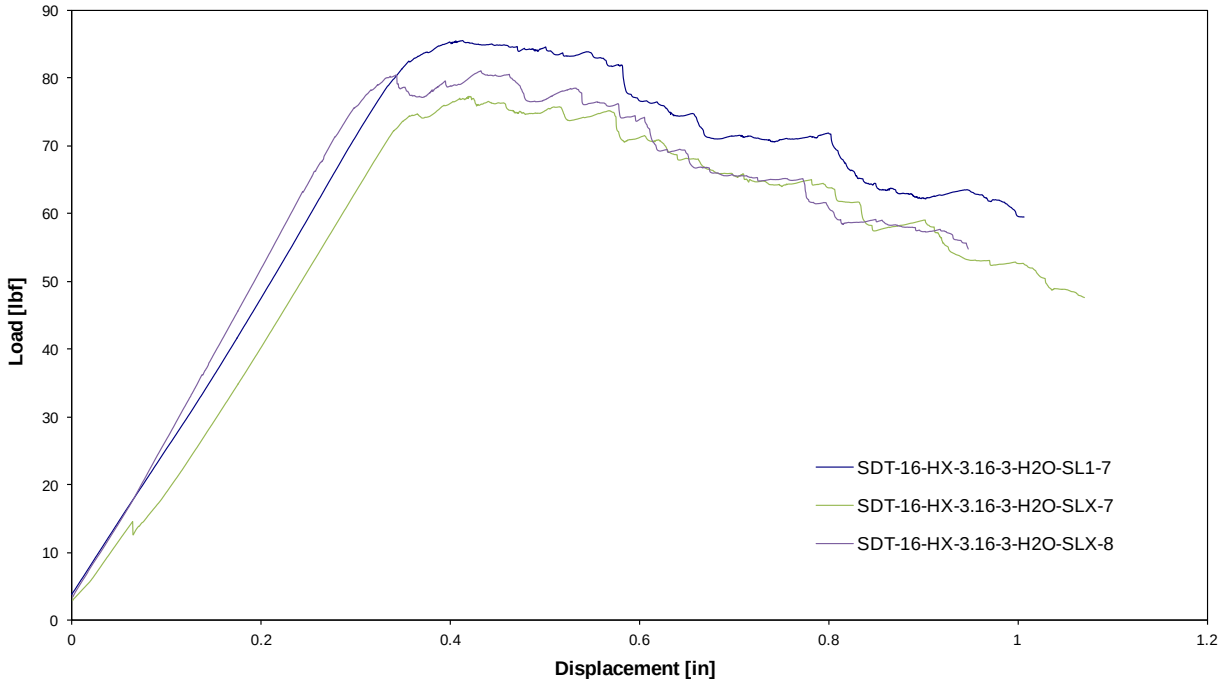

Figure C-63. Load vs. displacement curve for HRH-10–3/16–3.0 water ingressed (2.5″ prescribed crack)

C.4 HRH-10–3/16–6.0 DATA

C.4.1 HRH-10–3/16–6.0 BASELINE DATA

Table C-25. Test summary for HRH-10–3/16–6.0 baseline (2.5″ prescribed crack) precrack

Specimen	GIC (in-lb/in^2)			GIC (KJ/m^2)			Failure Mode
	NL	VIS	5%/max	NL	VIS	5%/max	
SDT-16-HX-3.16-6-BL-SL1-1	1.992	-	2.919	0.349	-	0.511	Mix of A and PO with a cell in C
SDT-16-HX-3.16-6-BL-SL1-2	2.336	-	3.351	0.409	-	0.587	Mix of A and PO with a cell in C
SDT-16-HX-3.16-6-BL-SL1-3	2.584	3.221	4.191	0.452	0.564	0.734	Primarily in A with a cell in PO
SDT-16-HX-3.16-6-BL-SL1-4	2.719	-	5.356	0.476	-	0.938	Primarily in A with a couple of cells in PO
SDT-16-HX-3.16-6-BL-SL1-5	2.237	-	4.267	0.392	-	0.747	Primarily in A with a couple of cells in PO
SDT-16-HX-3.16-6-BL-SL1-6	2.226	-	3.135	0.390	-	0.549	Primarily in A with a cell in PO
AVERAGE GIC	2.349	3.221	3.870	0.411	0.564	0.678	
STANDARD DEVIATION	0.264	-	0.915	0.046	-	0.160	
COEFFICIENT OF VARIATION (%)	11.230	-	23.637	11.230	-	23.637	

Table C-26. Test summary for HRH-10–3/16–6.0 baseline (2.5″ prescribed crack)

Specimen	GIC (in-lb/in^2)			GIC (KJ/m^2)			Failure Mode
	NL	VIS	5%/max	NL	VIS	5%/max	
SDT-16-HX-3.16-6-BL-SL1-1	2.348	6.594	7.439	0.411	1.155	1.303	Mix of A and PO
SDT-16-HX-3.16-6-BL-SL1-2	1.277	-	5.144	0.224	-	0.901	Mix of A and PO with last couple of rows in D
SDT-16-HX-3.16-6-BL-SL1-3	1.245	4.706	6.140	0.218	0.824	1.075	Primarily A with occasional PO, then a mix of A and PO with last couple of rows in D
SDT-16-HX-3.16-6-BL-SL1-4	1.496	5.299	5.414	0.262	0.928	0.948	Primarily A with occasional PO, then a mix of A and PO with last several rows in D
SDT-16-HX-3.16-6-BL-SL1-5	2.504	4.824	5.210	0.439	0.845	0.912	Mix of A and PO with last couple of rows in D
SDT-16-HX-3.16-6-BL-SL1-6	1.461	4.181	4.522	0.256	0.732	0.792	Primarily A with occasional PO, then a mix of A and PO with last several rows in D
AVERAGE GIC	1.722	5.121	5.645	0.302	0.897	0.989	
STANDARD DEVIATION	0.556	0.915	1.022	0.097	0.160	0.179	
COEFFICIENT OF VARIATION (%)	32.313	17.860	18.102	32.313	17.860	18.102	

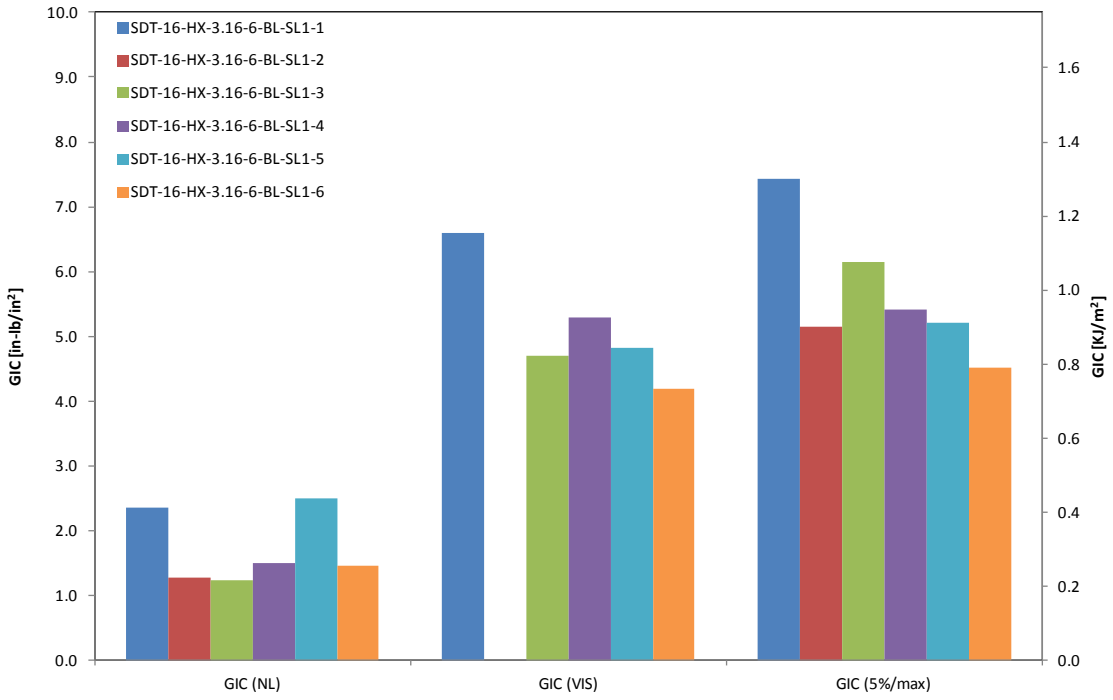

Figure C-64. GIC for HRH-10–3/16–6.0 baseline (2.5″ prescribed crack)

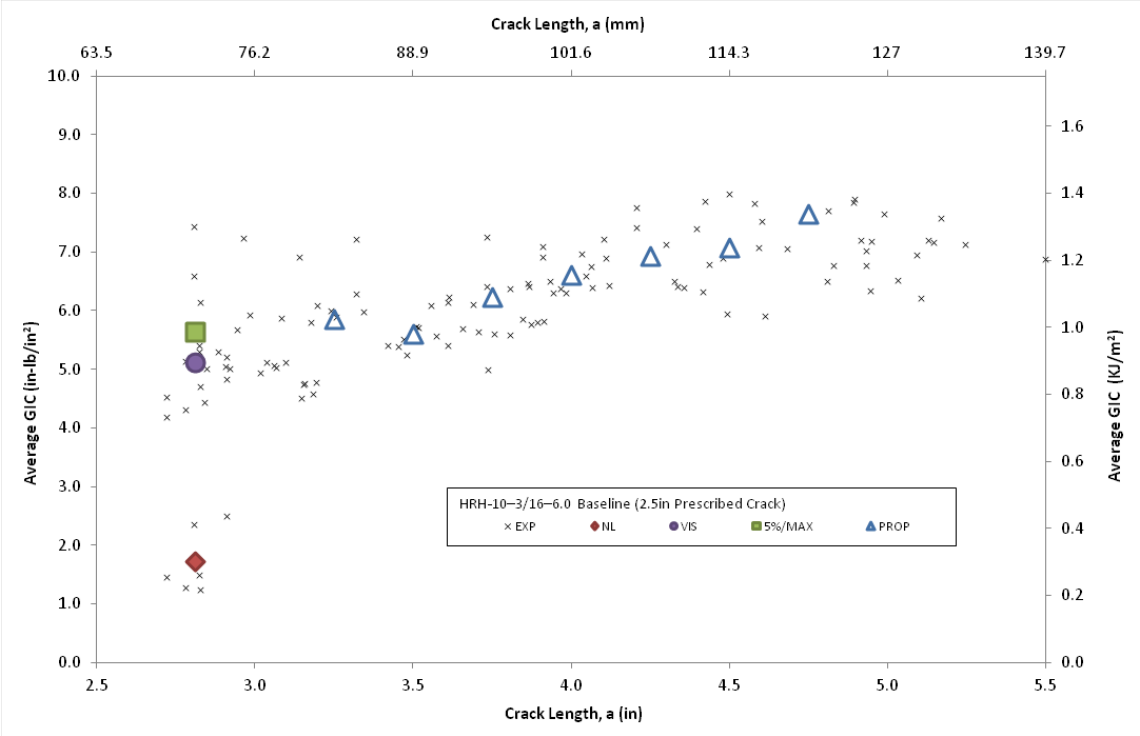

Figure C-65. Resistance curve for HRH-10–3/16–6.0 baseline (2.5″ prescribed crack)

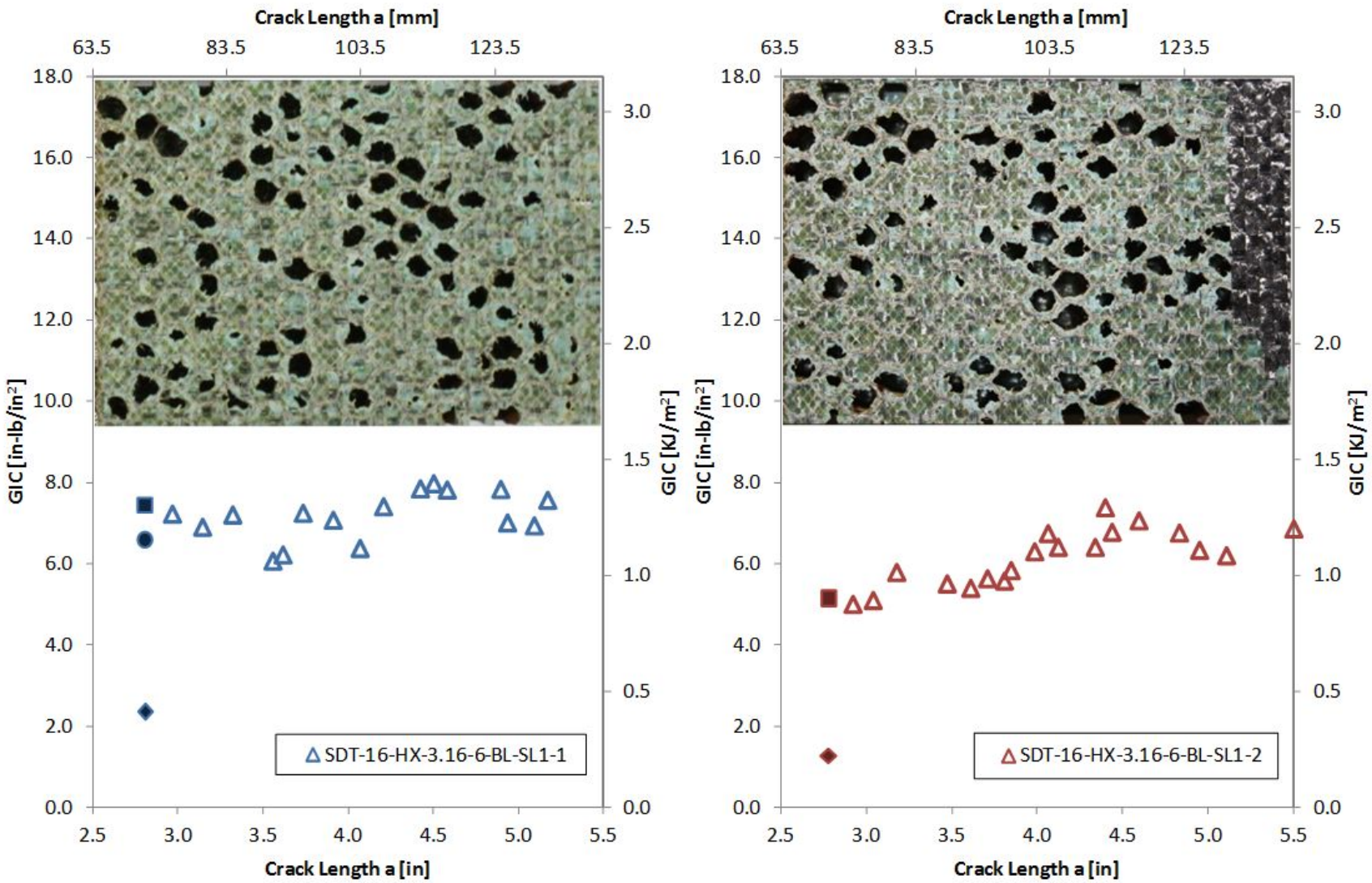

Figure C-66. Failure mode image and resistance curve for SDT-16-HX-3.16-6-BL-SL1-X #1 and #2

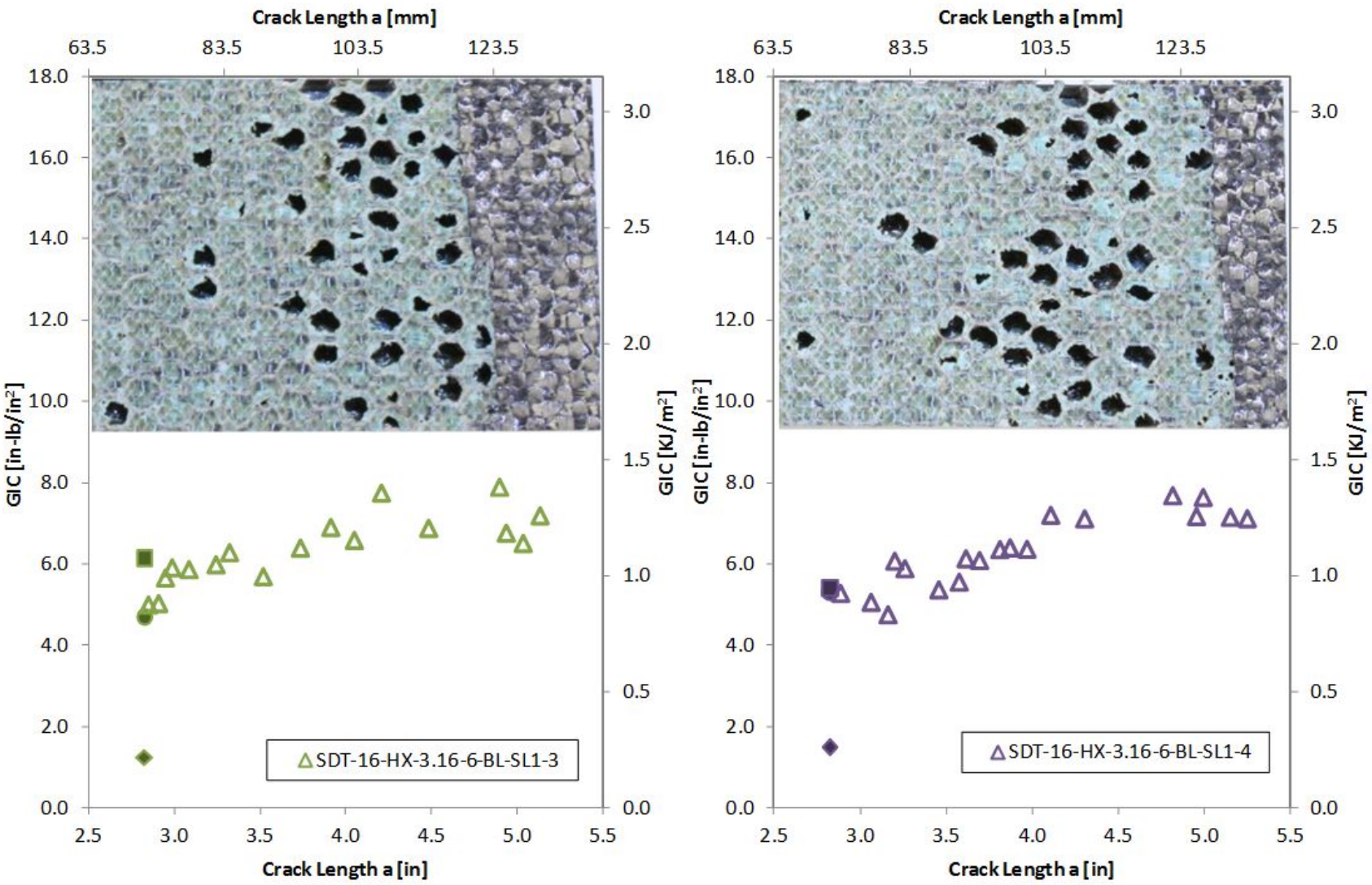

Figure C-67. Failure mode image and resistance curve for SDT-16-HX-3.16-6-BL-SL1-X #3 and #4

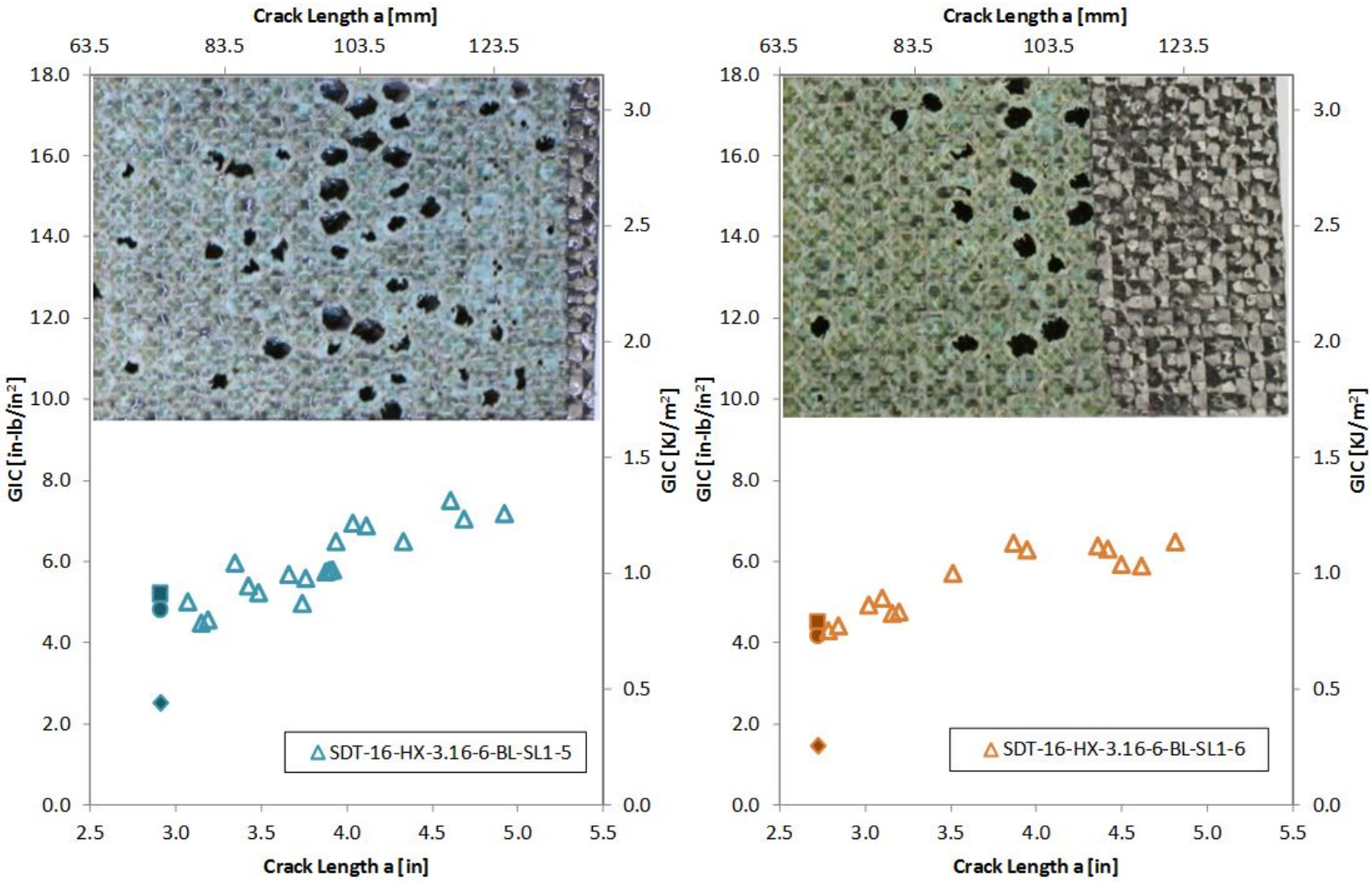

Figure C-68. Failure mode image and resistance curve for SDT-16-HX-3.16-6-BL-SL1-X #5 and #6

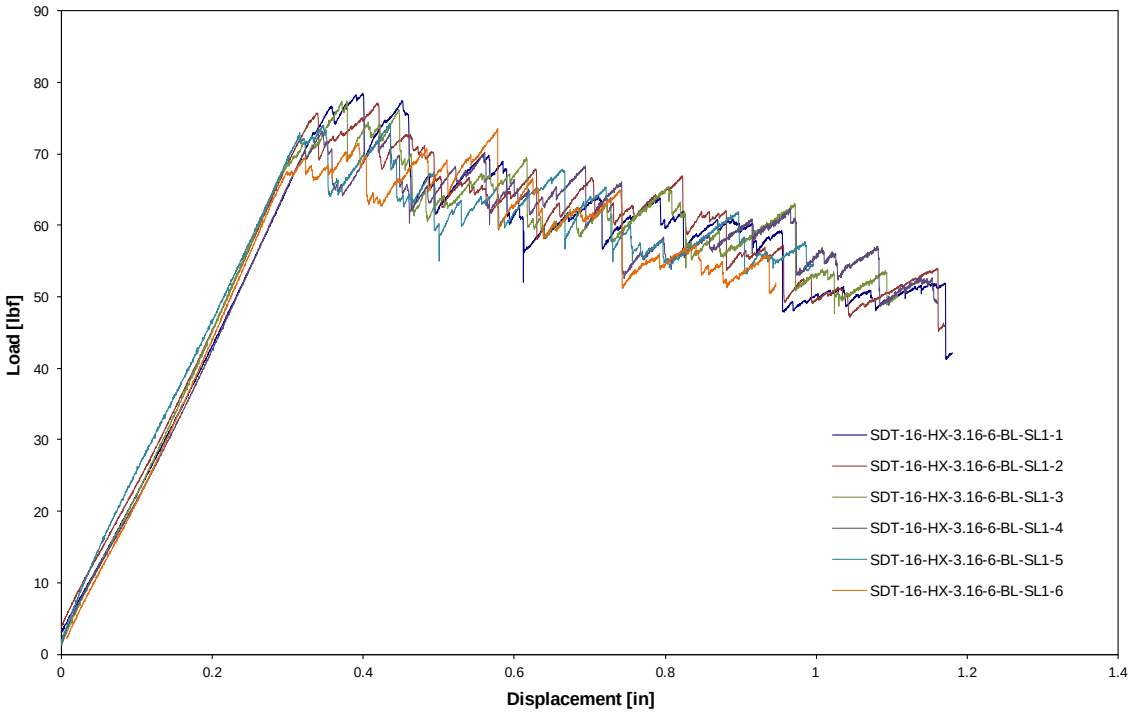

Figure C-69. Load vs. displacement curve for HRH-10–3/16–6.0 baseline (2.5″ prescribed crack)

C.4.2 HRH-10–3/16–6.0 FLUID-INGRESSED DATA

Table C-27. Test summary for HRH-10–3/16–6.0 fluid-ingressed (2.5″ prescribed crack) precrack

Specimen	GIC (in-lb/in^2)			GIC (KJ/m^2)			Failure Mode
	NL	VIS	5%/max	NL	VIS	5%/max	
SDT-16-HX-3.16-6-FI-SL1-2	1.662	-	2.468	0.291	-	0.432	Primarily in A with a few cells in PO
SDT-16-HX-3.16-6-FI-SL1-3	1.596	-	2.947	0.280	-	0.516	Primarily in A with a couple of cells in PO
SDT-16-HX-3.16-6-FI-SL1-4	1.813	-	2.640	0.318	-	0.462	Primarily in A with a cell in PO
SDT-16-HX-3.16-6-FI-SL1-5	1.696	-	2.426	0.297	-	0.425	Primarily in A with a cell in PO
SDT-16-HX-3.16-6-FI-SL1-6	1.488	-	2.154	0.261	-	0.377	Primarily in A with a couple of cells in PO
SDT-16-HX-3.16-6-FI-SL1-7	1.643	-	5.007	0.288	-	0.877	Primarily in A with several cells in PO
AVERAGE GIC	1.650	-	2.940	0.289	-	0.515	
STANDARD DEVIATION	0.108	-	1.046	0.019	-	0.183	
COEFFICIENT OF VARIATION (%)	6.542	-	35.568	6.542	-	35.568	

Table C-28. Test summary for HRH-10–3/16–6.0 fluid-ingressed (2.5″ prescribed crack)

Specimen	GIC (in-lb/in^2)			GIC (KJ/m^2)			Failure Mode
	NL	VIS	5%/max	NL	VIS	5%/max	
SDT-16-HX-3.16-6-FI-SL1-2	1.539	6.386	7.064	0.269	1.118	1.237	Mix of A and PO
SDT-16-HX-3.16-6-FI-SL1-3	1.423	6.136	6.772	0.249	1.075	1.186	Initially A, then a mix of A and PO; last few rows in D
SDT-16-HX-3.16-6-FI-SL1-4	1.296	6.045	6.674	0.227	1.059	1.169	Initially A, then a mix of A and PO; last few rows in D
SDT-16-HX-3.16-6-FI-SL1-5	1.103	-	4.940	0.193	-	0.865	Initially A, then a mix of A and PO; last few rows in D
SDT-16-HX-3.16-6-FI-SL1-6	1.008	-	4.399	0.176	-	0.770	Initially A, then a mix of A and PO; last few rows in D
SDT-16-HX-3.16-6-FI-SL1-7	1.523	5.589	6.050	0.267	0.979	1.060	Mix of A and PO; last few rows in D
AVERAGE GIC	1.315	6.039	5.983	0.230	1.058	1.048	
STANDARD DEVIATION	0.221	0.333	1.084	0.039	0.058	0.190	
COEFFICIENT OF VARIATION (%)	16.812	5.512	18.113	16.812	5.512	18.113	

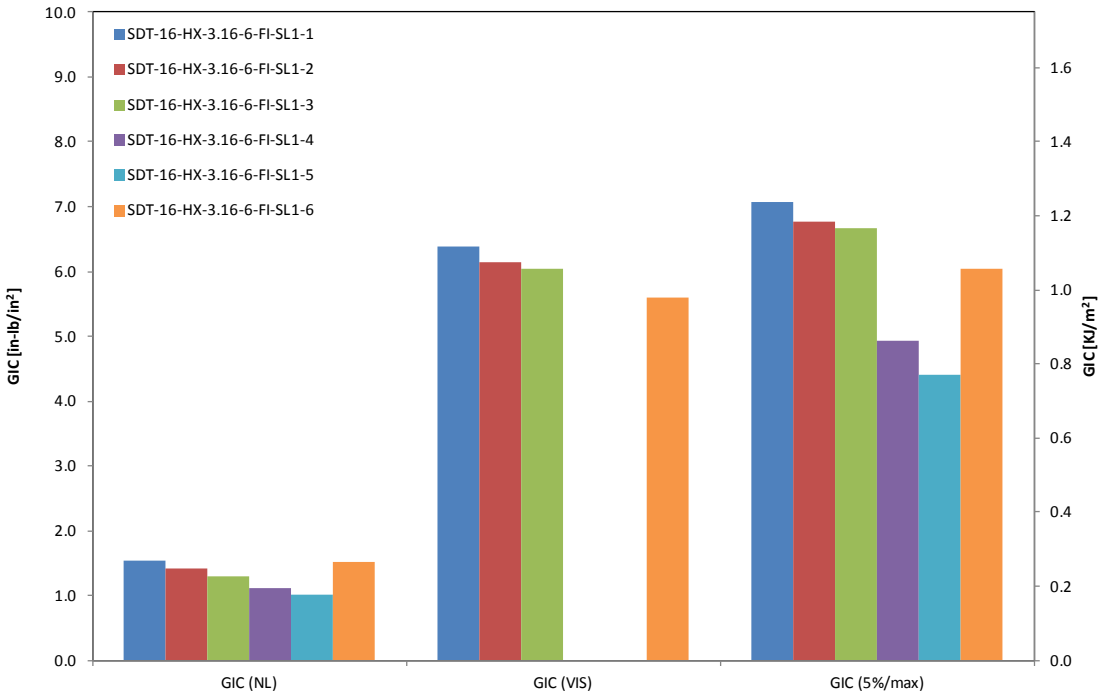

Figure C-70. GIC for HRH-10–3/16–6.0 fluid ingressed (2.5″ prescribed crack)

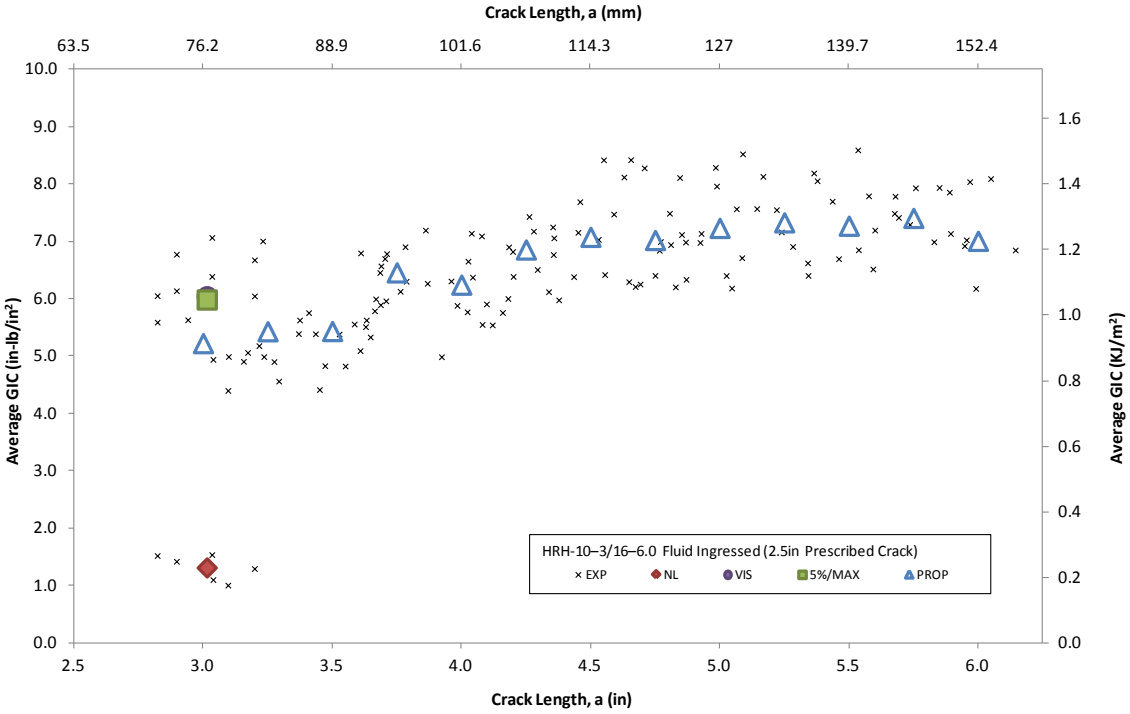

Figure C-71. Resistance curve for HRH-10–3/16–6.0 fluid ingressed (2.5″ prescribed crack)

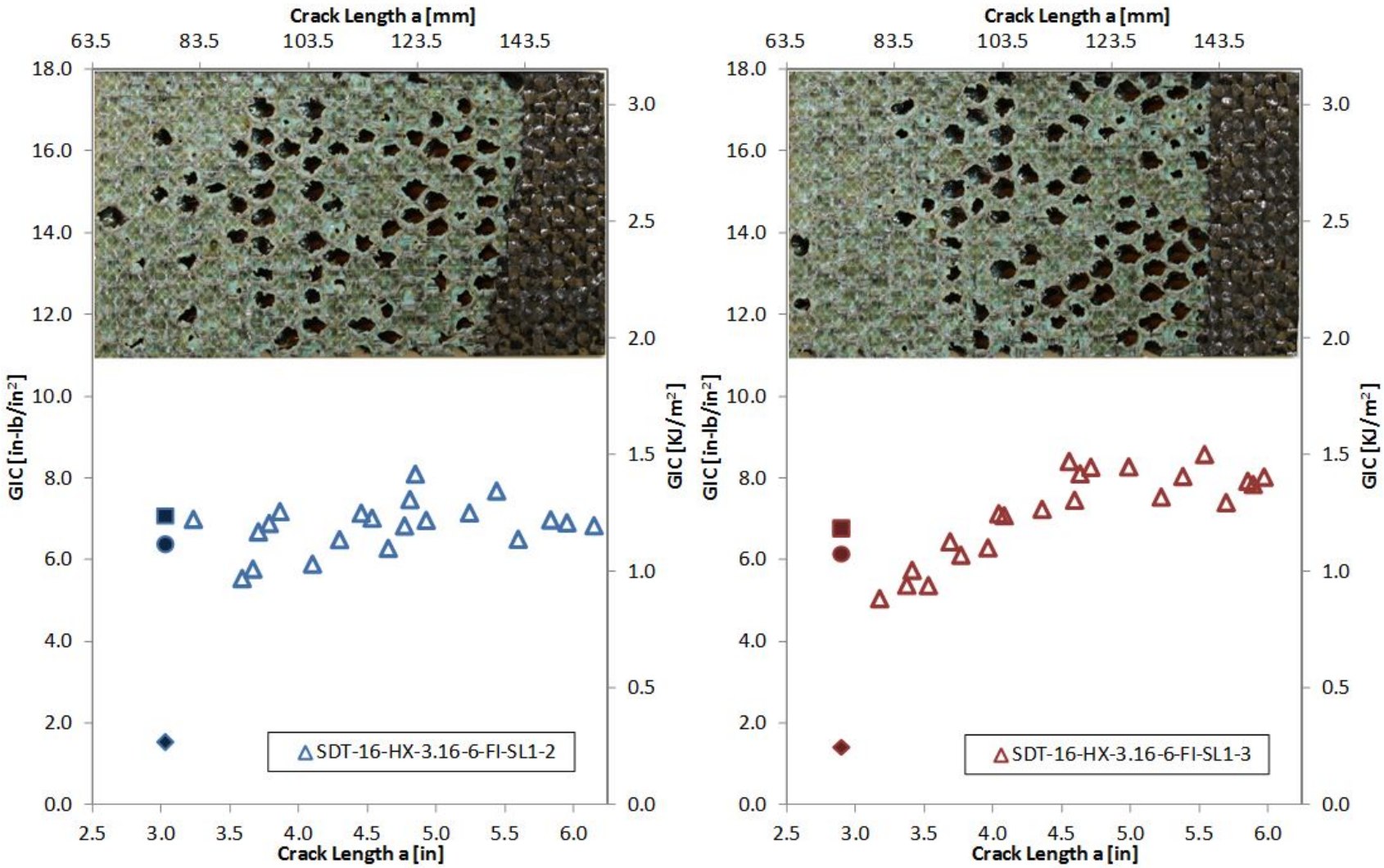

Figure C-72. Failure mode image and resistance curve for SDT-16-HX-3.16-6-FI-SL1-X #2 and #3

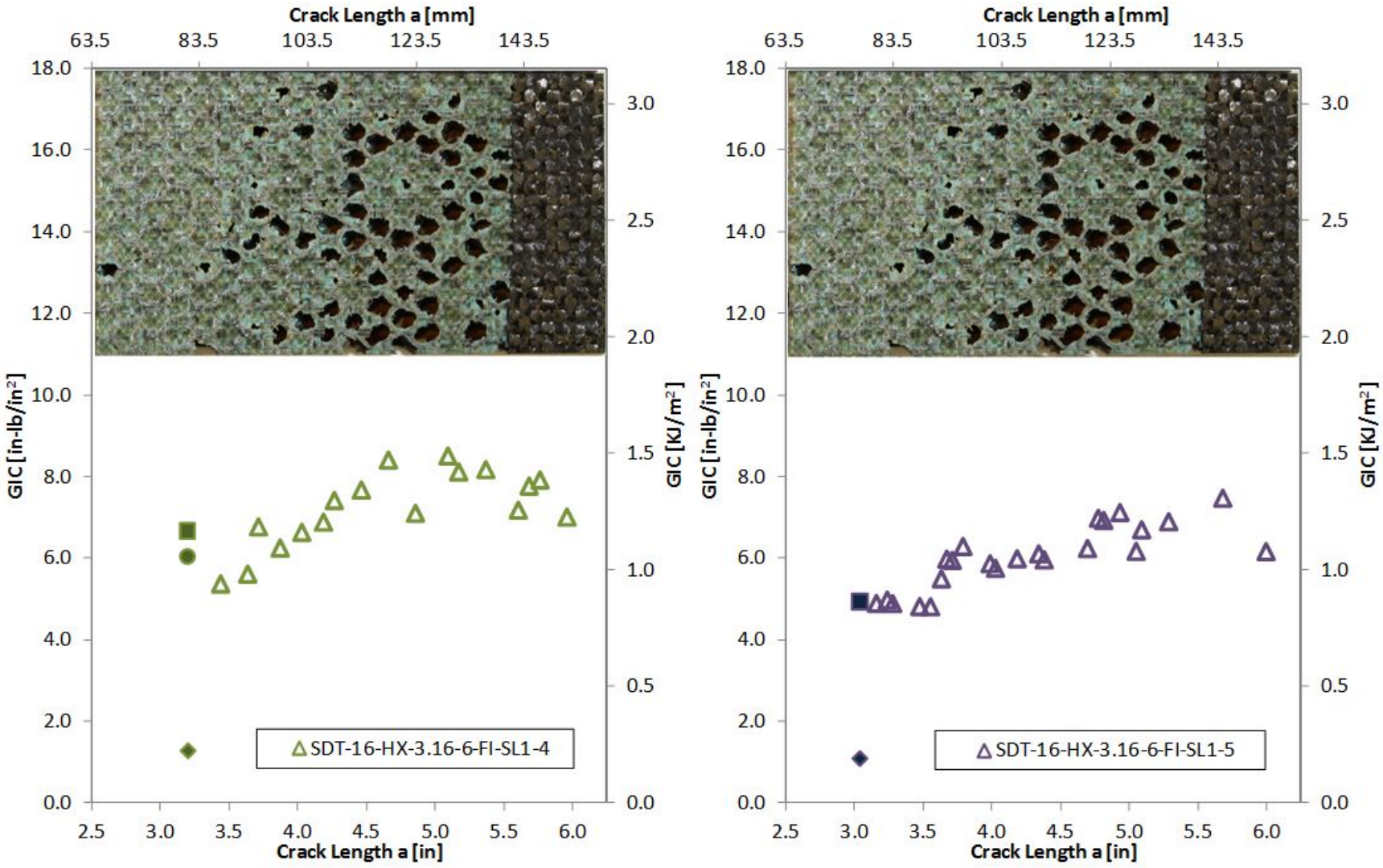

Figure C-73. Failure mode image and resistance curve for SDT-16-HX-3.16-6-FI-SL1-X #4 and #5

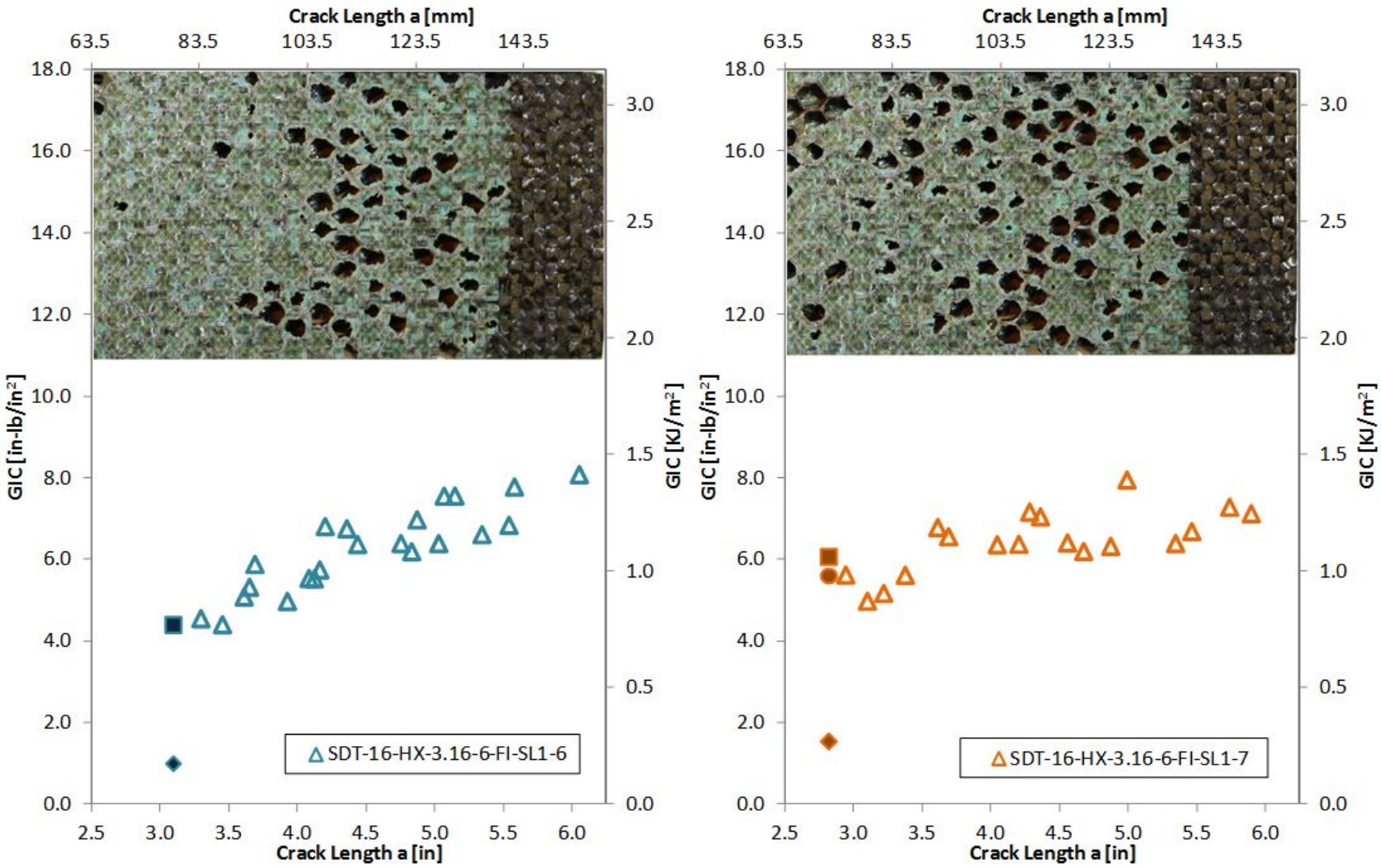

Figure C-74. Failure mode image and resistance curve for SDT-16-HX-3.16-6-FI-SL1-X #6 and #7

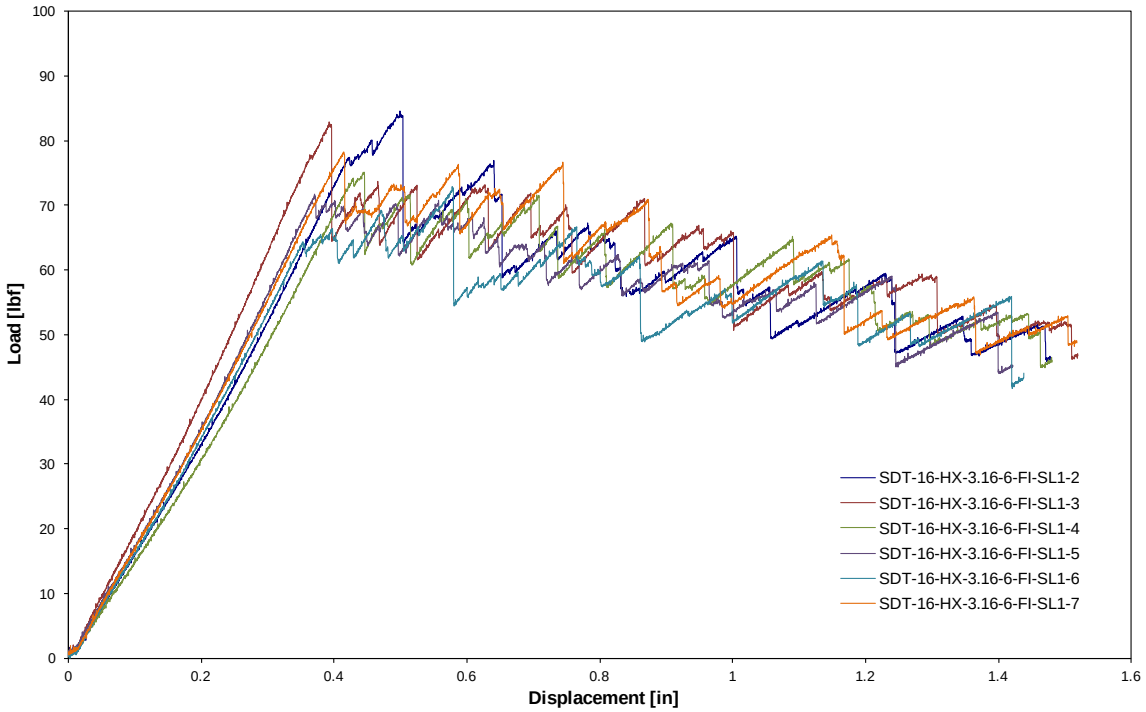

Figure C-75. Load vs. displacement curve for HRH-10–3/16–6.0 fluid ingressed (2.5″ prescribed crack)

C.4.3 HRH-10–3/16–6.0 EXTENDED FLUID-INGRESSED DATA

Table C-29. Test summary for HRH-10–3/16–6.0 extended fluid ingressed (2.5″ prescribed crack) precrack

Specimen	GIC (in-lb/in^2)			GIC (KJ/m^2)			Failure Mode
	NL	VIS	5%/max	NL	VIS	5%/max	
SDT-16-HX-3.16-6-EFI-SL1-7	-	-	-	-	-	-	
SDT-16-HX-3.16-6-EFI-SL1-8	1.643	-	2.685	0.288	-	0.470	Mix of A and PO
AVERAGE GIC	1.643	-	2.685	0.288	-	0.470	
STANDARD DEVIATION	-	-	-	-	-	-	
COEFFICIENT OF VARIATION (%)	-	-	-	-	-	-	

Table C-30. Test summary for HRH-10–3/16–6.0 extended fluid ingressed (2.5″ prescribed crack)

Specimen	GIC (in-lb/in^2)			GIC (KJ/m^2)			Failure Mode
	NL	VIS	5%/max	NL	VIS	5%/max	
SDT-16-HX-3.16-6-EFI-SL1-7	-	-	-	-	-	-	
SDT-16-HX-3.16-6-EFI-SL1-8	1.558	-	5.962	0.273	-	1.044	Mix of A and PO, then S
AVERAGE GIC	1.558	-	5.962	0.273	-	1.044	
STANDARD DEVIATION	-	-	-	-	-	-	
COEFFICIENT OF VARIATION (%)	-	-	-	-	-	-	

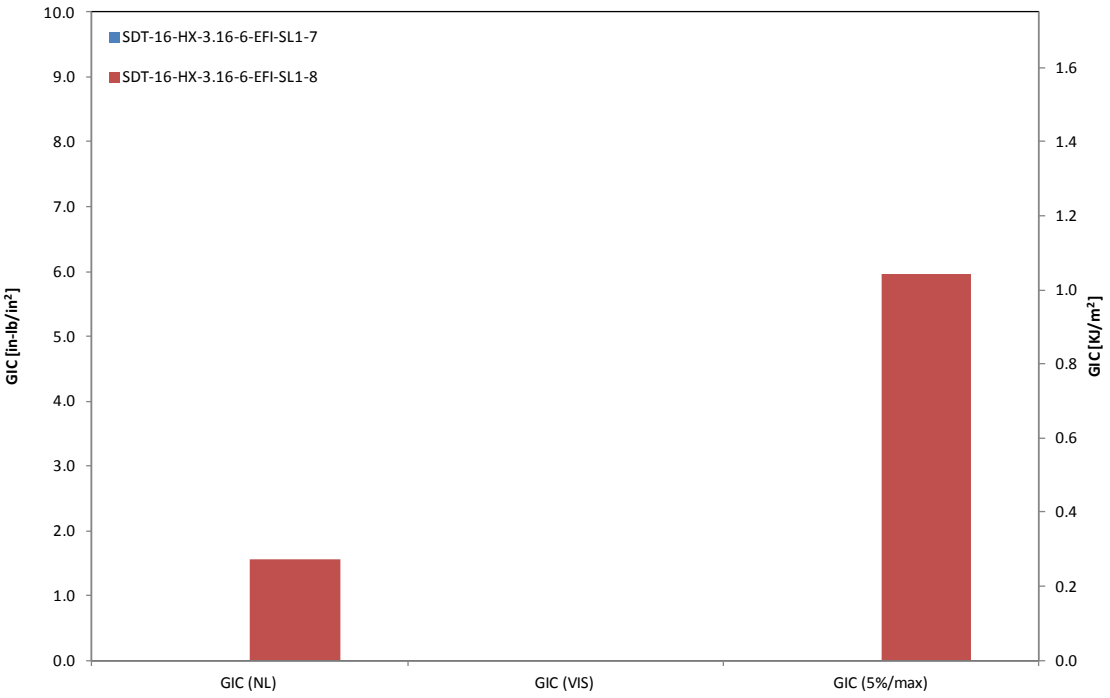

Figure C-76. GIC for HRH-10–3/16–6.0 extended fluid ingressed (2.5″ prescribed crack)

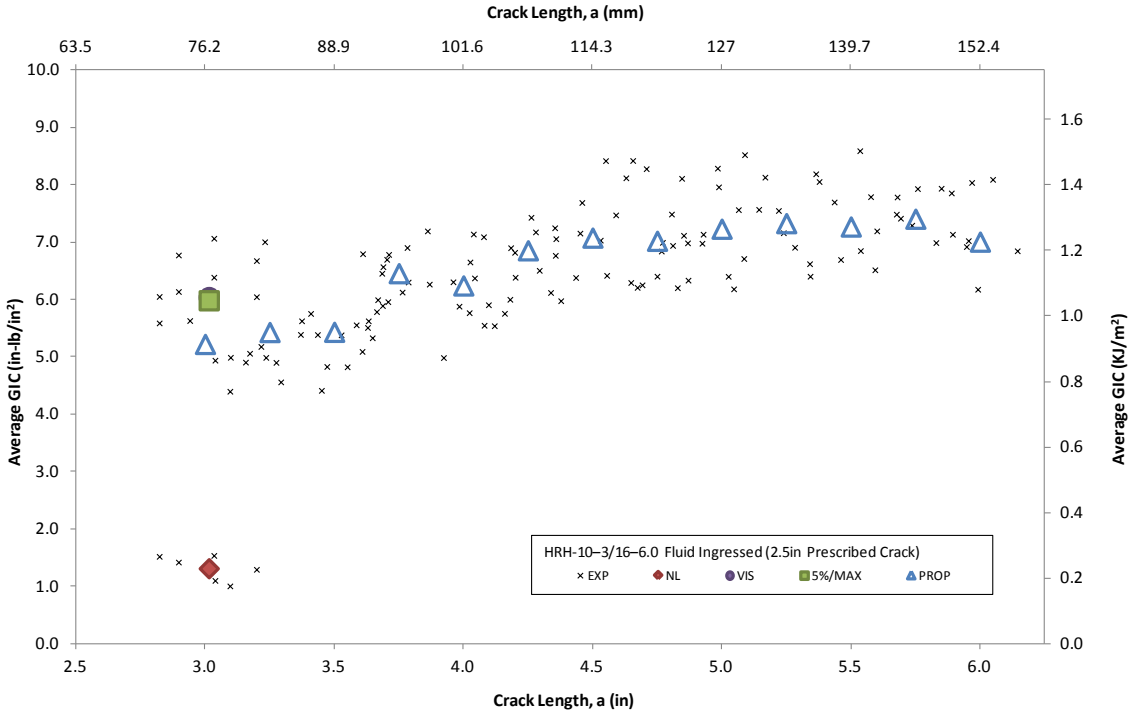

Figure C-77. Resistance curve for HRH-10–3/16–6.0 fluid ingressed (2.5″ prescribed crack)

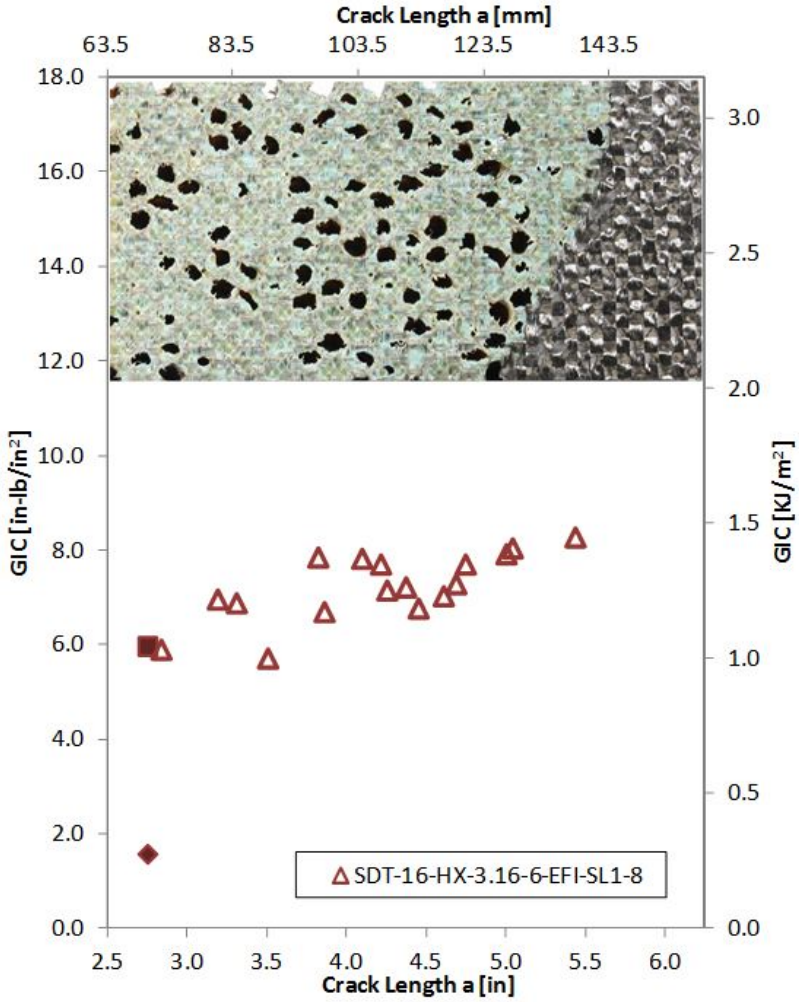

Figure C-78. Failure mode image and resistance curve for SDT-16-HX-3.16-6-EFI-SL1-X # 8

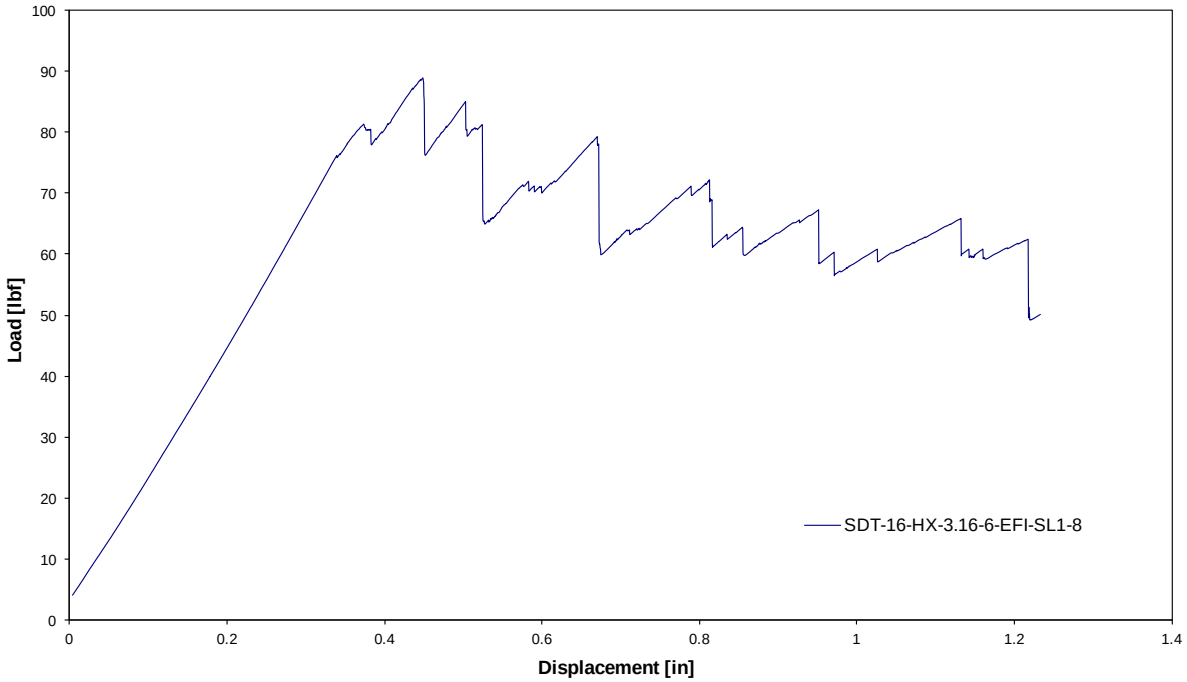

Figure C-79. Load vs. displacement curve for HRH-10–3/16–6.0 extended fluid ingressed (2.5″ prescribed crack)

C.4.4 HRH-10–3/16–6.0 WATER-INGRESSED DATA

Table C-31. Test summary for HRH-10–3/16–6.0 water (2.5″ prescribed crack) precrack

Specimen	GIC (in-lb/in^2)			GIC (KJ/m^2)			Failure Mode
	NL	VIS	5%/max	NL	VIS	5%/max	
SDT-16-HX-3.16-6-H2O-SL1-7	4.156	-	7.813	0.728	-	1.368	Mix of A and C
SDT-16-HX-3.16-6-H2O-SL1-8	3.814	-	4.575	0.668	-	0.801	Mix of A and PO
SDT-16-HX-3.16-6-H2O-SLX-7	3.200	-	6.173	0.560	-	1.081	Mix of A and C
SDT-16-HX-3.16-6-H2O-SLX-8	1.759	-	3.252	0.308	-	0.569	Mix of A and PO
AVERAGE GIC	3.232	-	5.453	0.566	-	0.955	
STANDARD DEVIATION	1.059	-	1.975	0.185	-	0.346	
COEFFICIENT OF VARIATION (%)	32.761	-	36.221	32.761	-	36.221	

Table C-32. Test summary for HRH-10–3/16–6.0 water (2.5″ prescribed crack)

Specimen	GIC (in-lb/in^2)			GIC (KJ/m^2)			Failure Mode
	NL	VIS	5%/max	NL	VIS	5%/max	
SDT-16-HX-3.16-6-H2O-SL1-7	1.379	-	10.524	0.242	-	1.843	Mix of A and PO, then S
SDT-16-HX-3.16-6-H2O-SL1-8	1.705	-	9.881	0.299	-	1.730	Mix of A and PO, then S
SDT-16-HX-3.16-6-H2O-SLX-7	2.053	-	9.318	0.359	-	1.632	Mix of A and PO
SDT-16-HX-3.16-6-H2O-SLX-8	1.720	-	8.876	0.301	-	1.554	Mix of A and PO, then S
AVERAGE GIC	1.714	-	9.650	0.300	-	1.690	
STANDARD DEVIATION	0.275	-	0.713	0.048	-	0.125	
COEFFICIENT OF VARIATION (%)	16.046	-	7.392	16.046	-	7.392	

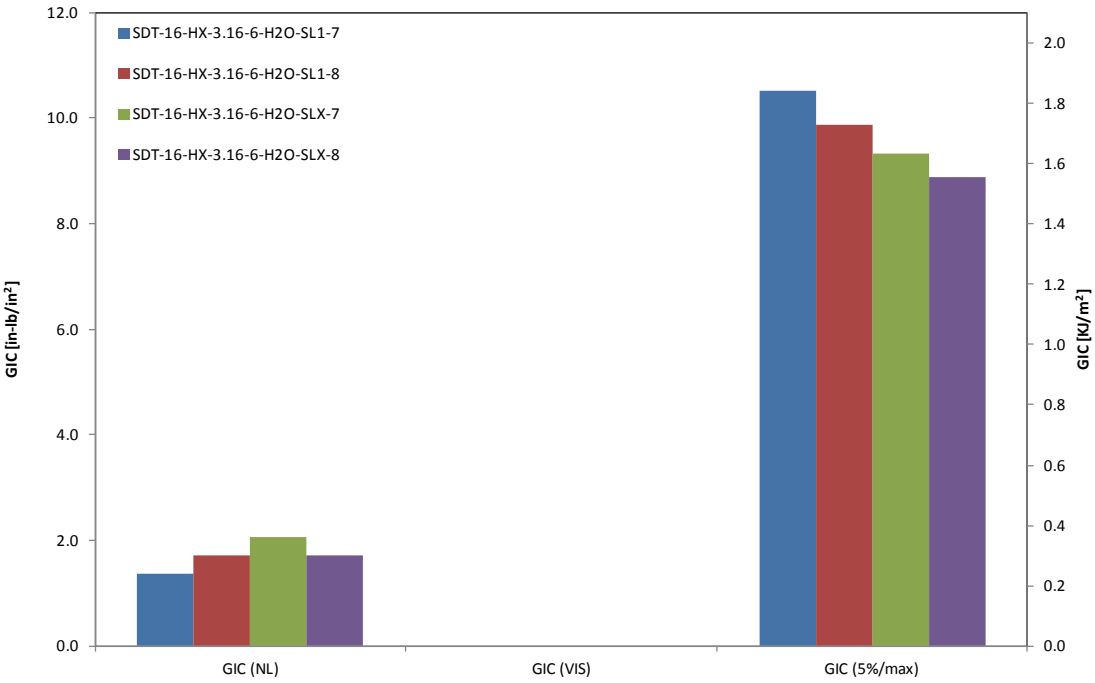

Figure C-80. GIC for HRH-10–3/16–6.0 water (2.5″ prescribed crack)

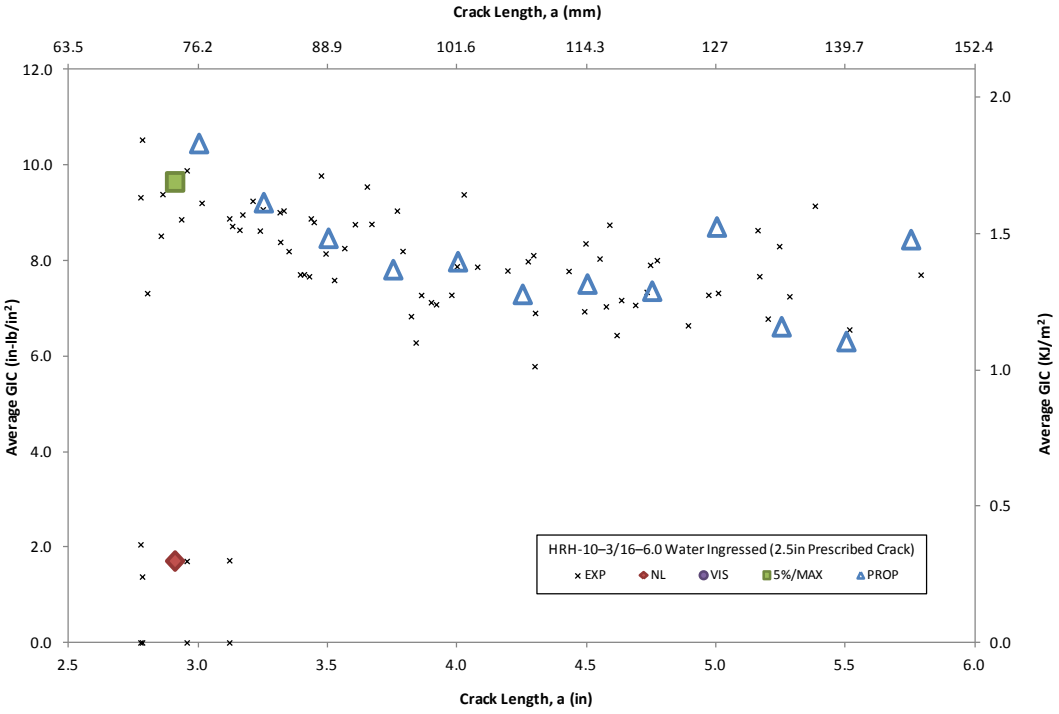

Figure C-81. Resistance curve for HRH-10–3/16–6.0 water (2.5″ prescribed crack)

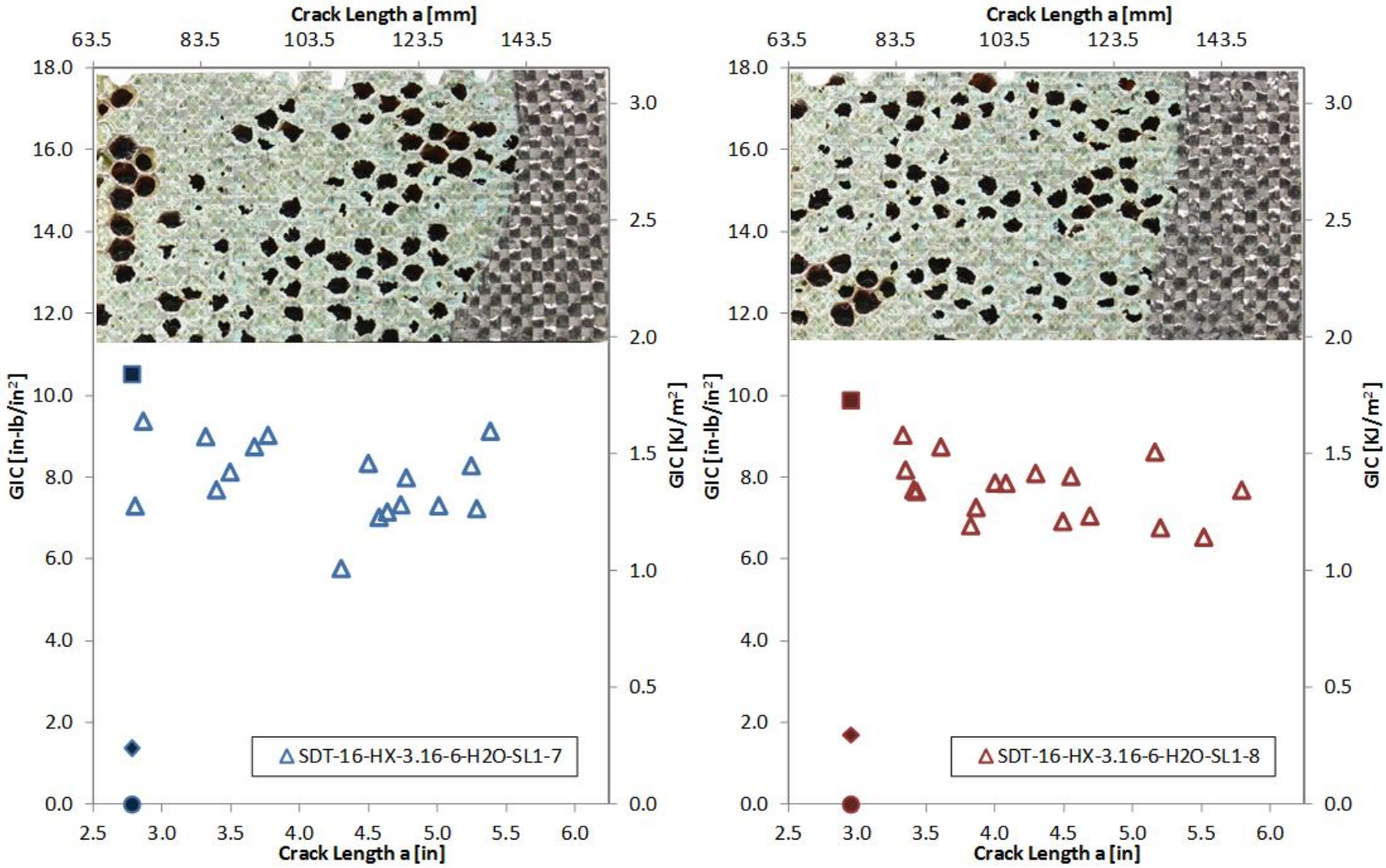

Figure C-82. Failure mode image and resistance curve for SDT-16-HX-3.16-6-H2O-SL1-X #7 and #8

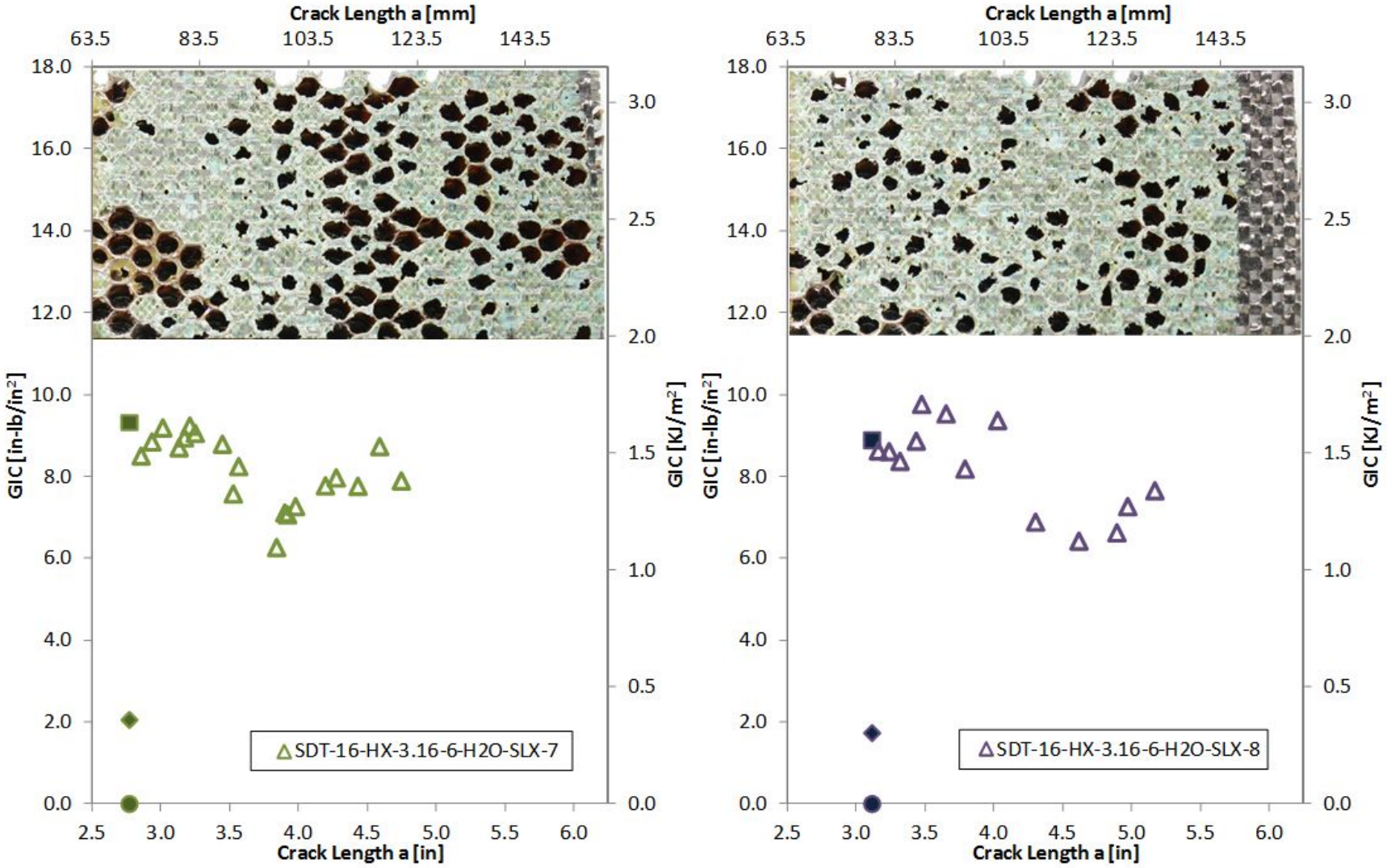

Figure C-83. Failure mode image and resistance curve for SDT-16-HX-3.16-6-H2O-SLX-X #7 and #8

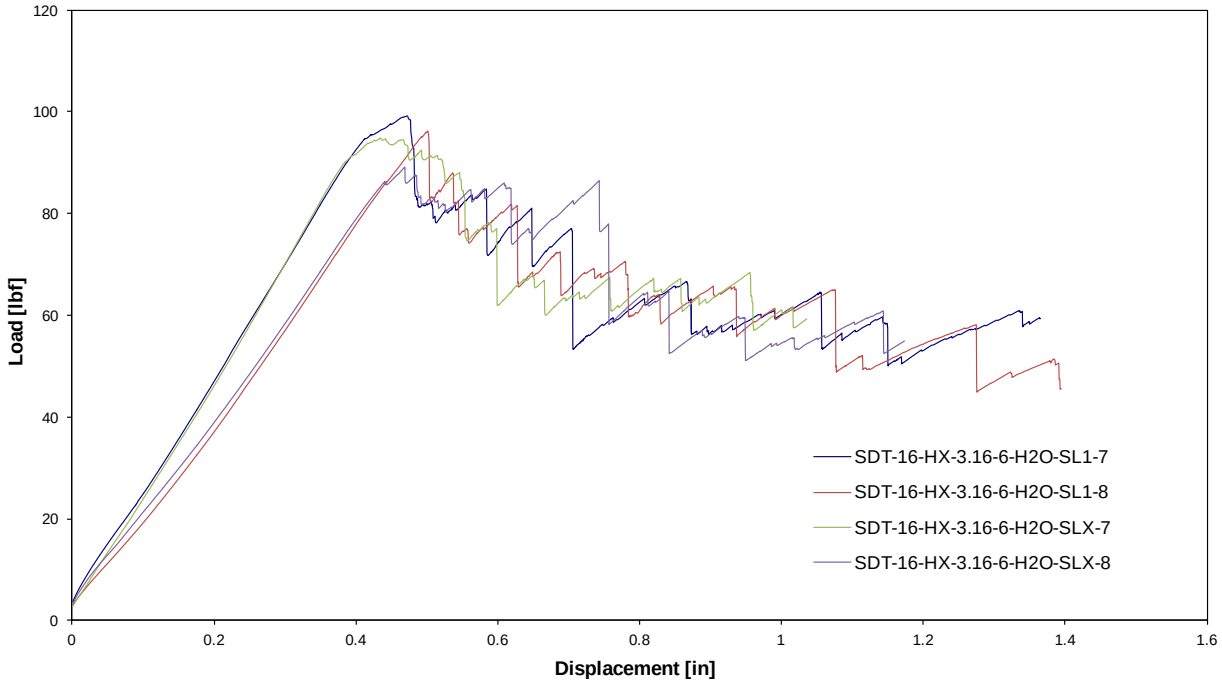

Figure C-84. Load vs. displacement curve for HRH-10–3/16–6.0 water (2.5″ prescribed crack)

C.5 HRH-10–3/8–3.0 DATA

C.5.1 HRH-10–3/8–3.0 BASELINE DATA

Table C-33. Test summary for HRH-10–3/8–3.0 baseline (2.5″ prescribed crack) precrack

Specimen	GIC (in-lb/in^2)			GIC (KJ/m^2)			Failure Mode
	NL	VIS	5%/max	NL	VIS	5%/max	
SDT-16-HX-3.8-3-BL-SL1-1	2.060	-	3.485	0.361	-	0.610	Primarily in A with a cell in PO
SDT-16-HX-3.8-3-BL-SL1-2	1.390	-	2.459	0.243	-	0.431	Primarily in A with a cell in PO
SDT-16-HX-3.8-3-BL-SL1-3	1.814	-	2.948	0.318	-	0.516	Primarily in A
SDT-16-HX-3.8-3-BL-SL1-4	1.456	-	2.485	0.255	-	0.435	Primarily in A with a cell in PO
SDT-16-HX-3.8-3-BL-SL1-5	1.518	-	2.508	0.266	-	0.439	Primarily in A
SDT-16-HX-3.8-3-BL-SL1-6	1.614	-	2.647	0.283	-	0.464	Primarily in A with a cell in PO
AVERAGE GIC	1.642	-	2.755	0.288	-	0.483	
STANDARD DEVIATION	0.252	-	0.401	0.044	-	0.070	
COEFFICIENT OF VARIATION (%)	15.373	-	14.540	15.373	-	14.540	

Table C-34. Test summary for HRH-10–3/8–3.0 baseline (2.5″ prescribed crack)

Specimen	GIC (in-lb/in^2)			GIC (KJ/m^2)			Failure Mode
	NL	VIS	5%/max	NL	VIS	5%/max	
SDT-16-HX-3.8-3-BL-SL1-1	1.280	2.627	3.430	0.224	0.460	0.601	Primarily in A with occasional PO and the last couple of rows in D
SDT-16-HX-3.8-3-BL-SL1-2	1.775	2.729	2.975	0.311	0.478	0.521	Primarily in A with occasional PO and the last couple of rows in D
SDT-16-HX-3.8-3-BL-SL1-3	1.653	3.082	3.306	0.289	0.540	0.579	Primarily A with a cell in PO, then primarily C with a cell in PO, then a mix of A, PO and C
SDT-16-HX-3.8-3-BL-SL1-4	1.878	-	2.830	0.329	-	0.496	Primarily in A with occasional PO and the last couple of rows in D
SDT-16-HX-3.8-3-BL-SL1-5	1.078	-	1.624	0.189	-	0.284	Primarily A with a couple of cells in PO, then primarily C
SDT-16-HX-3.8-3-BL-SL1-6	1.741	-	3.096	0.305	-	0.542	Primarily in A with occasional PO and the last couple of rows in D
AVERAGE GIC	1.567	2.813	2.877	0.274	0.493	0.504	
STANDARD DEVIATION	0.316	0.239	0.651	0.055	0.042	0.114	
COEFFICIENT OF VARIATION (%)	20.165	8.490	22.629	20.165	8.490	22.629	

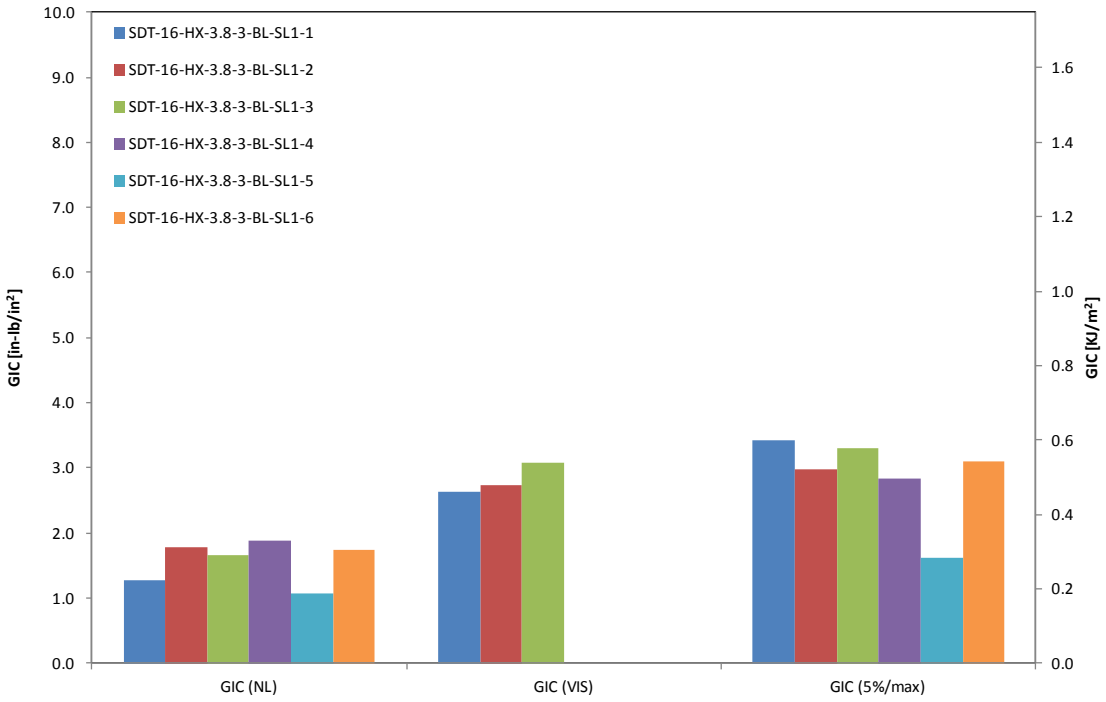

Figure C-85. GIC for HRH-10–3/8–3.0 baseline (2.5″ prescribed crack)

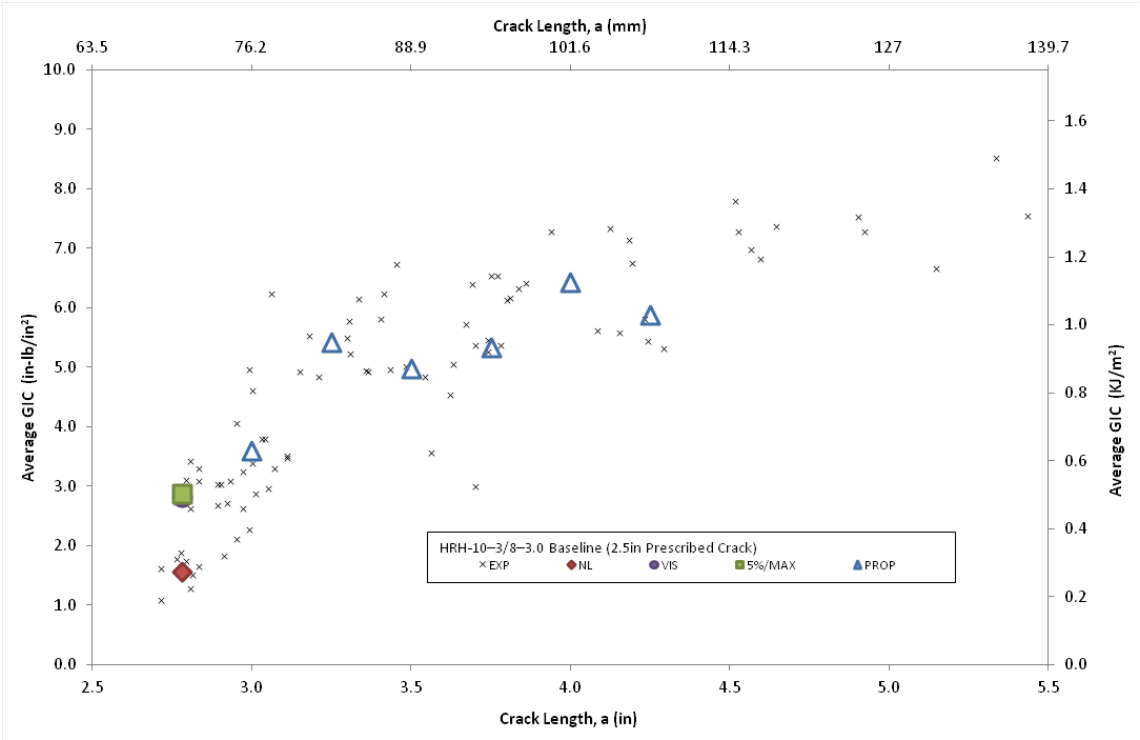

Figure C-86. Resistance curve for HRH-10–3/8–3.0 baseline (2.5″ prescribed crack)

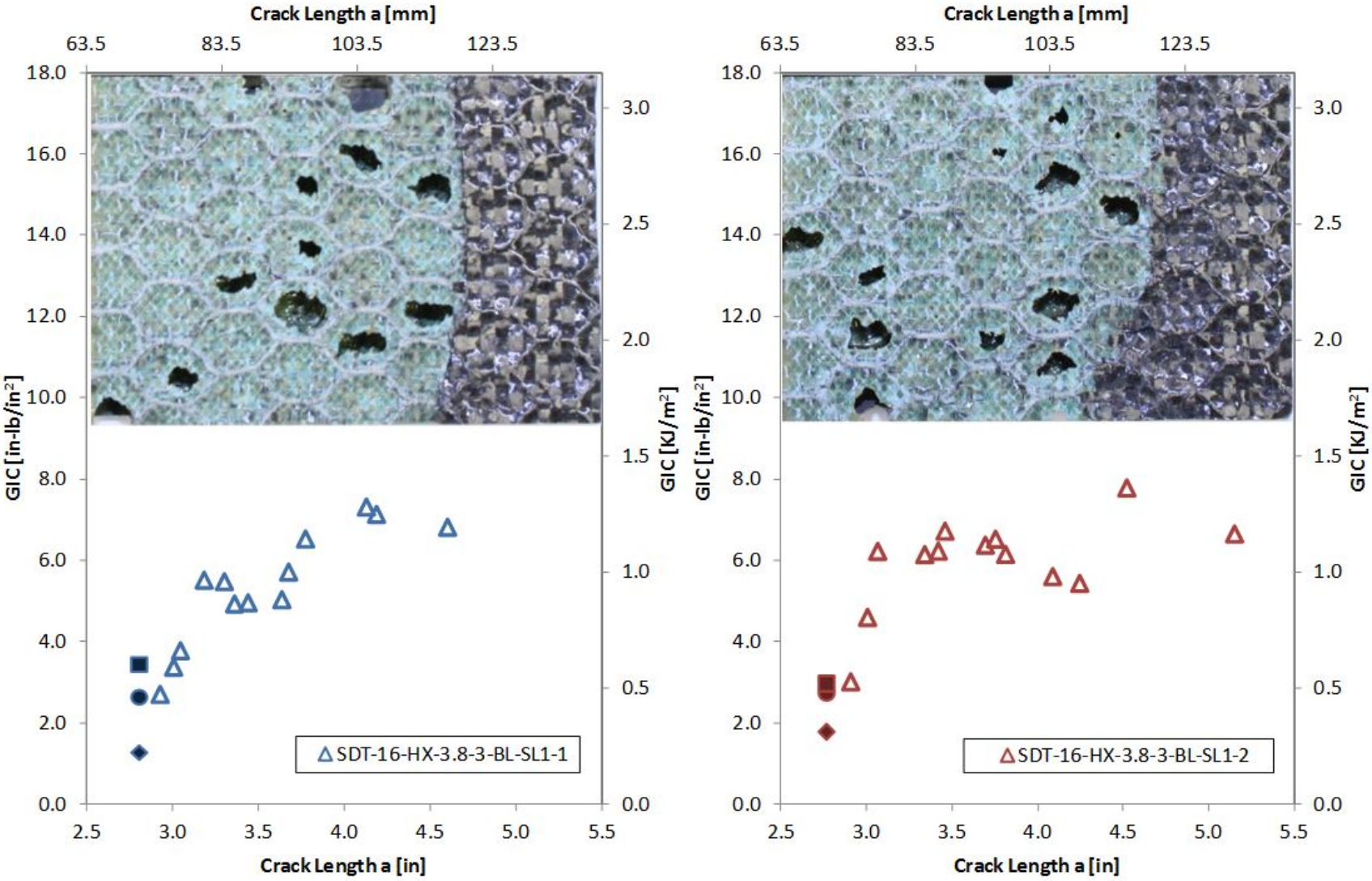

Figure C-87. Failure mode image and resistance curve for SDT-16-HX-3.8-3-BL-SL1-X #1 and #2

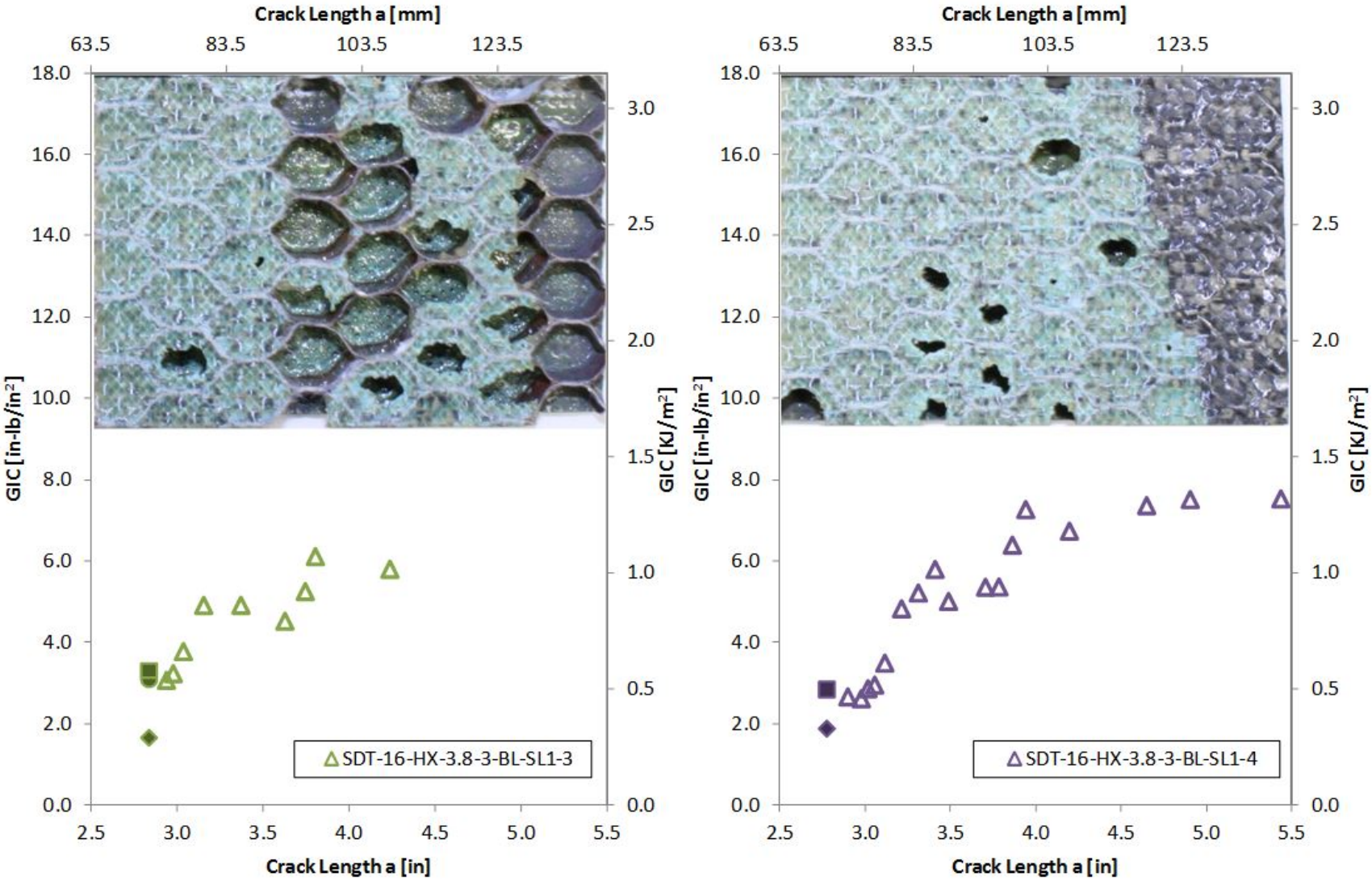

Figure C-88. Failure mode image and resistance curve for SDT-16-HX-3.8-3-BL-SL1-X #3 and #4

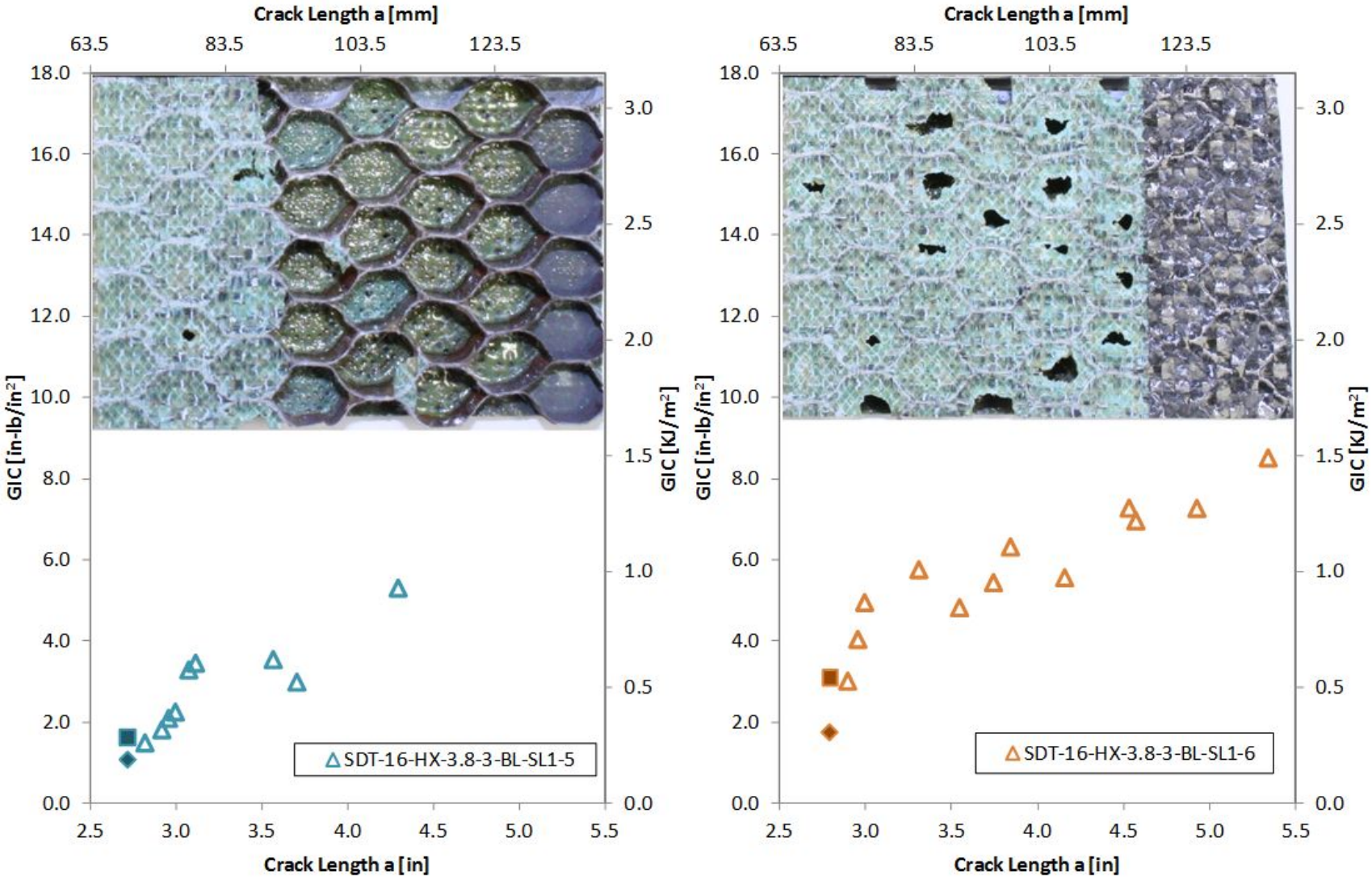

Figure C-89. Failure mode image and resistance curve for SDT-16-HX-3.8-3-BL-SL1-X #5 and #6

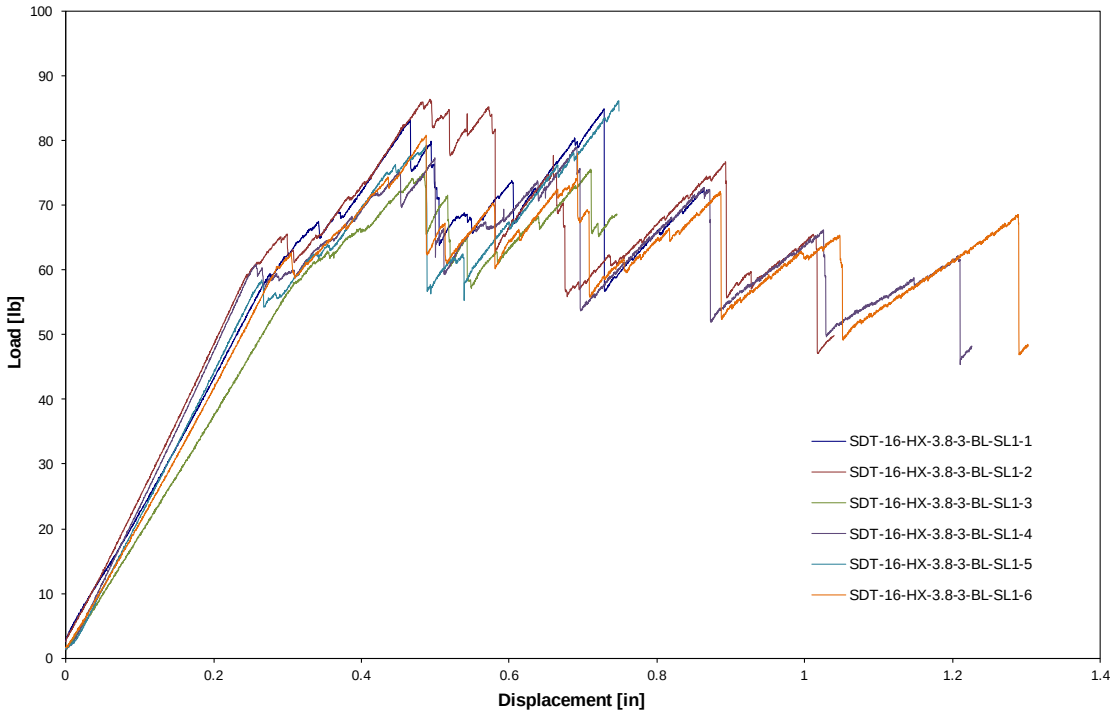

Figure C-90. Load vs. displacement curve for HRH-10–3/8–3.0 baseline (2.5″ prescribed crack)

C.5.2 HRH-10–3/8–3.0 FLUID-INGRESSED DATA

Table C-35. Test summary for HRH-10–3/8–3.0 fluid ingressed (2.5″ prescribed crack) precrack

Specimen	GIC (in-lb/in^2)			GIC (KJ/m^2)			Failure Mode
	NL	VIS	5%/max	NL	VIS	5%/max	
SDT-16-HX-3.8-3-FI-SL1-1	1.710	-	4.168	0.299	-	0.730	First row primarily in PO, then a mix of A and PO
SDT-16-HX-3.8-3-FI-SL1-2	1.666	-	2.985	0.292	-	0.523	Primarily in A with a couple of cells in PO
SDT-16-HX-3.8-3-FI-SL1-3	1.657	-	3.128	0.290	-	0.548	Primarily in A with several cells in PO
SDT-16-HX-3.8-3-FI-SL1-4	1.304	-	2.578	0.228	-	0.451	Primarily in A with several cells in PO
SDT-16-HX-3.8-3-FI-SL1-5	2.064	-	3.388	0.362	-	0.593	Primarily in A with a couple of cells in PO
SDT-16-HX-3.8-3-FI-SL1-6	2.125	-	2.697	0.372	-	0.472	Primarily in A
AVERAGE GIC	1.754	-	3.157	0.307	-	0.553	
STANDARD DEVIATION	0.302	-	0.575	0.053	-	0.101	
COEFFICIENT OF VARIATION (%)	17.215	-	18.217	17.215	-	18.217	

Table C-36. Test summary for HRH-10–3/8–3.0 fluid ingressed (2.5″ prescribed crack)

Specimen	GIC (in-lb/in^2)			GIC (KJ/m^2)			Failure Mode
	NL	VIS	5%/max	NL	VIS	5%/max	
SDT-16-HX-3.8-3-FI-SL1-1	2.257	-	5.543	0.395	-	0.971	Primarily in PO with several cells in A; last few rows in D
SDT-16-HX-3.8-3-FI-SL1-2	2.025	5.263	6.631	0.355	0.922	1.161	Mix of A and PO; last row in D
SDT-16-HX-3.8-3-FI-SL1-3	2.090	-	9.548	0.366	-	1.672	Mix of A and PO; last few rows in D
SDT-16-HX-3.8-3-FI-SL1-4	2.780	-	7.764	0.487	-	1.360	Mix of A and PO; last few rows in D
SDT-16-HX-3.8-3-FI-SL1-5	1.744	-	6.386	0.305	-	1.118	Initially primarily A, then primarily PO; last couple of rows in D
SDT-16-HX-3.8-3-FI-SL1-6	1.413	-	5.024	0.248	-	0.880	Initially primarily A, then primarily PO; last couple of rows in D
AVERAGE GIC	2.052	5.263	6.816	0.359	0.922	1.194	
STANDARD DEVIATION	0.464	-	1.638	0.081	-	0.287	
COEFFICIENT OF VARIATION (%)	22.626	-	24.032	22.626	-	24.032	

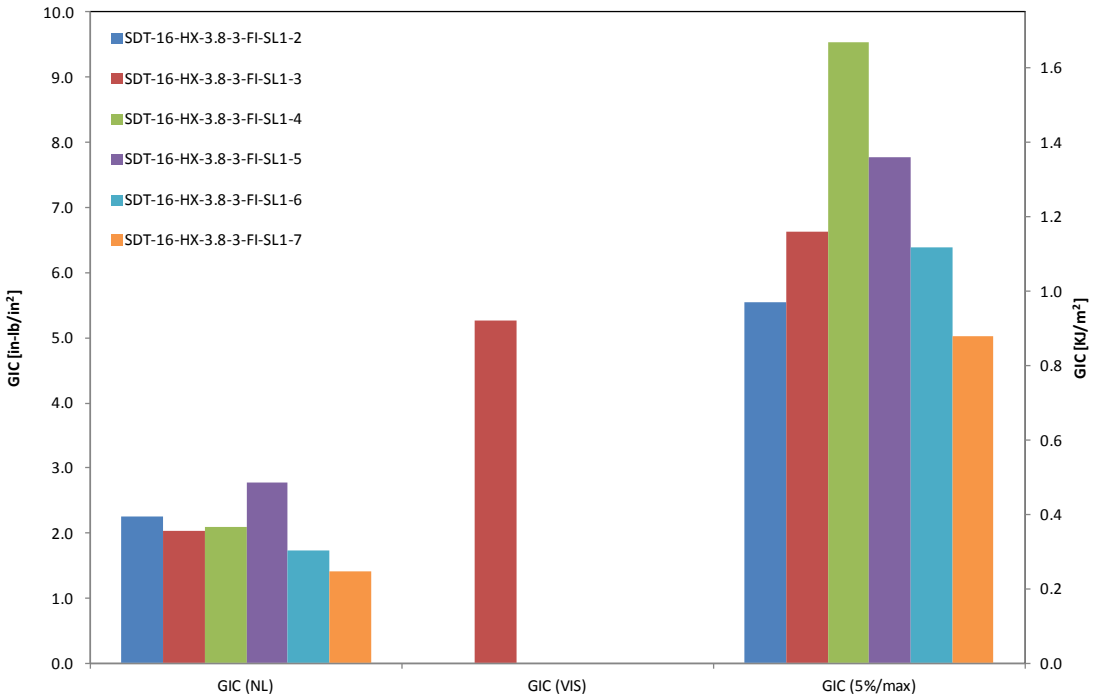

Figure C-91. GIC for HRH-10–3/8–3.0 fluid ingressed (2.5″ prescribed crack)

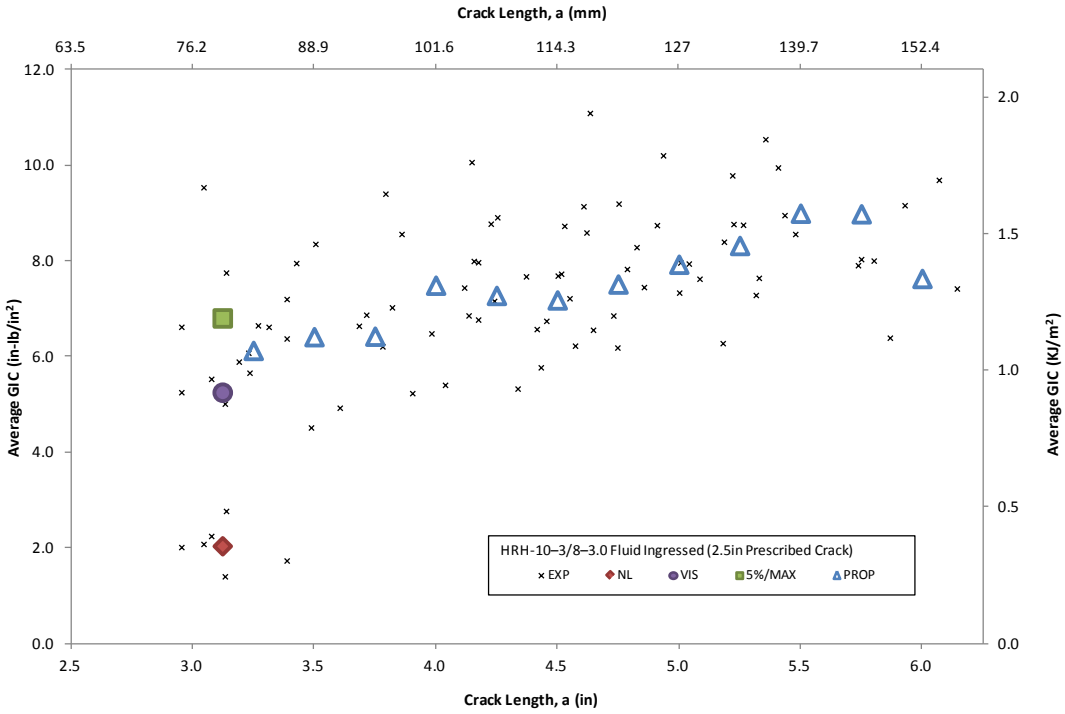

Figure C-92. Resistance curve for HRH-10–3/8–3.0 fluid ingressed (2.5″ prescribed crack)

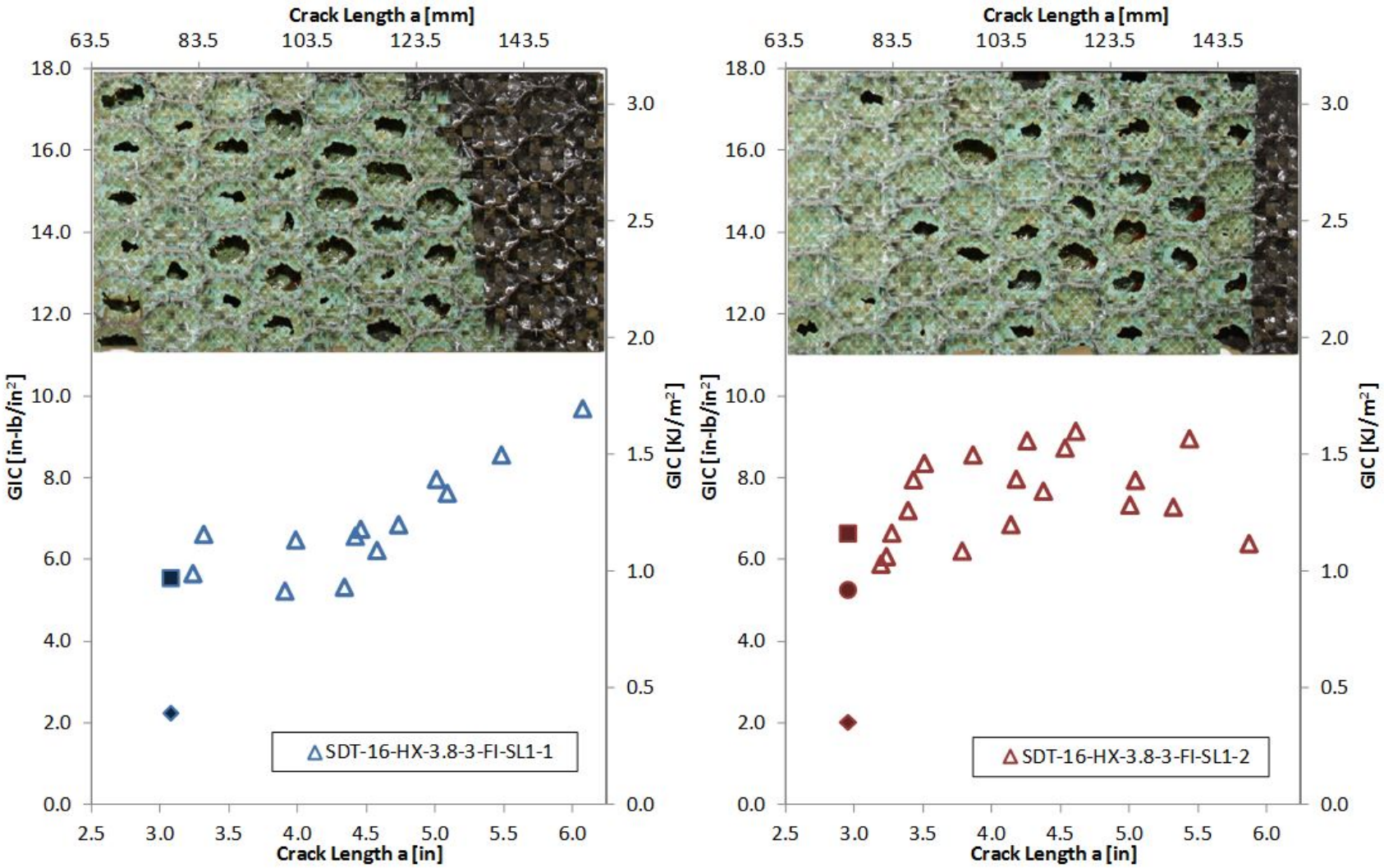

Figure C-93. Failure mode image and resistance curve for SDT-16-HX-3.8-3-FI-SL1-X #1 and #2

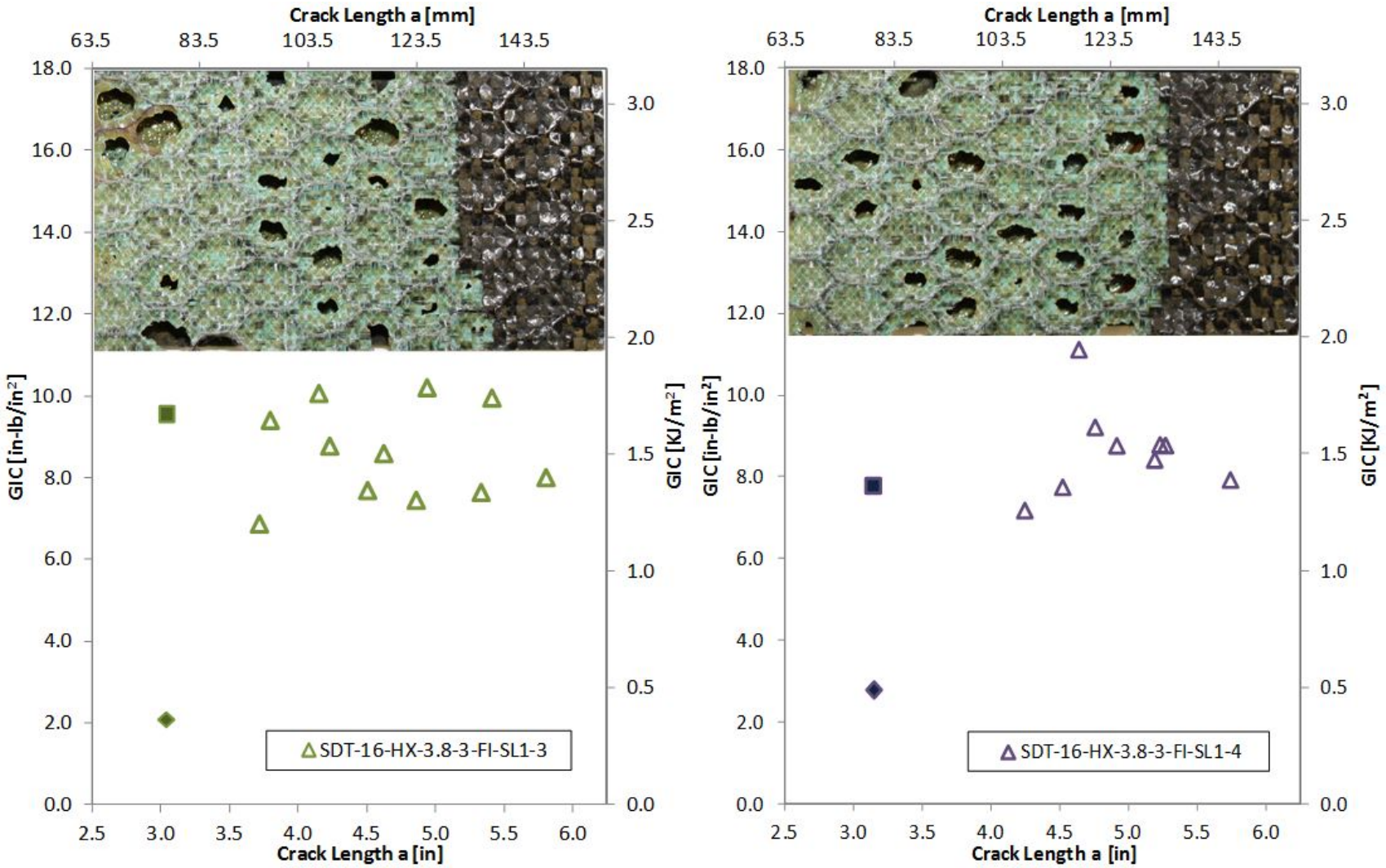

Figure C-94. Failure mode image and resistance curve for SDT-16-HX-3.8-3-FI-SL1-X #3 and #4

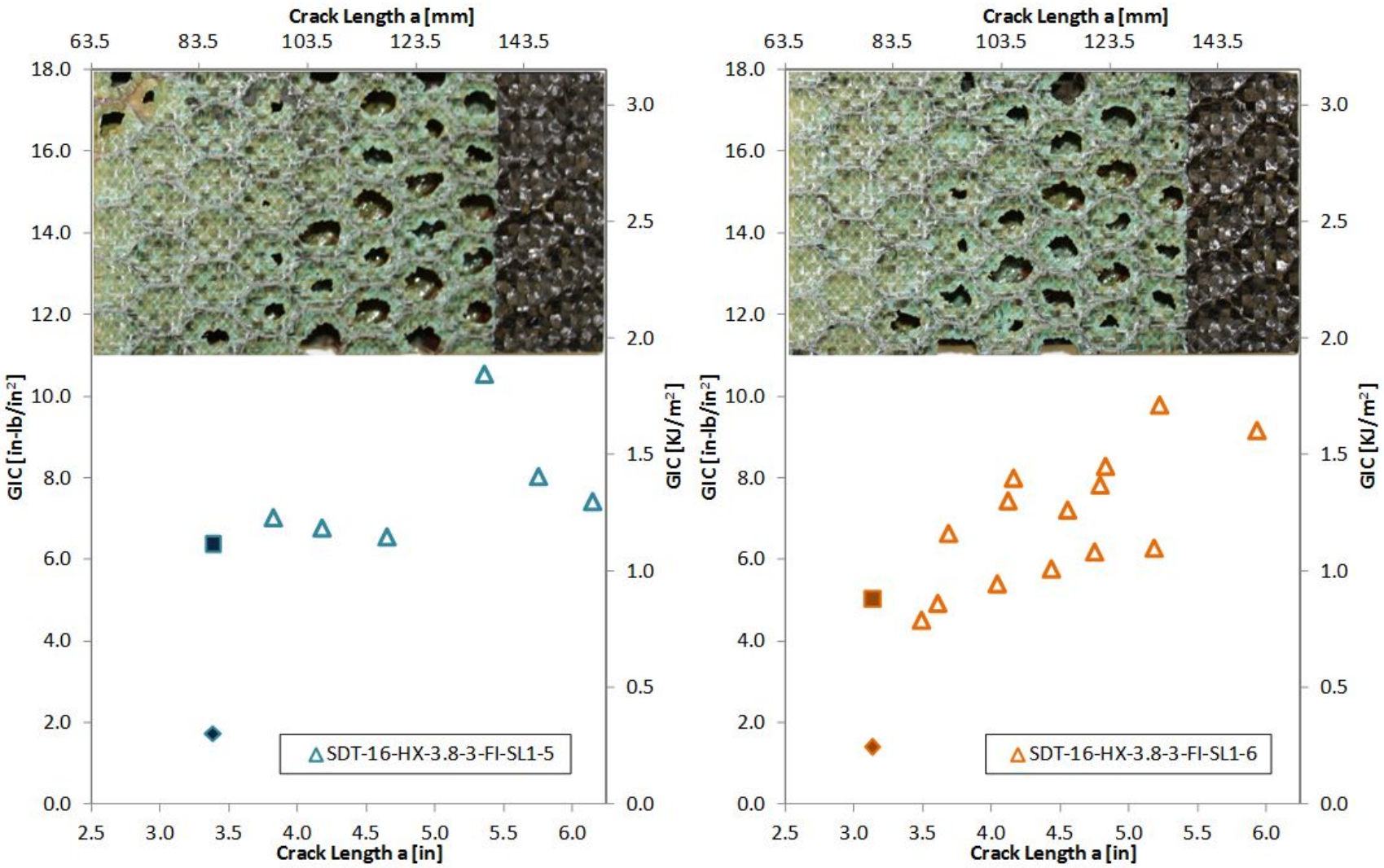

Figure C-95. Failure mode image and resistance curve for SDT-16-HX-3.8-3-FI-SL1-X #5 and #6

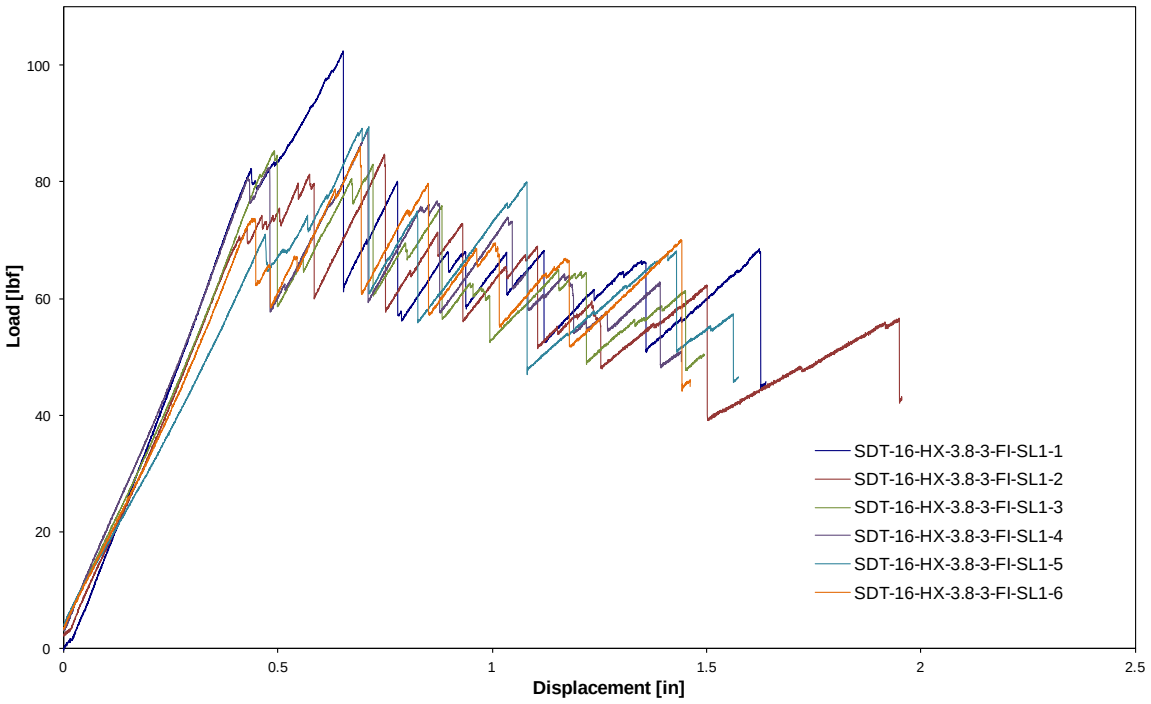

Figure C-96. Load vs. displacement curve for HRH-10–3/8–3.0 fluid ingressed (2.5″ prescribed crack)

C.5.3 HRH-10–3/8–3.0 EXTENDED FLUID-INGRESSED DATA.

Table C-37. Test summary for HRH-10–3/8–3.0 extended fluid ingressed (2.5″ prescribed crack) precrack

Specimen	GIC (in-lb/in^2)			GIC (KJ/m^2)			Failure Mode
	NL	VIS	5%/max	NL	VIS	5%/max	
SDT-16-HX-3.8-3-EFI-SL1-7	1.126	-	3.743	0.197	-	0.656	Primarily in A
SDT-16-HX-3.8-3-EFI-SL1-8	1.891	-	2.713	0.331	-	0.475	Primarily in A
AVERAGE GIC	1.509	-	3.228	0.264	-	0.565	
STANDARD DEVIATION	0.541	-	0.729	0.095	-	0.128	
COEFFICIENT OF VARIATION (%)	35.836	-	22.573	35.836	-	22.573	

Table C-38. Test summary for HRH-10–3/8–3.0 extended fluid ingressed (2.5″ prescribed crack)

Specimen	GIC (in-lb/in^2)			GIC (KJ/m^2)			Failure Mode
	NL	VIS	5%/max	NL	VIS	5%/max	
SDT-16-HX-3.8-3-EFI-SL1-7	2.193	-	5.591	0.384	-	0.979	Primarily in A, then a mix of A and PO, then C with a pocket of PO
SDT-16-HX-3.8-3-EFI-SL1-8	2.402	-	6.221	0.421	-	1.089	Primarily in A, then a mix of A and PO, then C
AVERAGE GIC	2.298	-	5.906	0.402	-	1.034	
STANDARD DEVIATION	0.148	-	0.445	0.026	-	0.078	
COEFFICIENT OF VARIATION (%)	6.426	-	7.538	6.426	-	7.538	

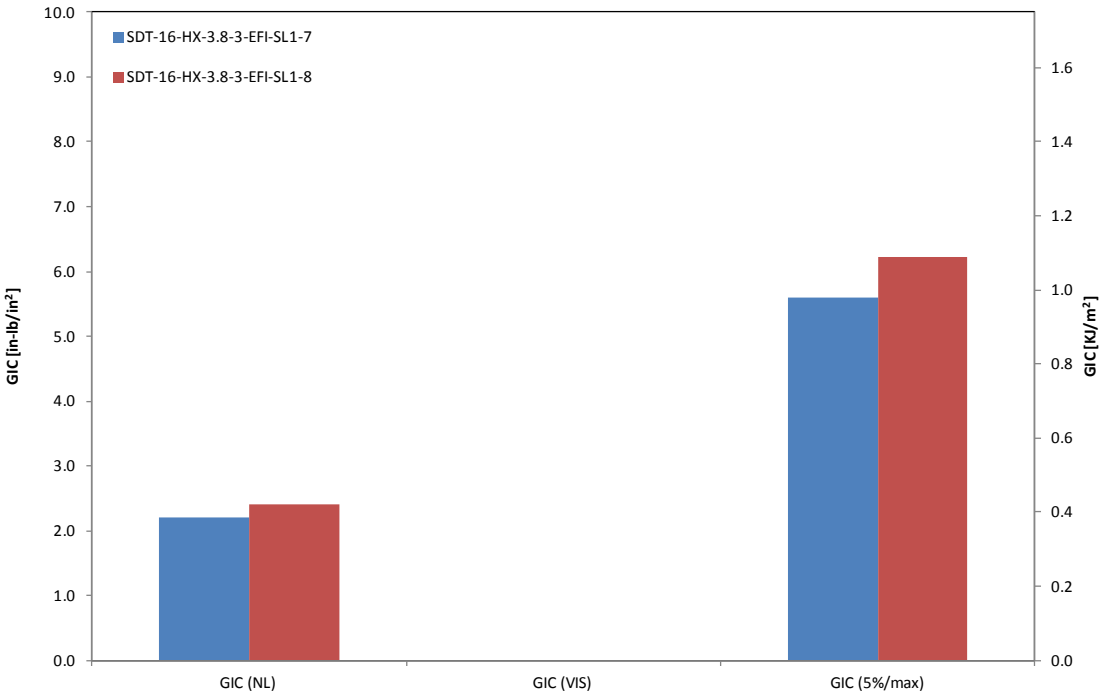

Figure C-97. GIC for HRH-10–3/8–3.0 extended fluid ingressed (2.5″ prescribed crack)

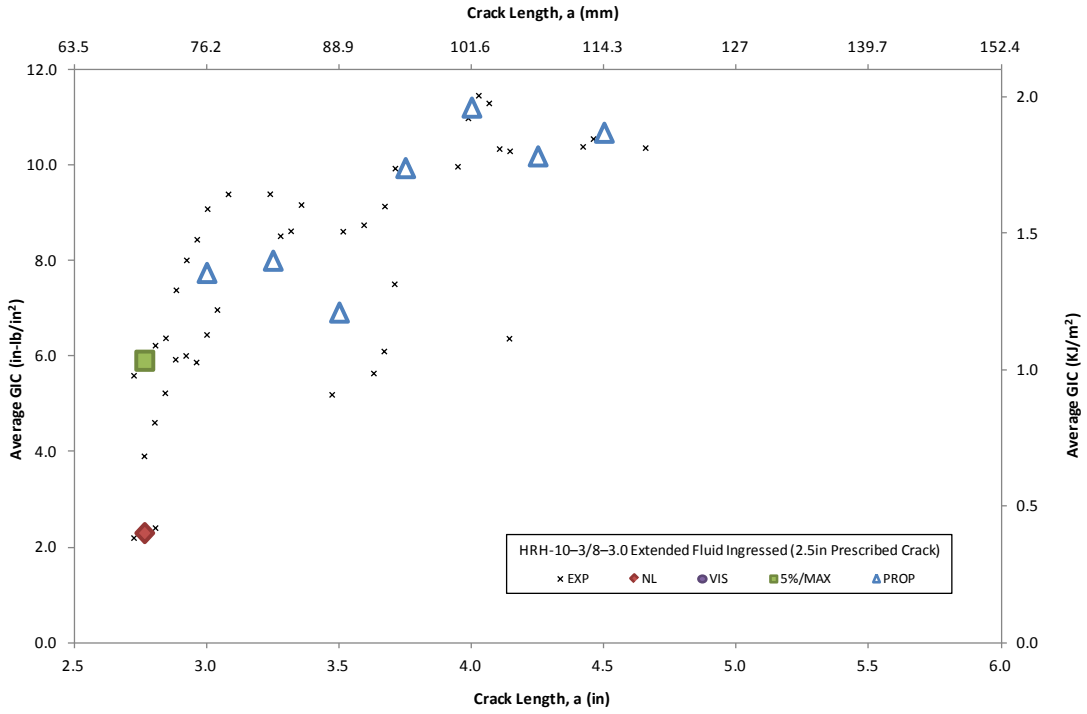

Figure C-98. Resistance curve for HRH-10–3/8–3.0 extended fluid ingressed (2.5″ prescribed crack)

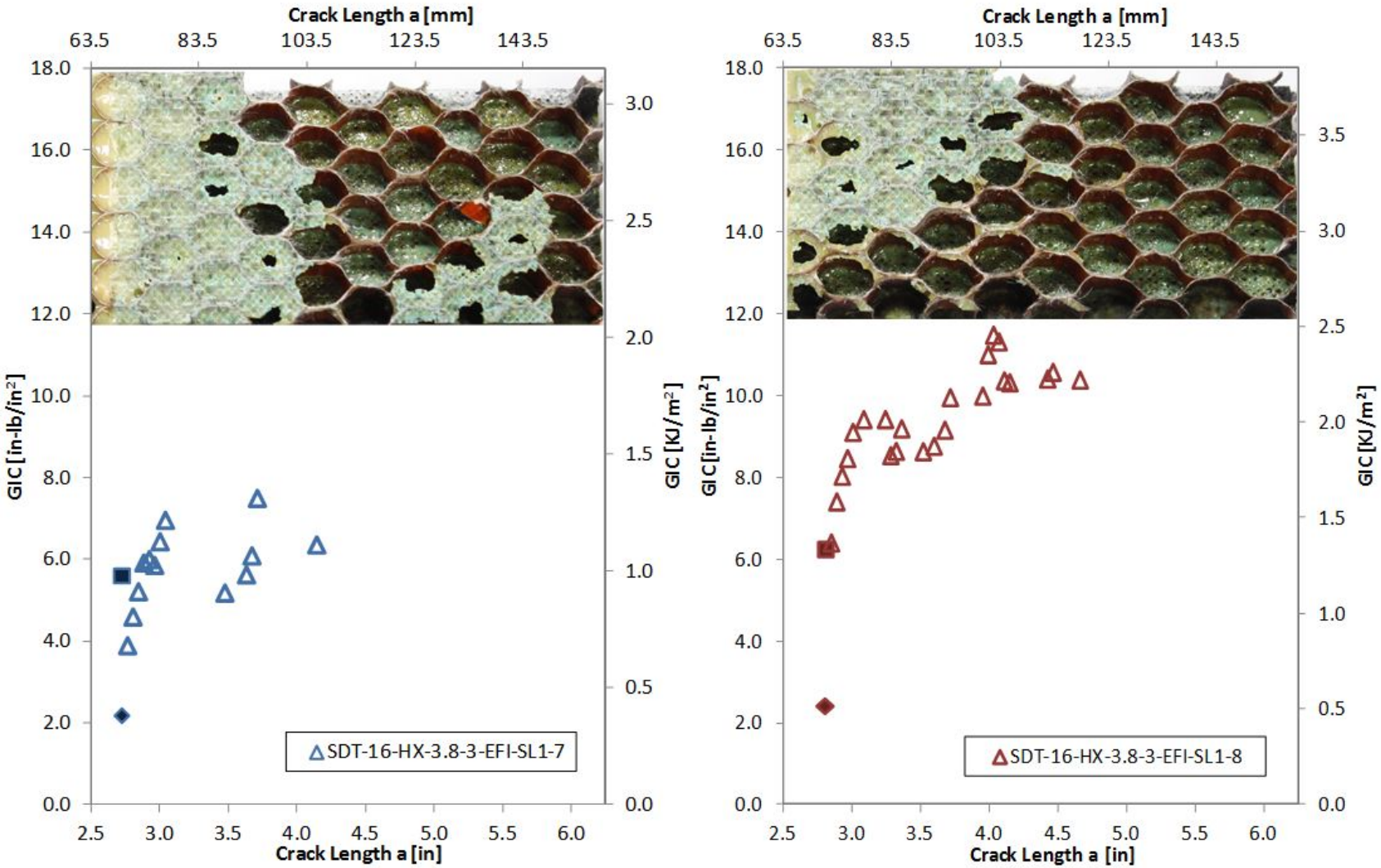

Figure C-99. Failure mode image and resistance curve for SDT-16-HX-3.8-3-EFI-SL1-X #7 and #8

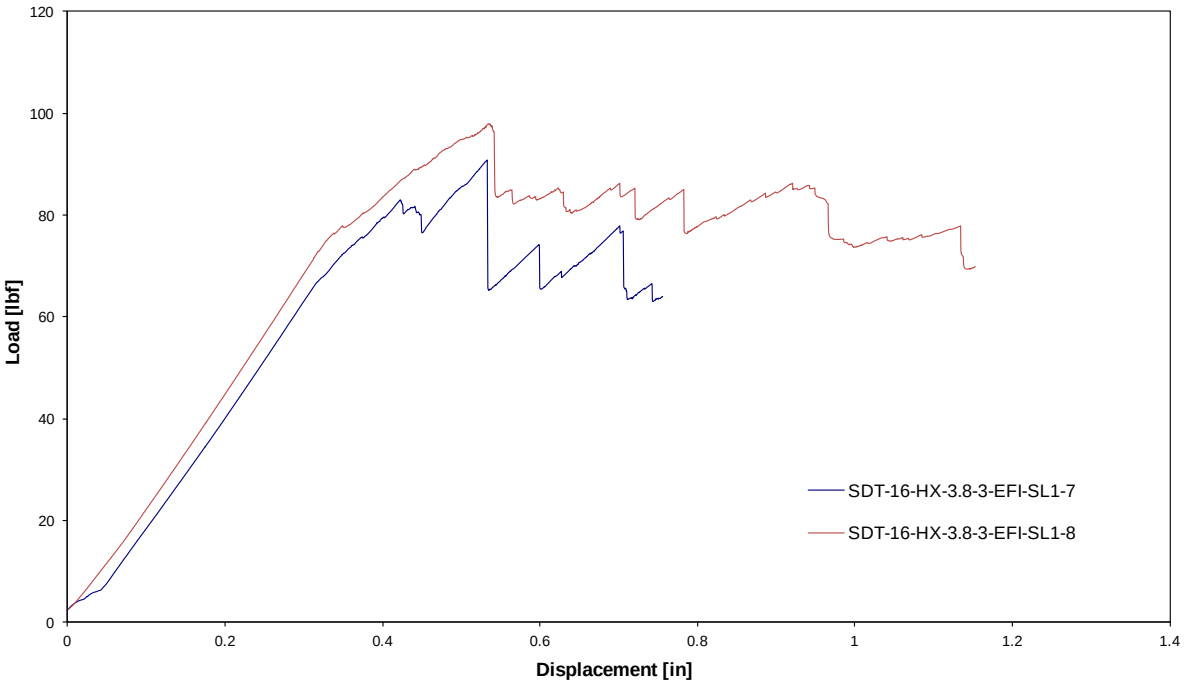

Figure C-100. Load vs. displacement curve for HRH-10–3/8–3.0 extended fluid ingressed (2.5″ prescribed crack)

C.5.4 HRH-10–3/8–3.0 WATER-INGRESSED DATA

Table C-39. Test summary for HRH-10–3/8–3.0 water ingressed (2.5″ prescribed crack) precrack

Specimen	GIC (in-lb/in^2)			GIC (KJ/m^2)			Failure Mode
	NL	VIS	5%/max	NL	VIS	5%/max	
SDT-16-HX-3.8-3-H2O-SL1-7	1.759	-	3.321	0.308	-	0.582	Primarily in C with a couple of cells in A
SDT-16-HX-3.8-3-H2O-SL1-8	1.705	-	N/A	0.299	-	N/A	Primarily in C with a couple of cells in A
SDT-16-HX-3.8-3-H2O-SLX-7	1.477	-	2.612	0.259	-	0.457	Primarily in C with a couple of cells in A
SDT-16-HX-3.8-3-H2O-SLX-8	1.692	-	2.164	0.296	-	0.379	Primarily in C with a couple of cells in A
AVERAGE GIC	1.658	-	2.699	0.290	-	0.473	
STANDARD DEVIATION	0.124	-	.583	0.022	-	0.102	
COEFFICIENT OF VARIATION (%)	7.480	-	21.615	7.480	-	21.615	

Table C-40. Test summary for HRH-10–3/8–3.0 water ingressed (2.5″ prescribed crack)

Specimen	GIC (in-lb/in^2)			GIC (KJ/m^2)			Failure Mode
	NL	VIS	5%/max	NL	VIS	5%/max	
SDT-16-HX-3.8-3-H2O-SL1-7	1.738	-	8.085	0.304	-	1.416	Mix of PO and C, then C
SDT-16-HX-3.8-3-H2O-SL1-8	1.613	-	6.715	0.282	-	1.176	Mix of PO and C, then C
SDT-16-HX-3.8-3-H2O-SLX-7	2.351	-	6.435	0.412	-	1.127	Mix of PO and C, then C
SDT-16-HX-3.8-3-H2O-SLX-8	3.009	-	4.227	0.527	-	0.740	Mix of PO and C, then C
AVERAGE GIC	2.178	-	6.366	0.381	-	1.115	
STANDARD DEVIATION	0.641	-	1.597	0.112	-	0.280	
COEFFICIENT OF VARIATION (%)	29.439	-	25.094	29.439	-	25.094	

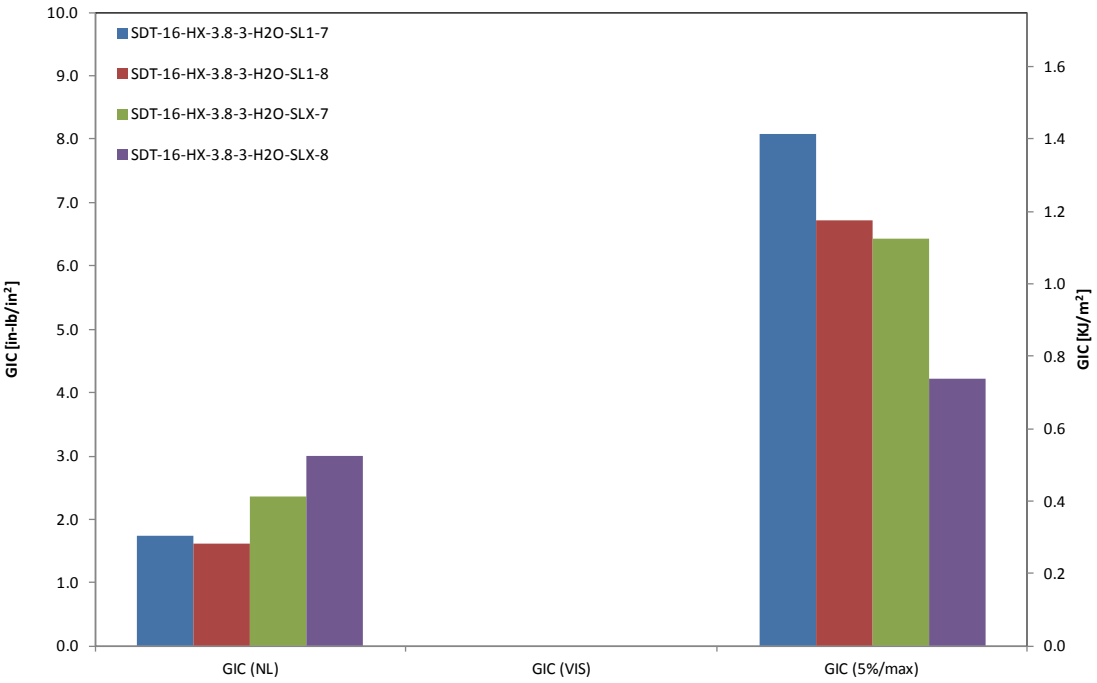

Figure C-101. GIC for HRH-10–3/8–3.0 water ingressed (2.5″ prescribed crack)

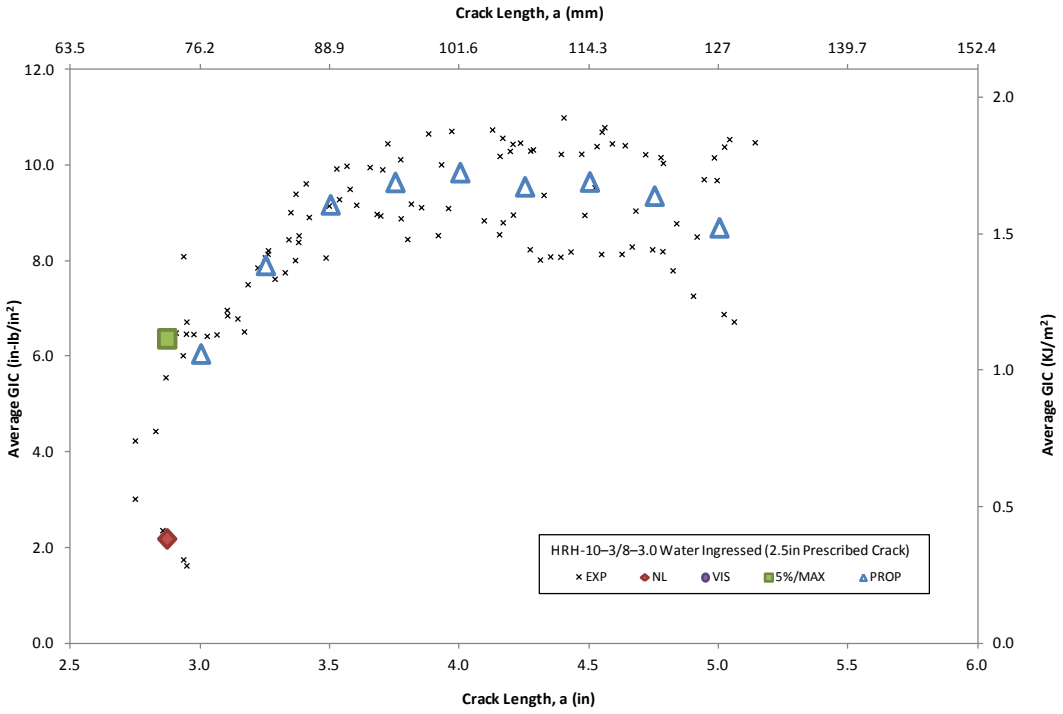

Figure C-102. Resistance curve for HRH-10–3/8–3.0 water ingressed (2.5″ prescribed crack)

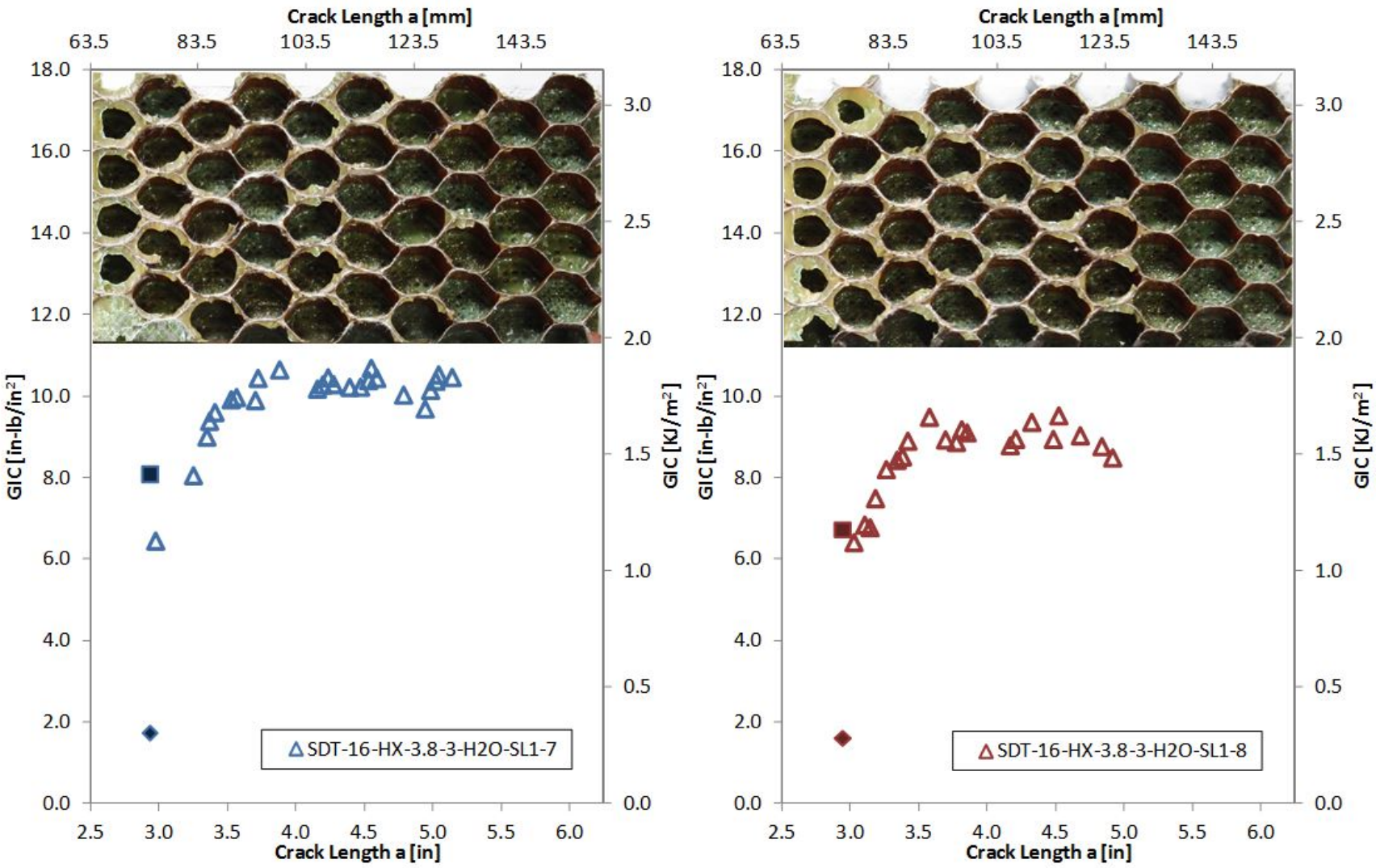

Figure C-103. Failure mode image and resistance curve for SDT-16-HX-3.8-3-H2O-SL1-X #7 and #8

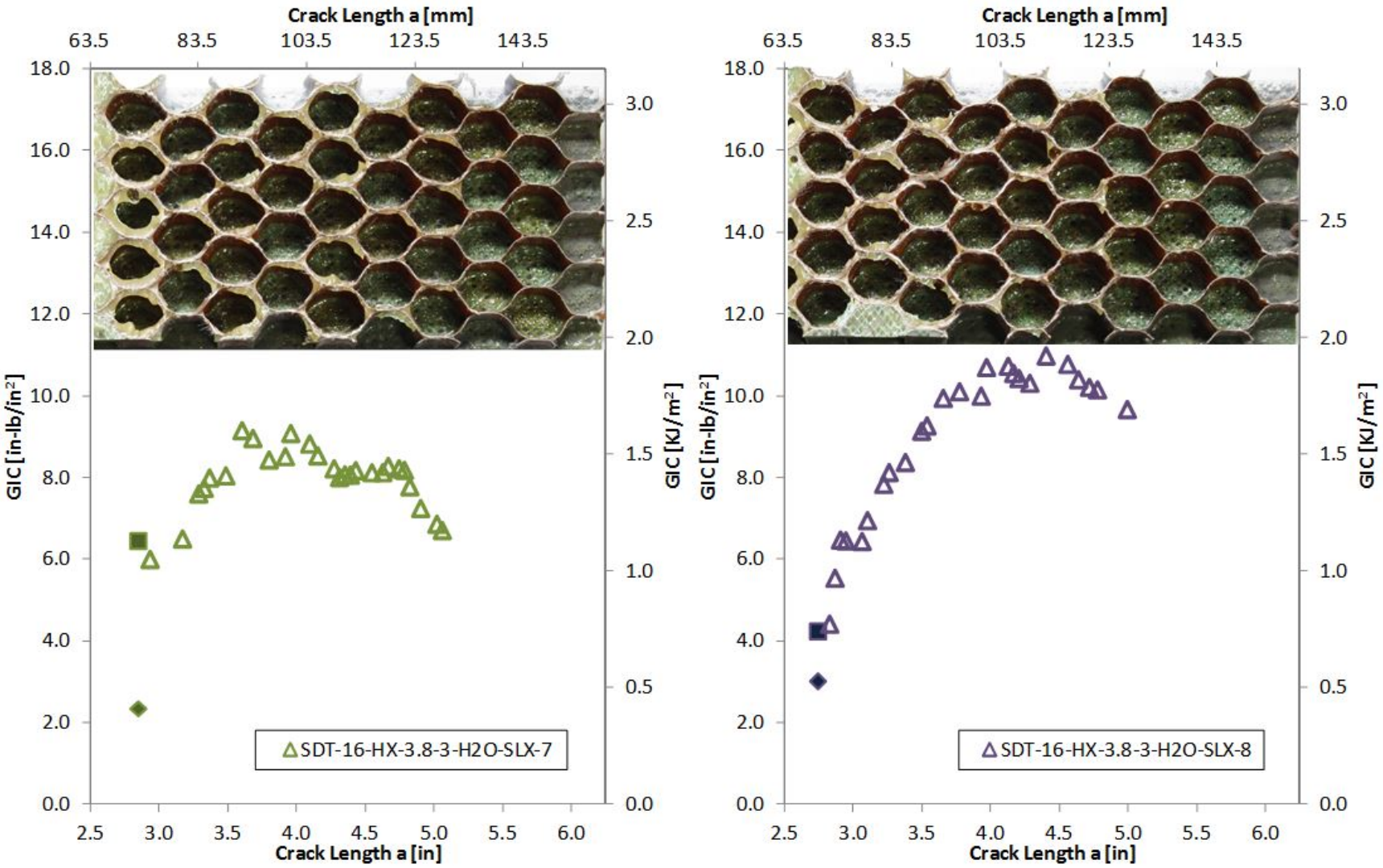

Figure C-104. Failure mode image and resistance curve for SDT-16-HX-3.8-3-H2O-SLX-X #7 and #8

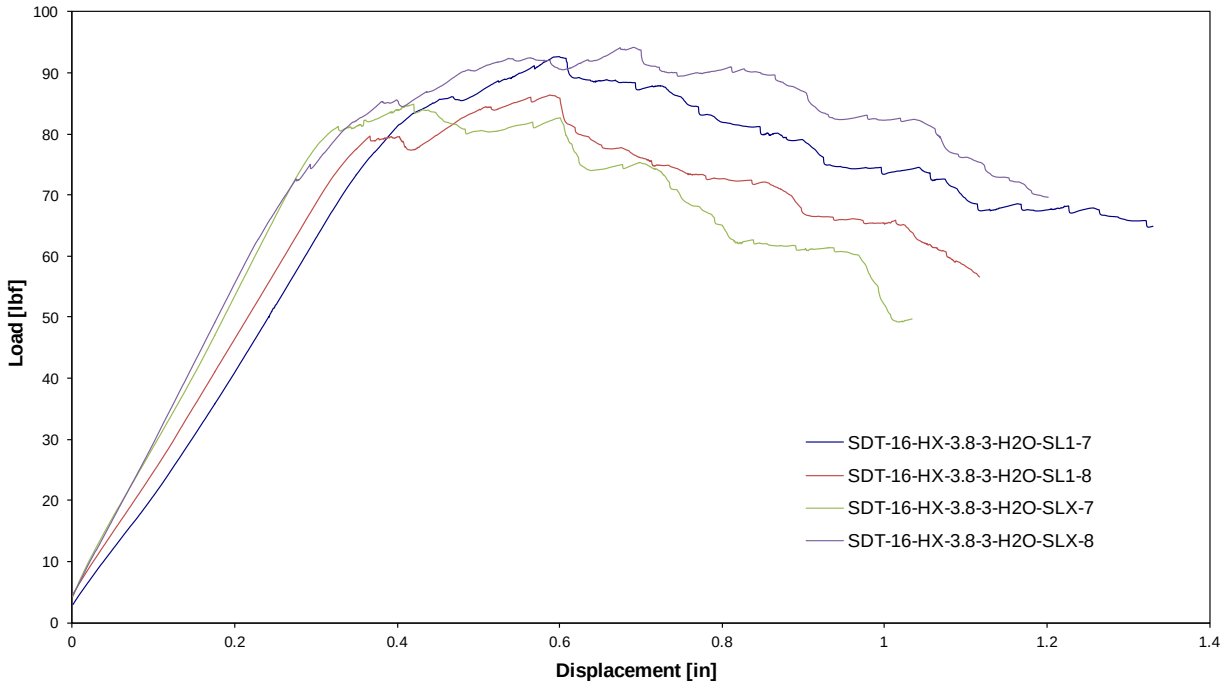

Figure C-105. Load vs. displacement curve for HRH-10–3/8–3.0 water ingressed (2.5″ prescribed crack)

APPENDIX D—STATIC RESULTS FOR THIN FACESHEET (4 PLY) AND HRH-10 OVER-EXPENDED CORES TESTED AS SINGLE-CANTILEVER BEAMS

Note that 4-ply material systems were tested with two prescribed crack lengths. Six baseline specimens were tested with 2.5″ prescribed cracks, and three baseline specimens were tested with 1″ prescribed cracks, referred to as “shortened.” The fluid-ingressed and extended fluid-ingressed specimens were all tested with a 1″ prescribed crack, still referred to as “shortened.”

D.1 HRH-10/OX–3/16–3.0 DATA

D.1.1 HRH-10/OX–3/16–3.0 BASELINE DATA

D.1.1.1 HRH-10/OX–3/16–3.0 Baseline Data (2.5″ Prescribed Crack)

Table D-1. Test summary for HRH-10/OX–3/16–3.0 baseline (2.5″ prescribed crack) precrack

Specimen	GIC (in-lb/in^2)			GIC (KJ/m^2)			Failure Mode
	NL	VIS	5%/max	NL	VIS	5%/max	
SDT-04-OX-3.16-3-BL-SL1-1	0.953	-	3.358	0.167	-	0.588	Primarily in A with a couple of cells in PO and several cells in C
SDT-04-OX-3.16-3-BL-SL1-2	1.058	-	3.546	0.185	-	0.621	First row a mix of A and PO; second row a mix of A, PO, and C
SDT-04-OX-3.16-3-BL-SL1-3	1.144	-	3.632	0.200	-	0.636	Primarily in C with multiple cells in A and one cell in PO
SDT-04-OX-3.16-3-BL-SL1-4	1.125	-	3.602	0.197	-	0.631	Primarily in A with a couple of cells in PO and several cells in C
SDT-04-OX-3.16-3-BL-SL1-5	1.116	-	3.787	0.195	-	0.663	Mix of A and C with a cell in PO
SDT-04-OX-3.16-3-BL-SL1-6	1.183	-	2.775	0.207	-	0.486	First row primarily A with a couple of cells in PO; second row a mix of A, PO, and C
AVERAGE GIC	1.096	-	3.450	0.192	-	0.604	
STANDARD DEVIATION	0.081	-	0.358	0.014	-	0.063	
COEFFICIENT OF VARIATION (%)	7.400	-	10.390	7.400	-	10.390	

Table D-2. Test summary for HRH-10/OX–3/16–3.0 baseline (2.5″ prescribed crack)

Specimen	GIC (in-lb/in^2)			GIC (KJ/m^2)			Failure Mode
	NL	VIS	5%/max	NL	VIS	5%/max	
SDT-04-OX-3.16-3-BL-SL1-1	0.635	2.141	2.301	0.111	0.375	0.403	Primarily C with a large pocket of A and PO and a few cells in A and PO
SDT-04-OX-3.16-3-BL-SL1-2	0.538	-	2.154	0.094	-	0.377	Primarily C with multiple cells in A and PO
SDT-04-OX-3.16-3-BL-SL1-3	0.412	1.282	1.421	0.072	0.224	0.249	Primarily C with a few small pockets in A and PO
SDT-04-OX-3.16-3-BL-SL1-4	0.524	-	2.008	0.092	-	0.352	Primarily C with several cells in A and PO
SDT-04-OX-3.16-3-BL-SL1-5	0.599	-	2.529	0.105	-	0.443	Primarily C with an occasional cell in PO
SDT-04-OX-3.16-3-BL-SL1-6	0.790	-	2.757	0.138	-	0.483	Primarily C with one pocket in A and PO, and a few cells in A and PO
AVERAGE GIC	0.583	1.712	2.195	0.102	0.300	0.384	
STANDARD DEVIATION	0.127	0.608	0.464	0.022	0.106	0.081	
COEFFICIENT OF VARIATION (%)	21.783	35.525	21.117	21.783	35.525	21.117	

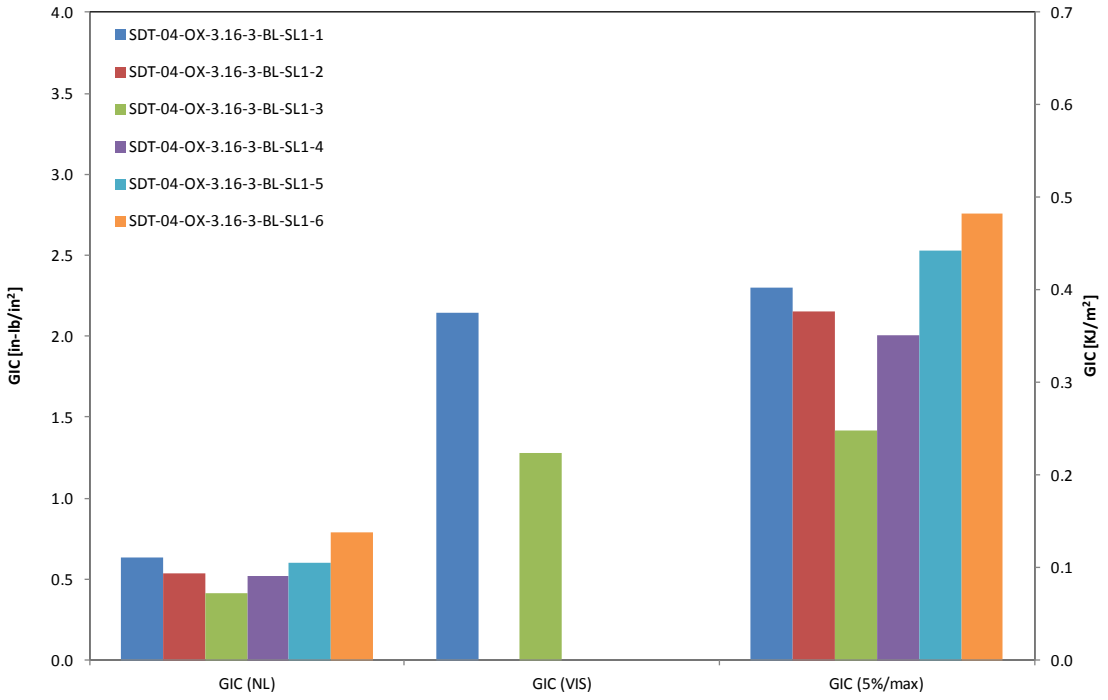

Figure D-1. GIC for HRH-10/OX–3/16–3.0 baseline (2.5″ prescribed crack)

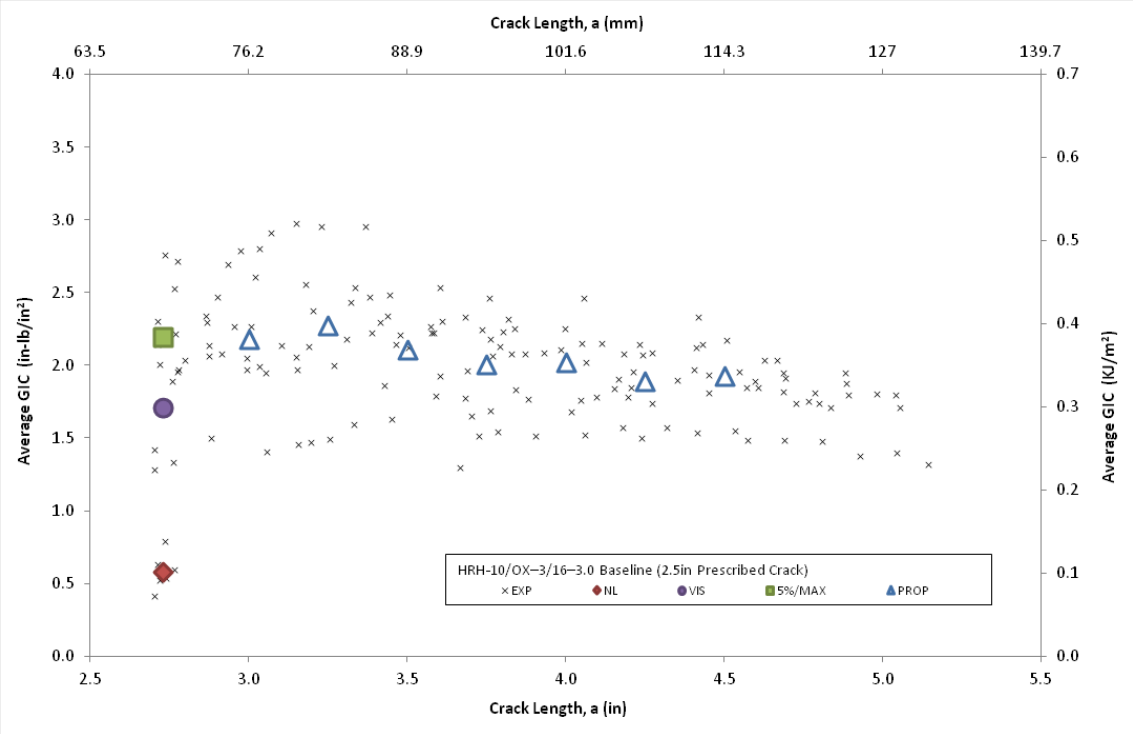

Figure D-2. Resistance curve for HRH-10/OX–3/16–3.0 baseline (2.5″ prescribed crack)

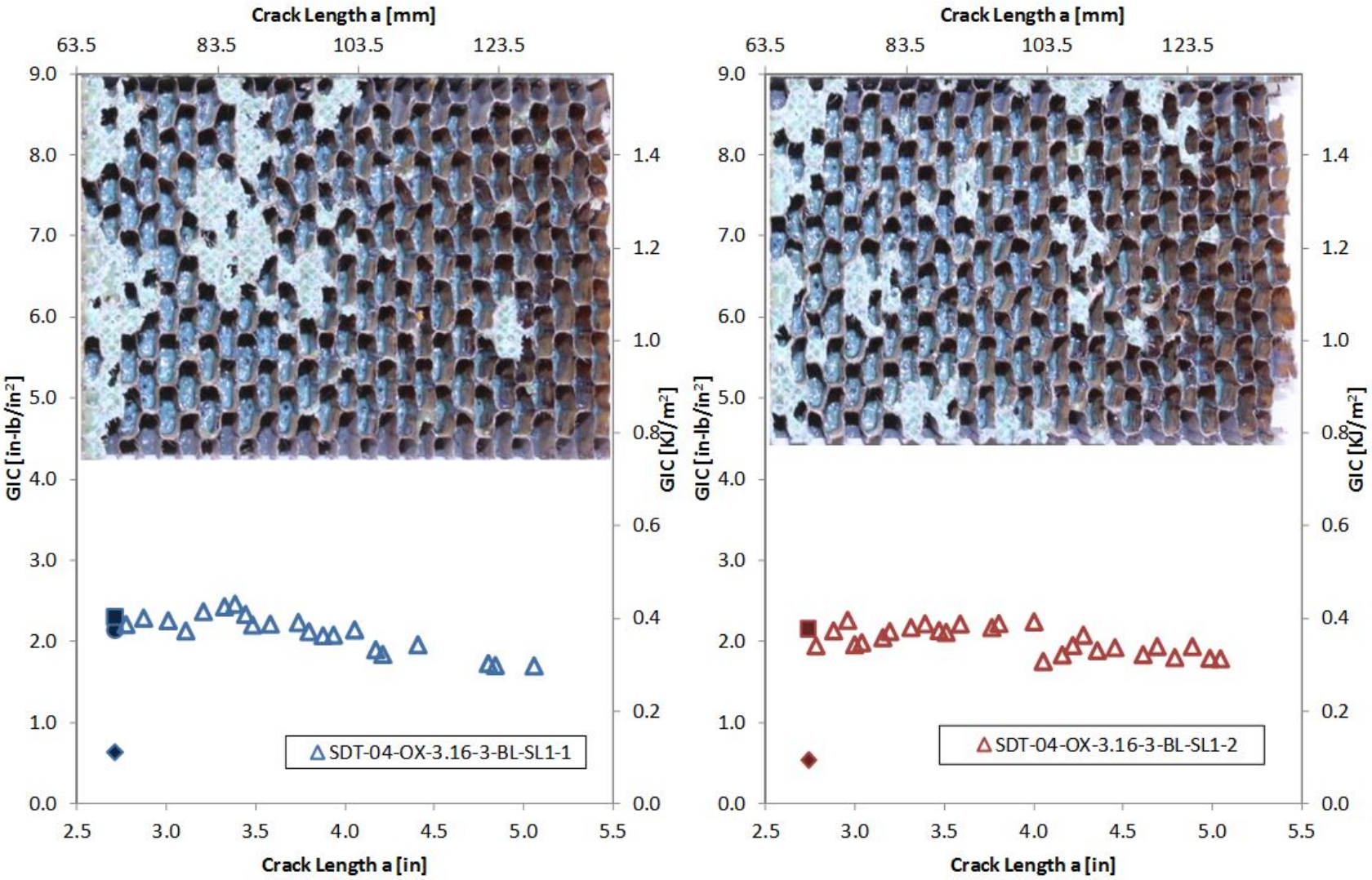

Figure D-3. Failure mode image and resistance curve of SDT-04-OX-13.16-3-BL-SL1-X #1 and #2

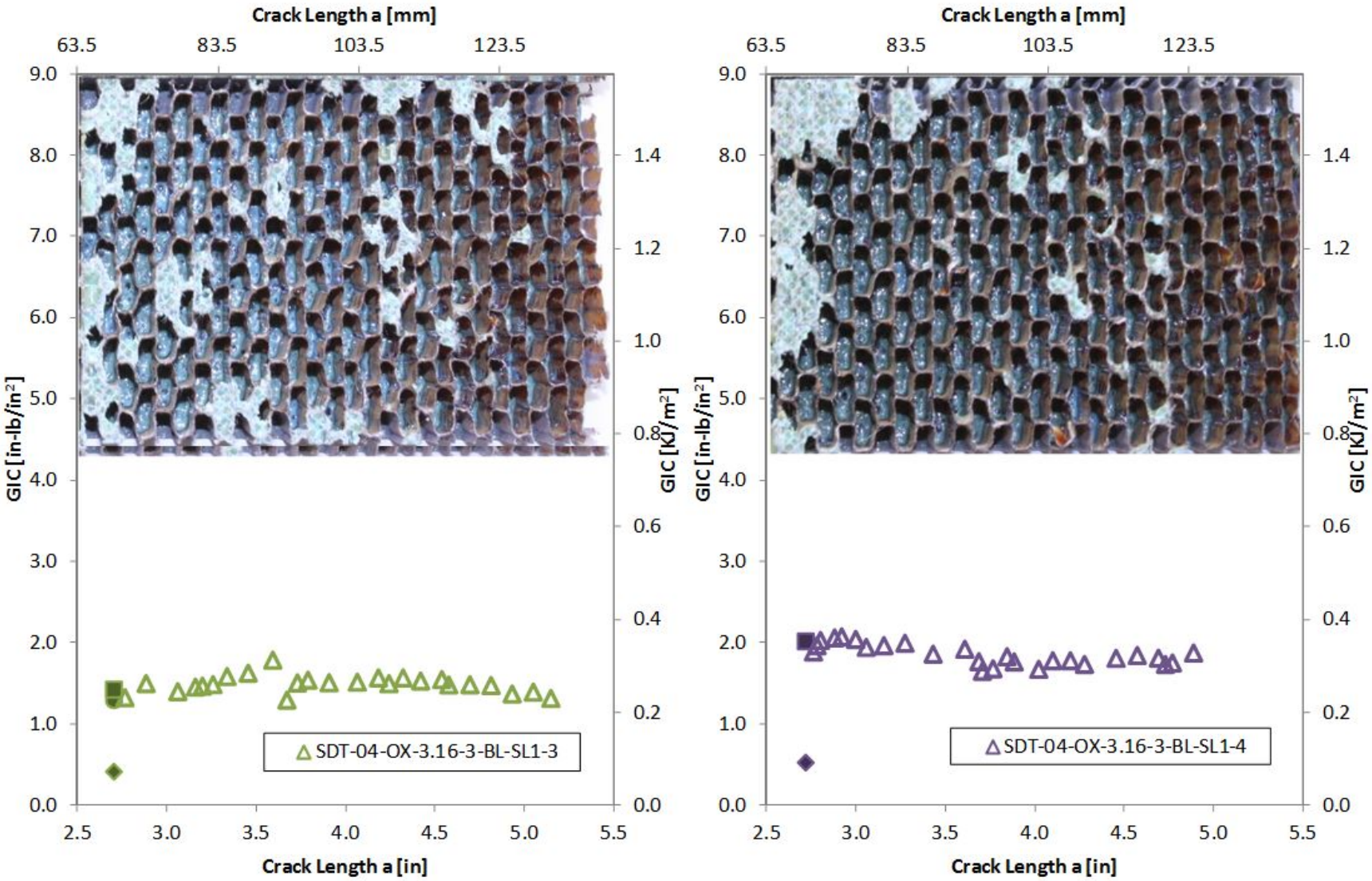

Figure D-4. Failure mode image and resistance curve of SDT-04-OX-13.16-3-BL-SL1-X #3 and #4

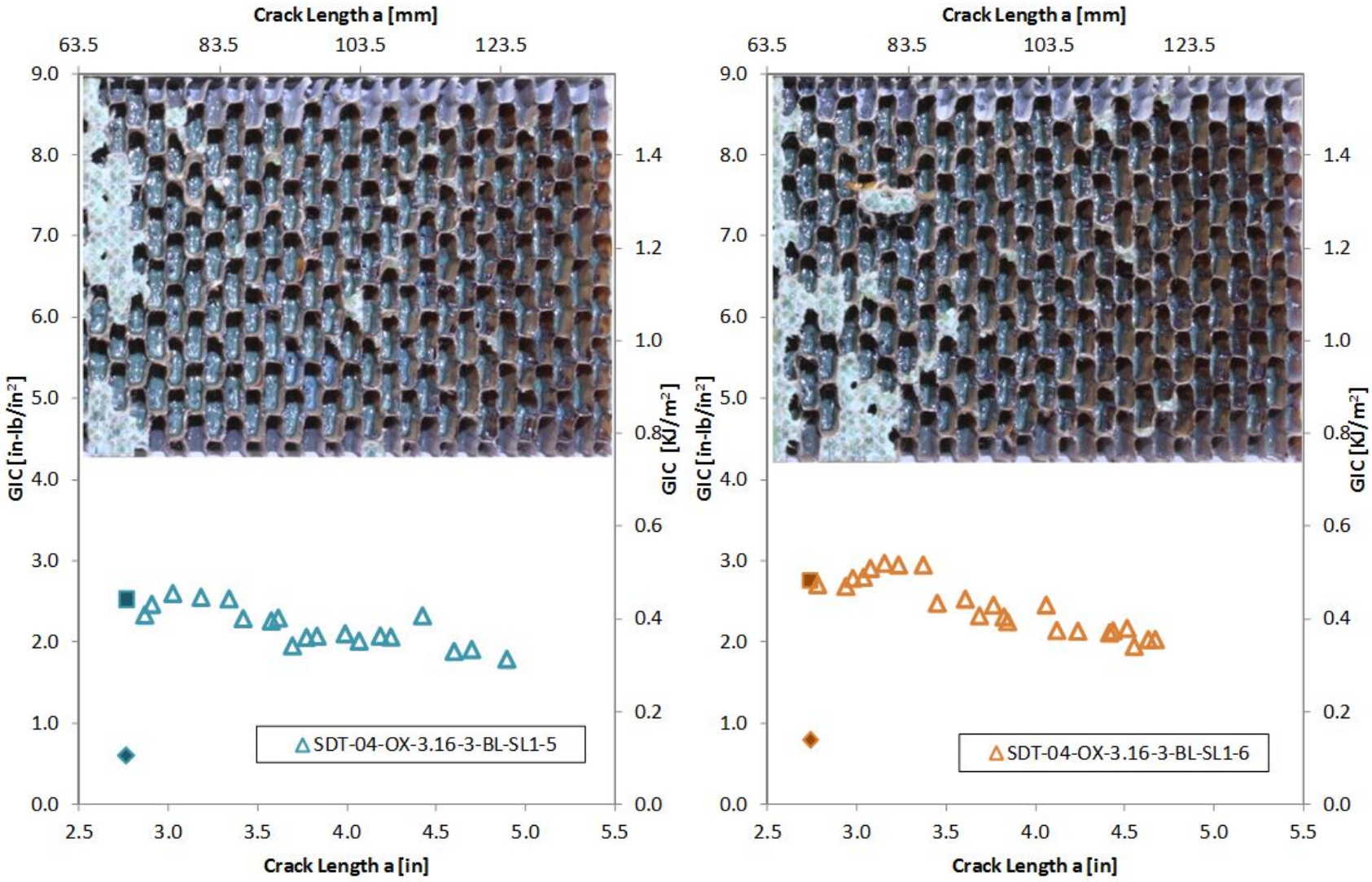

Figure D-5. Failure mode image and resistance curve of SDT-04-OX-13.16-3-BL-SL1-X #5 and #6

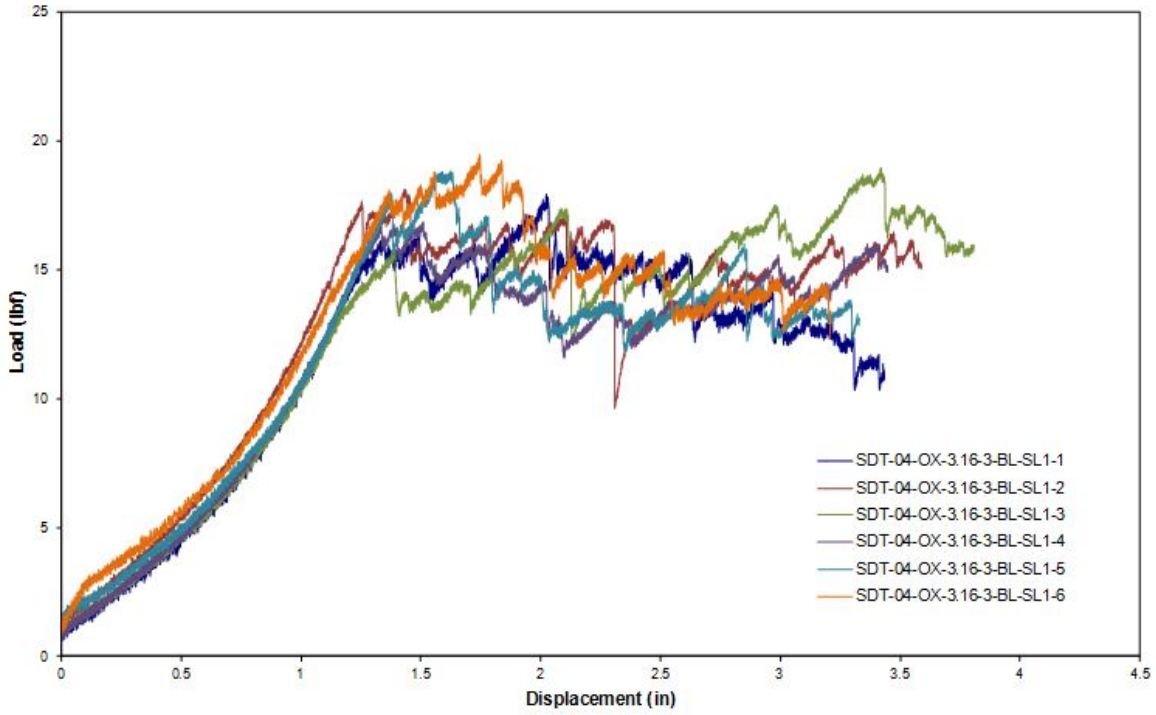

Figure D-6. Load vs. displacement curve for HRH-10/OX–3/16–3.0 baseline (2.5″ prescribed crack)

D.1.1.2 HRH-10/OX–3/16–3.0 Baseline Data (1.0-Inch Prescribed Crack—Shortened)

Table D-3. Test summary for HRH-10/OX–3/16–3.0 baseline (1″ prescribed crack—shortened) precrack

Specimen	GIC (in-lb/in^2)			GIC (KJ/m^2)			Failure Mode
	NL	VIS	5%/max	NL	VIS	5%/max	
SDT-04-OX-3.16-3-BL-SL1-7 (shortened)	3.597	-	5.866	0.630	-	1.027	Mix of A and PO
SDT-04-OX-3.16-3-BL-SL1-8 (shortened)	2.696	-	3.588	0.472	-	0.628	Mix of PO and C
SDT-04-OX-3.16-3-BL-SLX-7 (shortened)	3.161	-	3.336	0.554	-	0.584	Mix of A and C
AVERAGE GIC	3.151	-	4.263	0.552	-	0.747	
STANDARD DEVIATION	0.009	-	0.031	0.079	-	0.244	
COEFFICIENT OF VARIATION (%)	14.302	-	32.690	14.302	-	32.690	

Table D-4. Test Summary for HRH-10/OX–3/16–3.0 baseline (1″ prescribed crack—shortened)

Specimen	GIC (in-lb/in^2)			GIC (KJ/m^2)			Failure Mode
	NL	VIS	5%/max	NL	VIS	5%/max	
SDT-04-OX-3.16-3-BL-SL1-7 (shortened)	1.142	-	3.177	0.200	-	0.556	Primarily C after quick transition from mix of A and PO with a couple of cells in PO
SDT-04-OX-3.16-3-BL-SL1-8 (shortened)	1.086	-	2.933	0.190	-	0.514	Primarily C with a couple pockets of A
SDT-04-OX-3.16-3-BL-SLX-7 (shortened)	1.037	-	3.284	0.182	-	0.575	Primarily C with a couple pockets of A
AVERAGE GIC	1.088	-	3.131	0.191	-	0.548	
STANDARD DEVIATION	0.009	-	0.031	0.009	-	0.031	
COEFFICIENT OF VARIATION (%)	4.837	-	5.741	4.837	-	5.741	

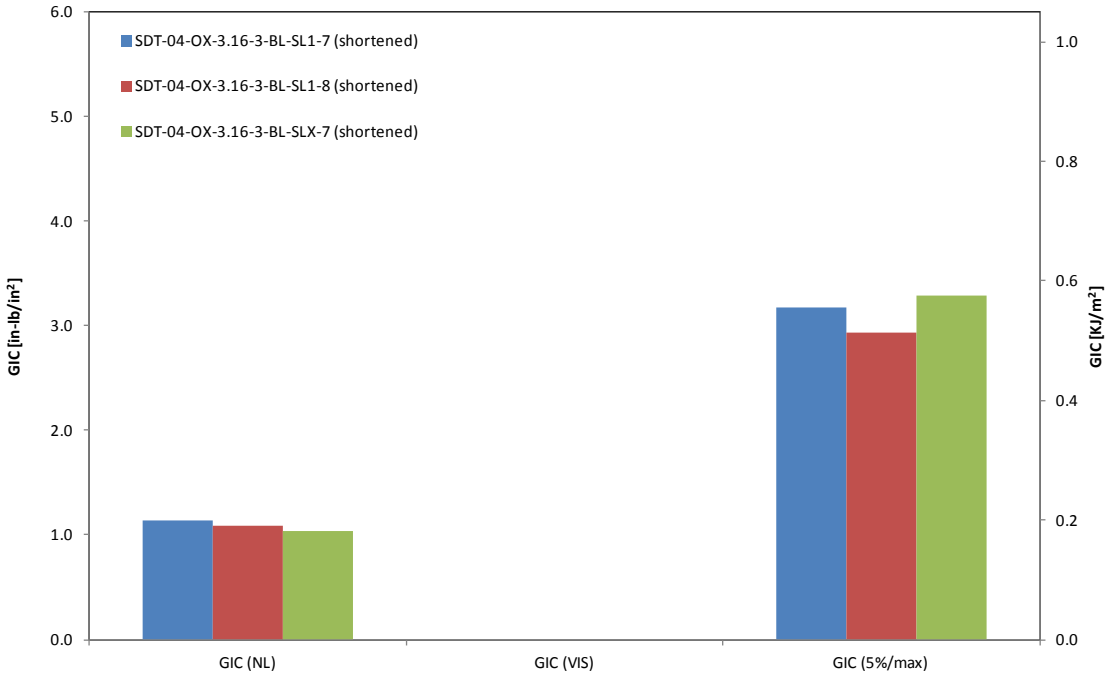

Figure D-7. GIC for HRH-10/OX–3/16–3.0 baseline (1″ prescribed crack—shortened)

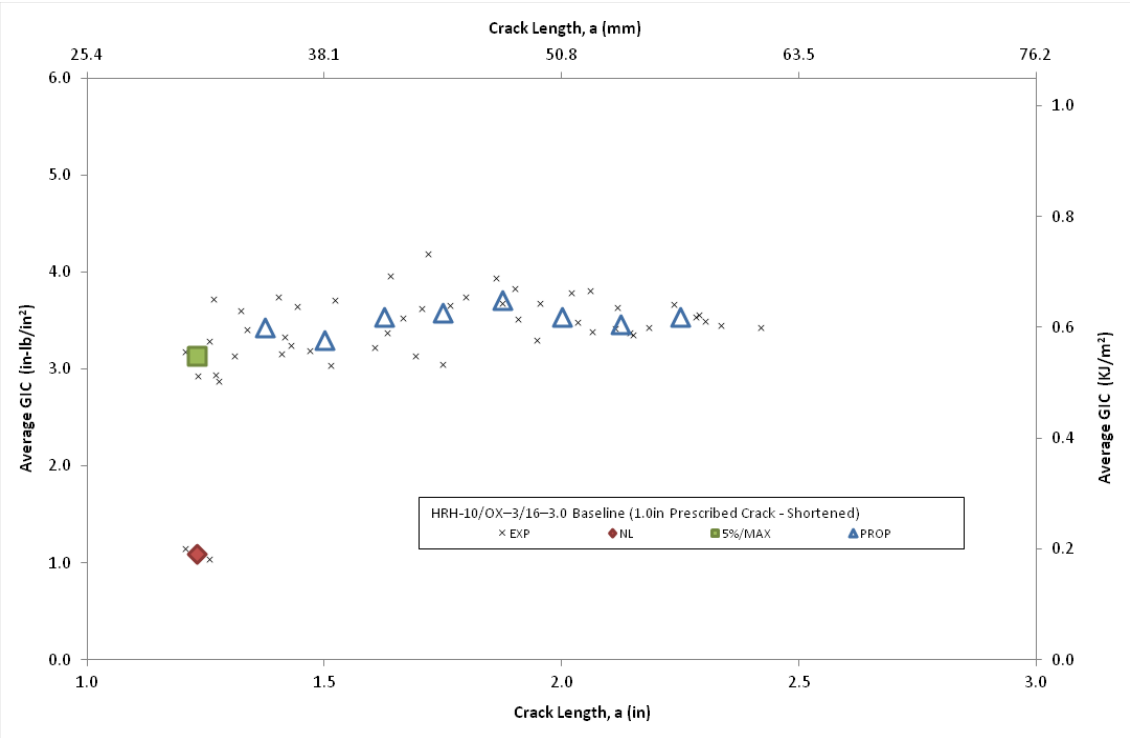

Figure D-8. Resistance curve for HRH-10/OX–3/16–3.0 baseline (1″ prescribed crack—shortened)

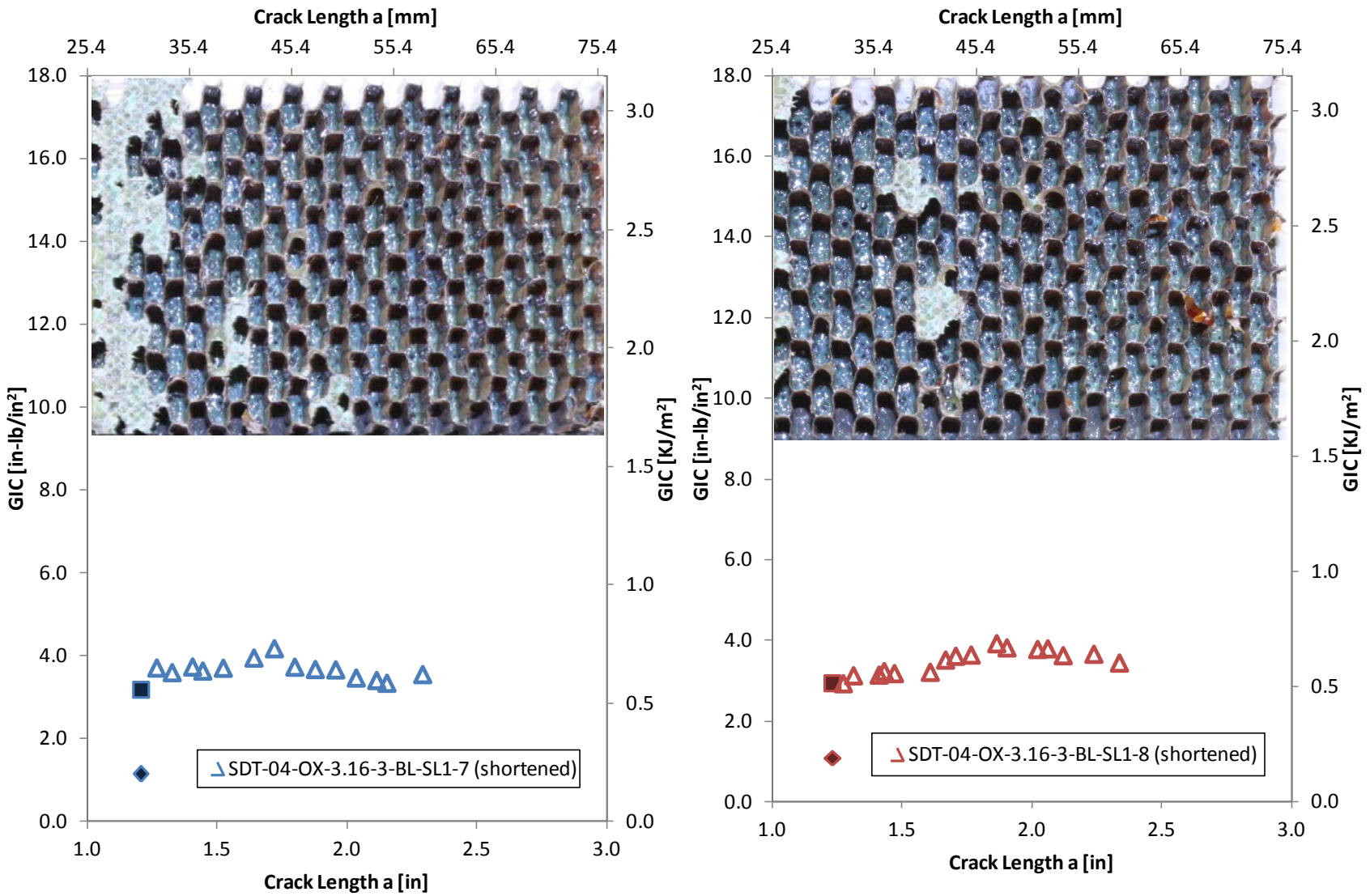

Figure D-9. Failure mode image and resistance curve of SDT-04-OX-3.16-3-BL-SL1-X (shortened) #7 and #8

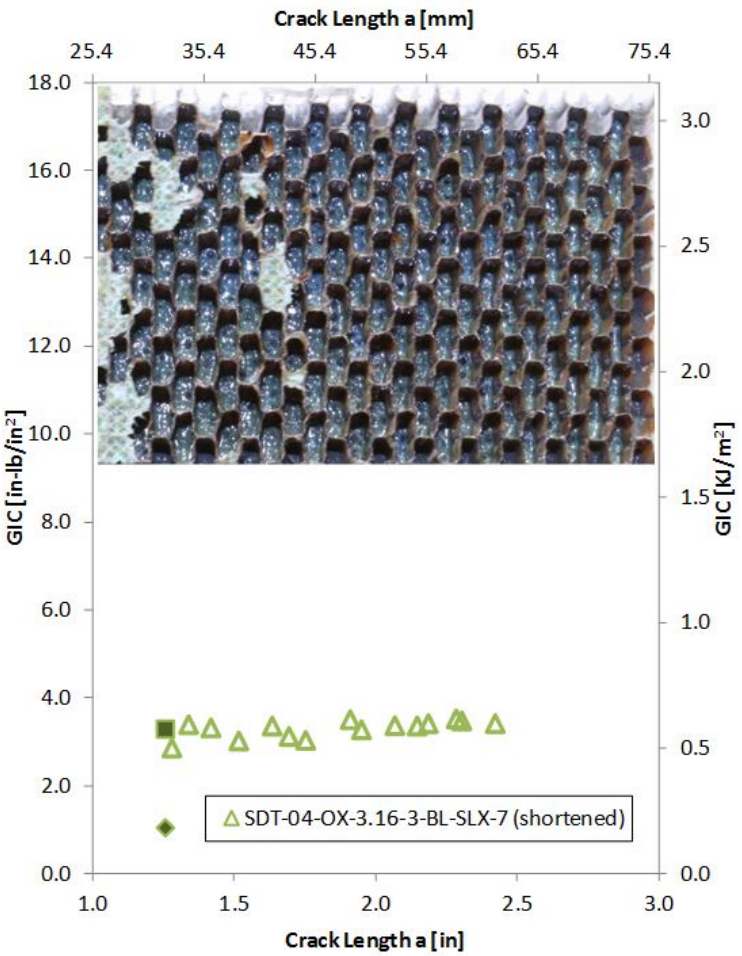

Figure D-10. Failure mode image and resistance curve of SDT-04-OX-3.16-3-BL-SLX-X #7 (shortened)

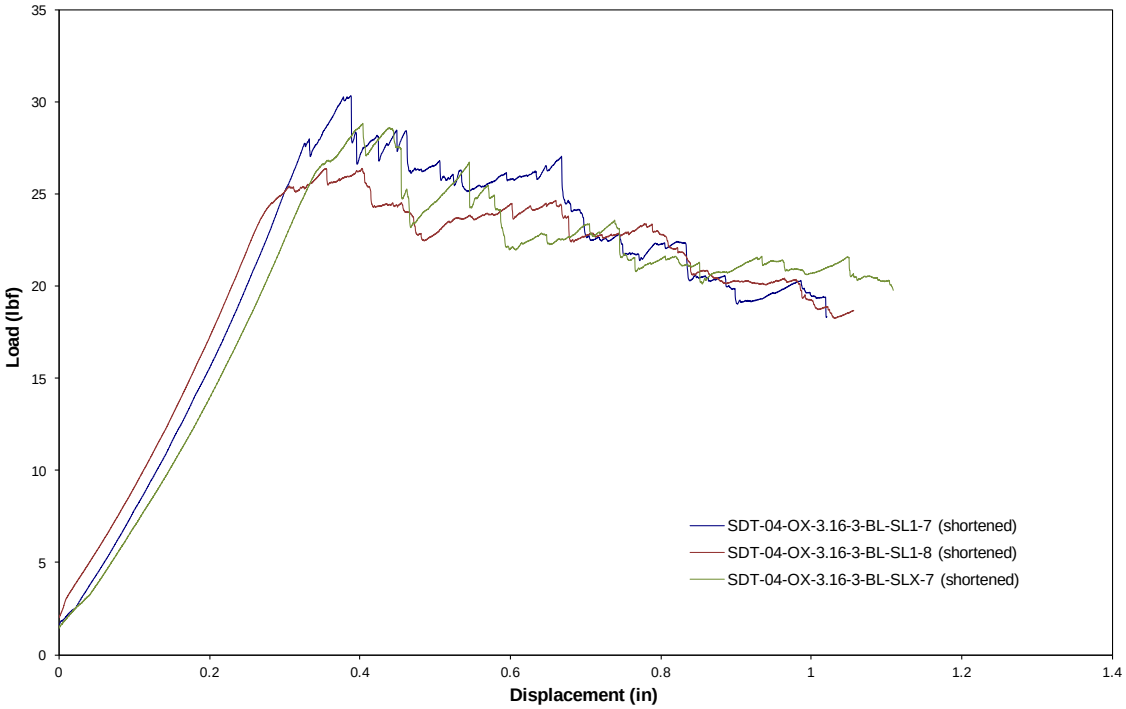

Figure D-11. Load vs. displacement curve for HRH-10/OX–3/16–3.0 baseline (1″ prescribed crack—shortened)

D.1.2 HRH-10/OX–3/16–3.0 FLUID-INGRESSED DATA

Table D-5. Test summary for HRH-10/OX–3/16–3.0 fluid ingressed (1″ prescribed crack—shortened) precrack

Specimen	GIC (in-lb/in^2)			GIC (KJ/m^2)			Failure Mode
	NL	VIS	5%/max	NL	VIS	5%/max	
SDT-04-OX-3.16-3-FI-SL1-1 (shortened)	0.746	-	2.700	0.131	-	0.473	Primarily in C with a couple of cells in A
SDT-04-OX-3.16-3-FI-SL1-2 (shortened)	1.533	-	3.168	0.268	-	0.555	Primarily in C
SDT-04-OX-3.16-3-FI-SL1-3 (shortened)	0.739	-	3.219	0.129	0.565	0.564	Primarily in C
SDT-04-OX-3.16-3-FI-SL1-4 (shortened)	0.791	-	3.177	0.139	-	0.556	Primarily in C
SDT-04-OX-3.16-3-FI-SL1-5 (shortened)	0.366	-	3.577	0.064	0.616	0.626	Primarily in C
SDT-04-OX-3.16-3-FI-SL1-6 (shortened)	0.924	-	3.426	0.162	0.533	0.600	Primarily in C with a few cells in A
AVERAGE GIC	0.850	-	3.211	0.149	0.571	0.562	
STANDARD DEVIATION	0.383	-	0.298	0.067	0.042	0.052	
COEFFICIENT OF VARIATION (%)	45.042	-	9.284	45.042	7.369	9.284	

Table D-6. Test summary for HRH-10/OX–3/16–3.0 fluid ingressed (1″ prescribed crack—shortened)

Specimen	GIC (in-lb/in^2)			GIC (KJ/m^2)			Failure Mode
	NL	VIS	5%/max	NL	VIS	5%/max	
SDT-04-OX-3.16-3-FI-SL1-1 (shortened)	0.746	-	2.700	0.131	-	0.473	Primarily in C
SDT-04-OX-3.16-3-FI-SL1-2 (shortened)	1.533	-	3.168	0.268	-	0.555	Primarily in C
SDT-04-OX-3.16-3-FI-SL1-3 (shortened)	0.739	3.226	3.219	0.129	0.565	0.564	Primarily in C with a cell in A
SDT-04-OX-3.16-3-FI-SL1-4 (shortened)	0.791	-	3.177	0.139	-	0.556	Primarily in C
SDT-04-OX-3.16-3-FI-SL1-5 (shortened)	0.366	3.518	3.577	0.064	0.616	0.626	Primarily in C
SDT-04-OX-3.16-3-FI-SL1-6 (shortened)	0.924	3.041	3.426	0.162	0.533	0.600	Primarily in C
AVERAGE GIC	0.850	3.262	3.211	0.149	0.571	0.562	
STANDARD DEVIATION	0.383	0.240	0.298	0.067	0.042	0.052	
COEFFICIENT OF VARIATION (%)	45.042	7.369	9.284	45.042	7.369	9.284	

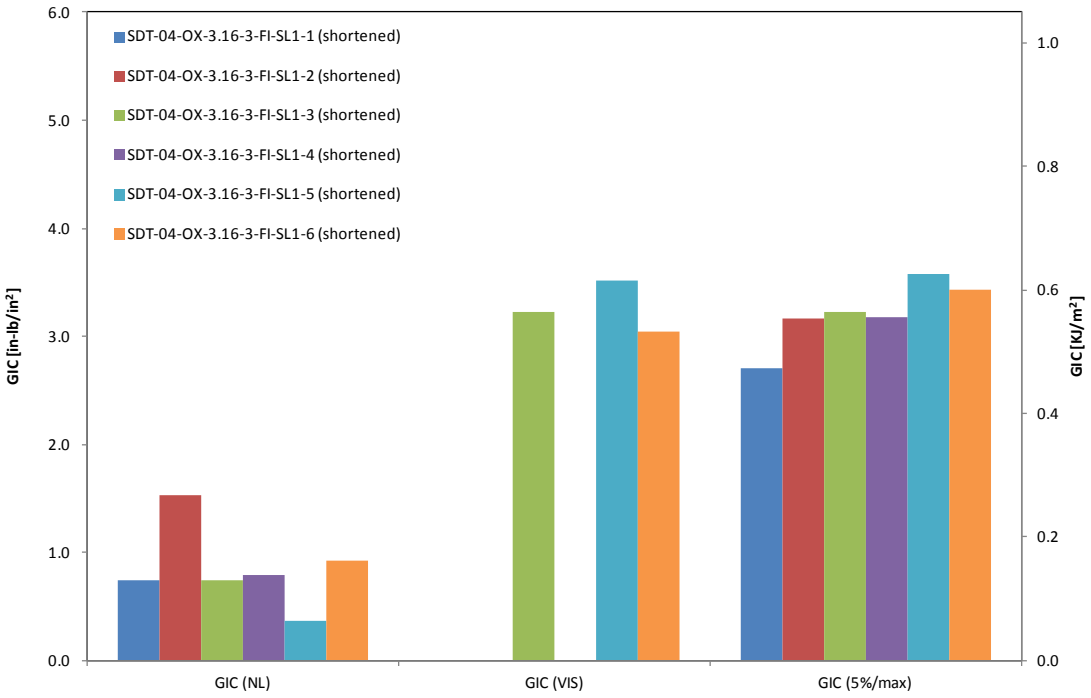

Figure D-12. GIC for HRH-10/OX–3/16–3.0 fluid ingressed (1″ prescribed crack—shortened)

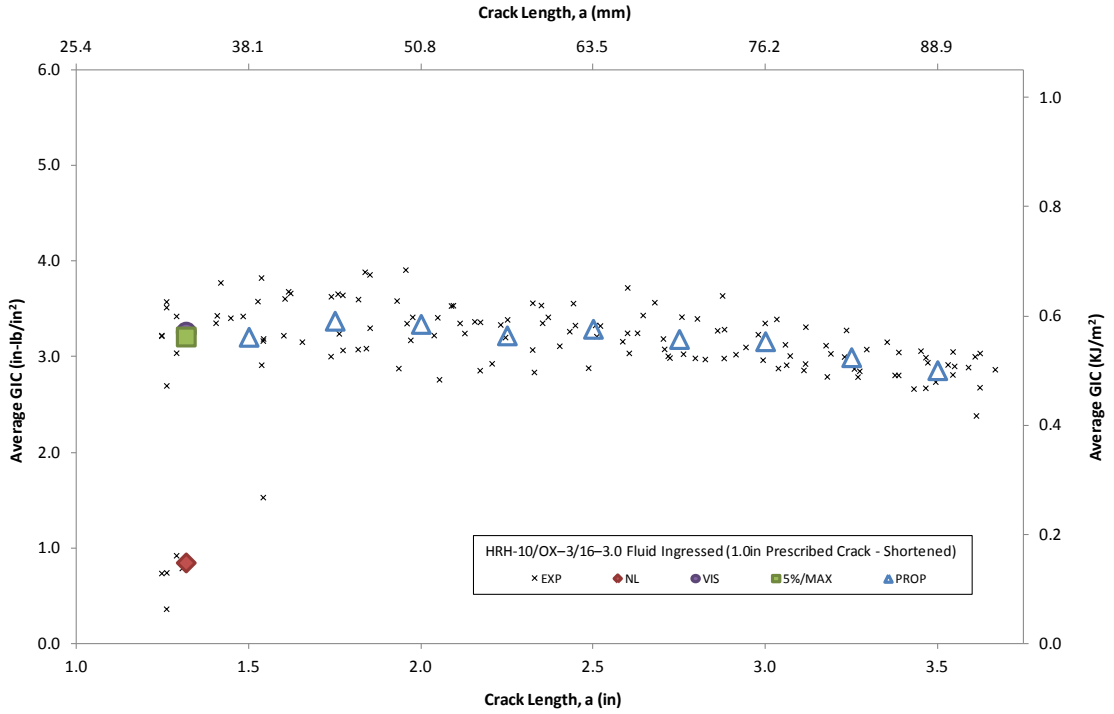

Figure D-13. Resistance curve for HRH-10/OX–3/16–3.0 fluid ingressed (1″ prescribed crack—shortened)

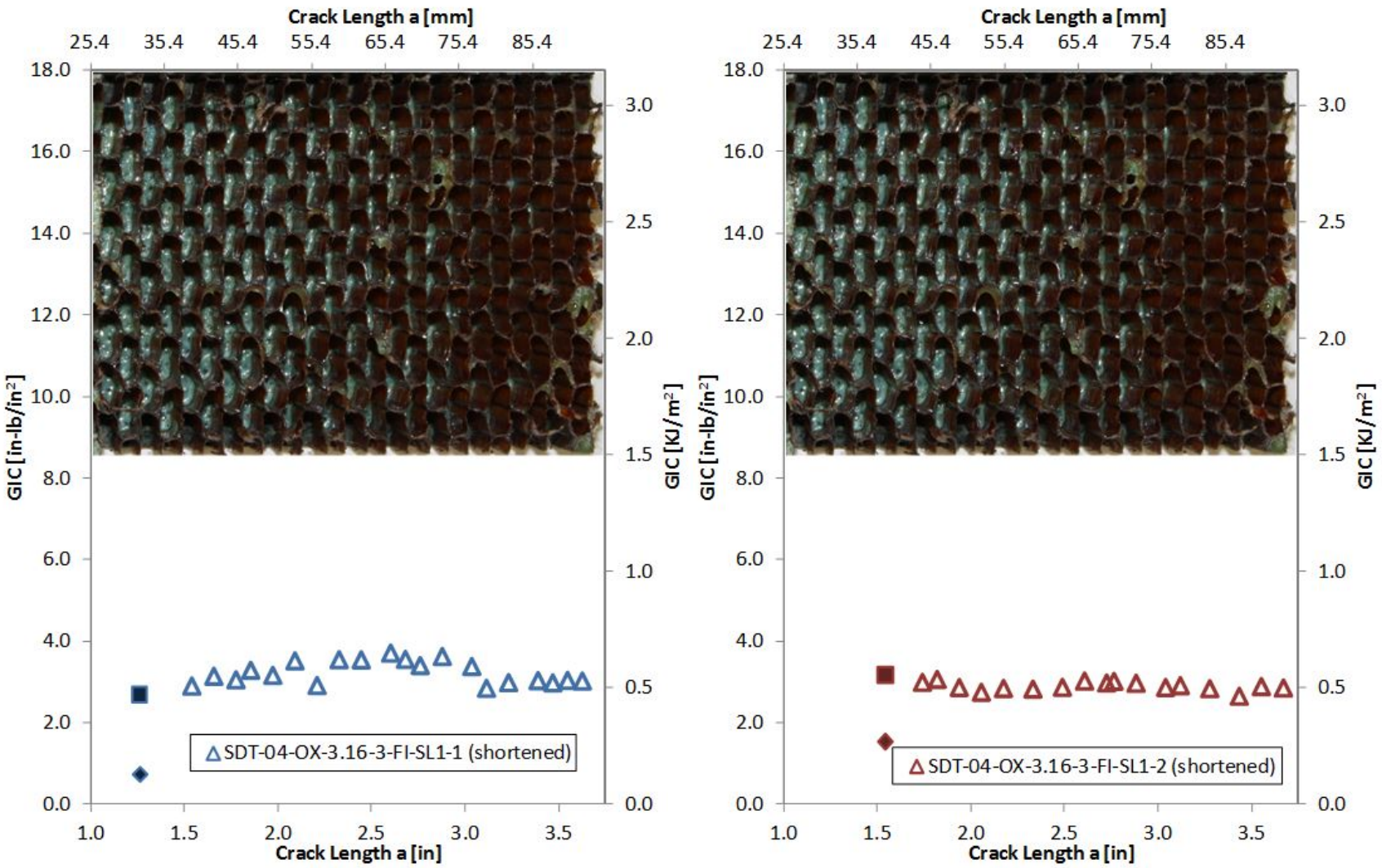

Figure D-14. Failure mode image and resistance curve of SDT-04-OX-3.16-3-FI-SL1-X (shortened) #1 and #2

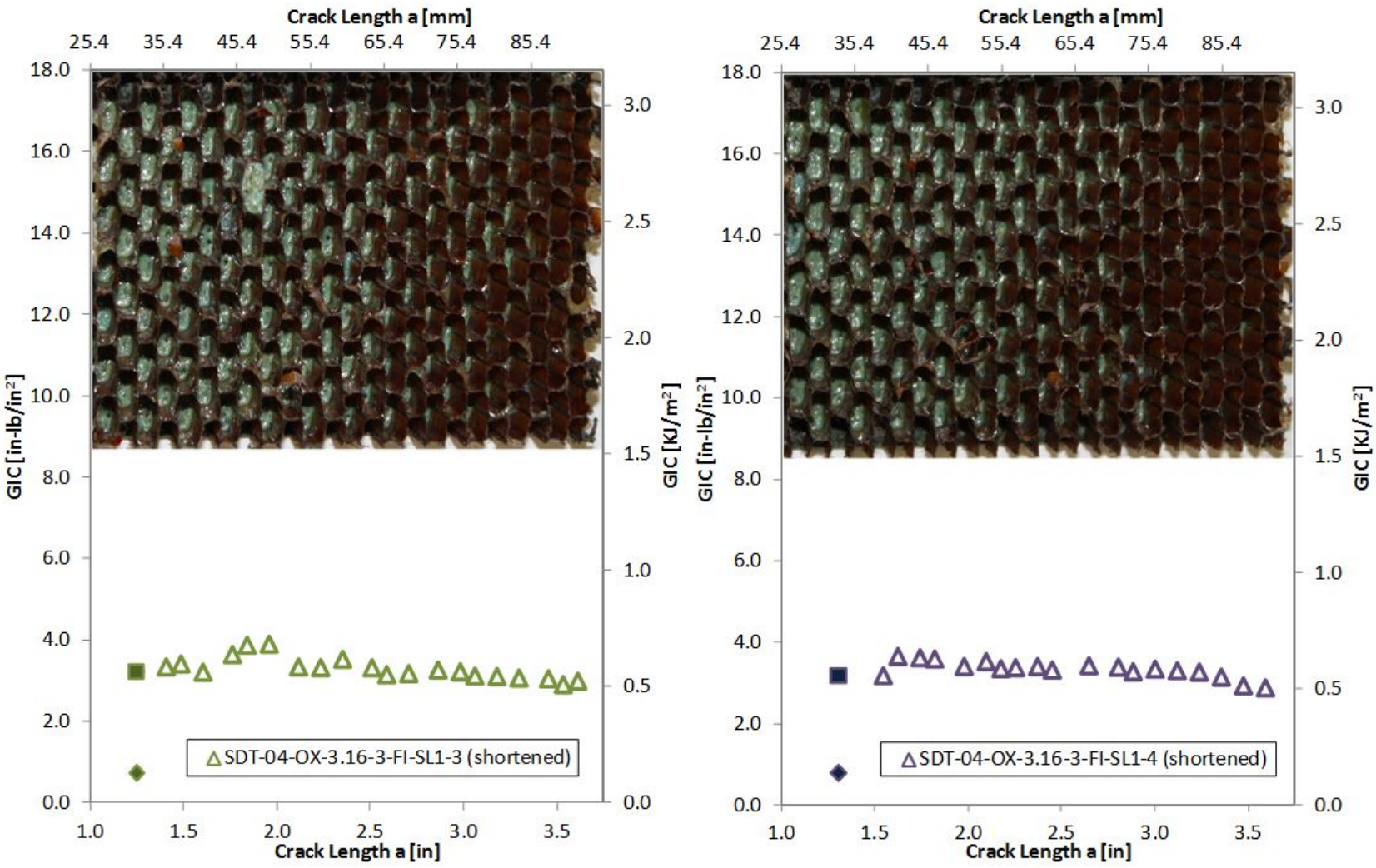

Figure D-15. Failure mode image and resistance curve of SDT-04-OX-3.16-3-FI-SL1-X (shortened) #3 and #4

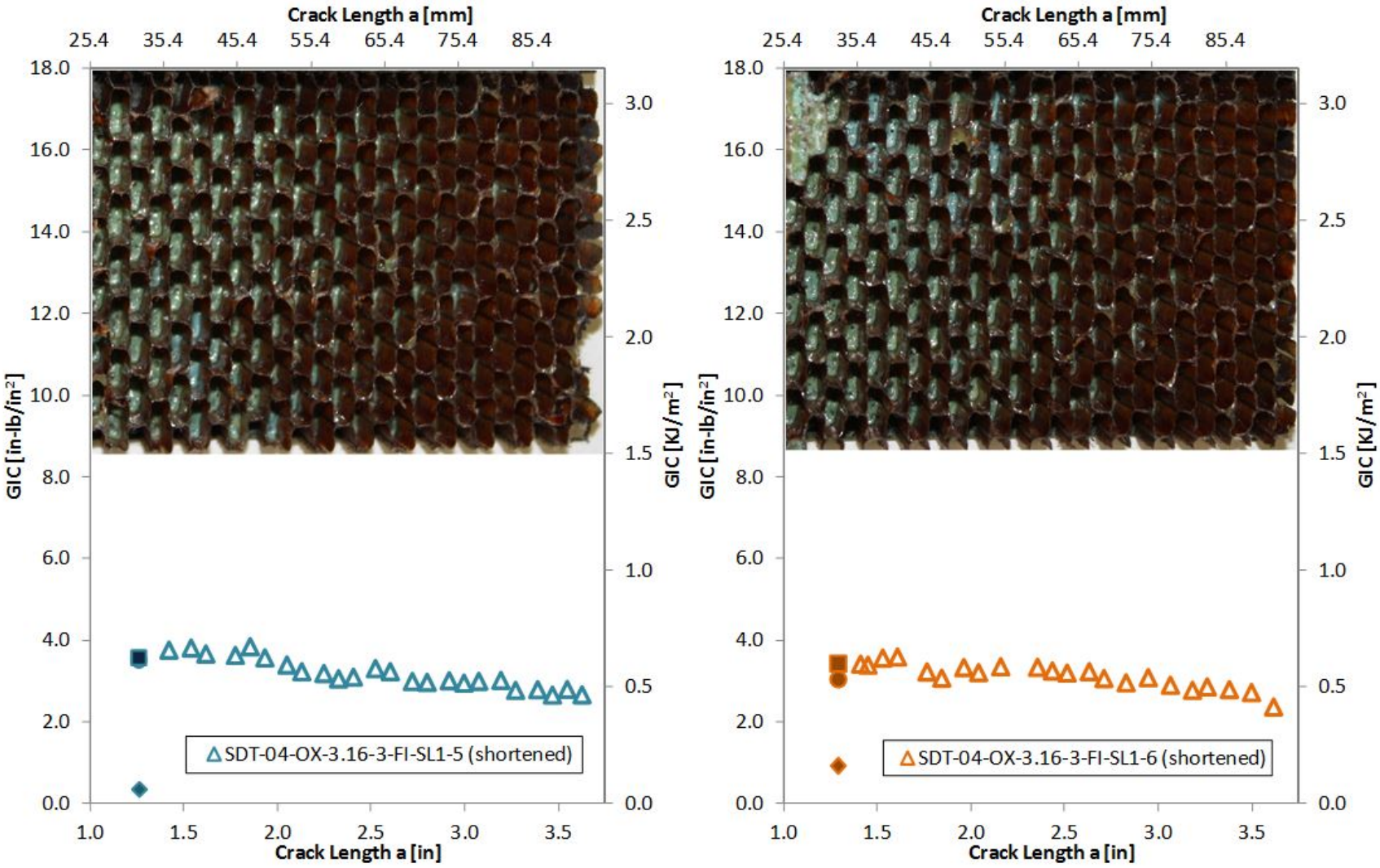

Figure D-16. Failure mode image and resistance curve of SDT-04-OX-3.16-3-FI-SL1-X (shortened) #5 and #6

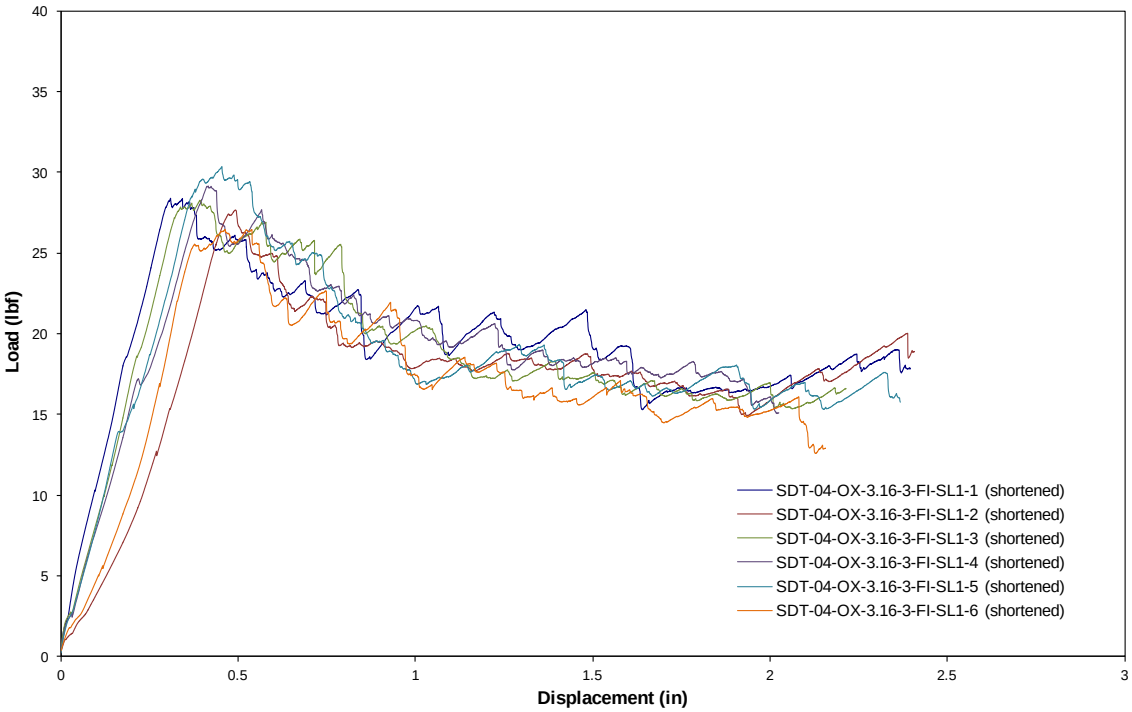

Figure D-17. Load vs. displacement curve for HRH-10/OX–3/16–3.0 fluid ingressed (1″ prescribed crack—shortened)

D.1.3 HRH-10/OX–3/16–3.0 EXTENDED FLUID-INGRESSED DATA

Table D-7. Test summary for HRH-10/OX–3/16–3.0 extended fluid ingressed (1″ prescribed crack—shortened) precrack

Specimen	GIC (in-lb/in^2)			GIC (KJ/m^2)			Failure Mode
	NL	VIS	5%/max	NL	VIS	5%/max	
SDT-04-OX-3.16-3-EFI-SL1-7 (shortened)	1.339	-	N/A	0.235	-	N/A	First row primarily in PO, second row primarily in C with a few cells in A
SDT-04-OX-3.16-3-EFI-SL1-8 (shortened)	0.724	-	1.905	0.127	-	0.334	Primarily in C
AVERAGE GIC	1.031	-	1.905	0.181	-	0.334	
STANDARD DEVIATION	0.435	-	-	0.076	-	-	
COEFFICIENT OF VARIATION (%)	42.212	-	-	42.212	-	-	

Table D-8. Test summary for HRH-10/OX–3/16–3.0 extended fluid ingressed (1″ prescribed crack—shortened)

Specimen	GIC (in-lb/in^2)			GIC (KJ/m^2)			Failure Mode
	NL	VIS	5%/max	NL	VIS	5%/max	
SDT-04-OX-3.16-3-EFI-SL1-7 (shortened)	1.003	-	4.000	0.176	-	0.701	Primarily in C
SDT-04-OX-3.16-3-EFI-SL1-8 (shortened)	0.591	-	2.866	0.103	-	0.502	Primarily in C
AVERAGE GIC	0.797	-	3.433	0.140	-	0.601	
STANDARD DEVIATION	0.292	-	0.802	0.051	-	0.140	
COEFFICIENT OF VARIATION (%)	36.576	-	23.359	36.576	-	23.359	

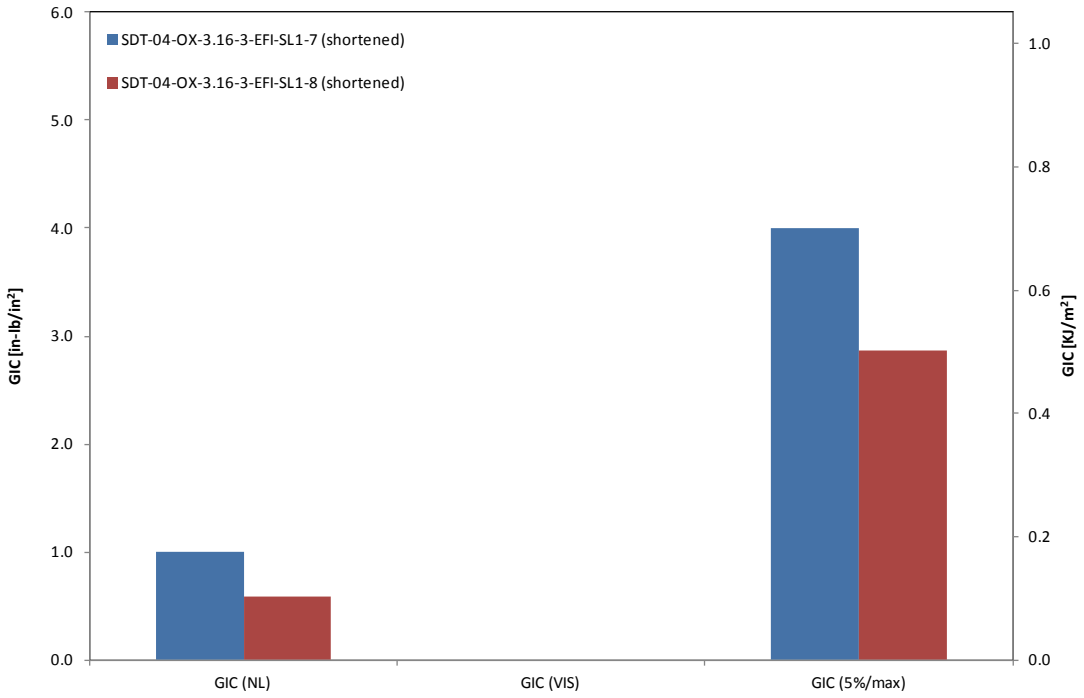

Figure D-18. GIC for HRH-10/OX–3/16–3.0 extended fluid ingressed (1″ prescribed crack—shortened)

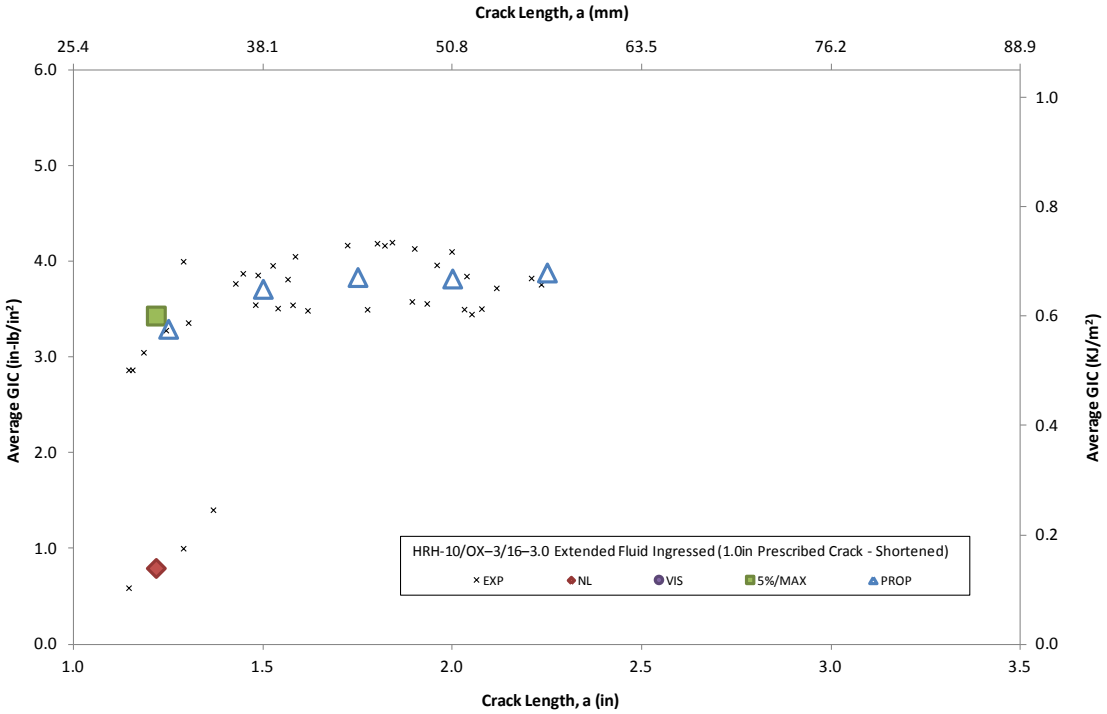

Figure D-19. Resistance curve for HRH-10/OX–3/16–3.0 extended fluid ingressed (1″ prescribed crack—shortened)

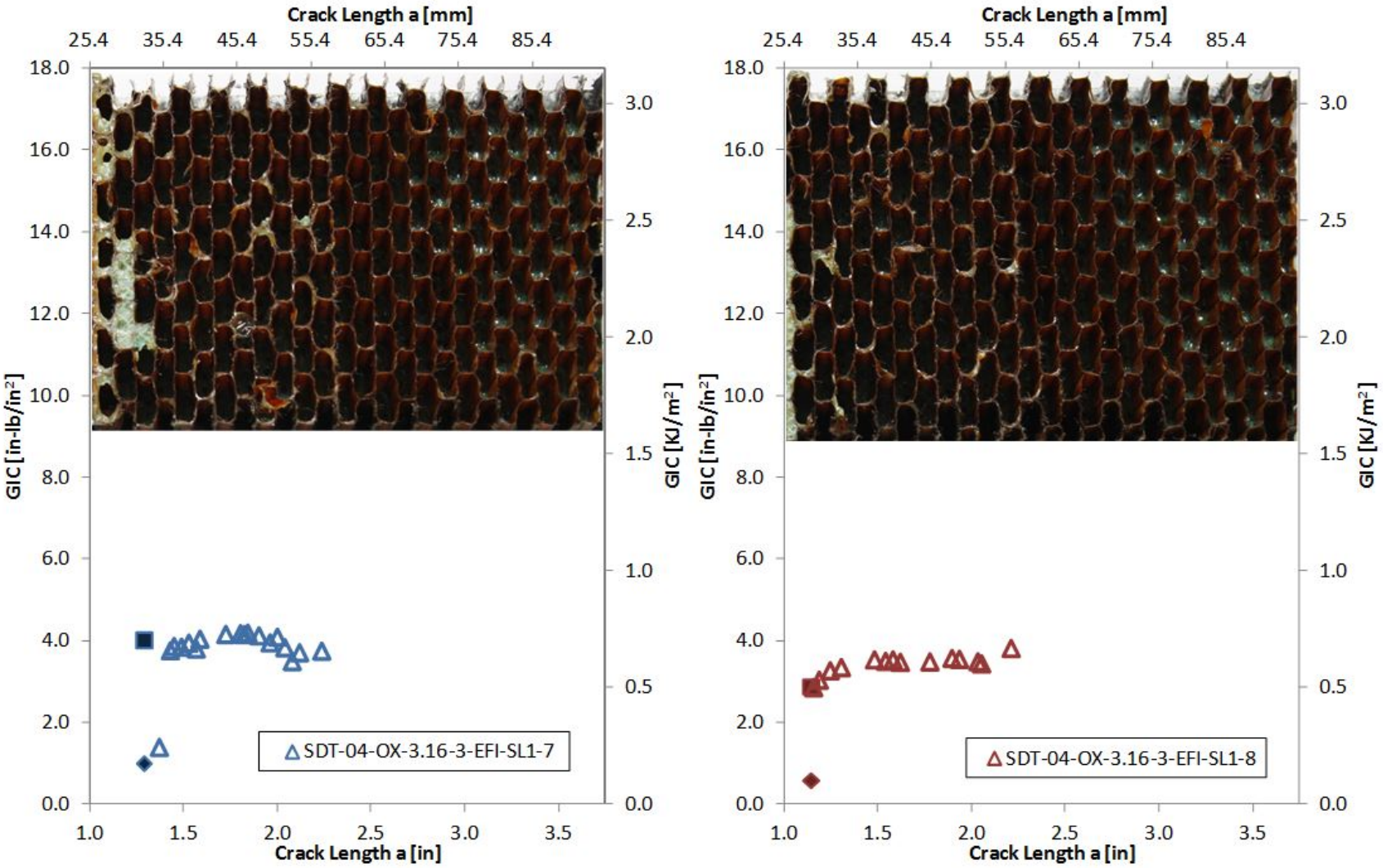

Figure D-20. Failure mode image and resistance curve of SDT-04-OX-3.16-3-EFI-SL1-X (shortened) #7 and #8

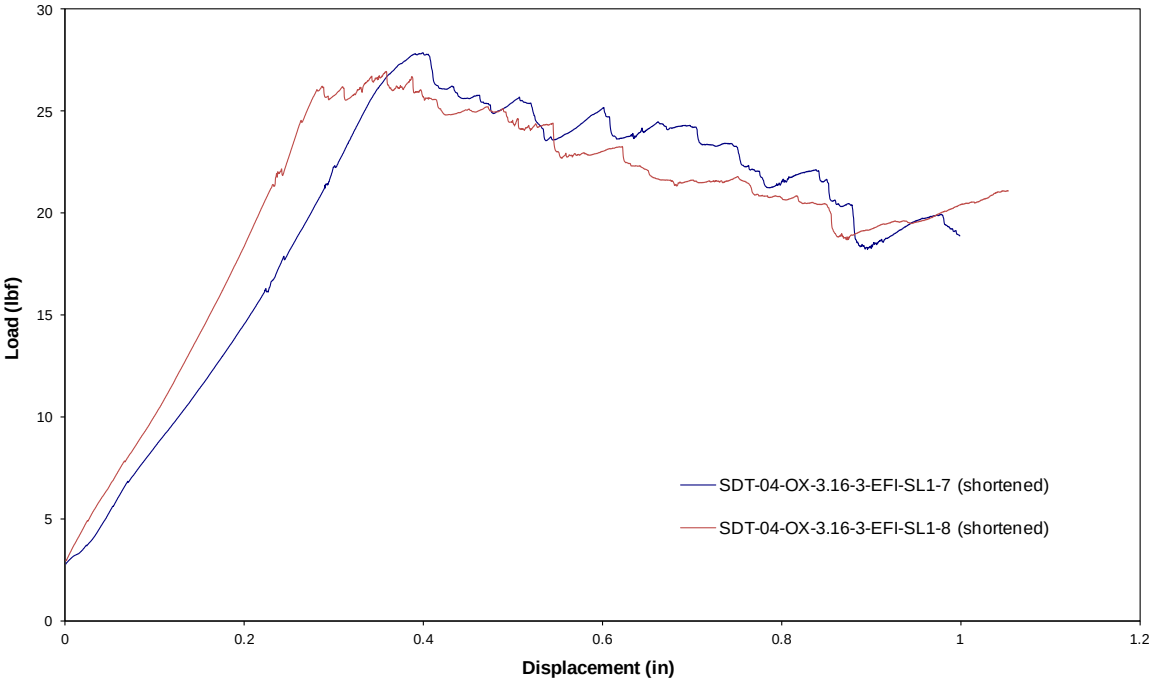

Figure D-21. Load vs. displacement curve for HRH-10/OX–3/16–3.0 extended fluid ingressed (1″ prescribed crack—shortened)

APPENDIX E—STATIC RESULTS FOR THICK FACESHEET (16-PLY) AND HRH-10 OVER-EXPANDED CORE TESTED AS SINGLE-CANTILEVER BEAMS

Note that 16-ply material systems were tested with one prescribed crack length. The baseline, fluid-ingressed, extended fluid-ingressed, and water-ingressed specimens were all tested with a 2.5″ prescribed crack.

E.1 HRH-10/OX–3/16–3.0 DATA

E.1.1 HRH-10/OX–3/16–3.0 BASELINE DATA

Table E-1. Test summary for HRH-10/OX–3/16–3.0 baseline (2.5″ prescribed crack) precrack

Specimen	GIC (in-lb/in^2)			GIC (KJ/m^2)			Failure Mode
	NL	VIS	5%/max	NL	VIS	5%/max	
SDT-16-OX-3.16-3-BL-SL1-1	3.515	-	4.382	0.616	-	0.767	First two rows primarily in A with a couple of cells in PO and C; third row a mix of A and C
SDT-16-OX-3.16-3-BL-SL1-2	2.763	-	3.949	0.484	-	0.691	First row primarily in A with a cell in C; second row a mix of A and C; third row in C
SDT-16-OX-3.16-3-BL-SL1-3	2.816	-	4.703	0.493	-	0.824	First row primarily in A; second row a mix of A and C; third row in C
SDT-16-OX-3.16-3-BL-SL1-4	3.152	-	3.698	0.552	-	0.648	Primarily in A with a couple of cells in C
SDT-16-OX-3.16-3-BL-SL1-5	2.979	-	3.991	0.522	-	0.699	Primarily in A with a couple of cells in C
SDT-16-OX-3.16-3-BL-SL1-6	2.478	-	3.586	0.434	-	0.628	Primarily in C
AVERAGE GIC	2.950	-	4.051	0.517	-	0.710	
STANDARD DEVIATION	0.357	-	0.422	0.063	-	0.074	
COEFFICIENT OF VARIATION (%)	12.101	-	10.414	12.101	-	10.414	

Table E-2. Test summary for HRH-10/OX–3/16–3.0 baseline (2.5″ prescribed crack)

Specimen	GIC (in-lb/in^2)			GIC (KJ/m^2)			Failure Mode
	NL	VIS	5%/max	NL	VIS	5%/max	
SDT-16-OX-3.16-3-BL-SL1-1	1.426	-	5.751	0.250	-	1.007	Primarily in C with a pocket of A
SDT-16-OX-3.16-3-BL-SL1-2	1.667	5.703	7.190	0.292	0.999	1.259	Primarily in C
SDT-16-OX-3.16-3-BL-SL1-3	1.735	-	7.000	0.304	-	1.226	Primarily in C
SDT-16-OX-3.16-3-BL-SL1-4	1.509	5.262	5.751	0.264	0.922	1.007	Primarily in C after quick transition from a mix of A and C
SDT-16-OX-3.16-3-BL-SL1-5	1.547	-	5.130	0.271	-	0.898	Primarily in C after a quick transition from a mix of A and C
SDT-16-OX-3.16-3-BL-SL1-6	1.359	-	5.281	0.238	-	0.925	Primarily in C
AVERAGE GIC	1.541	5.483	6.017	0.270	0.960	1.054	
STANDARD DEVIATION	0.142	0.312	0.873	0.025	0.055	0.153	
COEFFICIENT OF VARIATION (%)	9.221	5.685	14.512	9.221	5.685	14.512	

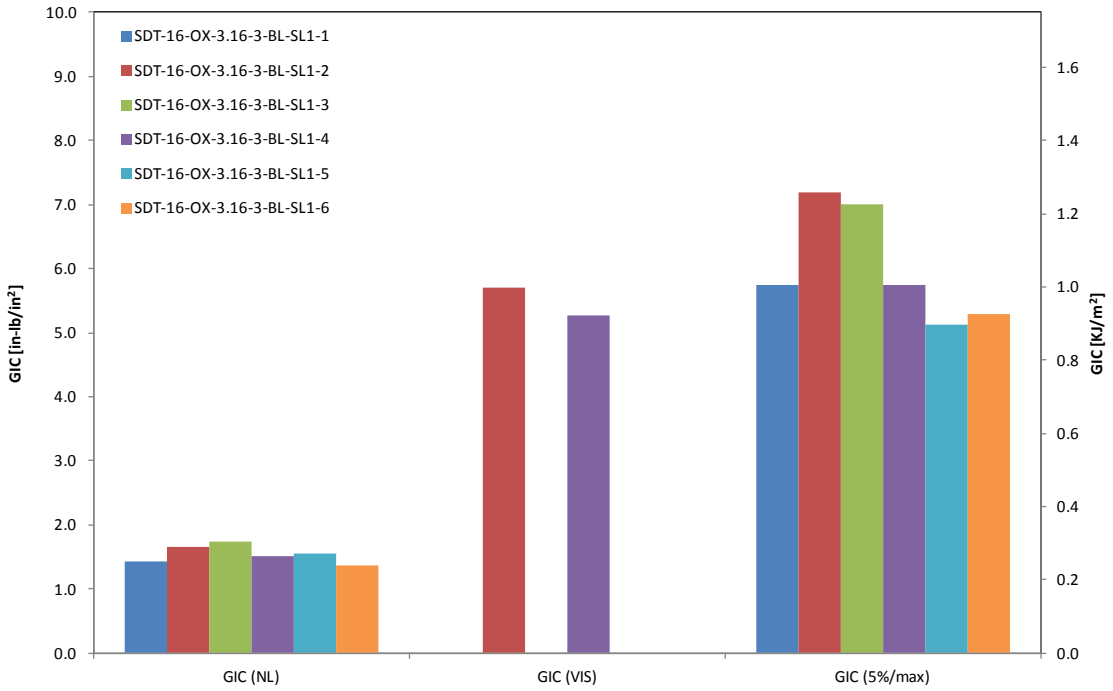

Figure E-1. GIC for HRH-10/OX–3/16–3.0 baseline (2.5″ prescribed crack)

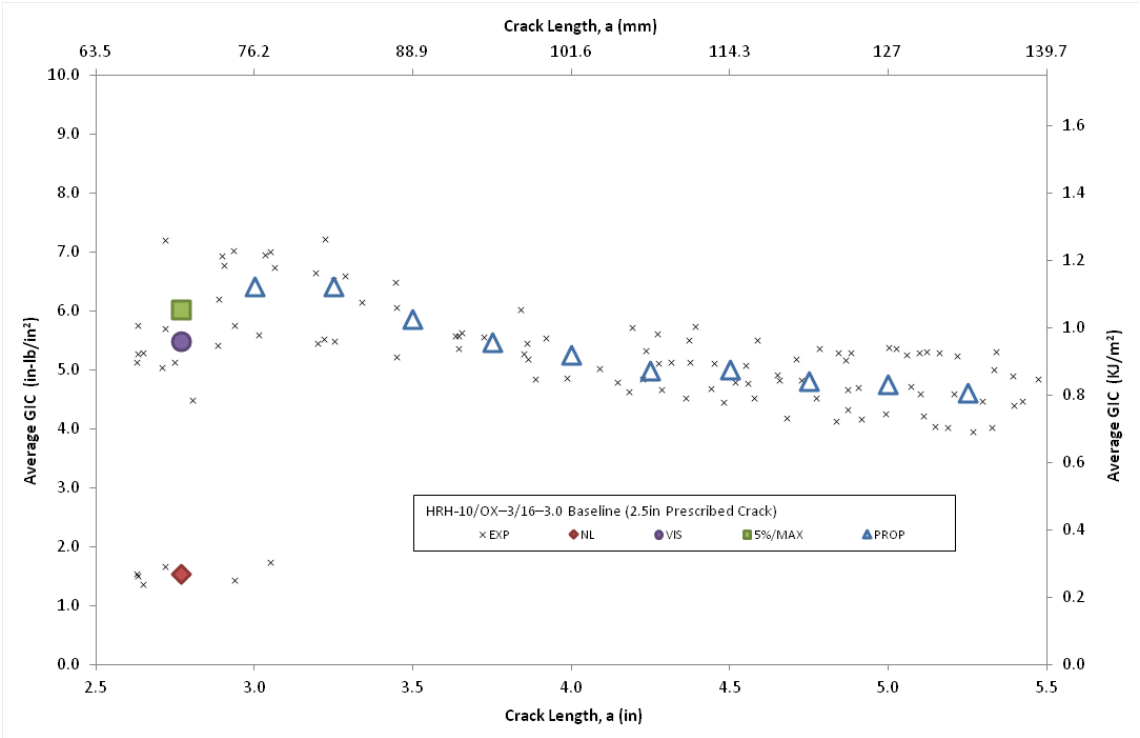

Figure E-2. Resistance curve for HRH-10/OX–3/16–3.0 baseline (2.5″ prescribed crack)

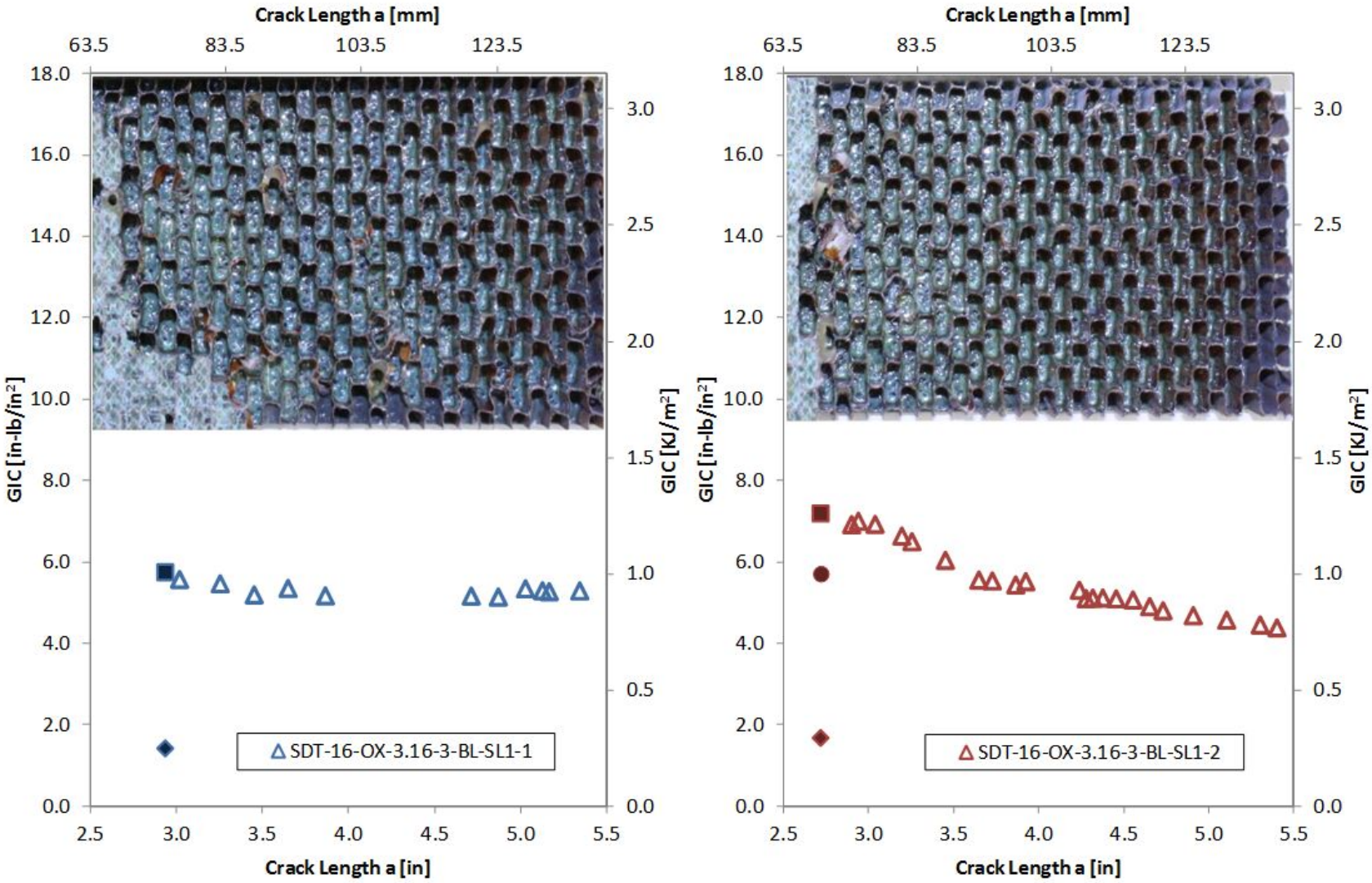

Figure E-3. Failure mode image and resistance curve of SDT-16-OX-3.16-3-BL-SL1-X #1 and #2

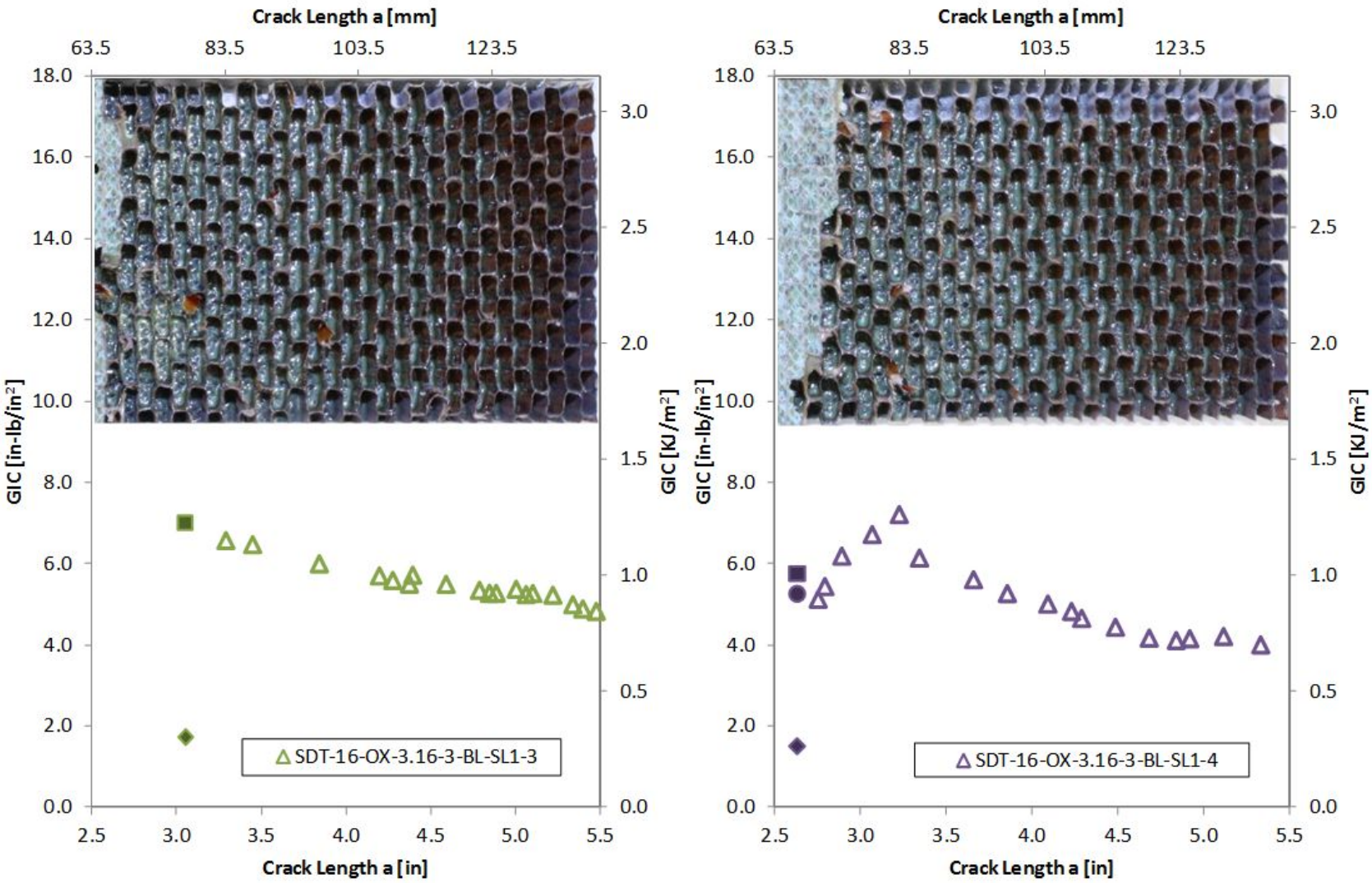

Figure E-4. Failure mode image and resistance curve of SDT-16-OX-3.16-3-BL-SL1-X #3 and #4

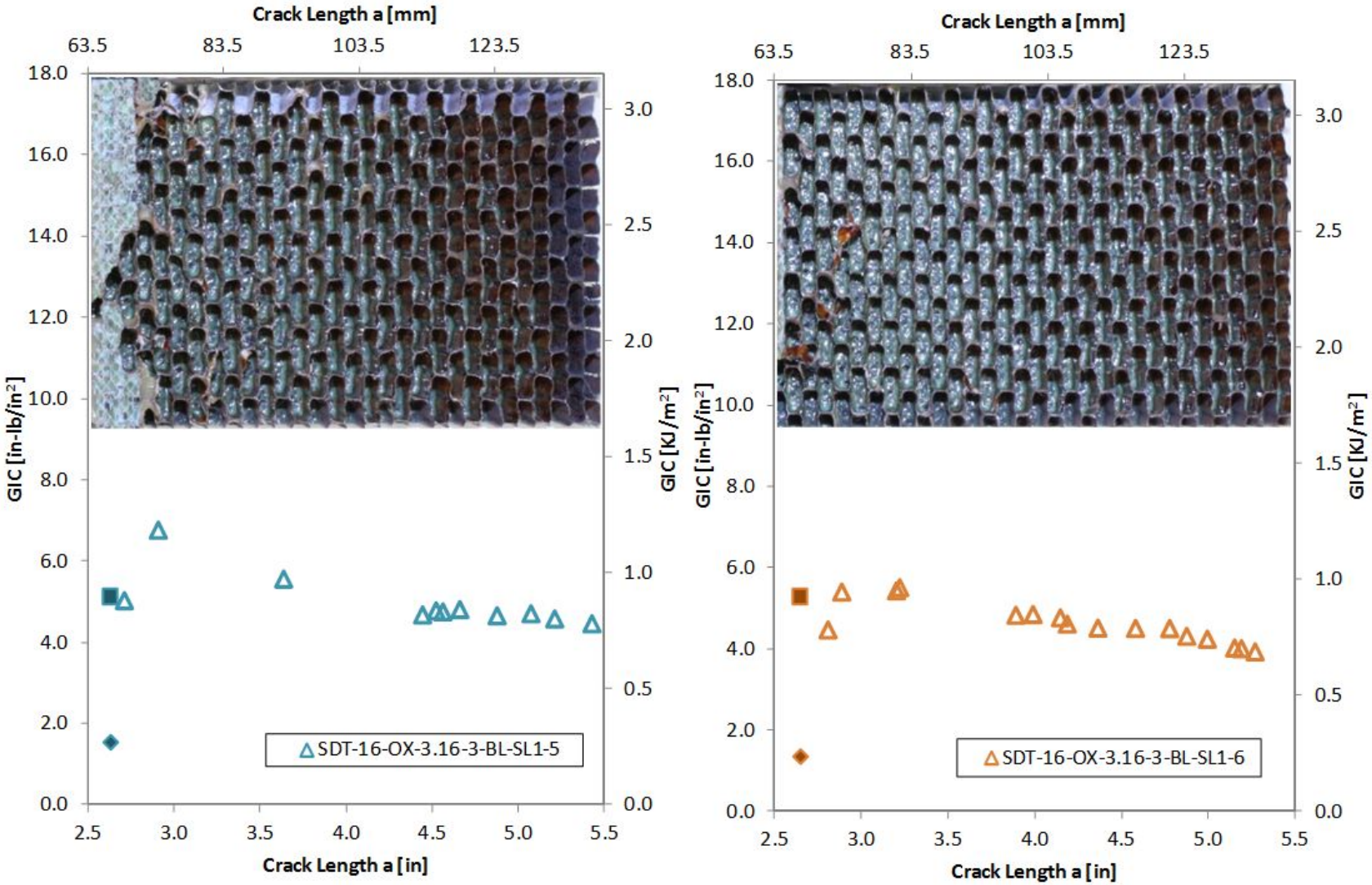

Figure E-5. Failure mode image and resistance curve for SDT-16-OX-3.16-3-BL-SL1-X #5 and #6

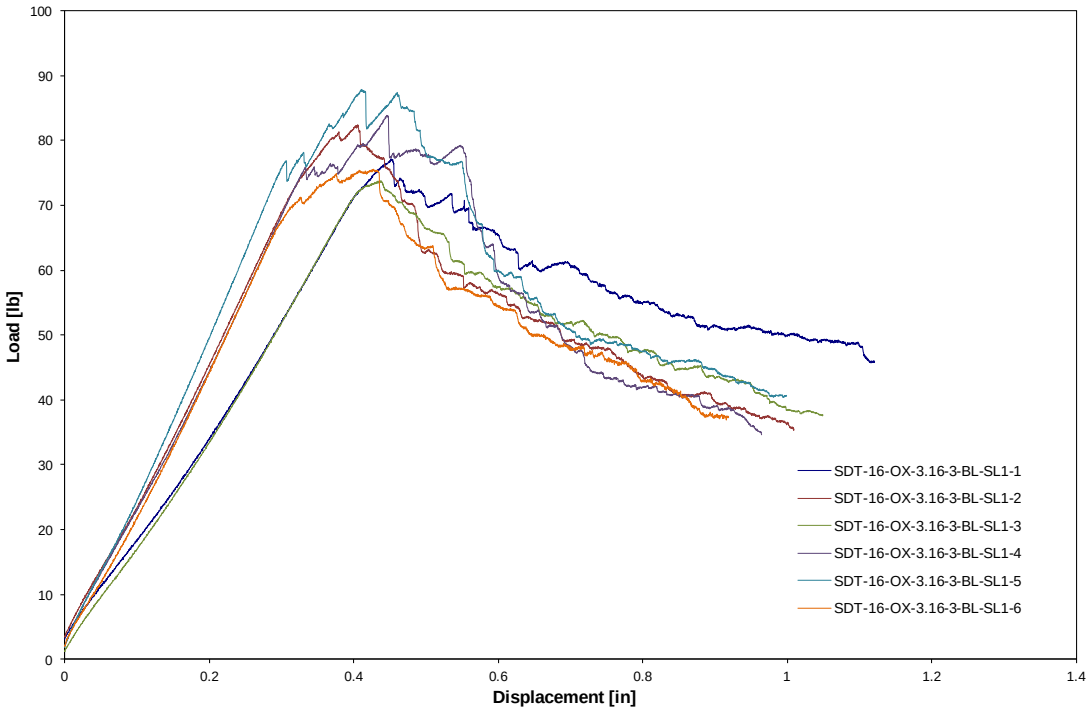

Figure E-6. Load vs. displacement curve for HRH-10/OX–3/16–3.0 baseline (2.5″ prescribed crack)

E.1.2 HRH-10/OX–3/16–3.0 FLUID-INGRESSED DATA

Table E-3. Test summary for HRH-10/OX–3/16–3.0 fluid ingressed (2.5″ prescribed crack) precrack

Specimen	GIC (in-lb/in^2)			GIC (KJ/m^2)			Failure Mode
	NL	VIS	5%/max	NL	VIS	5%/max	
SDT-16-OX-3.16-3-FI-SL1-2	1.452	-	2.297	0.254	-	0.402	Primarily in C
SDT-16-OX-3.16-3-FI-SL1-3	1.602	-	2.732	0.281	-	0.478	First row a mix of A and C, then primarily in C
SDT-16-OX-3.16-3-FI-SL1-4	1.681	-	3.251	0.294	-	0.569	Primarily in C with a cell in A
SDT-16-OX-3.16-3-FI-SL1-5	1.899	-	4.073	0.333	-	0.713	Primarily in C with a cell in A
SDT-16-OX-3.16-3-FI-SL1-6	1.675	-	3.669	0.293	-	0.643	Primarily in C
SDT-16-OX-3.16-3-FI-SL1-7	1.552	-	2.686	0.272	-	0.470	First row primarily in A, second row a mix of A and C, then primarily in C
AVERAGE GIC	1.643	-	3.118	0.288	-	0.546	
STANDARD DEVIATION	0.152	-	0.670	0.027	-	0.117	
COEFFICIENT OF VARIATION (%)	9.220	-	21.478	9.220	-	21.478	

Table E-4. Test summary for HRH-10/OX–3/16–3.0 fluid ingressed (2.5″ prescribed crack)

Specimen	GIC (in-lb/in^2)			GIC (KJ/m^2)			Failure Mode
	NL	VIS	5%/max	NL	VIS	5%/max	
SDT-16-OX-3.16-3-FI-SL1-2	1.087	-	4.203	0.190	-	0.736	Primarily in C
SDT-16-OX-3.16-3-FI-SL1-3	1.470	-	5.363	0.257	-	0.939	Primarily in C
SDT-16-OX-3.16-3-FI-SL1-4	0.873	4.572	5.192	0.153	0.801	0.909	Primarily in C
SDT-16-OX-3.16-3-FI-SL1-5	1.338	5.046	5.292	0.234	0.884	0.927	Primarily in C
SDT-16-OX-3.16-3-FI-SL1-6	1.375	5.787	5.878	0.241	1.013	1.029	Primarily in C
SDT-16-OX-3.16-3-FI-SL1-7	1.094	4.488	4.513	0.192	0.786	0.790	Primarily in C
AVERAGE GIC	1.206	4.973	5.074	0.211	0.871	0.889	
STANDARD DEVIATION	0.225	0.595	0.611	0.039	0.104	0.107	
COEFFICIENT OF VARIATION (%)	18.650	11.968	12.038	18.650	11.968	12.038	

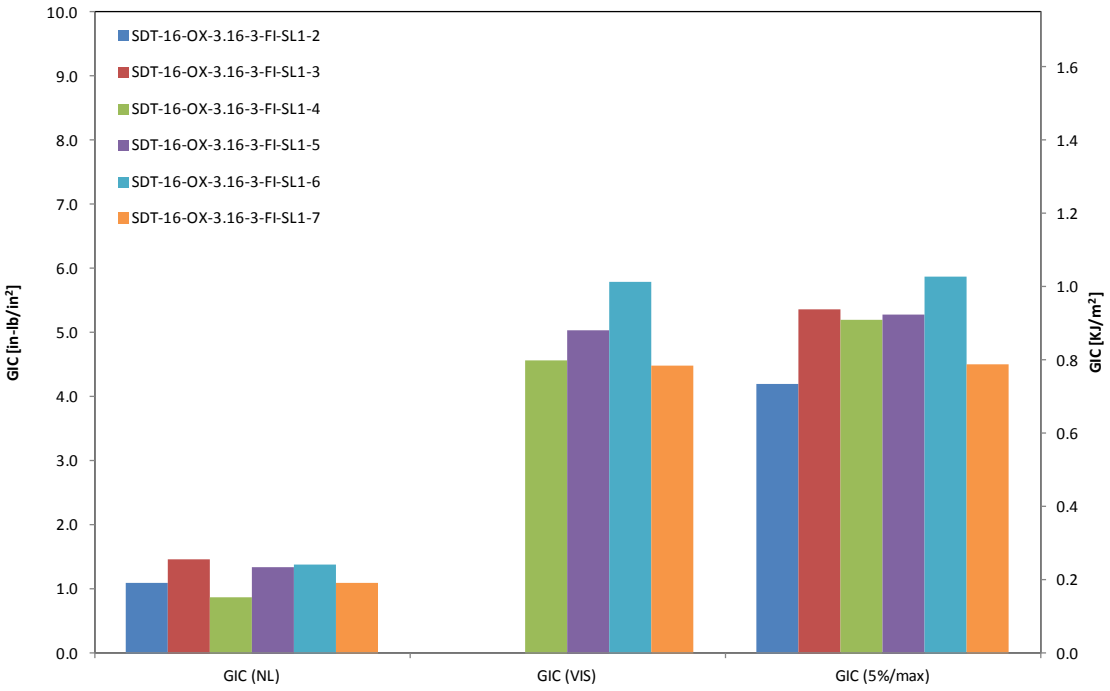

Figure E-7. GIC for HRH-10/OX–3/16–3.0 fluid ingressed (2.5″ prescribed crack)

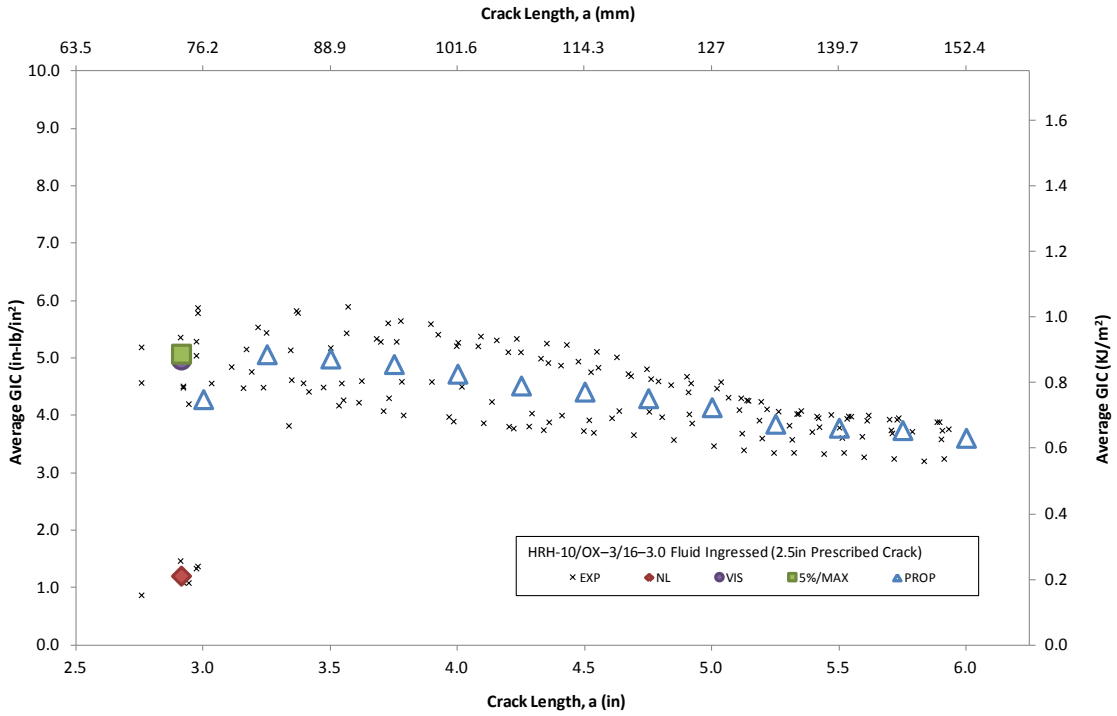

Figure E-8. Resistance curve for HRH-10/OX–3/16–3.0 fluid ingressed (2.5″ prescribed crack)

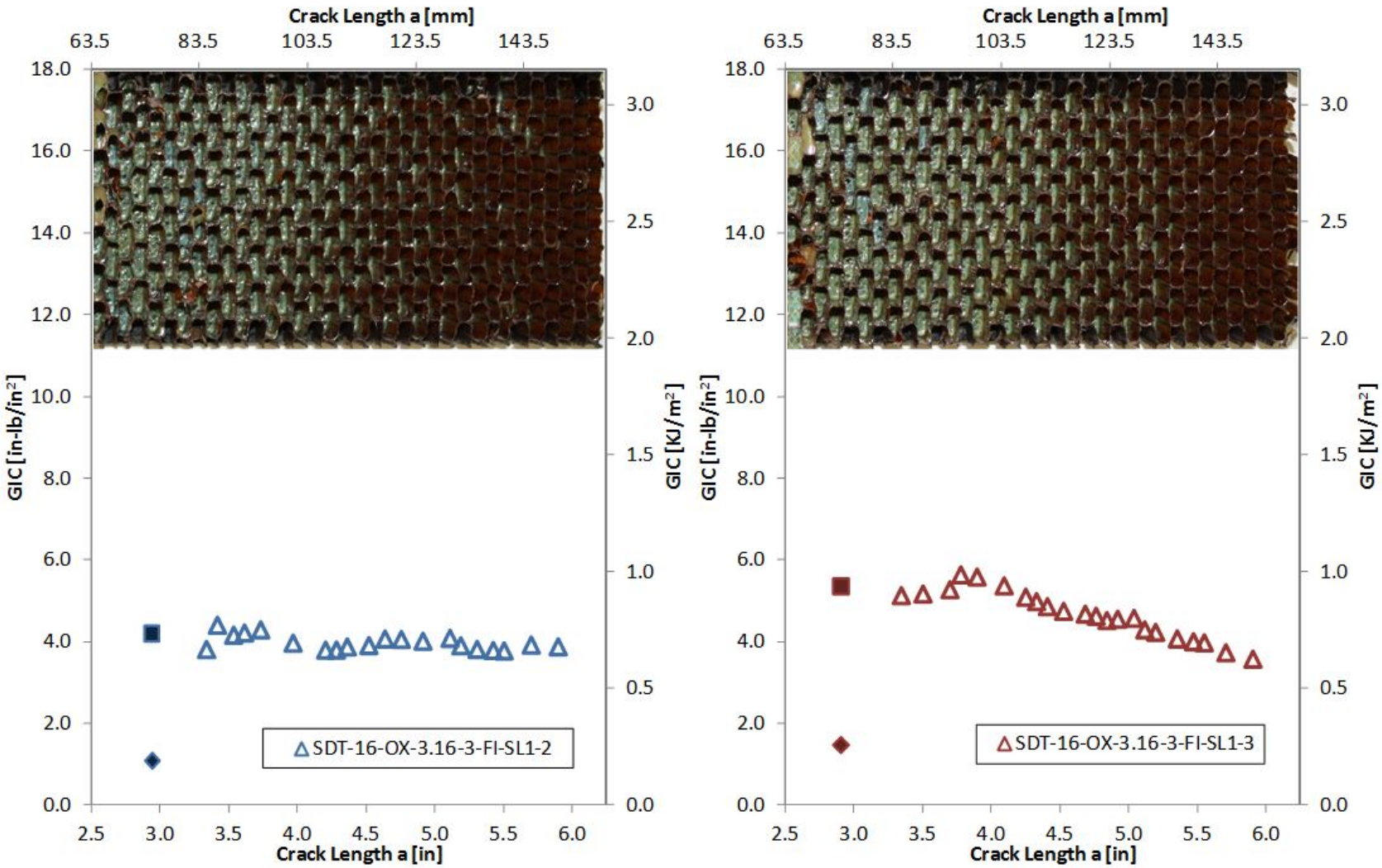

Figure E-9. Failure mode image and resistance curve of SDT-16-OX-3.16-3-FI-SL1-X # 2 and #3

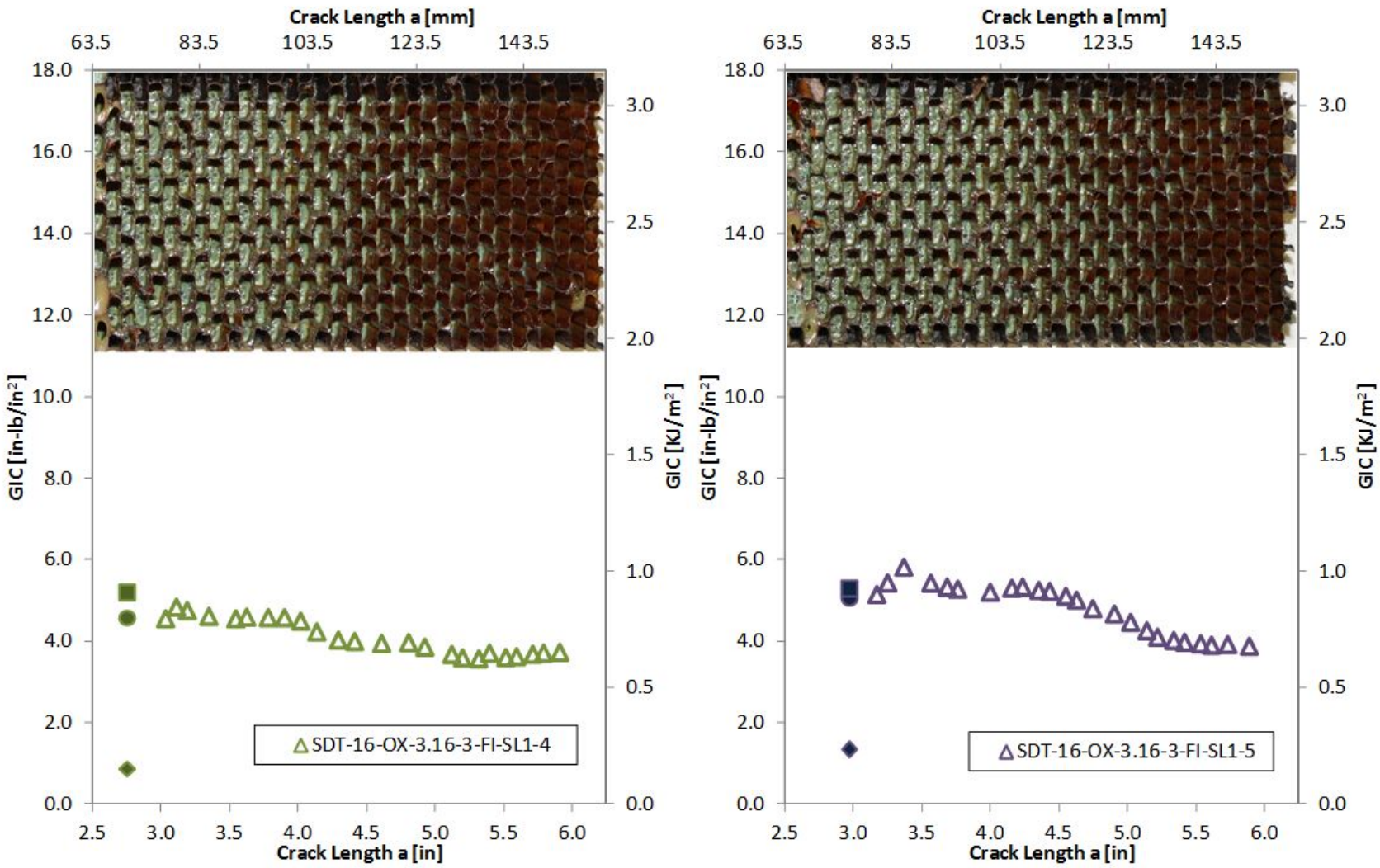

Figure E-10. Failure mode image and resistance curve of SDT-16-OX-3.16-3-FI-SL1-X # 4 and #5

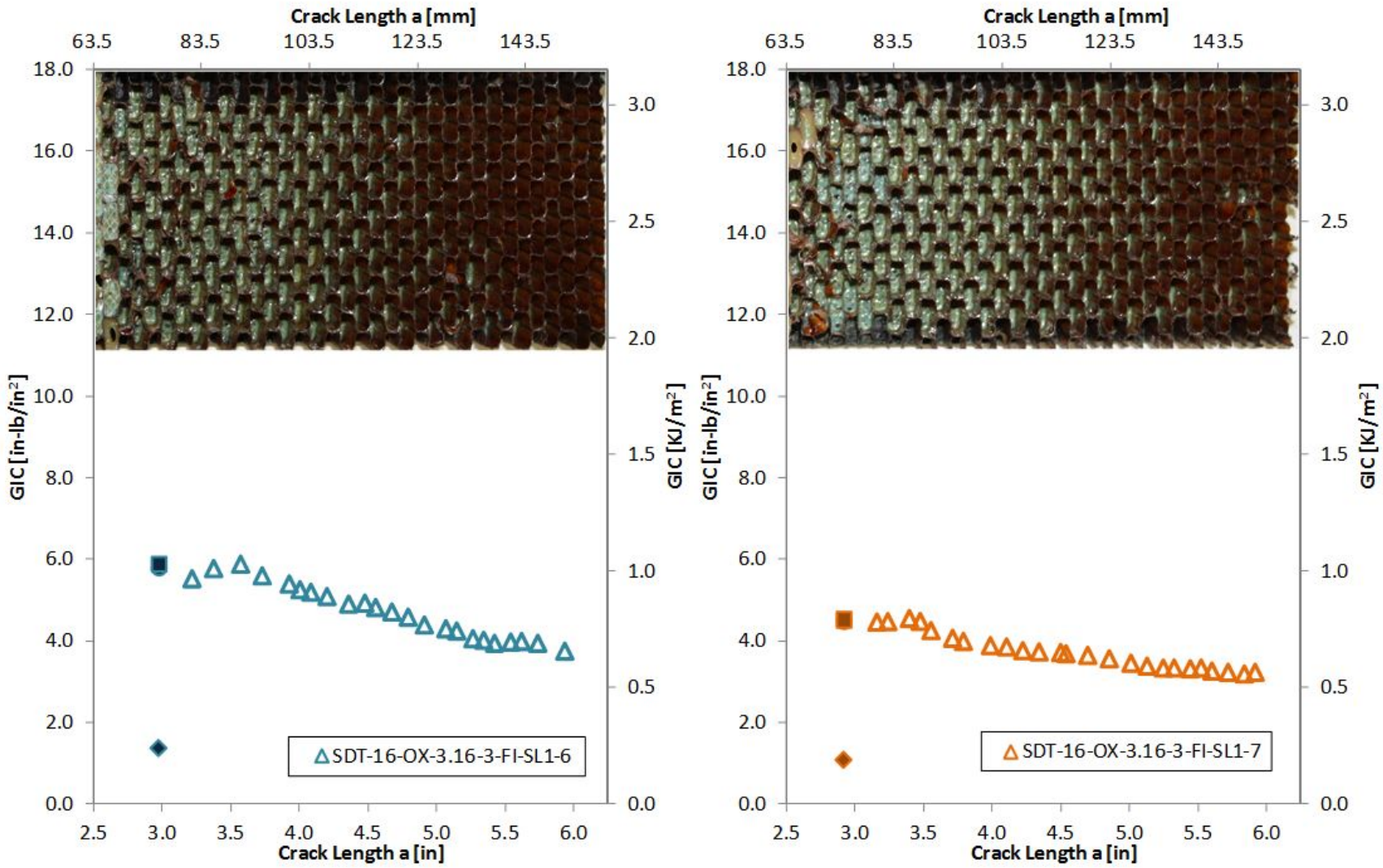

Figure E-11. Failure mode image and resistance curve of SDT-16-OX-3.16-3-FI-SL1-X # 6 and #7

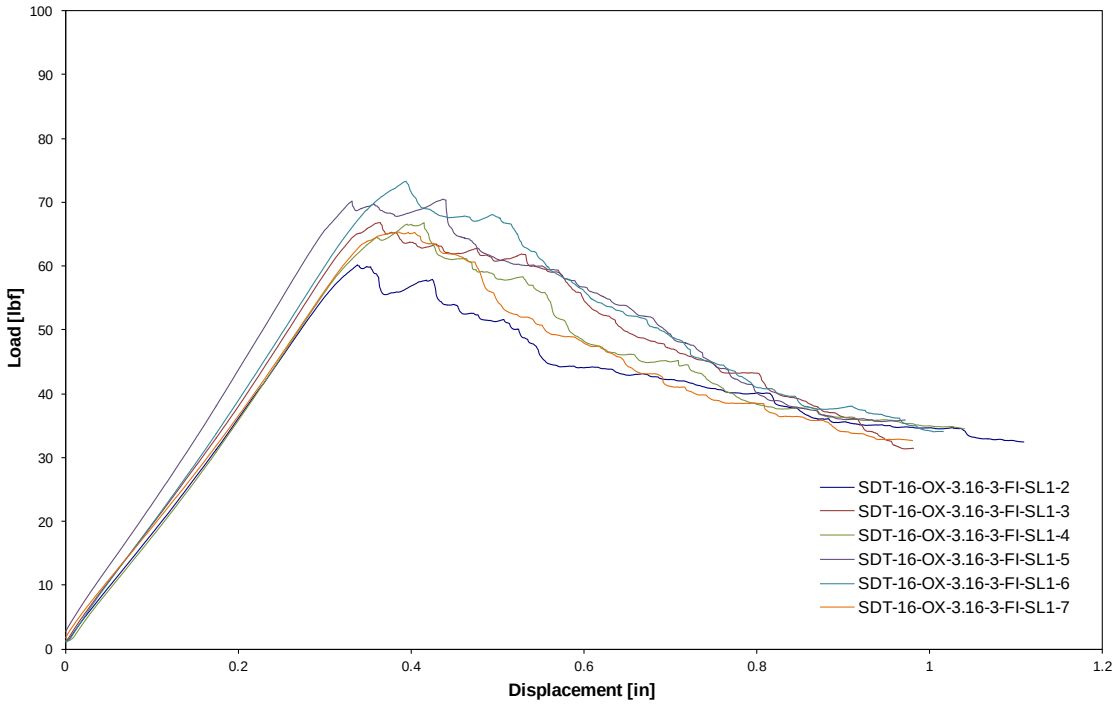

Figure E-12. Load vs. displacement curve for HRH-10/OX–3/16–3.0 fluid ingressed (2.5″ prescribed crack)

E.1.3 HRH-10/OX–3/16–3.0 EXTENDED FLUID-INGRESSED DATA

Table E-5. Test summary for HRH-10/OX–3/16–3.0 extended fluid ingressed (2.5″ prescribed crack) precrack

Specimen	GIC (in-lb/in^2)			GIC (KJ/m^2)			Failure Mode
	NL	VIS	5%/max	NL	VIS	5%/max	
SDT-16-OX-3.16-3-EFI-SL1-7	-	-	-	-	-	-	
SDT-16-OX-3.16-3-EFI-SL1-8	2.109	-	N/A	0.369	-	N/A	First row in A, second row a mix of A and C
AVERAGE GIC	2.109	-	-	0.369	-	-	
STANDARD DEVIATION	-	-	-	-	-	-	
COEFFICIENT OF VARIATION (%)	-	-	-	-	-	-	

Table E-6. Test summary for HRH-10/OX–3/16–3.0 extended fluid ingressed (2.5″ prescribed crack)

Specimen	GIC (in-lb/in^2)			GIC (KJ/m^2)			Failure Mode
	NL	VIS	5%/max	NL	VIS	5%/max	
SDT-16-OX-3.16-3-EFI-SL1-7	-	-	-	-	-	-	
SDT-16-OX-3.16-3-EFI-SL1-8	1.149	-	5.022	0.201	-	0.879	Primarily in C
AVERAGE GIC	1.149	-	5.022	0.201	-	0.879	
STANDARD DEVIATION	-	-	-	-	-	-	
COEFFICIENT OF VARIATION (%)	-	-	-	-	-	-	

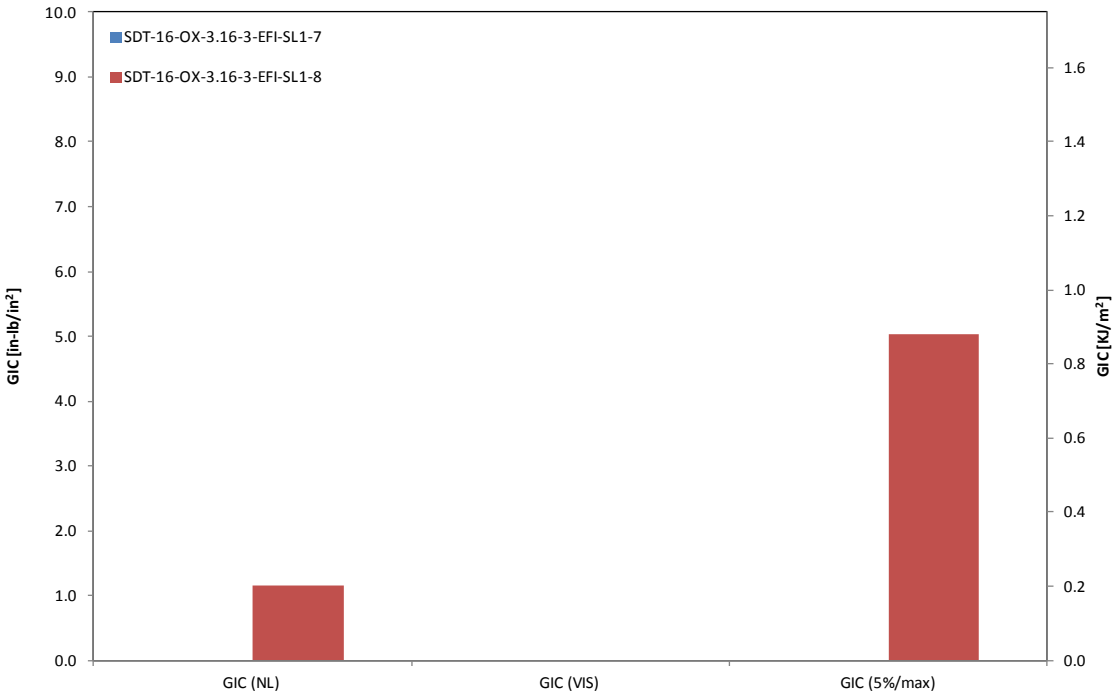

Figure E-13. GIC for HRH-10/OX–3/16–3.0 extended fluid ingressed (2.5″ prescribed crack)

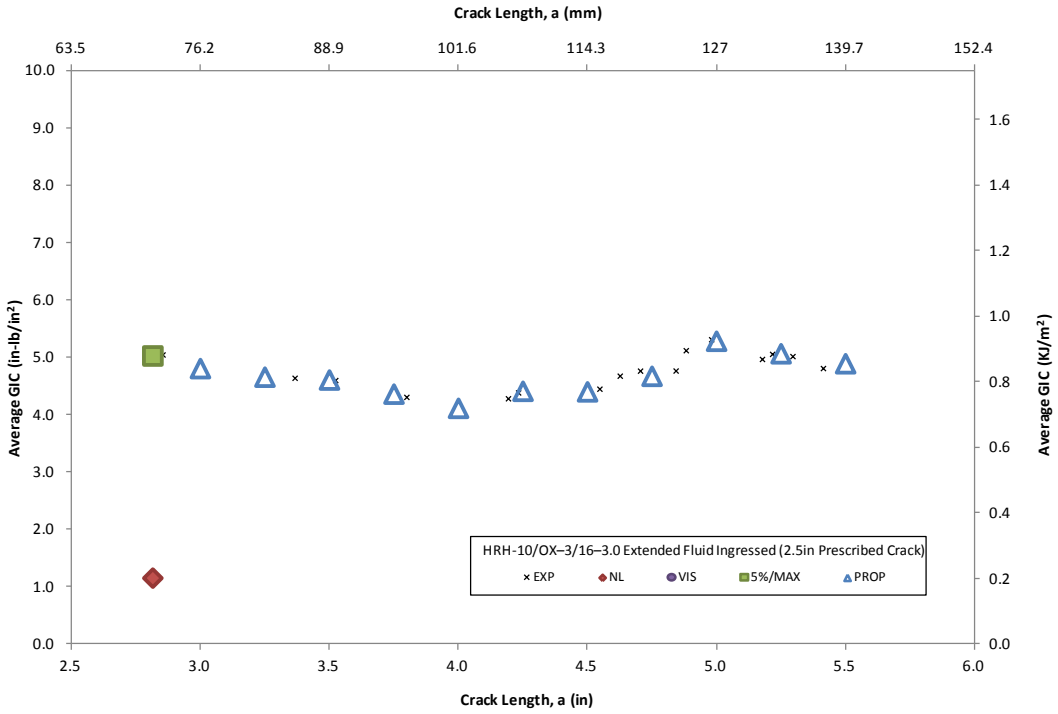

Figure E-14. Resistance curve for HRH-10/OX–3/16–3.0 extended fluid ingressed (2.5″ prescribed crack)

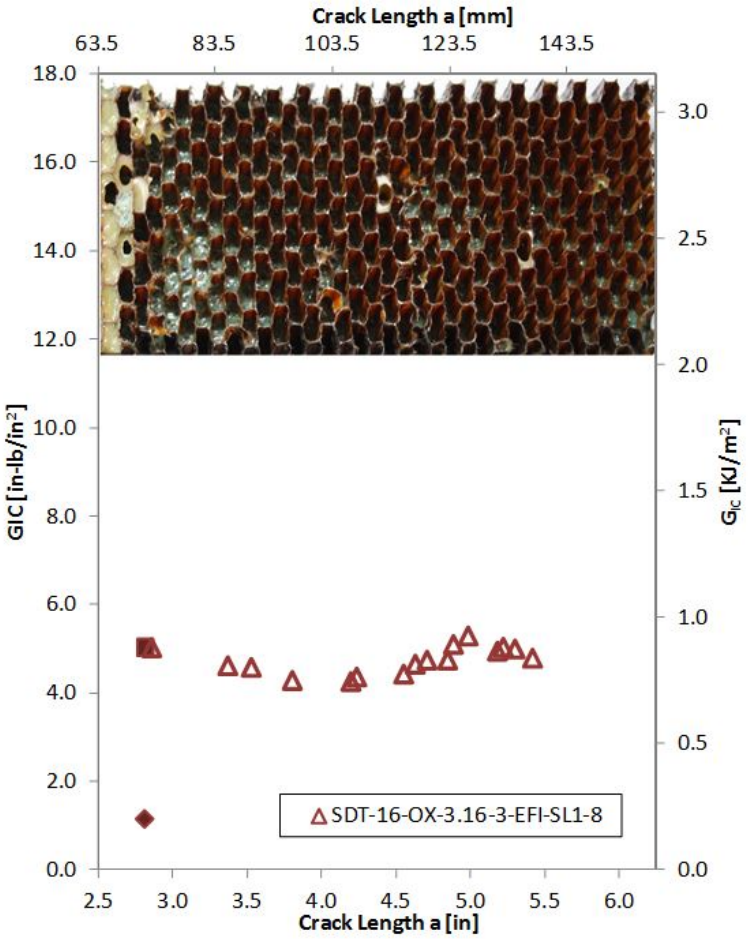

Figure E-15. Failure mode image and resistance curve of SDT-16-OX-3.16-3-EFI-SL1-X #8

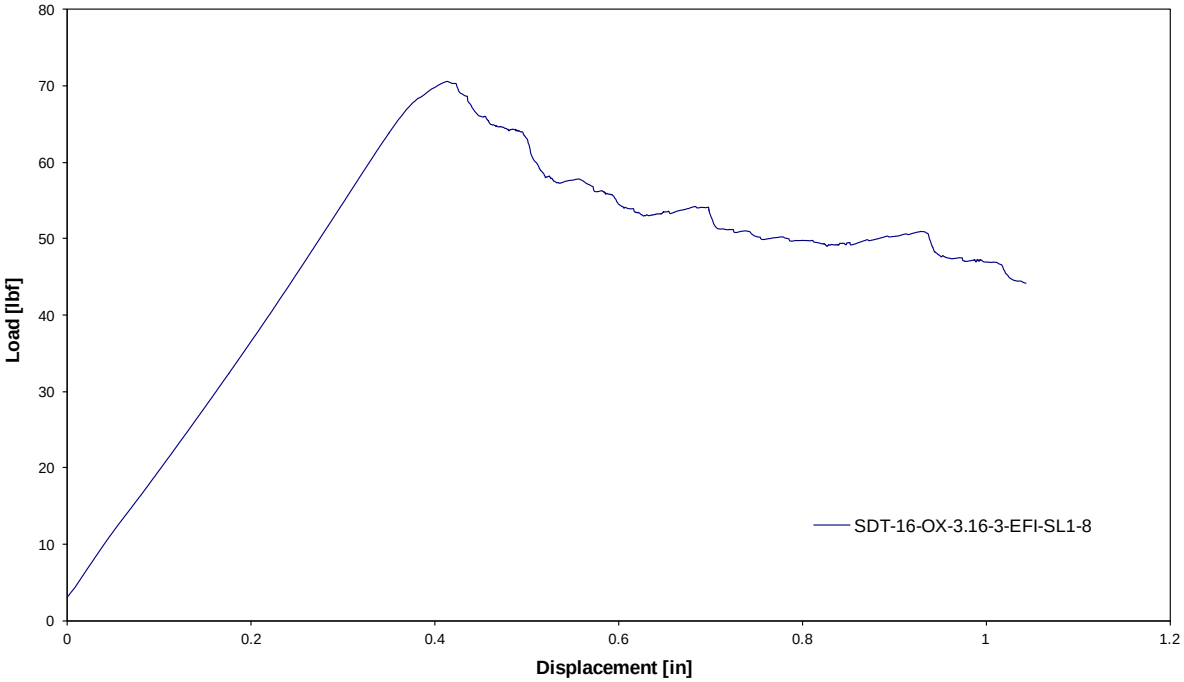

Figure E-16. Load vs. displacement curve for HRH-10/OX–3/16–3.0 extended fluid ingressed (2.5″ prescribed crack)

E.1.4 HRH-10/OX–3/16–3.0 WATER-INGRESSED DATA

Table E-7. Test summary for HRH-10/OX–3/16–3.0 water ingressed (2.5″ prescribed crack) precrack

Specimen	GIC (in-lb/in^2)			GIC (KJ/m^2)			Failure Mode
	NL	VIS	5%/max	NL	VIS	5%/max	
SDT-16-OX-3.16-3-H2O-SL1-7	3.013	-	4.091	0.528	-	0.716	Primarily in C
SDT-16-OX-3.16-3-H2O-SL1-8	1.477	-	2.207	0.259	-	0.387	Primarily in C
SDT-16-OX-3.16-3-H2O-SLX-7	1.598	-	3.053	0.280	-	0.535	Primarily in C
SDT-16-OX-3.16-3-H2O-SLX-8	1.663	-	2.712	0.291	-	0.475	Primarily in C
AVERAGE GIC	1.938	-	3.016	0.339	-	0.528	
STANDARD DEVIATION	0.721	-	0.796	0.126	-	0.139	
COEFFICIENT OF VARIATION (%)	37.205	-	26.406	37.205	-	26.406	

Table E-8. Test summary for HRH-10/OX–3/16–3.0 water ingressed (2.5″ prescribed crack)

Specimen	GIC (in-lb/in^2)			GIC (KJ/m^2)			Failure Mode
	NL	VIS	5%/max	NL	VIS	5%/max	
SDT-16-OX-3.16-3-H2O-SL1-7	1.647	-	4.848	0.288	-	0.849	Primarily in C
SDT-16-OX-3.16-3-H2O-SL1-8	1.901	-	4.635	0.333	-	0.812	Primarily in C
SDT-16-OX-3.16-3-H2O-SLX-7	2.003	-	5.093	0.351	-	0.892	Primarily in C
SDT-16-OX-3.16-3-H2O-SLX-8	1.845	-	4.394	0.323	-	0.770	Primarily in C
AVERAGE GIC	1.849	-	4.743	0.324	-	0.831	
STANDARD DEVIATION	0.150	-	0.298	0.026	-	0.052	
COEFFICIENT OF VARIATION (%)	8.104	-	6.285	8.104	-	6.285	

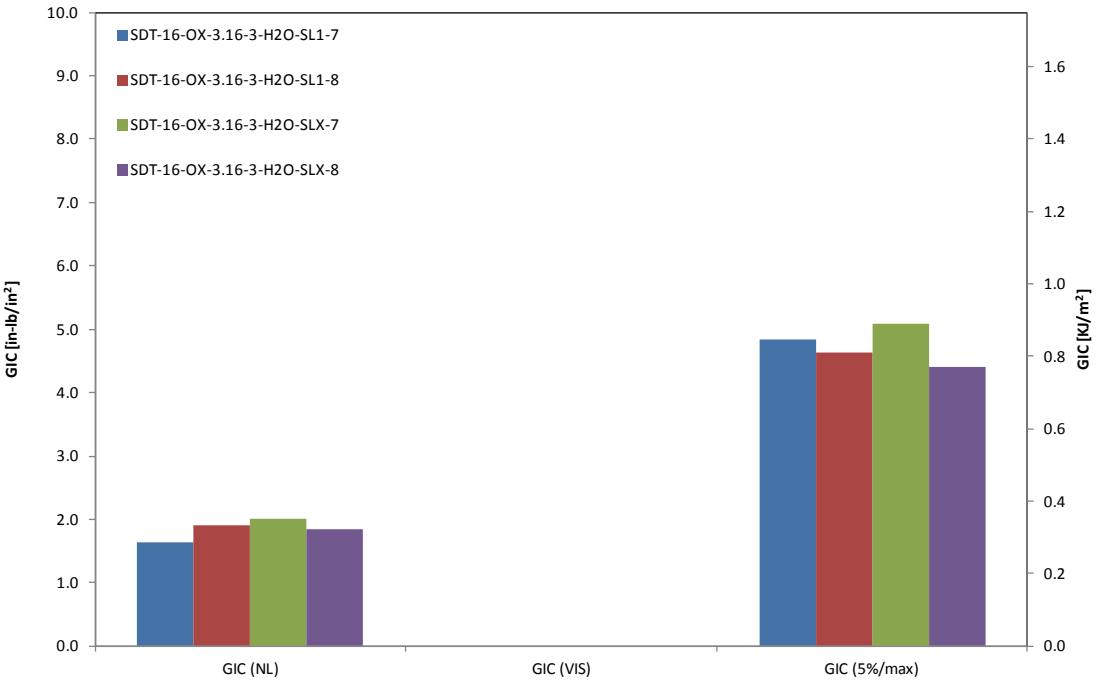

Figure E-17. GIC for HRH-10/OX–3/16–3.0 water ingressed (2.5″ prescribed crack)

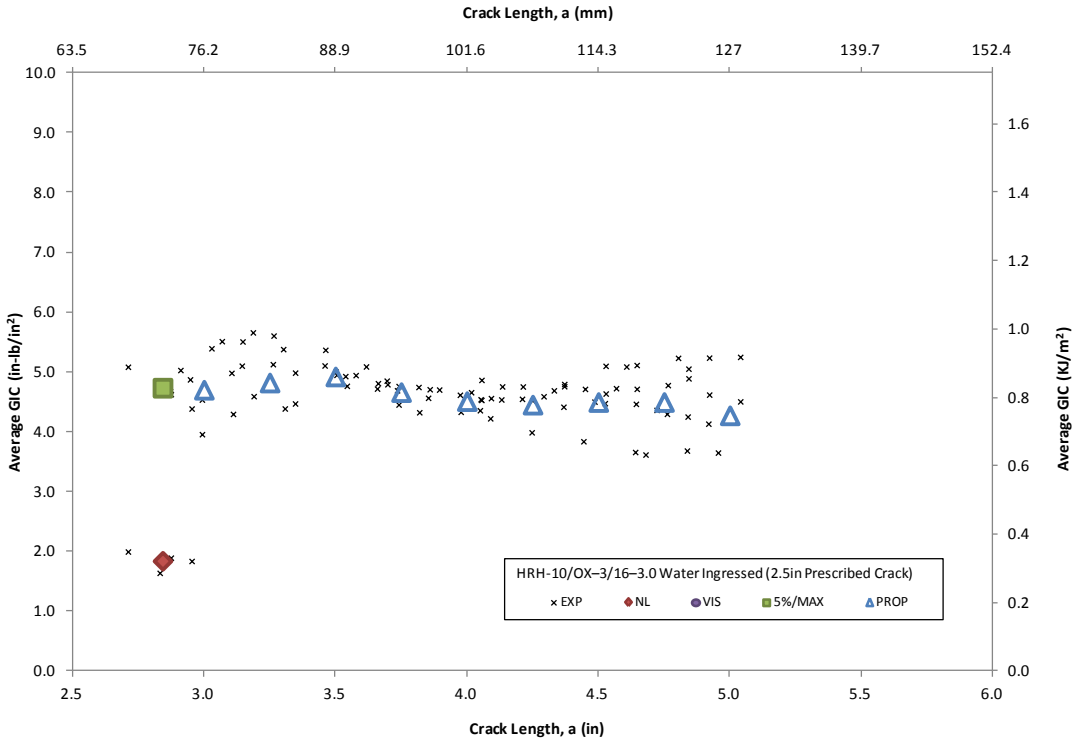

Figure E-18. Resistance curve for HRH-10/OX–3/16–3.0 water ingressed (2.5″ prescribed crack)

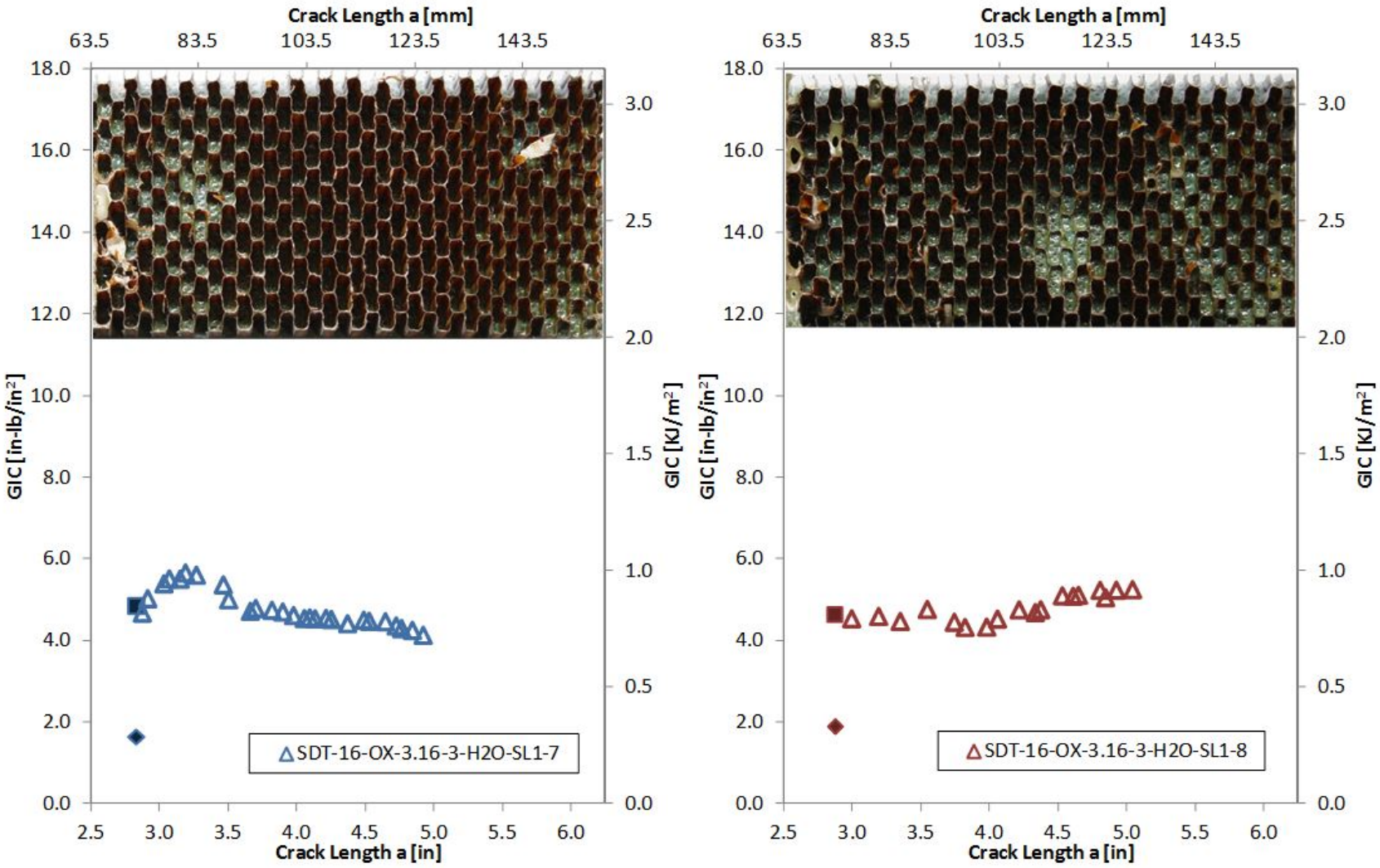

Figure E-19. Failure mode image and resistance curve of SDT-16-OX-3.16-3-H2O-SL1-X #7 and #8

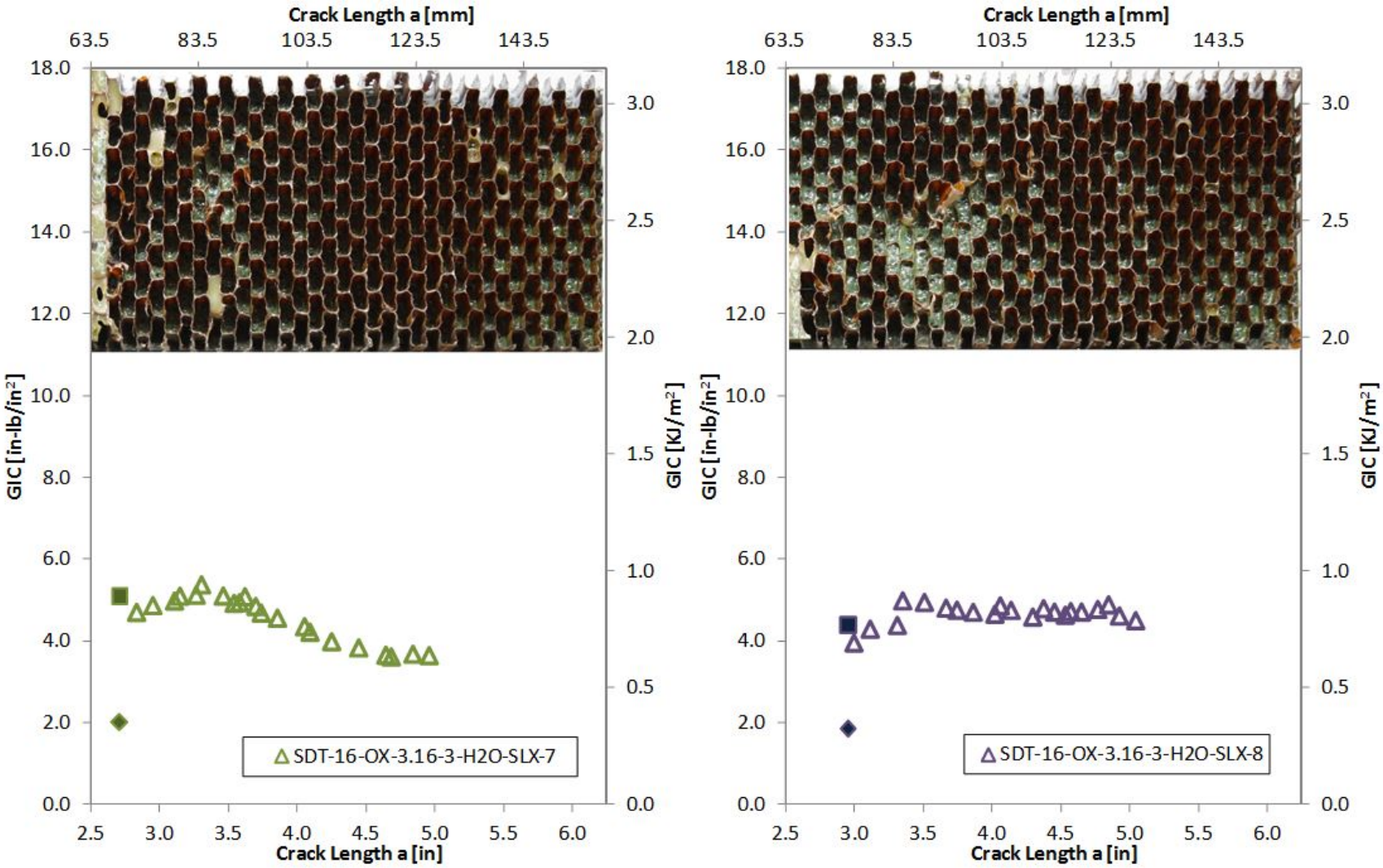

Figure E-20. Failure mode image and resistance curve of SDT-16-OX-3.16-3-H2O-SLX-X #7 and #8

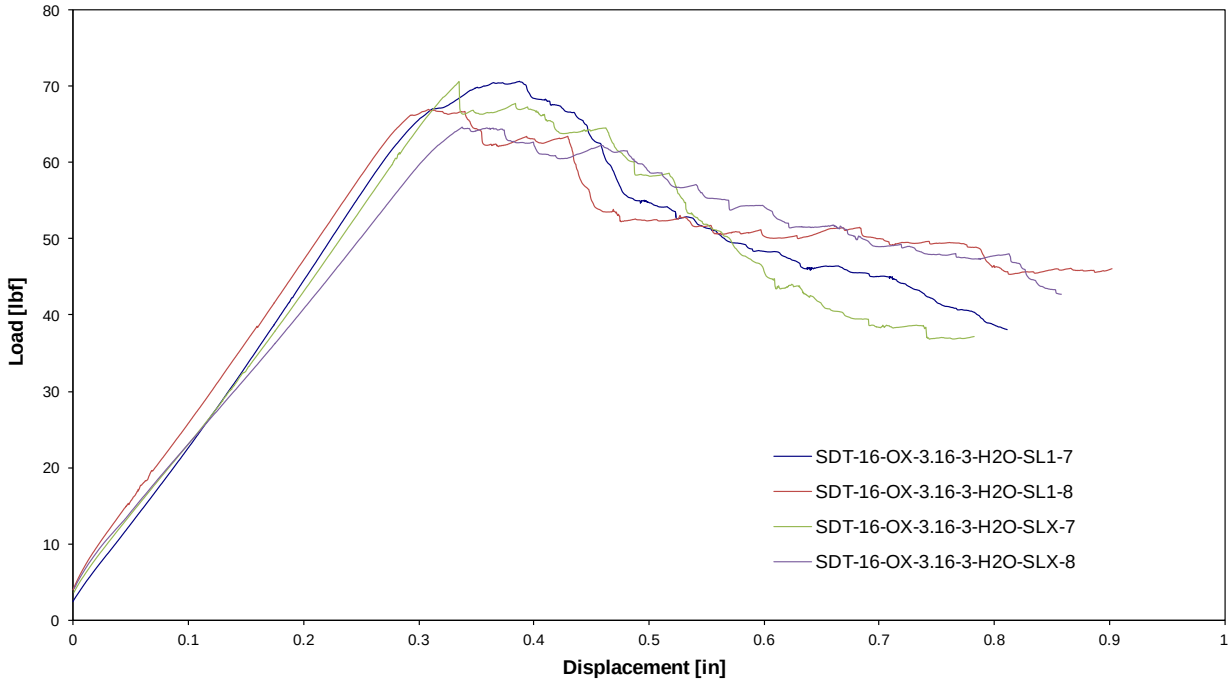

Figure E-21. Load vs. displacement curve for HRH-10/OX–3/16–3.0 water ingressed (2.5″ prescribed crack)

APPENDIX F—STATIC RESULTS FOR SUPPLEMENTAL TESTING OF DOUBLE-CANTILEVER BEAMS (DCB) AND FLATWISE TENSION (FWT) SPECIMENS

Note that DCB specimens were tested at two temperatures (room and elevated) and two environmental conditions (baseline and fluid ingressed).

F.1 DOUBLE CANTILEVER BEAM (DCB) DATA

F.1.1 LAMINATE DATA

F.1.1.1 Laminate RTD Baseline Data

Table F-1. Test summary for laminate RTD baseline precrack

Specimen	GIC (in-lb/in^2)			GIC (KJ/m^2)		
	NL	VIS	5%/max	NL	VIS	5%/max
SDT-LM-BL-RTD-SL1-1	1.315	-	1.985	0.230	-	0.348
SDT-LM-BL-RTD-SL1-2	0.844	-	1.393	0.148	-	0.244
SDT-LM-BL-RTD-SL1-3	0.754	-	1.579	0.132	-	0.277
SDT-LM-BL-RTD-SL1-4	1.002	1.917	1.943	0.175	0.336	0.340
SDT-LM-BL-RTD-SL1-5	0.884	-	2.031	0.155	-	0.356
SDT-LM-BL-RTD-SL1-6	1.590	1.782	2.482	0.278	0.312	0.435
AVERAGE GIC	1.065	1.850	1.902	0.186	0.324	0.333
STANDARD DEVIATION	0.322	0.096	0.381	0.056	0.017	0.067
COEFFICIENT OF VARIATION (%)	30.287	5.181	20.016	30.287	5.181	20.016

Table F-2. Test summary for laminate RTD baseline

Specimen	GIC (in-lb/in^2)			GIC (KJ/m^2)		
	NL	VIS	5%/max	NL	VIS	5%/max
SDT-LM-BL-RTD-SL1-1	1.489	3.118	3.456	0.261	0.546	0.605
SDT-LM-BL-RTD-SL1-2	2.635	-	2.784	0.461	-	0.488
SDT-LM-BL-RTD-SL1-3	1.835	-	2.864	0.321	-	0.502
SDT-LM-BL-RTD-SL1-4	1.230	3.294	3.379	0.215	0.577	0.592
SDT-LM-BL-RTD-SL1-5	2.196	-	2.866	0.385	-	0.502
SDT-LM-BL-RTD-SL1-6	2.223	-	2.820	0.389	-	0.494
AVERAGE GIC	1.935	3.206	3.028	0.339	0.561	0.530
STANDARD DEVIATION	0.519	0.124	0.304	0.091	0.022	0.053
COEFFICIENT OF VARIATION (%)	26.821	3.863	10.041	26.821	3.863	10.041

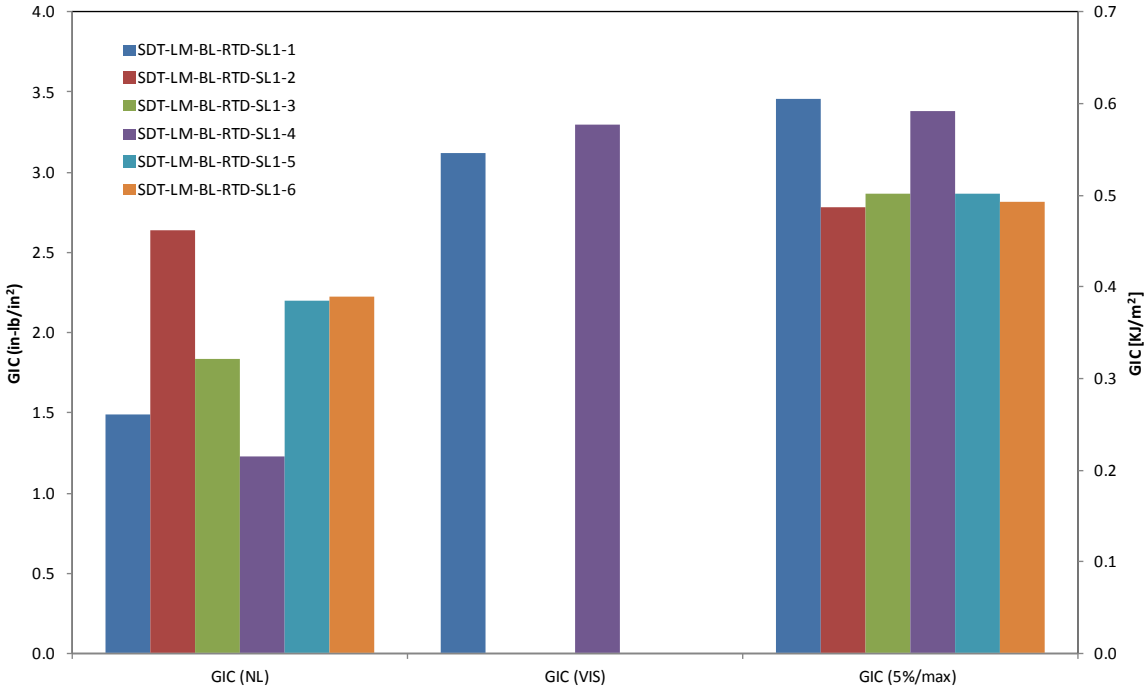

Figure F-1. GIC for laminate RTD baseline

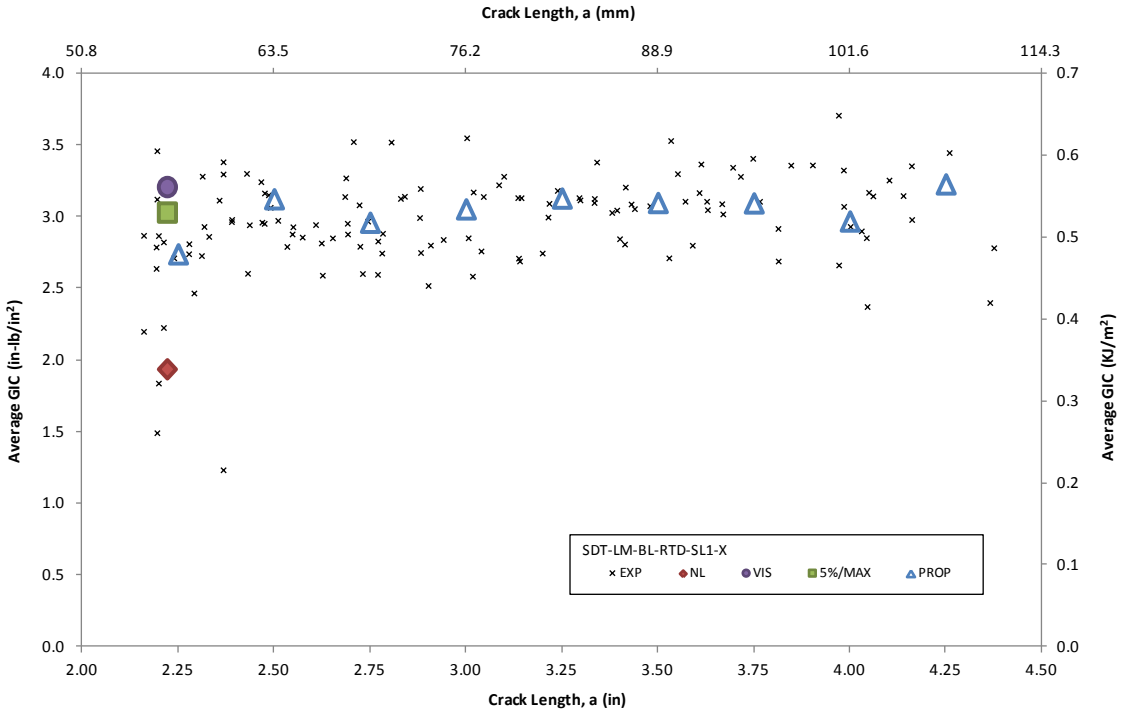

Figure F-2. Resistance curve for laminate RTD baseline

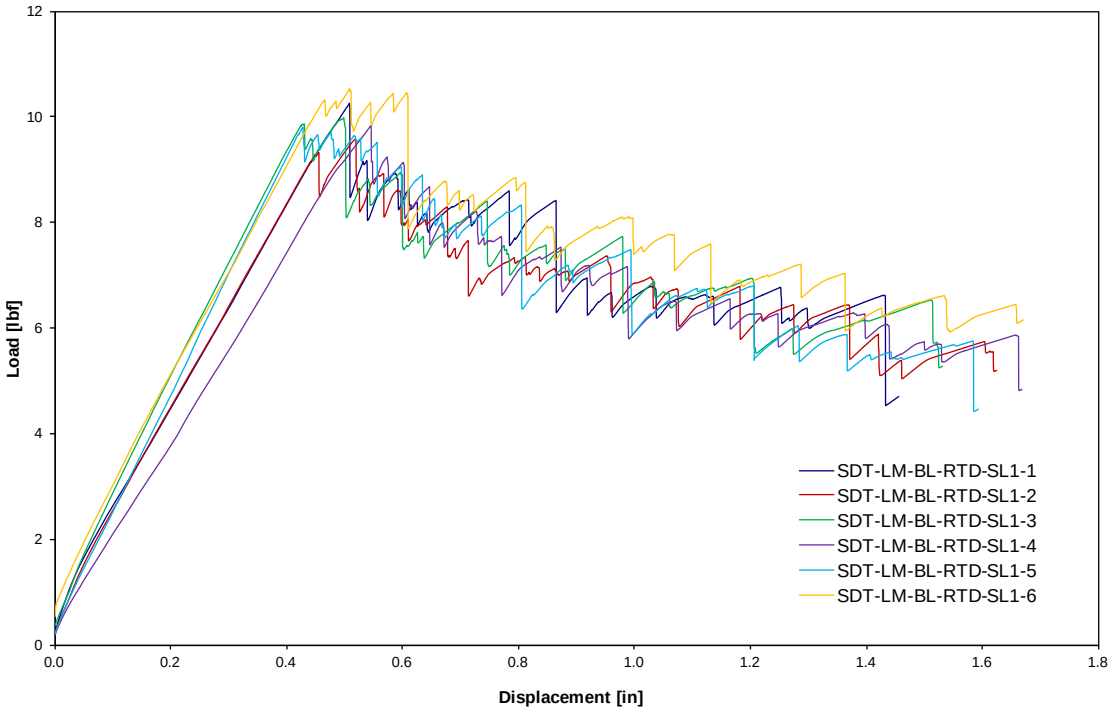

Figure F-3. Load vs. displacement curve for laminate RTD baseline

F.1.1.2 Laminate RTW Fluid-Ingressed Data

Table F-3. Test Summary for laminate RTW fluid-ingressed precrack

Specimen	GIC (in-lb/in^2)			GIC (KJ/m^2)		
	NL	VIS	5%/max	NL	VIS	5%/max
SDT-LM-FI-RTW-SL1-2	0.866	-	1.249	0.152	-	0.219
SDT-LM-FI-RTW-SL1-3	0.956	-	1.057	0.167	-	0.185
SDT-LM-FI-RTW-SL1-4	0.964	-	1.135	0.169	-	0.199
SDT-LM-FI-RTW-SL1-5	0.927	-	1.308	0.162	-	0.229
SDT-LM-FI-RTW-SL1-6	0.682	-	0.911	0.120	-	0.160
SDT-LM-FI-RTW-SL1-7	0.803	-	1.199	0.141	-	0.210
AVERAGE GIC	0.866	-	1.143	0.152	-	0.200
STANDARD DEVIATION	0.109	-	0.143	0.019	-	0.025
COEFFICIENT OF VARIATION (%)	12.550	-	12.536	12.550	-	12.536

Table F-4. Test summary for laminate RTW fluid ingressed

Specimen	GIC (in-lb/in^2)			GIC (KJ/m^2)		
	NL	VIS	5%/max	NL	VIS	5%/max
SDT-LM-FI-RTW-SL1-2	1.976	2.783	3.111	0.346	0.487	0.545
SDT-LM-FI-RTW-SL1-3	1.772	-	2.292	0.310	-	0.401
SDT-LM-FI-RTW-SL1-4	1.444	2.361	2.561	0.253	0.414	0.448
SDT-LM-FI-RTW-SL1-5	2.282	-	2.872	0.400	-	0.503
SDT-LM-FI-RTW-SL1-6	1.822	-	2.125	0.319	-	0.372
SDT-LM-FI-RTW-SL1-7	1.473	-	1.939	0.258	-	0.340
AVERAGE GIC	1.795	2.572	2.483	0.314	0.450	0.435
STANDARD DEVIATION	0.315	0.298	0.450	0.055	0.052	0.079
COEFFICIENT OF VARIATION (%)	17.576	11.594	18.118	17.576	11.594	18.118

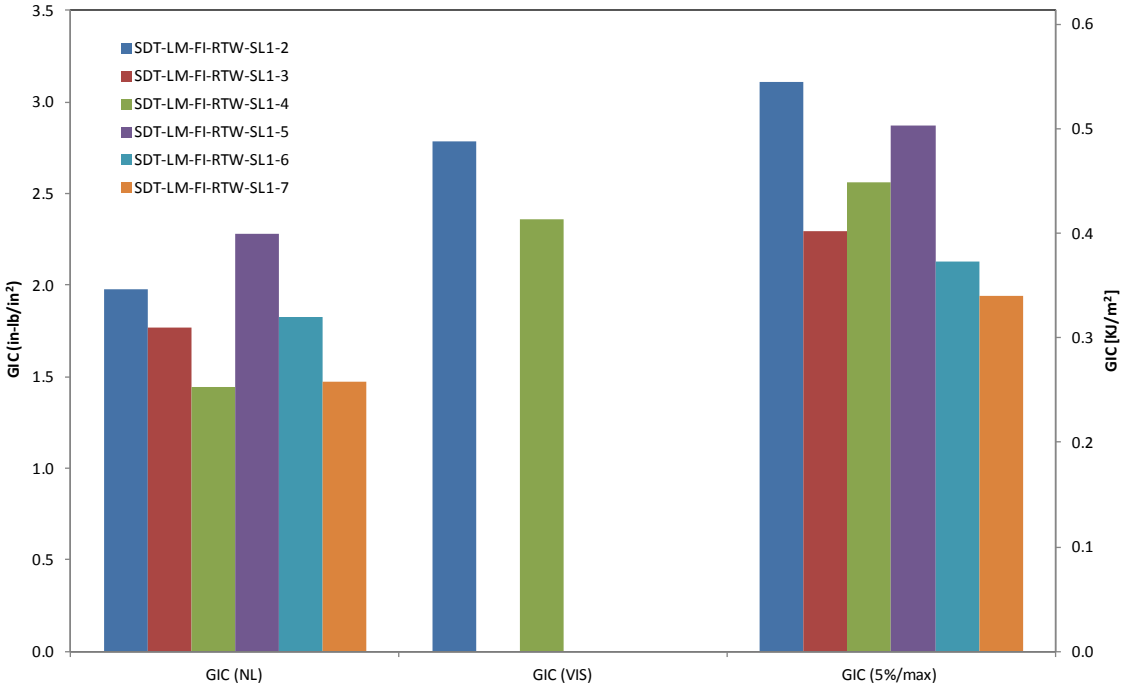

Figure F-4. GIC for laminate RTW fluid ingressed

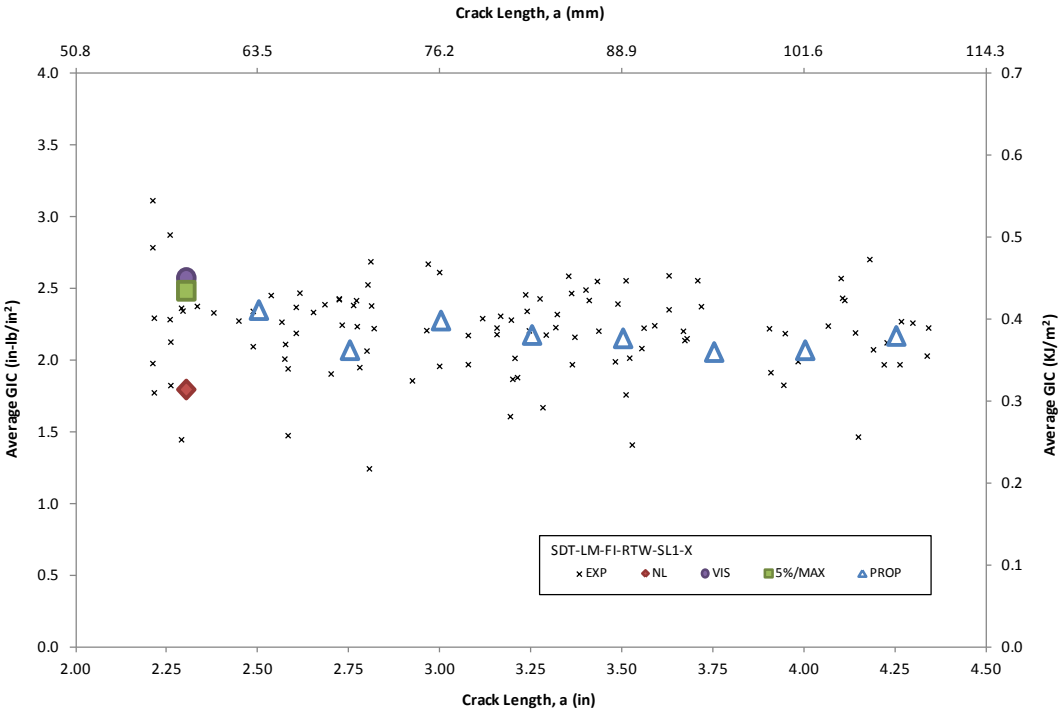

Figure F-5. Resistance curve for laminate RTW fluid ingressed

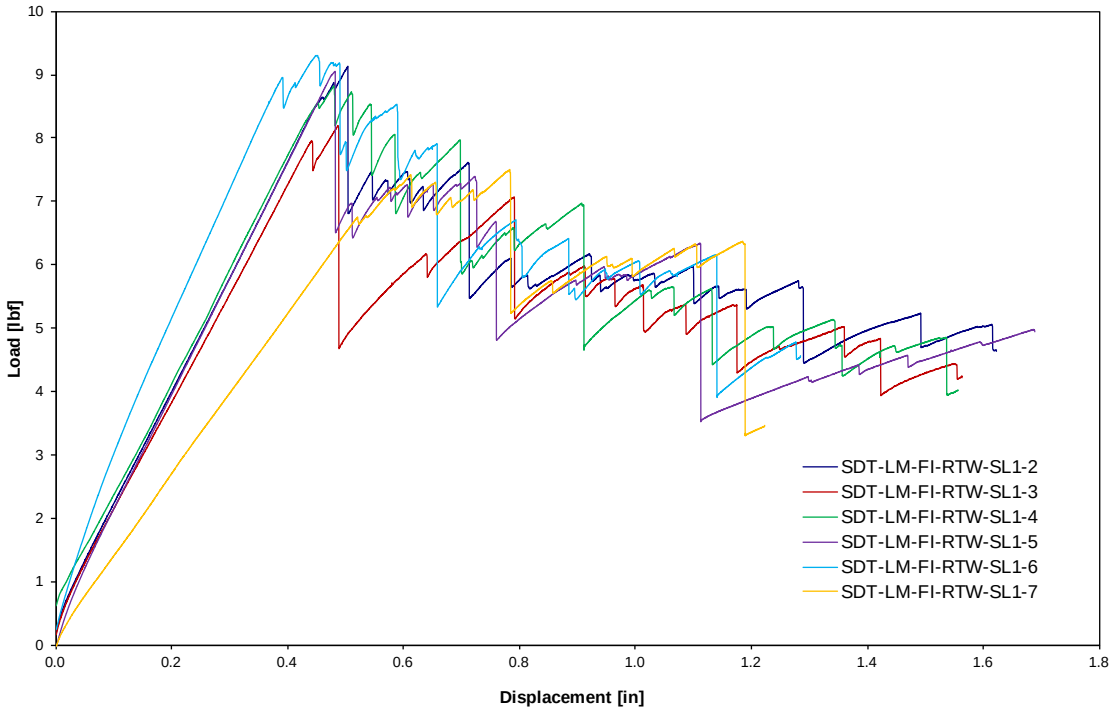

Figure F-6. Load vs. displacement curve for laminate RTW fluid ingressed

F.1.1.3 Laminate ETD Baseline Data

Table F-5. Test summary for laminate ETD baseline precrack

Specimen	GIC (in-lb/in^2)			GIC (KJ/m^2)		
	NL	VIS	5%/max	NL	VIS	5%/max
SDT-LM-BL-ETD-SL1-2	1.020	-	1.457	0.179	-	0.255
SDT-LM-BL-ETD-SL1-3	0.772	-	1.099	0.135	-	0.193
SDT-LM-BL-ETD-SL1-4	0.790	-	0.962	0.138	-	0.168
SDT-LM-BL-ETD-SL1-5	1.136	-	0.000	0.199	-	0.000
SDT-LM-BL-ETD-SL1-6	0.935	-	1.975	0.164	-	0.346
SDT-LM-BL-ETD-SL1-7	1.250	-	1.931	0.219	-	0.338
AVERAGE GIC	0.984	-	1.237	0.172	-	0.217
STANDARD DEVIATION	0.190	-	0.735	0.033	-	0.129
COEFFICIENT OF VARIATION (%)	19.290	-	59.379	19.290	-	59.379

Table F-6. Test Summary for Laminate ETD Baseline

Specimen	GIC (in-lb/in^2)			GIC (KJ/m^2)		
	NL	VIS	5%/max	NL	VIS	5%/max
SDT-LM-BL-ETD-SL1-2	0.803	-	2.184	0.141	-	0.382
SDT-LM-BL-ETD-SL1-3	1.269	-	2.480	0.222	-	0.434
SDT-LM-BL-ETD-SL1-4	1.509	-	2.131	0.264	-	0.373
SDT-LM-BL-ETD-SL1-5	1.386	-	1.886	0.243	-	0.330
SDT-LM-BL-ETD-SL1-6	1.918	-	2.133	0.336	-	0.373
SDT-LM-BL-ETD-SL1-7	0.900	-	2.153	0.158	-	0.377
AVERAGE GIC	1.298	-	2.161	0.227	-	0.378
STANDARD DEVIATION	0.410	-	0.190	0.072	-	0.033
COEFFICIENT OF VARIATION (%)	31.587	-	8.775	31.587	-	8.775

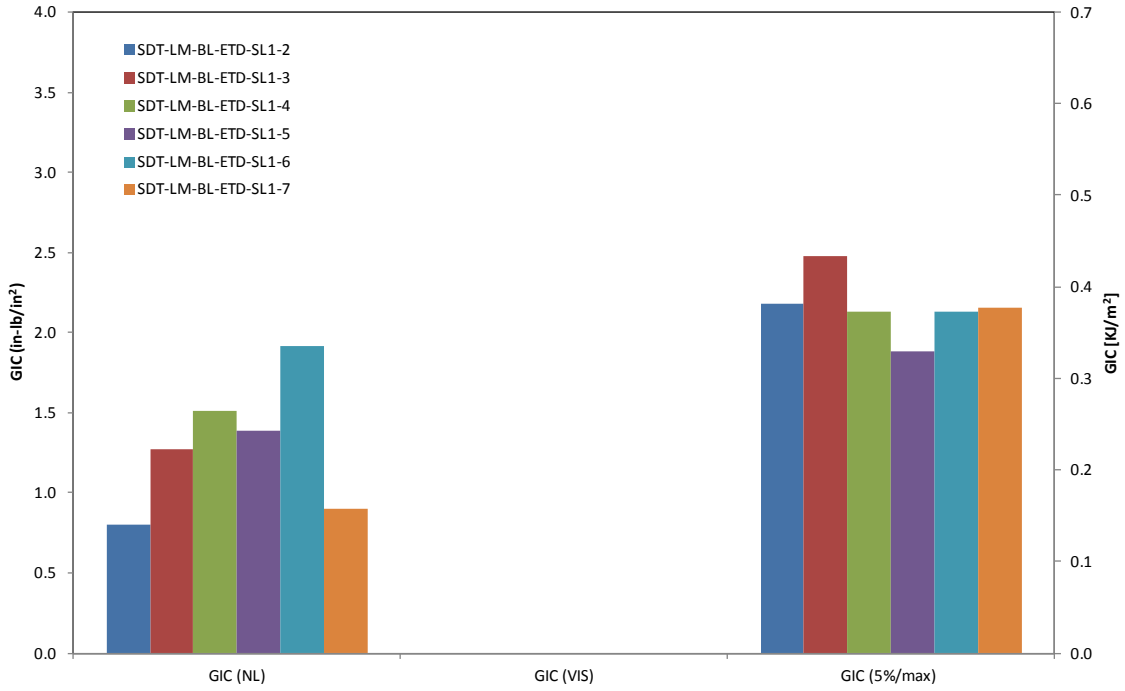

Figure F-7. GIC for laminate ETD baseline

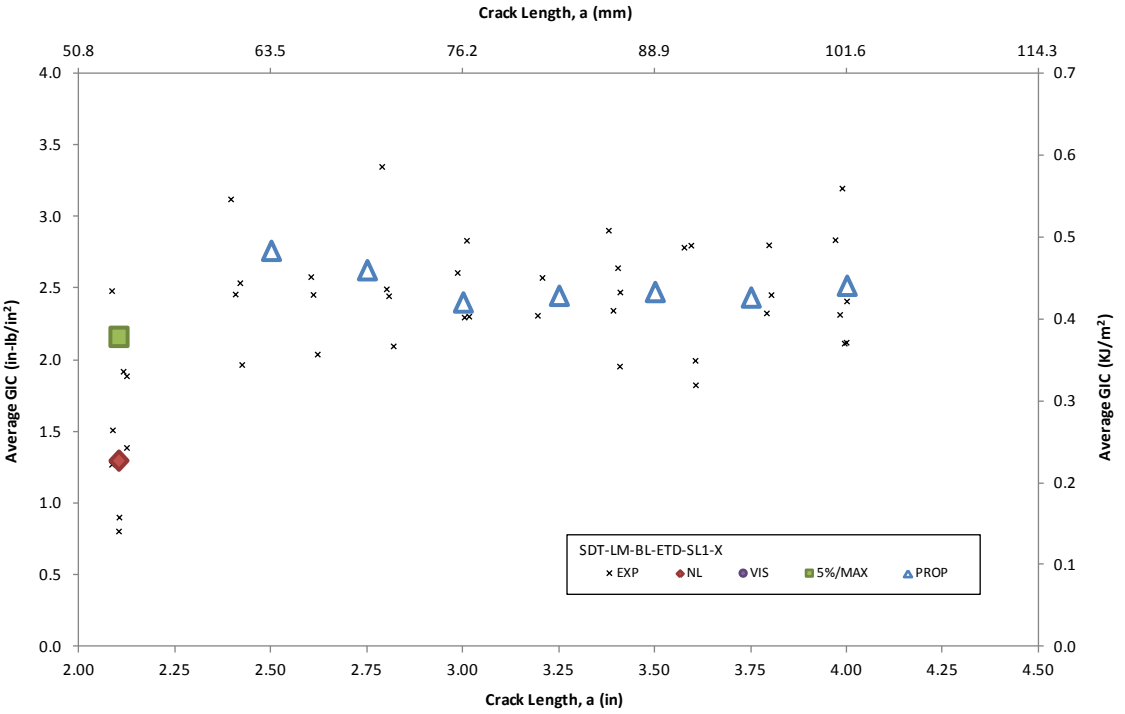

Figure F-8. Resistance curve for laminate ETD baseline

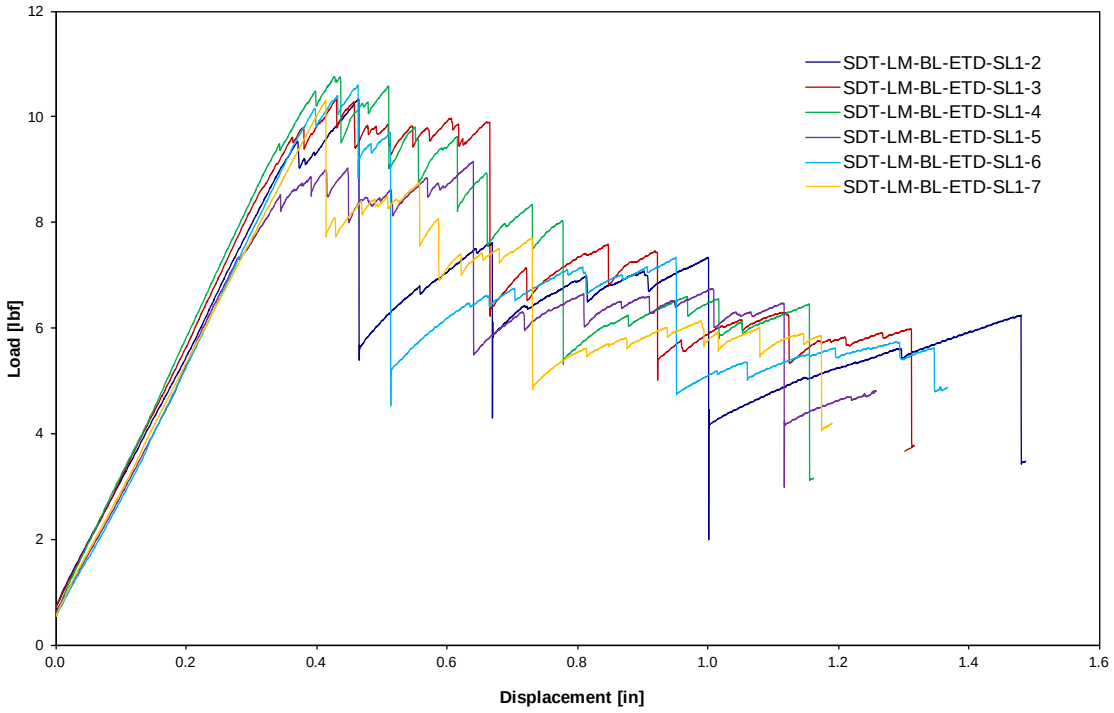

Figure F-9. Load vs. displacement curve for laminate ETD baseline

F.1.1.4 Laminate ETW Fluid-Ingressed Data

Table F-7. Test summary for laminate ETW fluid-ingressed precrack

Specimen	GIC (in-lb/in^2)			GIC (KJ/m^2)		
	NL	VIS	5%/max	NL	VIS	5%/max
SDT-LM-FI-ETW-SL1-1	1.348	-	1.693	0.236	-	0.296
SDT-LM-FI-ETW-SL1-2	0.864	-	1.430	0.151	-	0.250
SDT-LM-FI-ETW-SL1-3	0.631	-	1.042	0.110	-	0.183
SDT-LM-FI-ETW-SL1-4	0.827	-	1.852	0.145	-	0.324
SDT-LM-FI-ETW-SL1-5	-	-	1.452	-	-	0.254
AVERAGE GIC	0.917	-	1.494	0.161	-	0.262
STANDARD DEVIATION	0.305	-	0.307	0.053	-	0.054
COEFFICIENT OF VARIATION (%)	33.213	-	20.557	33.213	-	20.557

Table F-8. Test Summary for laminate ETW fluid ingressed

Specimen	GIC (in-lb/in^2)			GIC (KJ/m^2)		
	NL	VIS	5%/max	NL	VIS	5%/max
SDT-LM-FI-ETW-SL1-1	0.054	-	0.067	0.009	-	0.012
SDT-LM-FI-ETW-SL1-2	1.416	-	2.873	0.248	-	0.503
SDT-LM-FI-ETW-SL1-3	1.616	-	2.318	0.283	-	0.406
SDT-LM-FI-ETW-SL1-4	1.587	-	3.174	0.278	-	0.556
SDT-LM-FI-ETW-SL1-5	1.782	-	2.036	0.312	-	0.357
AVERAGE GIC	1.291	-	2.094	0.226	-	0.367
STANDARD DEVIATION	0.704	-	1.218	0.123	-	0.213
COEFFICIENT OF VARIATION (%)	54.494	-	58.189	54.494	-	58.189

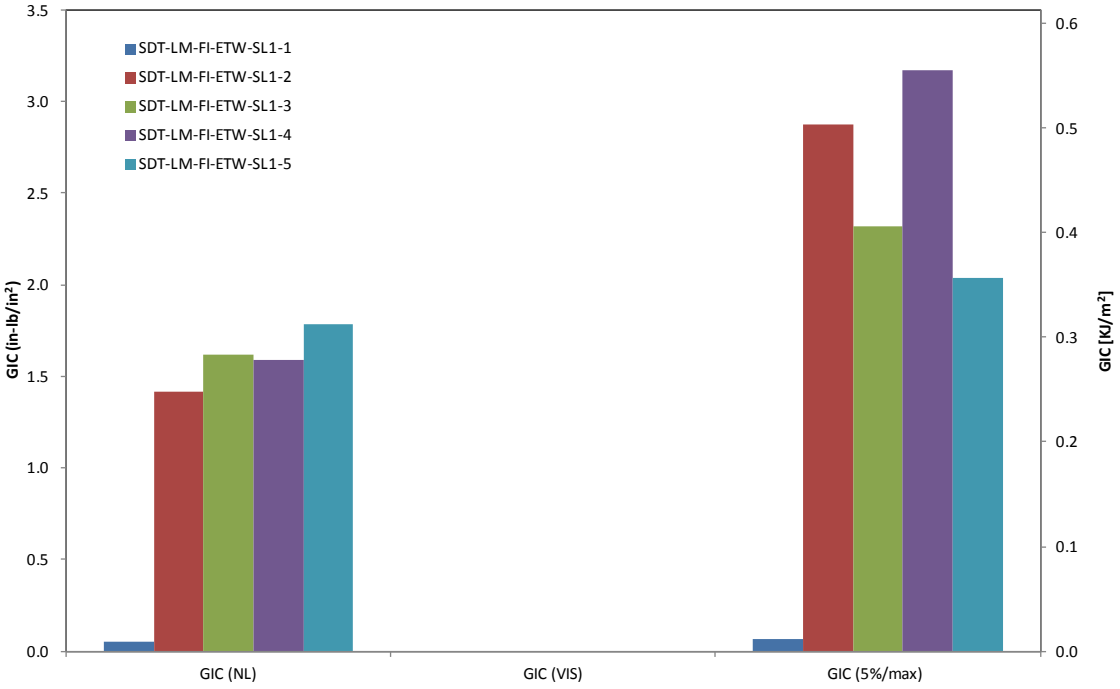

Figure F-10. GIC for laminate ETW fluid ingressed

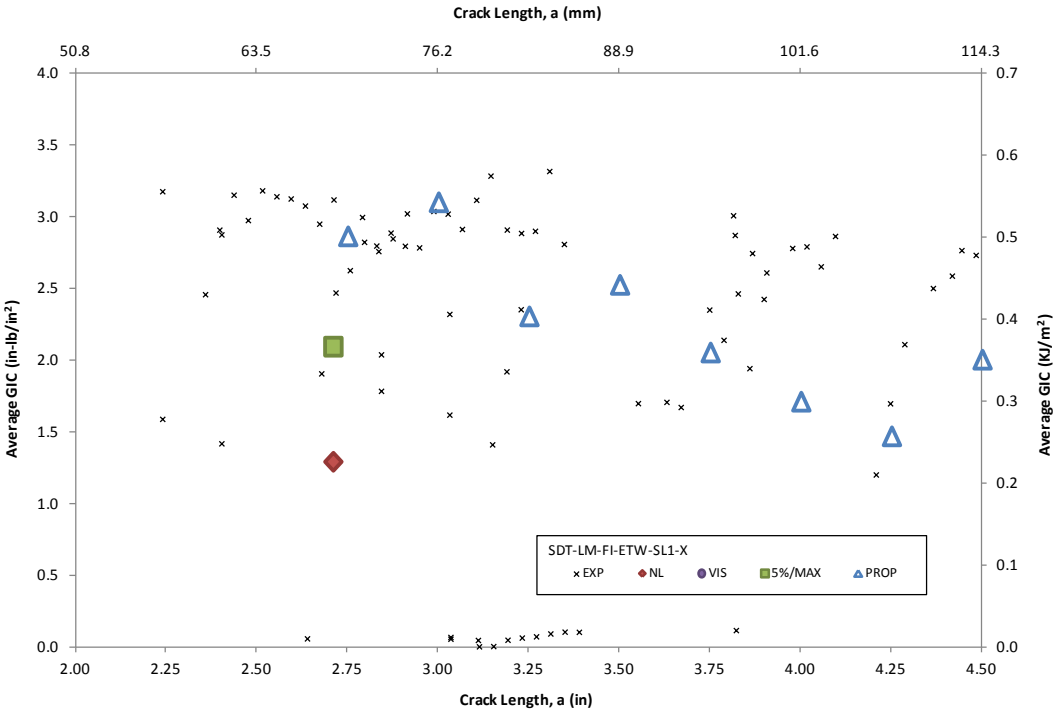

Figure F-11. Resistance curve for laminate ETW fluid ingressed

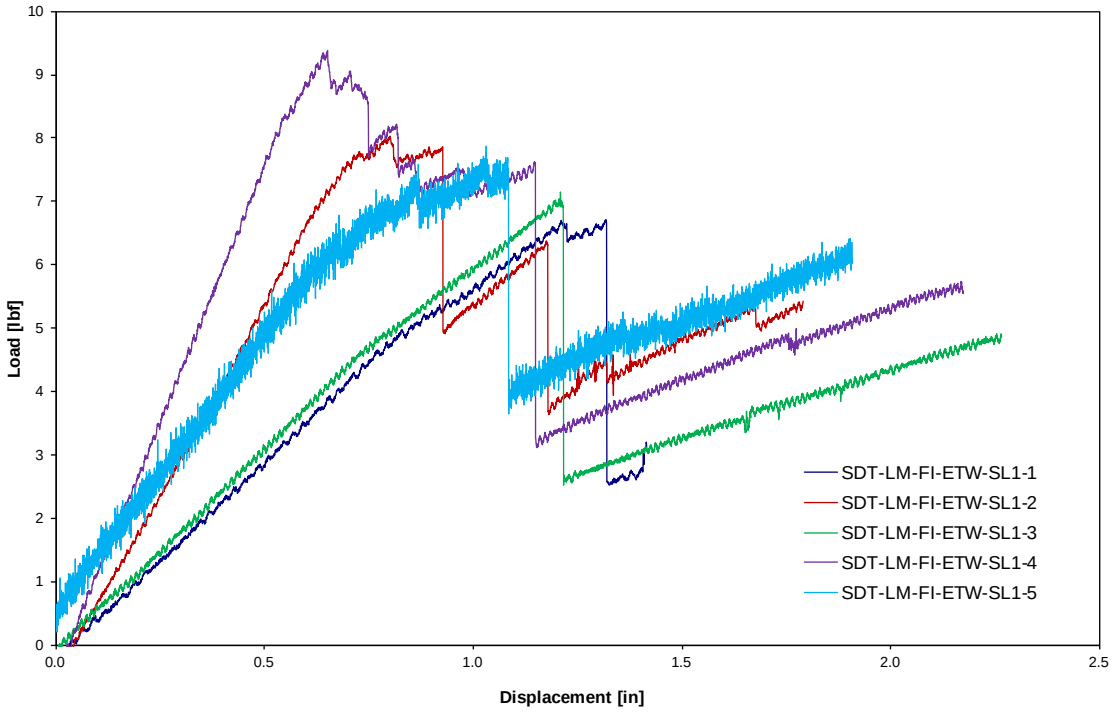

Figure F-12. Load vs. displacement curve for laminate ETW fluid ingressed

F.1.2 ADHESIVE DATA

F.1.2.1 Adhesive RTD Baseline Data

Table F-9. Test summary for adhesive RTD baseline precrack

Specimen	GIC (in-lb/in^2)			GIC (KJ/m^2)		
	NL	VIS	5%/max	NL	VIS	5%/max
SDT-AD-BL-RTD-SL1-2	5.500	-	5.851	0.963	-	1.025
SDT-AD-BL-RTD-SL1-3	5.336	-	6.596	0.934	-	1.155
SDT-AD-BL-RTD-SL1-5	5.271	-	6.696	0.923	-	1.173
SDT-AD-BL-RTD-SL1-6	3.681	-	6.082	0.645	-	1.065
SDT-AD-BL-RTD-SL1-7	3.704	-	4.342	0.649	-	0.760
SDT-AD-BL-RTD-SL1-8	4.236	5.251	5.308	0.742	0.920	0.930
SDT-AD-BL-RTD-SL1-9	3.365	-	5.486	0.589	-	0.961
AVERAGE GIC	4.442	5.251	5.766	0.778	0.920	1.010
STANDARD DEVIATION	0.907	-	0.814	0.159	-	0.143
COEFFICIENT OF VARIATION (%)	20.411	-	14.120	20.411	-	14.120

Table F-10. Test summary for adhesive RTD baseline

Specimen	GIC (in-lb/in^2)			GIC (KJ/m^2)		
	NL	VIS	5%/max	NL	VIS	5%/max
SDT-AD-BL-RTD-SL1-2	4.699	5.671	6.389	0.823	0.993	1.119
SDT-AD-BL-RTD-SL1-3	5.473	6.839	7.092	0.959	1.198	1.242
SDT-AD-BL-RTD-SL1-5	6.301	6.331	7.542	1.103	1.109	1.321
SDT-AD-BL-RTD-SL1-6	4.468	-	6.425	0.782	-	1.125
SDT-AD-BL-RTD-SL1-7	4.058	-	5.452	0.711	-	0.955
SDT-AD-BL-RTD-SL1-8	2.460	-	5.955	0.431	-	1.043
SDT-AD-BL-RTD-SL1-9	2.450	6.572	7.096	0.429	1.151	1.243
AVERAGE GIC	4.273	6.353	6.564	0.748	1.113	1.150
STANDARD DEVIATION	1.439	0.500	0.727	0.252	0.088	0.127
COEFFICIENT OF VARIATION (%)	33.685	7.873	11.080	33.685	7.873	11.080

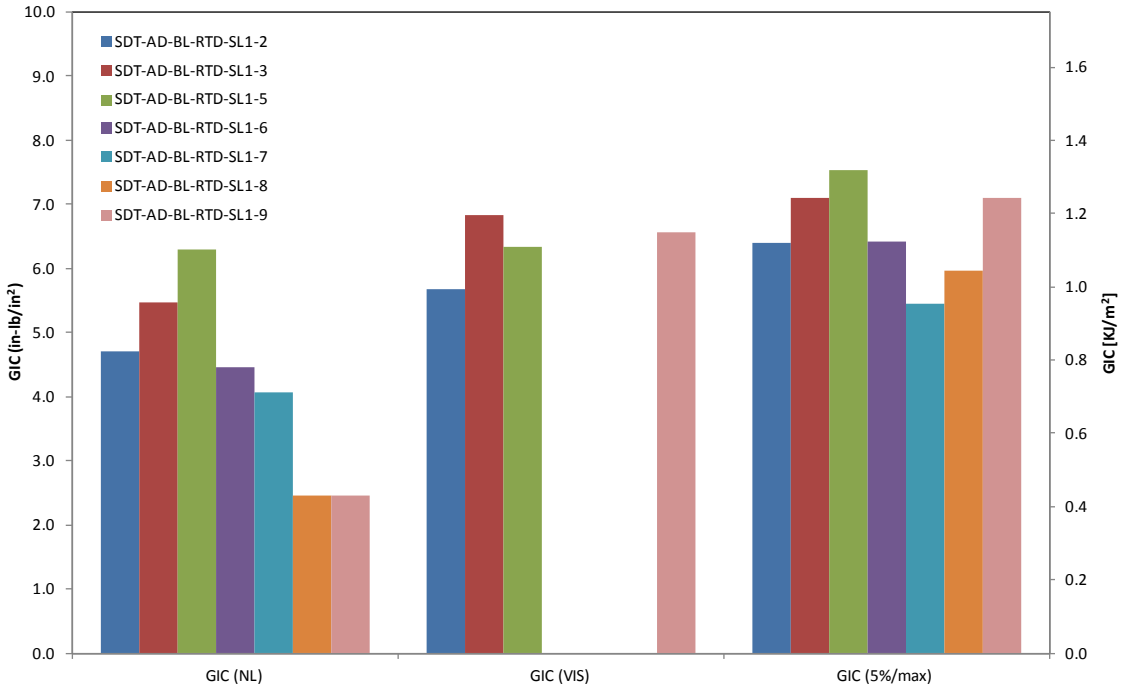

Figure F-13. GIC for adhesive RTD baseline

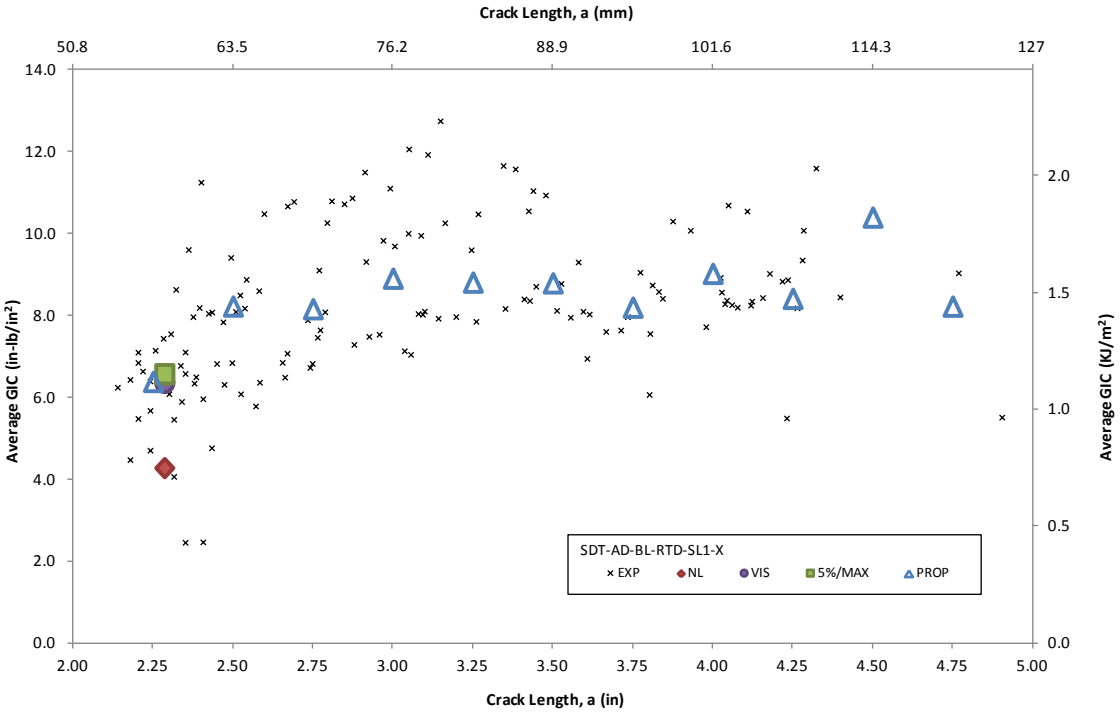

Figure F-14. Resistance curve for adhesive RTD baseline

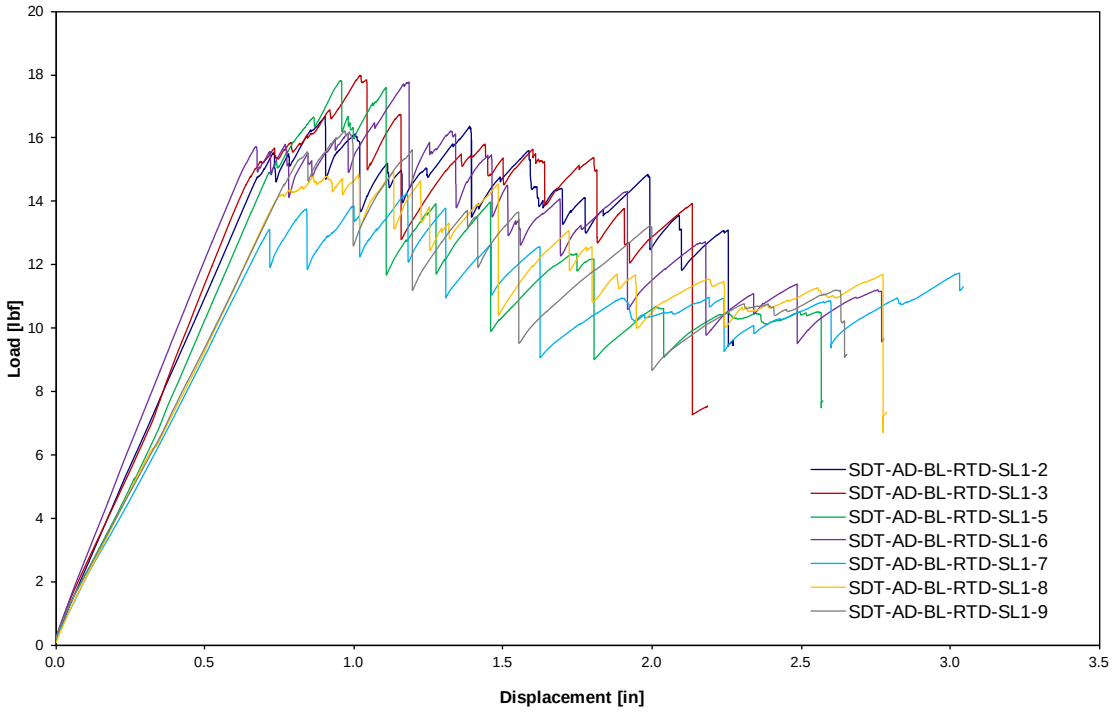

Figure F-15. Load vs. displacement curve for adhesive RTD baseline

F.1.2.2 Adhesive RTW Fluid-Ingressed Data

Table F-11. Test summary for adhesive RTW fluid-ingressed precrack

Specimen	GIC (in-lb/in^2)			GIC (KJ/m^2)		
	NL	VIS	5%/max	NL	VIS	5%/max
SDT-AD-FI-RTW-SL1-1	3.313	-	4.127	0.580	-	0.723
SDT-AD-FI-RTW-SL1-2	5.376	-	6.400	0.941	-	1.121
SDT-AD-FI-RTW-SL1-3	2.914	-	3.923	0.510	-	0.687
SDT-AD-FI-RTW-SL1-4	6.054	-	7.647	1.060	-	1.339
SDT-AD-FI-RTW-SL1-5	4.960	-	7.035	0.869	-	1.232
SDT-AD-FI-RTW-SL1-6	5.105	-	6.098	0.894	-	1.068
AVERAGE GIC	4.620	-	5.872	0.809	-	1.028
STANDARD DEVIATION	1.233	-	1.528	0.216	-	0.268
COEFFICIENT OF VARIATION (%)	26.683	-	26.024	26.683	-	26.024

Table F-12. Test summary for adhesive RTW fluid ingressed

Specimen	GIC (in-lb/in^2)			GIC (KJ/m^2)		
	NL	VIS	5%/max	NL	VIS	5%/max
SDT-AD-FI-RTW-SL1-1	1.257	5.680	5.744	0.220	0.995	1.006
SDT-AD-FI-RTW-SL1-2	1.192	-	5.633	0.209	-	0.986
SDT-AD-FI-RTW-SL1-3	1.576	5.620	6.654	0.276	0.984	1.165
SDT-AD-FI-RTW-SL1-4	1.935	5.122	6.431	0.339	0.897	1.126
SDT-AD-FI-RTW-SL1-5	1.979	-	5.434	0.347	-	0.952
SDT-AD-FI-RTW-SL1-6	1.062	-	5.935	0.186	-	1.039
AVERAGE GIC	1.500	5.474	5.972	0.263	0.959	1.046
STANDARD DEVIATION	0.393	0.306	0.476	0.069	0.054	0.083
COEFFICIENT OF VARIATION (%)	26.172	5.597	7.974	26.172	5.597	7.974

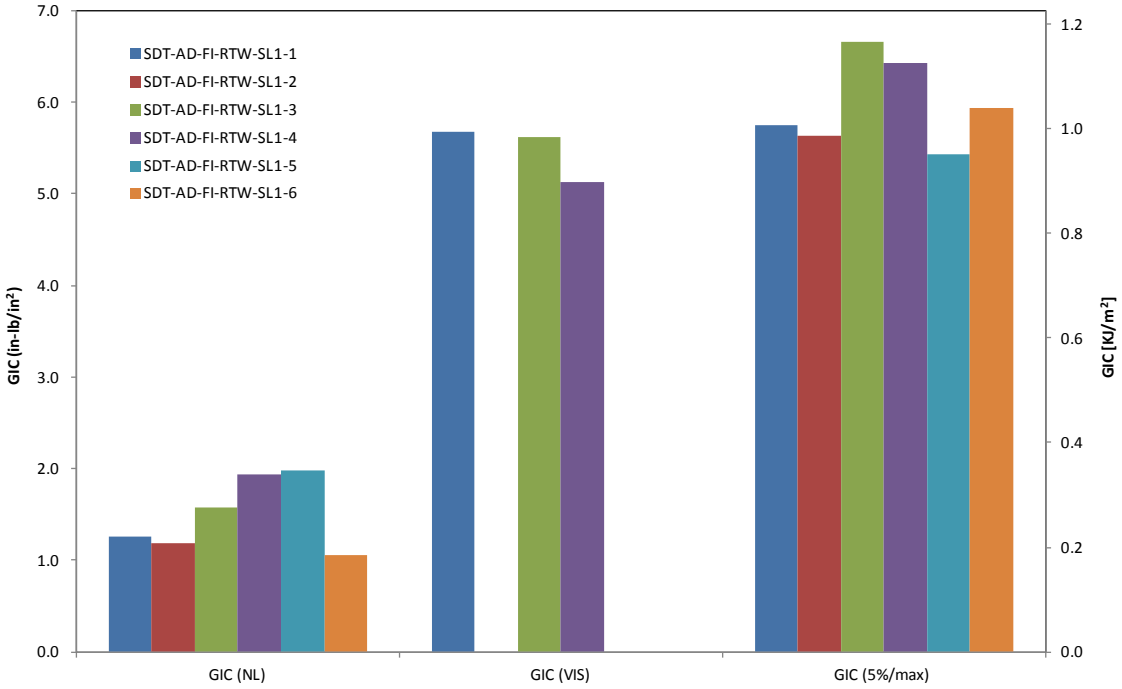

Figure F-16. GIC for adhesive RTW fluid ingressed

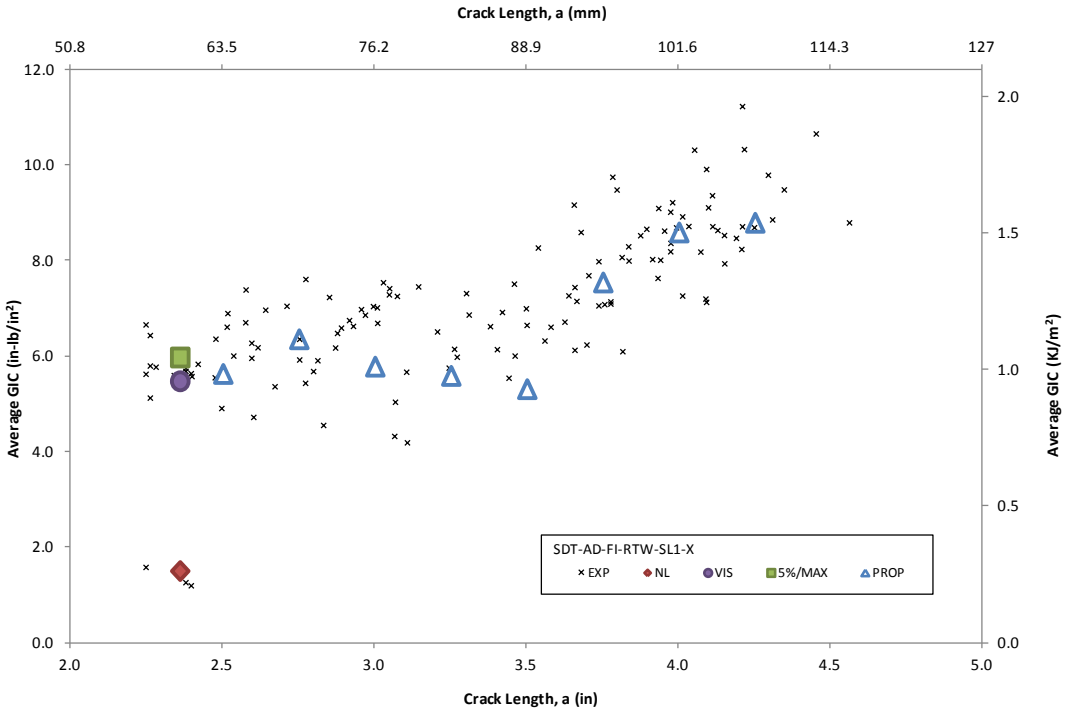

Figure F-17. Resistance curve for adhesive RTW fluid ingressed

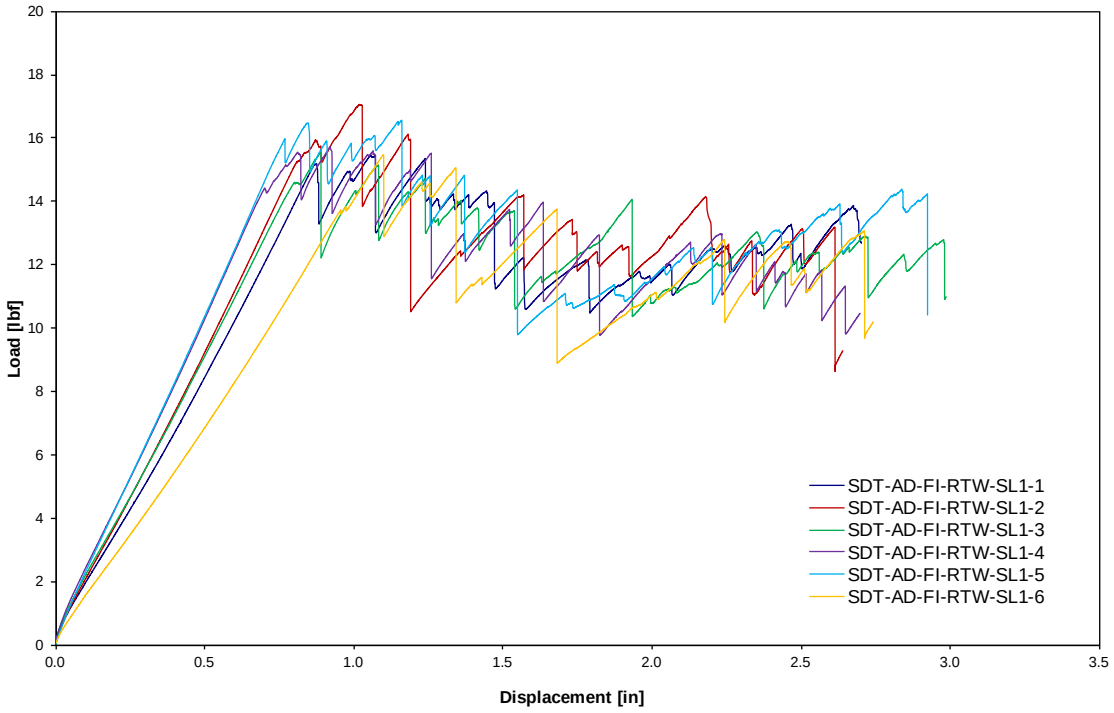

Figure F-18. Load vs. displacement curve for adhesive RTW fluid ingressed

F.1.2.3 Adhesive ETD Baseline Data

Table F-13. Test summary for Adhesive ETD baseline precrack

Specimen	GIC (in-lb/in^2)			GIC (KJ/m^2)		
	NL	VIS	5%/max	NL	VIS	5%/max
SDT-AD-BL-ETD-SL1-1	3.054	-	5.435	0.5349	-	0.9518
SDT-AD-BL-ETD-SL1-2	3.572	-	6.090	0.6256	-	1.0665
SDT-AD-BL-ETD-SL1-3	3.944	-	5.733	0.6906	-	1.0040
SDT-AD-BL-ETD-SL1-4	3.527	-	6.342	0.6177	-	1.1106
SDT-AD-BL-ETD-SL1-5	3.225	-	5.704	0.5648	-	0.9990
SDT-AD-BL-ETD-SL1-6	3.334	-	4.651	0.5839	-	0.8145
AVERAGE GIC	3.443	-	5.659	0.603	-	0.991
STANDARD DEVIATION	0.311	-	0.587	0.055	-	0.103
COEFFICIENT OF VARIATION (%)	9.044	-	10.379	9.044	-	10.379

Table F-14. Test summary for adhesive ETD baseline

Specimen	GIC (in-lb/in^2)			GIC (KJ/m^2)		
	NL	VIS	5%/max	NL	VIS	5%/max
SDT-AD-BL-ETD-SL1-1	4.034	-	5.043	0.707	-	0.883
SDT-AD-BL-ETD-SL1-2	3.373	-	6.258	0.591	-	1.096
SDT-AD-BL-ETD-SL1-3	5.331	-	7.309	0.934	-	1.280
SDT-AD-BL-ETD-SL1-4	4.095	-	6.893	0.717	-	1.207
SDT-AD-BL-ETD-SL1-5	3.202	-	5.335	0.561	-	0.934
SDT-AD-BL-ETD-SL1-6	3.805	-	6.597	0.666	-	1.155
AVERAGE GIC	3.973	-	6.239	0.696	-	1.093
STANDARD DEVIATION	0.754	-	0.888	0.132	-	0.156
COEFFICIENT OF VARIATION (%)	18.986	-	14.240	18.986	-	14.240

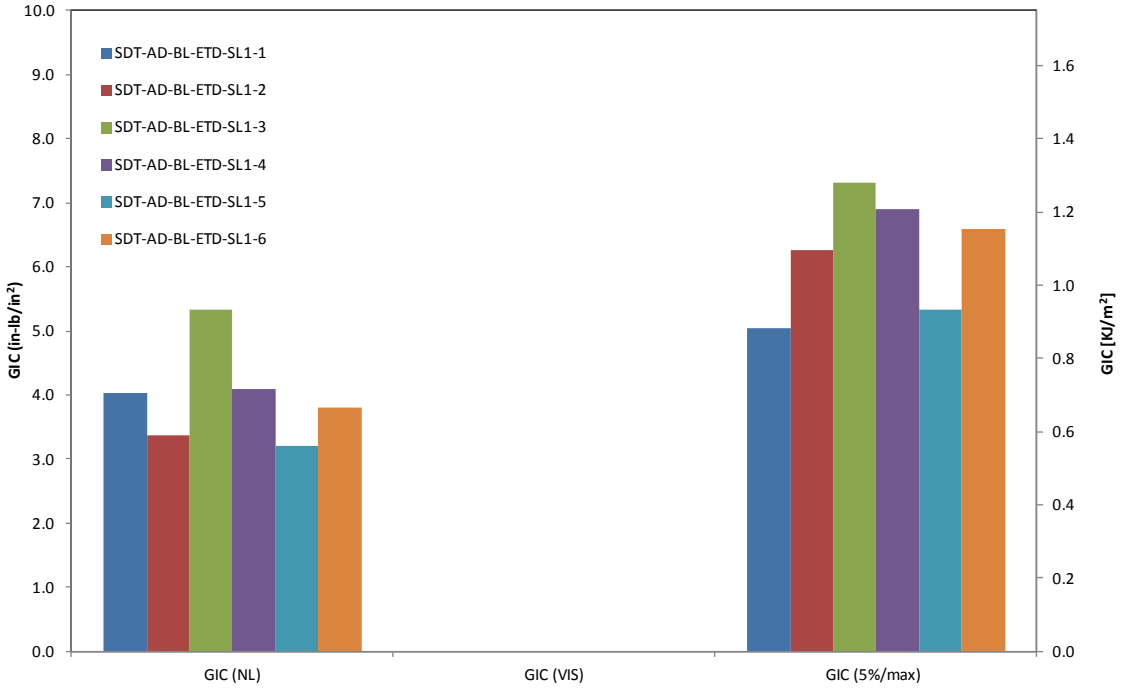

Figure F-19. GIC for adhesive ETD baseline

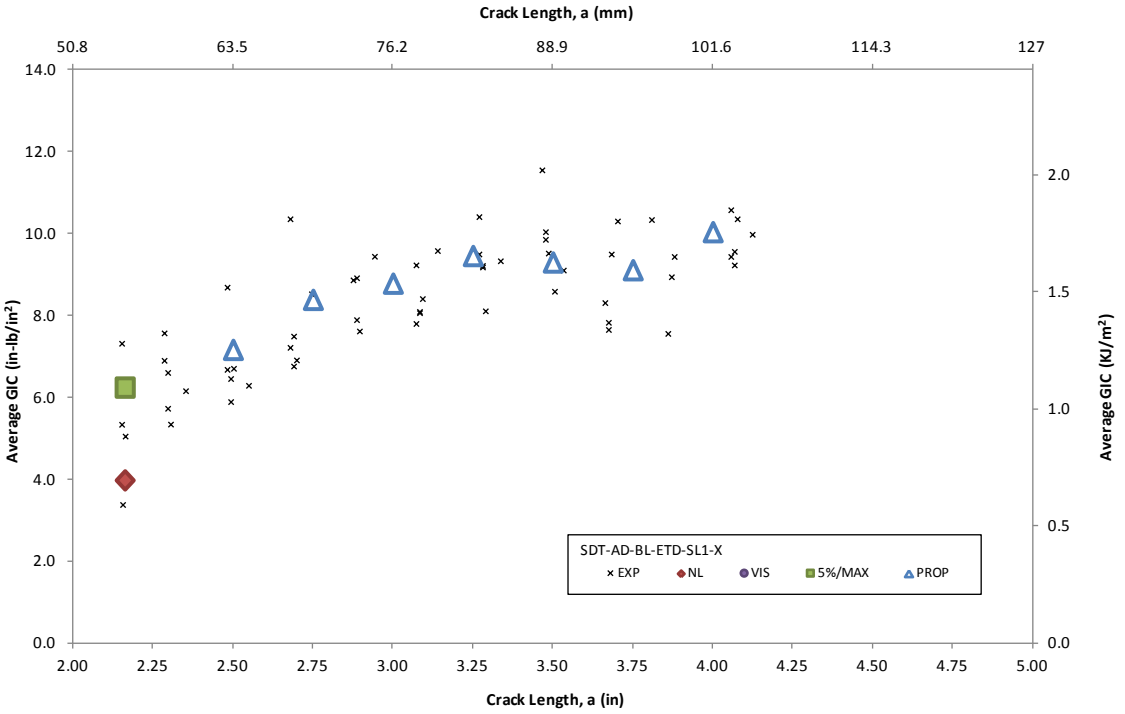

Figure F-20. Resistance curve for adhesive ETD baseline

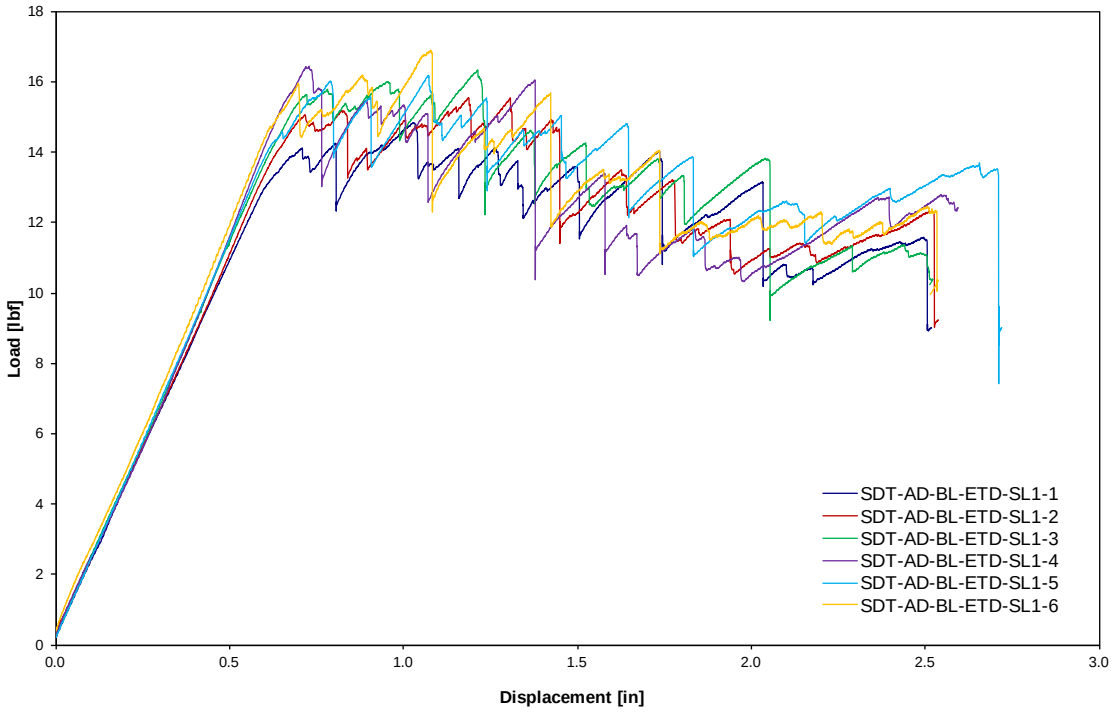

Figure F-21. Load vs. displacement curve for adhesive ETD baseline

F.1.2 Adhesive ETW Fluid-Ingressed Data

Table F-15. Test summary for adhesive ETW fluid-ingressed precrack

Specimen	GIC (in-lb/in^2)			GIC (KJ/m^2)		
	NL	VIS	5%/max	NL	VIS	5%/max
SDT-AD-FI-ETW-SL1-1	4.143	-	6.987	0.725	-	1.224
SDT-AD-FI-ETW-SL1-2	4.169	-	6.314	0.730	-	1.106
SDT-AD-FI-ETW-SL1-3	2.742	-	5.212	0.480	-	0.913
SDT-AD-FI-ETW-SL1-4	-	-	-	-	-	-
SDT-AD-FI-ETW-SL1-5	3.071	-	5.496	0.538	-	0.963
SDT-AD-FI-ETW-SL1-6	3.788	-	6.563	0.663	-	1.149
AVERAGE GIC	3.583	-	6.114	0.627	-	1.071
STANDARD DEVIATION	0.646	-	0.741	0.113	-	0.130
COEFFICIENT OF VARIATION (%)	18.023	-	12.122	18.023	-	12.122

Table F-16. Test summary for adhesive ETW fluid ingressed

Specimen	GIC (in-lb/in^2)			GIC (KJ/m^2)		
	NL	VIS	5%/max	NL	VIS	5%/max
SDT-AD-FI-ETW-SL1-1	2.275	-	4.112	0.398	-	0.720
SDT-AD-FI-ETW-SL1-2	3.122	-	5.668	0.547	-	0.993
SDT-AD-FI-ETW-SL1-3	3.092	-	5.621	0.542	-	0.984
SDT-AD-FI-ETW-SL1-4	3.150	-	5.727	0.552	-	1.003
SDT-AD-FI-ETW-SL1-5	2.553	-	4.624	0.447	-	0.810
SDT-AD-FI-ETW-SL1-6	2.511	-	4.550	0.440	-	0.797
AVERAGE GIC	2.784	-	5.050	0.488	-	0.884
STANDARD DEVIATION	0.382	-	0.704	0.067	-	0.123
COEFFICIENT OF VARIATION (%)	13.728	-	13.939	13.728	-	13.939

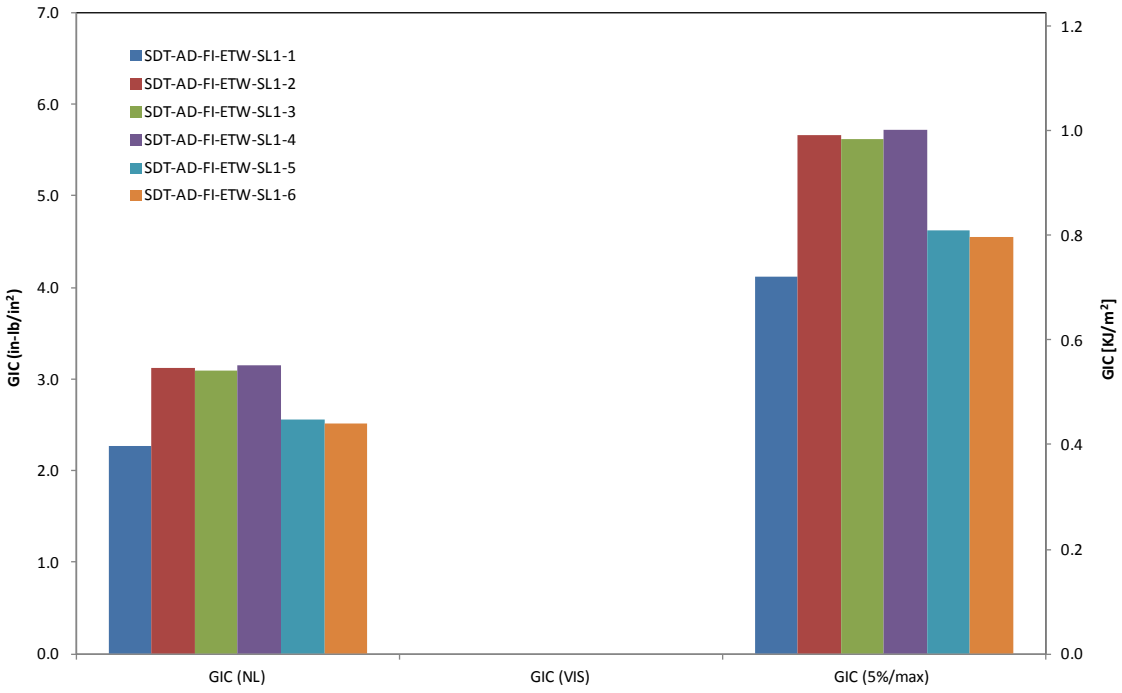

Figure F-22. GIC for adhesive ETW fluid ingressed

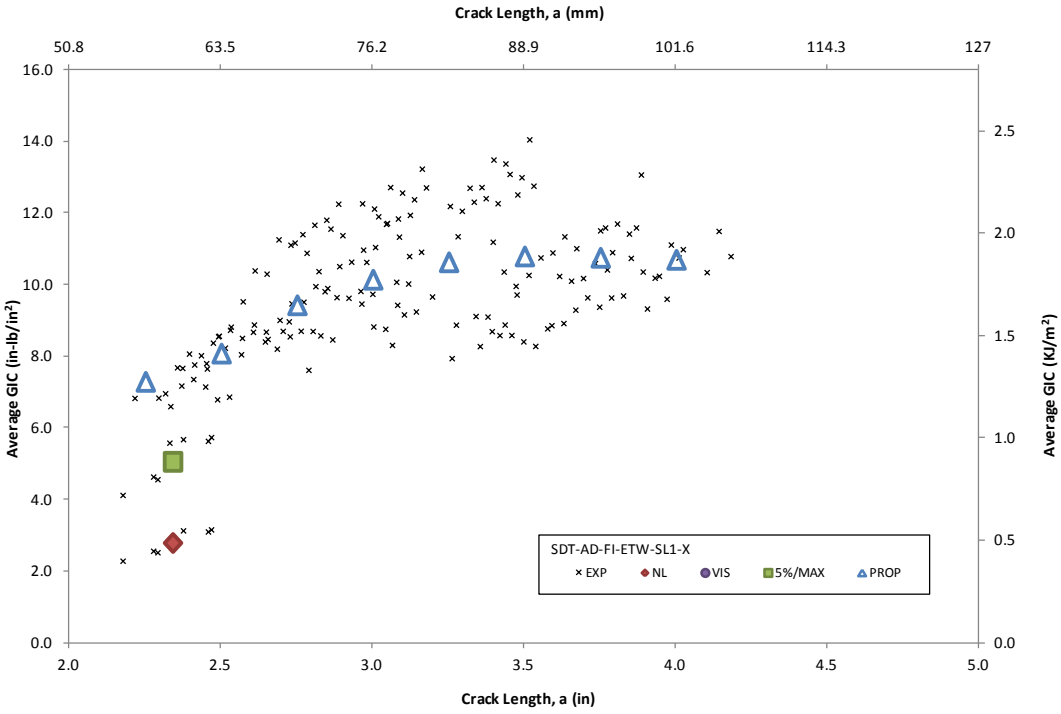

Figure F-23. Resistance curve for adhesive ETW fluid ingressed

Figure F-24. Load vs. displacement curve for adhesive ETW fluid ingressed

F.2 FLATWISE TENSION (FWT) DATA

F.2.1 HRH-10–1/8–3.0 DATA

F.2.1.1 HRH-10–1/8–3.0 Baseline Data

Table F-17. Test summary for HRH-10–1/8–3.0 baseline

Specimen	Flatwise Tensile Strength (ksi)
SDT-04-HX-1.8-3-BL-FWT-SL1-1	0.398
SDT-04-HX-1.8-3-BL-FWT-SL1-2	0.393
SDT-04-HX-1.8-3-BL-FWT-SL1-3	0.370
SDT-04-HX-1.8-3-BL-FWT-SL1-4	0.371
SDT-04-HX-1.8-3-BL-FWT-SL1-5	0.373
SDT-04-HX-1.8-3-BL-FWT-SL1-6	0.372
AVERAGE FLATWISE TENSILE STRENGTH	0.379
STANDARD DEVIATION	0.012
COEFFICIENT OF VARIATION (%)	3.252

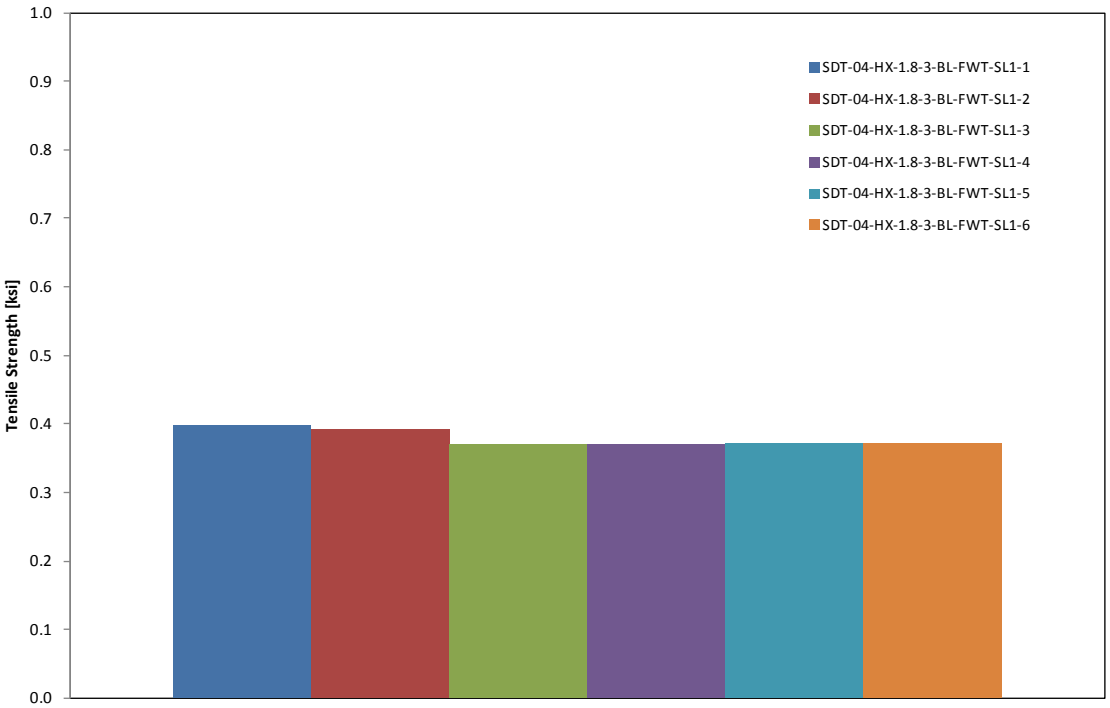

Figure F-25. Flatwise tensile strength for HRH-10–1/8–3.0 baseline

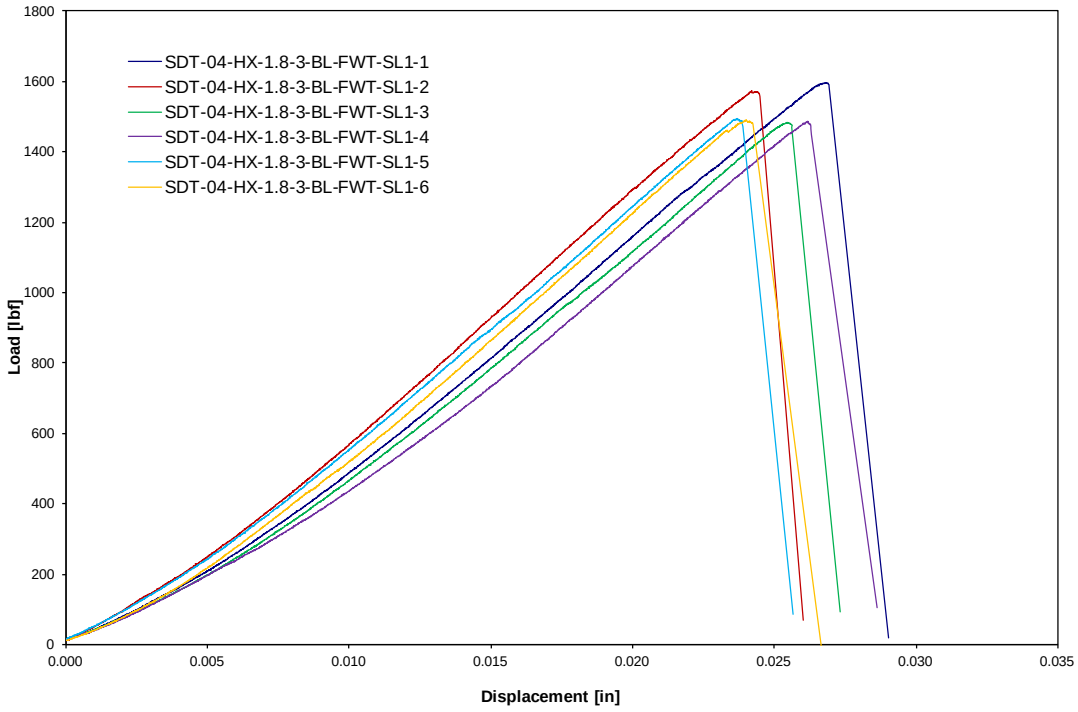

Figure F-26. Load vs. displacement curve for HRH-10–1/8–3.0 baseline

F.2.1.2 HRH-10–1/8–3.0 Fluid-Ingressed Data

Table F-18. Test summary for HRH-10–1/8–3.0 fluid ingressed

Specimen	Flatwise Tensile Strength (ksi)
SDT-04-HX-1.8-3-FI-FWT-SL1-1	0.334
SDT-04-HX-1.8-3-FI-FWT-SL1-2	0.333
SDT-04-HX-1.8-3-FI-FWT-SL1-3	0.332
SDT-04-HX-1.8-3-FI-FWT-SL1-4	0.319
SDT-04-HX-1.8-3-FI-FWT-SL1-5	0.344
SDT-04-HX-1.8-3-FI-FWT-SL1-6	0.347
AVERAGE FLATWISE TENSILE STRENGTH	0.335
STANDARD DEVIATION	0.010
COEFFICIENT OF VARIATION (%)	3.001

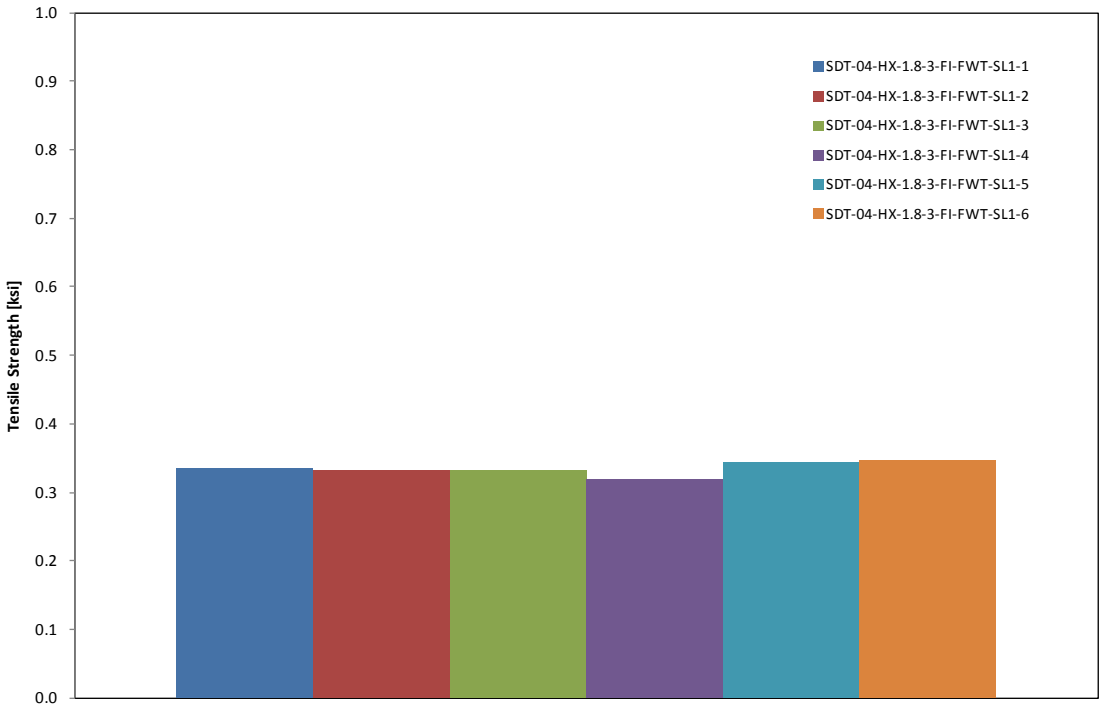

Figure F-27. Flatwise tensile strength for HRH-10–1/8–3.0 fluid ingressed

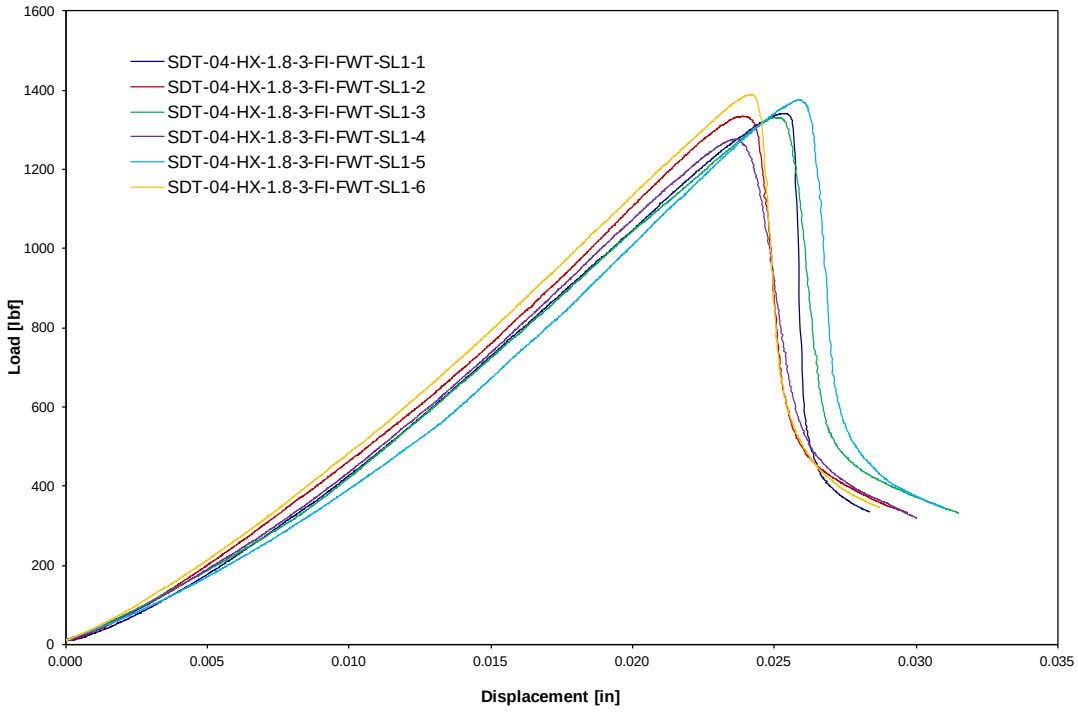

Figure F-28. Load vs. displacement curve for HRH-10–1/8–3.0 fluid ingressed

F.2.2 HRH-10–3/16–2.0 DATA

F.2.2.1 HRH-10–3/16–2.0 Baseline Data

Table F-19. Test summary for HRH-10–3/16–2.0 baseline

Specimen	Flatwise Tensile Strength (ksi)
SDT-04-HX-3.16-2-BL-FWT-SL1-1	0.223
SDT-04-HX-3.16-2-BL-FWT-SL1-2	0.240
SDT-04-HX-3.16-2-BL-FWT-SL1-3	0.234
SDT-04-HX-3.16-2-BL-FWT-SL1-4	0.217
SDT-04-HX-3.16-2-BL-FWT-SL1-5	0.222
SDT-04-HX-3.16-2-BL-FWT-SL1-6	0.234
AVERAGE FLATWISE TENSILE STRENGTH	0.229
STANDARD DEVIATION	0.009
COEFFICIENT OF VARIATION (%)	3.934

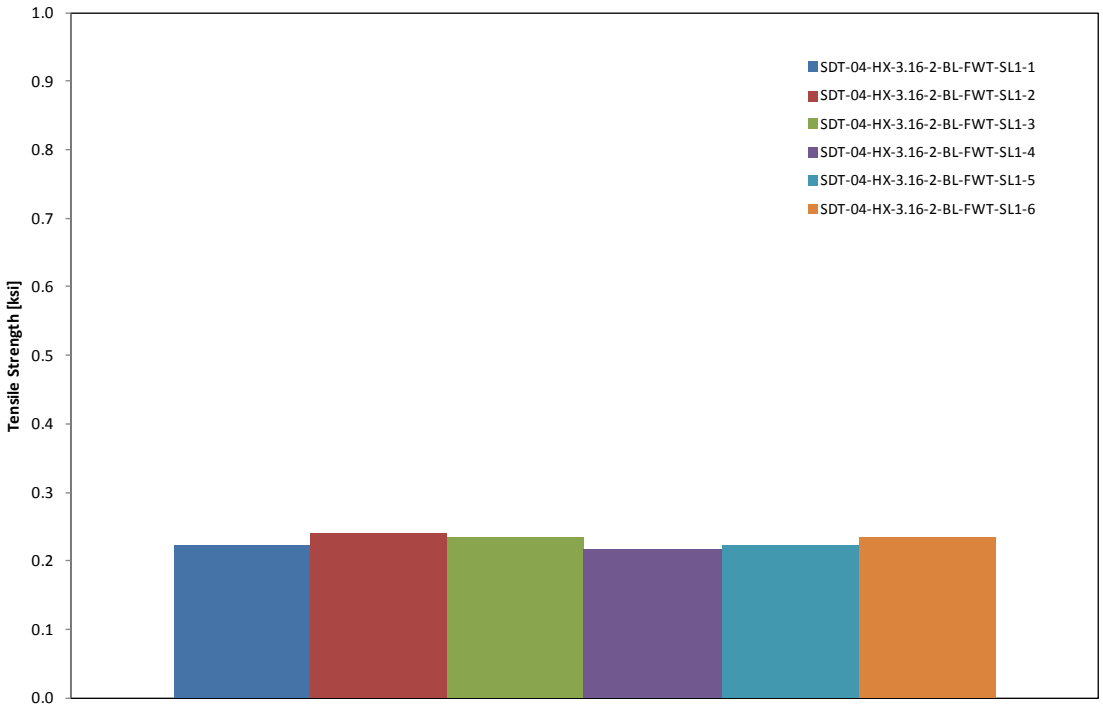

Figure F-29. Flatwise tensile strength for HRH-10–3/16–2.0 baseline

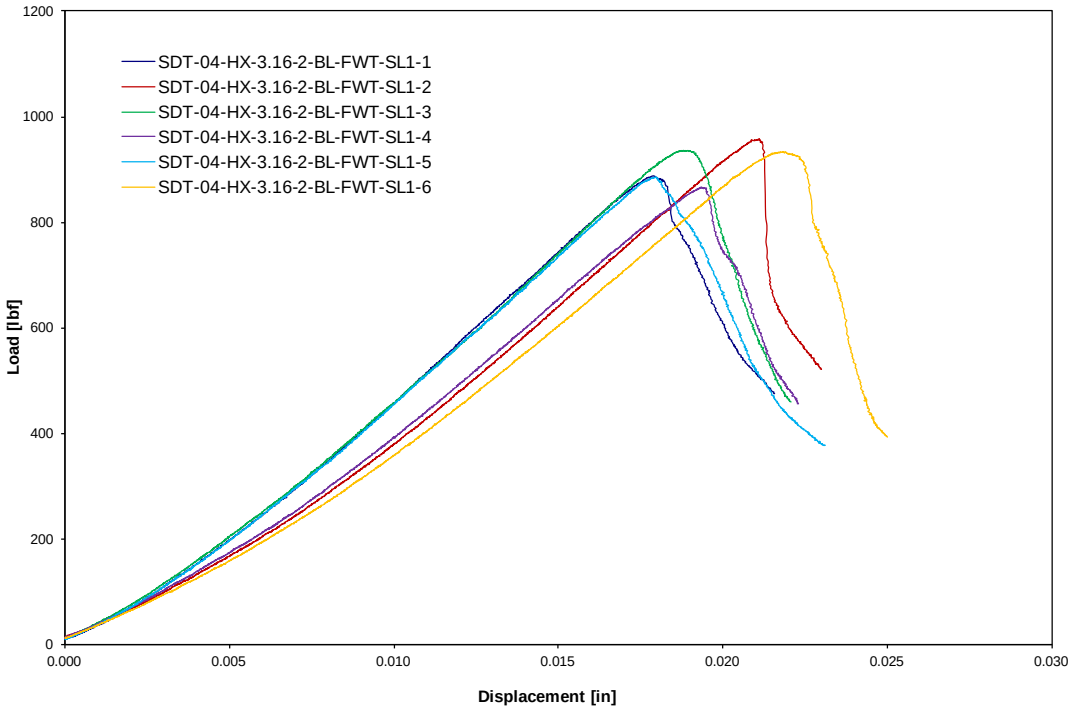

Figure F-30. Load vs. displacement curve for HRH-10–3/16–2.0 baseline

F.2.2.2 HRH-10–3/16–2.0 Fluid-Ingressed Data

Table F-20. Test summary for HRH-10–3/16–2.0 fluid ingressed

Specimen	Flatwise Tensile Strength (ksi)
SDT-04-HX-3.16-2-FI-FWT-SL1-1	0.192
SDT-04-HX-3.16-2-FI-FWT-SL1-2	0.219
SDT-04-HX-3.16-2-FI-FWT-SL1-3	0.195
SDT-04-HX-3.16-2-FI-FWT-SL1-4	0.191
SDT-04-HX-3.16-2-FI-FWT-SL1-5	0.215
SDT-04-HX-3.16-2-FI-FWT-SL1-6	0.217
SDT-04-HX-3.16-2-FI-FWT-SL1-7	0.200
AVERAGE FLATWISE TENSILE STRENGTH	0.206
STANDARD DEVIATION	0.012
COEFFICIENT OF VARIATION (%)	5.970

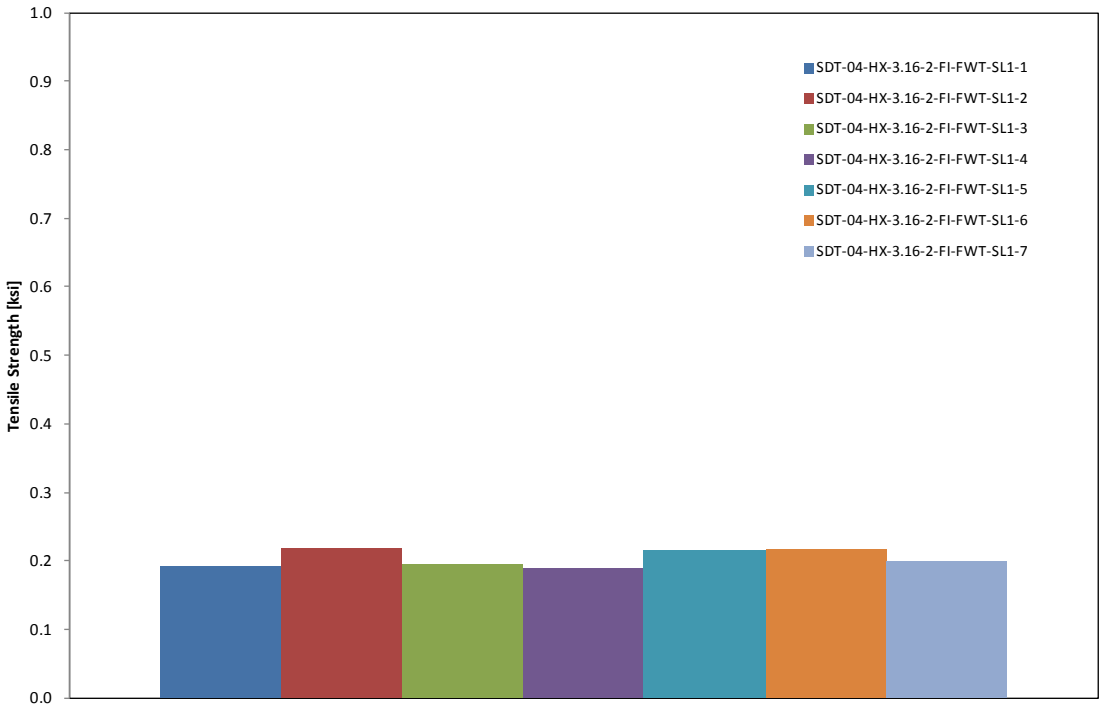

Figure F-31. Flatwise tensile strength for HRH-10–3/16–2.0 fluid ingressed

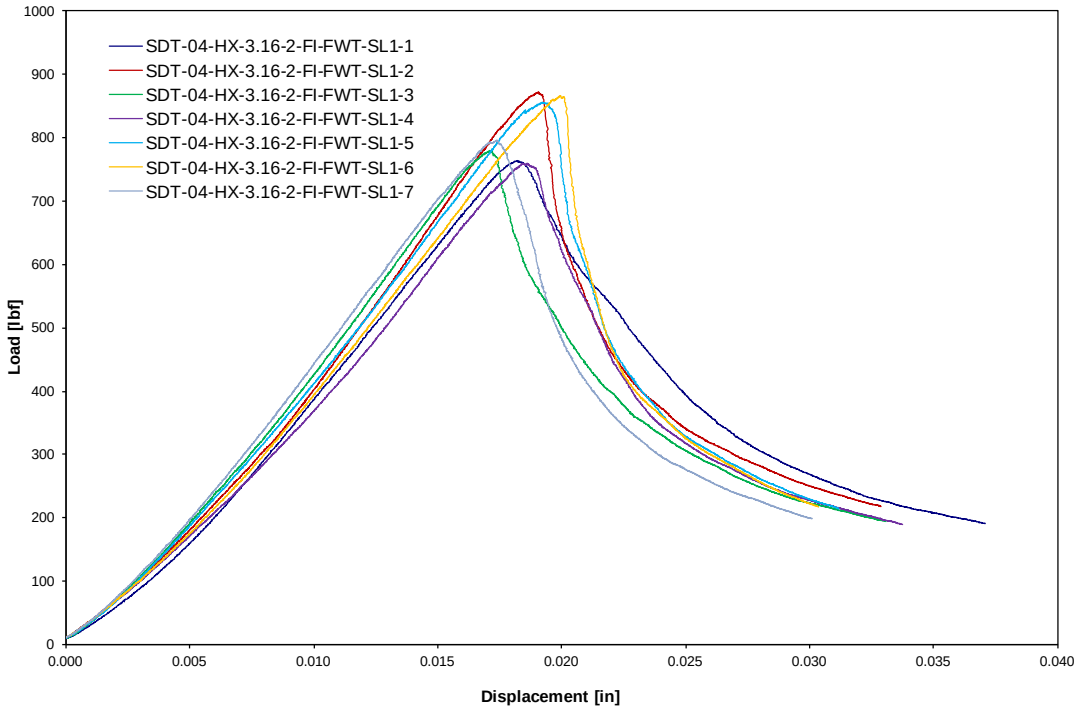

Figure F-32. Load vs. displacement curve for HRH-10–3/16–2.0 fluid ingressed

F.2.3 HRH-10–3/16–3.0 DATA

F.2.3.1 HRH-10–3/16–3.0 Baseline Data

Table F-21. Test summary for HRH-10–3/16–3.0 baseline

Specimen	Flatwise Tensile Strength (ksi)
SDT-04-HX-3.16-3-BL-FWT-SL1-1	0.357
SDT-04-HX-3.16-3-BL-FWT-SL1-2	0.356
SDT-04-HX-3.16-3-BL-FWT-SL1-3	0.349
SDT-04-HX-3.16-3-BL-FWT-SL1-4	0.359
SDT-04-HX-3.16-3-BL-FWT-SL1-5	0.356
SDT-04-HX-3.16-3-BL-FWT-SL1-6	0.354
AVERAGE FLATWISE TENSILE STRENGTH	0.355
STANDARD DEVIATION	0.004
COEFFICIENT OF VARIATION (%)	0.985

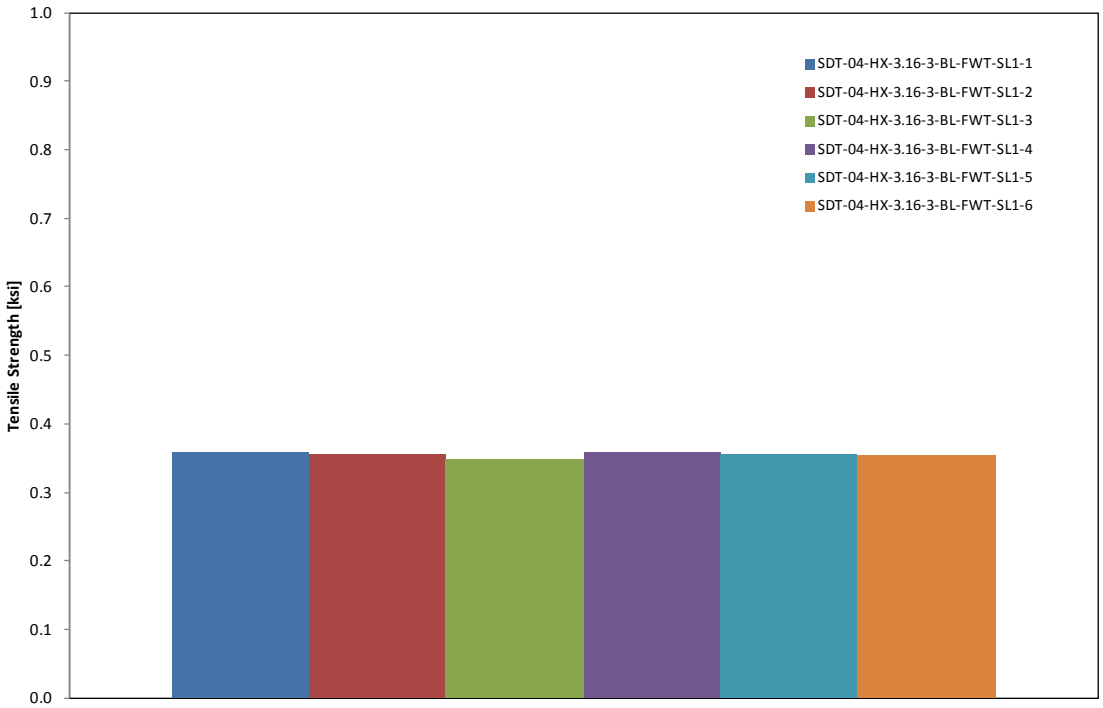

Figure F-33. Flatwise tensile strength for HRH-10–3/16–3.0 baseline

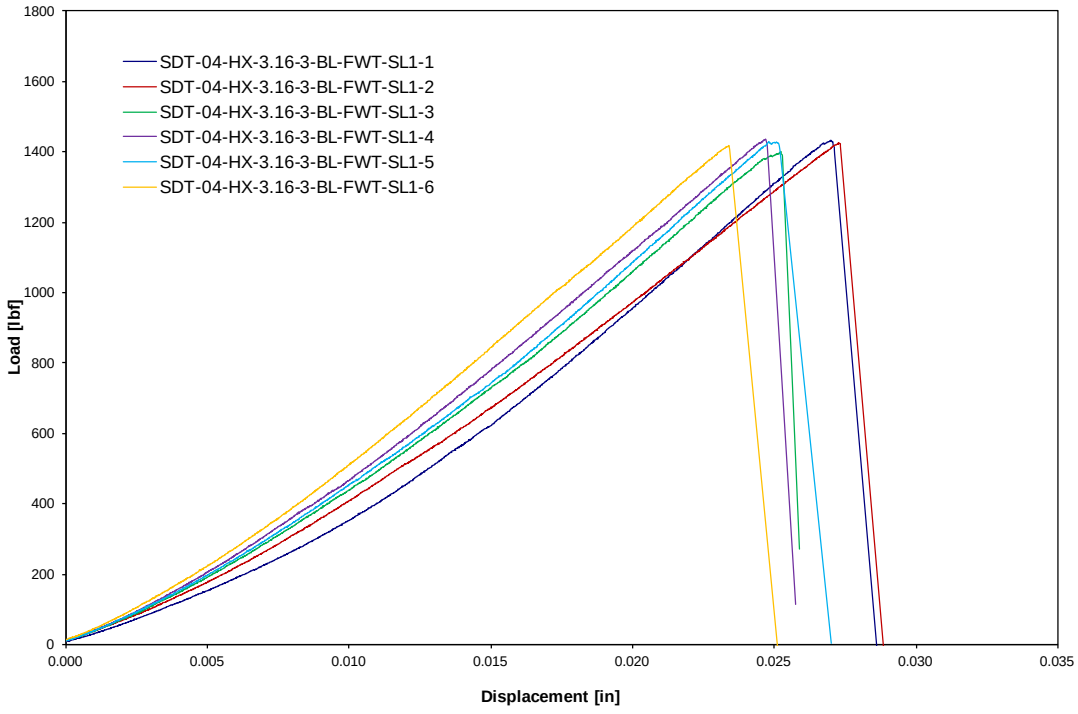

Figure F-34. Load vs. displacement curve for HRH-10–3/16–3.0 baseline

F.2.3.2 HRH-10–3/16–3.0 Fluid-Ingressed Data

Table F-22. Test summary for HRH-10–3/16–3.0 fluid ingressed

Specimen	Flatwise Tensile Strength (ksi)
SDT-04-HX-3.16-3-FI-FWT-SL1-1	0.315
SDT-04-HX-3.16-3-FI-FWT-SL1-2	0.341
SDT-04-HX-3.16-3-FI-FWT-SL1-3	0.323
SDT-04-HX-3.16-3-FI-FWT-SL1-4	0.332
SDT-04-HX-3.16-3-FI-FWT-SL1-5	0.337
SDT-04-HX-3.16-3-FI-FWT-SL1-6	0.331
SDT-04-HX-3.16-3-FI-FWT-SL1-7	0.297
AVERAGE FLATWISE TENSILE STRENGTH	0.327
STANDARD DEVIATION	0.016
COEFFICIENT OF VARIATION (%)	4.879

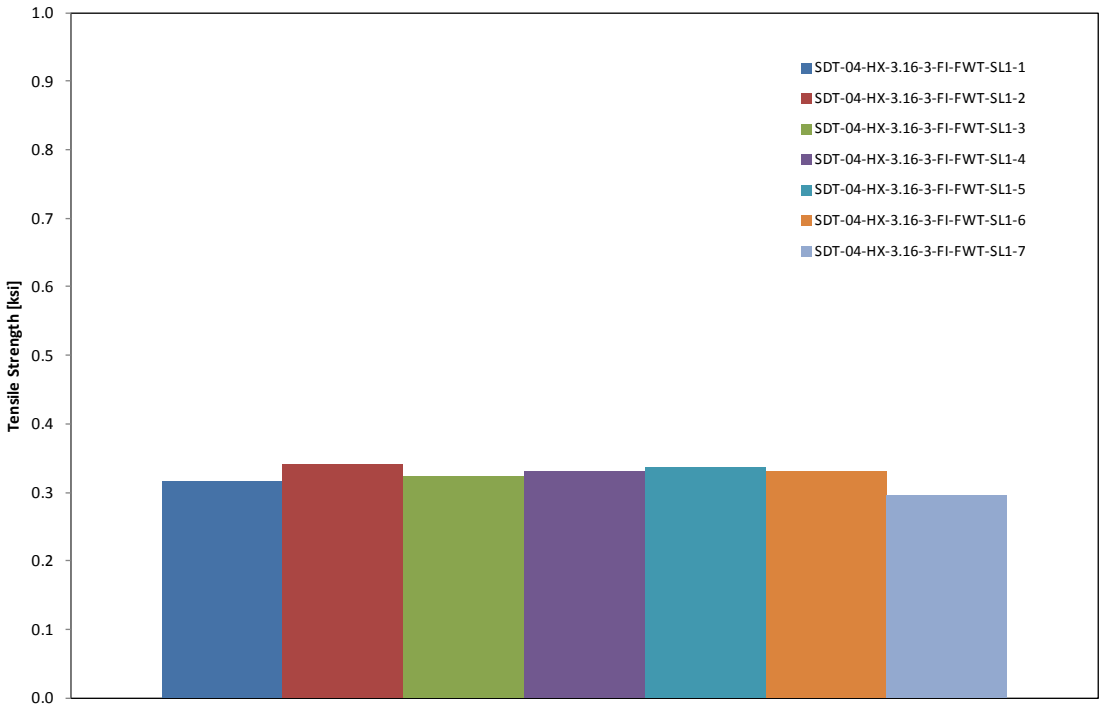

Figure F-35. Flatwise tensile strength for HRH-10–3/16–3.0 fluid ingressed

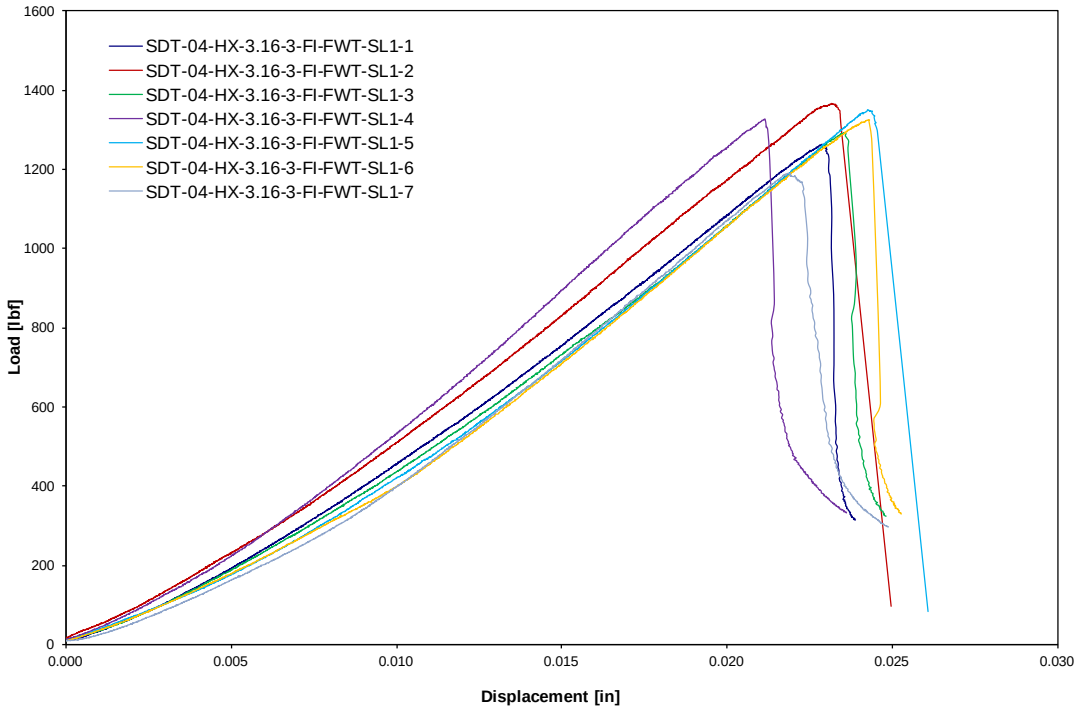

Figure F-36. Load vs. displacement curve for HRH-10–3/16–3.0 fluid ingressed

F.2.4 HRH-10–3/16–6.0 DATA

F.2.4.1 HRH-10–3/16–6.0 Baseline Data

Table F-23. Test summary for HRH-10–3/16–6.0 baseline

Specimen	Flatwise Tensile Strength (ksi)
SDT-04-HX-3.16-6-BL-FWT-SL1-1	0.743
SDT-04-HX-3.16-6-BL-FWT-SL1-2	0.742
SDT-04-HX-3.16-6-BL-FWT-SL1-3	0.750
SDT-04-HX-3.16-6-BL-FWT-SL1-4	0.714
SDT-04-HX-3.16-6-BL-FWT-SL1-5	0.713
SDT-04-HX-3.16-6-BL-FWT-SL1-6	0.700
AVERAGE FLATWISE TENSILE STRENGTH	0.727
STANDARD DEVIATION	0.020
COEFFICIENT OF VARIATION (%)	2.819

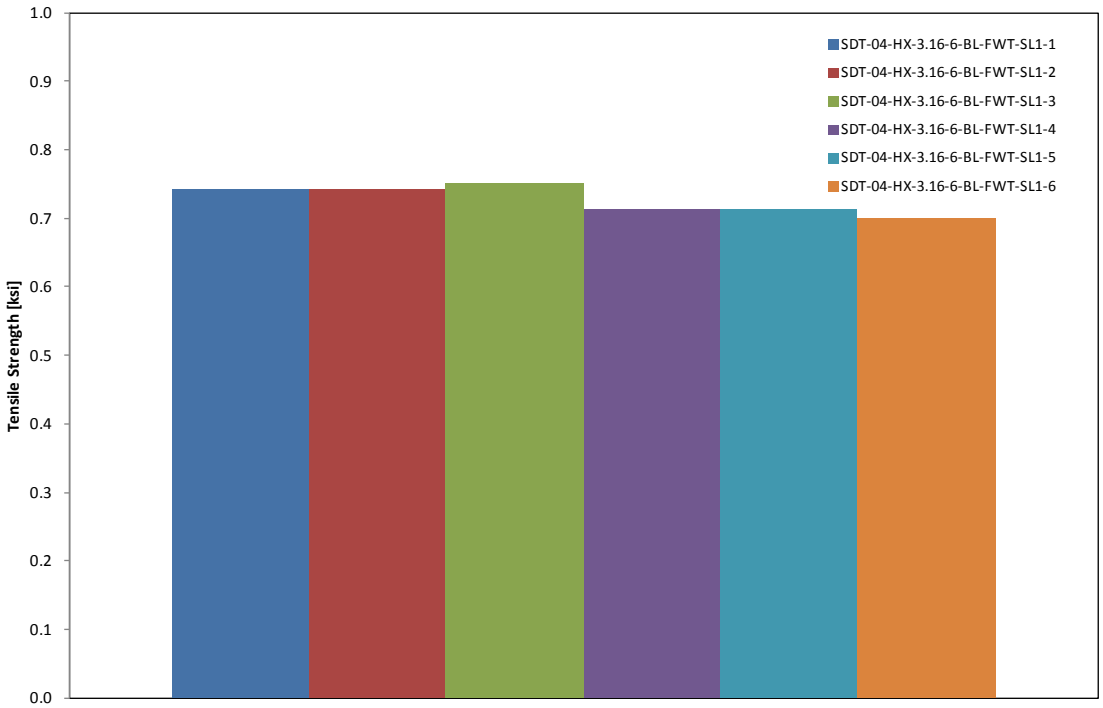

Figure F-37. Flatwise tensile strength for HRH-10–3/16–6.0 baseline

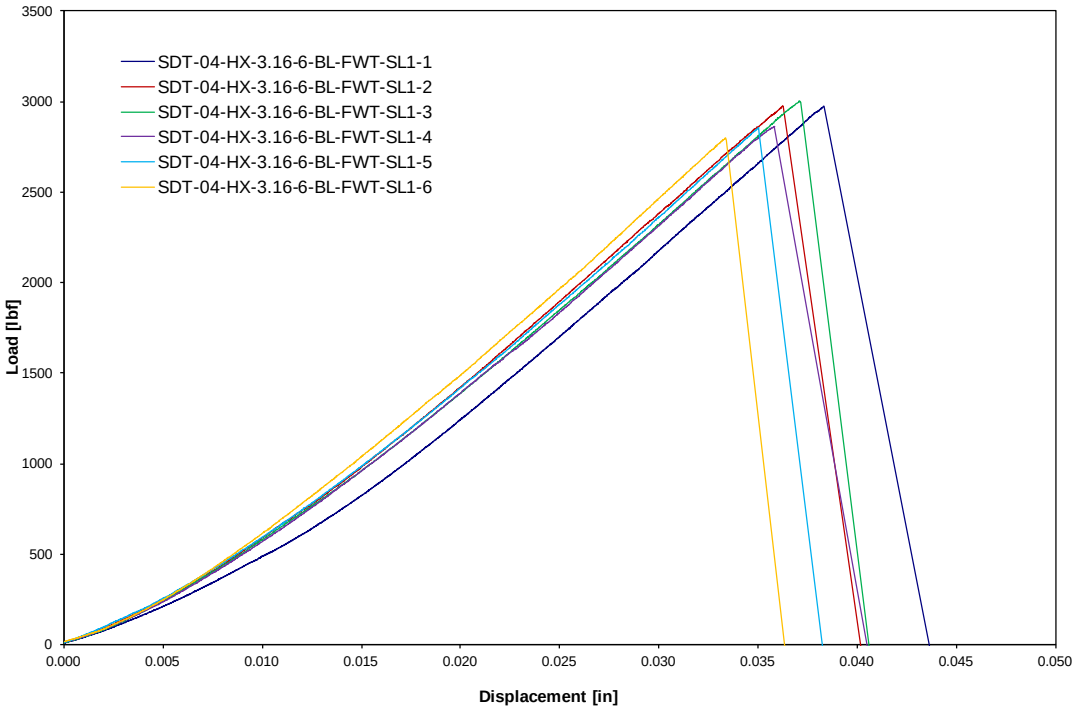

Figure F-38. Load vs. displacement curve for HRH-10–3/16–6.0 baseline

F.2.4.2 HRH-10–3/16–6.0 Fluid-Ingressed Data

Table F-24. Test summary for HRH-10–3/16–6.0 fluid ingressed

Specimen	Flatwise Tensile Strength (ksi)
SDT-04-HX-3.16-6-FI-FWT-SL1-1	0.705
SDT-04-HX-3.16-6-FI-FWT-SL1-2	0.707
SDT-04-HX-3.16-6-FI-FWT-SL1-3	0.717
SDT-04-HX-3.16-6-FI-FWT-SL1-4	0.710
SDT-04-HX-3.16-6-FI-FWT-SL1-5	0.719
SDT-04-HX-3.16-6-FI-FWT-SL1-6	0.719
AVERAGE FLATWISE TENSILE STRENGTH	0.713
STANDARD DEVIATION	0.006
COEFFICIENT OF VARIATION (%)	0.889

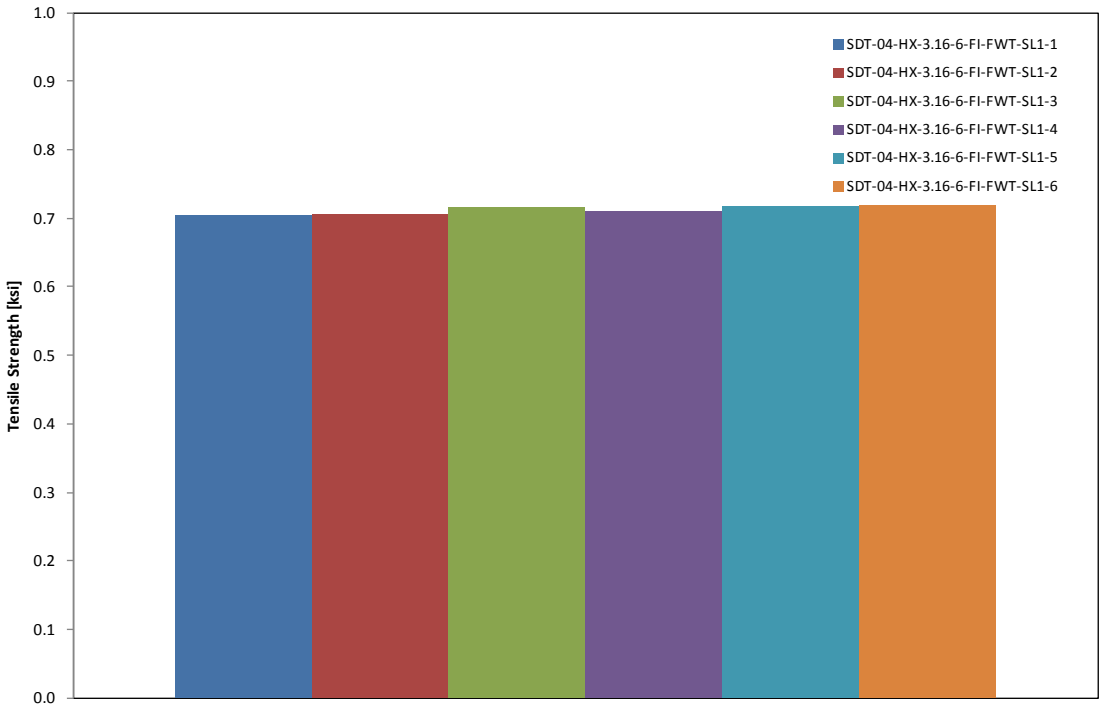

Figure F-39. Flatwise tensile strength for HRH-10–3/16–6.0 fluid ingressed

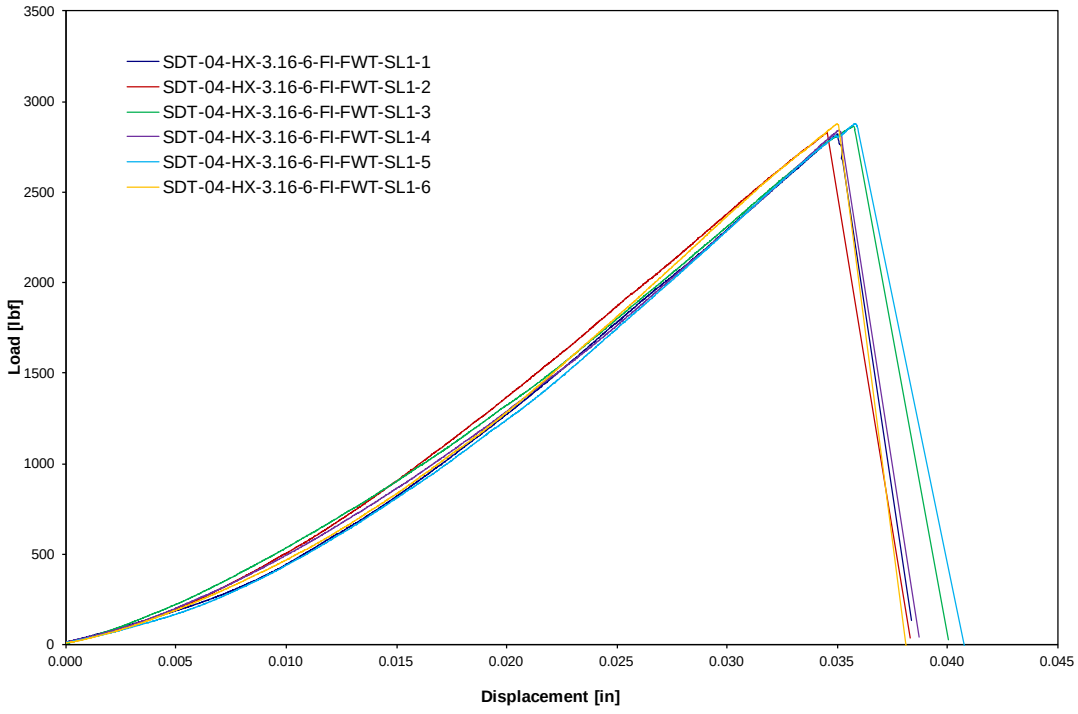

Figure F-40. Load vs. displacement curve for HRH-10–3/16–6.0 fluid ingressed

F.2.5 HRH-10–3/8–3.0 DATA

F.2.5.1 HRH-10–3/8–3.0 Baseline Data

Table F-25. Test summary for HRH-10–3/8–3.0 baseline

Specimen	Flatwise Tensile Strength (ksi)
SDT-04-HX-3.8-3-BL-FWT-SL1-1	0.284
SDT-04-HX-3.8-3-BL-FWT-SL1-2	0.300
SDT-04-HX-3.8-3-BL-FWT-SL1-3	0.308
SDT-04-HX-3.8-3-BL-FWT-SL1-4	0.310
SDT-04-HX-3.8-3-BL-FWT-SL1-5	0.309
SDT-04-HX-3.8-3-BL-FWT-SL1-6	0.295
AVERAGE FLATWISE TENSILE STRENGTH	0.301
STANDARD DEVIATION	0.010
COEFFICIENT OF VARIATION (%)	3.408

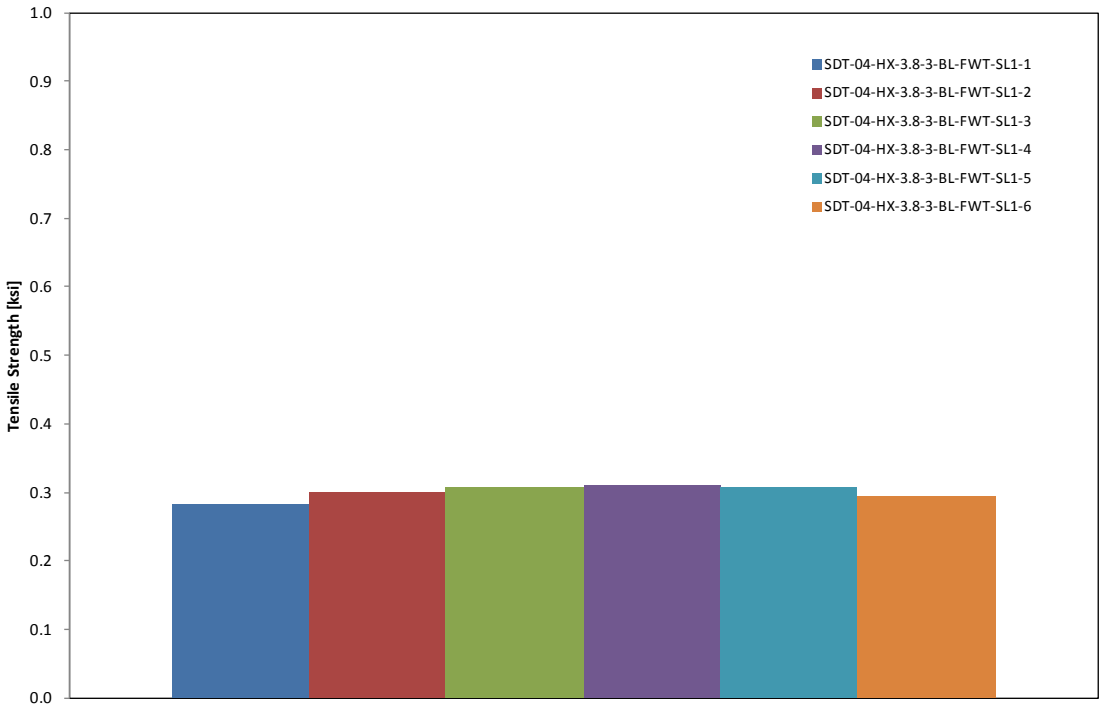

Figure F-41. Flatwise tensile strength for HRH-10–3/8–3.0 baseline

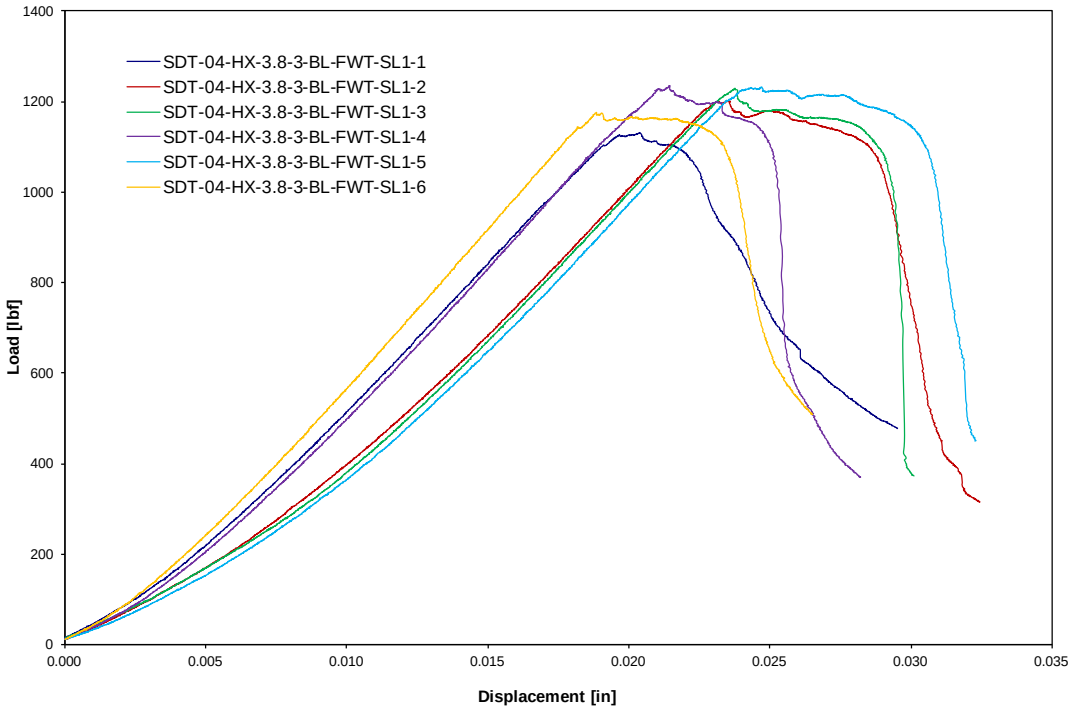

Figure F-42. Load vs. displacement curve for HRH-10–3/8–3.0 baseline

F.2.5.2 HRH-10–3/8–3.0 Fluid-Ingressed Data

Table F-26. Test summary for HRH-10–3/8–3.0 fluid ingressed

Specimen	Flatwise Tensile Strength (ksi)
SDT-04-HX-3.8-3-FI-FWT-SL1-1	0.239
SDT-04-HX-3.8-3-FI-FWT-SL1-2	0.248
SDT-04-HX-3.8-3-FI-FWT-SL1-3	0.256
SDT-04-HX-3.8-3-FI-FWT-SL1-4	0.255
SDT-04-HX-3.8-3-FI-FWT-SL1-5	0.264
SDT-04-HX-3.8-3-FI-FWT-SL1-6	0.241
SDT-04-HX-3.8-3-FI-FWT-SL1-7	0.234
AVERAGE FLATWISE TENSILE STRENGTH	0.250
STANDARD DEVIATION	0.011
COEFFICIENT OF VARIATION (%)	4.472

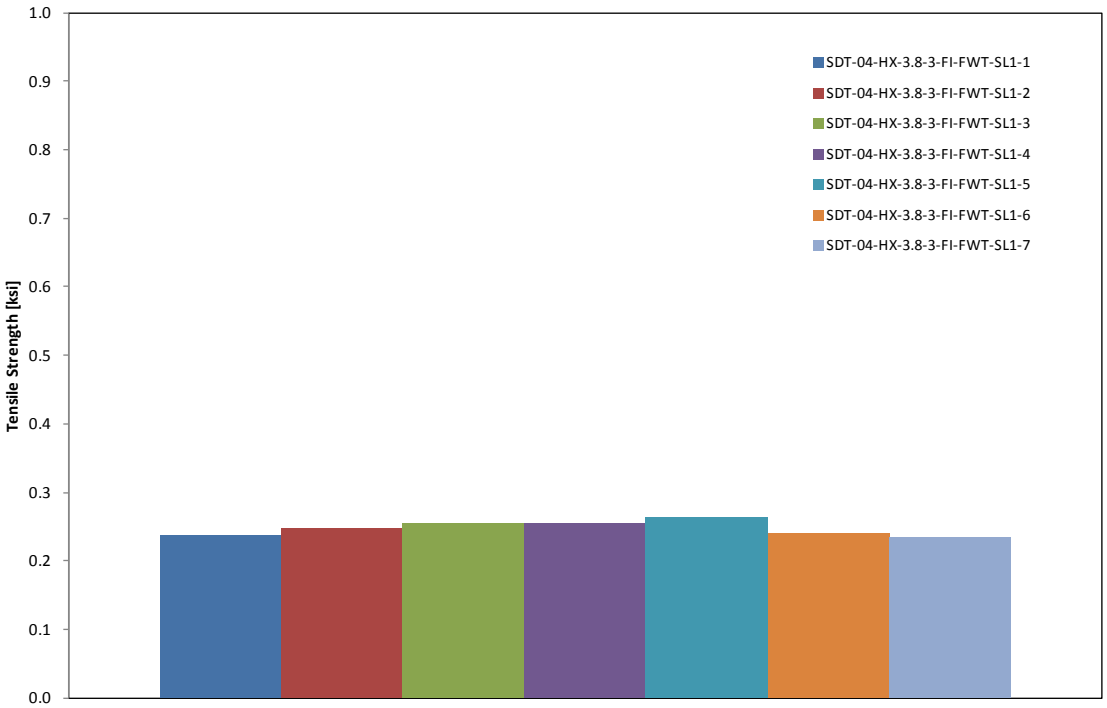

Figure F-43. Flatwise tensile strength for HRH-10–3/8–3.0 fluid ingressed

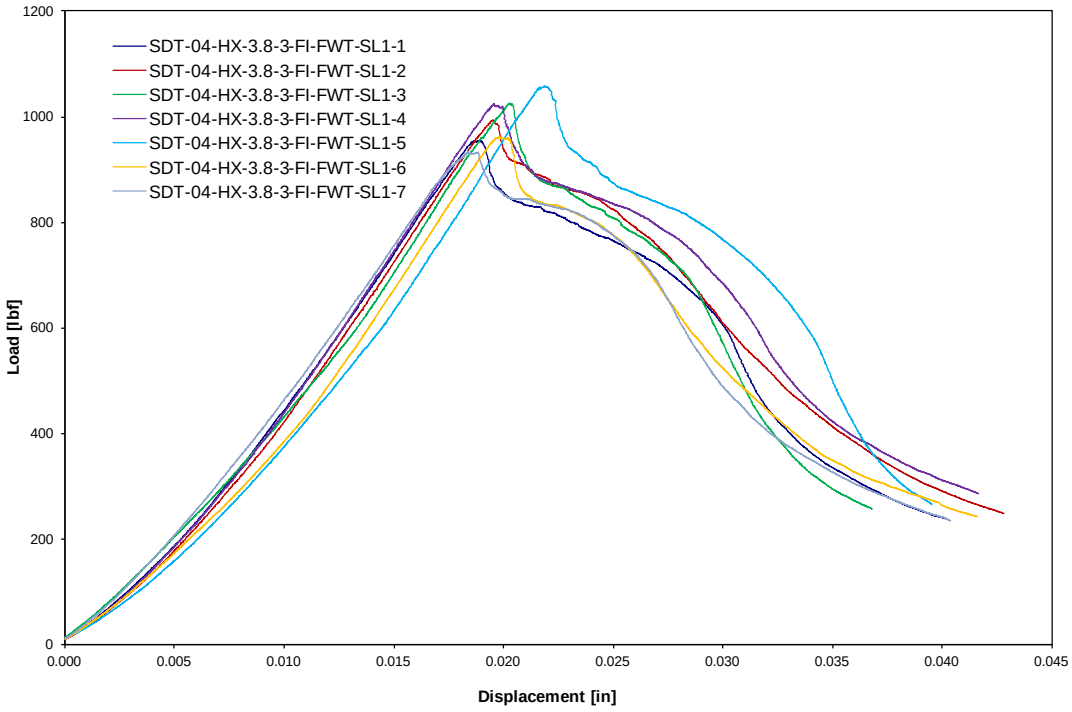

Figure F-44. Load vs. displacement curve for HRH-10–3/8–3.0 fluid ingressed

F.2.6 HRH-10/OX–3/16–3.0 DATA

F.2.6.1 HRH-10/OX–3/16–3.0 Baseline Data

Table F-27. Test summary for HRH-10/OX–3/16–3.0 baseline

Specimen	Flatwise Tensile Strength (ksi)
SDT-04-OX-3.16-3-BL-FWT-SL1-1	0.313
SDT-04-OX-3.16-3-BL-FWT-SL1-2	0.284
SDT-04-OX-3.16-3-BL-FWT-SL1-3	0.285
SDT-04-OX-3.16-3-BL-FWT-SL1-4	0.262
SDT-04-OX-3.16-3-BL-FWT-SL1-5	0.342
SDT-04-OX-3.16-3-BL-FWT-SL1-6	0.285
AVERAGE FLATWISE TENSILE STRENGTH	0.295
STANDARD DEVIATION	0.028
COEFFICIENT OF VARIATION (%)	9.479

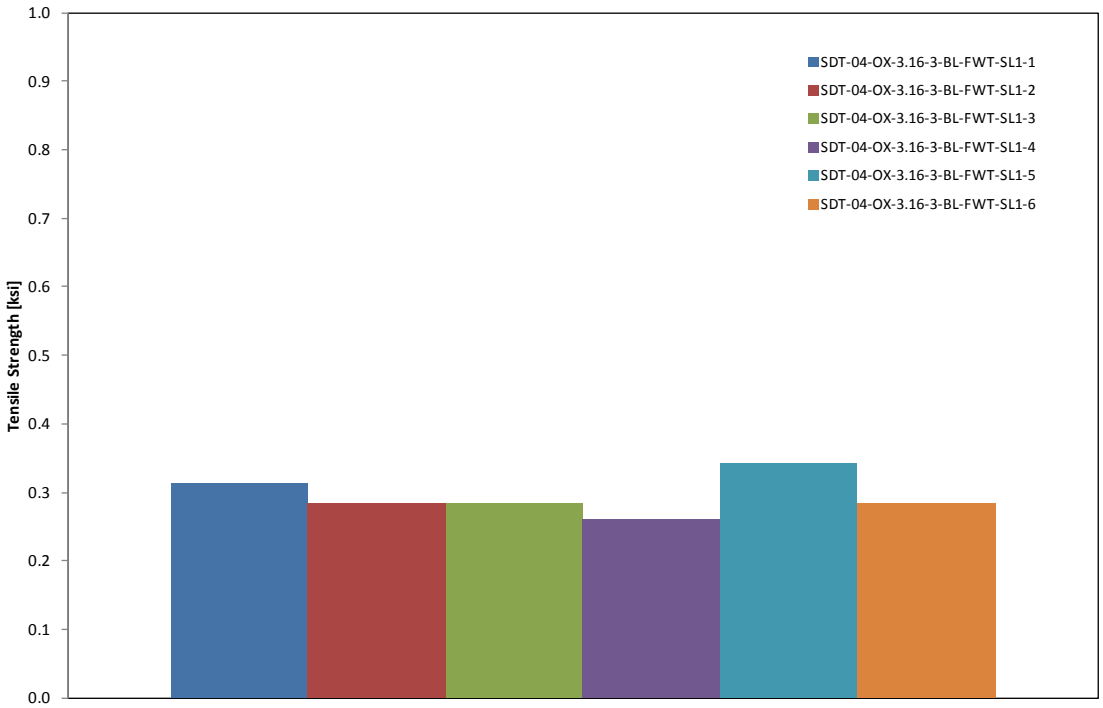

Figure F-45. Flatwise tensile strength for HRH-10/OX–3/16–3.0 baseline

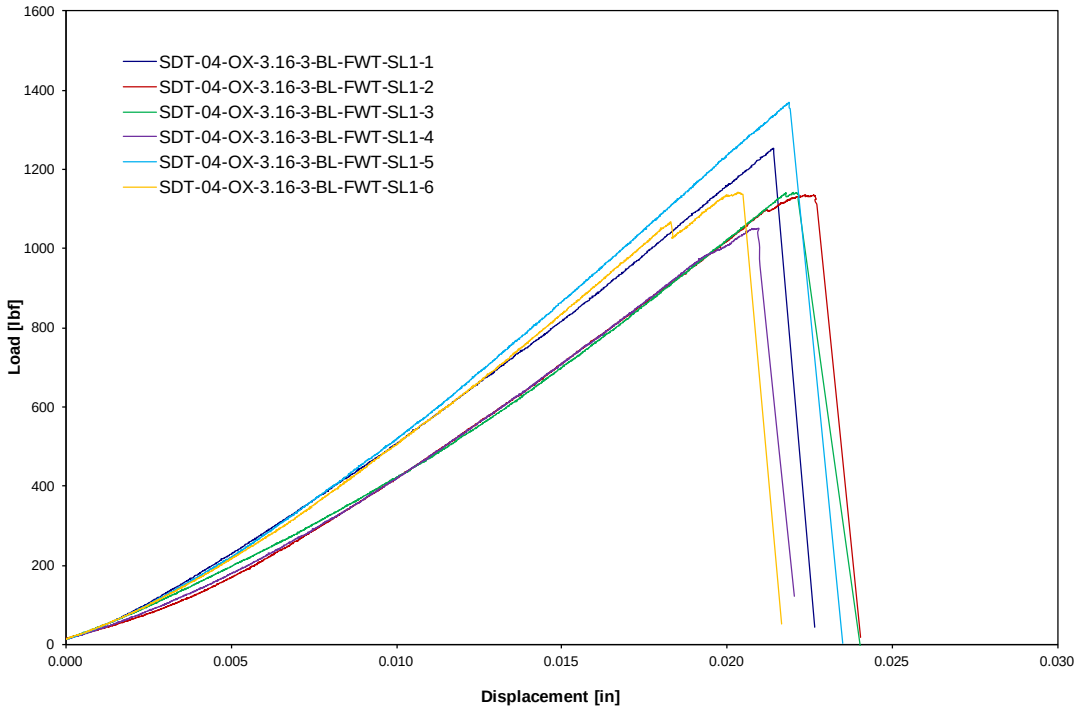

Figure F-46. Load vs. displacement curve for HRH-10/OX–3/16–3.0 baseline

F.2.6.2 HRH-10/OX–3/16–3.0 Fluid-Ingressed Data

Table F-28. Test summary for HRH-10/OX–3/16–3.0 fluid ingressed

Specimen	Flatwise Tensile Strength (ksi)
SDT-04-OX-3.16-3-FI-FWT-SL1-1	0.334
SDT-04-OX-3.16-3-FI-FWT-SL1-2	0.315
SDT-04-OX-3.16-3-FI-FWT-SL1-3	0.340
SDT-04-OX-3.16-3-FI-FWT-SL1-4	0.302
SDT-04-OX-3.16-3-FI-FWT-SL1-5	0.361
SDT-04-OX-3.16-3-FI-FWT-SL1-6	0.359
AVERAGE FLATWISE TENSILE STRENGTH	0.335
STANDARD DEVIATION	0.024
COEFFICIENT OF VARIATION (%)	7.016

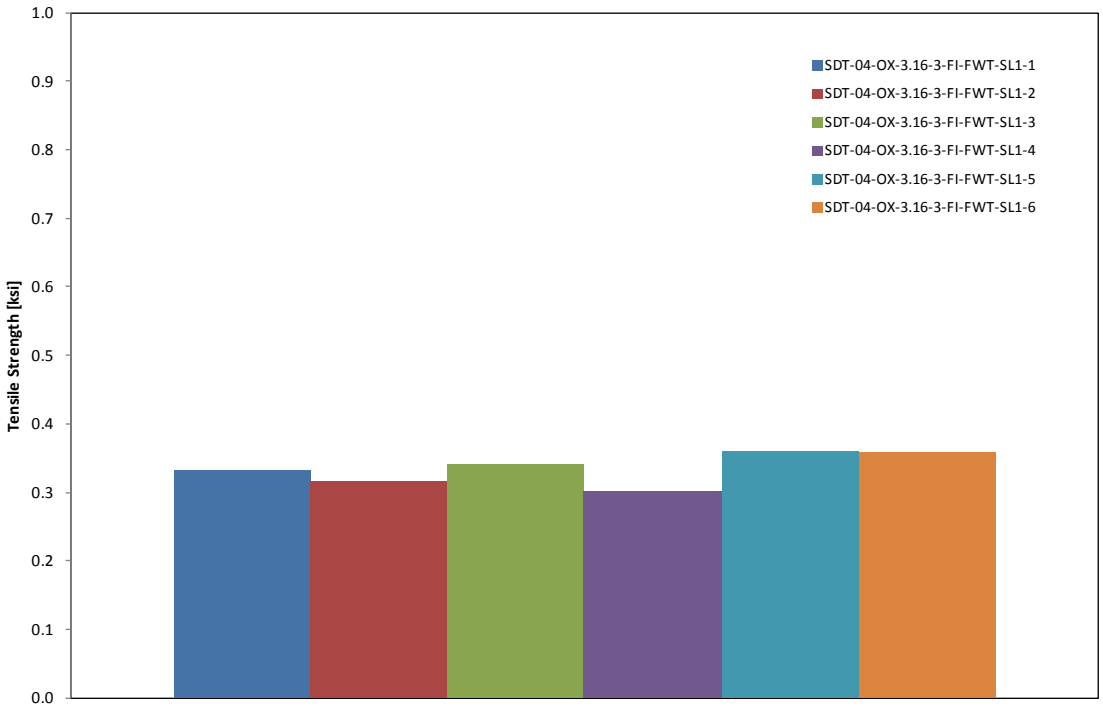

Figure F-47. Flatwise tensile strength for HRH-10/OX–3/16–3.0 fluid ingressed

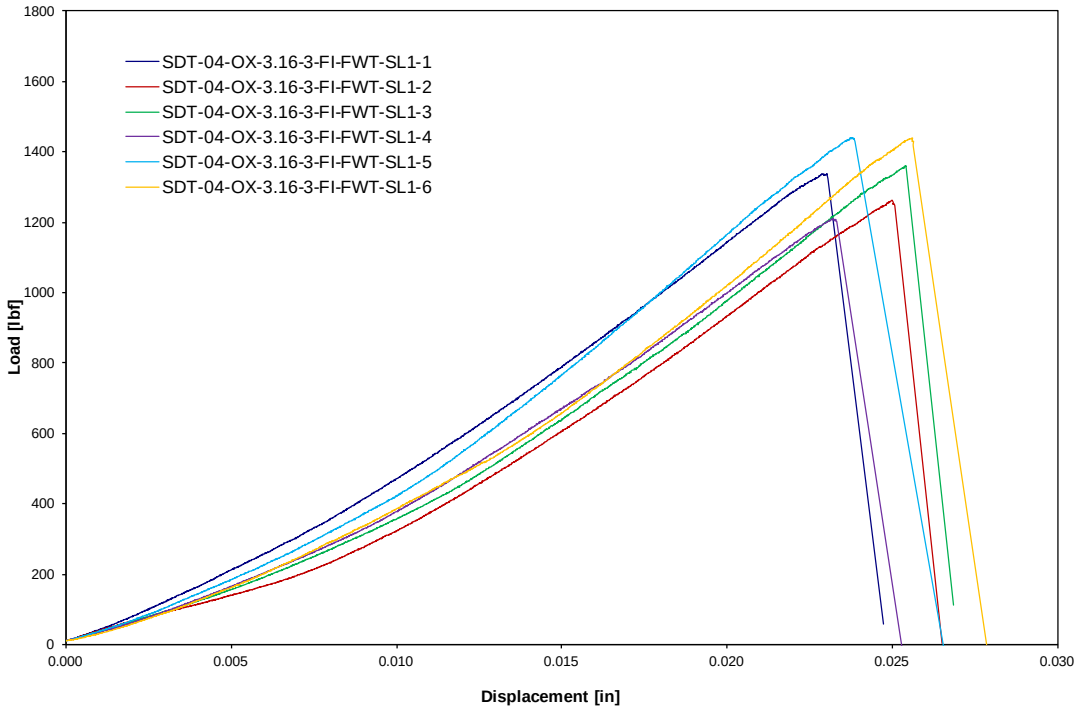

Figure F-48. Load vs. displacement curve for HRH-10/OX–3/16–3.0 fluid ingressed